Controlling reactive materials by crystallisation and hosting

Martin, Alan

Award date:
2014

Awarding institution:
University of Bath

Controlling Reactive Materials by Crystallisation and Hosting

Thesis submitted for the degree of Doctor of Philosophy

Alan Richard Guthrie Martin

University of Bath
Department of Chemistry
Supervisor: Professor C. C. Wilson

April 2014

Declaration

The research described in this thesis was conducted by the author at the University of Glasgow between October 2009 and May 2011 and at the University of Bath between May 2011 and May 2013. It represents the author's original and independent work, except where a specific reference is made to the contrary. No part of this thesis has been submitted previously in support of a degree at this or any other university.

_____

Alan R. G. Martin

Table of Contents

Acknowledgements

There are a lot of people who should feature prominently on this page. A lot of people who helped, supported and guided me through not only this thesis, but the last four years in its entirety. It was not easy, and not particularly fun at times, however the number of people ready to offer help and that I could really rely upon was truly appreciated.

Firstly the people who actually helped with the research, I will always be grateful to. Lynne Thomas – never has there been a postdoc so helpful and underappreciated, you helped me to understand and apply crystallography and were never afraid to tell me how bad my writing was. Your colourful assortment of corrective pens (never red) will be missed. Of course Chick, your help, encouragement and good cop to Lynne's bad could never be overvalued. Without your input, understanding and efforts, this would never have left the ground, and for that I am truly thankful. Chick, you are now the last man standing, well at least from north of the wall! Thank you!

I would like to thank the people that I had the pleasure of spending time in an office with every day. In Glasgow, where I learned from the best: Big Craig "from the Falkirk Council" – my first mentor, Bryan – "Diabetes is not just a way of living – it's a valid excuse" and also Lorretta, Martin, Javier, Marc and the unforgettable Ioana, whom I will never play cards with again! In Bath there was Louise "Big Hammers" Hamdy, Anneke "Happy Klappy", "Heavy-weight" Kate, classy "Chaz", Pilar and her eagles, Lucy – everyone's little sister, and Karen. And of course there were the ones that spanned the two locations with me, Andrew – "let's crash this ceilidh", Andras – "I can outrun a bull", and "Wee" Craig – or "Batman" as he preferred to be called. You were all a constant and yet welcome distraction that I couldn't have done without, even the project students…

My family, Mum, Dad, Brother and grandparents. How can you put a value on the support of the people who will care for you regardless of the outcome? Even several hundred miles away, they can be there in a heartbeat, particularly if something goes wrong and you need someone, even without asking. Your confidence in me is at times overwhelming, and I only hope that I can live up to all of your expectations and hopes for me, as you more than deserve your faith in me to be justified. You may never read this thesis, and if you do, you probably won't understand it, but you all contributed to it in some way and it is for you all.

Finally, Stephanie. Without this research we would never have met, and if we had never met, I doubt I would have managed this research, so all in all it's a good thing we did. For three years you have watched me stress and strain, through illness and a wrenching two year long distance relationship. Neither of us wanted me to go but we made the most of what little time we did get together. As a result however, Bath will always be a special place for us and this thesis will hopefully symbolise the start of what will be a long happy life together. That is, if you will continue to put up with me. I personally don't know how you manage it.

To all of you, coffee, tea, noodles, chocolate, all the scouts and scout leaders that cheered me up over the years on the weekends away from computers, X-rays and science, and to those people that I have forgotten to mention, a massive thank you.

Abstract

The research herein presents an approach to stabilising reactive materials by engineering and designing strategies for forming multi-component materials containing the reactive molecules by use of their non-covalent intermolecular interactions. These interactions may be utilised as part of a design approach to create new materials of more beneficial physical and chemical properties for the desired application.

The reactive materials focussed on in this research are organic peroxyacids, in particular peroxyacetic acid, *meta*-chloroperbenzoic acid and 6-phthalimidoperoxyhexanoic acid. The stabilities of these target materials under different conditions are probed to find a suitable environment for crystallisation experiments. Crystal structures of the materials were isolated and characterised and the peroxyacids were subsequently cocrystallised with materials chosen to interact with the target molecules to form new molecular complexes, including carboxylic acids, π stacking materials and metal salts.

A hosting approach was also employed to form multi-component systems containing these materials, crystallising them with larger, stable, structure-generating compounds with the aim of intercalating the reactive molecules in their stable structure. To this end, urea based compounds, cyclodextrins and Montmorillonite clay were investigated as hosting materials. Candidate multi-component materials were synthesised which successfully retain peroxyacid reactivity.

A second set of materials studied was agrichemicals, which also frequently have reactive character, in which a change in physical properties was pursued by the method of forming new crystalline complexes. Five new crystalline agrochemical molecular complexes were synthesised and tested for thermal stability in comparison to the original materials to assess for changes in properties of the multi-component materials.

List of figures

List of tables

1. Introduction

1.1 Scope

The outline of the research presented in this thesis is to assess the feasibility of using crystal engineering approaches and techniques to directly target reactive materials of commercial interest with an aim to altering their physical or chemical properties in such a manner as to enhance or modify the stability of the material in the solid state, with potential implications also for the solution state stability. The approach adopted in this work has primarily focused on solid state methods for product characterisation, predominantly using X-ray crystallography, in order to assess the impact of induced hydrogen bonding on the target materials by full structure elucidation and evaluation of products from synthesis by medium to high throughput X-ray powder diffraction screening methods, providing rapid indications of whether new materials have formed through solid state interactions, or by chemical reaction.

1.2 What is a reactive material?

The reactive materials described in this research, refer to selected organic chemicals of commercial interest which react readily under relatively mild reaction conditions to affect a desired function. In such circumstances, the reactivity of the material is inherently important in the reaction and often forms the rate determining step in a process. As a result, these materials can often prove difficult to work with safely or difficult to store for extended periods and can thus be less than practical in their normal state required for their function as a reagent in their proposed reaction. This research has primarily focussed on peroxyacids, also called peracids, and in particular a subset of these functional materials, the organic peroxyacids (or organic peracids). These materials are of great commercial relevance and interest as oxidizing agents in synthetic[1-3] and household applications[4, 5] reaching from cosmetics[6] to industrial bleaching[7]. Another set of reactive materials studied in this work are agrichemicals, particularly chlorophenoxyacetic acids, widely used as herbicides in which solubility over time is important as a time-release mechanism in the soil[8]. These agrichemicals can be highly affected by sudden rainfall, resulting in dissolution and loss of the material to the environment and thus reacting in higher concentrations than is needed. In this case, this research is focussed on changing the physical properties of these materials to attempt to make the solubility more suited to the application.

1.3 Working with reactive materials and stability

The instability inherent to reactive molecules is beneficial to their usefulness and activity. Although the reactivity is highly desirable at one point of the reaction, it can cause difficulties, for example in its preparation, storage, or dispersal[9, 10]. Working with peroxides in particular can potentially be hazardous as the highly energetic materials become unstable at elevated temperatures leading to explosions, and thus great care must be taken when working with them and their synergistic products[11]. The goal of modifying their physical properties to increase their stability is therefore useful for their application as well as for their potential safety and storage.

1.3.1 Organic peroxides

Organic peroxides are a well-known class of materials. They are highly energetic materials that are potentially very dangerous with a characteristic unpleasant sharp smell, however they have a wide range of potential uses. Synthetic methodologies regularly take advantage of their reactive attributes in the synthesis of polymers[12], utilising their ability to generate free radicals as initiators[13]; however their main use by far is by the consumer industry in the application of their reactivity by formulation of peroxides into cleaning agents and detergents. It is their oxidising power that is key to their usefulness in this application, chemically oxidising unsaturated fats, oils and colour from fabrics during the cleaning process[4].

The most reactive and hence unstable of all organic peroxides is the organic peroxyacid. They are commercially available and readily employed as a result of their ease of use[12] and within the field of consumer detergents, of particular interest, is the potential for organic peroxy acids to work as low temperature laundry bleaches[14]. Unsurprisingly, the application of this goal has proved problematic for the industry and the main problem lies in the inability to control the reactive peroxyacid effectively. Decomposition of the peroxyacid in the formulation renders the detergent less effective over time as the peroxide activity is lost, leaving only the parent acid without the oxidizing ability of the reactive material[10]. This has the result of greatly limiting shelf life of any mixture containing the peroxide compound[9]. The strong oxidising ability also poses compatibility issues between the reactive component and the other materials present, such as perfumes[15] and enzymes, leading to a need to seek a medium for storage of the oxidising material separate of the other components, or by only selecting components in the formulation that the reactive material will not readily oxidise. These issues have yet to be overcome in any reliable or commercially viable way and it is therefore within that area

that this research on these particular reactive materials is focussed. Three different peroxyacids have been studied: peroxyacetic acid, meta-chloroperbenzoic acid and 6-phtalimidoperoxyhexanoic acid (Figure 1). These peroxyacids are all very reactive, but have very different molecular characteristics such as size, shape and functionality.

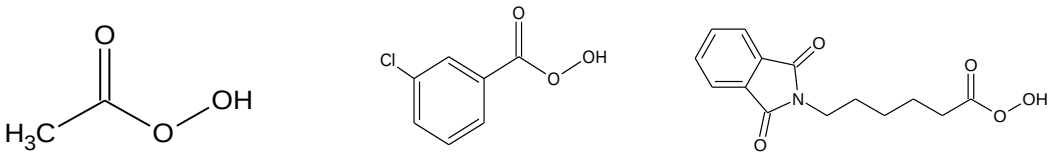

Figure 1 - Peroxyacetic acid, m-chloroperbenzoic acid and 6-phthalimidoperoxyhexanoic acid.

Organic peroxy acids can be generalised by the notation $R(CO_3H)_n$ where R can be substituted with an alkyl, aryl, cycloalkyl or heterocycle and n is 1 or 2 (Figure 2). They are normally named after their parent acid prefixed by either "peroxy" or "per", denoting that the acid functionality has been oxidised.

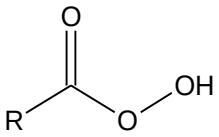

Figure 2 - Generic peroxyacid molecular formula.

The simplest peroxyacids may be synthesised by the reaction of the parent carboxylic acid with 30%-98% hydrogen peroxide with an acid catalyst in a reversible reaction between the parent acid and the peracid[12], as can be seen for peroxyacetic acid (Figure 3).

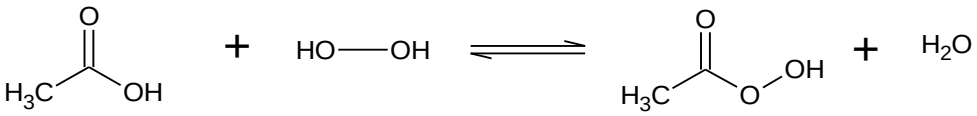

Figure 3 - Reaction scheme for oxidation of acetic acid to form peroxyacetic acid

As this is an equilibrium reaction, the concentration and proportion of the hydrogen peroxide has an important role to play in the eventual concentration of peroxyacid. It is therefore necessary during synthesis to maintain a high concentration of hydrogen peroxide to ensure sufficiently high conversion of the parent acid. Upon creation of the peroxyacids, they are typically purified by distillation and fractional freezing, obviously taking great care to avoid thermal decomposition and potential explosions. Larger parent acids are less soluble in aqueous hydrogen peroxide, and can instead be prepared by the same reaction, but using sulphuric acid, or the more powerful acid catalyst methane sulfonic acid, as a solvent to aid dissolution and accelerate conversion. Other preparation methods, in which diacyl peroxides have a risk of forming, may be employed using sodium

peroxide whilst chilling the reaction under strictly controlled stoichiometric conditions. Preparations of peroxybenzoic acids are relatively simple and commercially attractive, as they follow the same reaction as a small chain aliphatic peroxyacid, with only the addition of hydrogen peroxide required, which may be further catalysed by stimulating the radical reaction initiation with ultraviolet light, various metals or salts[11, 12].

The equilibrating nature of the synthesis of peroxyacids means that during storage and decomposition of the peroxyacid, the reaction is reversed. Water, present from environmental sources, aids in pushing the equilibrium in the reverse direction, towards the formation of the parent acid and thus affecting the yield of peroxyacid (Figure 4). During synthesis this is combatted by the use of water azeotroping solvents, a factor key to the crystallisation of these materials. Prevention of the decomposition is a significant element in the development of these materials, not only for storage, but for their likely use in aqueous suspensions.

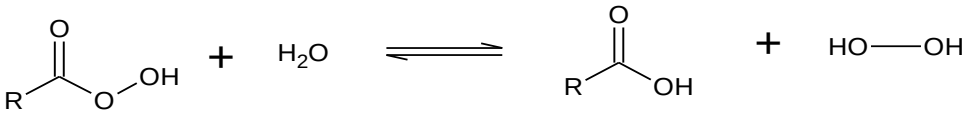

Figure 4 - Reversed reaction of formation of a peroxyacid, emphasising the role of the "decomposition reaction" in the presence of excess H_2O.

1.3.1.1 The chemical activity of peroxyacids

Peroxyacids by nature are very good oxidising agents and react with a large range of materials. They are used for a wide range of reactions and are commonly used for epoxidations and hydroxylations of many organic compounds including, but not limited to acetates, amines, nitroso compounds, oximes, imines, azo compounds, aldehydes, azines, hydrazones, phenols, esters, ketones and ketoacids. A common example in which this reactivity is used is in the Baeyer-Villiger reaction (Figure 5)[16].

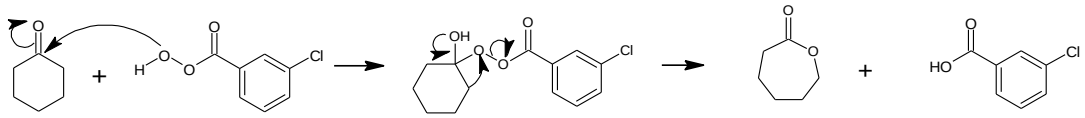

Figure 5 - The Baeyer-Villiger reaction mechanism.

Analysis of this reaction indicates the potential for the terminal oxygen of the peroxyacid molecule to act as an electron donor, nucleophilically attacking the carbonyl at the carbon position, disrupting the double bond[1]. The nucleophilicity of the terminal oxygen is the driving force of the oxidation and hence the reactivity of the peroxyacid family of molecules.

A second common reaction of peroxyacids is the Prilezhaev epoxidation reaction, the mechanism of which is quite different (Figure 6).

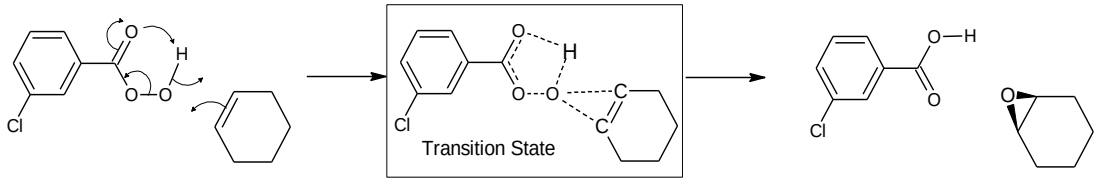

Figure 6 - Prilezhaev epoxidation of cyclohexene by meta-chloroperbenzoic acid.

In the Prilezhaev reaction, an intramolecular hydrogen bond forms within the peroxyacid group in solution, resulting in a high degree of polarisation of the group, leading to the generation of a highly electrophilic terminal oxygen atom that attaches through the shown "butterfly" transition state across a double bond. The peroxyacid will attack any double bond, however the more substituted the bond is, the more stable it will be with the peroxyacid. It is important to note that oxidation by peroxyacids is not considered to be a radical driven reaction due to the high activation energies required for homolytic cleavage of the peroxide bonds which does not support the kinetics of observed oxidation reactions[1]. Again it is shown that the basicity of the terminal oxygen is crucial in the reaction, and as thus was an obvious target for stabilisation of the peroxyacids.

Solvent is also known to have an important role to play in the reaction of peroxyacids. With respect to the present work, the peroxy group has been shown in many cases to be assisted by altering the polarisation of the terminal oxygen by a polar solvent molecule, with the solvent molecule itself being an integral part of the transition state of the oxidation reaction, as with the oxidation of aromatic amines (Figure 7)[1].

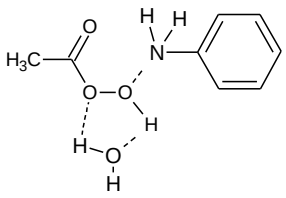

Figure 7 - Transition state in oxidation of an aromatic amine by a peroxyacid showing solvent (water) involvement.

The mechanism confirms that this is not a radical oxidation, as when radical inhibitors are added, no effect is observed and the reaction proceeds unhindered. A similar effect is observed with alcohols. The hydroxyl group on the alcohol in the oxidation of a sulphide acts similarly to the water molecule in the transition state shown in Figure 7, with the oxygen and the hydrogen of the alcohol hydrogen bonding to the non-terminal oxygen and the peroxy-hydrogen (Figure 8).

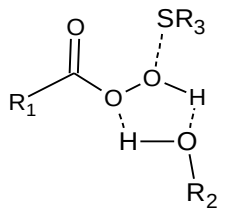

Figure 8 - Ring transition state present upon oxidation of a sulfide with an alcohol solvent environment.

In basic solvents, such as dioxane and DMF, an open chain intermolecular hydrogen bond intermediate is formed, with the basic oxygen bonded to the acidic hydrogen of the peroxy group (Figure 9).

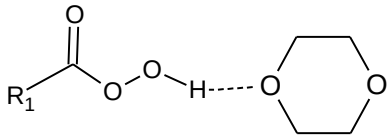

Figure 9 - Open chain intermolecular hydrogen bond intermediate comprising of a generic peroxyacid and 1,4-dioxane.

The hydrogen bonding to a basic solvent reduces the rate of the reaction, showing that the reactivity is decreased by the inclusion of basic solvents[2, 17].

These observations indicate that not only will the choice of solvent be crucial in working with these reactive materials, but also that they may be modified by interaction of the functional group through hydrogen bonding. These arrangements observed in these mechanisms in the solution phase, show which possible hydrogen bonding motifs may be reinforced or created in the solid phase in order to target reducing the reactivity of this family of molecules.

1.3.2 Agrochemicals

The second family of materials studied in this research is agrochemicals, or active agrochemical ingredients, AAI's. The term agrochemical can literally mean any chemical that is used in agriculture but within the context of this research, it refers solely to the subcategory of pesticides, herbicides and fungicides. The field of AAI's is a closely scrutinised one, that over recent years has come under a great deal of public and resulting legislative pressure to regulate and control the chemicals being deployed, to ensure they are used effectively, safely and conveniently. This entails having knowledge of, and being able to predict accurately the bioactivity, solubility and dispersibility of the materials being used. With the delivery method for these materials generally spraying over exposed land, environmental factors such as the weather and rainfall have a dramatic effect upon the dosage and permeability of the materials into the soil and surrounding environment[8].

Heavy rainfall in particular can remove the compounds completely from the target location, allowing water soluble materials to seep rapidly into groundwater, eliminating their effectiveness and contaminating other areas and waterways within a matter of hours[18]. The usefulness of any given agrochemical is therefore a complex balance between several factors, chiefly the solubility, the bioavailability, the physical stability, safety and of course cost[8].

Many attempts have been made over the years to ensure these goals are achieved, with varying degrees of success. These have included granulation, microencapsulation, and use of concentrates, emulsions, wettable powders and suspensions[8]. All of these, however, have dealt with altering the formulation of the material and not the physical properties at the molecular level. Much of the research outlined here focusses upon modification of the physical properties of the primary material directly.

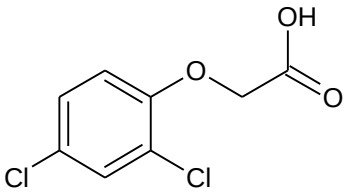

Figure 10 - 2,4-Dichlorophenoxyacetic acid (2,4-D).

The chosen family of materials for study in this research is that of the phenoxyacetic acid herbicide family. This includes the material 2,4-dichlorophenoxyacetic acid (2,4-D; Auxin) (Figure 10). This material is by far the most commonly used herbicide and was the first in the family of phenoxyacetic acids to be synthesised, from a reaction of chloroacetic acid and 2,4-dichlorophenol. It is a synthetic plant hormone which regulates growth by absorption through the leaves of a broad leaf plant such as a weed. The environmental properties of 2,4-D are well known and it is recorded to have a half-life of 10 days upon application in a controlled environment. However, it is water soluble and this has led to it leeching into water supplies.

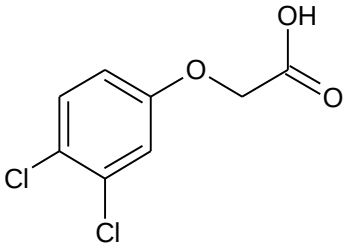

Figure 11 - 3,4-Dichlorophenoxyacetic acid (3,4-D).

The second material in this family studied is that of 3,4-Dichlorophenoxyacetic acid (3,4-D) (Figure 11). 3,4-D is an isomer of 2,4-D and is less commonly used. It is a less water soluble analogue and is typically used as a replacement in areas where rainfall is high due to its similar chemistry yet higher stability.

One particular methodology that has not been widely applied to these materials is that of modification of the reactivity or stability by crystal engineering methods, in the solid form before formulation methods have been applied. Alteration of the melting point of these materials has a direct effect upon the water solubility, so modification of the chemical structure will in turn affect the water solubilities of the materials[19]. This research into these materials is largely focussed upon this methodology. Crystal engineering techniques are employed through medium throughput crystallisation to modify the crystal form of the material in a way that will affect the melting point (and hence solubility) in a favourable way, also assessing any outcomes the structural motifs have upon the stability of the molecules.

1.4 Achieving control of reactive materials via structural modification

The stability of a material in the solid state is not only dependent upon the chemical characteristics (functionality and reactivity) of the molecule, but also upon its interaction with other molecules of the same type, or of different molecules present. Intermolecular interactions can have a dramatic effect upon the stability and physical properties of a material. Implementing this observation in a practical methodology is thus a theoretically plausible concept for altering the physical properties of any given target material, providing an understanding of the preferred interactions of the target molecule, allowing these to be predicted and adequately understood. A target material could potentially be matched with any secondary material with favourable interactions, and in particular in the solid crystalline form, could form a new intermolecularly stabilised complex with distinct physical characteristics, whilst retaining the chemical character (and effectiveness) of the individual molecules.

Intermolecular interactions are normally relatively weak in comparison to covalent bonding, and could be seen as “temporary molecular binding” for a reactive material, stabilising its physical properties in the solid state, yet upon dissolution releasing the target molecule. This would essentially offer the capability to switch on and off the modification of the material, and hence its modified reactivity. It was the aim of this research to use this approach, as has become more commonplace in the pharmaceutical industry, to target the given reactive materials to form complexes using intermolecular interactions.

There are of course many types intermolecular interactions, however the ones used for design within the context of this research are outlined here and can be considered tools in a molecular solid state crystal designing toolbox for the creation of new crystalline materials with modified properties.

1.4.1 Hydrogen bonding

Although much weaker than a covalent bond, the hydrogen bond is considered the strongest of the intermolecular interactions[20] and thus the most important structure directing factor in molecular solids. It is also highly directional, allowing not only for molecular recognition in design, but also orientation prediction of the assembled forms[20].

Hydrogen bonding is a donor-acceptor interaction that has similarities to the characteristics of a Brønsted-Lewis acid, through the presence of a proton donor (D) and a proton acceptor (A)[21]. The interaction originates from a difference in electronegativity of the donor atom and a bonded hydrogen. The difference in electronegativity creates a withdrawing of electron density from the hydrogen to the donor, resulting in a partial de-shielding of the hydrogen atom creating a dipole. The partially unshielded hydrogen atom is then susceptible to interaction with the acceptor atom, which may be any atom with available lone pairs of electrons or polarisable π electrons. This leads to the formation of an attractive bond between the donor and acceptor atoms with a hydrogen atom positioned between the two (denoted D–H···A), at a point that may be influenced by several factors. Very strong hydrogen bonds (HBs) share some characteristics of covalent bonds, but HBs can also be as weak as van der Waals forces; the majority of hydrogen bonding interactions lie between these extremes[21]. They may exist as intermolecular or intramolecular HBs and are competitive, i.e. a stronger, more geometrically favourable, hydrogen bond interaction will prevail over a weaker one, in the absence of other structural considerations. In general hydrogen bonds are predominantly linear and the D···A distance should be less than the sum of the van der Waals radii for the donor and the acceptor.

Hydrogen bonds are generally classified into three categories – strong, medium and weak, however in reality, it is a continuum with no real physical boundaries between the categories. The categories defined by Jeffrey[21] however are generally a useful descriptor and they are outlined here in Table 1.

Table 1 - Properties of strong medium and weak hydrogen bonds[21]

Bond category	Strong	Medium	Weak
D-H···A characteristic	Mostly covalent	Mostly electrostatic	Electrostatic
Bond lengths	D-H ≈ H···A	D-H < H···A	D-H << H···A
H···A (Å)	1.2-1.5	1.5-2.2	2.2-3.2
D···A (Å)	2.2-2.5	2.5-3.2	3.2-4.0
Bond angles (°)	175-180	130-180	90-150
Bond energy (kcal mol^{-1})	14-40	4-15	<4

A strong hydrogen bond may be formed (with typical D···A distances of less than ~2.5 Å for O···O and less than ~2.55 Å for N···O) by donors with a deficiency in electron density or an acceptor with a particularly high electron density, such as –O$^{\delta-}$-H$^{\delta+}$ and O^{-}-P. The large amount of electronegativity on the donor atom de-shields the hydrogen atom effectively giving it a greater δ^{+} charge which is attracted to the negative charge on the acceptor atom. They may also be the result of a "forced strong hydrogen bond" where the conformation pushes the donor and acceptor closer together than would be expected for the types of donor and acceptor included[21].

A moderate strength hydrogen bond is much more common, with donor – acceptor distances of between around 2.5 Å and 3.2 Å they are considered a softer interaction, generally occurring between neutral donor and acceptor atoms, such as –O-H···O=C, where the acceptor has free electron pairs which are able to assist in the bond interaction.

A weak hydrogen bond is the result of a smaller difference of electronegativity between the covalently bonded hydrogen and the donor atom. An example of this would be a -C-H donor. It may be the case that no lone pair is available as acceptor, and in such instances a polarisable π electron orbital, such as in an aromatic ring or a double bond may be the acceptor. Weak HB distances fall into the region of 3.2 Å to 4.0 Å and are directional, distinguishing them from van der Waals interactions of similar strength[21].

The distinction between these three classes allows for a description of a bond which gives a primary indication of strength of the intermolecular interactions. Hydrogen bonded molecules with stronger interactions are more tightly bound and it follows that they are more stable, although designing a structure with stronger interactions is more complicated than merely choosing the strongest donors and acceptors.

HB geometry is not always a single D–H···A interaction, for example in bifurcated hydrogen bonds, where there are two donors to one acceptor or two acceptors to one donor (Figure 12).

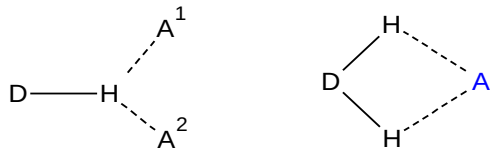

Figure 12 - A generalised example of a single donor-double acceptor bifurcated bond and a double donor-single acceptor bifurcated bond.

In a bifurcated single donor hydrogen bond the hydrogen atom is shared between the two acceptors, lying is a position closest to the stronger of the two acceptors, on a plane between the two, assuming there are no other external influences upon the bond. In a particularly strong bifurcated hydrogen bond of this type, the position of the hydrogen atom may be spread between the two acceptors in the plane of the donor and acceptor atoms. Alternatively, the hydrogen atom may be positionally disordered over two sites. In a double donor-single acceptor bond, two hydrogen atoms on the same donor atom may interact with a single acceptor atom[22]. This is recognised by a D-H angle that is different to that which would be expected by VSEPR theory, i.e. the D-H bonds are bent towards the acceptor.

In order to describe the often complex hydrogen bonding patterns and motifs present in a 3D crystal structure, a simple method of presenting these can be employed. The method used within the crystallographic community is known as graph set notation. The graph set notation effectively defines the morphology of hydrogen bonded arrays within the structure as well as their constituent donors and acceptors[23]. The motif is identified and one repeating unit is used to generate the notation.

- For intermolecular hydrogen bonds, the designator (X) C, R or D is assigned, corresponding to either a chain, ring or dimer morphology respectively.
- For an intramolecular hydrogen bond, an S designation is given.
- The number of hydrogen bond donors (d) and acceptors (a) is assessed and recorded as superscripts and subscripts, respectively
- The number of atoms in the repeating unit is recorded in parentheses (Y)

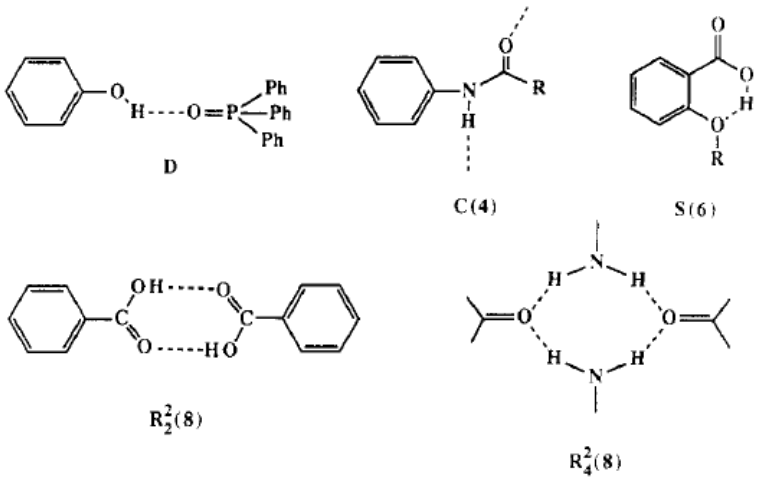

Figure 13 - A sample of example motifs and their corresponding graph set notations[23].

Thus the eventual graph set is recorded in the form $X^d_a(Y)$ (Figure 13). An example of this is the common motif displayed by a carboxylic acid dimer (Figure 13, lower left), which would be defined as a $R^2_2(8)$ motif, being a ring morphology with two hydrogen bonding donors, two hydrogen bonding acceptors and eight atoms in total forming the ring.

1.4.2 Π interactions

Molecules with π electrons, either in a delocalised π cloud or in the π orbital lobes of a multiple bond may interact with each other. Although significantly weaker than hydrogen bonding, these π electron interactions, or π-π bonds, are significant and useful for molecular stacking. They π electrons of two neighbouring molecules, such as aromatic rings may interact with each other even in the presence of hydrogen bonding to the σ bonds of the system. The molecules of a π-π bonded material approach each other such as to maximise this interaction within the allowances of stronger interactions and steric obstacles. Given free rein, the molecules would tend to stack indirectly over each other so that the π orbitals would interlock most effectively – in the case of benzene, this would mean the rings would stack directly on top of each other (Figure 14, left) however when the ring becomes substituted, this is offset.

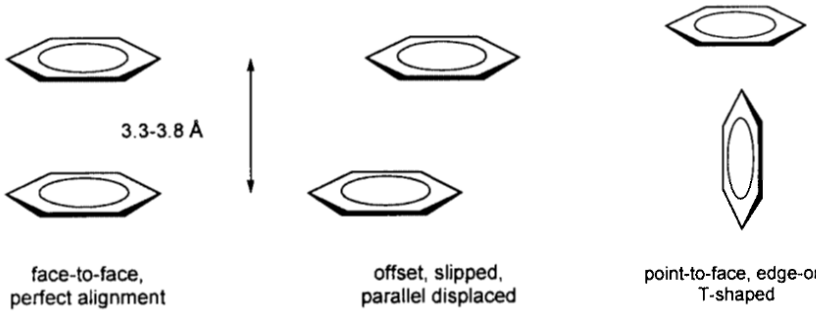

Figure 14 - Illustration of π-π stacking interactions and a perpendicular π-σ interactions of aromatic rings[24].

Depending on detailed electron distributions, aside from stacking planar to each other, the planes may be skewed (Figure 14, centre) or somewhat perpendicular (Figure 14, right), allowing for edge to face π-σ interactions[24, 25]. Where π-π stacking is involved in a parallel arrangement, the accepted distance limits for a significant interaction are 3.3 Å - 3.8 Å, limited by the attractive nature of the π – σ charge band and the Pauli repulsion of the π-π negative charged fields (Figure 15), with an average bond energy of approximately 2 kJ mol^{-1}.

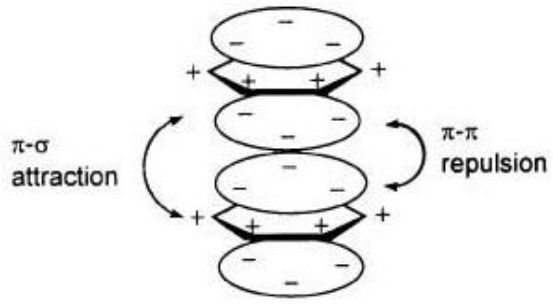

Figure 15 - Pauli attraction and repulsion effects in stacked aromatic rings[24].

In molecules where there is a large amount of aromatic character, the π-π stacking interactions may dominate over weaker or less abundant hydrogen bonding, becoming the primary driving force in the structural arrangement of the crystal.

1.4.3 Halogen interactions

One final type of significant intermolecular interaction found in the materials studied here, is that of halogen interactions. Halogen to halogen interatomic distances in crystalline materials are often significantly less than the sum of the van der Waals radii for the two halogen atoms. As a result of this they are regarded a “close contact”. This interaction may merely be a result of the greater strength interactions directing the packing, but the halogen interactions are known to have a smaller, though not insignificant directing

influence upon the crystal structure. These may exist between symmetrical pairings of interacting halogens, such a Cl···Cl, I···I or Br···Br, or an unsymmetrical interactions between two different halogen types such as Cl···Br. These interactions are categorised into two classes.

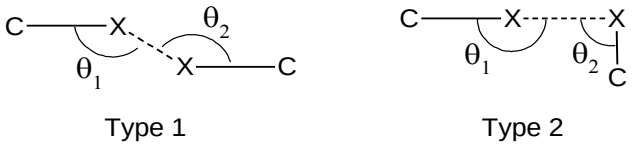

Figure 16 - Illustration of halogen-halogen interaction types.

By the definition given by Desiraju [26], type 1 describes an interaction between two halogen atoms where the angle between the carbon-halogen bond and the halogen-halogen contact, θ, is equal for both molecules: $\theta_1=\theta_2$. It is generally accepted that a type 1 contact is a consequence of crystallographic symmetry, with the halogen atom interaction across an inversion centre. Type 2 is the description given to an arrangement where one of the angles θ is approximately equal to 180° and the other is approximately equal to 90°; the example of $\theta_1\approx180°$, $\theta_2\approx90°$ is shown in Figure 16. Type 2 halogen bonding results from a polarisation of adjacent halogen atoms from anisotropic non-spherical flattening of the electron density causing attraction; these can be regarded as donor-acceptor interactions[27].

Also to be considered are more classical donor-acceptor interactions involving halogens. In such instances a covalently bonded halogen (X) may interact with an electron rich donor (D) in the form D···X-Y, where Y is the atom covalently bonded to the halogen. This, similarly to hydrogen bonding, is a result of the differences in electronegativity between the two covalently bonded atoms, resulting in formation of a dipole, creating an electropositive halogen, attracted to the donor site. Such an interaction can have varying strengths depending upon the atom types and differences in electronegativities. They thus span a large bond energy range (5-180 kJ mol^{-1}) [28].

1.5 Crystal engineering

A field that has potential for changing the physical properties of the given target materials in order to alter the reactivity is Crystal Engineering. The aim is to design rationally the solid state crystal structure of the target materials by influencing available intermolecular interactions with the introduction of secondary materials to incorporate into the lattice. This method of engineering crystals has had much success over recent years, particularly in the pharmaceutical industry[29, 30-35], in modifying solid forms of active ingredients in order to

tune physical properties to those beneficial for the desired application and is becoming commonplace in the process of producing new, efficient, stable forms of active components. The field of crystal engineering was defined by Desiraju to have three facets, that of studying intermolecular interactions, the study of packing modes with the aim of defining a strategy and the study of crystal properties and how they may be fine-tuned corresponding to modifications in the packing[20].

Integration of a secondary component into a crystal structure is known to have a wide array of physicochemical effects and is thus suited well to the research detailed within this thesis. Physicochemical properties known to be influenced by modification of the crystal structure include solubility[31, 36], bioavailability[31, 37], density, refractive index, conductivity (both thermal and electrical), melting points[32], and, influencing some of these, free energy[27, 31], chemical potential and thermal stability[35, 38]. The reduction of reactivity has been achieved with other materials within the literature through solid state modification by crystal engineering methods however it is by no means commonly adopted. Co-crystallisation in particular has be used to quench reactivity of photodecarbonylation reactions[39], and the use of halogen bonding in combination with π-π stacking has been used in an attempt to control the reactivity in the solid state[40].

This approach addresses the way molecular building blocks are arranged in a designed optimal superstructure, and as such it is a semi-synthetic methodology that identifies molecular building blocks of favourable molecular properties and intermolecular interaction capability which can be combined with a chosen primary material in a directed self-assembly of a new, designed, crystalline product[41]. Aside from the legal ramifications of designing "new materials" that may be patented from older materials, hence giving them a new lease of life[33, 35], crystal engineering is well suited as a method of providing a delivery method for a primary active component as the process does not necessitate the breaking of covalent bonds, hence no chemical changes are imposed upon a primary material, therefore retaining its intrinsic activity as an individual component whilst changing its solid state properties[33]. Of course an influencing factor in the design of a new material by crystal engineering is that of reversibility; the gained stability of a reactive material, once achieved, must be able to be reversed. The methods chosen here must facilitate such an easy return to the reactive state upon application. In most cases this would be a dissolution process, releasing the reactive material from the intermolecular interactions of the stabilised material upon dissociation from the host or secondary influencing material.

The primary driving force in the design of supramolecular structures is usually hydrogen bonding. Although other interactions are significant, it is to be expected when an attempt is made to predict a final outcome of a crystallisation, that the strongest interactions will have the greatest influence over the final structural arrangement. The empirical observation of predictable robust hydrogen bonding motifs has led to the creation of a guiding set of rules for supramolecular structure prediction that were outlined by Etter in 1990[23]. The Etter rules for self-assembly of molecules containing hydrogen bonding sites are as follows:

1. All good proton donors and acceptors are used for hydrogen bonding;
2. Six membered ring intramolecular hydrogen bonds form in preference to intermolecular hydrogen bonds;
3. The best proton donors and acceptors remaining after intramolecular hydrogen bonds are formed will form intermolecular hydrogen bonds to one another.

These are augmented with additional rules for specific interactions[23]. Those rules are easily explained and make sense: for the first rule, it makes logical sense that no interaction potential should remain unused; for the second rule, an intramolecular bond would be formed first, as the molecule need no seek for an intermolecular interaction, when a geometrically favourable one within the same molecule is available; the third rule follows from the first.

The concept of a molecular synthon[42] is a useful one within this context and describes an arrangement of molecular components of which the molecular interactions are known and reliably form a bonding pattern between them. The synthon may be between the active material and another material present in the crystallisation and as such is a building tool in the larger crystal structure. Depending upon the available bonding sites upon the molecules, the interactions may self-assemble in the presence of each other in a way as to maximise the use of the interactions, forming one large crystalline material containing more than one component. As such when designing a molecular arrangement, the choice of the secondary synthons is one of, if not the most important step. A secondary molecule's interacting sites must be matched to the primary material in order to express favourable interactions and generate a synthon. A crystallisation of two molecules may have multiple possible synthons as the hydrogen bonding may have unexpected preferential attraction or hindering features that prevent or drive the desired structure forming (Figure 17).

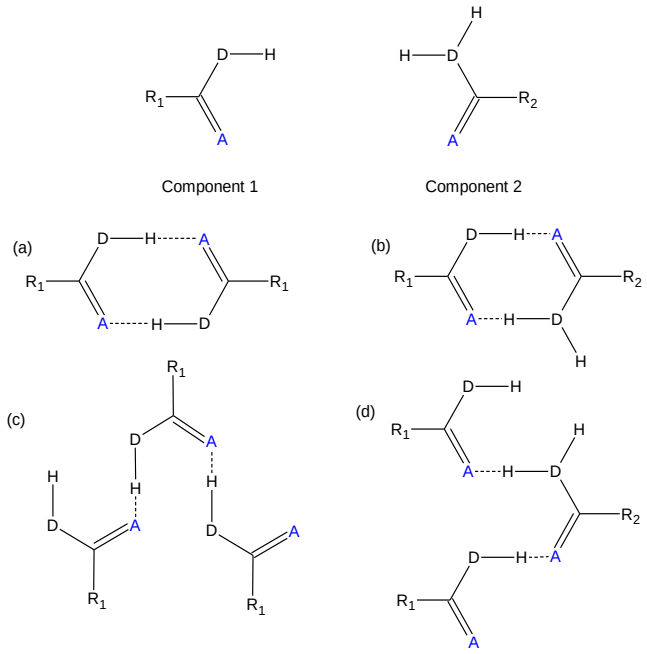

Figure 17 - An example of two molecules generating multiple synthons. (a) Component 1 self dimerised, (b) a ring generated by the dimerisation of components 1 and 2, (c) component 1 recrystallising to form a pure component 1 chain, (d) components 1 and 2 alternating to form a multi component catemeric chain

The interaction between components with favourable hydrogen bonding potential however is a competitive process. This can have the effect of either helping or hindering formation of a designed material. If the available hydrogen bonding pattern of a particular molecule in its pure state allows it to favourably hydrogen bond to itself, such as in a carboxylic acid where reliable dimerisation is observed[43,44] (Figure 17), the relative energetic facility for it to do so may be greater than for it to hydrogen bond to another molecule, hence the material would recrystallise on its own without any inclusion of a secondary material at all, following the most energetically efficient route. For this reason, molecules are chosen that exhibit a degree of complementarity, levelling the energetic playing field to allow crystallisation of the materials together, or if possible, making them more energetically favourable to co-form than to recrystallise in a pure state[45].

This necessitates matching the hydrogen bond donor and acceptor sites in the primary and secondary components, aiming to introduce partners for molecular recognition through these in the solution state where the self-assembly process is taking place, leading to pre association and coalescence in the solid state[20]. Predicting likely interactions may be aided by the use of preliminary crystallisations of a material and observation of the outcomes. However, for statistical analysis and collation of similarly featured materials and crystal structures, it is becoming increasingly more efficient and reliable to assess likely interactions of a given material computationally. The Cambridge Structural Database[46] has thus been widely utilised here, and has proved valuable in assessing which types of

interactions a given material is likely to prefer, by assessing all recorded interactions of that material known and optionally including those similar to the target material[47]. This field is now entering a point where prediction of new materials that are resultant from a crystal engineering experiment is becoming a real possibility[48].

The arrangement of the synthons defined by the crystal engineering technique may result in the formation of several different types of final structure, the most common of which are illustrated in Figure 18.

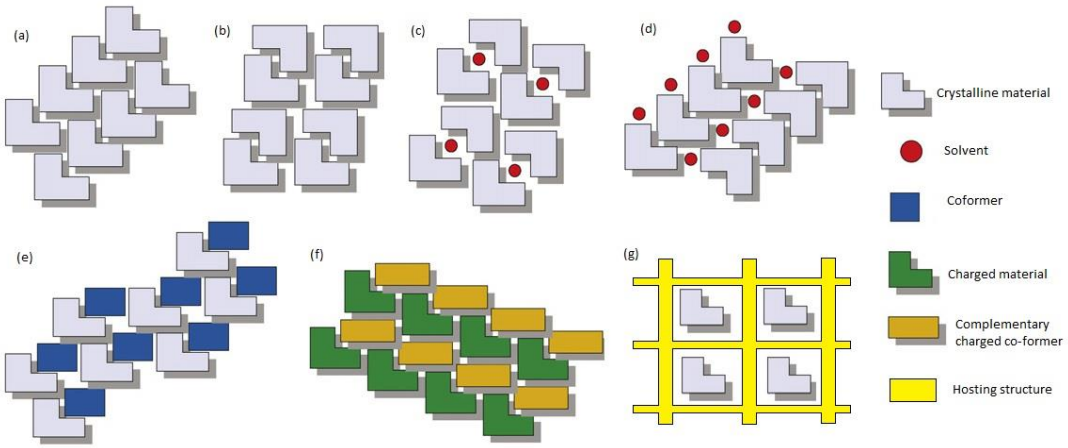

Figure 18 - Illustration of various engineered crystal structure outcomes.

Figure 18 (a) and (b) represent recrystallisations of a single material. As is represented by the motifs, there may be more than one possible arrangement of the material: polymorphs. A polymorphic material expresses itself in more than one arrangement of the crystal structure and bonding motifs resulting in different molecular arrangements and conformations, designated as distinctly different phases[49]. This is equally true of single component materials and multi component materials. As a result of different molecular interactions, they have different physical properties and are energetically different, representing minima in a potential energy landscape where they are separated by a activation energy[50]. Interconversion between polymorphs is possible and without a complete polymorph screening, it is impossible to definitively know whether an observed phase of a material is the most stable form, or meta-stable[51]. It is suggested, although not confirmed, that "every compound has different polymorphic forms and that, in general, the number of forms known for a given compound is proportional to the time and money spent in research on that compound"[52]. Although this comment is speculative, a lack of understanding of the polymorphic nature of materials has led to financially disastrous consequences for pharmaceutical companies[53], with polymorphic transformations

occurring out-with the control of the manufacturers, leading to a change in physical properties of a crystalline product to those that were ultimately undesirable[54].

Figure 18 (c) and (d) show inclusion of solvent within a crystal structure, a common occurrence in both single and multi-component crystallisations. This may occur in several different ways. The solvent may be included in a solvate as part of the hydrogen bonded network, and as such would be included in any graph set notation describing the hydrogen bonding motifs (Figure 18(d)). This may occur with inclusion of the crystallisation solvent, or in those crystallisations which involve the use of hygroscopic solvents, it is not uncommon for water to be absorbed from the atmosphere and incorporated into the structure. Water molecules readily incorporate themselves into a crystal structure because of their versatile hydrogen bonding capabilities and their small size. Incorporation of other solvents is also regularly observed, however it is only about 10% as prevalent[55]. The presence of a strongly hydrogen bonding solvent within the structure often becomes an integral part of the hydrogen bonded structure as a whole[56-58] and may prove vital to its stability, bonding itself strongly to the molecular components, preventing its loss by heating or causing structural collapse with its loss from the structure[58]. In the second type of solvent inclusion within a crystal structure, a solvent molecule becomes incorporated within a pore or void in the structure (Figure 18c)[59]. A structure may assemble around a solvent and be porous on the molecular scale allowing disordered solvent molecules to be located within multiple positions or to occur freely throughout a pore, channel or void without any strong HB interactions identified in the crystal structure. In such a material it is usually easier to remove a solvent from a void by heating a sample, promoting escape and in some cases displacement of one solvent within a material with another. The inclusion of large amounts of loosely bound water within the crystalline structure is fairly common in large biological molecules. The large amount of solvent water present and its disordered nature in these structures often prevents complete assignment of all solvent electron density to precise coordinates, a fact equally true of non-biological structures[60, 61].

Figure 18 (e), (f) and (g) represent molecular complexes corresponding to a co-crystal, a charged ionic material or a salt, and an inclusion complex respectively. These will be discussed in greater depth as a result of their extensive use within this research.

1.5.1 Co-crystals, Cocrystallisations and Molecular-Complexes

Co-crystallisation, represented by schematic (Figure 18(e)) is defined as the deliberate bringing together of two different molecules into a single crystalline solid “without making or breaking covalent bonds”[62]. The result of such an experiment, if successful, is the

creation of a crystalline material that may be referred to under certain conditions as a "co-crystal", however this term is somewhat ambiguous and there is much debate as to whether "co-crystal", despite its popularity, is the correct term at all[63]. The ambiguity stems from the fact that the term co-crystal has and may refer to several different phenomenon within the literature: a composite-crystal[64] consisting of two discrete crystal forms, connected at the molecular level, or a crystal structure of two separate materials to form one multi-component crystal structure in which the two co-formers are intermolecularly bonded to each other within the lattice throughout one domain. A second definition also requires that the co-molecules must originate as solid at ambient conditions[57] and thus excludes solvates and hydrates as well as charged materials and metal ions[44]. As an attempt to avoid this ambiguity, within the course of this research the terms "multi-component crystal" and "molecular complex" will be used to describe such a material, with the addition of the word "solvate" or "hydrate" as required. The use of the term co-crystal, if used, will only apply in the event that the structure being defined consists of neutral molecules where there has been no proton transfer and the molecules remain unchanged in their new intermolecular arrangement with each other.

The term co-crystallisation however, is less ambiguous and is used extensively to describe the multi-component synthesis of a solid crystalline material containing both (or all) components, for example an active pharmaceutical ingredient and stabilising co-molecule(s). It is considered a softer synthesis methodology as there is no intentional breaking of covalent bonds in the selection of the crystallisation conditions. However, as has been observed, bond breaking reactions can occur, leading to the formation of entirely new materials which may or may not end up forming molecular complexes.

A co-crystallisation may be carried out by different methods, the most typical of which is by evaporation, the method primarily employed within this research (described in detail in Chapter 2). The concentration of a solution containing two co-molecules is gradually reduced by loss of solvent to the atmosphere, causing supersaturation, nucleation and subsequent co-crystallisation. Other methods include dry solid grinding and solvent drop grinding (a solvent catalysed variant of mechanochemical grinding), where mechanical energy is used to crystallise the two components together[65], sonochemical co-crystal formation[66] and simply melting the two components together[34]. The resulting properties of the formed materials can be very different from those of the original components. and the solid mechanochemical co-crystallisation method has been seen as a greener route to co-crystals of interest as a result of the minimised or eliminated use of expensive solvents[67]

Co-crystallisation has had particular success in the pharmaceutical industry as it is ideally suited to the preferred solid dosage form of the consumer distribution of active pharmaceuticals, whilst the dissolution and dissociation of the co-molecules within the human body allows release of the API in un-modified form, allowing its function to be completed. The technique has been utilised to alter aqueous solubility in many cases as well as melting behaviour in anti-cancer medication[68], anti HIV drugs[69] and aspirin[70]. Co-crystallisation has also been used as a separation tool for purifying materials and selectively removing synthons from reactions, thus controlling concentrations[71] including the decaffeination of coffee[72]. In the agrochemical industry, there has been new interest in the use of co-crystals over recent years, with patents taken out on new co-crystals of active agrochemical ingredients[73] where more favourable modified physical properties have been achieved. As such the creation of molecular complexes, or specifically co-crystals of agrochemicals and reactive materials seems well suited to the aims of this work.

Of particular relevance to highly reactive materials, the use of co-crystallisation has been applied to explosives, propellants, pyrotechnics and other energetic materials with stabilising effects[74] including the use of one highly reactive material to stabilise another. It follows that this method could therefore be used for the crystal engineering of highly reactive peroxyacids if the correct co-component with sufficient complementarity can be found.

1.5.2 Salt formation

The difference between a salt (Figure 18(f)) and a co-crystal is that of charge. Although both material types are multi component molecular complexes and are overall charge neutral, upon co-crystallisation a material may be formed in which both components are oppositely charged. The materials may have originated as charged species in solution, a neutral solid salt, or two neutral molecules, however upon solid crystallisation a charge assisted network is formed. Not all molecules within the molecular complex may be ions; materials may exist where there are charged and neutral components present throughout the structure, however overall charge neutrality is always maintained. An organic material balancing a positively charged ion may typically deprotonate, particularly with carboxylic acids, to form a $RCOO^-$ anion.

Two neutral organic materials may also become an ionised molecular complex as a result of a proton transfer effect from one material to the other, the degree of which varies creating a “salt-co-crystal continuum” of ionisation with co-crystals with no proton transfer at one extreme and complete proton transfer at the other, creating a salt[75]. The probability of a

co-crystallisation resulting in a co-crystal or a salt can be predicted to a limited extent by analysis of the difference between the pK_a values (ΔpK_a) of the two co-components.

Equation 1 - Calculation of the difference in pK_a in a given cocrystallisation experiment

$$\Delta pK_a = pK_a[protonated\ base] - pK_a[acid]$$

The difference in pK_a as shown in Equation 1 when applied to a cocrystallisation experiment containing two materials, one which will act as a base and one which will act as an acid, will give a primary numerical assessment of the strength of the proton transferring ability of the pairing. If this number is greater than 2 or 3, from empirical observations, it is predicted that a salt complex will form[75, 76]. The closer the value is to zero or below, the more likely the cocrystallisation is to form a non-ionic co-crystal. However, the pK_a is not the only deciding factor. For ΔpK_a values between 0 and 3 the continuum type nature is truly observed where there is a large overlap in cocrystallisations forming a co-crystal or a salt. This can be seen in the analysis by Cruz-Cabeza[76] where a survey of 6465 crystal structures from the CSD[46] were assessed for their ΔpK_a and whether proton transfer had occurred (Figure 19).

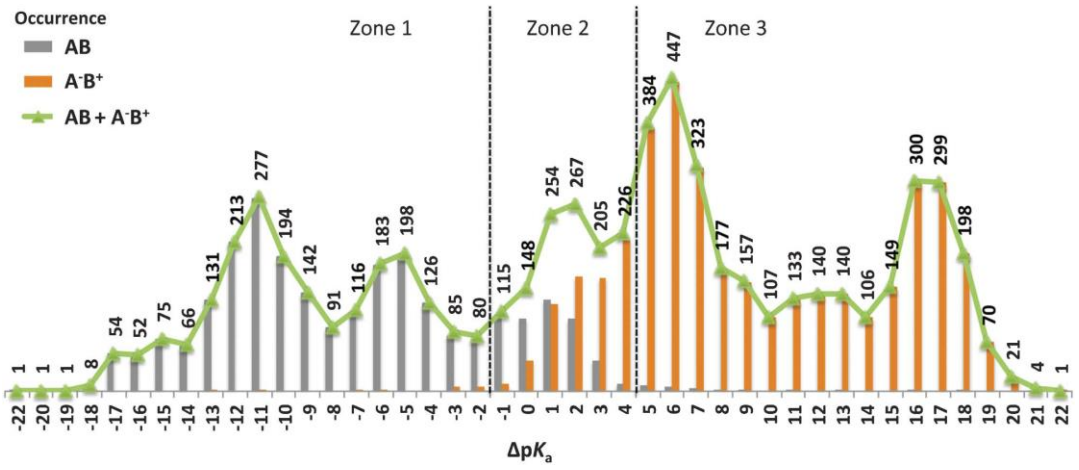

Figure 19 - Plot of 6465 co-crystals and salts from the CSD and their corresponding ΔpK_a [76].

In Figure 19, zone 1, representing ΔpK_a of less than -1, there is a 99.1% probability of a co-crystal forming exclusively. In zone 3, corresponding to a ΔpK_a greater than 4, there is a 99.2% chance of a salt forming exclusively, with an approximate 40/60 % probability of a co-crystal/salt forming, respectively, in the range of ΔpK_a between -1 and 4 inclusive[77].

There are of course factors to consider other than pK_a and it must be noted that pK_a is an (aqueous) solution, not solid-state, parameter. As can be expected, steric parameters[78] as well as thermal conditions must have an influence on the hydrogen transfer ability. Hydrogen bonds, like any other bonds, upon increasing temperature exhibit thermal

vibrations. The increase in temperature produces a spreading out of the hydrogen position along the axis of the bond, leading to ambiguity in its definitive position and distance from donor and acceptor. In general this can be clarified by cooling to low temperatures (20K) during collection of a crystal structure. This reduces the thermal motion, allowing for a more accurate position to be defined. There have been examples however, such as in the complex pentachlorophenol and 4-methylpyridine in which a proton is observed to exhibit transfer at low temperatures but not at temperatures above 90K, leading to a lack of definition of whether the complex is entirely a co-crystal or a salt[75]. Problems also arise from molecular complexes with different stoichiometric ratios. In such cases, only some of the synthons may exhibit proton transfer, such as in the 2:1 complex of fumaric acid and anilinium[79] where there is incomplete deprotonation of the fumaric acid molecules resulting in overall charge balance, but with the complex having the character of both a co-crystal and a salt. In some definitions this would still be called a salt however, as a "pair of molecules are ionised"[80].

The characteristics of changing the physical properties of a material by salt formation has long been used and parallels that of co-crystallisation, and in particular the pharmaceutical industry have used it for controlling formulations in distribution[81]. Its use as a crystal engineering tool is as valid as that of the aim of creating co-crystals, providing deprotonation of a target or primary material does not compromise its efficacy permanently or permanently change the chemical behaviour of the material upon application.

1.5.3 Inclusion complex (hosting)

Figure 18(g) represents a hosted complex. This is a generalised term covering many different situations. The first of these is a molecular inclusion approach. Co-crystallisation of a smaller target molecule with a secondary co-molecule which includes a large empty volume within its molecular structure can physically encapsulate the target material within this space, assuming the interior wall of the volume is compatible with the target material, i.e. the intermolecular interactions of the target material are attracted to those on the inside of the void. There are several families of large molecules that are ideal for this type of co-crystallisation and are commonly used. These include, but are not limited to, cyclodextrins[60, 82], modified cyclodextrins[83], crown ethers[84, 85] and cucurbiturils[86]. They are termed inclusion complexes as the larger material forms the majority of the structure. The included component may alter the overall structure somewhat, but the main interactions are with the hosting material itself.

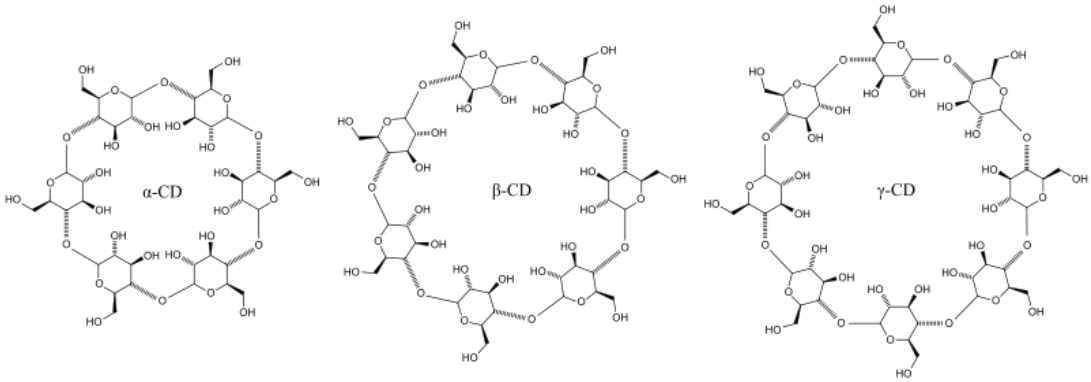

Figure 20 - Unmodified α, β and γ – cyclodextrins.

In the cyclodextrin family (Figure 20), it is typical for the ring shaped molecule to stack with other cyclodextrin molecules in opposite directions forming a barrel structure. Depending on the type of cyclodextrin used, the size of the barrel may be chosen to best suit the molecule being hosted. The included material is hosted within the hydrophobic void generated by this stacking and as such is locked in and protected from external influence (Figure 21).

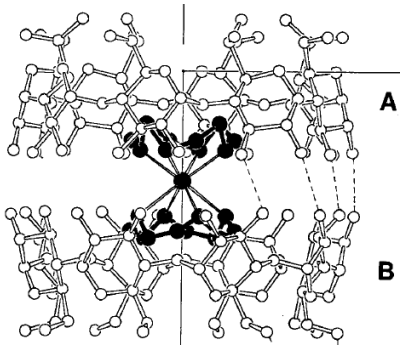

Figure 21 – γ-cyclodextrin inclusion complex showing two inverted γ-cyclodextrin molecules A and B forming a barrel-like structure[85].

Not only does hosting a material within a guest molecule protect the included material by physically encapsulating it within the void in the sold state, but as with other co-crystals the physical properties are modified with respect to the hosting material.

The second type of complex is that of urea inclusion compounds. For many years urea and its related family of molecules have been noted for their ability to form tubular channelled structures in which secondary materials can be hosted. In contrast to the hosting molecules noted above, the urea series are small molecules, forming extended open architectures by exploiting the strong hydrogen bonding potential for interaction with each other. The urea type compounds are known to form a predictable hexagonal hydrogen bonded tubular structure (Figure 22), similar to a honeycomb design, with a cross surface

revealing a tunnel type void with an inner wall diameter (defined by the van der Waals surface) of between 5.5 and 5.8 Å [87].

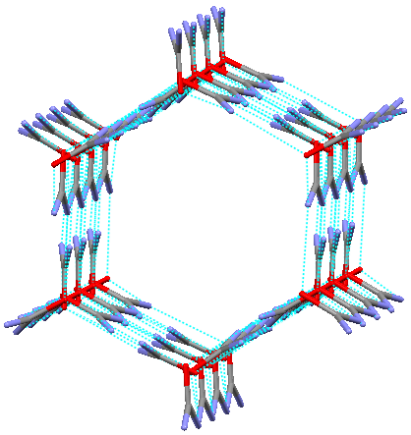

Figure 22 - Crystal structure of Urea revealing the tubular void.

The void is sufficiently large for aromatic molecules to be incorporated into the channel, such as with glipizide[87], without disrupting the crystal structure, which maintains its original parameters with small distortions resulting from bulky guests[88]. They are particularly well suited to molecules resembling large aliphatic chains which may rotate their orientation within the void forming a disordered or periodic arrangement, aligning the chain with the channel[89]. Inclusion is not favoured, however, for non-chain molecules or those with bulky side groups. Their preference for inclusion of long chain molecules is so strong that these complexes have been used for separation of linear alkanes from mixtures[90]. The inclusion compounds based upon urea form the crystalline tunnels around the molecules during the crystallisation phase, the hosted material aiding in the structural integrity of the urea channels. A typical synthesis of such a structure would employ slow evaporation of a solvent, or alternatively slow cooling of methanolic solutions containing urea (approx. 2M), and the desired guest, provides well-formed hexagonal needles, prisms or plates. The crystals however tend to contain substantial amounts of methanol within the channels, as a result of its ability to flow freely through the comparatively larger diameter channel[91]. This is not the case for larger solvent molecules such as DMSO, DMF and propanol. An alternative method, described later, is to use solvent drop grinding methods, with methanol as a catalytic amount of solvent, for liquid guests and low volatility solids[91].

It has been shown that upon removal of the material from inside the void, the structure collapses and recrystallises in its pure crystalline phase[90]. Thiourea, closely related to urea, also forms the same host type channelled structure, but due to the larger size of the molecule, the guest materials that can be incorporated are larger. Thiourea channels have

been observed to host molecules as large as ferrocenes, cyclohexanes and other organometallics as well as easily incorporating benzene[90]; the channel size can thus be tuned to suit the intended guest material. Another feature of thiourea inclusion materials is the divergence from the strictly tunnelled structure, with the channels incorporating a slight bulge which constricts the channels. The structure could thus be considered as an arrangement of smaller cages, increasing stability of the guest material by reducing disorder[90].

This method has been used previously to host diacyl-peroxides, where the structure of the included material within the host material was mediated by hydrogen bonding within the inner wall of the urea complex, regulating guest-guest interaction[91]. Photolysis has been known to occur in such situations, generating radicals within the channels which may not escape to further the reaction, allowing their study[92].

The limiting size of urea inclusion structures, however, poses potential problems and adaptations have been attempted to allow for larger guest intercalation, for example using bis-urea macrocycles (Figure 23). The connection of two urea molecules by an organic substrate forming a cyclic ring results in the crystallisation of a macrocyclic tubular stack, producing hosting channels with an internal diameter between urea molecules, aided by π stacking at a distance which may be altered depending on the size of the organic substrate used [93, 94].

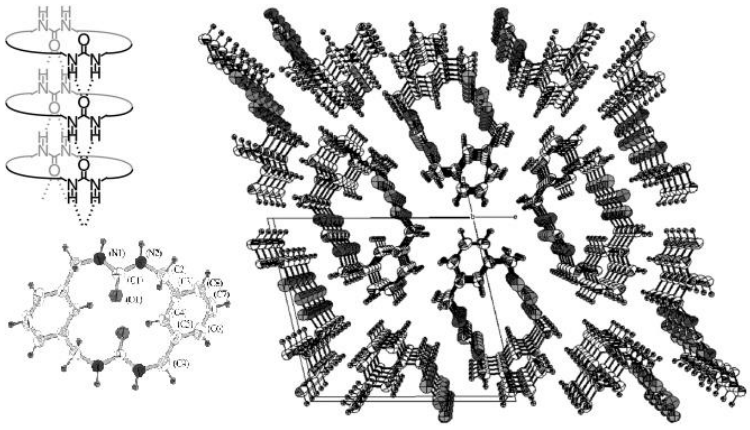

Figure 23 - Bis-urea macrocyclic molecule producing a channelled structure upon stacking[93].

One further extension of this is to link such generated stacks and nanotubes together with a further strongly bonded parameter, to form the material into a fully three dimensionally coordinated framework or "molecular scaffold" (Figure 18(g)). As with the other void creating methodologies, the adaptability of these materials, resulting from the ability to customise produced voids by selecting constructing molecules of desirable functionalities,

making voids more or less attractive to the intercalated material, is the key to their use and popularity. The most commonly known type of these materials, achieving great interest in the last decade is the field of metal-organic frameworks, or MOFs for convenience, also termed coordination polymers and hybrid organic-inorganic materials. Within these structures, the strong bonding network provides robustness and a pre-assembled well defined highly crystalline structure which like the other clathrate types, lends such stability to the included material. Like previously described materials, they are generally assembled in situ around the material to be intercalated, often under solvothermal conditions aided by the directionality and rigidity of bonding of the framework forming materials, These materials are generally favoured for their porosity, which only applies if the material can allow the intercalate to enter and then leave the network without the destruction of the network itself[95].

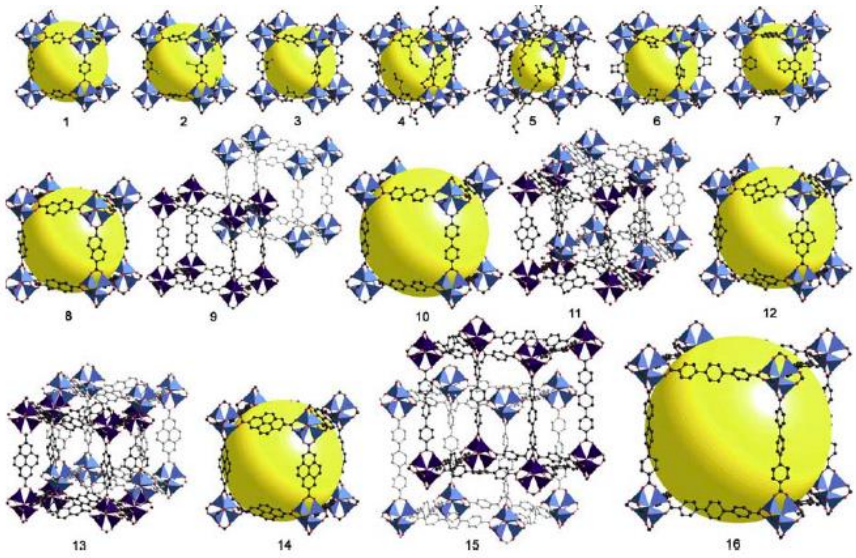

Figure 24 - Illustration of consecutively larger organic substrates incorporated into the molecular framework creating a larger intermolecular void (represented by yellow spheres)[95].

One such material of particular interest due to its adaptability, ease of construction and benign nature is that of the somewhat recently published edible MOFs, a family of materials that are inexpensive and not harmful to the "end consumer"[96].

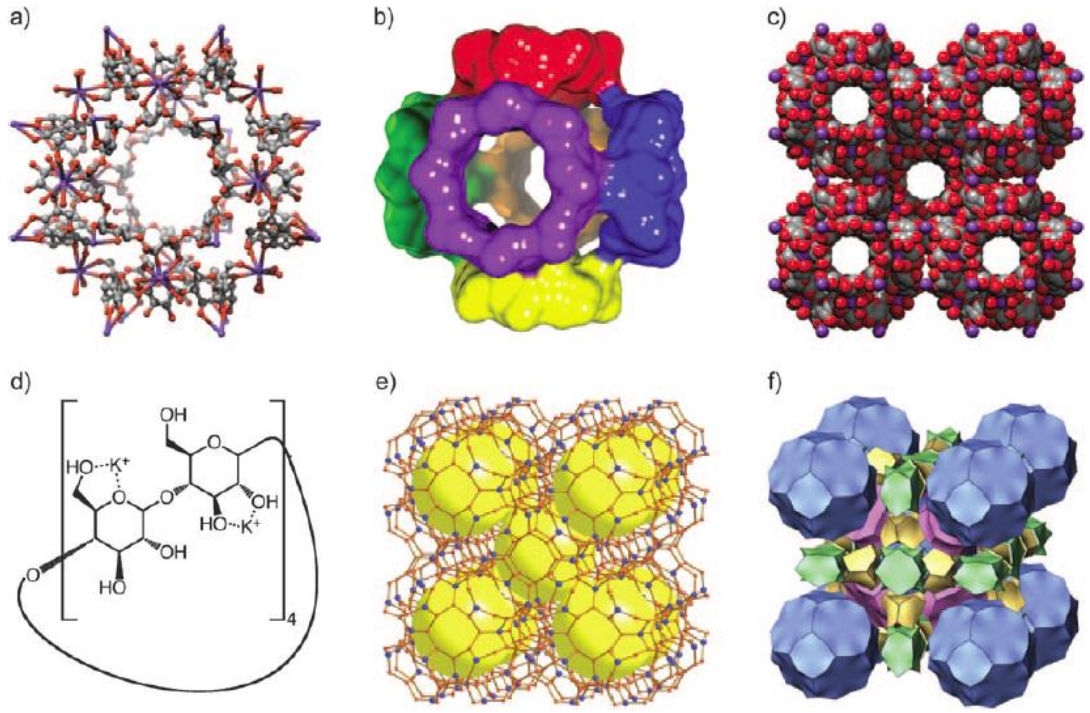

Figure 25 - Non-toxic edible MOFs from gamma-cyclodextrins and eight coordinate K^+ ions.

These materials are attractive as MOFs as they use smaller non-toxic metals that are more abundant and renewable organic materials produced by natural methods, such as potassium and cyclodextrins, are utilised to form the superstructure. As is seen in Figure 25 (a) a large spherical superstructure is generated by linking the hydroxyl groups (d) on the primary (smaller) face of the cyclodextrin rings as well as glycosidic ring oxygen atoms by ionic association with the potassium ions. The potassium ions further coordinate to the secondary outer faces resulting in eight oxygen coordination (e). This produces cages with inner voids (c) of a diameter of 0.9nm with pores of 0.78nm and 0.42nm in which small neutral molecules may be stored[96].

1.6 Structural analysis of targeted materials

Choosing the correct methodology for stabilisation of the target material with all cases relies upon an in depth understanding of the interactions involved and how they will affect outcomes of crystallisation experiments with these materials.

1.6.1 Peroxyacids

The structural chemistry of peroxyacids has not been widely studied, with only 16 known crystal structures held in the CSD, many of which lack the important hydrogen positions on the vital peroxide group. Nonetheless, several structure determinations of pure peroxy acids have been reported, such as peroxypelargonic acid[97], (Figure 26).

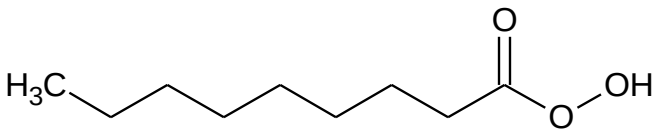

Figure 26 - Peroxypelargonic acid.

As an example of the confusing collection of data available, the active site of the molecule, the CO_3H, was thought by Swern[12] to exhibit evidence of dimerisation similar to that observed with carboxylic acids (Figure 27).

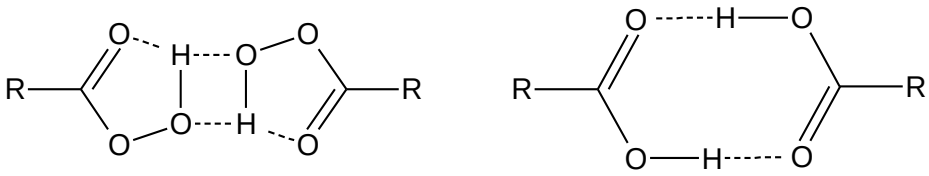

Figure 27 - (left) hydrogen bonded peroxyacid dimers - (right) carboxylic acid dimerisation.

The assumed dimerisation would give weight to a methodology of hydrogen bonding to induce stability, by promoting self-supporting peroxyacid units in a way similar to the well-used carboxylic acid dimerisation[98], a commonly utilised crystal engineering strategy, providing a predictable hydrogen bonding motif for intermolecular association. Upon closer investigation of the interaction observed in the supporting data however, it can be observed that this is not the case. Instead, as seen in Figure 28, the crystal structure of peroxypelargonic acid collected in 1965 by Jeffrey[97], it can almost be understood how when viewed from a certain orientation, the mistake of assuming that molecules exist as dimers could be made, however when rotated to view from other angles, it becomes clear that this simply is not the case.

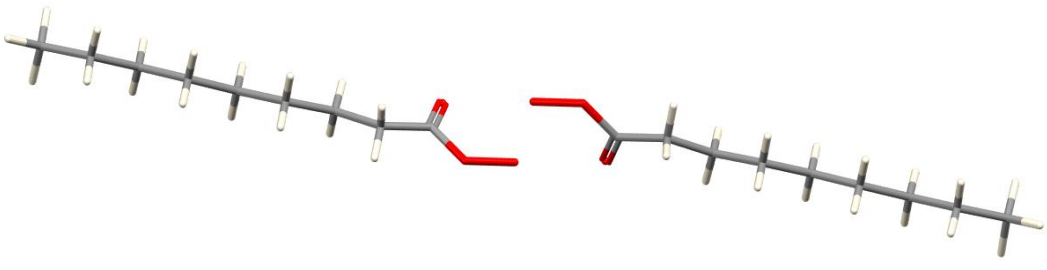

Figure 28 - Hydrogen bonded "Dimer" observed from the b axis in the crystal structure of peroxypelargonic acid between two neighbouring molecules.

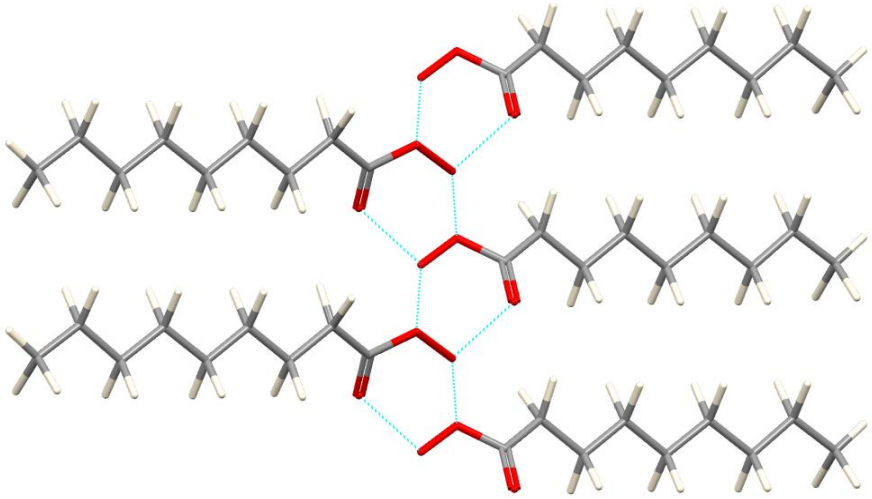

Figure 29 - Peroxypelargonic acid viewed along c-axis highlighting the true hydrogen bonding network.

The literature defines the carbonyl as being involved in an intermolecular hydrogen bond to the terminal hydrogen of the peroxyacid functional group of a neighbouring molecule. Since the hydrogen atom is not modelled in the supplementary data for the structure, the distance measured from the carbonyl to the neighbouring basic oxygen, with the hydrogen atom present somewhere between the two, presumably on the side of the basic oxygen, of 2.746Å – a moderate strength hydrogen bond. The endmost single bonded oxygen, the basic oxygen as described earlier, participates in an intramolecular hydrogen bond to the terminal hydrogen of the dimerised peroxy acid. Dipole moment data also indicates that the peroxy acids are approximately coplanar to each other, with the terminal hydrogen sitting out of the plane[97]. It is not possible to confirm this from the crystal structure (Figure 29), as the terminal hydrogen position is undetermined. The peroxy acid component of the molecule forms a hydrogen bonded spiralling chain around the screw axis, with a moderate strength HB between the basic oxygen and the acidic oxygen of a neighbouring group, with O1 – O1 distance of 2.875Å, also considered a moderate strength hydrogen bond, showing indication that the hydrogen may be directed towards it also forming a bifurcated hydrogen bond (Figure 30). The hydrocarbon chains lie parallel to each other and show no further significant interactions aside from steric packing effects.

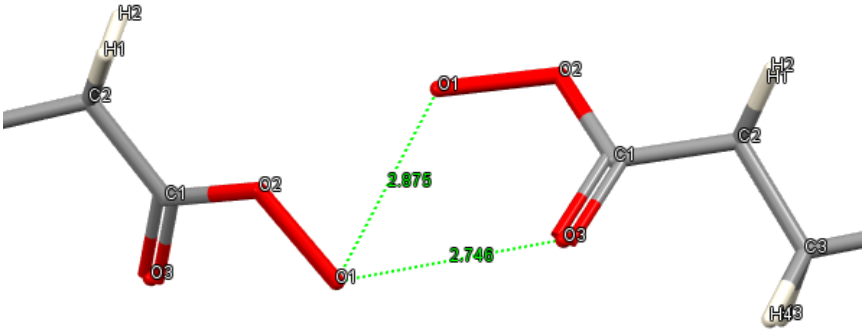

Figure 30 - Hydrogen bond distances between two neighbouring peroxypelagonic acid molecules.

The interactions observed of the terminal hydrogen, are examined in the study of the crystal structures of four p-amidoperbenzoic acids[99], following the general structure outlined in Figure 31 for the cases where n=1-4. In each of these it is observed that the dimerisation present in peroxypelargonic acid is not observed and instead all four examples exhibit hydrogen bonded chains as the primary motif.

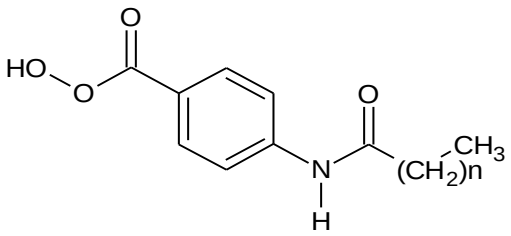

Figure 31 - General formula of p-Amidoperbenzoic acid family

The first in the family, p-acetamidoperbenzoic acid has a moderate strength hydrogen bond, with an O-O distance (O1···H6-O4) of 2.574Å, from the carbonyl at the start of the aliphatic chain to the terminal hydrogen of a neighbouring group. This is further verified by the presence of the terminal peroxy hydrogen within the plane of the hydrogen bond. The hydrogen bonding motif is then completed as a chain by the weaker yet still moderate strength hydrogen bond with a N-O (N1-H1···O2) distance of 2.937Å between the carbonyl of the peroxyacid group to the amino hydrogen (Figure 32).

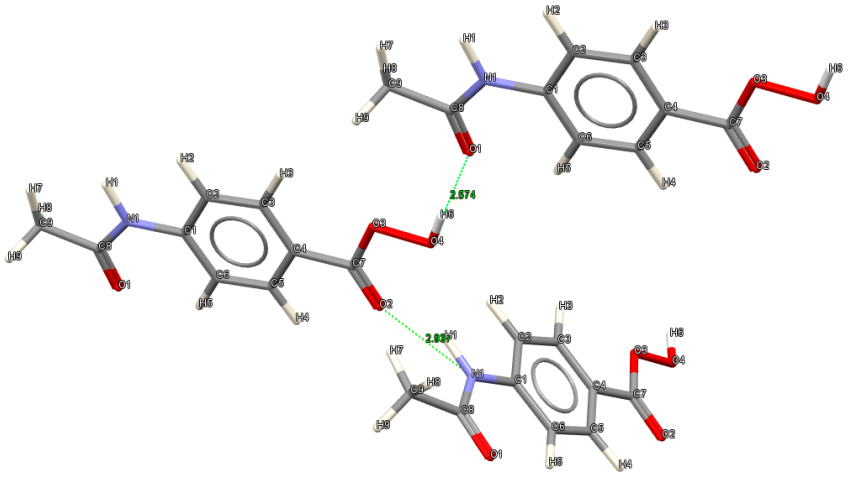

Figure 32 - Hydrogen bonded chain motif of p-acetamidoperbenzoic acid.

These features are observed in all recorded structures of this family in the CSD, with π-π stacking along the a-axis and steric manipulation of the orientation of the molecules by the increasing aliphatic chain length, affecting the packing within the solid state. The cases where n=1 and n=2 exhibit similar packing (Figure 33), where the molecules align themselves in an alternating 90° orientation to each other whilst maintaining the chain structure perpendicular to the plane generated by this feature. For n=3 and n=4, this packing is no longer present, with the n=3 case exhibiting a sandwich structure, with the molecules in their entirety forming parallel sheets, as shown in (Figure 34) supported by π-π stacking at a distance of 3.440Å, within the accepted range of such interactions, and the n=4 case stacked in alternating directions with a skewed, stacked scissor like arrangement.

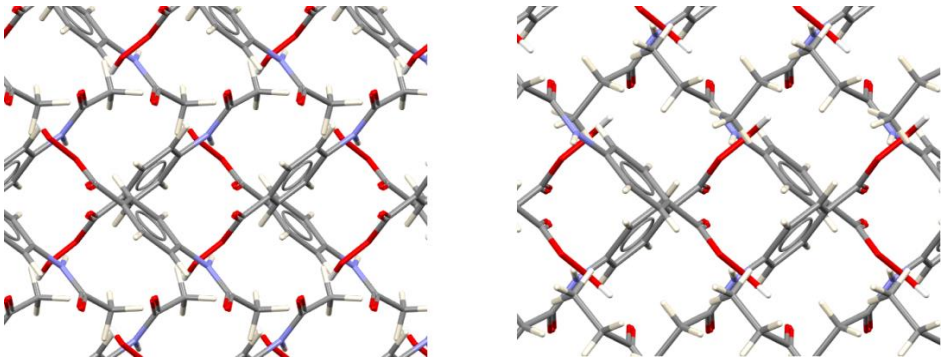

Figure 33 - Crystal structures viewed along the c-axis showing similar packing for p-acetamidoperbenzoic acid (left) and p-propanamidoperbenzoic acid (right).

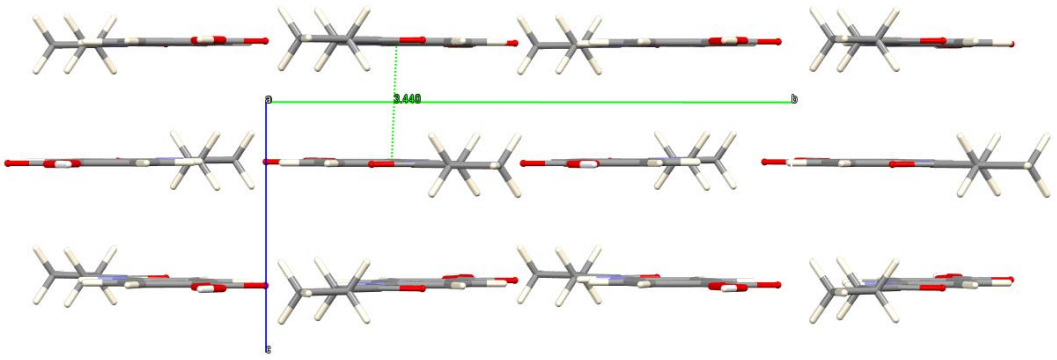

Figure 34 - Crystal structure of p-butanamidoperbenzoic acid viewed along a-axis.

For the nitroperoxybenzoic acids, only the ortho-nitro and para-nitro structures are reported. o-nitroperoxybenzoic acid shows a similar motif as the peroxyacids above. Once again a chain is formed by the hydrogen bond generated between the terminal hydrogen of the peroxyacid and the carbonyl of the peroxyacid group of the neighbouring molecule (Figure 35).

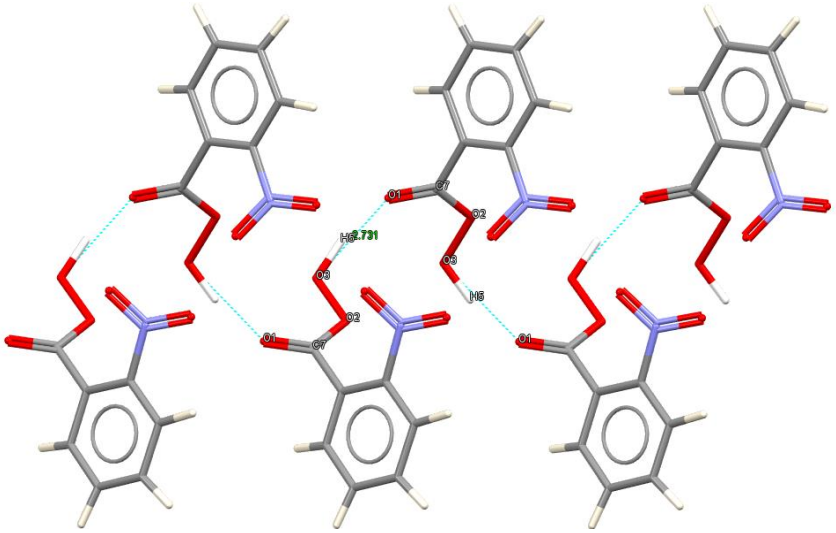

Figure 35 - Hydrogen bonded chain motif observed in o-nitroperbenzoic acid.

The measured distance from O1 to O3 is 2.731Å, again a moderate strength hydrogen bond. The nitro group does not interact with the peroxyacid and only forms interactions in the form of short contacts to neighbouring aromatic hydrogens (Figure 36).

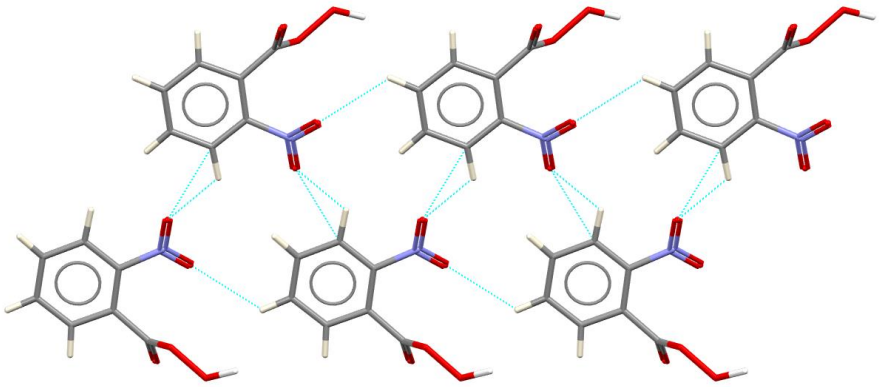

Figure 36 - Close contact interactions present between nitro group and aromatic hydrogens as viewed along the c-axis of o-nitroperbenzoic acid.

The crystal structure of p-nitroperbenzoic acid has a different hydrogen bonding arrangement. The motif observed is very similar to that observed in peroxypelargonic acid, described earlier. The primary interaction of the chain motif is a hydrogen bond between the peroxyacid carbonyl and the terminal peroxy hydrogen of the next molecule. This interaction is again of moderate strength with an O1··O3 distance of 2.740Å (Figure 37).

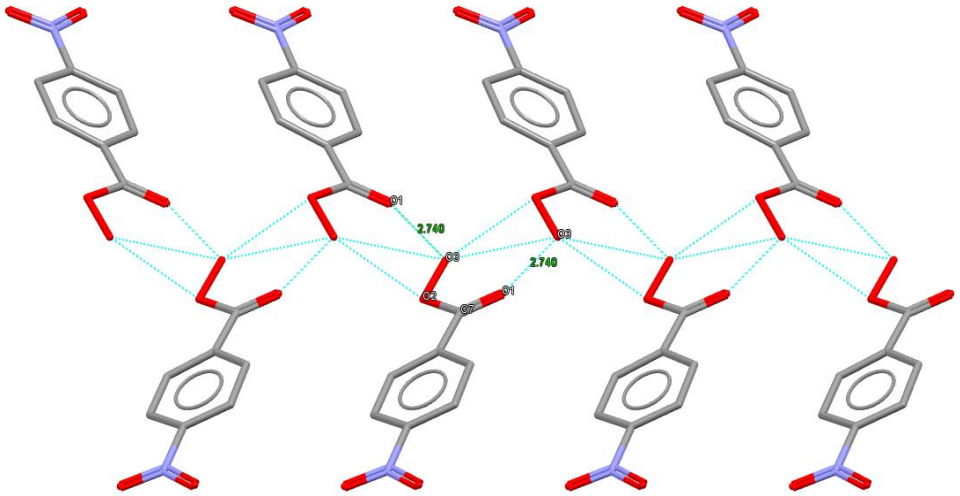

Figure 37 - Primary hydrogen bonding motif observed along the c-axis of p-nitroperoxybenzoic acid.

This primary peroxyacid interaction is supplemented within the structure by weaker interactions between nitro groups in a herringbone fashion with a close contact from the oxygen of one nitro group to the nitrogen of the next with a distance of 3.063Å (Figure 38).

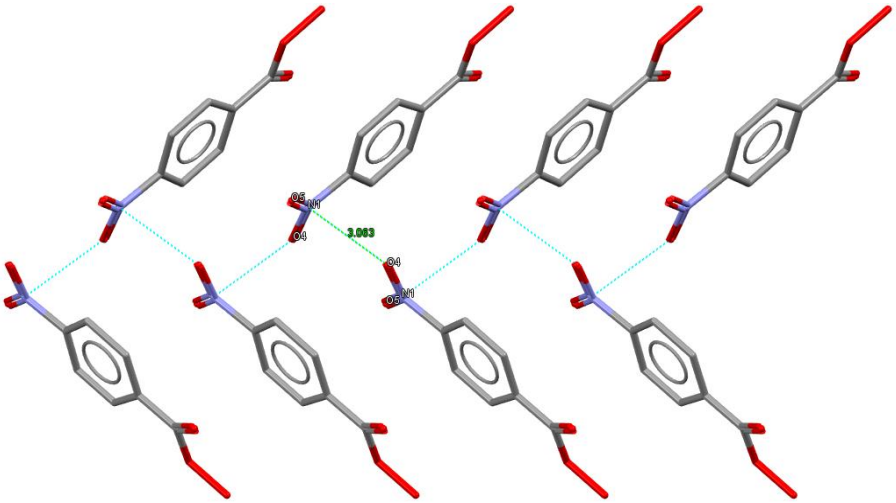

Figure 38 - p-nitroperbenzoic acid viewed along the b-axis showing the herringbone arrangement of the nitro groups.

One of the final families of peroxyacids characterised and present in the CSD are the 3-oxo-1,2-benzisothiazole-2-peroxycarboxylic acid 1,1-dioxides which have the general molecular structure shown in Figure 39.

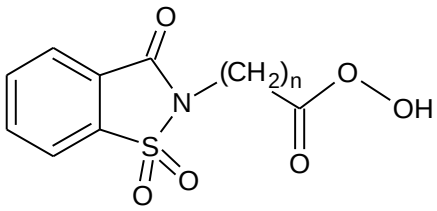

Figure 39 - General formula of the 3-oxo-1,2-benzisothiazole-2-peroxycarboxylic acid 1,1-dioxides.

A series of three of these compounds have been studied by single crystal X-ray diffraction, the smallest of which is 3-oxo-1,2-benzisothiazole-2(3H)-perethanoic acid 1,1-dioxide (n=1).

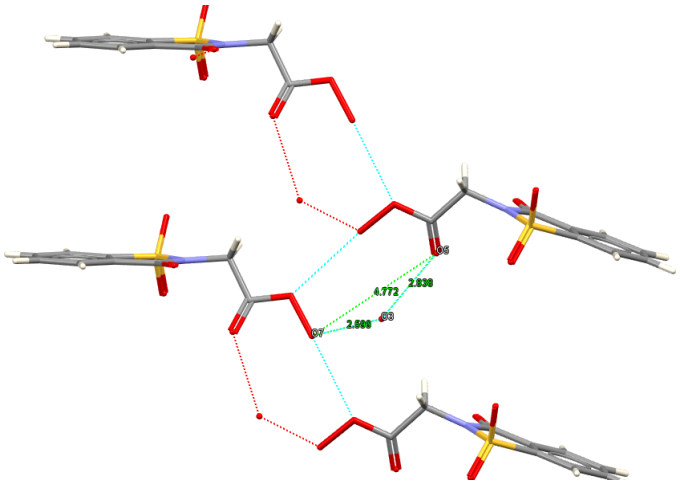

Figure 40 - 2-Saccharinperacetic acid monohydrate viewed along the c-axis.

In this case, the chain arranged hydrogen bonding motif is distinctly different in the inclusion of a bond bridging water molecule between the peroxyacid carbonyl and the terminal peroxy oxygen (the terminal peroxy hydrogen position has not been determined) depicted in Figure 40. The water molecule has the effect of bridging a gap between the "normal" position of the peroxyacid regular hydrogen bond donor/acceptor motif O7···O5. As a result of other bulky packing effects, this distance is increased to 4.772Å – beyond the range of even weak hydrogen bonds, instead forming two hydrogen bonds, one from O5···O3 (2.838Å) and one from O3···O7 (2.599Å) and joining the two molecules with two moderate strength hydrogen bonds. As the hydrogens have not been accurately determined, the directionality of the bonds cannot be confirmed. Another possibility is that the terminal hydrogen of the peroxyacid group could be directed towards the non-basic peroxide oxygen of the neighbouring peracid. The water molecule also exhibits a close contact with the aliphatic C-H on a third molecule, further stabilising its position. The S=O groups also point towards both another aliphatic C-H and the carboxylic carbon on a peroxy group, creating infinite chains.

The second in the family, n=2, exhibits an entirely different motif, presumably resulting from the increased aliphatic chain length allowing a more efficient packing arrangement. In this case (Figure 41) it can be seen that the peroxyacid functional group does not interact with any other peracid oxygens, unlike all other structures observed. The terminal peroxy hydrogen is then definitively directed and thus hydrogen bonded to the carbonyl upon the 3-oxo-benzothiazole part of the next molecule with an O2···O5 distance of 2.618Å.

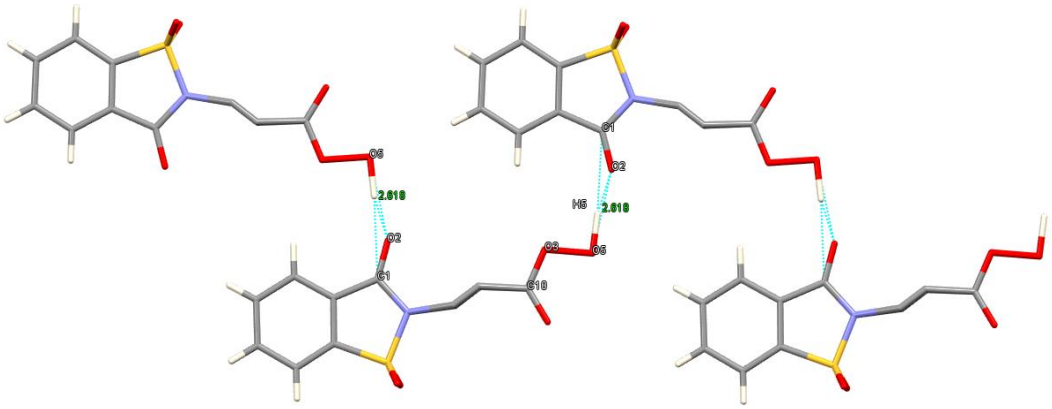

Figure 41 - Crystal structure of N-Saccharinperpropanoic acid showing primary hydrogen bonding motif.

This shows that not only will the peroxyacid hydrogen bond with other peroxyacid functional groups, but also with any sufficiently electronegative carbonyls. The carbonyl oxygen in the peroxyacid group exhibits a close contact with an aromatic C-H of a neighbouring molecule. The molecular structure, with the exception of the sulphur oxygen

bonds, is planar creating hydrogen bonded planes with only π-π stacking interactions between the planes. There is also symmetrical disorder present in the aliphatic chain, however it has no effect upon the position or orientation of the functional parts of the molecule.

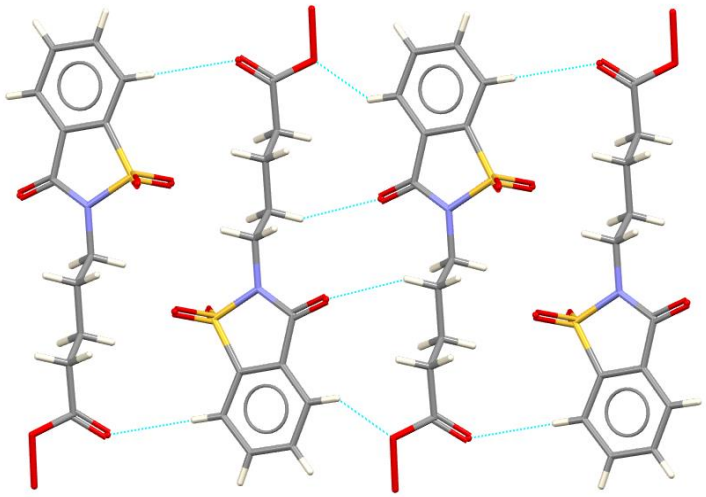

Figure 42 – Antiparrallel dimers of N-Saccharinperpentanoic acid as viewed along a-axis.

In the third of this family whose structure is known (n=4; 3-oxo-1,2-benzisothiazole-2(3H)-perpentanoic acid 1,1-dioxide), the peroxyacid functional group does not play a prominent role in the structural architecture. Figure 42 shows how the molecules are aligned alongside each other stacked anti-parallel to one another. This allows close contact interactions between the non-terminal peroxyacid oxygen and an aromatic C-H at either end of the rotated molecule forming dimers which are reinforced by the carbonyl on the five-membered ring interacting with an aliphatic C-H. On the other side of the molecules, the peroxyacid carbonyl also interacts with an aromatic C-H, forming chains, and also with an aliphatic C-H out of the plane. As before, π-π stacking is also present in the structure. There are no specific interactions with the terminal peroxide OH group in this example.

In the known crystal structures of such materials, the primary interaction of the peroxyacid functionality thus appears almost invariably to be moderate strength hydrogen bonds between the terminal basic oxygen of the peroxyacid group to either a neighbouring peroxyacid carbonyl, or other electronegative carbonyl within the structure. The exception to this is for cases where the steric interactions of the remainder of the molecules dominates, preventing such interactions taking place.

1.6.1.1 Compounds of interest

The peroxyacid compounds to be studied are outlined here. The primary material targeted for stabilisation is 6-phthamilidoperoxyhexanoic acid. Of particular interest for its utilisation as a potential low temperature laundry bleach, its crystal structure was collected along with three other members of the same phthalimidoaliphatic peroxyacids by Feeder and Jones in 1996[14]. The molecular formula of 6-phtalimidoperoxyhexanoic acid (Figure 43) shows the features of the family of molecules – a peroxyacid head, a phthalimido tail and an aliphatic hydrocarbon backbone of varying length – with the 6-phthalimidoperoxyheaxanoic acid being the six-membered aliphatic chain example. The steric characteristics will play a role in assembly of these molecules, as well as π stacking effects, alongside the predicted peroxyacid interaction behaviour as highlighted by the other materials surveyed above. The material is a white solid at room temperature with a purity of 70-100% on average.

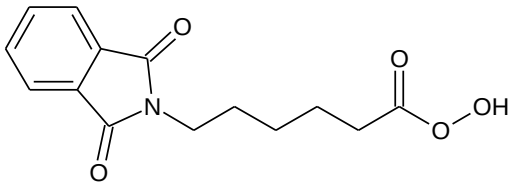

Figure 43 - Molecular structure of 6-phthalimidoperoxyhexanoic acid.

The second material under study is meta-chloroperbenzoic acid (Figure 44). MCPBA is a common oxidising agent, routinely used in organic synthesis. In contrast to its frequency of use, the study of its solid state properties is limited, with no crystal structure reported in the CSD. Again the peroxyacid group should be the most significant interaction of this molecule, however the presence of the aromatic ring and the chlorine atom opens the molecule to the possibilities of π stacking interaction and halogen interactions. At room temperature it exists as a white solid that is quick to draw water from the air to give it a sticky texture, thus working with it can prove difficult. These difficulties may be overcome by aiming to develop a method of co-crystallisation with a secondary material that can be used for the phthalimidoperoxyacids in general.

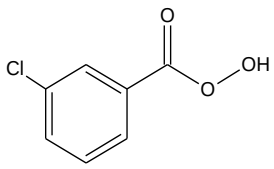

Figure 44 - MCPBA: meta-chloroperbenzoic acid.

The third and final peroxyacid under study is that of the simplest of all peroxyacids, peroxyacetic acid. Peroxyacetic acid is a liquid at room temperature, typically supplied in equilibrium with acetic acid, and thus technically any material formed by a cocrystallisation containing it would be a solvate of the presumably solid co-former. Any stabilisation of the peroxyacid functional group would potentially apply to all peroxyacids, no matter their secondary functionalities. The material therefore gives us the ability to study the peroxyacid group itself, unhindered by secondary interactions, relying only upon the motifs generated by the peroxyacid group. As it is a liquid at ambient conditions, no crystallographic data of peroxyacetic acid have been obtained.

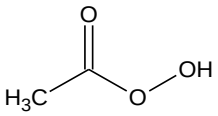

Figure 45 - Peroxyacetic acid.

1.6.1.2 Known crystal structures containing the target materials

In order to fully understand and be able to predict the interactions of 6-phthalimidoperoxyhexanoic acid, the family of molecules of which it is a member have been examined. In the reported structures of the family of molecules, none of the terminal peroxy hydrogens are reported. In 3-phthalimidoperoxyhexanoic acid, hydrogen bonding at the peroxyacid end of the molecule is observed between the terminal basic oxygen of the peroxyacid group and the carbonyl of the phthalimido group with an O···O distance of 2.779Å (Figure 46) with the hydrogen assumed to be located between the two atoms, on the peroxyacid side. The peroxycacid carbonyl is not the HB acceptor in this structure as would be expected from previous observations.

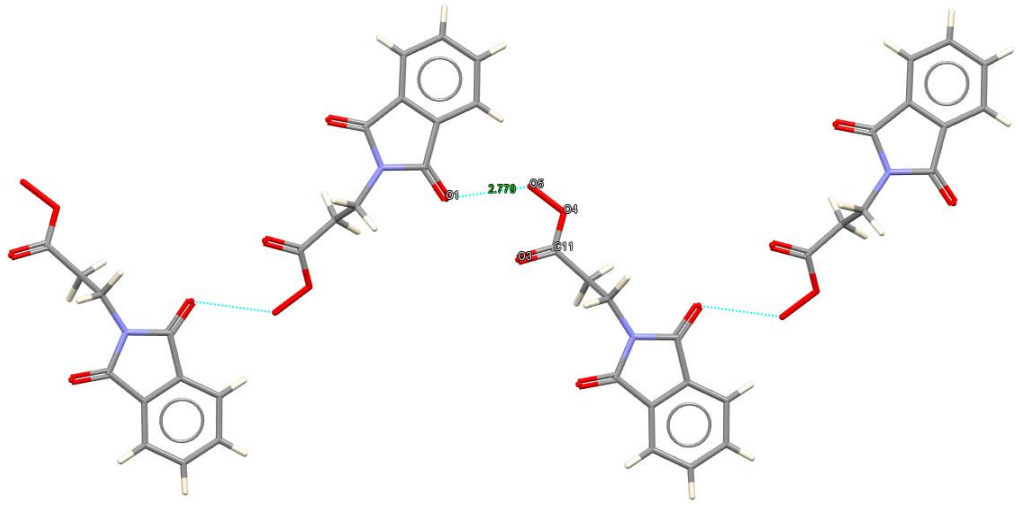

Figure 46 - 3-phthalimidoperoxypropanoic acid viewed along a-axis showing hydrogen bond between phthalimido O1 and basic peroxyacid O5.

This motif is also observed in the next molecule in the series, 4-phthalimidoperoxybutanoic acid, but in this case the molecules are aligned in a parallel arrangement (Figure 47) as opposed to the alternating direction seen in the previous member of the series. The hydrogen bond distance in this example is 2.753Å, again a moderate strength interaction.

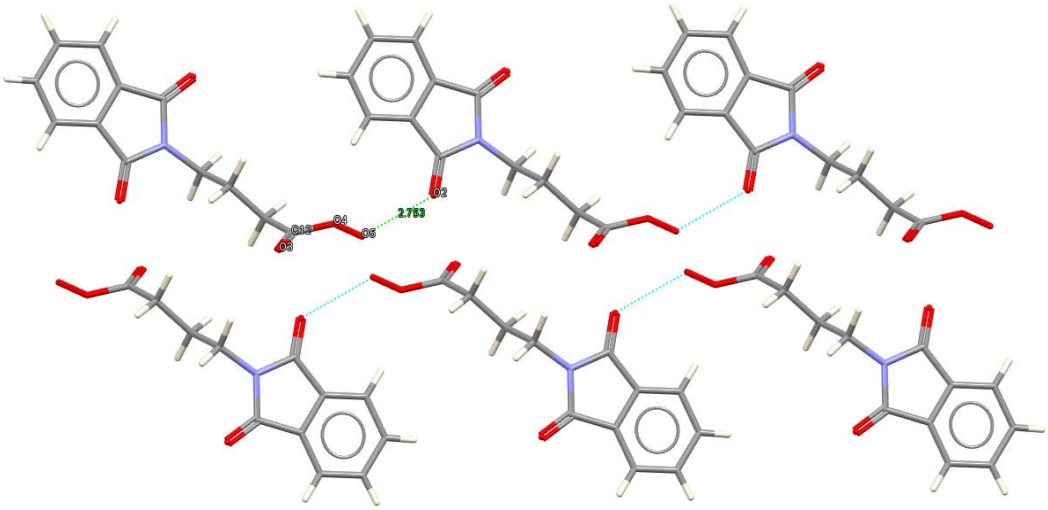

Figure 47 - 4-phthalimidoperoxybutanoic acid showing O2···O5 hydrogen bond distance.

As the chain backbone length increases within the series from four carbons to five, the peroxyacid bonding motif changes to the more common motif seen in peroxyacids. The primary hydrogen bond is located between carbonyl O3 of a neighbouring molecule and terminal peroxyacid oxygen O5 with a O···O bond distance of 2.715Å, a moderate strength hydrogen bond. The terminal peroxyacid oxygen is also within moderate to weak hydrogen bonding distance of 3.002Å to the non-terminal acidic oxygen of the neighbouring peroxyacid in the opposite direction, resulting in ambiguity as to whether the peroxy

hydrogen is located in this interaction O5-H···O4 or in the predicted carbonyl interaction O5-H···O3 (Figure 48). It is assumed that the hydrogen is in fact directed towards the more electronegative carbonyl however the ambiguity can only be eliminated by a determination of the proton position. The assembly of the structure is further aided by steric factors and by interaction of the π-π stacking phthalimido groups which fall within accepted π stacking distances, at 3.602Å.

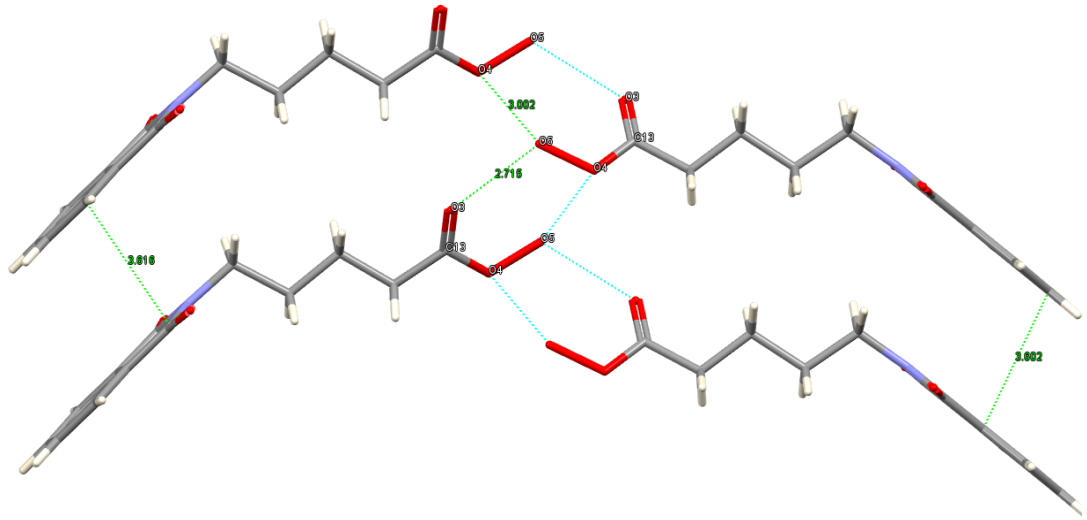

Figure 48 - 5-phthalimidoperoxypentanoic acid as seen along the a-axis showing the hydrogen bonded chain motif aided by π-π stacking.

The larger backbone of the molecule also lends itself to this packing arrangement, with the aliphatic chains separating the channels of hydrogen bonding interactions generated by the peroxyacid groups from the channels of phthalimido π-π stacking.

The final molecule in this family studied is the target molecule itself, 6-phthalimidoperoxyhexanoic acid. The existing structure in the CSD, like the rest of the family, does not determine the terminal peroxyacid hydrogen position. As such the full structure of this molecule was studied as part of this research. The main features of the previously known structure will be discussed here.

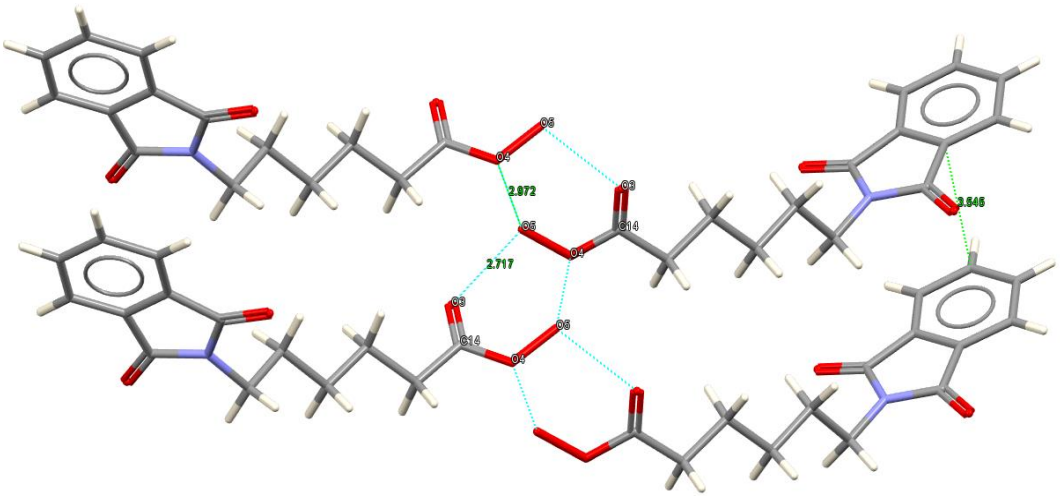

Figure 49 - 6-phtalimidoperoxyhexanoic acid as viewed along the a-axis showing hydrogen bonding channels.

The structure is very similar to that of the previous member in the family, with the terminal basic oxygen of the peroxyacid group forming a moderate strength hydrogen bond that is closer in distance to the carbonyl of a neighbouring peroxyacid group (Figure 49). The O5···O3 bond distance is 2.717Å and is likely the direction in which the hydrogen atom is located. The other possible hydrogen bond orientation has a larger bond distance between O5···O4 of 2.972Å and therefore is the weaker of the interactions. Also similarly to the previous member of the series, the aliphatic chain orients the molecules to allow a channel of hydrogen bonding to be formed, and π-π interactions that lie within the accepted π-π stacking range. Unlike the previous member of the series however, the phthalimido groups are angled in the opposite direction, resulting from the increased carbon atom in the aliphatic chain.

All of the molecules within the phthalimidoperoxyaliphatic acid family have the characteristic phtalimido group, which is in itself relatively well studied and the interactions it is likely to have may be assessed more statistically. The phthalimido group presents significant intermolecular interaction potential which could be exploited for crystal engineering purposes.

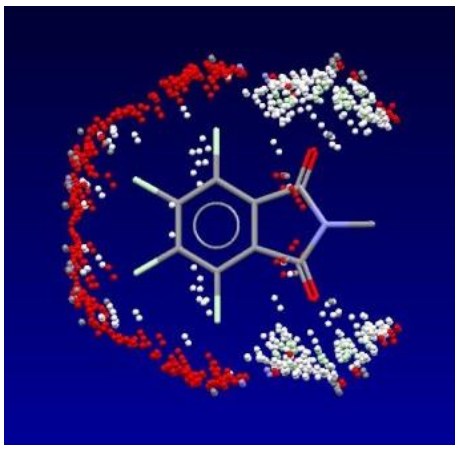

Figure 50 – Collated atomic short contacts of a phtalimido group as shown in isoStar, with red spheres representing close oxygen contacts and white spheres representing hydrogen atom positions from recorded crystal structures in the CSD.

As can be seen in Figure 50, an isoStar plot of non-bonded interactions as collated from the CSD[100], the interactions around the phthalimido group are of two general types. Aside from the red oxygen interactions around the aromatic hydrogens on the 6-membered ring in which the hydrogens are acting merely as hydrogen bond donors to another molecule, the predominant interactions are those that are primarily hydrogen bond-like in nature, around the carbonyls at the head of the group. These interactions (Figure 51) mainly originate from standard hydrogen bond donors N-H···O, O-H···O but also a few C-H···O interactions.

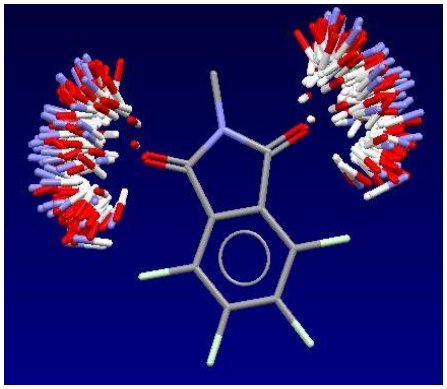

Figure 51 - Interactions of phthalimido group directed towards the carbonyls.

It may be taken from this evidence and from the hydrogen bonding density distribution map of these interactions (Figure 52) that the carbonyls are obviously the main area of interaction for the phthalimido molecule, as expected from their high electronegativity, and is likely increased by the aromatic nature of the group and the delocalisation of the lone pair on the nitrogen.

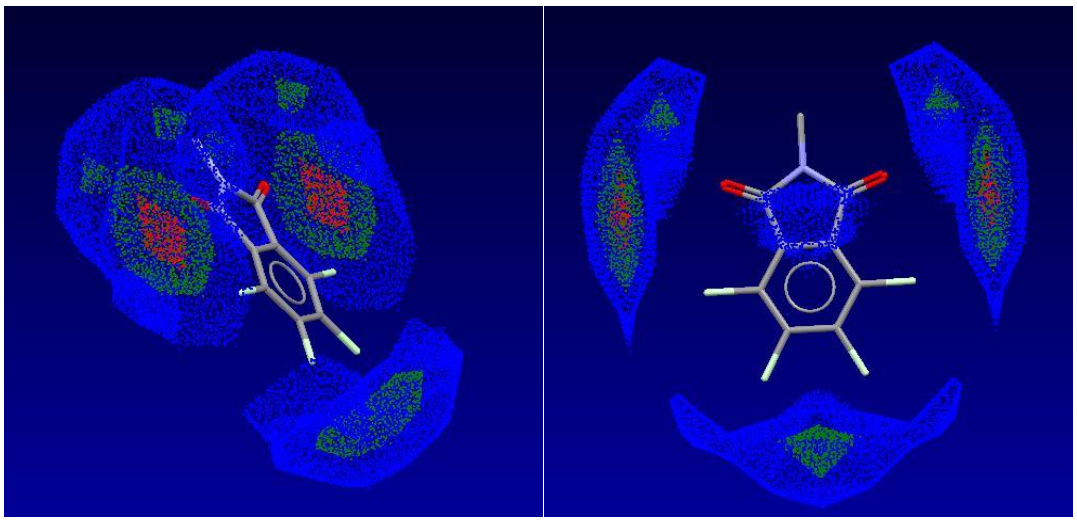

Figure 52 - Hydrogen bonding density distribution map representing close contacts around phtalimido functional groups for all known CSD structures.

Secondary to the hydrogen bonding interactions in terms of influence is the aromatic character of the phtalimido group itself.

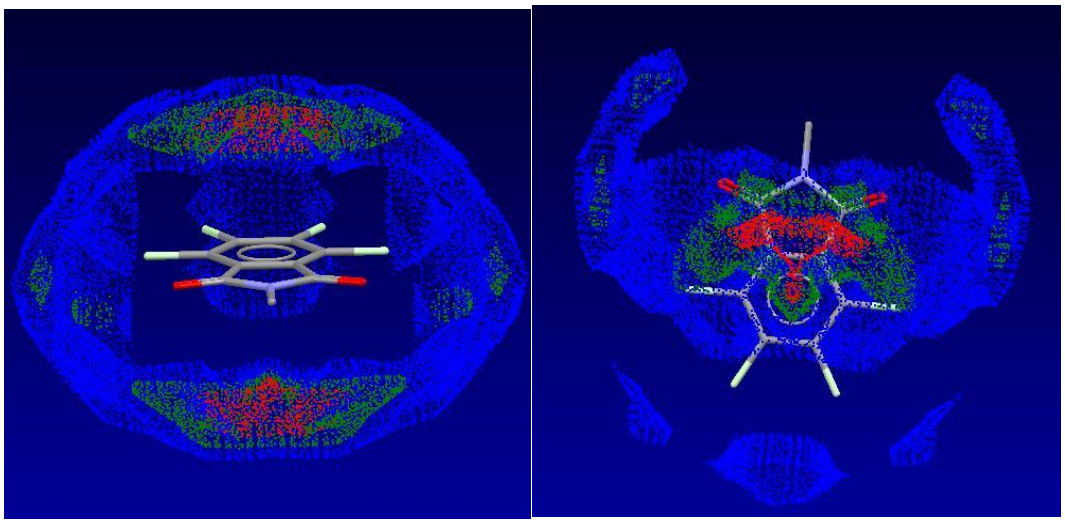

Figure 53 - C-H interaction density plots for the phtalimido functional group.

From the plots of interaction density (Figure 53), where red regions show the highest density of C-H interactions with the phthalimido groups, it can be observed that the most focussed areas of these types of short contacts are situated above and below the planes of the rings, most likely originating from π-π stacking. This is therefore an important interaction that must be considered with these molecules, as has been noted with the phthalimidoperoxyaliphatic acids in their pure structures.

There is no solid state crystal structure on record for meta-chloroperbenzoic acid, and so one of the aims in studying this material was to determine this structure. Leading from the observation of the hydrogen bonding motifs in all other peroxyacids recorded in the CSD, it

can be predicted that the crystal structure of MCPBA should exhibit similar characteristics. In particular it could be expected that the terminal peroxyacid hydrogen will be hydrogen bonded to the carbonyl of a neighbouring molecule, likely forming a catemeric chain that would be assisted by π-π stacking originating from the aromatic ring. It is unclear at this point what effect the chlorine atom substituted on the aromatic ring will have upon the structure other than obvious steric effects resulting from its larger atomic radius.

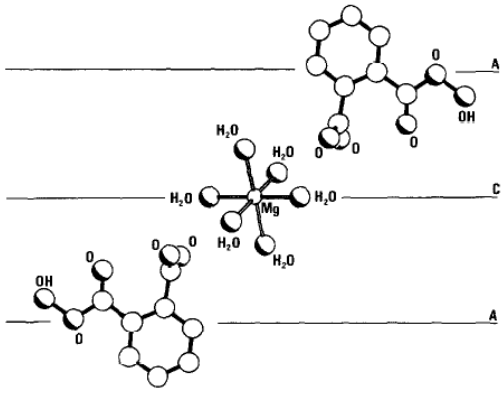

Figure 54 - Diagrammatic representation of the molecular arrangement in 2-carboxylato-peroxybenzoic acid[101].

The closest resembling material to MCPBA within the CSD is that of 2-carboxylato-monoperoxy benzoic acid, which is known to form a 2:1 structure with magnesium hexahydrate[101] (Figure 54). Unfortunately the atomic coordinates and atom parameters are not available for a more complete evaluation. It appears, however, that the main interaction within the association to the magnesium complex is only via the carboxylate group, but interaction between the peroxyacid groups must be expected.

Peroxyacetic acid, being a liquid, has no crystal structure known, and it was not expected that it would be possible to collect this within this research due to its volatile nature.

No known structures containing any of these three target materials as a component in a multi component crystallisation are known to exist. However, it can be assumed that any material to be used as a co-former in a multi-component experiment should contain either a carbonyl for interaction with the terminal peroxyacid hydrogen, or in the cases of the phtalimidoperoxyaliphatic acids and meta-chloroperbenzoic acid, have a delocalised π electron character available for interaction with the phthalimido and the aromatic groups respectively. With the 6-phtalimidoperoxyhexanoic acid, it was predicted that any co-forming molecule will not only be competing with the carbonyl-terminal hydrogen peroxyacid functional group interactions, but also the phthalimido carbonyls present within the target material structure. Secondary components that may be utilised in attempts to

form new multi-component materials may include those with either of these characteristics or a combination of both, including, but not limited to, carboxylic acids, ketones, and quinones.

1.6.2 Agrochemicals

As mentioned above two agrochemical compounds are studied as target materials within this research. They are both structurally very similar, being isomers of each other. The materials being targeted for stabilisation by cocrystallisation are 2,4-dichlorophenoxyacetic acid (2,4-D; Figure 10 and 3,4-dichlorophenoxyacetic acid Figure 11).

The main points of interaction can be easily identified as being the hydrogen bond donor/acceptor group of the carboxylic acid, the electronegative lone pairs on the aromatic oxygen substituent and of course the aromatic chlorine atoms as well as the π-π stacking potential originating from the benzene ring. It is easily predicted that the carboxylic acid will be the dominant hydrogen bonding interaction in a like-for-like multi-component crystallisation, likely forming the familiar $R^2_2(8)$ ring motif with another carboxylic acid molecule. It would be sensible therefore to attempt co-crystallisation experiments with other carboxylic acids.

Analysis of the pure materials, aided by study of their known structure in the CSD[102] shows this to be the case. With 2,4-D it can be observed (Figure 55) that dimers are formed via a double moderate strength hydrogen bonded ring between the carboxylic acid groups, with the $R^2_2(8)$ motif and O-H···O bond distances of 2.633Å.

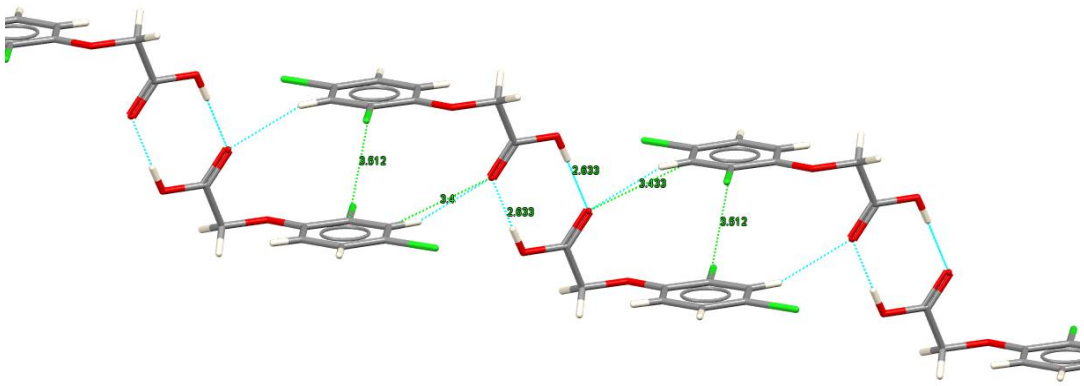

Figure 55 - Hydrogen bonding motif in 2,4dichlorophenoxyacetic acid as viewed along c-axis.

The carboxylic acid carbonyl also makes a short contact to the aromatic C-H between the two chlorine atoms of a neighbouring dimer of C-H···O distance 3.433 Å, a weak interaction. The dimers are arranged in a stacked interlocking pattern, held in place by π-π stacking interactions of 3.512Å.

Figure 56 - 2,4-dichlorophenoxyacetic acid highlighting angle of carboxylic acid group from the plane of the benzene ring.

In the crystal structure, the chain angle is 112.12° , as would be expected for such a bond but with the rotation around the oxygen resulting in the plane of the benzene rings being perpendicular to each other in the dimer unit whilst allowing for the primary hydrogen bonding interactions (Figure 56).

The structure of pure 3,4-D[103] has both similarities and distinct differences to that of 2,4-D. The main interaction is again the $R^2_2(8)$ hydrogen bonding motif between two carboxylic acid groups as would be expected, with a moderate strength O-H···O HB with a bond distance of 2.636Å, creating dimer units as before.

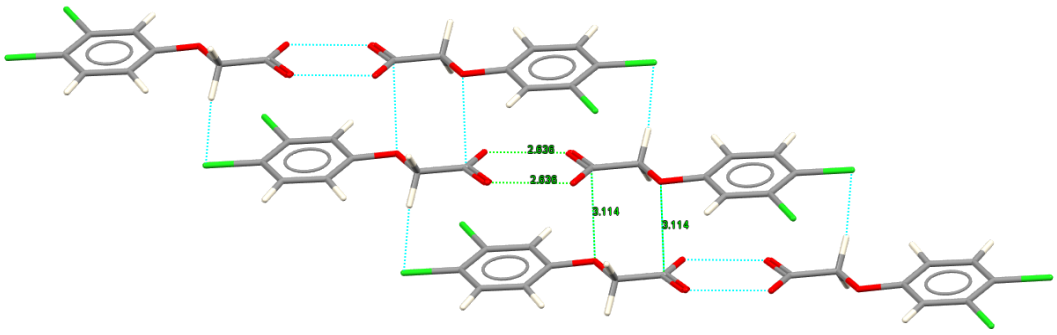

Figure 57 - Crystal structure and primary interactions with measured distances in 3,4-dichlorophenoxyacetic acid.

The $R^2_2(8)$ dimer motifs are sandwiched by a dimer above and below, parallel to the direction of the hydrogen bonding, allowing alignment of the alkoxy oxygen with the carboxylic carbon producing a packing motif of parallel stacked dimers at a distance of 3.114Å, slightly stronger than the accepted π-π stacking interactions but of a comparable spacing (Figure 57).

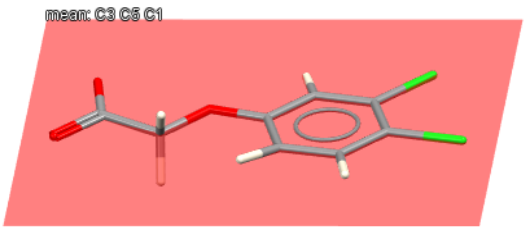

Figure 58 - 3,4-dichlorophenoxyacetic acid in the pure crystalline state with a plane generated through the benzene ring.

The structure is more two dimensional in nature than that of 2,4-D (Figure 58). The entire molecule lies in plane with the benzene ring and follows through the hydrogen bonding motif to the entire dimer and the structure as a whole. This structure lacks the acidic hydrogen atom determination, however with the motif observed, it can be certain that the hydrogen is in plane with the rest of molecule on the hydrogen bond.

1.6.2.1 Known crystal structures containing the target materials

These two target materials, 2,4-D and 3,4-D are known to have been included in multi component molecular complexes in both their protonated and unprotonated form. 2,4-D has been shown to form discrete ionised salts with six materials recorded in the CSD, where the charged 2,4-D is molecularly separate and not chelated to the secondary material. These materials are a hydrated potassium salt, a benzimidazolium salt, an ammonium salt, a 3-hydroxypyridinium salt, and a salt with dicyclohexylammonium[104, 105, 106, 107]. The final complex in which the molecule exists as a discrete ion is one in which a second ion of the molecule is also coordinated to a compound containing two charged manganese centres. In all of these instances, with the exception of the hydrated ammonium salt where it is planar like pure 3,4-D, the molecule retains its bent conformation in the final structure.

In its protonated form, 2,4-D has been shown to form six multi-component molecular complexes, two of which are substituted β-cyclodextrin hosted materials in which the 2,4-D is located within the barrel of the much larger β-cyclodextrin molecule whilst maintaining its twisted conformation[108]. It is also observed to have formed complexes with 2-aminopyrimidine[109], 4,4-bipyridine[110], 4-aminobenzoic acid and triphenylphosphine oxide[104] of which only the 4,4-bipyridine and the 4-aminobenzic acid force planar geometry upon the 2,4-D molecule. There are also 14 structures of 2,4-D in the CSD in which it is deprotonated and coordinated to a metal centre. Of these structures, four of the metal centres are copper, three are cobalt, two are zinc, two are nickel, with one example of each of vanadium, silver and tin.

3,4-D in comparison has fewer known molecular complexes on record. There are two known molecular complexes in which 3,4-D remains protonated, one of which is triphenylphosphine oxide[111] and the other 2-aminopyrimidine[109]. In the triphenylphospine oxide, the molecular attraction is via a short moderate strength hydrogen bond of O-H···O distance 2.597Å between the phosphine oxygen and the acidic hydrogen of the 3,4-D. The molecular complex with 2-amidopyrimidine has a more complicated hydrogen bonding interaction network: there is a an $R^2_2(8)$ hydrogen bonding motif present between the two synthons with an O-H···N short hydrogen bond of length 2.540Å and a longer, moderate strength N-H···O bond of 2.893Å forming a dimer between the two molecules. Two dimers are then further connected by a weak hydrogen bond of 3.390Å between the remaining unbounded amino hydrogen and the alkoxy oxygen of two neighbouring dimers forming a block of four molecules whose only further interactions are chlorine-chlorine interactions and π-π stacking from all four of the molecules (Figure 59).

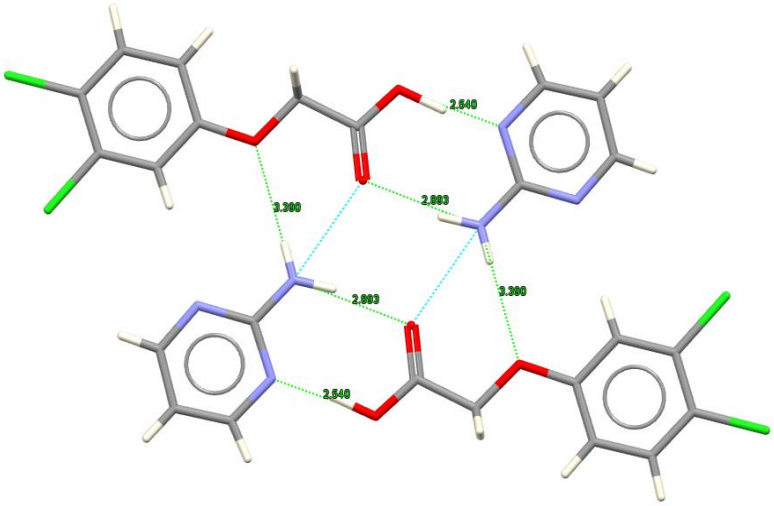

Figure 59 - 3,4-D 2-Aminopyrimidine molecular complex showing hydrogen bond distances of primary interactions.

There is only one example in which 3,4-D exists as a discrete deprotonated material, in a complex with zoxazolamine[112]. The deprotonation is the result of a proton transfer in the plane of a short strong hydrogen bond (2.546Å) in the observed $R^2_2(8)$ motif that is once again observed with the carboxylic acid functional group. The second hydrogen bond in the motif, weaker in comparison at 2.795Å, again aids in the formation of dimers.

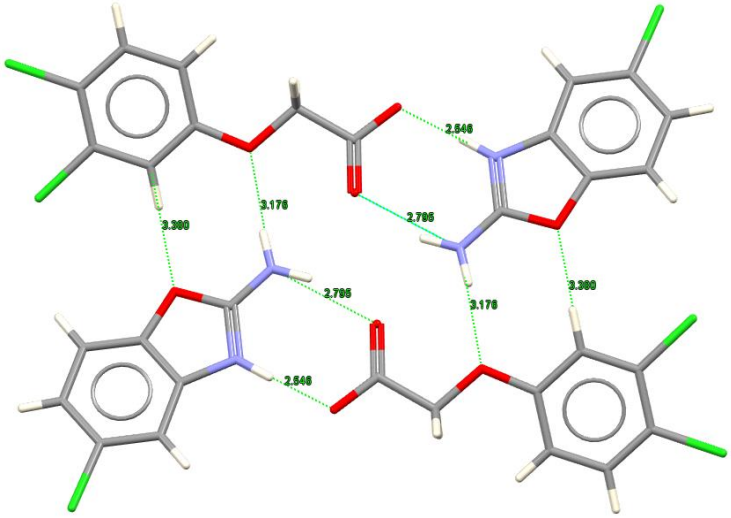

Figure 60 - Zoxazolamine 2-(3,4-dichlorophenoxy)acetate showing primary intermolecular interactions.

The dimers (Figure 60) are again interconnected in pairs by weaker hydrogen bonding interactions present between amino hydrogens and alkoxy oxygens (3.176Å) and aromatic hydrogens to the secondary oxygen in the 5 membered ring of the zoxazolamine (3.380Å). 3,4-D is known to coordinate to only one metal centre, manganese.

In summary, both 2,4-D and 3,4-D are quite versatile molecules with much potential for intermolecular interaction with a variety of materials including acids, amines, amides and both transition group and alkali metals. Given that both molecules have the potential to be deprotonated, one particular area of interest that was therefore studied was that of interaction with proton sponge materials, which primarily use nitrogen lone pair interactions to form short strong hydrogen bonds to the acidic hydrogen of carboxylic acid molecules to the point in which the hydrogen is transferred to the proton sponge molecule and a salt complex is formed.

2. Analytical Theory

A range of techniques have been employed to characterise the products from the experimental work carried out in this work. With the expected diversity of materials produced, medium to high throughput techniques to study the large number of samples were needed, highlighting the more relevant and interesting products for further study. Materials which were highlighted as previously unknown or those which gave information on the behaviour and reactivity of the materials under study were then further characterised fully by X-ray diffraction techniques, along with other supporting analytical methods.

2.1 Crystallography

The crystalline nature of the products in a large proportion of the samples provides a method of precise analysis through crystallographic methods. A crystalline structure is one that is defined as having a distinct motif of atoms repeated in three dimensions throughout the material in its solid state forming a lattice. When represented in its smallest volume, the dimensions of this repeating motif in the x, y and z directions can be represented by the basis vectors **a**, **b** and **c** and the angles between these, α, β and γ (Figure 61). These vectors can operated any point in the lattice to translate to the next equivalent position or lattice point in the extended structure[113].

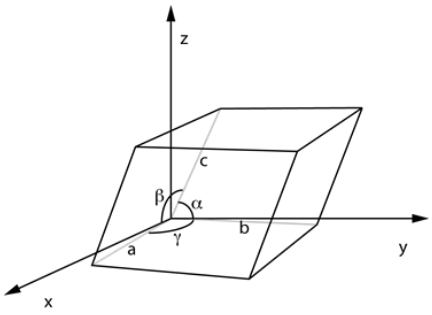

Figure 61 - A unit cell showing vectors a, b and c with corresponding angles α, β and γ, forming a box in the x, y and z axes.

The physical volume described by these vectors is referred to as the unit cell, the building block which through translation creates the extended lattice. The contents of the unit cell can thus be described in relation to the vectors a, b and c in fractional coordinates (x,y,z) of those vectors. An atom described in a unit cell with these fractional coordinates will be at the same fractional coordinates throughout the entire crystal.

Symmetry present within the lattice gives rise to seven possible crystal systems which in turn express themselves in the shape of the unit cell, as shown for the seven unit cells in

Figure 62, and the geometry of the external faces of crystal itself[114]. The seven crystal systems exhibit restrictions on their cell dimensions and angles to allow for the various symmetry elements (

Table 2). Convention states that aside from symmetry considerations, all dimensions should be as small, and angles as close to 90°, as possible.

Crystal System	Essential Symmetry	Restrictions on Unit Cell Dimensions	Restriction on unit cell angles	Possible lattice centring
Triclinic	None	$a \neq b \neq c$	$\alpha \neq \beta \neq \gamma \neq 90°$	P
Monoclinic	One two-fold rotation and/or mirror	$a \neq b \neq c$	$\alpha = \gamma = 90°$	P, C (I)
Orthorhombic	Three two-fold rotation and/or mirror	$a \neq b \neq c$	$\alpha = \beta = \gamma = 90°$	P, C (A), F, I
Tetragonal	One four-fold rotation	$a = b \neq c$	$\alpha = \beta = \gamma = 90°$	P, I
Rhombohedral	One three-fold rotation	$a = b = c$	$\alpha = \beta = \gamma \neq 90°$	P (R)
Hexagonal	One six-fold rotation	$a = b \neq c$	$\alpha = \beta = 90°; \gamma = 120°$	P
Cubic	Four three-fold rotation axes	$a = b = c$	$\alpha = \beta = \gamma = 90°$	P, I, F

Table 2 - The seven possible crystal systems and their restrictions on the unit cell dimensions along with their possible Bravais lattice types (Lattice centring in parenthesis may be converted to standard cell centring by modification of axes)[113-115].

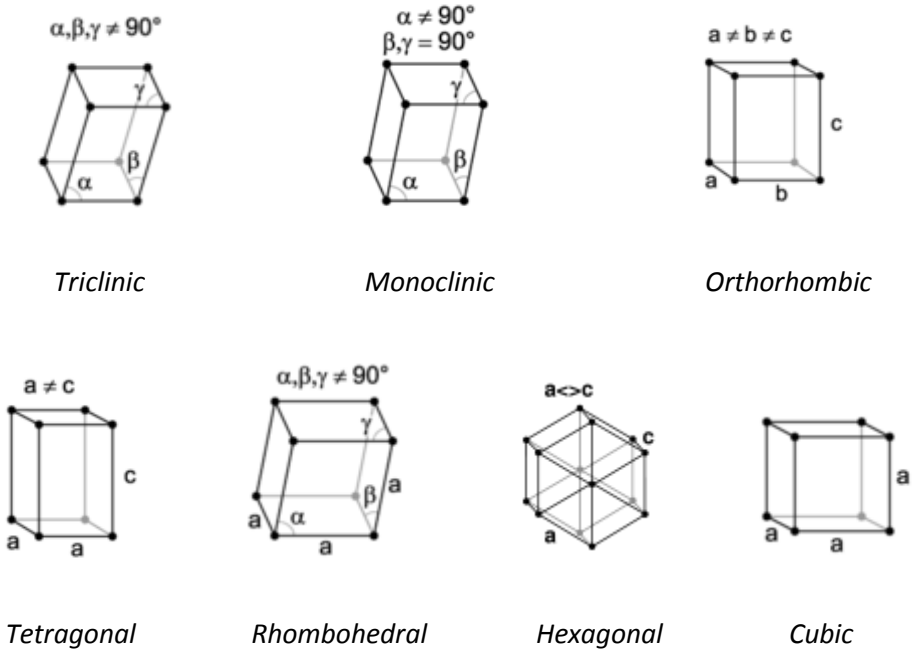

Figure 62 – Primitive unit cell shapes imposed by restrictions generated from symmetry.

In some cases, a primitive unit cell lattice (P) may not fully address the symmetry present. In these, further lattice points may be added into the cell description by increase of volume, adding to the six primitive lattices, an additional eight centred lattices to produce the fourteen Bravais Lattices. The lattices are described to be A, B or C centred if a lattice point is present on the a, b or c faces respectively and F centred if a there is a lattice point on all faces. If the lattice point is at its (body) centre, it is I centred[113]. Any further symmetry in a crystal structure is within the cell itself.

Although the unit cell may be the smallest translating volume within the structure, it is in the majority of cases not the smallest unique part of the structure. The asymmetric unit is the smallest unique part of the crystal structure which, through symmetry operations, can generate the unit cell and through translation, the structure as a whole. The presence of rotation, reflection and inversion, along with combined rotations and translations – screw axes – and reflections and translations – glide planes (Figure 63), leads to the subdivision of the lattice types to 230 possible unique space groups [116], defining all possible arrangements of an asymmetric unit [117].

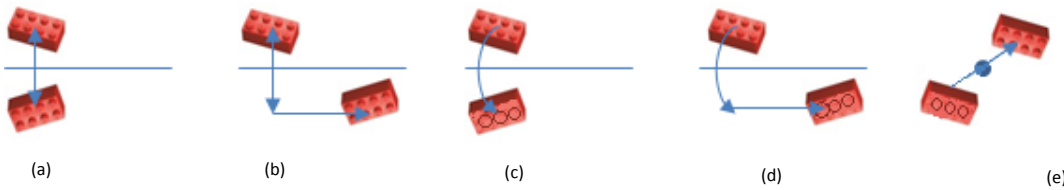

Figure 63 - Representation of possible symmetry elements present within the unit cell (a) reflection, (b) glide plane - reflection and translation, (c) rotation, (d) screw axis - rotation and translation, (e) inversion centre.

The nature of the crystallinity in organic, inorganic and metallic materials is such that the unit cell generated by the lattices under observation is of the size (3-40 Å[113]) comparable to the wavelength of X-ray radiation. As a result, the lattice can act as a three dimensional diffraction grating causing constructive and destructive interference effects on a coherent X-ray beam and hence can be studied by X-ray diffraction.

2.2 X-ray Diffraction

In laboratory based experiments, monochromatic X-rays are typically generated using a sealed X-ray vacuum tube in which a high voltage (30-60 kV) is passed through a metal anode (Figure 64).

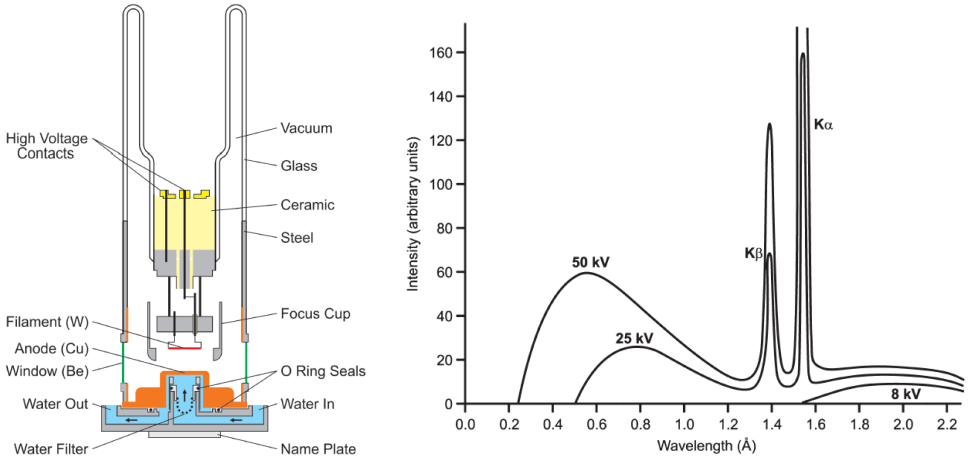

Figure 64 - Cutaway of a standard high vacuum X-ray tube with Cu anode and plot of wavelength against intensity showing characteristic K peaks [113].

The type of metal anode chosen for a particular experiment is dependent on the wavelength of radiation required. Commonly for small molecule experiments, a molybdenum or copper target is used, with different characteristic wavelengths depending on the energy difference between the electron shells in the target material (Table 3). In order to achieve an intense monochromated beam of X-rays, the radiation is tuned either using a filter, or more commonly a single crystal of graphite or other suitable material orientated to the beam such that only the more intense Kα radiation wavelength meets the conditions for constructive interference and is therefore reflected, collimated and used in the experiment.

Anode type	$K\alpha^1$ (Å)	$K\alpha^2$ (Å)	$K\bar{\alpha}$ (Å)
Molybdenum	0.70926	0.713543	0.71069
Copper	1.54051	1.54433	1.54178
Iron	1.93597	1.93991	1.93728

Table 3 - Kα wavelengths of commonly used X-ray tube sources, along with averaged 2:1 weighted Kα [113].

The two X-ray diffraction techniques used in this work, single crystal X-ray diffraction and powder X-ray diffraction, rely upon the same initial principle. An X-ray beam incident on a crystal interacts with the regular array of concentrations of electron density in the lattice, notably around atoms and in covalent bonds. The degree to which the beam of X-rays interacts is dependent on the relative abundance of electron density and thus is proportional to the atomic number. Materials with heavier elements, for example containing heavier metals, therefore diffract X-rays better than those which have fewer electrons, such as organic materials with only carbon, hydrogen and oxygen. Scattering

from the regular planes of a crystal results in constructive and destructive interference patterns as shown by the Bragg condition, Figure 65.

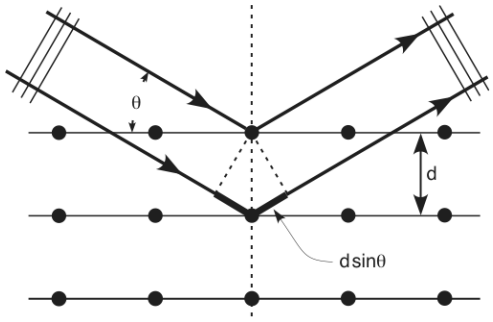

Figure 65 - Illustration of the Bragg construction for diffraction from a set of crystal planes.

For constructive interference to occur, coherent X-rays incident on the parallel planes of spacing *d* at an angle θ to the plane are diffracted (reflected) with a path difference of 2*d*sinθ between parallel planes; for constructive interference to occur, this must equal an integral number of wavelengths (Equation 2).

Equation 2 – The Bragg equation for constructive interference

$$n\lambda = 2d_{hkl}\sin\theta\,; \quad (n = 0,1,2,3\ldots)$$

Equation 3 – Rearrangement of the Bragg equation, to give the scattering angle at which diffraction from particular lattice spacings will be observed

$$\sin\theta = \frac{\lambda}{2} \times \frac{1}{d_{hkl}}$$

In three dimensions, these planes can be labelled with the Miller indices *h, k* and *l,* and results in discrete reflections satisfying the Bragg equation: nλ=2d_{hkl}*sin*θ for a particular set of (*hkl*) planes. A regular pattern of spots, or reflections, is thus observed at the detector. The separations between reflections are related inversely to the lattice [113], hence it is named "the reciprocal lattice". From the measurement of spacings of the diffraction pattern, it is therefore possible to calculate the spacing of the lattice and infer its symmetry from the symmetry of the pattern.

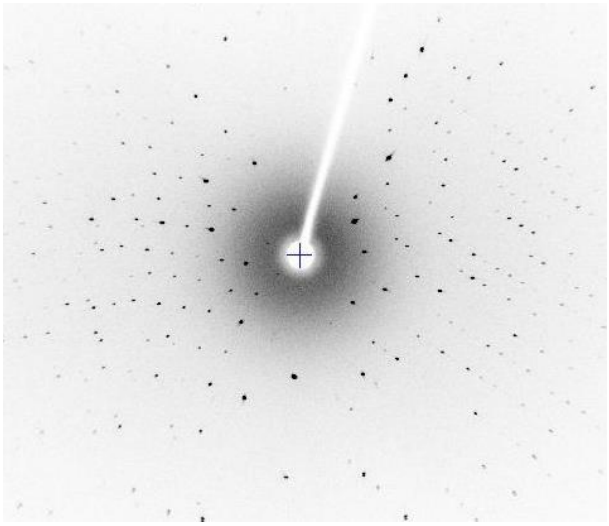

Figure 66 - Reciprocal lattice as observed *via* reflections measured on an image plate detector.

This can be presented using the Ewald Construction (Figure 67). It follows from observation that upon diffraction, the scattering vector $\boldsymbol{S_0}$ is equal to a reciprocal lattice vector $\boldsymbol{S}$, a consequence of the orientation of the lattice parameters in the sample. A sphere of radius $\frac{\mathbf{1}}{\boldsymbol{\lambda}}$ centred at the point of diffraction, will at its edge (the position of the detector) satisfy the Bragg equation for production of constructive interference. When a lattice point on the reciprocal lattice is placed on this point **(0,0,0)**, any other points in the lattice that overlay the surface of the sphere also satisfy the Bragg conditions for constructive interference and a reflection is observed. It is then possible by rotating the orientation of the crystal and correspondingly the reciprocal lattice, to allow for the lattice points to be observed and have their intensities measured by the detector.

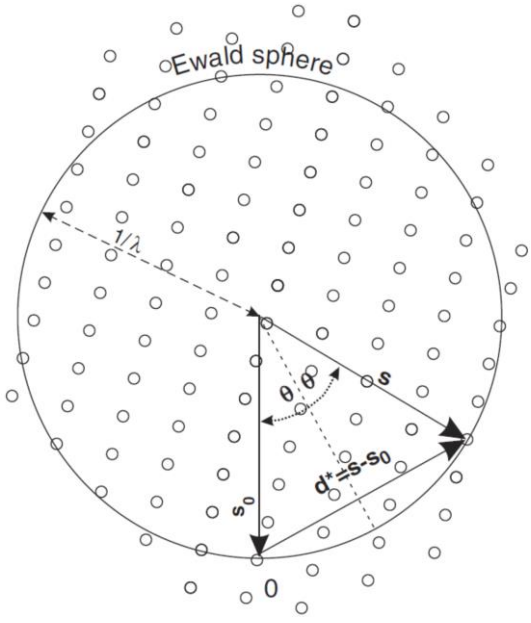

Figure 67 - Ewald Sphere construction with 0 as the reciprocal lattice origin[113].

Lattice points which cannot be rotated to intersect with the surface of the sphere cannot be observed as they cannot satisfy Bragg's Law for the given wavelength of incident radiation. To increase the number of reflections accessible, i.e. which are within the Ewald sphere, the incident wavelength must be decreased, giving access to measurements of lower d-spacings.

The position of the reflections and their intensities contains the information both to calculate the dimensions and symmetry of the crystal lattice, and its contents within the unit cell. The information on the unit cell contents is held within the intensities of the reflections in the reciprocal lattice, related to the electron density by Fourier transform. The observed diffraction pattern is the Fourier transform of the electron density and is defined in terms of the structure factor F_{hkl} at a defined reciprocal lattice point hkl.

Equation 4 – The structure factor components (amplitude and phase)

$$F_{hkl} = |F_{hkl}| \cdot e^{[i\phi_{hkl}]}$$

The structure factor consists of two components, amplitude $|F_{hkl}|$ and phase ϕ_{hkl} (Equation 4), for each reflection and is calculated by summing the electron density $\rho(xyz)$ at every point in the unit cell multiplying by $e^{[2\pi i(hx+ky+lz)]}$ and then integrating for the entire cell volume (Equation 5).

Equation 5 – The structure factor as the Fourier transform of the electron density

$$F_{hkl} = \int_{cell} \rho(xyz) \cdot e^{[2\pi i(hx+ky+lz)]}\, dV$$

In turn, the diffraction pattern is related by an inverse Fourier transform to the electron density (Equation 6), where V is the volume of the unit cell.

Equation 6 - Electron density expressed as a reverse Fourier transform of the structure factor

$$\rho(xyz) = \frac{1}{V}\sum_{h,k,l} F_{hkl} \cdot e^{[2\pi i(hx+ky+lz)]}$$

From the experiment, the intensities can be measured directly by integration of the reflections, but the phase information is lost for each reflection. Consequently it is not possible to directly perform a reverse Fourier transform of the diffraction pattern to directly view the electron density. This is what is known as the "Phase Problem". The process of solving a crystal structure is a method of accurately estimating these missing phases in order to match a calculated structure to an observed structure as accurately as

possible, comparing Fourier transforms to form accurate electron density maps by atom assignment that can be justified by the observed reflections.

2.3 Structure elucidation and refinement

The phase problem is not trivial to solve and methods for doing so are necessarily iterative. Whilst originally computationally time consuming and expensive, they are now routinely employed with little effort as computational power has increased. The most commonly used techniques for routine structure solution from experimental data are Patterson methods, Direct methods and Charge-Flipping (otherwise referred to as "Dual-Space methods").

2.3.1 Patterson Methods

The Patterson method relies upon the basic principle that the observed amplitudes in the diffraction pattern, $|F_{hkl}|$, are squared, ignoring the phases initially, generating a map of peaks corresponding to inter-atomic vectors. The magnitude of the peaks is proportional to the electron densities of the atoms and thus to the product of the atomic numbers of the two atoms involved. This generates a set of interatomic vectors through the Patterson function, ρ_{uvw} (Equation 7).

Equation 7 – The Patterson function

$$\rho_{uvw} = \frac{1}{V}\sum_{hkl}|F_{hkl}|^2 \cdot \cos[2\pi(hu + kv + lw)]$$

Once the phase information has been defined, it can be related to the cell origin. The maxima on the Patterson maps, the Harker peaks, define the ends of the interatomic vectors. The largest of the Harker peaks correspond to the vector of the largest atom with itself and are used to normalise all other vector magnitudes; interatomic vectors between larger, more electron rich atoms are easier to define. Smaller atomic pairings are thus harder to define, being "lost" in the background. This leads to the Patterson method sometimes being referred to as the "Heavy Atom method" and it is generally considered to be only practical if there are one or two heavy atoms in the asymmetric unit that differ significantly in electron density from the rest of the atoms present. With the Patterson maxima identified, they can be interpreted to give some atomic positions and approximate phases can be generated. These can be used to generate a reverse Fourier transform and thus generate a calculated map of electron density which, by comparison to the observed electron density map, serves as a first step for further refinement and interpretation as more atoms are identified and included in the calculation.

2.3.2 Direct Methods

A more generalised approach to solving a structure, without the need to rely upon heavy atoms being present, is using "Direct Methods". The methods are termed "Direct" as they directly solve the phase problem by utilising the relationships between observed intensities of reflections. The method is statistical in nature and relies on two fundamental principles: at any point in the crystal structure, the electron density cannot be negative, and electron densities are located in well-defined maxima, corresponding to atomic positions. The Sayre equation, Equation 8, based on these principles, shows that the structure factor for a particular reflection, F_{hkl}, is a summation of the products of all pairs of reflections that contribute to it.

Equation 8 - The Sayre Equation

$$F_{hkl} = k \sum_{h'k'l'} F_{h'k'l'} \cdot F_{h-h',k-k',l-l'}$$

As the structure factor relies upon all reflections relating to it, it is important that as much information is collected in the experiment as possible. This includes harder-to-observe, high θ angle reflections, however as they are weaker, their contribution is less than the stronger, often smaller angle, reflections. For cases where a pair of reflections that are both very strong are being utilised to calculate a third reflection that is also very strong, the relationship gives a good indication as to the phase of the structure factor; this is the triplet relationship. For centrosymmetric structures it is reduced to assigning positive or negative values. Three reflections, S_{321}, S_{210} S_{111}, are related to each other by the following equality: $S_{321} = S_{210} \cdot S_{111}$. If the two reflections 210 and 111 are the same sign, 321 will be positive, a phase angle of 0°. If they have opposite signs, 321 will be negative with a phase angle of 180°. These initial relationships are set up for multiple sets of reflections, initially with random phases and a few strong reflections with definitively assigned phases, and changed in an iterative way to assign which is the most probable, and thus the remaining phases are determined approximately. From the initial set of phases, an electron density map is generated, allowing visualisation of the results for identification and correction of any molecular shapes and atom assignments. For non-centrosymmetric structures, the procedure is similar however the phase angle is not restricted simply to be positive or negative. Direct methods are thus usually applied in an iterative, multisolution manner in which some strong reflections are given starting sets of phase angles and solutions corresponding to permutations of these are computed and evaluated.

Equation 9- Probability that a phase is correctly determined

$$p = \frac{1}{2} + \frac{1}{2}\tanh\left[\frac{1}{\sqrt{N}} E_H E_{H'} E_{H-H'}\right]$$

Direct methods tend to work best with materials that have no more than about 300 non hydrogen atoms, as the probability of correctly determining a phase is inversely proportional to the square root of the number of atoms, *N*, in the unit cell (Equation 9).

2.3.3 Charge Flipping (Dual-Space Methods)

Charge-flipping is considered a simpler yet considerably more computationally expensive method of solving a crystal structure than more traditional Patterson or Direct methods that has only become particularly useful in the past few years due to the greatly increased processing potential of modern computers[117]. It is a method that uses both direct and reciprocal space to determine the phases and as thus is alternatively named "Dual-Space iterative methods". It is a method that relies upon several logical constraints upon the data which allow for construction of a meaningful set of phases for solution. The constraints are outlined below in both direct and reciprocal space:

Reciprocal Space Constraints:

- Amplitude constraints – amplitudes observed in the experiment pose a constraint on the electron densities

Direct Space Constraints:

- Positivity constraint – electron densities must always remain positive, negative electron densities are meaningless
- Sparseness constraint – The unit cell will be mostly empty with a limited defined amount of positions of localised electron density

The solution problem then becomes a matter of finding a suitable set of electron densities that comply with the amplitude constraints, and as closely as possible complying with some of the direct space constraints. Any sets of electron densities that fulfil these constraints are called "constrained sets". Finding a correct set is a matter of finding a minimum where the constraints in both real and reciprocal space match up well, without falling into local minima. The standard charge-flipping algorithm is outlined here[116]:

1. All the experimental amplitudes are assigned random phases and all unobserved amplitudes are given a value of zero
2. The electron density is calculated by inverse Fourier transform, from the observed amplitudes and assigned phases

3. The resulting electron densities are then modified by flipping the density of all points where the value of electron density is meaningless, i.e. below a set threshold, or is negative
4. Structure factors are generated by Fourier transform of the modified electron density map
5. A new set of structure factors are then obtained by using the observed experimental amplitudes with the calculated phases resultant from the flipping process, and these are iterated through the cycle from step 2 until the process converges between observed and calculated amplitudes.

This method has the advantage of not relying upon knowledge of the symmetry in the unit cell before solution which at times can be ambiguous. The symmetry is determined after the fact, as it can be observed in the calculated electron densities[118]. The limit on the size of unit cell is only dependent upon computational power, with structures containing thousands of atoms in the unit cell known to be routinely solved by the method. As the method relies upon a large amount of measured accurate amplitudes, it is not as suitable for use on an incomplete data set as Direct Methods.

2.3.4 Structure completion and refinement

Once a proportion of the atoms within the unit cell have been determined, the structure can be recycled through an iterative Fourier process, taking the forward Fourier transform of the new model produces a new set of calculated amplitudes and phases, and the previous set is discarded. This can be repeated until all atoms are found. Refinement of the structure most commonly is carried out using least-squares techniques, in which the atomic parameters in the model (for example, positions in the unit cell, and thermal parameters) are varied to give best agreement with the observed structure factor data set. Several cycles of refinement are typically required until the shifts in the parameter being varied are sufficiently minimal and the refinement is said to have converged. The quality of the refinement is governed by the similarity between the two sets of structure factor values from the observed experimental data, F_0, and the calculated data from Fourier transform of the calculated electron density, F_c. The R-factor is the term used to describe this quantification and is a calculation of the summation of the observed structure factors, F_0, minus the calculated structure factors F_c, normalised by the sum of the observed structure factors, usually expressed as a percentage (Equation 10).

Equation 10 - Calculation of R-Factor

$$R = \frac{\sum_{hkl}\big||F_0| - |F_c|\big|}{\sum_{hkl}|F_0|}$$

Weighting of error in the experiment must also be taken into consideration at this stage. For calculation of the R-factor, it is therefore important to state which reflections were actually used. The most common way to decide which reflections are used are by taking only the structure factors that are greater than three times the error (σ) in the measurement of them, $F_0 > 3\sigma(F_0)$. The weighted R-factor, wR_2, is used to assess the quality of the weighted refinement (Equation 11).

Equation 11 - Calculation of the weighted R-factor

$$wR_2 = \sqrt{\frac{\sum_{hkl} w(F_0^2 - F_c^2)^2}{\sum_{hkl} w(F_0^2)^2}}$$

The weighted R-factor is much more sensitive to smaller errors in the proposed model such as missing hydrogen atoms. One further quantification of the structure similarity is the "goodness of fit", *S*. This, shown in Equation 12, is the sum of the difference in weighted structure factors divided by the number of reflections (*m)*, minus the number of parameters (*n)* used to define the structure (or the over-determination of the structure). The goodness of fit is close to 1 for a correctly assigned structure.

Equation 12 - Calculation of the goodness of fit

$$S = \sqrt{\frac{\sum_{hkl} w(F_0^2 - F_c^2)^2}{m - n}}$$

solved structures may have missing or inaccurate atom assignments. Fourier methods are used to find other atoms or features contributing electron density that is not currently assigned. In the early stages of structure completion, an "Fobs" Fourier can be calculated using the observed structure factor amplitudes with the set of phases calculated from the available partial model. This normally reveals further atoms which can then be added to the model and the procedure repeated until all non-hydrogen atoms are found. Towards the end of the structure determination, after initial refinement (see below), a Fourier map is calculated from the differences between the observed and calculated structure factors. This greatly highlights any areas where further assignments need to be made or modified to eliminate differences in the two sets of values. In particular, assignment of hydrogen atoms is typically performed using this method where they can be reliably observed as peaks of residual unaccounted electron density. However as they only have one electron and thus do not contribute much to the overall electron density, they are harder to observe and can sometimes be absent, requiring the assignment of "fixed" idealised hydrogen atoms to be generated.

Initially atoms in the calculated structure are defined using the x, y and z coordinates and a further parameter defining the radius of a sphere from that point to account for the spread of electron density originating from thermal or isotropic vibrations of the atom. Although this is a convenient way to first model non-hydrogen atoms, it is not particularly realistic. This is therefore improved by assigning anisotropic displacement parameters; in total six parameters per atom[114], defining an ellipsoidal shape (Figure 68). This gives a better approximation of the atom thermal displacements. Anisotropic thermal parameters are normally not applied to hydrogen atoms, since they have only one electron associated with them, which is, in addition, participating in covalent bonding to the parent atom in the molecule.

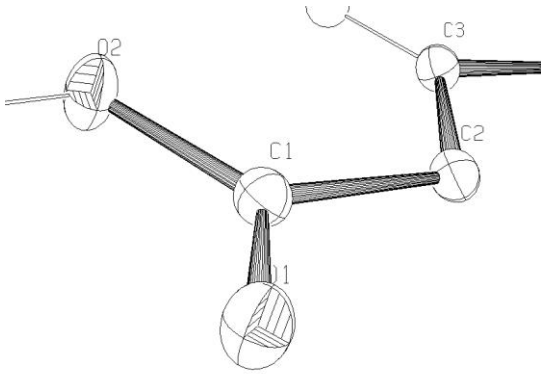

Figure 68 - Anisotropic thermal ellipsoids showing 50% probability of electron density position

2.3.5 Disorder and occupancy

It is relatively common for crystals to exhibit disorder within their structure where a percentage of the cells within it, or an entire domain of the crystal is ordered differently from the bulk. In cases where the long range order dominates and it is only a small portion of the structure that is disordered, it is usually possible to model the material with a generalised crystal structure representing the time-averaged arrangement of the material that is observed at the measured temperature and pressure[114].

The presence of disorder within a solved structure that has not been accounted for is usually detected by the appearances of irregularities in the structure, such as small or larger than normal isotropic parameters for atoms, or unusual elongated ellipsoids in anisotropic atom models.

This can be accounted for in the crystal structure model by assigning partial atoms to positions of disorder to accurately model the electron density.

2.3.6 Interpretation and analysis of the structure

Upon determination of the atom positions, it is possible to interpret the structure using visualisation software. From the size, shape and positions of the thermal and vibrational displacement parameters, the interaction between the Wan der Waals radii and comparing them to known physical constants, it is possible to analyse the connectivity and behaviour of the molecules within the crystals. In sufficiently high quality data, it is possible to measure the length and the angle of hydrogen bonds and their influence upon the local and global structure. The standard visualisation tool for single crystal structures used here has been "Mercury" from the CCDC[119] as it provides an effective and convenient array of features and abilities for analysing and displaying crystallographic information.

2.5 Powder X-ray diffraction

Powder X-ray diffraction (XRPD) is an extremely powerful characterisation tool used extensively throughout this research for medium throughput screening of crystalline samples, allowing for identification of new materials for further study.

In powder diffraction, the sample is essentially an averaged mixture of single crystallites of the material in all possible orientations, giving the appearance of continuous rings of intensity, termed Debye-Scherrer rings (Figure 69).

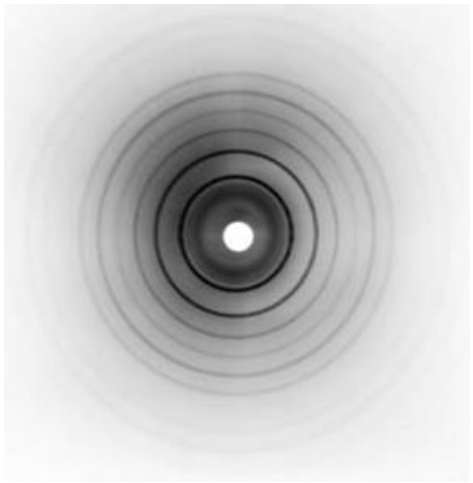

Figure 69 - Powder X-ray diffraction image clearly showing Debye-Scherrer rings around direct beam

The observed rings are a result of the Bragg reflections generated from each individual single crystal, however the polycrystalline material produces multiple sets of Bragg reflections and the patterns appear overlaid on top of each other and rotated around the direct beam position at 0° on the θ axis, Figure 70[113].

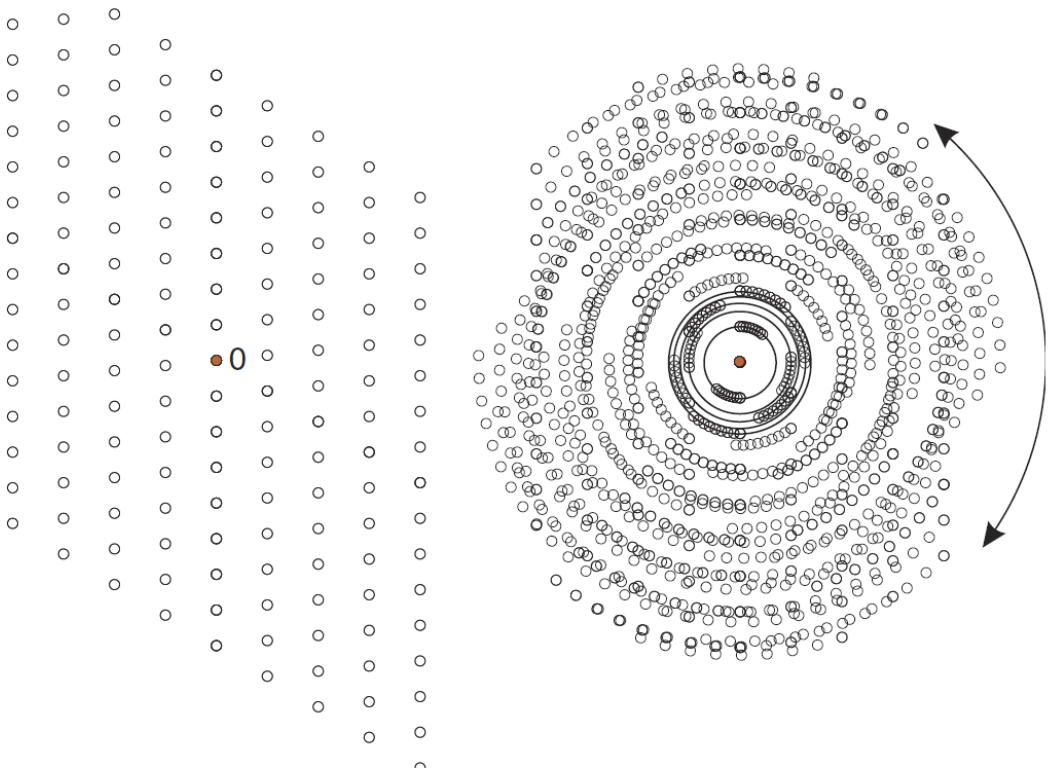

Figure 70 - Simulated observed reflections of a single crystal multiplied to represent crystallites rotated about the direct beam position

The resultant image therefore generates a one dimensional data set corresponding to a cross section through the rings, with only the intensity of the rings and a measured angle, 2θ, measured from the direct beam position, Figure 71. As the rings are a result of the Bragg peak positions, their angle is proportional to the unit cell geometries and can be used to measure the dimensions of the cell via Rietveld refinement. As these properties are characteristic of the crystal structure of the materials being analysed, they are extremely useful as a fingerprinting technique.

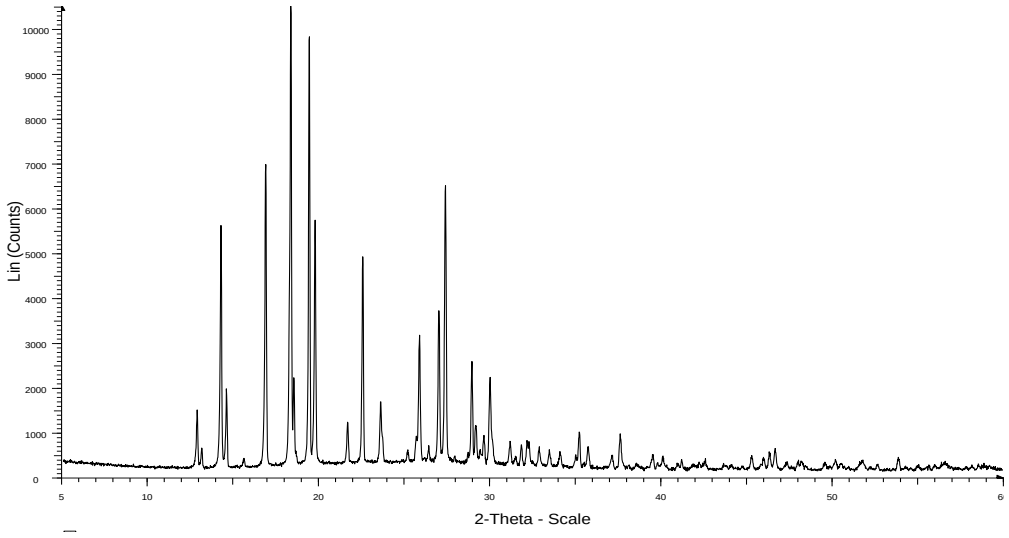

Figure 71 - Example X-ray powder diffraction pattern. A one dimensional plot of the intensity measured in counts as a function of 2θ.

When a mixture of materials is analysed, it is possible, if one or more of the components are known, to isolate the individual patterns corresponding to the each component and identify which materials are responsible for each of the Bragg peaks. This allows for identification of new materials by subtraction of known peaks leaving only peaks corresponding to the un-matched material. Although a full three dimensional structure cannot be obtained from such a method, it can be used to match it to a characterised material from single crystal data. The intensities of the individual components making up a complete pattern also gives information as to the proportion of materials present, allowing for quantification, however, care must be taken as the intensity, being a consequence of the intensity of the individual Bragg reflections, is proportional to the electron densities of the atoms within the structure. Single phase powder diffraction data of sufficiently high quality can also be used to solve the structure of a crystalline material. There are two main approaches to solving structures from powder diffraction measurements. The first of which is a more conventional approach where individual reflection intensities are extracted from the diffraction data and the structure is solved using Patterson or direct methods. This approach was used as early as 1948 by Zachariasen[120] to solve the structure of α-CrPO4. This could be done due to the relatively simple systems involved with minimal peak overlap in the scattering pattern. Where larger more complex samples are involved, it becomes a lot more difficult to be able to distinguish the individual peaks. The second approach is a more recent development and is referred to as the "direct space" strategy. It involves the calculation of a predicted structure and comparison of its calculated diffraction data to the measured diffraction data. The similarity between the two sets of data is quantified and given a figure such as a profile R factor. The simulated structure is then

modified in order to minimise the difference between the two sets of data until the structure is solved. This is a "global optimisation" method, in which the techniques range from a simple grid search to more complex methods such as simulated annealing and genetic algorithms[121]. This direct space method is based on the approach suggested by David is incorporated in computer software for this application such as DASH[122]. These methods however could not be used in this research due to the varied interfering mixtures of materials possibly present in the samples being analysed.

The main use of XRPD in this research will be by comparison of observed patterns to calculated patterns from known structures of starting materials in structural databases, where they exist, or by comparison to the raw or recrystallized starting materials. This allows for rapid identification of whether a recrystallisation, reaction or cocrystallisation has occurred.

2.6 Auto-statistical analysis of powder diffraction data

As a consequence of the generation of vast quantities of X-ray powder diffraction data collected from the screening process, it was necessary for interpretation of the data within the contents of this research to use statistical analysis software in cases where the data was of sufficient quality for powder pattern matching. The software used for this purpose was PolySNAP-3 [123], for its qualitative and quantitative abilities, its phase compositional analysis features, as well as its adaptability to multiple forms of data including XRPD, DSC, Raman and IR. It is able to take a collection of sample powder patterns and through provision of the starting material powder patterns, can identify the individual sample patterns corresponding to starting materials, clustering them together as similar patterns, separating those which have no remaining starting materials as new materials as well as identifying those which are a mixture and which are amorphous. With mixed component patterns, it is further able to separate patterns within the sample pattern that correspond to known phases or materials and give a percentage compositional analysis, identifying unknown phases also present and estimating a percentage composition for those also. Unlike some other programs with similar features, PolySNAP-3 is capable of full profile pattern matching as well as matching by comparison of the most intense Bragg peaks. This has obvious benefits of being able to generate more comprehensive matches of multi-components mixtures, inclusion of weaker peaks from the "fingerprint region" of the patterns, as well as the ability to choose to match by intense peaks only, when the background in the samples are too high even after the software's inbuilt background subtraction has attempted correction. The patterns are matched by a numerical

assignment of “similarity” which is generated by comparing every sample pattern to every other within the data set and assigning a weighted mean of correlation coefficients to each pairing. Those with a high correlation coefficient are clustered together and are given a similarity ranking. The results are then able to be viewed numerically or visually using various graphical outputting options, the most useful of which, is the dendrogram (Figure 72).

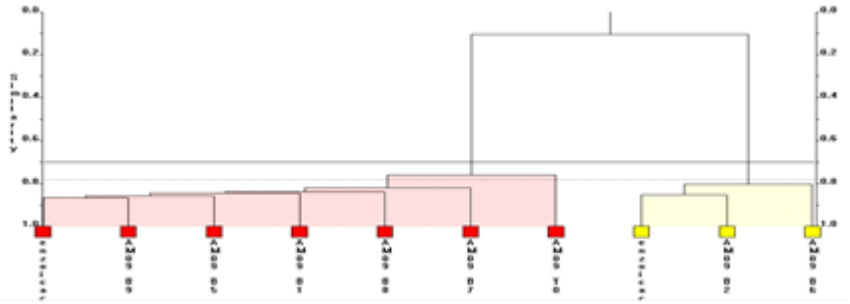

Figure 72 - An example PolySNAP-3 dendrogram output with samples clustered according to similarity

Limitations, however, were encountered when in utilising this software when comparing data from different diffractometers. Characteristic features in the diffraction patterns specific to each instrument lead to lower than expected similarity figures when comparing data from two different sources, leading to clustering of data from different diffractometers. In essence the issue is oversensitivity of the technique. This was partially overcome by only matching data within certain, characteristic free, regions within the patterns and preparation of data by background subtraction by other software before inputting it into the PolySNAP software. More reliably, identification of phases was verified by visual comparison of the samples to their components as in some cases, use of the software was limited by the systematic errors in the collection.

New compounds identified by the statistical analyses are highlighted for further study, for example by isolation for single crystal characterisation methods. These methods complement each other well, as the compositional analysis and quantification can give an assessment of how much decomposition has occurred or how much starting material remains after each experiment has taken place.

2.7 Raman and infrared spectroscopy

In certain circumstances, X-ray diffraction is not a suitable choice for analysis and spectroscopic methods may be used to study the materials. Although they are not as definitive and unambiguous as single crystal X-ray diffraction, they can provide much useful information on bond interactions in non-crystalline materials as well as phase identification

by comparison to reference spectra and libraries. Both infrared and Raman spectroscopy were employed to aid characterisation of new compounds.

2.7.1 Infrared Spectroscopy

Infrared spectroscopy (IR) utilises the absorption of EM radiation by molecules at characteristic resonant frequencies that are directly related to the connectivity of the atoms within the compound and hence characteristic of functional groups and often associated with individual bond vibrations. The wavelengths of radiation absorbed by each chemical bond within the structure are a direct consequence of the bond strength and the masses of the atoms that are bonded, as well as their molecular environment. Many functional groups can be identified by their vibrational frequencies expressed as peaks in an IR spectrum and thus compound identification may be achieved without the need for crystallisation, or even solidity. The characteristic peaks, corresponding to vibrations within the molecules (normal modes), are exhibited in the infrared region of the electromagnetic spectrum between 4000cm^{-1} and 400cm^{-1} [124].

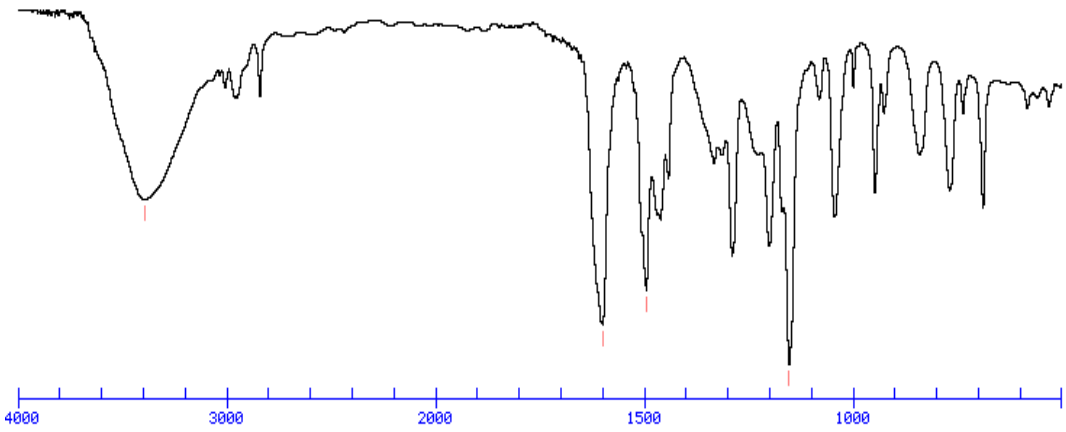

Figure 73 - Example IR spectrum of a compound showing a broad O-H peak at 3400cm^{-1}.

Typically solid samples are placed in a coherent IR beam tuned to the area of the spectrum wishing to be studied. Absorption of IR radiation at a frequency corresponding to the energy of a vibrational mode is registered as an absorbance by comparison of the transmitted beam to a reference beam.

Fourier transform IR (FTIR) can increase the sensitivity IR measurements by employing a Michaelson interferometer to simultaneously irradiate the sample with the entire required range of radiation, as opposed to a standard scanning method through the range. The interference pattern generated by recombination with the reference beam can then be converted by Fourier transform to produce a plot that is very similar to a standard IR

spectrum. It has the benefit of decreasing the needed sample size and allowing a more rapid collection of a spectrum with a decreased sample preparation.

Hydrogen bonds effects are observed within an IR spectrum by analysis of the O-H or the N-H bands which characteristically appear at the high frequency end of the spectrum as a result of the low mass of the hydrogen atom. The strength of a hydrogen bond may be observed by analysis of the frequency of these bands. A stronger hydrogen bond will increase the O-H or N-H bond length, lowering the vibration frequency, leading to a broader, more intense adsorption band.

2.7.2 Fourier Transform Raman Spectroscopy

Fourier transform Raman spectroscopy is a similar yet complementary technique to infrared spectroscopy. As before noted, electromagnetic radiation is incident on a molecule it interacts with the vibrational modes of that molecule. As a result of the Raman Effect, a photon of the specific frequency may excite the electronic state of a molecule from a ground state to a higher energy state. Upon relaxation it emits a photon of a different energy and consequently returns to a different rotational or vibrational state than the original ground state. As a result, a percentage of the photons scattered by the sample will exhibit a change in frequency.

If the system returns to a more energetic state than that of the original state, a photon of a lower frequency will be emitted from the sample. This is termed as a Stokes shift. If it is less energetic, the frequency of the emitted photon will be higher, causing an anti-Stokes shift to be observed. The Raman scattering intensity is determined by the observed change in polarisability between the two states.

Similarly to X-ray powder diffraction, Raman scattering provides fingerprint information on small samples by analysing peak positions and comparing them to pure references. It is a very powerful tool for determining the presence of very small changes between samples, such as in differentiation between two polymorphs of the same material by observing changes in the intermolecular frequencies and also changes in hydrogen bonding within the structure[125] which can be further investigated through other complementary techniques such as single crystal X-ray diffraction.

2.8 Electron microscopy

Scanning Electron Microscopy (SEM) is a visual tool for observation and measurement of particles within samples. Like an optical microscope with photons, an electron beam may be used to create a magnified image of an object, however in place of optical lenses and mirrors, a beam of electrons may be bent by a magnetic field allowing scanning of the

surface of a sample. This has the effect of knocking off electrons from the surface which are collected in a positively charged anode which modulates the electron beam in a cathode ray tube, synchronous with the scanning beam on the sample. The result is the production of a greatly magnified image of the target with a typical resolution of approximately 10nm which may be used for measurements of particle size or microscopic features[126].

2.9 Thermal analysis

Two thermal analysis techniques – differential scanning calorimetry (DSC) and hot stage microscopy – were used to study the materials collected in order to identify the existence of new products and to aid characterisation of mixed component materials.

2.9.1 Differential Scanning Calorimetry

DSC is an extremely useful screening technique for identification of new materials and analysis of mixed phase materials. It is an analytical technique that relies on the thermo-chemical properties of the material being analysed and may be used for identification of melting points, phase transitions and solid to solid transitions of single or multi component samples in the solid state.

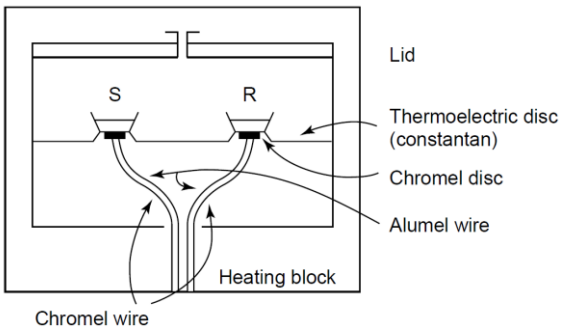

Figure 74 - Diagrammatic display of standard Heat-flux DSC equipment[127]

In heat-flux DSC, a sample (S), be it amorphous or crystalline, is incrementally heated or cooled in a temperature controlled furnace as a function of time, at a chosen programmed rate along with a reference pan (R) (Figure 74). The difference in heat flow required to maintain the two pans at the same temperature is recorded and thus the thermal behaviour of the sample is observed by comparison. When the sample undergoes a transition between phases, there will be a change in the heat required to maintain the pans at the same temperature, a result of either exothermic or endothermic transitions. An endothermic transition would thus give a negative heat flow peak, indicating a phase transition possibly corresponding to a melt. On a cooling cycle and occasionally on a

heating cycle, re-crystallizations show a peak in the positive heat flow direction, representative of an exothermic transition such as a recrystallisation (Figure 75).

The areas under these observed peaks give a direct measure of the enthalpy of transition between phases. DSC can be utilised to detect multiple phases in a sample, such as starting materials, products or polymorphs, as a DSC plot of a mixed phase sample would show individual thermal events corresponding to the separate materials, or a unique new melting point, belonging to a new material such as a cocrystal, in general distinct from the melting points of the starting materials[128]. Normally, a sample plot would be compared to a reference DSC plot of the starting materials to allow identification of the thermal events.

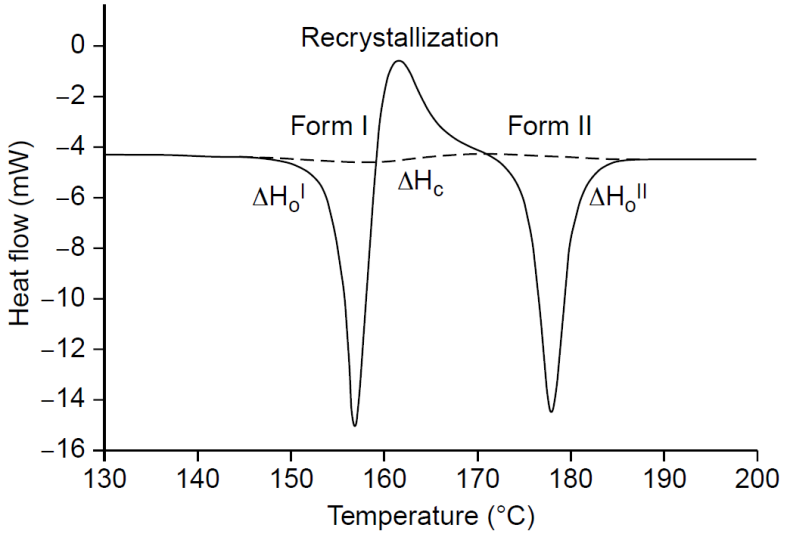

Figure 75 - DSC plot showing exothermic cooling transitions with an upward pointing positive heat flow and endothermic melting with a downward pointing negative heat flow[127].

DSC is able to distinguish individual polymorphs of a single material, as they will normally have different melting points due to different intermolecular interactions. A more stable polymorph will have stronger interactions and thus be more thermally stable, resulting in a higher melting point. It is also possible through DSC to observe transitions between polymorphs using the same principle, observing melting, crystallisations and further melting on a single scan. This relatively rapid technique is particularly useful for screening a large number of samples to identify compounds of interest for further analysis and for providing stability information on materials formed from crystallisation experiments.

2.9.2 Hot-stage microscopy

Hot stage microscopy, similarly to DSC, provides information of transitions in phases by thermally modifying the environment whilst making observations upon physical changes in the material, determining the thermodynamic landscape for a system. It is a form of

thermoptometry as a small sample is placed within a calibrated furnace and heated through a chosen programmed temperature cycle whilst making visual observations of the material as it is recorded with an optical microscope[129]. Changes in the material at thermal events may be observed visually; for example, the melting of the material can be directly observed. This is an excellent complementary thermal technique to DSC as the thermal events observed in DSC can be targeted with the temperature regime and studied in order to ascertain the behaviour of the material that results in the thermal event[129]. This can help combat occasionally ambiguous DSC result interpretations that can lead to confusion in conclusions[30]. It is possible using this technique easily to observe evolution of solvent from porous crystalline materials[130] and also to watch transitions in polymorphs as they occur. By application of the "mixed fusion method" it is also an effective way to identify phase behaviour in two component systems[131].

3. Techniques and instrumentation

3.1 Sample preparation

Several different crystallisation methods were used throughout this research with the aim of creating stable molecular complexes of reactive materials and studying their behaviour with additional chosen components. These methods each have their own advantages and disadvantages, which are outlined in this section. These techniques form the basic standard procedure followed throughout the majority of the research detailed here and any modification to these core methods will be stipulated in the specific experiment descriptions.

3.1.1 Temperature controlled medium throughput crystallisation

The main technique used for preparation of new materials was that of temperature controlled evaporative crystallisation on a medium throughput scale. This is a standard approach used to produce crystalline products for structural elucidation in small molecule crystallography and one that is commonly used within the crystallographic community. In particular, the methods employed here can be classed as combinatorial self-assembly of multi component crystals. It is the most flexible method and can be easily adapted to direct a crystallisation towards a particular structure or polymorph of interest[132]. Aside from its adaptability, the overwhelming advantage of this method is its simplicity and hence repeatability, allowing for parallel batches of crystallisations with small adaptations to each sample to be initiated within a short time scale.

The general procedure for generating a batch of crystallisation experiments, whether involving single or multiple components, is as follows:

- A set of experiment parameters is decided upon for a combinatorial or single component crystallisation, generally consisting of 10-20 individual experiments, each with a differing set of environmental variables, such as an array of different solvents and temperatures of crystallisation, maximising the possibility of obtaining the desired complex and optimising crystal growth. The choice of solvent is dependent on the reactivity and solubility of the target materials.
- Into a clean, new, 7ml glass vial, typically of order 0.00025 moles of the reactive material is weighed accurately along with the relevant molar quantity of the co-component (if required), depending on the target component ratio in the product (it should be noted that the resulting molar ratio in the crystallised product does not necessarily reflect the stoichiometry of the initial solution preparation). It is important

that a clean new sample vial is used to eliminate contamination by any extraneous components, which could lead to the degradation of the reactive material, and to eliminate scratches and other nucleation points from within the vessel, leading to growth of fewer, less flawed individual crystals for analysis.

- The chosen solvent is added slowly to each vial and dissolution is encouraged by several methods.
    - Stirring/vortex mixing – the vial is quickly agitated by a motor / magnetic stirrer creating a vortex within the sample
    - Sonication – sound energy is transferred into the sample through the vial, which is partially immersed within a bath of water, greatly agitating any particulate matter within it, aiding dissolution
    - Heating – the sample may be heated gently on a hot plate with a constantly controlled temperature, by gently warming with the palm of a hand through the glass vial, or by raising the temperature of the sonication bath. Great care must be taken with the materials studied here, due to the reactivity of the materials and their tendency to decompose at relatively low temperatures.
    - In some cases where the solubility of a material is very limited, the addition of a few drops of a second solvent in which it is more soluble may be required to aid dissolution.

  In all cases, the volume of the solvent level is kept to the absolute minimum, no more than 6ml, to allow faster supersaturation once sufficient evaporation has occurred. Dissolution may be checked by transmission of a low intensity laser, such as a laser pointer, through the sample vial. If the sample is completely dissolved, no specular reflection beam will be observed. If complete dissolution cannot be achieved due to impurities, filtration may be attempted before the crystallisation is allowed to proceed however this can affect the stoichiometric ratio of components in the starting preparation.

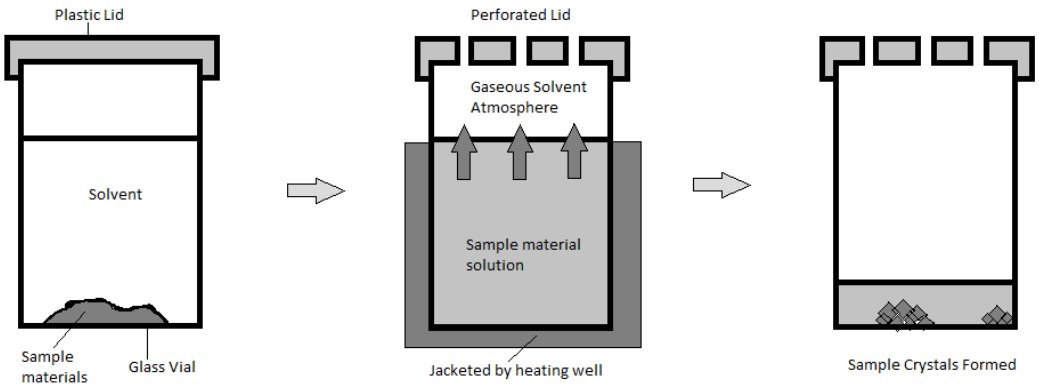

Figure 76 - Cutaway diagram of sample preparation and crystal growth procedure for medium throughput temperature controlled crystallisations, from left to right: pre-dissolution – solvent is added to the solid materials; plastic lid of vial is perforated to allow for evaporation and placed in a heating well to control temperature; crystals are formed in the vial upon evaporation of the solvent past the supersaturation point.

- Once the sample is completely dissolved (Figure 76), the plastic lid is perforated and the sample vial is placed within a multi-well heating unit, set at a controlled temperature (Figure 77), left in a fridge or left at ambient temperature for the duration of the crystallisation. The crystals (which in this work are often subject to decomposition) are to some extent protected from the atmosphere during the crystallisation by the evaporating solvent, which displaces any air from the vial. The solvent is allowed to evaporate completely. Once the solvent has become supersaturated, crystallisation will occur as the reducing solvent can no longer retain the quantity of material, releasing crystallite seeds from which larger crystals will grow as more of the material assembles on the surface of the seeds.

Figure 77 - Samples are placed in temperature controlled hot plates set at a constant temperature with custom made blocks for the duration of the crystallisation.

- Once all solvent is evaporated, the vial containing the solid product material is removed from the temperature controlled environment and stored at ambient

conditions until analysis (Figure 78). If single crystals have been formed, these are analysed by single crystal X-ray diffraction, while representative samples of all resulting compounds are analysed by X-ray powder diffraction.

Figure 78 - Crystallised experiment samples produced from the medium throughput crystallisation technique awaiting analysis at ambient temperature.

This method represents a simple self-assembly approach to synthesising the desired crystalline molecular complexes. In the context of the present work, it also avoids adding excessive amounts of energy to the sample, thus limiting decomposition or reactivity. If a desired crystal form cannot be obtained by the initial set of conditions chosen, the experiment can be easily altered by changing the chosen temperatures and solvents. As reactive materials were being studied, the scale of this method also meets the need to use only small amounts of material, limiting possible unforeseen reactivity that may be hazardous.

In cases where experiments were better suited to a smaller scale crystallisation, 1.5ml scale solvent crystallisations were carried out in a Reactarray Microvate Solo (Figure 79), with temperatures available from -30°C to 150°C in 12 independently controlled rows of 4 cells, resulting in a simultaneous capability of 48 individual crystallisation experiments.

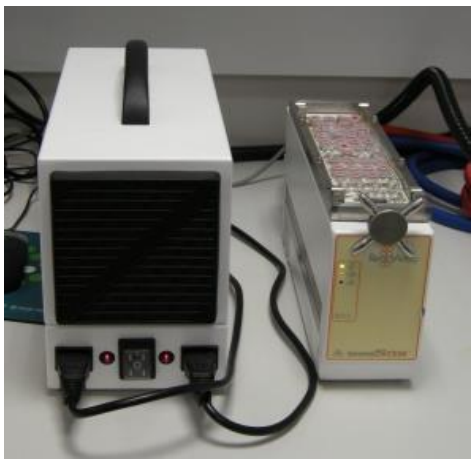

Figure 79 - Reactarray Microvate Solo.

This piece of apparatus was extremely useful as a temperature gradient could also be set for each row before reaching the set crystallisation holding temperature, allowing a cooling supersaturation to be reached in a crystallisation, preventing crashing out of starting materials immediately upon rapid cooling.

If larger crystals of a material were needed for study, seeding crystallisation, where a small crystal is placed in a saturated solution of the same material to promote growth of a particular crystal or form, was utilised. This has the effect of greatly accelerating the nucleation rate determining step of the crystallising process, and the seeding method is extremely useful in competitive processes, where it can be used to select a favoured solid form. Intentional seeding with one polymorph is often the most successful way of preferentially producing that form rather than any others. However, in general this was avoided where possible as extra steps in preparation of the sample can lead to contamination of the materials and exposure to atmosphere leading to further decomposition of the reactive component. For the majority of cases, the standard crystallisation method was sufficient for the creation of suitable materials for analysis.

3.1.2 Mechanochemical grinding and solvent drop grinding

When use of solvents must be avoided, either due to incompatibility or insolubility of components, the mechanochemical grinding method may be employed. First highlighted as a useful synthesis technique for the formation of hydrogen bonded co-crystals of picric acid by Rastogi[133] in 1963, it is an underused yet incredibly powerful method of achieving crystalline forms of compounds of interest that are unachievable through normal solution methods. An explanation of this phenomenon, proposed by Braga[134], is that the heat generated in the course of a mechanochemical process can induce localised melting of the crystal, thus the reaction takes place in the liquid phase although solid products are

eventually recovered [134]. This can be observed in the application of the method where often the mixture of samples can become sticky during the grinding process before returning to a solid.

The method can be performed manually, with a mortar and pestle, or by a ball mill. Both of these have proved effective, however throughout this research, only the manual method has been employed (Figure 80). The relatively simple general procedure for the method is as follows:

- The raw material components are weighed out accurately in equimolar quantities into a mortar;
- The components are gently mixed to homogenise the sample;
- A timer is started and the materials are manually ground with a pestle constantly for three minutes, ensuring all material is equally treated;
- The resulting powder is removed from the mortar and placed in a sealed glass vial until analysis.

Figure 80 - Apparatus required for a mechanochemical solvent free grinding experiment.

There are several modifications to the method that may aid complex formation, including the addition of catalytic amounts of a suitable solvent before grinding, which can increase the success of compound formation. This would suggest a second solution phase synthesis route to the target compounds.

The sample produced is characterised primarily by X-ray powder diffraction methods which easily identify the presence of new materials, but fully characterising the new material can prove difficult due to the microcrystalline state of the sample. As proposed in Figure 81 by Braga, once a polycrystalline material has been created and confirmed, it may be used to seed a solution based crystallisation of the reagents, leading to growth of larger crystals which may be fully characterised by single crystal X-ray diffraction methods.

Figure 81 - Solvent free grinding as an approach to producing larger cocrystals of a complex of interest[134].

Due to the energetic instability of the peroxide compounds studied here, however, any solvent free or solvent assisted grinding must be done in a carefully controlled environment and with small quantities in order to avoid energising the material to the point of decomposition.

3.2 Instrumentation

3.2.1 Single crystal X-ray diffraction

Generating a fully characterised crystal structure of a material necessitates the selection of a high quality crystal. Often this requires several trial crystals to be screened. First, these are examined by microscope under a polarising filter to ensure the crystal is single and to detect any flaws that may cause be indicative of the presence of a multiple crystal or of twinning, which would adversely affect the diffraction experiment. Secondly unit cell screening is run on a diffractometer. An ideal crystal should be on average be between 0.2mm and 0.5mm in multiple dimensions, appear transparent and clear with well-defined edges. When viewed through a polarised microscope, the entire crystal should appear as one domain with no obvious flaws or cracks and when it is rotated 90°, light passing through it should extinguish completely in one motion. Though several mounting methods are possible, in this research, single crystals were mounted on a glass fibre using either Fomblin®, a high-viscosity oil, or with vacuum grease for loading into a single crystal diffractometer.

Three laboratory based single crystal X-ray diffractometers were used in this research. These are outlined here:

3.2.1.1 Rigaku R–axis Rapid diffractometer

The main diffractometer used was a Rigaku R-axis Rapid diffractometer, using a molybdenum X-ray tube with a Kα radiation of wavelength 0.71073 Å, using a fine focus graphite monochromator. The diffractometer was fitted with a curved image plate detector set at 127.4mm from the crystal (Figure 82), allowing simultaneous collection of data over a large area of reciprocal space in a single image. The diffractometer was equipped with an Oxford Cryosystems 700 series liquid nitrogen cooled Cryostream, allowing for data collection temperatures between 80K and 400K using laminar flow of cooled N_2 gas from the cold head directly over the crystal. Unless otherwise stated, screening and collection was carried out at 100K. The operation of the hardware and the interpretation of the images is carried out through the Rigaku CrystalClear 2.0 software environment[135].

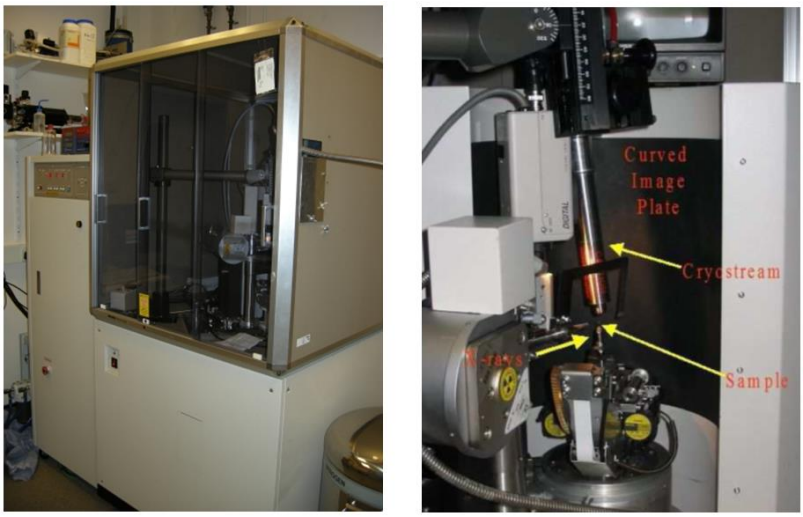

Figure 82 - Rigaku R-axis Rapid single crystal X-ray diffractometer.

The crystal is placed upon the glass fibre mount on a goniometer and centred directly in the path of the X-ray beam. The Cryostream rapidly cools the temperature of the crystal to 100K (or other chosen temperature) ready for collection of images. An initial set of typically four images is collected for determination of the unit cell of the material. The image exposure time is chosen dependent on multiple factors: the diffracting strength of the material under study, the size of the crystal and the intensity of the X-ray radiation. A typical exposure time for a single image of an organic material can be anywhere between 1 and 5 minutes. From the matrix of collected images, the spot positions are determined and a preliminary unit cell is calculated and refined. The unit cell may then be compared to those of the starting materials to see if it is a recrystallized reagent, or whether it is a crystal of a new material or new form. If the unit cell does not match those of starting

materials or known products, the unit cell may then be searched for in the Cambridge Structural Database[136] to see if it has previously been encountered. The initial images will also give an indication of poor crystallinity that has not been identified through microscopy, such as twinning, poor mosaicity and diffuse scattering. These will represent themselves in the image respectively as double peaks, spread out intensities and as broad features or additional peaks.

At this point if the crystal has been determined to have a previously unknown unit cell and a full data collection is required, a data collection strategy is calculated by the CrystalClear software by using the preliminary unit cell of the structure and optimising the collection by application of the knowledge of its lattice symmetry. The optimised collection strategy typically has a minimum d-spacing resolution of 0.7 Å, with a redundancy of five. The images, as with the matrix, can be exposed for typically between 10 and 30 minutes to collect full sets of reflections of sufficiently high intensity compared to the background. Once the data have been collected, the images are integrated using the CrystalClear software, producing a list of reflections and corresponding intensities. The data are corrected for background contribution, and an absorption correction applied using the multi-scan absorption correction method ABSCOR[137]. This information is then passed to the crystal solution software for determination of the structure.

3.2.1.2 Bruker Kappa APEX II

The second single crystal X-ray diffractometer used was a Bruker Kappa Apex II, 4-circle geometry diffractometer fitted with a Molybdenum sealed tube X-ray source with a Kα radiation of 0.71073 Å directed through a fine focus graphite monochromator and an APEX II charge-coupled device (CCD) detector. Measurement temperatures of 28K-100K are accessible using Helium gas and 100K-300K using a nitrogen generator with the equipped Oxford Cryosystems N-HeliX cryostat (Figure 83).

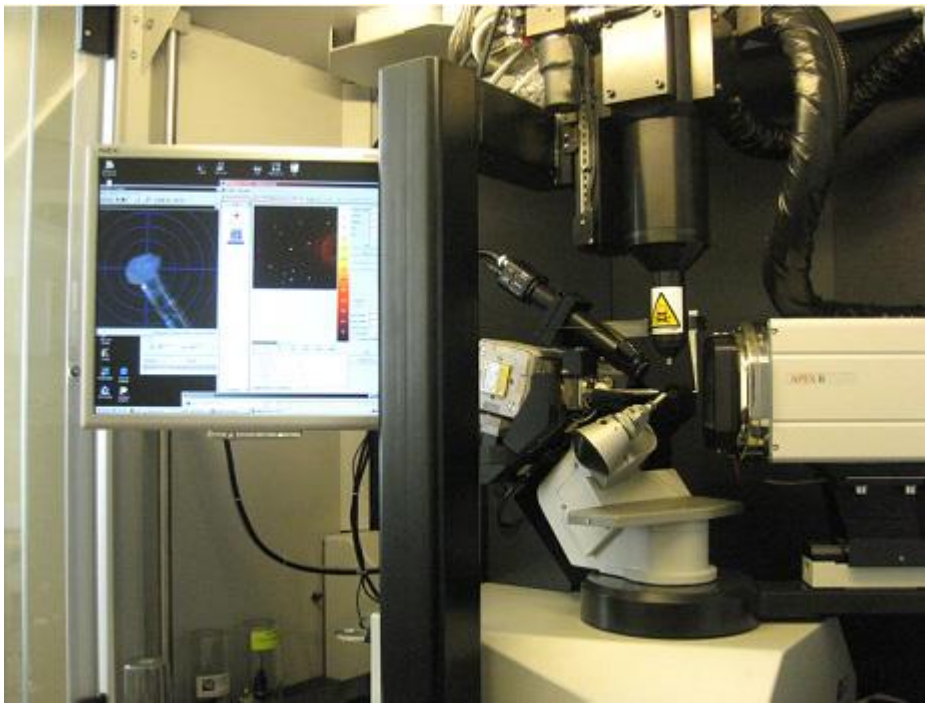

Figure 83 - Bruker Kappa APEX II single crystal X-ray diffractometer with Oxford Cryosystems N-HeliX cryostat.

The experimental procedure adopted is very similar to that used on the Rigaku R-axis Rapid diffractometer with obvious differences as a result of the different detector type. The APEX II CCD detector collects a much smaller area of reciprocal space in a single image and thus a much greater number of images must be obtained in order to collect a complete data set. The Bruker AXS APEX II software suite[138], uses on average 36 images during the matrix collection for unit cell determination in comparison to the four used on the Rigaku. However the collection time for each image is much shorter with exposure times between 10 and 30 seconds per image. Unlike the Rigaku however, the detector may be moved and the sample-detector distance altered to best suit the desired collection strategy. The data are integrated in a similar way with the Bruker AXS software and corrected using the SADABS[139] multi-scan absorption correction method.

3.2.1.3 Bruker-Nonius KappaCCD

The third single crystal X-ray diffractometer employed is the Bruker-Nonius KappaCCD diffractometer (Figure 84), which is the older predecessor of the Bruker Kappa APEX II and again uses a molybdenum sealed tube X-ray source with Kα radiation of 0.71073 Å, directed through a fine focus graphite monochromator, but uses a less advanced KappaCCD detector.

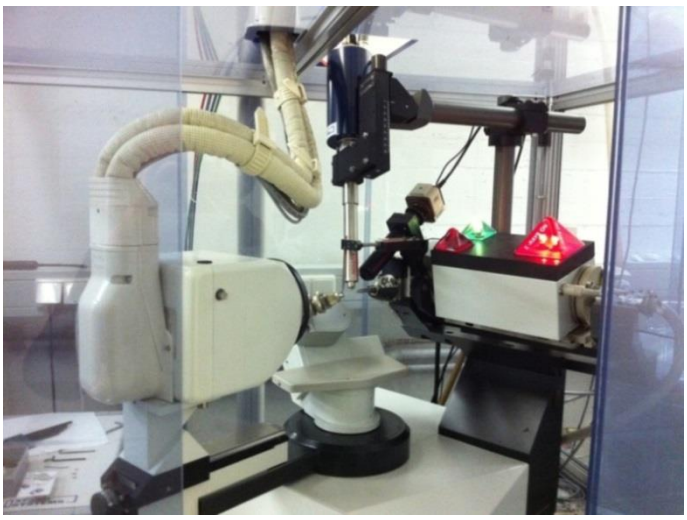

Figure 84 - Bruker-Nonius KappaCCD diffractometer.

The instrument used was fitted with an Oxford Cryosystems 500 series liquid nitrogen cooled Cryostream, allowing for data collection temperatures between 80K and 400K. The data were collected in an almost identical way to that employed on the APEX II, but with the COLLECT[140], HKL Denzo and Scalepack software[141]. Absorption correction was performed with SADABS[139].

The data obtained by these three diffractometers was interpreted through the WinGX interface[142] utilising SHELXS-97[142], SHELXS-86[143] or SIR-92[144] to solve the structure by direct methods, or SUPERFLIP[145] to solve using dual-space methods. All structures were refined using SHELXL-97[146].

3.2.2 Powder X-ray diffraction

Powdered materials were analysed primarily by powder X-ray powder diffraction (XRPD). XRPD was used to determine whether product material was crystalline, and whether it represented a previously unknown unit cell or a recrystallisation or decomposition product. XRPD patterns are more representative of the whole sample, but in consequence can represent the diffraction from several components that may be present. This can make the patterns more difficult to isolate and interpret.

The procedure for collection of a XRPD pattern on any of the three diffractometers used (see below) is as follows: a representative sample of the material is placed within a mortar and pestle and gently ground to homogenise the sample, reducing the microcystallites present within the sample to an average size and evenly distributing the components, assuming more than one component is present. The sample is then loaded, typically, into a 0.7mm glass capillary (0.3mm, 0.5mm and 1.0mm capillaries were also used where

appropriate). If a sample was sticky and proved impossible to load by this method, it was rolled onto a thin glass fibre which was mounted instead of a capillary. Samples once loaded were placed on a goniometer and centred in the X-ray beam of the diffractometer. The sample is rotated during the data collection in order to minimise any preferred orientation effects on the diffraction pattern.

Samples were subjected to fast screening in which the diffraction was measured in the 2θ range from 5° and 50°. A standard sample scan speed employed was 2° per minute which in most cases gave a reasonable pattern for analysis. Weakly diffracting materials were given a longer exposure of 1° per minute, increasing where necessary up to 0.5° per minute, giving an improved peak intensity to background ratio.

3.2.2.1 Bruker D8 Advance

The primary powder X-ray diffractometer used was a Bruker D8 Advance (Figure 10), using a Cu sealed tube source providing Kα radiation of 1.54056 Å, equipped with a VANTEC-1 X-ray detector. The samples were measured in capillary stage transmission geometry with a 1mm anti-divergence slit on the beam.

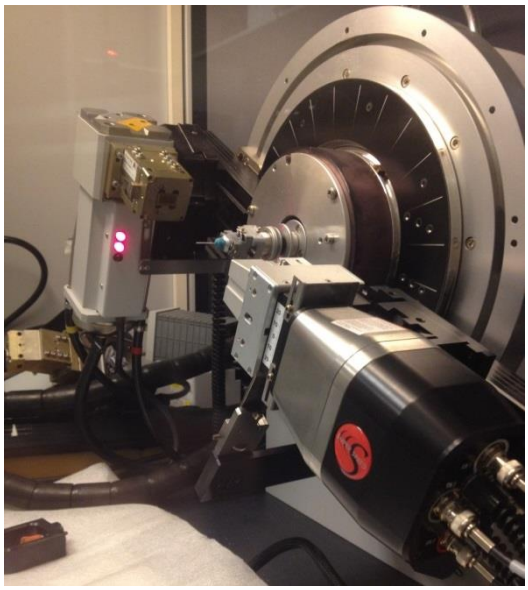

Figure 85 - Bruker D8 Advance X-ray powder diffractometer with VANTEC-1 detector in transmission geometry with capillary stage in use.

The hardware was controlled by the Bruker DIFFRAC^{plus} XRD Commander software environment[147], outputting the diffraction patterns as .raw files for analysis.

Two of these diffractometers were used over the course of this research. This presented a problem as one of the diffractometers exhibited a much higher background with a distinctive profile compared to the other.

3.2.2.2 PANalytical X'pert Pro

The second type of X-ray diffractometer used was a PANalytical X'pert Pro (Figure 11), again with a Cu sealed tube source providing Kα radiation of 1.54056Å. The X'pert was fitted with a scintillation counter detector and set to transmission geometry when required for capillary sample stage setup. Similarly to the Bruker D8, a 1mm slit size was used to limit the width of the beam.

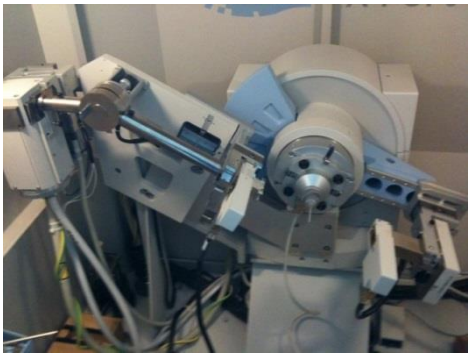

Figure 86 - PANalytical X'pert Pro in transmission geometry

The hardware was operated during collection by the PANalytical X'pert "Data Collector" control software, outputting .xrdml files for analysis by the PANalytical Highscore Plus interpretation software[148].

3.2.2.3 BTX Benchtop XRD

A small number of samples were analysed by a "BTX Benchtop XRD" compact X-ray diffraction / X-ray fluorescence system (Figure 87). This small diffractometer, equipped with a Cobalt source scanned from 5°-55° in 2θ and was able to analyse a ~20mg organic sample via an integrated sample chamber, vibrated to randomise the orientation of the crystallites.

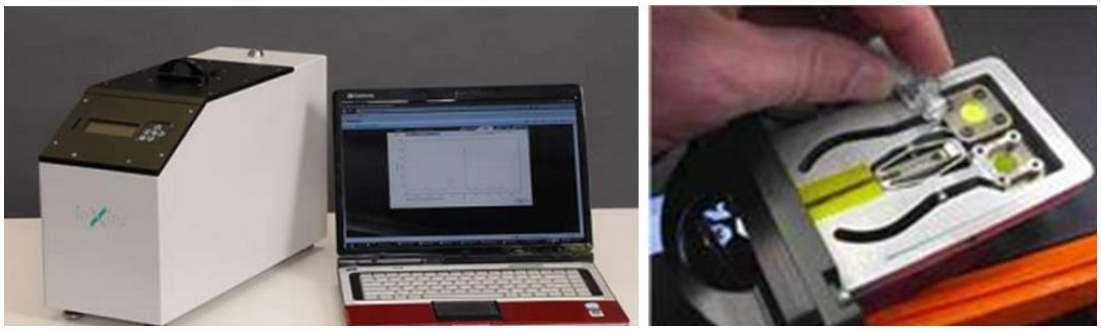

Figure 87 - BTX Benchtop XRD with vibrating sample stage[149].

The Benchtop XRD was unable to accommodate capillary geometry and was used on a trial basis to allow comparison with sample materials collected on the other powder X-ray

diffractometers. Any data collected on this instrument that is discussed will be specifically indicated.

The analysis of XRPD data was found to be best interpreted using the PANalytical Highscore Plus software[148] and the PolySNAP3[123] statistical analysis software due to their adaptability to different data file types output by the different types of diffractometer.

3.2.3 Thermal Analysis

3.2.3.1 Differential Scanning Calorimetry

DSC was carried out on selected samples on a TA Instruments Q20 Tzero differential scanning calorimeter, using heat flux based measurement (Figure 88). 5mg – 15 mg of material, representative of the entire sample being studied, was weighed accurately and hermetically sealed into a Tzero aluminium pan with a Tzero lid and press. Using a cleaned set of tweezers, the sample pan was placed manually into the temperature cell on the sample mount along with a blank, empty reference pan. The sample was then sealed into the cell and subjected to a temperature regime as described in the experiment to slightly above the melting point of the most thermally stable starting material present. The samples were analysed using the TA Instruments Universal Analysis 2000 data analysis tool[150] supplied with the calorimeter.

Figure 88 - TA Instruments Q20 DSC.

3.2.3.2 Hot-Stage microscopy

Hot stage microscopy was performed using a Leica DM2700 M microscope fitted with an Infinity 2 CCD camera for optically recording videos of thermal events. The samples, either single crystals or small amounts of powder, were prepared on a slide and subjected to a temperature regime dependent on the sample composition, similar to that used in a DSC experiment, as described above. This was carried out in a Mettler-Toledo FP900

thermosystem utilising a FP82HT hot stage transmission oven controlled by a FP90 processor (Figure 89).

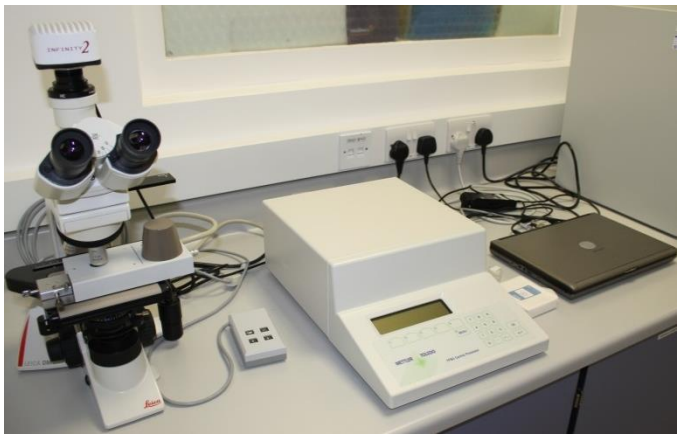

Figure 89 – Leica DM2700 M microscope with Mettler-Toledo FP900 thermosystem hot stage.

A limiting factor of the hot stage microscopy technique is that the samples chosen for mounting on the slide within the oven are not always fully representative of the entire bulk of the material. This results in the need for multiple measurements when 100% purity cannot be verified.

3.2.4 Spectroscopy

Small representative samples were analysed by Infrared and Raman spectroscopy where required. Sample size was no larger than 3-5 mg.

3.2.4.1 Infrared spectroscopy

The infrared spectra of samples were collected on one of several Thermo Scientific infrared spectrometers fitted with an ATR accessory allowing for analysis of very small samples and without preparation, aside from mixing to ensure a the sample was representative of the bulk of the material. Samples spectra are recorded several times and an average is taken to remove anomalous features in the spectra. A background scan was subtracted from all spectra to remove the background produced by the apparatus and produce a flattened baseline.

3.2.4.2 Raman optical microscopy

Raman spectra were collected on a HORIBA LabRAM HR confocal microscope (Figure 90). Standard scan parameters utilised a Ventus 532 laser system, 100mW 532.17nm laser set at 25% optical density to ensure the organic samples were not destroyed. The confocal aperture was set to 100µm and 600x, 50x and 10x objective lenses were available for observation by a Synapse CCD detection system. The best spectra resulted when studying a single crystal sample of a pure material. Sampling at different positions on a slide of a

material with a mixture of components provided different spectra corresponding to the different individual materials. Multiple measurements were thus made within a sampling to ensure the spectra were representative of the bulk of the sample.

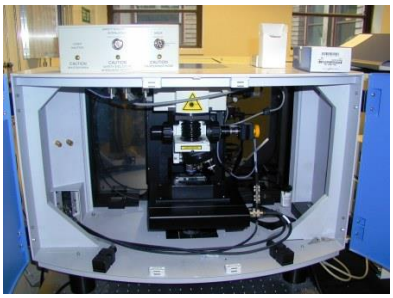

Figure 90 - HORIBA LabRAM HR confocal microscope.

Both IR and Raman samples were later analysed using the PolySNAP3 software, allowing background removal and statistical analysis, including the clustering of similar spectra.

3.2.5 Electron Microscopy

For imaging by scanning electron microscopy, a small portion of each sample was dusted onto a sample holder and coated before placing in the SEM chamber of a Philips/FEI XL30 ESEM (Figure 91), offering a magnification of between 10x and 40000x with a resolution of 3.5nm. The samples were coated with a gold/palladium coating using a Polaron SC7640 sputter coater to avoid melting and dispersion in the high vacuum chamber by the electron beam.

Figure 91 - Philips/FEI XL30 ESEM

Images produced by the SEM were analysed visually for features within the sample and measurements of artefacts and pore sizes.

4. Crystallisation of Reactive Materials

Working with reactive materials requires care in understanding all aspects of the behaviour of the molecule under study. Very little previous research has been conducted in the solid state properties of the extremely reactive organic peroxyacids and doubtless this is a result of their inherent instability, not only on their own in their pure form, but also with solvents in which dissolution may be attempted, pH conditions, temperature and ultimately any secondary materials into which they are brought into contact. This places limitations on the type of materials used in attempting to stabilise reactive peroxyacids, but with no complete understanding of these molecules available, selecting the correct environment for crystallisation of these materials must involve a broad screening process. Systems that do not retain the molecule's efficacy must be eliminated and systems that initially maintain its stability pursued.

In particular with the highly reactive organic peroxyacids, as observed in the crystal data that is available from Feeder and Jones[14], there has been shown to be a need to re-crystallise the phthalimidoperoxyaliphatic acids of interest in order to collect more accurate data to determine the behaviour of the terminal peroxyacid hydrogen, which was missing from the original data, and to re-discover the reaction conditions utilised to isolate the stable solid crystalline form in the first instance. The literature corresponding to these materials only states that the crystals were provided by an external source to the crystallographer[14] and thus the method of crystallising these materials, without allowing them to decompose to the parent acid, was confirmed in this work.

The model material *meta*-chloroperbenzoic acid also had to be isolated and crystallised in order to understand its hydrogen bonding motifs, allowing assessment and potential manipulation of any prevalent motifs to bring forward into a crystal engineering strategy for co-crystallisation of the molecule. It was also important to gather this information as it was likely that the recrystallised material may occur regularly in analysis of resulting materials, therefore a structure and powder pattern of the recrystallised pure MCPBA would be necessary.

The solubilities and single crystal structures of the second class of materials under study – agrichemicals – were already known and therefore this step was not required.

4.1 Solvent effects on reactive materials

4.1.1 *Meta*-chloroperbenzoic acid

In order to find a suitable crystallisation environment for *meta*-chloroperbenzoic acid (MCPBA) and to obtain crystals suitable for single crystal X-ray diffraction, an array of solvents were selected for preliminary assessment of the stability of the material and used in a set of evaporative crystallisation experiments with MCPBA in its delivered form, supplied by Sigma Aldrich.

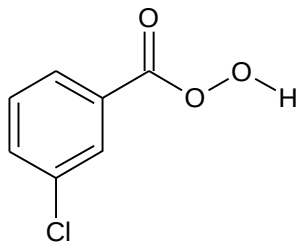

MCPBA

Figure 92 - Molecular structure of *meta*-chloroperbenzoic acid (MCPBA).

4.1.1.1 Overview of solvents chosen for screening

Initially, a standard array of frequently used lab solvents was chosen for crystallisation of MCPBA. Methanol, ethanol and propanol were selected due to the observed solubility of the material in these solvents and their relative inertness. To this selection, acetone was added as a standard laboratory use solvent. Acetone in particular was highlighted as a potential solvent which could not be oxidised, supported by evidence from existing crystallographic data[14] where carbonyl groups within a solid-state structure were known to interact with the peroxyacid group without reacting, and the robustness of the solvent in general.

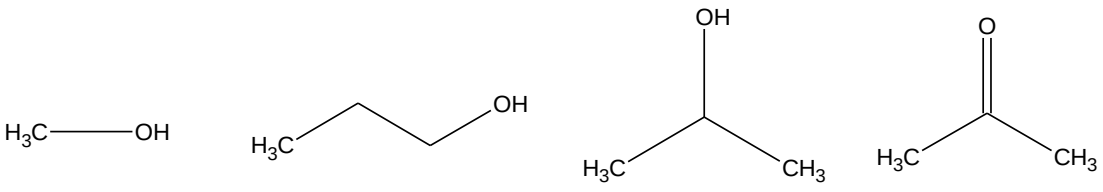

Methanol Ethanol Isopropanol Acetone

Figure 93 - Initial solvents chosen for dissolution and crystallisation study with MCPBA by evaporative crystallisation.

These solvents were used to dissolve the MCPBA and the solutions allowed to slowly evaporate at both room temperature to assess the stability under ambient conditions, and

a reduced temperate of 4°C to decrease the available energy available to the system for decomposition.

4.1.1.2 Statistical analysis of resulting compounds

The resulting solids were analysed by X-ray powder diffraction and analysed for similarity in PolySNAP3[123]. All patterns obtained may be found in Appendix 1. The powder data collected shows evidence of clustering of the X-ray powder patterns into two distinct categories (Figure 94).

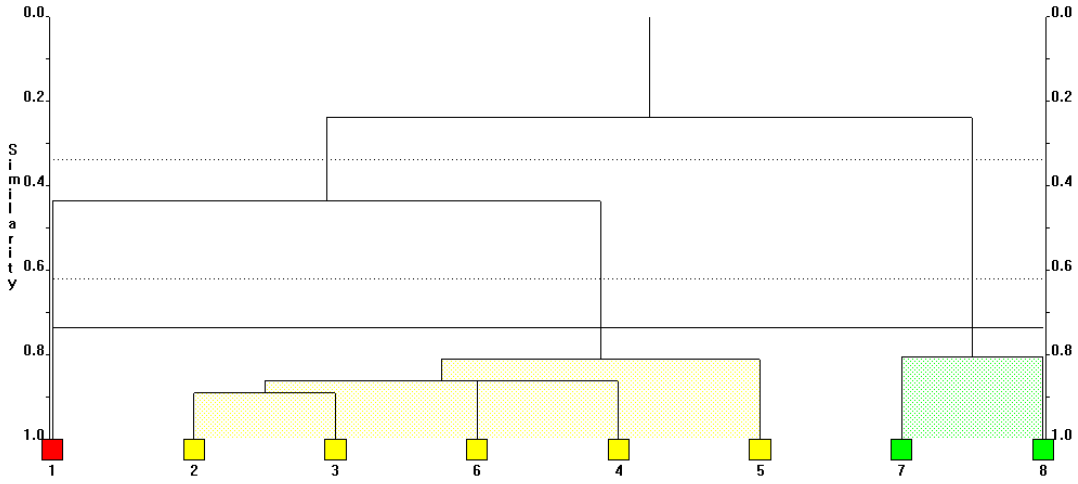

Figure 94 – PolySNAP 3 clustering analysis of x-ray powder patterns of materials collected from the attempted recrystallisation of MCPBA in selected solvents.

The yellow cluster indicated in the dendrogram (Figure 94) corresponds to the samples resulting from MCPBA recrystallized in methanol at 4°C, AM01_02[i], ethanol and isopropanol at ambient room temperature and 4°C, AM01_03 to AM01_06 respectively. The yellow clustered patterns correlate at greater than a 78.0% similarity match. The comparison of these patterns (Figure 95) confirms their excellent match to one another.

[i] For convenience, sample codes indicated are as used in the synthesis / crystallisation experiments. The materials they represent will always be clear from the context.

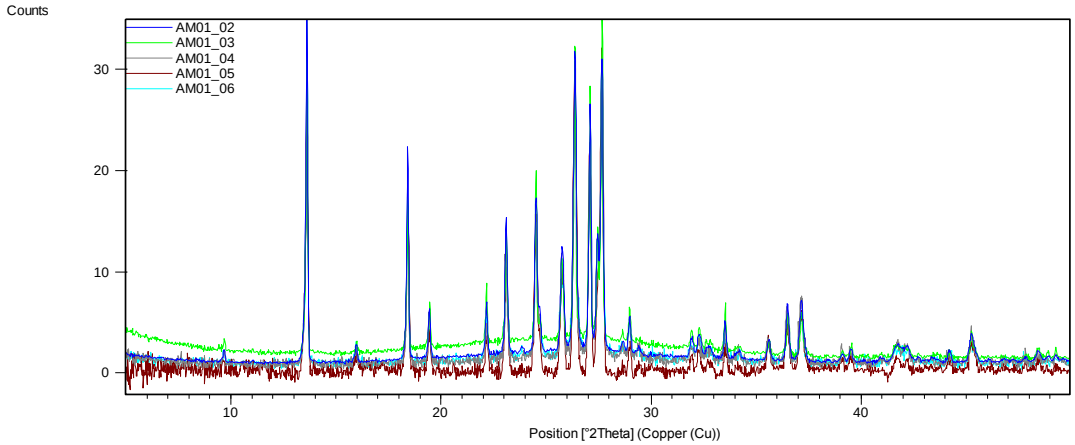

Figure 95 - Overlay of X-ray powder patterns from the identified yellow cluster (AM01_02 - AM01_06).

The red coded sample, identified as 1 in the dendrogram, corresponds to AM01_01 – MCPBA recrystallised in methanol at room temperature. Although the pattern is only at greatest, a 55.8% similarity match to the patterns within the yellow cluster, upon visual examination and comparison (Figure 96) the sample shows a very close match to the main peaks of the yellow clustered samples but with a much greater background noise resulting from a greater amorphous content. This sample can therefore, for qualitative analysis, be clustered with the yellow coded samples.

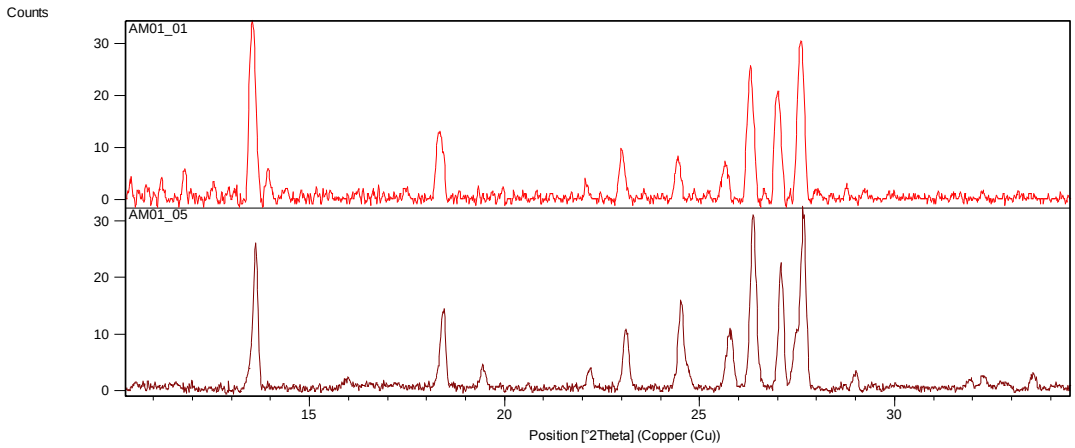

Figure 96 - Comparison of samples AM01_01 and AM01_05 – MCPBA crystallised in MeOH at room temperature and in propanol at room temperature.

The patterns from the yellow cluster match closely to that of the *meta*-chloroperbenzoic acid decomposition material, the parent acid, 3-chlorobenzoic acid as shown by a comparison with a representative sample from the set (Figure 97). These solvents were therefore not suitable for recrystallisation of the MCPBA on its own under the selected conditions.

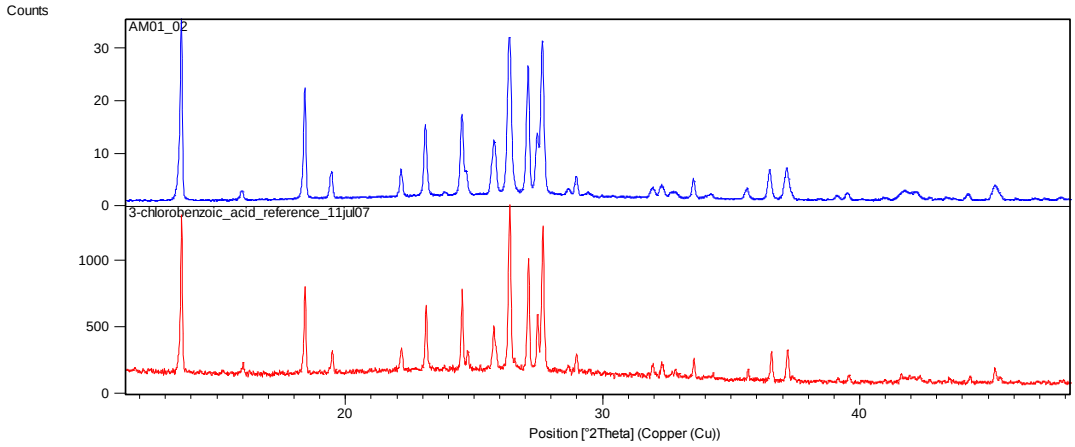

Figure 97 - A representative XRPD scan of the yellow cluster (AM01_02) compared with a reference pattern for 3-chlorobenzoic acid.

The green cluster (7 and 8 in Figure 94) represents samples AM01_07 and AM01_08, where the *meta*-chloroperbenzoic acid was crystallised in acetone at room temperature and 4°C respectively. These samples match with 80.4% similarity. The patterns do not show any resemblance to the decomposition product, 3-chlorobenzoic acid and may correspond to the recrystallised peroxyacid. Upon isolation of a single crystal of this material, it was analysed by single crystal X-ray diffraction and identified as the target *meta*-chloroperbenzoic acid, the structure of which is not recorded in the CSD[46]. Comparison of the simulated XRPD pattern from the single crystal structure generated to the samples within the green cluster show an excellent match with a slight shift in peak positions resulting from the decrease in unit cell size from cryogenic cooling of the single crystal at 100K, thus confirming the successful recrystallisation of MCPBA from acetone at both room temperature and 4°C (Figure 98).

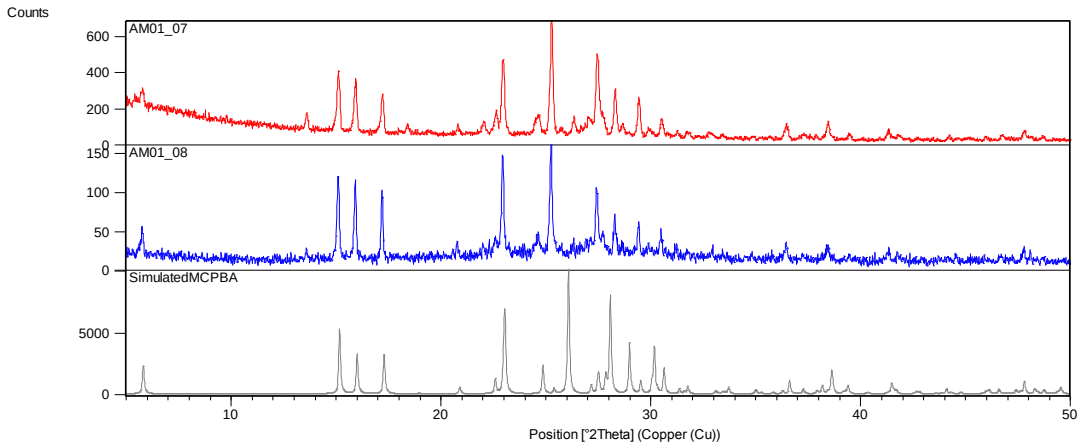

Figure 98 - Comparison of clustered room temperature XRPD patterns of recrystallised MCPBA samples (AM01_07 and AM01_08) to a simulated XRPD pattern generated from the solved structure of MCPBA from single crystal XRD data at 100K.

From the initial results, acetone is the only solvent in which the target peroxyacid crystallised successfully. From the comparison with the simulated MCPBA XRPD patterns, all peaks correspond to peaks that should be present within the with the exception of the addition of a few small peaks in AM01_07 (Figure 98). Comparing this sample to the reference XRPD pattern for 3-chlorobenzoic acid, it appears that a small amount of decomposition has in fact taken place in the room temperature acetone recrystallisaiton as these extra peaks match the strongest peaks observed in crystalline 3-chlorobenzoic acid (Figure 99).

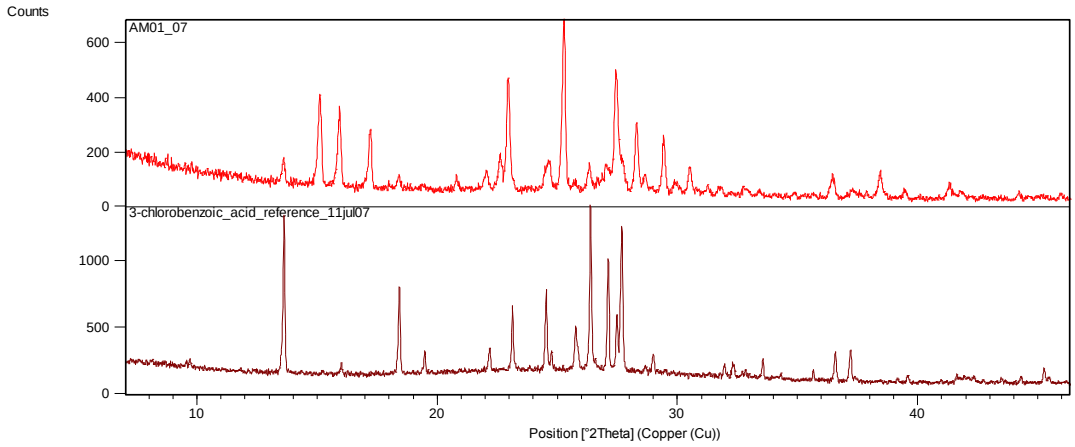

Figure 99 - XRPD pattern of AM01_07 compared to a reference pattern for 3-chlorobenzoic acid.

This would be consistent with the fact that the starting material is in equilibrium with the parent acid. This effect appears also to be present within the 4°C crystallisation, but to a smaller extent.

The study of MCPBA solvent interaction was subsequently extended to methanol at 4°C and room temperature with the addition of hydrogen peroxide to the solution. It was hoped that this would aid in the stabilisation of the MCPBA by pushing the decomposition equilibrium in a reverse direction, towards the formation of the peroxyacid, preventing, or at least making unfavourable, the formation of the parent 3-chlorobenzoic acid. It was already observed that these crystallisation conditions, in the absence of hydrogen peroxide, produce only the parent acid as a product, thus any retention of MCPBA would be a direct result of the addition of the hydrogen peroxide.

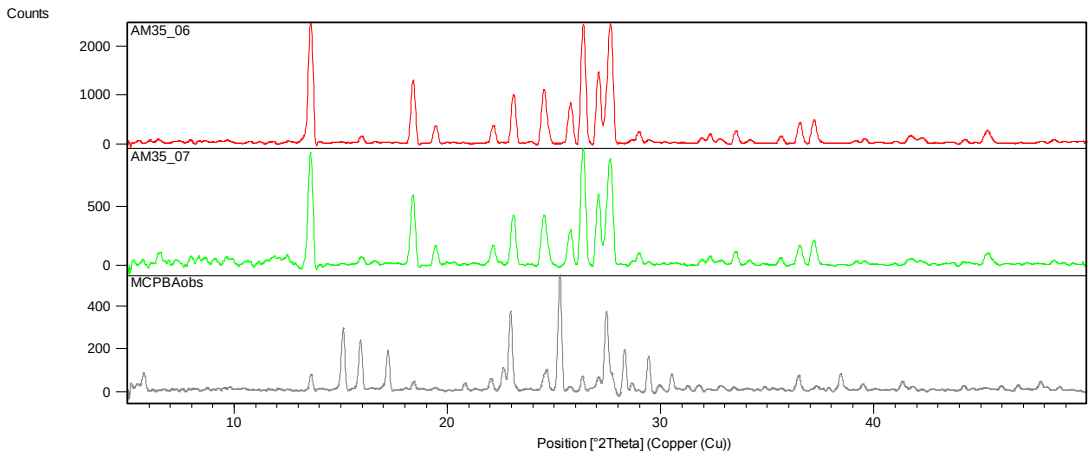

Figure 100 - AM35_06 and AM35_07, MCPBA recrystallised in methanol at 4°C and room temperature respectively with the addition of HOOH, compared with MCPBA.

As can be seen in Figure 100, this had a minimal effect, if any upon the samples from recrystallisation in methanol, with the addition of hydrogen peroxide insufficient to effectively minimise the decomposition in the polar methanol solvent. The application of a small excess of HOOH to a crystallisation is, however, a logical step and was therefore utilised in most subsequent crystallisations.

4.1.1.3 Analysis of isolated structures

For the samples obtained from the small scale solvent screening of *meta*-chloroperbenzoic acid, the majority of the crystallisations resulted in decomposition to 3-chlorobenzoic acid. However that was not the only solvent interaction observed, with .reaction products also obtained under certain conditions. One frequent such product was TATP – triacetone-triperoxide, also discussed here.

3-Chlorobenzoic acid

Although the structure of 3-chlorobenzoic acid is known, for which two data sets exist within the CSD, both were collected at room temperature. The structure was therefore recollected at 100K, in line with the standard collection temperature for single crystal X-ray diffraction in this research, and in the research group as a whole.

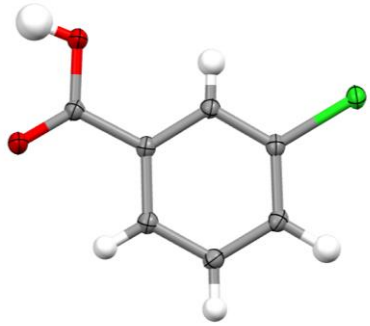

Figure 101 - Crystal structure asymmetric unit of 3-chlorobenzoic acid.

A crystal structure of 3-chlorobenzoic acid (Figure 101) was obtained from a single crystal representative of the bulk of the sample, isolated from the recrystallisation of MCPBA in methanol at 4°C, AM01_02, and determined by single crystal X-ray diffraction at a temperature of 100K. The structure of the material was reconfirmed to be monoclinic with a space group $P2_1/c$ (

Table 4). The asymmetric unit of the crystal structure comprises one full 3-chlorobenzoic acid molecule, and thus there are four molecules present within the unit cell. As would be expected, the acidic group of the molecule is protonated. Disorder of the chlorine atom on the 3 position of the benzene ring was observed, and modelled in terms of a 180° rotation of the aromatic part of the molecule resulting in two possible positions of the chlorine atom, alternating from the 3 to a 5 position. When the disorder is modelled, it leads to a 94% occupancy of the chlorine atom at the 3 position and a resulting 6% occupancy at the 5 position. This, however, has no real relevance to the hydrogen bonding motifs observed within the structure.

Table 4 - Crystal structure collection data for 3-chlorobenzoic acid.

Compound	**3-Chlorobenzoic acid**
Formula	$C_7H_5O_2Cl$
Crystallisation Conditions	MCPBA, Methanol at 4°C
Molecular weight / $gmol^{-1}$	156.56
Temperature (K)	100
Space Group	$P2_1/c$
a (Å)	3.7649(6)
b (Å)	15.991(3)
c (Å)	11.0242(18)
α (°)	90
β (°)	94.056(9)
γ (°)	90
Volume ($Å^3$)	662.04(19)
Z	4
Z'	1
θ range/˚	2.25-34.58
Reflections Collected	22577
Independent	2695
Refln (obs.I>2theta(I))	2299
R_{int}	0.0593
Parameters	107
GooF on F^2	1.068
R_1 (Observed)	0.0420
R_1 (all)	0.0491
wR_2 (all)	0.1198

The primary interaction within the structure is the predictable and familiar $R^2_2(8)$ carboxylic acid dimerization motif (Figure 102), associating two carboxylic acid molecules via two moderate strength hydrogen bonds at an O···H-O distance of 2.652(2)Å and an angle of 178(3)°, with the hydrogen atom clearly associated with O2, being at a distance of 0.86(3)Å to the donor and 1.79(3)Å to the acceptor O1. The two dimerised 3-chlorobenzoic acid molecules associate such as to create a planar arrangement of the two molecules, with an inversion centre in the middle of the hydrogen bonding motif.

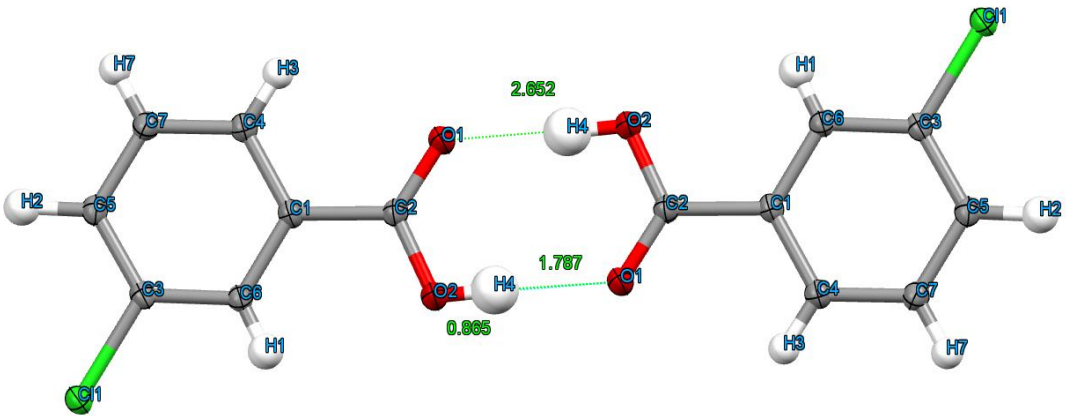

Figure 102 - 3-chlorobenzoic acid dimerisation motif with associated hydrogen bond distances.

O1 additionally interacts with the aromatic hydrogen at the 4 position on the aromatic ring, H2, creating a weak C-H···O interaction at an overall acceptor to acceptor distance of 3.368(2)Å and an angle of 148(2)° (Figure 103).

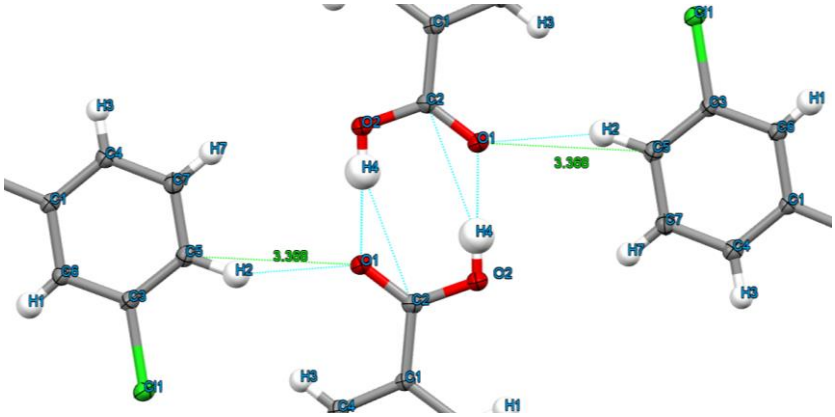

Figure 103 - 3-chlorobenzoic acid dimer interaction with aromatic hydrogen H2 parallel with the main dimer.

This O1···H2 interaction is close to being planar with the main dimer but neighbouring molecules are displaced by 0.819Å to each other, produces a stepping arrangement of dimers alternating orientation to form infinite chains (Figure 104) stacking on top of each other down the *a*-axis.

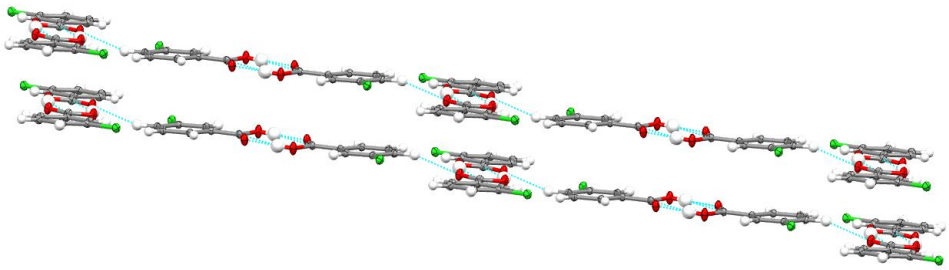

Figure 104 - Stepping arrangement of 3-chlorobenzoic acid dimers.

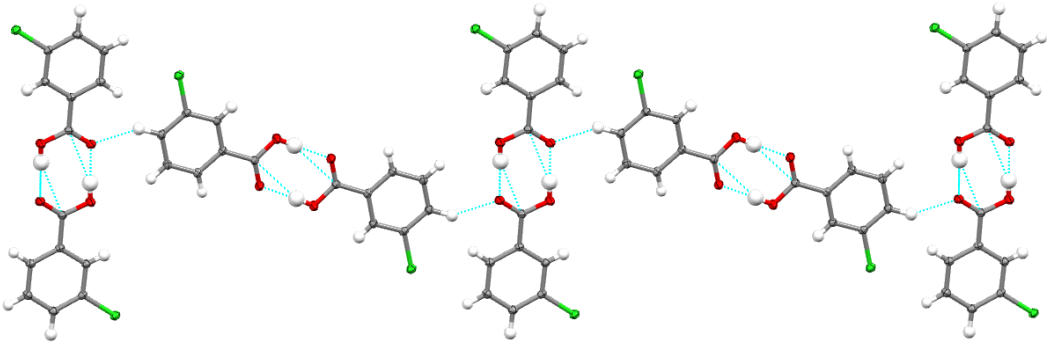

Figure 105 - Alternating dimers of 3-chlorobenzoic acid arranged along the stepping chains viewed down the direction of the *a*-axis.

As viewed down the *a*-axis (Figure 105), the alternating orientation of the dimers along the infinite stepping chains can be appreciated. These chains stack directly on top of each other down the *a*-axis thus generating sheets of hydrogen bonded molecules.

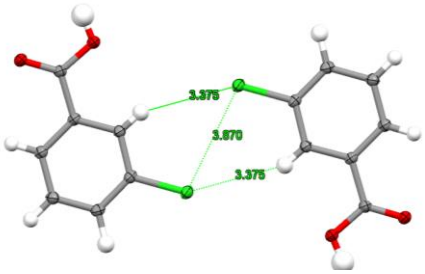

Figure 106 - Chlorine interactions within 3-chlorobenzoic acid.

The chlorine atoms in the molecule are not involved in significant intermolecular interactions (Figure 105). They lie within the structure at a distance of 3.8703(7)Å to each other, greater than the sum of their van der Waals radii. This is also true of their closest intermolecular interaction with the aromatic hydrogen at the 2 position, which has a distance of 3.38(2)Å. The only interactions in which the van der Waals radii do overlap, are intramolecular, such as with the neighbouring hydrogen atoms within the aromatic ring.

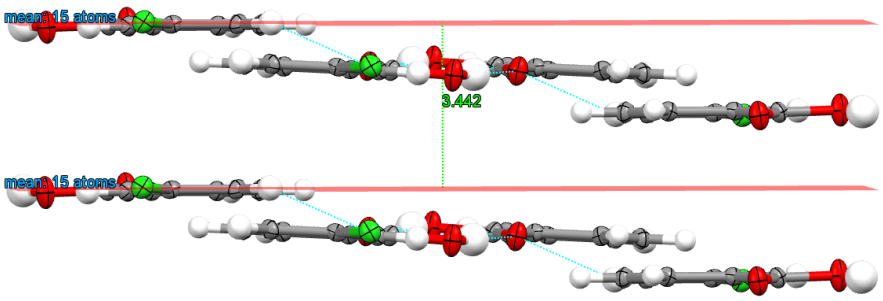

Figure 107 - Planes generated by stacked from symmetry equivalent benzene rings of 3-chlorobenzoic acid molecules in two stacked sheets with the distance measured between the two, indicative of the π-π stacking distance.

The aforementioned stacking of the sheets is facilitated by π-π stacking at a distance of 3.442Å between the planes generated by stacked molecules (Figure 105). The π-π stacking arrangement between the sheets is skewed as shown in Figure 108, where two adjacent sheets are coloured red and blue. There are no obvious voids or channels within the structure aside from between the π-π interacting sheets.

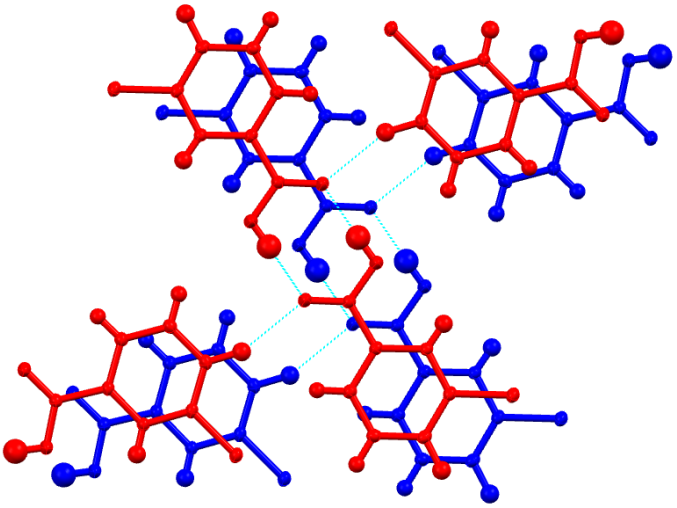

Figure 108 - Skewed stacking of two sheets (red and blue) of 3-chlorobenzoic acid.

Triacetone-triperoxide (TATP)

One unexpected side reaction that occurred frequently, not necessarily within the solvent screening process, but when acetone was used as a solvent to crystallise MCPBA or any of the other peroxyacids, was the formation of the highly energetic material triacetone-triperoxide – TATP. TATP is a highly unstable molecule which is very sensitive to concussion and ignition, and is used a primary and main charge explosive[151]. The danger associated with the occurrence of this material as a by-product of crystallisations was limited by the crystallisation technique used, with each sample isolated in an individual reaction vessel on very small scale.

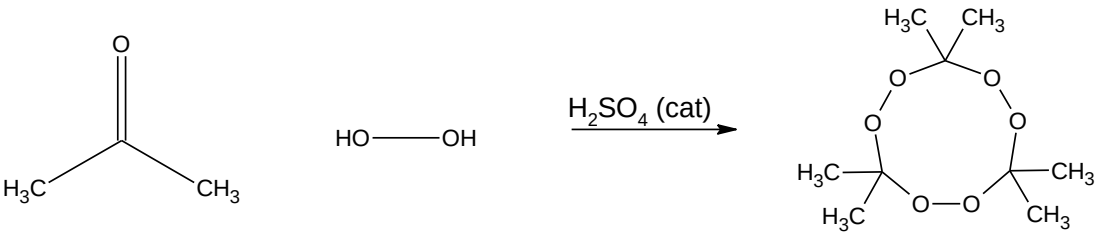

Figure 109 - Standard reaction scheme for synthesis of triacetone-triperoxide.

The standard synthesis of triacetone-triperoxide is by reaction of hydrogen peroxide solution with acetone in the presence of a sulphuric acid catalyst (Figure 109). Within the course of this research however, these reaction conditions are not present, and instead the acetone must react with hydrogen peroxide released from decomposition of the peroxyacid. The formation of TATP was noted mainly in cases where the co-component was a carboxylic acid, thus the synthesis seems to be catalysed also by much weaker carboxylic acids. The side reaction under the crystallisation conditions within acetone is therefore as follows (Figure 110):

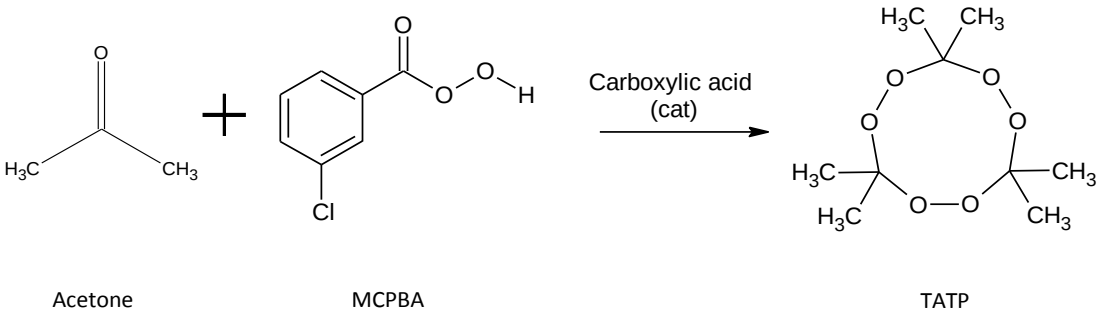

Figure 110 - Synthesis of TATP under crystallisation conditions for MCPBA.

TATP is a highly polymorphic material, with at least 6 known forms recorded[151]. The form observed in the reaction conditions here, however consistently has reduced unit cell parameters of polymorph b described in the CSD, although the CSD entry for that form is in space group Cmca, whereas the structure collected here was better solved as $P2_1/c$. Also, in disagreement with the provided description, this polymorph was previously obtained by thermal conversion over a course of weeks at 20°C, whereas the crystals collected here were all the result of a temperature controlled evaporative crystallisation in acetone.

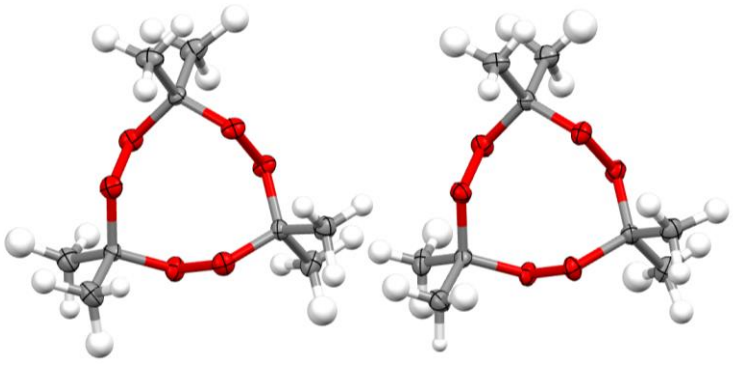

Figure 111 - Asymmetric unit of collected X-ray crystal structure of triacetone-triperoxide as viewed down the *b*-axis.

Table 5 - Crystal structure collection data for Triacetone-triperoxide

Compound	**Triacetone-triperoxide**
Formula	$C_9H_{18}O_6$
Crystallisation Conditions	Side product from crystallisation of 2-chlorobenzoic acid in acetone at 4°C with peroxyacetic acid
Molecular weight / $gmol^{-1}$	222.24
Temperature (K)	100
Space Group	$P2_1/c$
a (Å)	15.9136(6)
b (Å)	10.5446(4)
c (Å)	15.5134(6)
α (°)	90
β (°)	118.4660(10)
γ (°)	90
Volume ($Å^3$)	2288.46(14)
Z	8
Z'	2
θ range/°	1.46-24.7
Reflections Collected	43772
Independent	3834
Refln (obs.I>2theta(I))	2980
R_{int}	0.0562
Parameters	415
GooF on F^2	1.180
R_1 (Observed)	0.0629
R_1 (all)	0.0793
wR_2 (all)	0.1712

In the chosen unit cell setting, $P2_1/c$ (Table 5), there exist two independent molecules of TATP within the asymmetric unit. Both of the molecules are considered to be in the right handed D_3 conformation (Figure 111), as described by Reany *et al.*[151], with all oxygen bonds in a downward stepping orientation when the ring of the molecule is followed clockwise resulting in a right handed D_3 molecular symmetry and a right handed helical arrangement of the structure.

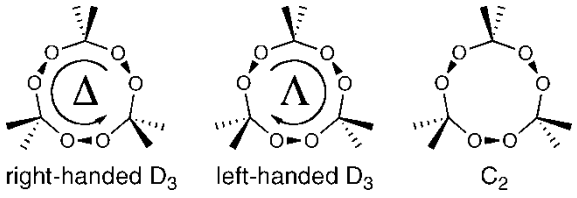

Figure 112 - Stable conformers of TATP[151].

There is also indication that there may be a small amount of disorder in the molecule between the conformers, which generates residual electron density not fully accounted for by this model, particularly noticeable around the oxygen positions, and also apparent by re-

orientation of the methyl groups resulting from alternating between step-up and step-down geometry of the O-O bonds.

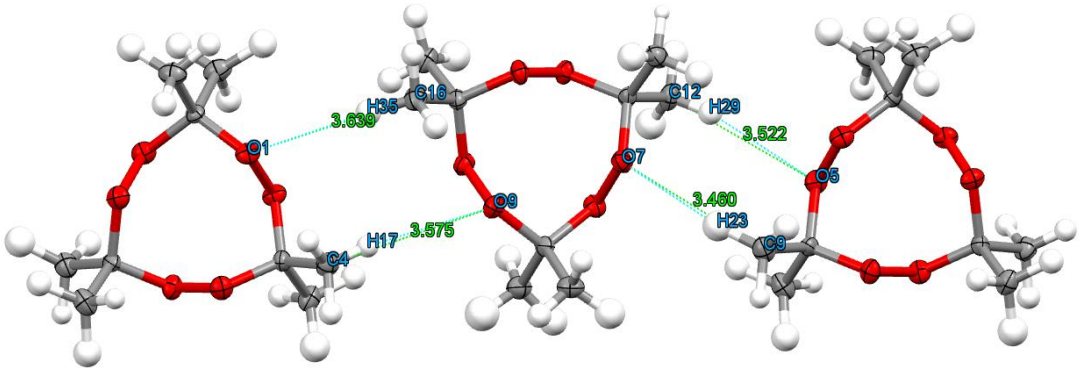

Figure 113 - Hydrogen bonding present in collected structure of TATP, polymorph b.

There are 4 unique intermolecular hydrogen bonds within this structure (Figure 112). They span between adjacent TATP molecules in pairs, linking inverted molecules in a chain perpendicular to the *b*-axis. Each of the bonds are methyl C-H···O interactions. C16-H35···O1 has an overall bond distance of 3.639(4)Å and an angle of 177(4)°, which is paired with a complementary bond C4-H17···O9 of 3.575(4)Å (166(4)°). This creates a weakly bonded $R^2_2(10)$ motif between the two inverted molecules. The other set of interactions are on the other side of the molecules and are slightly stronger than their counterparts. Again both are C-H···O interactions. The C12-H29···O5 bond distance is measured at 3.522(6)Å (167(4)°) and complemented by the strongest of the interactions C9-H23···O7 at a distance of 3.460(6)Å (173(4)°). This produces a second ring motif with a $R^2_2(8)$ configuration. The chains of TATP molecules stack on top of each other, with two layers per unit cell, thus the distance between the planes generated by the chains is 5.2725(4)Å – half the distance of the *b*-axis (Figure 114).

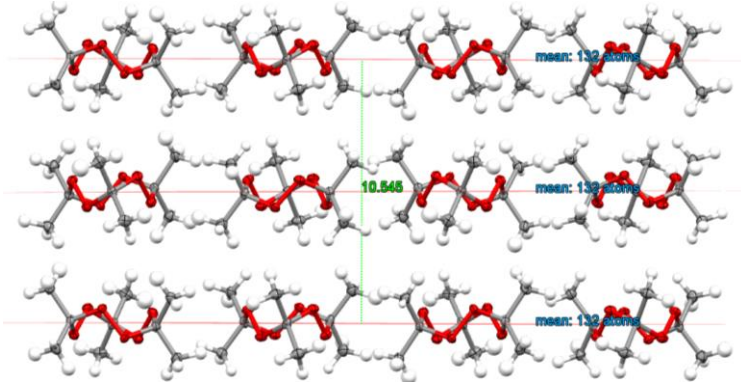

Figure 114 – Extended structure of TATP viewed along the *c*-axis showing planes generated by hydrogen bonded chains. The distance measured is between the top and bottom chain, the b-axis length of the unit cell.

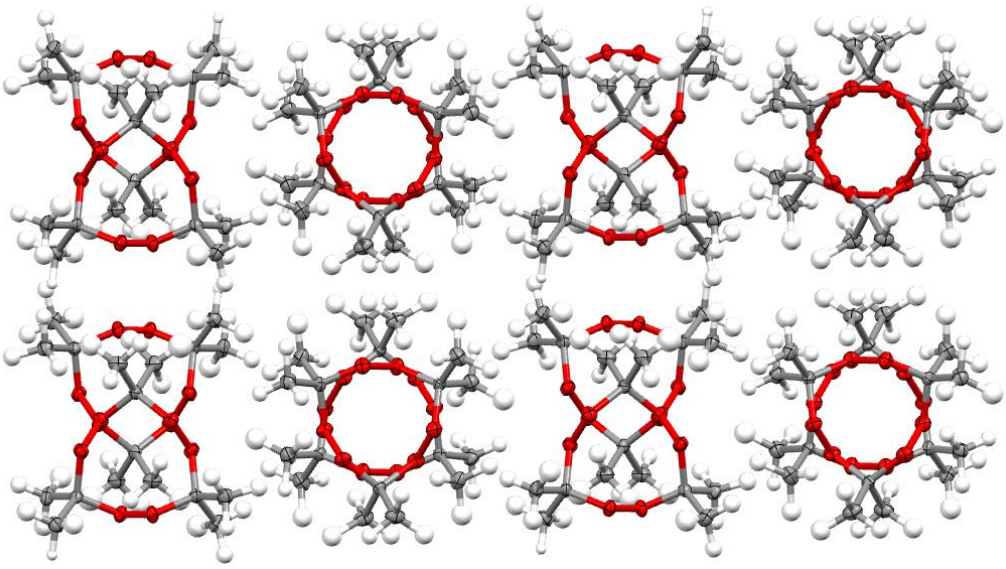

Figure 115 - Three layers of TATP chains viewed down the b-axis of the collected TATP structure.

Viewed down the direction of the *b*-axis (Figure 115), it can be observed that the molecules stack on top of each other in two distinct arrangements. The first type, the "snowflake" arrangement is created when the molecules stack directly above each other rotated 180°, giving the appearance of a circular centre of oxygen atoms with six protruding equally spaced methyl group pairs. This gives the appearance of channels extending the length of the b-axis, however at a channel size of approximately 3Å, the void is almost completely filled by Van der Waals radii of the oxygen atoms, leaving very little space for any inclusion. In the second stacking arrangement, the molecules do not overlay directly, however are still rotated by 180° with each consecutive layer. In the second arrangement, the methyl groups at one "point" of the molecule overlays with the void of the next creating an overall larger footprint than the snowflake, when viewed from this direction.

To an extent the oxygen atoms are isolated from any significant interactions by the arrangement of the methyl groups, which by arranging the molecules into chains introduces bands of methyl hydrogens. This is particularly evident in Figure 113, where bands of hydrogens between the layers introduce a significant separating gap into the structure.

As this material is highly polymorphic, it makes sense for all polymorphs of this material to be referenced to when using acetone as a solvent for crystallisation of peroxyacids. This is easily achieved by looking for the presence of the corresponding XRPD patterns of these polymorphs in the sample X-ray powder diffraction patterns – in contexts such as this, the value of using pattern matching software such as PolySNAP3 is obvious.

4.1.2 6-Phthalimidoperoxyhexanoic acid

There is little published information on the main material under study, 6-phthalimidoperoxyhexanoic acid (PAP), and as mentioned in the introduction, the position of the peroxy hydrogen atom was not determined in previous studies[14]. Similarly to MCPBA, the stability of PAP in solvent environments as for crystallisation experiments was not known, and a similar screening process for solvents was required.

4.1.2.1 Overview of solvents chosen for screening

As this was the main target material under study, a broader screen of solvents was chosen for study to maximise the potential of finding a compatible solvent to work with throughout the co-crystallisation experiments. As with the screening of *meta*-chloroperbenzoic acid, an initial two temperature regime was also adhered to in order to minimise the available energy in the system which may lead to activation of a decomposition reaction. The standard room temperature re-crystallisation was supplemented by a 4°C recrystallisation for each solvent, with the exception of morpholine, which is a solid at this temperature.

The solvents chosen for recrystallisation of PAP were: methanol, ethanol, isopropanol, acetone, methyl acetate, ethyl acetate, diethyl ether, chloroform, morpholine and dioxane. This included an array of standard lab solvents, as well as the use of acetates, which are known to be used during the synthesis of the material, and as such were expected to favour its stability.

Drawing parallels with the MCPBA screening, the use of acetone as a solvent was expected to produce positive results in this screening, leading to recrystallisation of the PAP. A wider range of recrystallisation conditions for acetone were thus prepared. Also in line with the previous screening, the introduction of hydrogen peroxide to selected recrystallisations was attempted in order to maintain the equilibrium of the peroxyacid/parent acid in favour of the production or retention of the target material.

An overview for the selection of solvents and conditions for the recrystallisation of PAP is presented in Table 6, with those conditions in which hydrogen peroxide was added, HOOH, shaded grey:

Table 6 - Solvent screening recrystallisation parameters for 6-phthalimidoperoxyhexanoic acid

Sample ID	Recrystallisation solvent	Temperature	PolySNAP3 ID
AM24_01	Methanol	4°C	1
AM24_02	Methanol	Room temperature	2
AM24_03	Ethanol	4°C	3
AM24_05	Isopropanol	4°C	4
AM24_06	Isopropanol	Room temperature	5
AM24_07	Chloroform	4°C	6
AM24_08	Chloroform	Room temperature	7
AM24_09	Acetone	4°C	8
AM24_10	Acetone	Room temperature	9
AM24_11	Diethyl Ether	4°C	10
AM24_12	Diethyl Ether	Room temperature	11
AM24_13	Ethyl Acetate	4°C	12
AM24_14	Ethyl Acetate	Room temperature	13
AM24_16	Morpholine	Room temperature	14
AM24_17	1,4-Dioxane	4°C	15
AM24_18	1,4-Dioxane	Room temperature	16
AM32_03	Acetone	4°C	17
AM32_04	Acetone	4°C	18
AM32_05	Acetone	Room temperature	19
AM32_06	Acetone	Room temperature	20
AM32_07	Acetone	30°C	21
AM32_08	Acetone	50°C	22
AM32_09	Methyl Acetate	4°C	23
AM32_10	Methyl Acetate	Room temperature	24
AM32_11	Methyl Acetate	30°C	25
AM32_12	Methanol and HOOH	4°C	26
AM32_14	Methanol and HOOH	30°C	27
AM32_15	Ethanol and HOOH	4°C	28
AM32_16	Ethanol and HOOH	Room temperature	29
AM32_17	Ethanol and HOOH	30°C	30

4.1.2.2 Statistical analysis of resulting compounds

The resulting solids collected from the recrystallisations were analysed by X-ray powder diffraction methods and analysed statistically using the PolySNAP 3 software. All XRPD patterns corresponding to this screening may be found in Appendix 1.

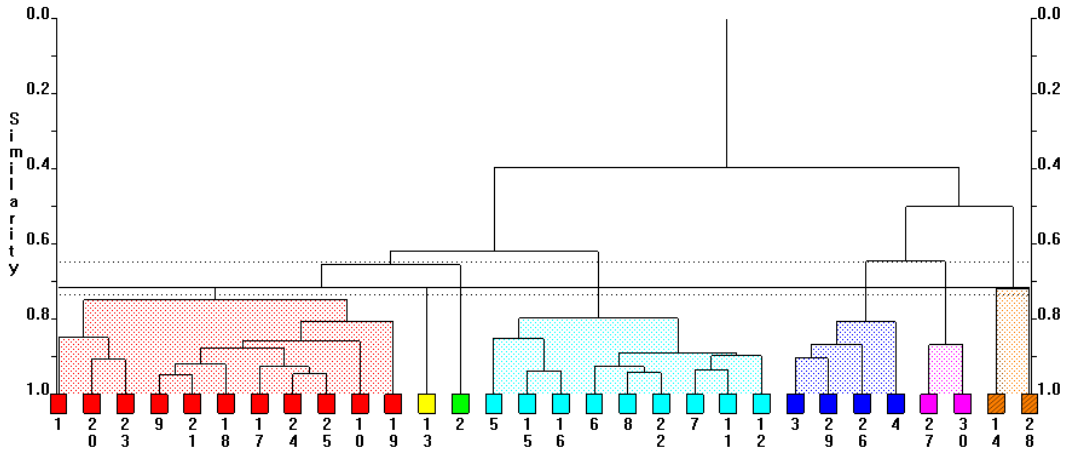

Figure 116 – PolySNAP 3 clustering analysis of X-ray powder patterns of materials collected from the attempted recrystallisation of 6-phthalimidoperoxyhexanoic acid in selected solvents as described in Table 6 with the cluster cut level set to 72% similarity.

The dendrogram presented from the analysis of the XRPD data (Figure 116), where the scan number corresponds to the system used for recrystallisation as detailed under the column "PolySNAP ID" in Table 6, when the percentage similarity cut off level is set to 72%, as suggested by the analysis, shows several distinct groupings amongst the materials. The first group, clustered as red and referred to as group A, consists of 11 samples, detailed in Table 7.

Table 7 - Resultant materials recrystallised from 6-phthalimidoperoxyhexanoic acid clustered within group A

Sample ID	Recrystallisation solvent	Temperature	PolySNAP3 ID
AM24_01	Methanol	4°C	1
AM24_10	Acetone	Room temperature	9
AM24_11	Diethyl Ether	4°C	10
AM32_03	Acetone	4°C	17
AM32_04	Acetone	4°C	18
AM32_05	Acetone	Room temperature	13
AM32_06	Acetone	Room temperature	20
AM32_07	Acetone	30°C	21
AM32_09	Methyl Acetate	4°C	23
AM32_10	Methyl Acetate	Room temperature	24
AM32_11	Methyl Acetate	30°C	25

When the patterns in group A are analysed (Figure 117), they appear to all have the same main component peaks, with the exception of the least similar pattern in the grouping, corresponding to sample AM32_05. All scans however show a similar presence of the main peaks and relative intensities.

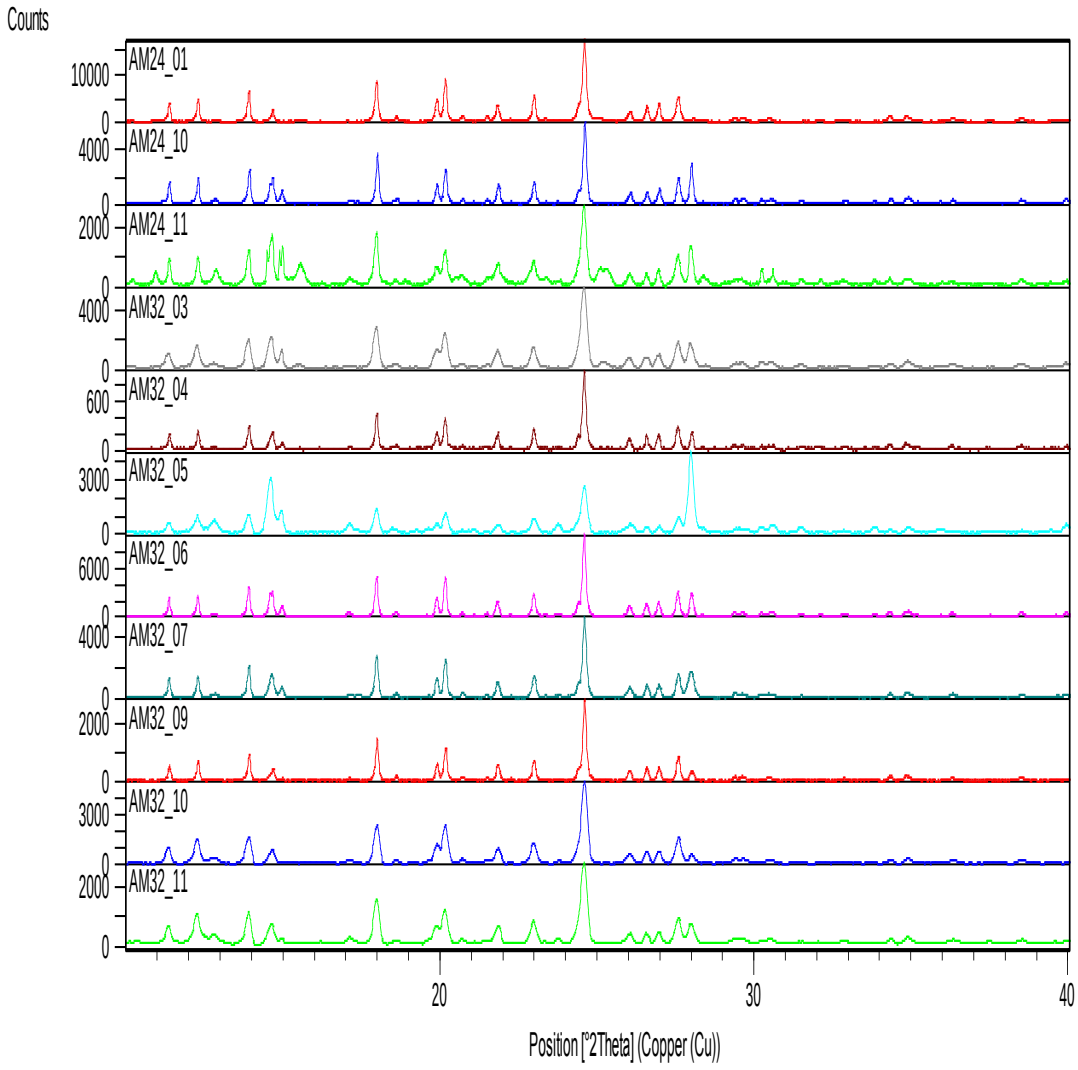

Figure 117 - XRPD patterns of collected materials from recrystallisation of 6-phthalimidoperoxyhexanoic acid clustered in group A.

When compared to a simulated powder X-ray diffraction pattern of the known crystal structure of PAP (Figure 118), confirmed by the assignment of the majority of the peaks that this is the main component within group A samples. Thus for the crystallisation conditions corresponding to this group, the peroxyacid is successfully recrystallised. Figure 118 shows the comparison of a representative pattern from group A and the simulated pattern, from which it can be observed that there are two peaks that are not representative of the reference pattern. These peaks, at 14.9° and 28.0°, do not correspond to any other known pattern, including those of 6-phthalimidohexanoic acid or any of the known forms of TATP. However, the sample that features these peaks most strongly is AM32_05, recrystallisation of PAP with acetone at room temperature, exactly the same conditions as AM35_06, in which these peaks are much smaller. It is possible is that these peaks could be the result of the presence of a small amount of an impurity in the

batch of PAP provided. This would be consistent with the fact that a small amount is present in all XRPD patterns of recrystallisations, albeit at different levels.

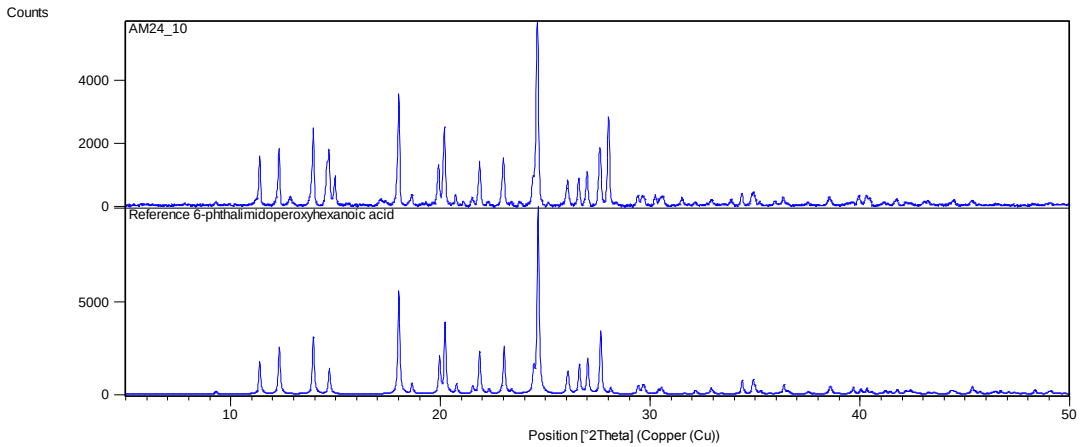

Figure 118 - Comparison of a XRPD sample representative of cluster group A with a simulated XRPD pattern from the reference crystal structure of 6-phthalimidoperoxyhexanoic acid.

These results from cluster group A show that the PAP is most stable in acetone, methyl acetate and, quite surprisingly, methanol at 4°C. The successful recrystallisation in methanol is unexpected as the model compound MCPBA showed fairly complete conversion to the parent acid under these conditions.

The second set of groupings, B and C – yellow and green respectively in Figure 116 – correspond to the samples outlined by the crystallisation conditions in Table 8 (with the colour coding retained).

Table 8 - Resultant materials recrystallised from 6-phthalimidoperoxyhexanoic acid clustered within groups B and C.

Sample ID	Recrystallisation solvent	Temperature	PolySNAP3 ID
AM24_02	Methanol	Room temperature	2
AM24_14	Ethyl Acetate	Room temperature	13

These conditions produced materials which show all the major peak correlations to recrystallised PAP, but as the samples were substantially more amorphous, their similarity was indicated to be less (Figure 119) at only 65%. Again it can be noted that in sample AM24_14, recrystallisation in ethyl acetate at room temperature, the unidentified peaks are of a greater intensity.

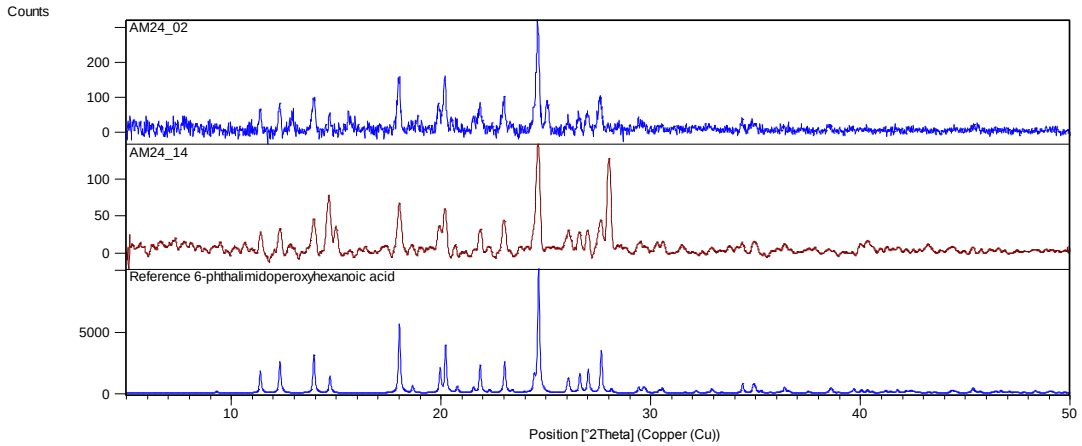

Figure 119 - XRPD patterns collected of samples in cluster groups B and C compared with the reference simulated XRPD pattern of 6-phthalimidoperoxyhexanoic acid.

Cluster group D, light blue (Figure 116), consists of nine samples, all with a similarity to each other greater than 79% with their crystallisation conditions as detailed in Table 9.

Table 9 - Resultant materials recrystallised from 6-phthalimidoperoxyhexanoic acid clustered within group D

Sample ID	Recrystallisation solvent	Temperature	PolySNAP3 ID
AM24_06	Isopropanol	Room temperature	5
AM24_07	Chloroform	4°C	6
AM24_08	Chloroform	Room temperature	7
AM24_09	Acetone	4°C	8
AM24_12	Diethyl Ether	Room temperature	11
AM24_13	Ethyl Acetate	4°C	12
AM24_17	1,4-Dioxane	4°C	15
AM24_18	1,4-Dioxane	Room temperature	16
AM32_08	Acetone	50°C	22

Cluster group D represents samples with a mixture of materials, which as a result have patterns similar to each other. The samples identified all show the presence of the impurity peak, as well as possible evidence of PAP within the sample in combination with the parent acid "decomposed PAP" – 6-phthalimidohexanoic acid or its hydrated crystal form (Figure 120). As such these crystallisation conditions, and their unpredictability for retention of the peroxyacid, are unsuitable for crystallisation of PAP, with perhaps the exception of AM24_09 – recrystallisation in acetone at 4°C, which by analysis of the XRPD pattern shows more retention of the peroxyacid with only minor decomposition to the parent acid.

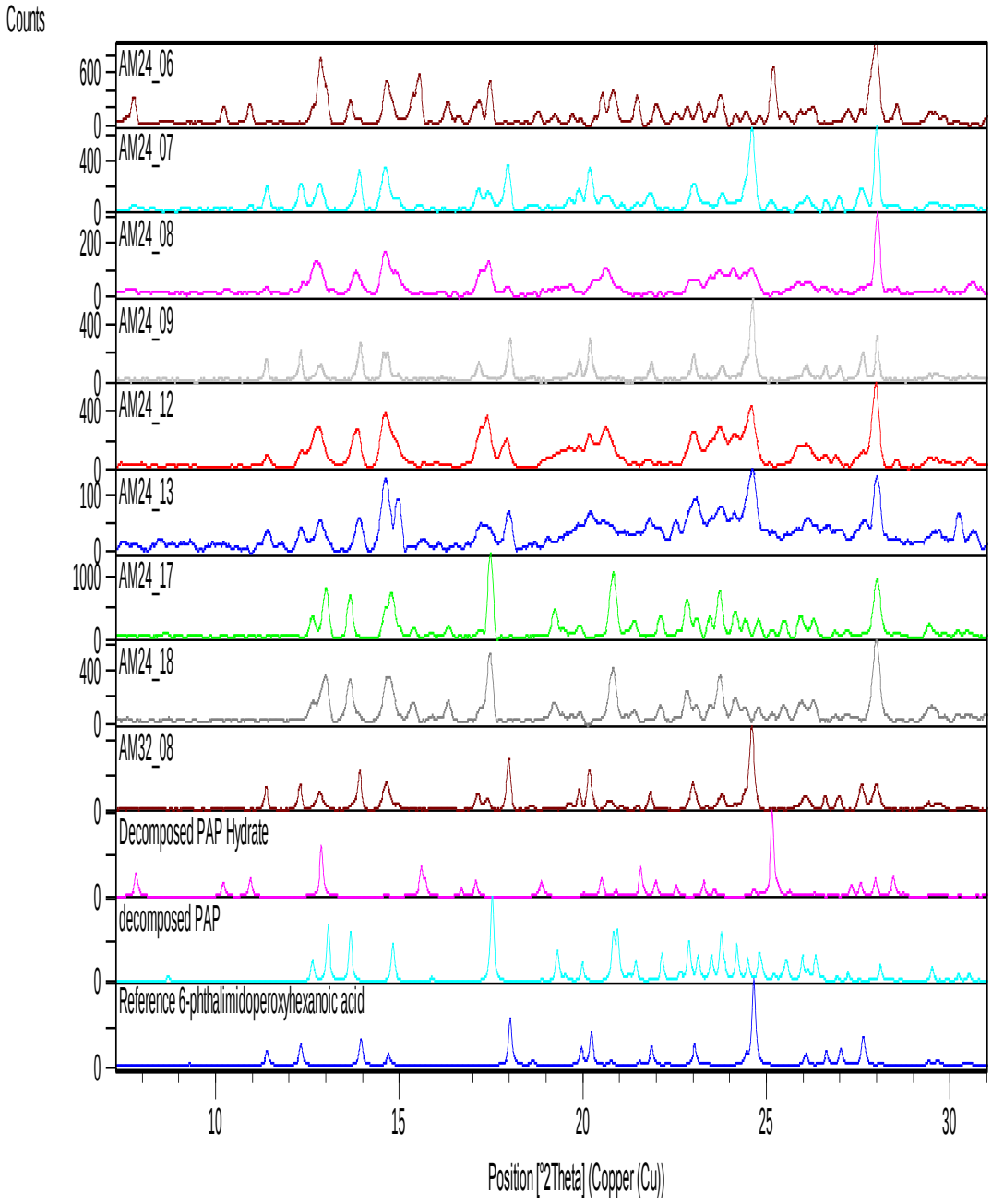

Figure 120 - XRPD patterns resultant materials recrystallised from 6-phthalimidoperoxyhexanoic acid clustered within group D compared to 6-phthalimidoperoxyhexanoic acid, its parent acid and a hydrate of the parent acid.

Cluster group E, dark blue, consists of four patterns with greater than 80% similarity. These samples, with their crystallisation conditions shown in Table 10 and their XRPD patterns shown in Figure 121 all have an excellent similarity to the simulated XRPD pattern of the known crystal structure of the decomposed PAP breakdown product 6-phthalimidohexanoic acid hydrate[152].

Table 10 - Resultant materials recrystallised from 6-phthalimidoperoxyhexanoic acid clustered within group E

Sample ID	Recrystallisation solvent	Temperature	PolySNAP3 ID
AM24_03	Ethanol	4°C	3
AM24_05	Isopropanol	4°C	4
AM32_12	Methanol and HOOH	4°C	26
AM32_16	Ethanol and HOOH	Room temperature	29

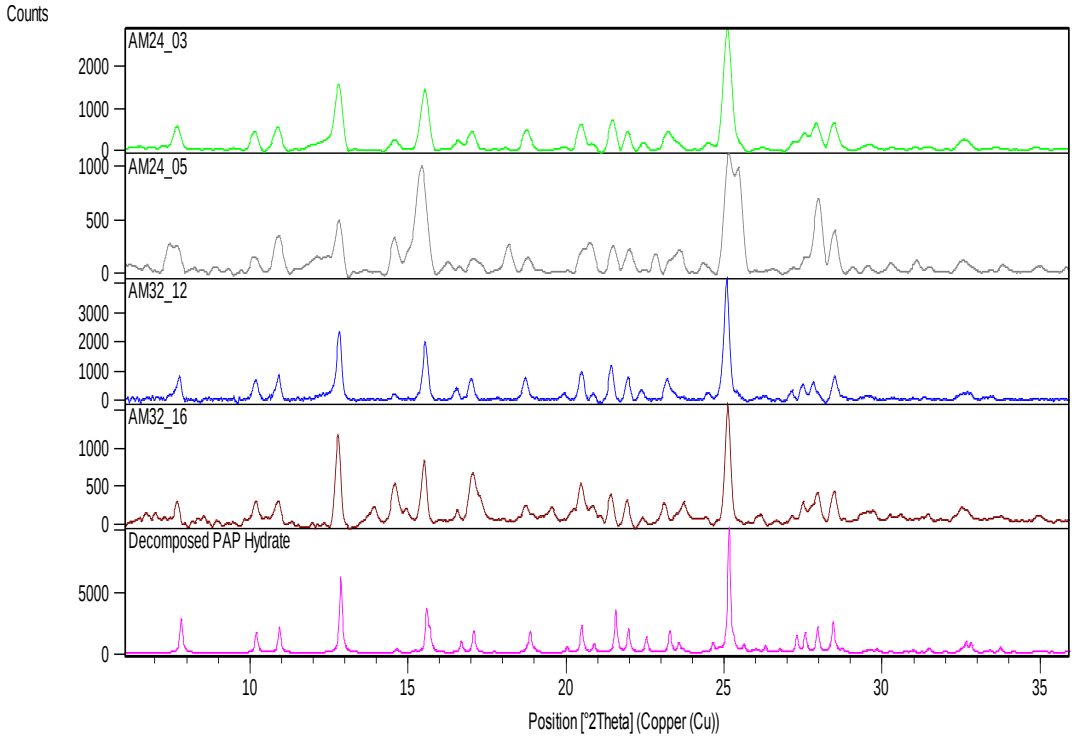

Figure 121 - XRPD patterns resultant materials recrystallised from 6-phthalimidoperoxyhexanoic acid clustered within group E compared to the simulated XRPD pattern of the known crystal structure of the decomposed PAP form 6-phthalimidohexanoic acid monohydrate.

Cluster group F, in magenta, consists of two samples, AM32_14 and AM32_17. Both of these samples are from crystallisation of PAP in an alcohol with the addition of hydrogen peroxide at 30°C (Table 11). These samples both result in a decomposition of the material to the parent acid, with AM32_14 producing a high purity of 6-phthalimidohexanoic acid monohydrate and AM32_17 producing a mixture of the same hydrate and as well as the anhydrous crystal form (Figure 122). There is no remaining peroxyacid in either of these samples.

Table 11 - Resultant materials recrystallised from 6-phthalimidoperoxyhexanoic acid clustered within group F

Sample ID	Recrystallisation solvent	Temperature	PolySNAP3 ID
AM32_14	Methanol and HOOH	30°C	27
AM32_17	Ethanol and HOOH	30°C	30

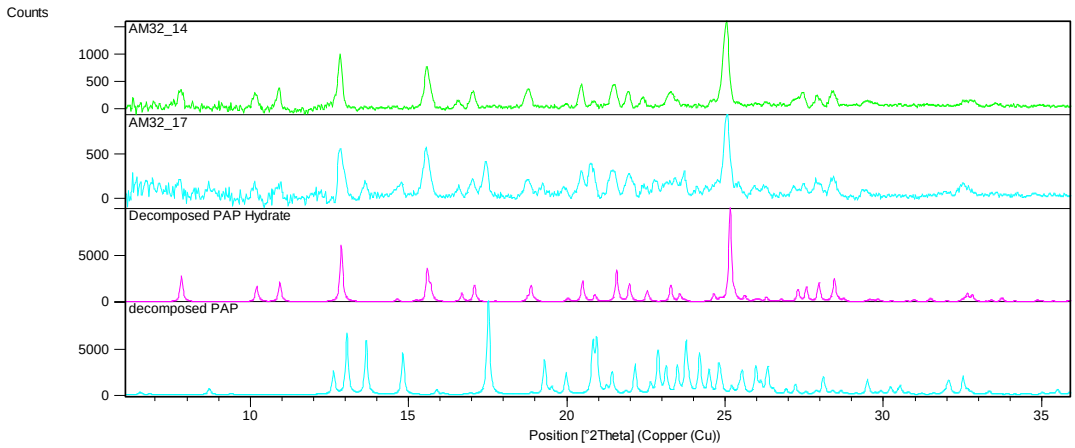

Figure 122 - XRPD patterns resultant materials recrystallised from 6-phthalimidoperoxyhexanoic acid clustered within group F compared to the simulated XRPD pattern of the known crystal structure of decomposed PAP forms 6-phthalimidohexanoic acid monohydrate and 6-phthalimidohexanoic acid.

The remaining cluster group, G, in orange is another small cluster of two samples: AM24_16 and AM32_15, both of which are from seemingly unrelated crystallisation conditions (Table 12). Both of these samples, however, show the presence of a new material, which does match any of the other known or expected decomposition products.

Table 12 - Resultant materials recrystallised from 6-phthalimidoperoxyhexanoic acid clustered within group G

Sample ID	Recrystallisation solvent	Temperature	PolySNAP3 ID
AM24_16	Morpholine	Room temperature	14
AM32_15	Ethanol and HOOH	4°C	28

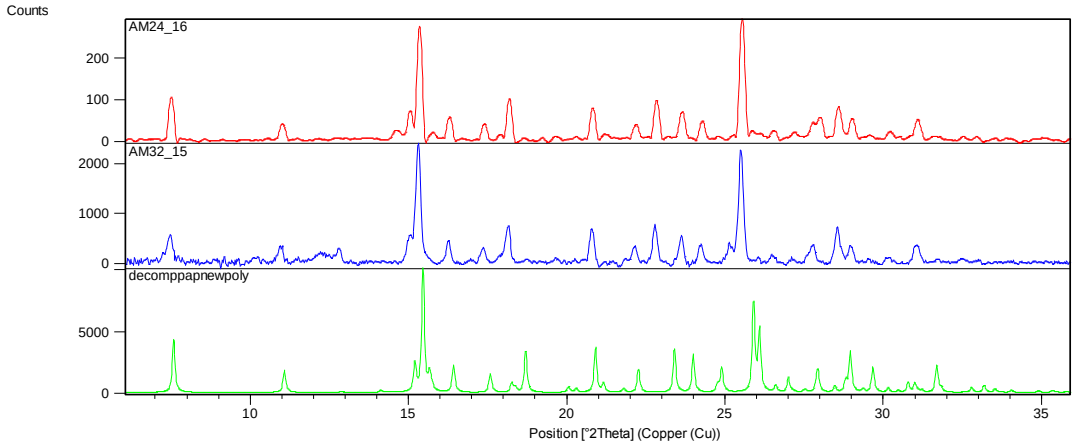

Figure 123 - XRPD patterns resultant materials recrystallised from 6-phthalimidoperoxyhexanoic acid clustered within group G compared to the simulated XRPD pattern of a new polymorph of 6-phthalimidohexanoic acid monohydrate.

The new product was analysed by single crystal X-ray diffraction and identified to be a new, unknown polymorph of the decomposed PAP product 6-phthalimidohexanoic acid monohydrate, which was an excellent match for the XRPD patterns of these two samples (Figure 123).

4.1.2.3 Analysis of isolated structures

As noted in the previous section, there were several materials isolated by the solvent screening process of 6-phthalimidoperoxyhexanoic acid identified by X-ray powder diffraction methods. These structures are described here with their characteristic crystallographic packing:

6-Phthalimidohexanoic acid

The main decomposition product of PAP, this material was encountered regularly throughout this research. As this compound has already been studied by Feeder and Jones[153], and recorded within the CSD, a recollection of the structure was not required for production of a simulated XRPD pattern for the analysis and assessment of decomposition products of the peroxyacid. It is, however, appropriate at this point to study the structure and interactions of the kwown structure of his material (CSD ref. code VUNZEJ10[153]).

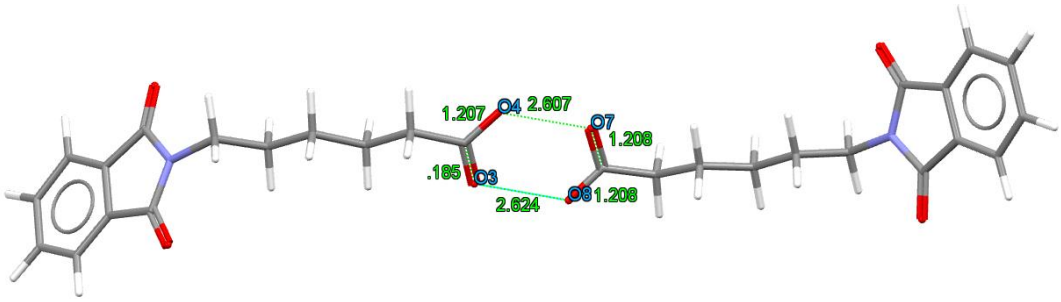

Figure 124 - Known crystal structure of 6-phthalimidohexanoic acid[153]

The structure of 6-phthalimidoperoxyhexanoic acid is likely to share interaction characteristics with the parent acid (6-phthalimidohexanoic acid), due to the high similarity between the two molecules. The phthalimido group and the aliphatic chain remain unchanged from the peroxyacid molecule with the same interaction sites. The only change in the structure is the loss of the basic oxygen atom from the peroxyacid functional group and resulting change in position of the terminal hydrogen onto the acidic oxygen, forming the parent carboxylic acid. As would be expected with the carboxylic acid functional group and synthons being present, the carboxylic acid $R^2_2(8)$ motif once again is the dominant interaction within the structure. This occurs between the two unique molecules of 6-phthalimidohexanoic acid in the asymmetric unit of the $P2_1/c$ structure. The two primary hydrogen bonds are formed between O4-H···O7 and O8-H···O3 with bond distances, from oxygen to oxygen, of 2.61(2)Å and 2.62(2)Å respectively (Figure 124). Upon closer inspection (Figure 125), it can be observed that the bond lengths between the C-O covalent bonds are not equivalent in the two molecules. The distances C28-O7 and C28-O8 in one molecule are equal at 1.21(2)Å, which would be unexpected for a carboxylic acid group.

Such an arrangement would usually only be present in a deprotonated carboxylic acid where the residual charge is delocalised over the entire O-C-O group. This leads to ambiguities as to the existence and, if present, the positioning of the acidic hydrogen atom on the molecule. By analysis of the second molecule the observed distances of the C-O bonds , 1.18(2)Å and 1.21(3)Å are not significantly different within the measured 3σ error and thus cannot be verified as to having double or single bond character.

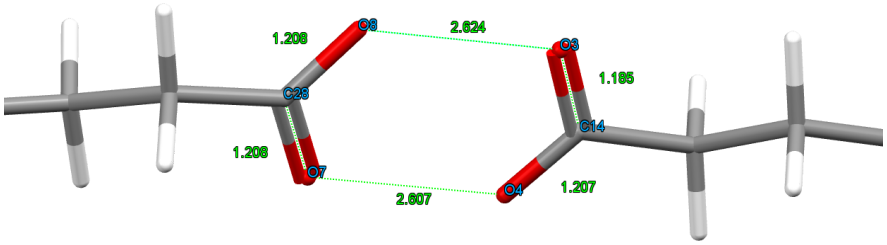

Figure 125 - $R^2_2(8)$ ring motif present between the two unique molecules of 6-phthalimidohexanoic acid in the asymmetric unit.

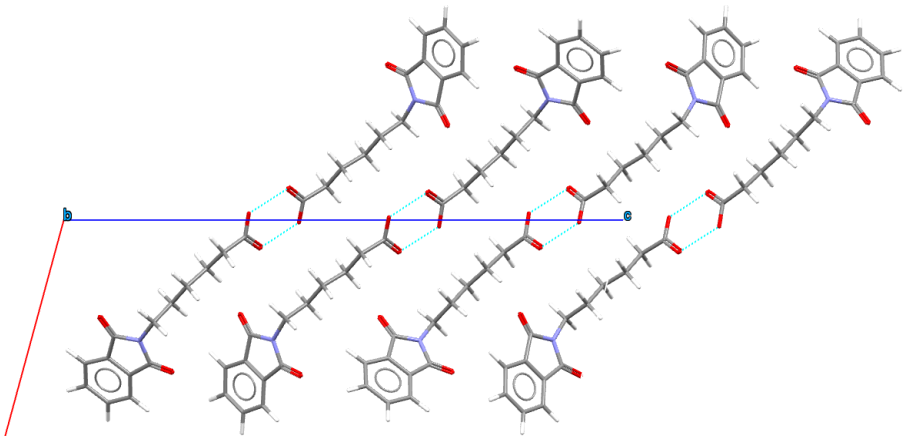

Figure 126 - 6-phthalimidohexanoic acid as viewed down the *b*-axis.

The two hydrogen bonds of moderate strength, as defined by Jeffrey[21], associate the two unique molecules of 6-phthalimidohexanoic acid together to form dimers which alternate in orientation along the *c*-axis and stack on top of each other down the *b*-axis (Figure 126).

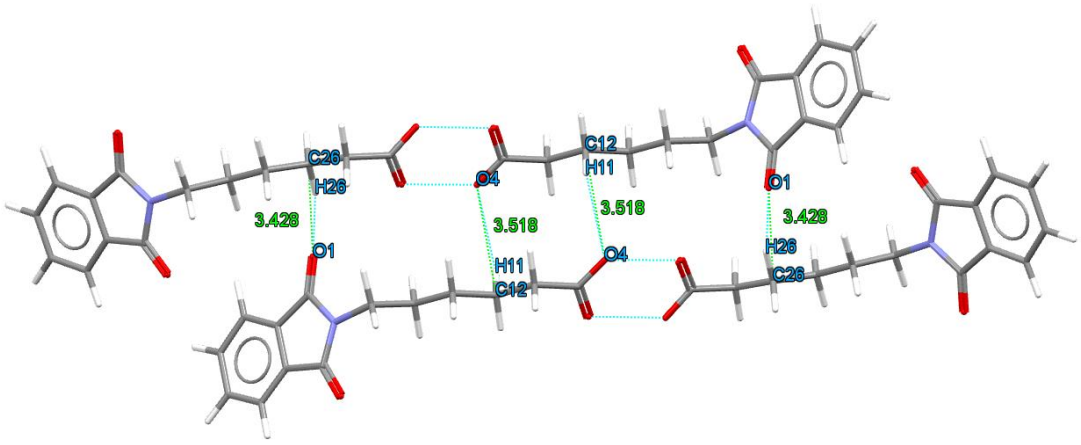

Figure 127 - Interactions between neighbouring paired 6-phthalimidoheaxanoic acid dimers.

Between neighbouring pairs of molecules, there are interactions from the aliphatic chain to both the phthalimido group and the carboxylic acid of the next dimer (Figure 127). The two interactions are along the plane of the *c*-axis and are mirrored in the two dimers to produce four interactions. The strongest of these interactions is C26-H26···O1, an aliphatic C-H from third carbon in the chain interacting with the phthalimido carbonyl measuring 3.43(2)Å between non hydrogen atoms. The second pair of interactions are again between the third carbon of the aliphatic chain, but of the second molecule, C12, and the single bonded oxygen, O4, of a symmetry equivalent molecule. This forms a C12-H11···O4 bond of overall distance 3.52(2)Å.

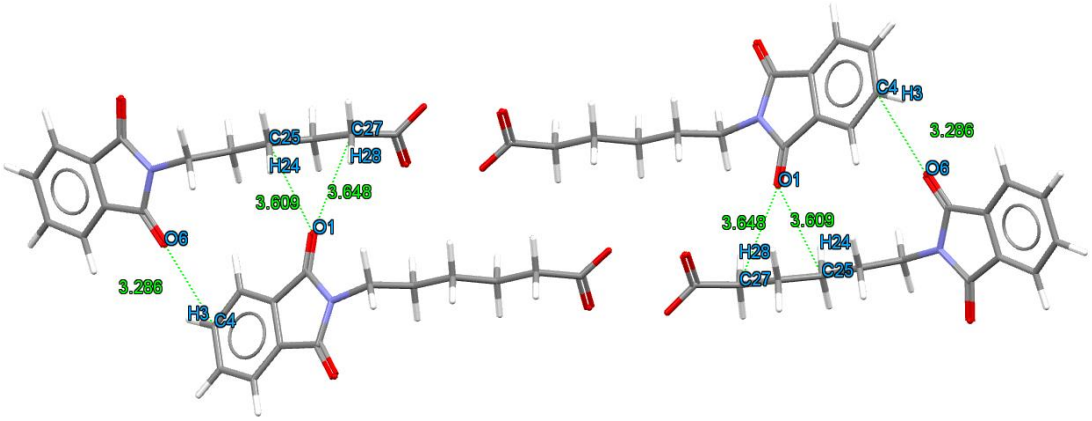

Figure 128 - Second set of interactions between the 6-phthalimidohexanoic acid dimers.

The second set of interactions between the dimers occurs along the same plane, however to the dimer set above the previous, resulting in the interaction to the second side of the dimer. As shown in Figure 128, there are three specific interactions, of C-H···O type, one between the carbonyl O6 of the phthalimido group and an aromatic C-H of the phthalimido group on a neighbouring dimer, C4-H3···O6 at a distance of 3.29(2)Å. The remaining set of interactions is present between O1, the phthalimido carbonyl of the second dimer and two

aliphatic C-H groups and the second and fourth carbon atoms of the chain, C27 and C25. These interactions are of approximately similar strength, at 3.65(2)Å and 3.61(2)Å respectively. As in the previous dimer, these three interactions are mirrored at the other end of the dimer pairs, resulting in six interactions between them. The last set of interactions between the dimers is as shown in Figure 129.

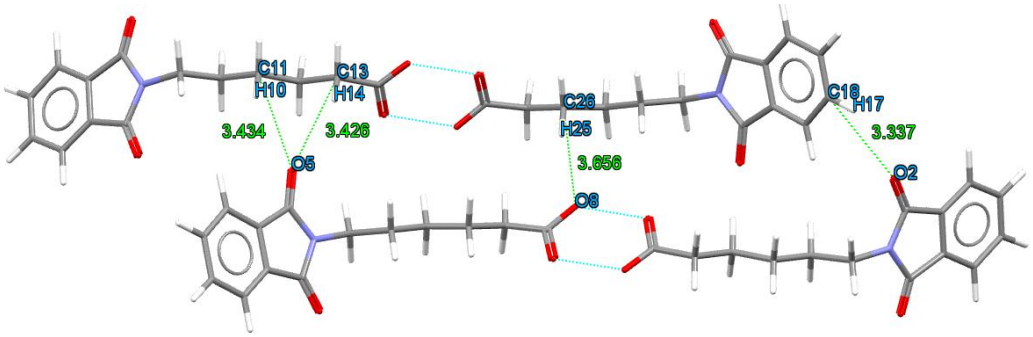

Figure 129 - Highlighted interactions between the dimers of 6-phtalimidohexanoic acid.

O5, a phthalimido carbonyl, exhibits two C-H···O interactions with C11 and C13, both at an overall distance of 3.43(2)Å. There is also an interaction between phthalimido carbonyl O2 and C18 at a distance of 3.34(2)Å and a further interaction to the unassigned hydroxyl carbon of the carboxylic acid dimer group, C26-H25···O8 at a distance of 3.66(2)Å. All of these are relatively weak interactions.

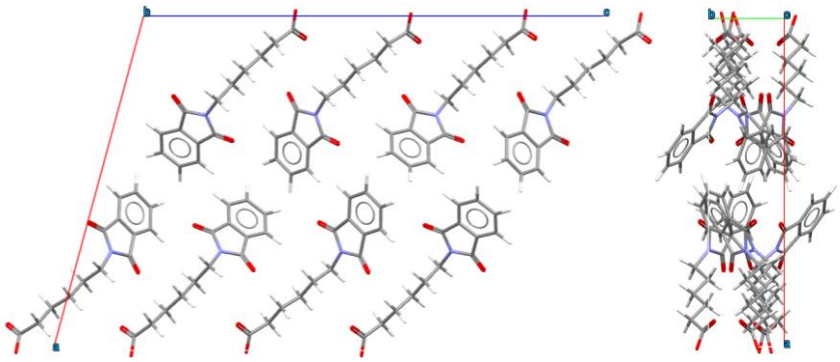

Figure 130 - Unit cell of 6-phthalimidohexanoic acid viewed down the *b*-axis (left) and down the *c*-axis (right).

The phthalimido ends of the molecule align along the *c*-axis, however when viewed down this axis, it can be seen that the arrangement of the groups shows no direct overlay of the molecules (Figure 130).

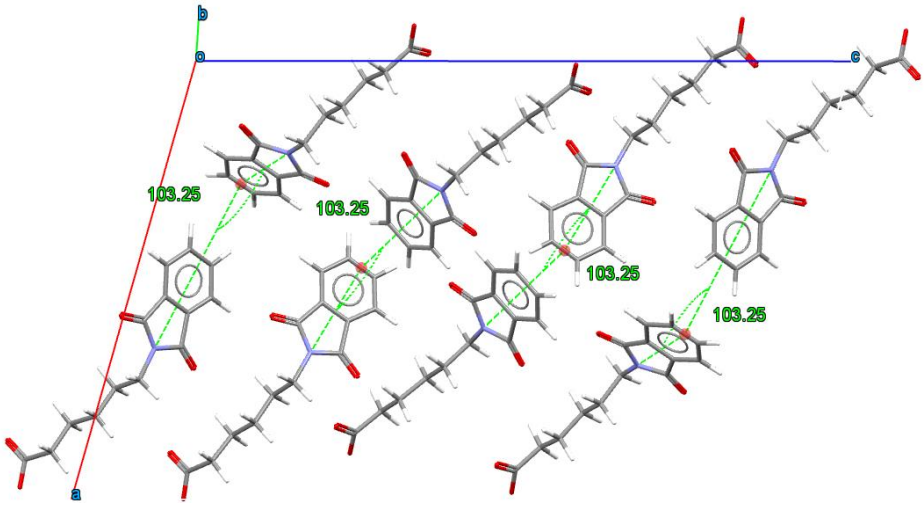

Figure 131 - Angles measured between planes generated by phthalimido groups in 6-phthalimidohexanoic acid.

The angle between the aligned phthalimido groups is equivalent in all molecular pairings within the unit cell at an angle of 103.25° (Figure 130) forming a “point to face” interaction between each molecule forming a “zipper” arrangement of phthalimido groups down the *b*-axis (Figure 132).

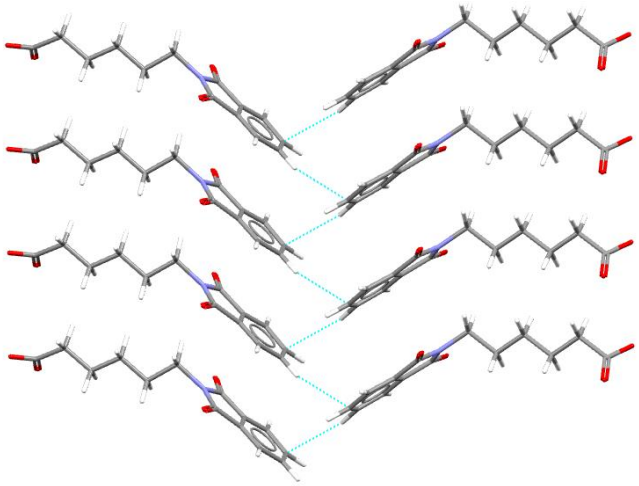

Figure 132 - "Zipper" arrangement of phthalimido groups present along the *b*-axis of 6-phthalimidohexanoic acid

This arrangement results in a skewed π-π stacking of the phthalimido rings at distances of 3.62(3)Å and 3.85(2)Å. The unit cell parameters of the CSD structure are shown in Table 13.

Table 13 - Details of the crystal structure of 6-phthalimidohexanoic acid[153]

Compound	**6-Phthalimidohexanoic acid**
Formula	$C_{14}H_{15}N_1O_4$
Molecular weight / gmol^{-1}	261.27
Temperature (K)	283-303
Space Group	$P2_1/c$
a (Å)	21.055(8)
b (Å)	4.662(1)
c (Å)	28.067(9)
α (°)	90
β (°)	105.22(3)
γ (°)	90
Volume (*Å^3*)	2658.380
Z	8
Z'	2
R_1 (Observed)	0.08

The primary driving force in the packing arrangement is evidently the hydrogen bonding of the carboxylic acid group, however the flexibility of the aliphatic chain allows for this whilst permitting efficient packing of the phthalimido group.

6-Phthalimidohexanoic acid hydrate

The statistical analysis also showed the presence of a PAP decomposition product as a monohydrate with two distinct crystal forms. The first form was already isolated by Feeder and Jones[152] and recorded in the CSD, however the XRPD pattern of the second material is distinctly different, and is identified as 6-phthalimidohexanoic acid monohydrate form II, with the previously recorded structure designated form I (Figure 133).

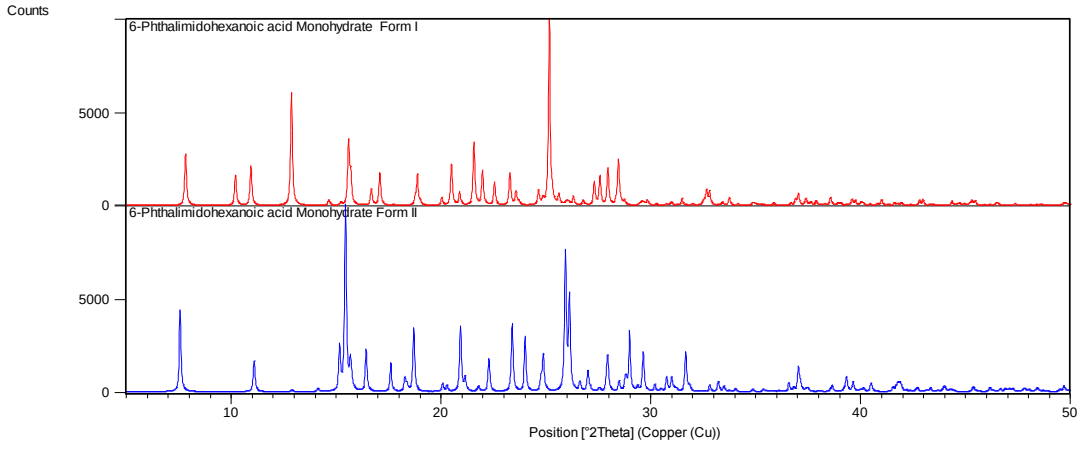

Figure 133 – XRPD patterns of 6-phthalimidohexanoic acid monohydrate forms I and II.

Crystals of Form II were isolated from crystallisation using morpholine as a solvent via slow evaporative crystallisation at room temperature. The details of the structure and data collection parameters are compared between forms in Table 14.

Table 14 – Crystal structure collection data of 6-phthalimidohexanoic acid monohydrate forms I and II

Compound	**6-Phthalimidohexanoic acid monohydrate Form I** [152]	**6-Phthalimidohexanoic acid monohydrate Form II**
Formula	$C_{14}H_{15}N_1O_4 – H_2O$	$C_{14}H_{15}N_1O_4 – H_2O$
Crystallisation Conditions	Crystallisation from acetic acid at room temperature	Decomposition of 6-phthalimidoperoxyhexanoic acid from crystallisation in morpholine at room temperature
Molecular weight / $gmol^{-1}$	279.1	279.1
Temperature (K)	295	100
Space Group	$P2_1/c$	P-1
a (Å)	8.771(3)	6.9672(5)
b (Å)	22.553(5)	8.5418(7)
c (Å)	7.257(2)	12.4428(9)
α (°)	90	109.156(6)
β (°)	99.33(6)	94.369(5)
γ (°)	90	95.813(6)
Volume ($Å^3$)	1417	689.31(9)
Z	4	2
Z’	1	1
θ range/˚	8-12	1.75-22.79
Reflections Collected	4362	11037
Independent	4126	1862
Refln (obs.I>2theta(I))	1734	1487
R_{int}	0.031	0.0717
Parameters	199	248
GooF on F^2	unknown	1.134
R_1 (Observed)	0.054	0.0492
R_1 (all)	Unknown	0.0681
wR_2 (all)	0.054	0.1124

The two forms are chemically identical, with very similar structural features and motifs, both consisting of one molecule of 6-phthalimidohexanoic acid and one water molecule in the asymmetric unit (Figure 134).

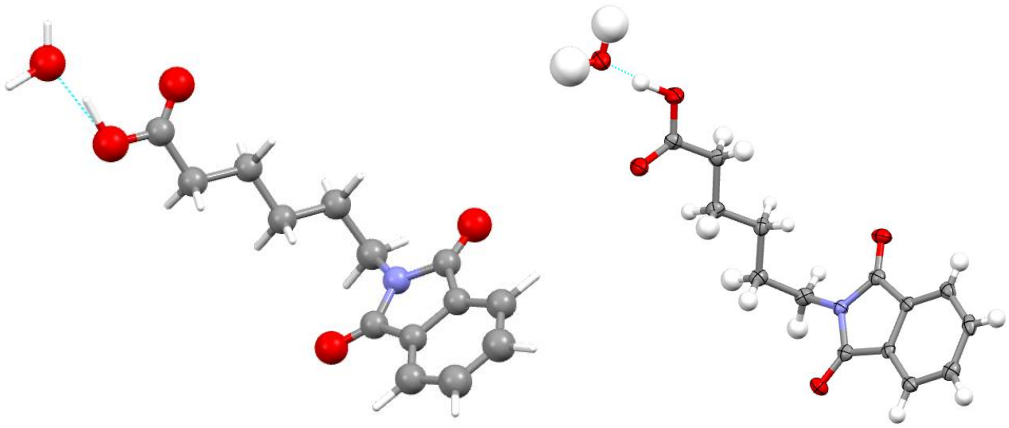

Figure 134 - Asymmetric units of 6-phthalimidohexanoic acid monohydrate forms I (left) and II (right).

The molecules show slight differences in geometry, likely a result of packing characteristics and the different temperatures of data collection.

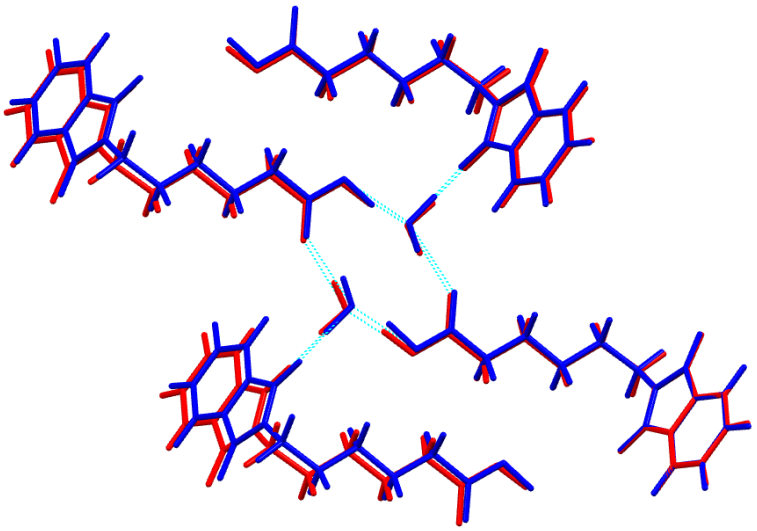

Figure 135 - Structures of 6-phthalimidohexanoic acid monohydrate overlaid with form I in blue, and form II in red.

Both forms of the monohydrate are similar in the fact that they exhibit a short moderate strength hydrogen bond to the water molecule from the hydroxyl hydrogen of the carboxylic acid functional group. These are of a similar length: in form I the distances measured between O(141)-H(141)···O(1) is 2.595(4)Å and O(1)-H(201)···O(140) is 2.769(4)Å, forming a water-incorporated ring motif with a $R^4_4(12)$ arrangement (Figure 136). The water molecules, O(1), form further hydrogen bonds to O(8) of the phthalimido group at an oxygen to oxygen distance of 2.745(5)Å.

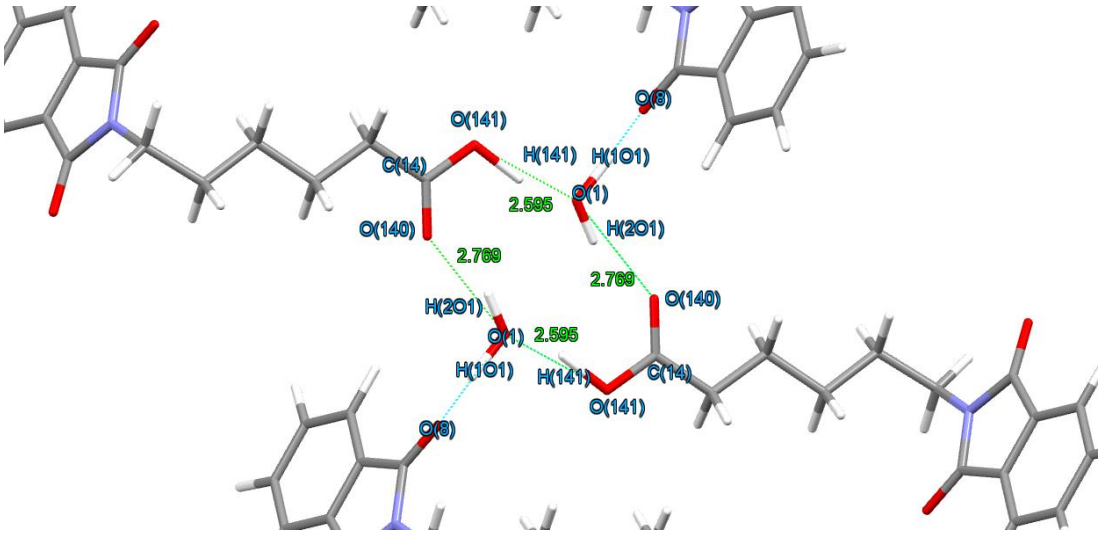

Figure 136 - Hydrogen bonding motif present in Form I of 6-phthalimidohexanoic acid monohydrate.

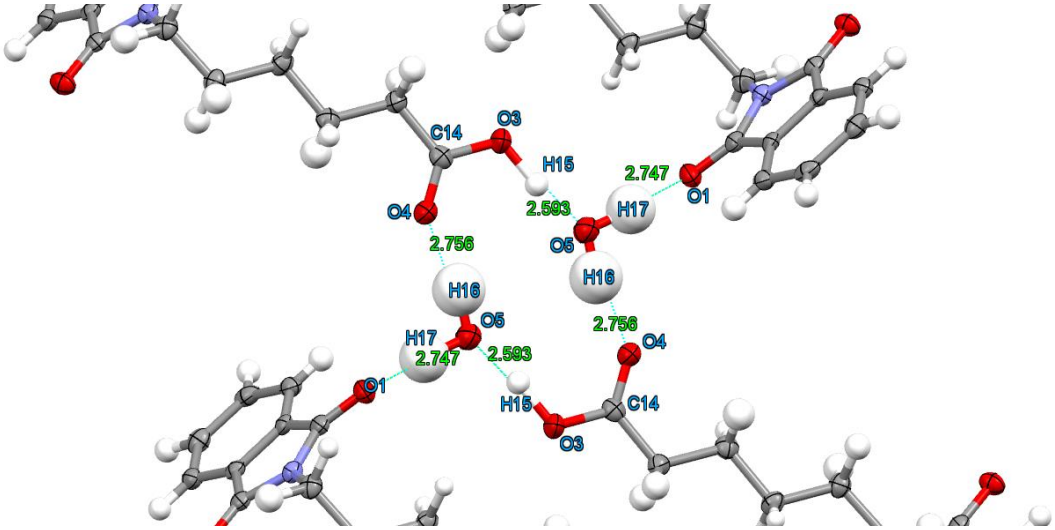

Figure 137 - Hydrogen bonding motif present in Form II of 6-phthalimidohexanoic acid monohydrate.

The motif in Form II is similar, with only minor differences (Figure 137). The distances measured between O(3)-H(15)···O(5) is 2.5932(2)Å (171(3)°) and O(5)-H(16)···O(4) is 2.7556(2)Å (168(6)°), forming a water-incorporate ring motif with a $R^4_4(12)$ arrangement. The water molecules, O(5), form further hydrogen bonds to O(1) of the phthalimido group at an oxygen to oxygen distance of 2.747(2)Å (168(5)°).

The differences in the structures arise from the arrangement of these groups with each other, seen through differing orientations of the phthalimido groups.

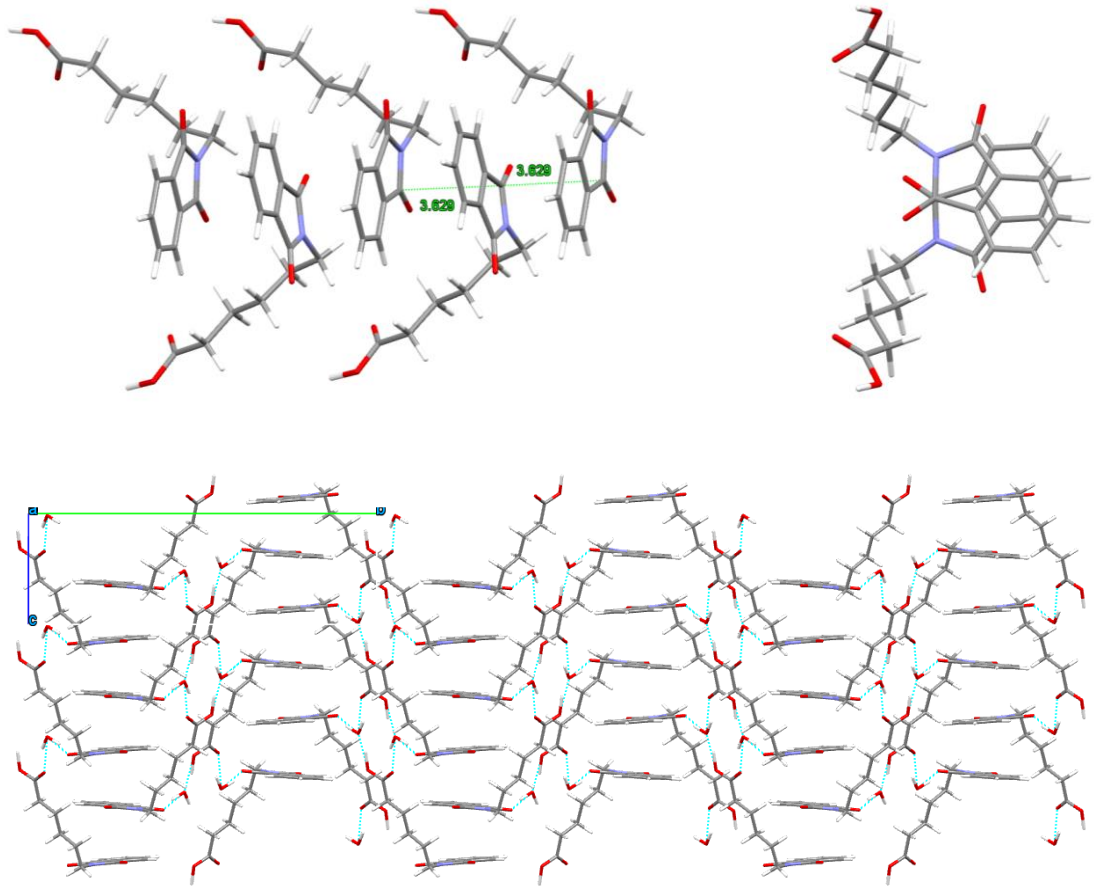

Figure 138 – Stacking of phthalimido groups in 6-phthalimidohexanoic acid in form I viewed down the *a*-axis (top left), *c*-axis (top right) and an expanded view down the *a*-axis (bottom).

In Form I, the phthalimido groups stack on top of each other with the aliphatic chains progressing in the same direction, the groups only rotating partially such as the chains are always to the same side of the stacked molecules. The phthalimido groups are at a vertical spacing of 3.629(4)Å.

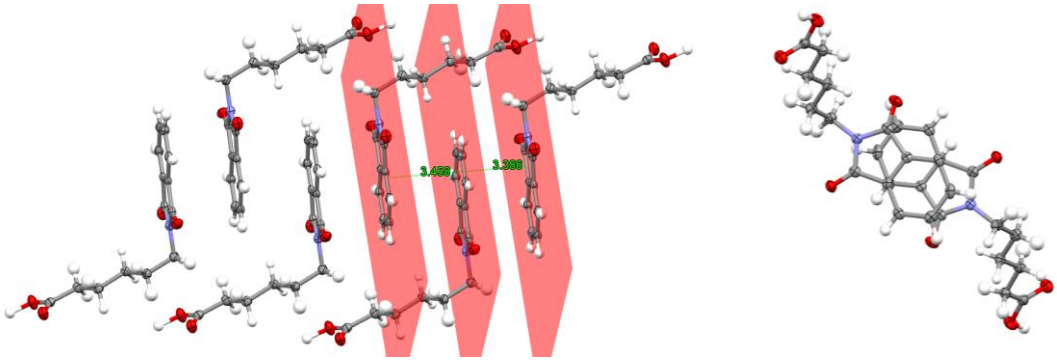

Figure 139 - Stacking of phthalimido groups in 6-phthalimidohexanoic acid in form II as viewed down the *b*-axis (left) and *a*-axis (right).

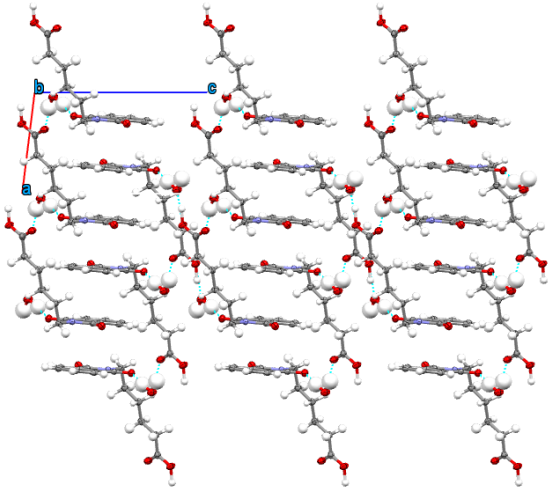

Figure 140 - Stacking of phthalimido groups in 6-phthalimidohexanoic acid in form II as viewed down the *b*-axis.

In form II however the phthalimido groups alternate in orientation so that the aliphatic chains change side and direction. As a result the phthalimido groups themselves are stacked at 180° to each other at spacings of 3.458Å and 3.386Å. This dramatic change in packing causes the difference in crystal structure between the two polymorphs.

4.2 Acidic and basic effects on reactive peroxides

The effects of addition of excess strong acid and strong base in a solvent that has proven instability with the crystallised peroxyacid material was also investigated. Both MCPBA and PAP were crystallised in methanol and ethanol in the presence of both hydrochloric acid and sodium hydroxide to assess the amount of decomposition of the target material that occurred under each condition.

4.2.1 Effect of introduction of hydrochloric acid and sodium hydroxide on MCPBA

Addition of hydrochloric acid to attempted recrystallisations of MCPBA in methanol and ethanol, conditions which in absence of the strong acid have been observed to allow decomposition of the material, was explored to assess whether introduction of acidic conditions would allow for better retention of the peroxyacid. The XRPD patterns of representative samples of these materials are recorded in Appendix 1, and analysed in Figure 141.

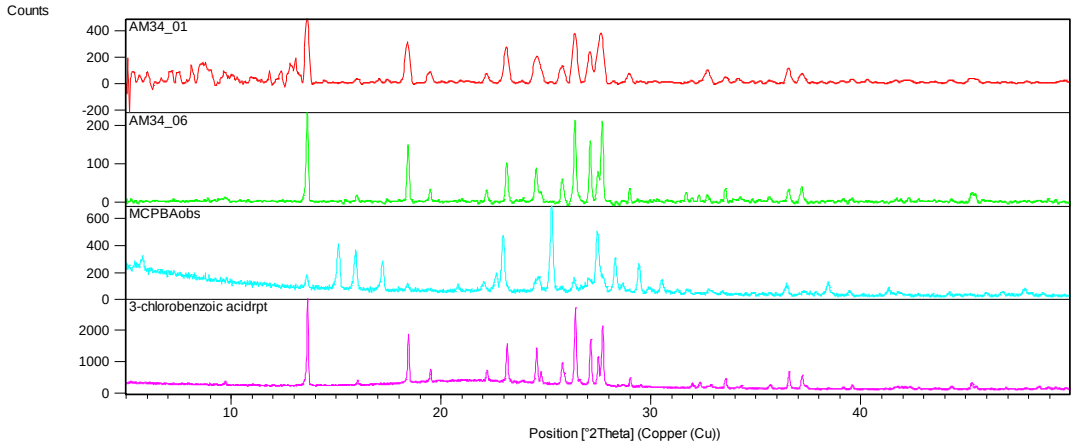

Figure 141 - XRPD patterns collected of crystallisations of MCPBA in methanol (red) and ethanol (green) with the addition of hydrochloric acid at room temperature, compared to sample patterns of MCPBA (blue) and 3-chlorobenzoic acid (magenta).

As can be noted from the XRPD patterns, both of the samples recrystallized from methanol and ethanol have resulted in a complete conversion to the parent acid, 3-chlorobenzobenzoic acid. It is evident from the scans that no traces of MCPBA are retained in the final product.

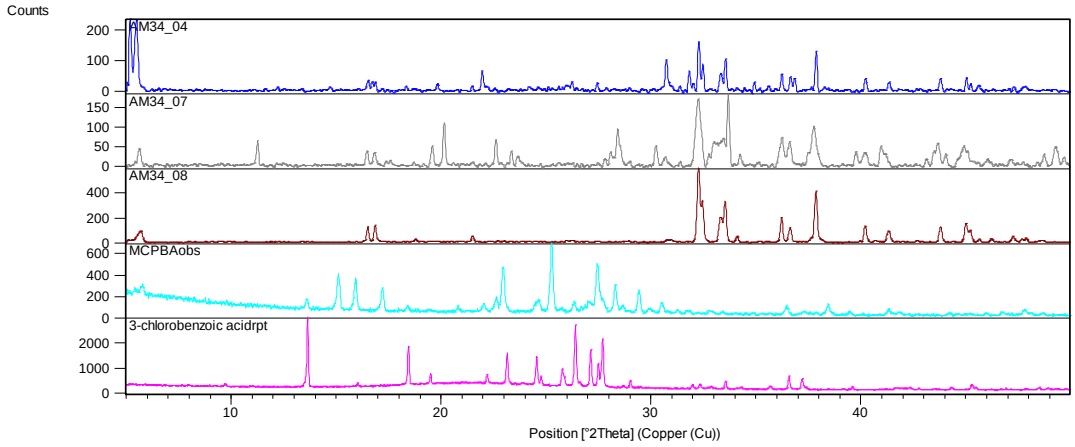

Figure 142 - XRPD patterns collected of crystallisations of MCPBA in methanol at room temperature (blue) and ethanol at 4°C (grey) and room temperature (brown) with the addition of sodium hydroxide, compared to sample patterns of MCPBA (blue) and 3-chlorobenzoic acid (magenta).

With the addition of sodium hydroxide to the same crystallisation conditions, formation of an entirely new material is observed. This material seems to be present in absence of peaks from either MCPBA and 3-chlorobenzoic acid (Figure 142), but the samples have poor crystallinity and it may be the case that other materials present in the representative samples are more amorphous or weakly diffracting in comparison. The crystalline material present was identified by manual powder pattern recognition (from comparison to known

materials in the ICSD[154]) to be sodium carbonate monohydrate. As shown in Figure 143, there is a very strong correlation between this XRPD pattern and the samples recorded.

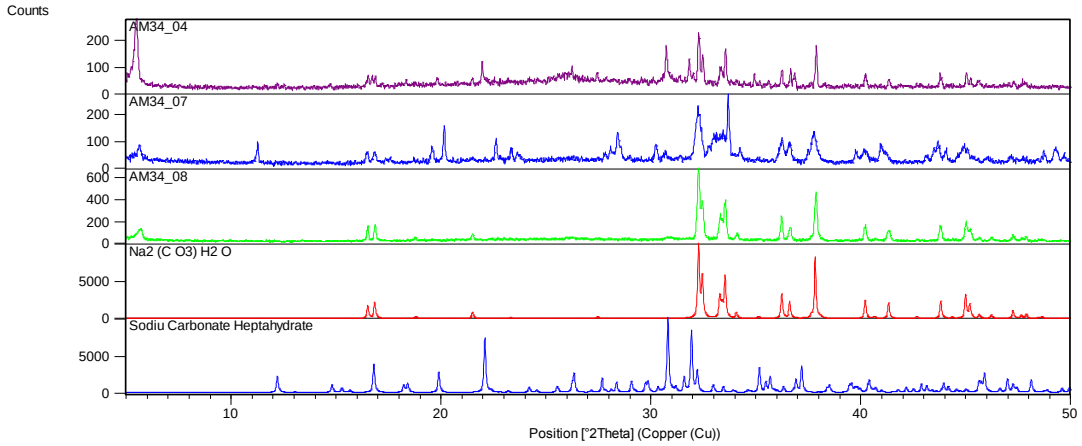

Figure 143 - XRPD patterns collected of crystallisations of MCPBA in methanol at room temperature (purple) and ethanol at 4°C (blue, second from top) and room temperature (green) with the addition of sodium hydroxide, compared a simulated XRPD pattern from the crystal structures of sodium carbonate monohydrate (red) and sodium carbonate heptahydrate (blue, bottom).

The samples also all contained varying amounts of sodium hydroxide heptahydrate (Figure 143). This material was isolated from a later complementary screening under the same conditions with PAP, however indications of its strongest peaks are present in the samples of recrystallised MCPBA to which sodium hydroxide had been added.

4.2.2 Effect of introduction of hydrochloric acid and sodium hydroxide on 6-phthalimidoperoxyhexanoic acid

A similar screening process was performed upon 6-phthalimidoperoxyhexanoic acid (PAP), adding hydrochloric acid and sodium hydroxide to the recrystallisations in methanol and ethanol at both 4°C and room temperature.

The results from the experiments with the hydrochloric acid addition are interesting. The first of the samples, with the target material crystallised in methanol at 4°C, is a very good match to the PAP decomposition product 6-phthalimidohexanoic acid monohydrate form I, thus under these conditions not only is there decomposition of the target material, but also water has been incorporated into the structure (Figure 144).

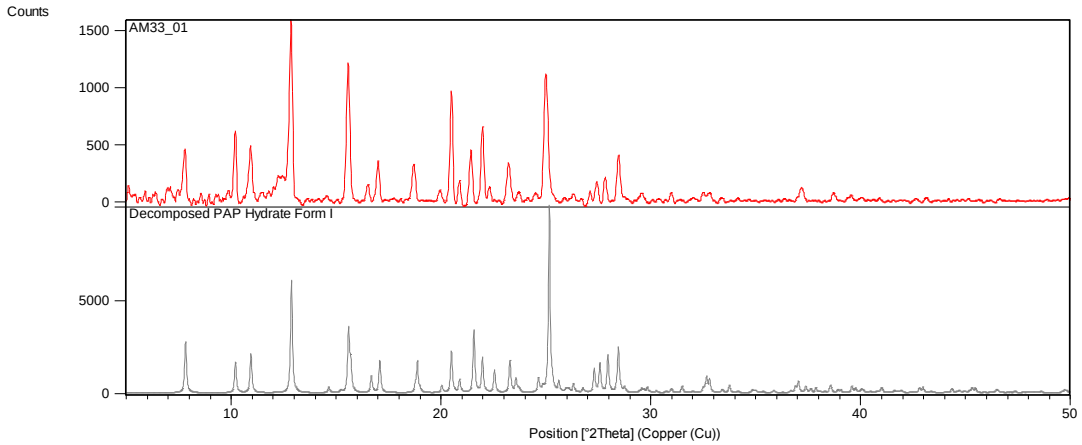

Figure 144 - XRPD patterns collected of crystallisation of 6-phthalimidoperoxyhexanoic acid in methanol at 4°C with the addition of hydrochloric acid (red) compared with a simulated XRPD pattern from the crystal structure of 6-phthalimidohexanoic acid monohydrate form I (grey).

The other three resultant materials, however, do not match this pattern (Figure 145). Recrystallisation of the peroxyacid in methanol at room temperature, as well as in ethanol at both 4°C and room temperature, with hydrochloric acid added, has resulted in a material where the XRPD pattern does not match the target material, its parent acid or either of the two decomposed PAP hydrates.

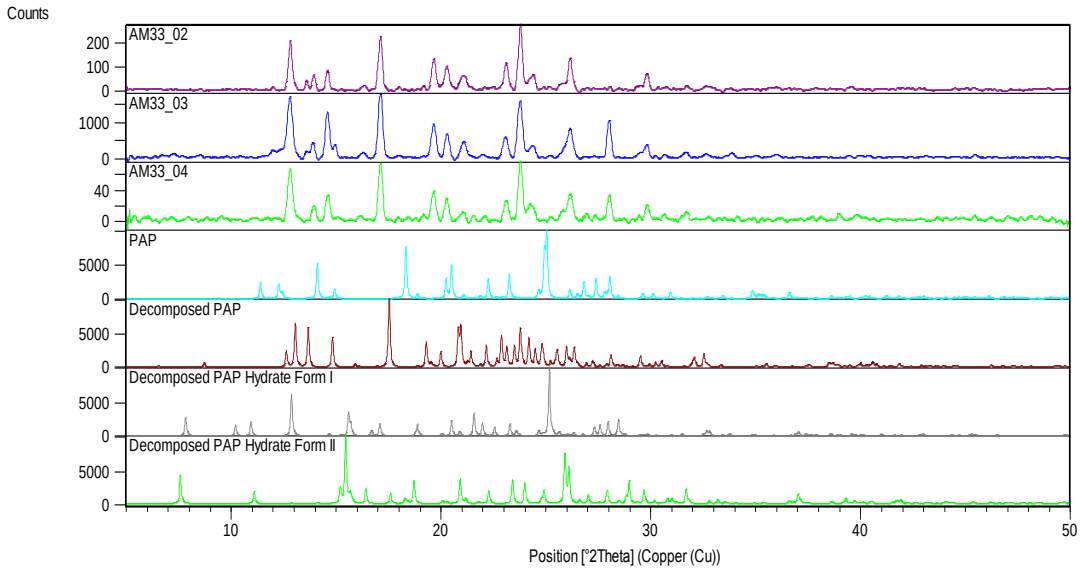

Figure 145 - XRPD patterns of 6-phthalimidoperoxyhexanoic acid in methanol at room temperature (AM33_02; purple), and in ethanol at 4°C (AM33_03; blue) and room temperature (AM33_04; green upper), all with the addition of hydrochloric acid, compared with those from 6-phthalimidoperoxyhexanoic acid (light blue), 6-phthalimidohexaanoic acid (dark red) and its two hydrates (grey, and green lower)

The pattern most closely resembles that of 6-phthalimidohexanoic acid, but it is clear that it is not a good match. This material may therefore be either another undiscovered polymorph of 6-phthalimidohexanoic acid or its hydrates, or a chloride salt of the parent

acid. It can be concluded that in each circumstance, addition of a strong acid is a detriment to the retention of the peroxyacid.

When crystallised in the presence of sodium hydroxide, again a transformation is found to have taken place in the material. Collected powder X-ray diffraction patterns of representative samples show no presence of the peroxyacid of any of its known decomposition products in their known forms (Figure 146).

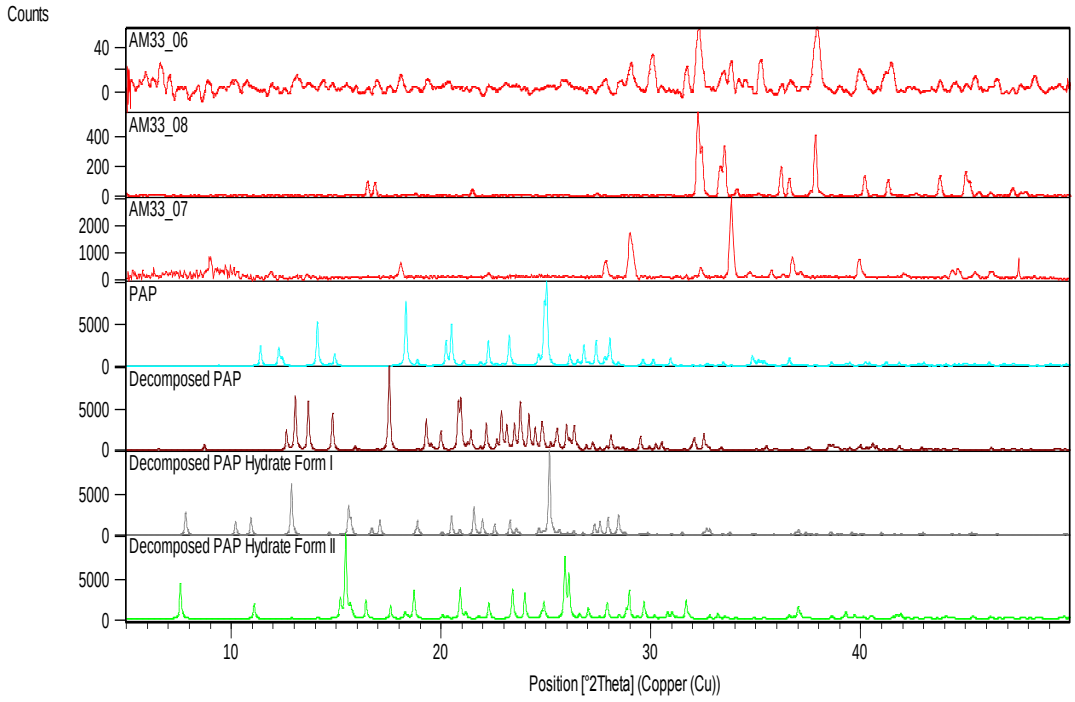

Figure 146 - XRPD patterns of 6-phthalimidoperoxyhexanoic acid with the addition of sodium hydroxide in methanol and ethanol at room temperature (AM33_06 (red upper) & AM33_08; red middle), and in ethanol at 4°C (AM33_07; red lower) compared with 6-phthalimidoperoxyhexanoic acid (light blue), 6-phthalimidoheaxanoic acid (dark red) and its two hydrates (grey and light green).

The XRPD patterns of these materials, although showing a high background level, have primary peaks at a very high angle, suggestive of a small unit cell. It is evident that the two recrystallisations at room temperature have produced the same material which again closely resembles sodium carbonate monohydrate, whereas the crystallisation at 4°C has produced a different material which could not be identified.

From the recrystallisation of PAP in MeOH at 4°C with NaOH present, single crystals were obtained that were suitable for single crystal X-ray diffraction. The following structure solution was obtained from data collected on the Rigaku Single crystal X-ray diffractometer at 100K using an Oxford Cryosystems Cryostream (Table 15).

Table 15 - Crystal structure data for sodium carbonate heptahydrate

Compound	Sodium Carbonate Heptahydrate
Formula	$C_1 H_{14} Na_2 O_{10}$
Crystallisation Conditions	Recrystallisation of 6-phthalimidoperoxyhexanoic acid in MeOH at 4°C with NaOH present
Molecular weight / $gmol^{-1}$	232.10
Temperature (K)	100K
Space Group	P b c a
a (Å)	6.97960(10)
b (Å)	14.49430(10)
c (Å)	19.3246(2)
α (°)	90
β (°)	90
γ (°)	90
Volume ($Å^3$)	1954.95(4)
Z	8
θ range/˚	2.108- 27.603
Reflections Collected	32142
Independent	2238
Refln (obs.I>2theta(I))	2119
R_{int}	0.1172
Parameters	161
GooF on F^2	1.0095
R_1 (Observed)	0.0179
R_1 (all)	0.0192
wR_2 (all)	0.0560

Sodium carbonate heptahydrate is commonly known as “soda ash” and is most commonly synthesised using the Solvay Process[155], from sodium chloride and calcium carbonate, but as neither of these components are present in the crystallisation, it must follow a different reaction mechanism. The sodium must originate from the sodium hydroxide, however the presence of the carbonate molecule must be from a decomposition of the target material, or more likely a reaction of the methanol solvent. The methanol is likely oxidised by the liberated hydrogen peroxide from the decomposition of the PAP to oxygenate the carbon of the methanol molecule, transforming it to a tertiary oxidised carbon, the negatively charged carbonate ion. This then crystallises with two positively charged sodium ions and the remaining water molecules are either taken from the solution as a result of the decomposing peroxyacid, the used hydrogen peroxide, or absorbed from the atmosphere into the crystal structure. This proposed reaction mechanism would also hold for the MCPBA recrystallisations with sodium hydroxide.

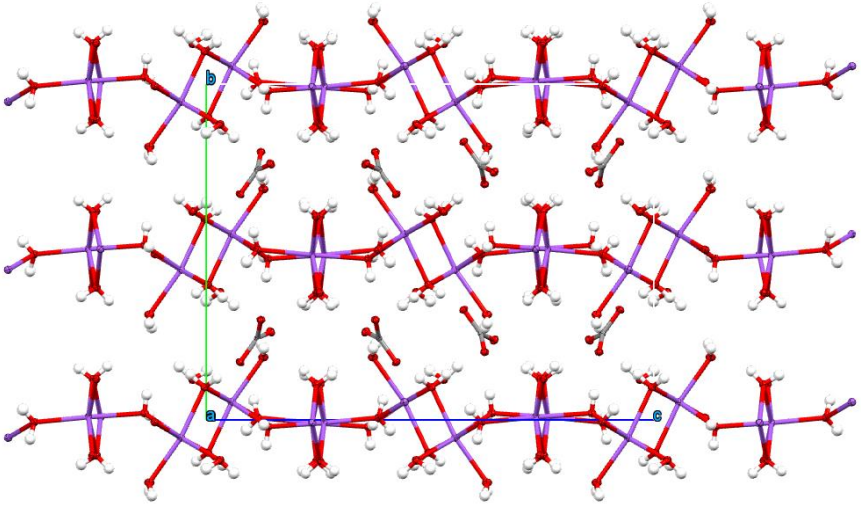

Figure 147 - Unit cell of the collected structure of sodium carbonate heptahydrate from the recrystallisation of 6-phthalimidoperoxyhexanoic acid in methanol at 4°C with the addition of NaOH.

The crystal structure of this material, determined for confirmation, has no real implications to this research and did not merit further structural investigation.

4.3 Crystal structure of *meta*-chloroperbenzoic acid

The crystal structure of *meta*-chloroperbenzoic acid, was obtained from samples obtained from an evaporative crystallisation in acetone at 4°C. The crystals themselves were very plate-like and consequently it was difficult to select a sufficiently high quality crystal for a detailed un-twinned collection and subsequent structure solution. The following structure represents the best of the isolated crystals analysed by X-ray diffraction.

4.3.1 Summary of diffraction experiment and data

This X-ray crystal structure (Table 16) was collected on a Bruker AXS Apex II single crystal X-ray diffractometer at a collection temperature of 100K. The crystals were clear and colourless and with a plate morphology.

Table 16 - Crystal structure collection data for *meta*-chloroperbenzoic acid

Compound	***Meta*-chloroperbenzoic acid**
Formula	$C_7H_5O_3Cl_1$
Crystallisation Conditions	Crystallised by slow evaporation in acetone at 4°C
Molecular weight / $gmol^{-1}$	172.57
Temperature (K)	100
Space Group	$P2_1/c$
a (Å)	3.9254(17)
b (Å)	5.920(2)
c (Å)	30.427(11)
α (°)	90
β (°)	93.31(2)
γ (°)	90
Volume ($Å^3$)	705.9(5)
Z	4
Z'	1
θ range/˚	1.34-28.12
Reflections Collected	17385
Independent	1678
Refln (obs.I>2theta(I))	1406
R_{int}	0.346
Parameters	120
GooF on F^2	1.073
R_1 (Observed)	0.1040
R_1 (all)	0.1175
wR_2 (all)	0.2491

The final R-factor is rather high for this structure, but the data quality is sufficient for determination of both non-hydrogen and hydrogen positions, allowing a structural analysis of the material. The heavily twinned nature of these crystals and difficulty in producing a sufficiently high quality crystal are possible reasons for the lack of an existing X-ray crystal structure for this material.

4.3.2 Analysis of the structure and interactions of MCPBA

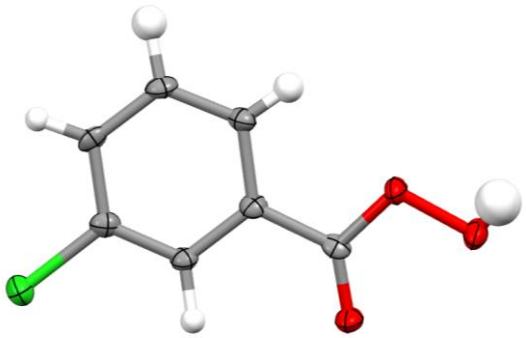

Figure 148 - Crystal structure of *meta*-chloroperbenzoic acid (MCPBA).

The crystal structure of *meta*-chloroperbenzoic acid (MCPBA) is monoclinic with a space group of $P2_1/c$. The asymmetric unit of the structure contains only one molecule of MCPBA in the asymmetric unit, with a fully protonated peroxyacid group identified (Figure 148).

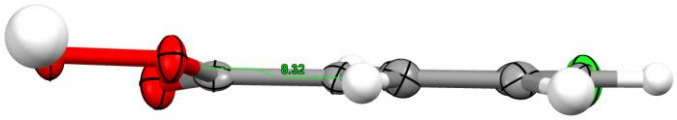

Figure 149 - MCPBA molecule viewed along the plane of the aromatic ring

The molecule itself is almost planar, with only a rotation of 8.3(7)° of the peroxyacid functional group from the plane of the benzene ring and the chlorine atom (Figure 149).

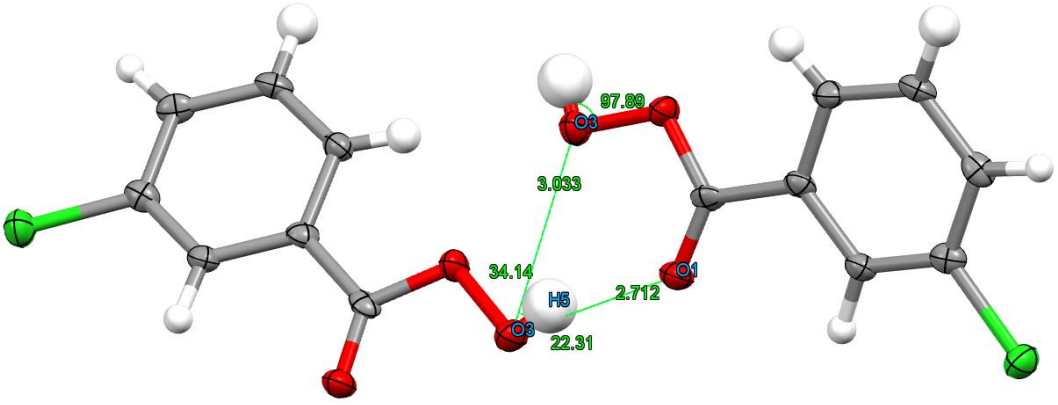

Figure 150 - Hydrogen bonding of peroxyacid group in MCPBA viewed along a-axis

When viewed perpendicular to the plane defined by the molecules, the hydrogen bonding motif can be observed. The basic oxygen of the peroxide group, O3, forms an asymmetric bifurcated hydrogen bond motif comprising a weaker bond with the basic oxygen of the neighbouring molecule, also O3, and a stronger hydrogen bond with the carbonyl of the same neighbouring molecule, O1 (Figure 150). The interaction with the carbonyl is the

stronger of the two, at a distance of 2.712(6)Å (O3-H5···O1); the bent nature of this hydrogen bond (O-H-O angle 158(9)°) allows the formation of the second interaction making the bond bifurcated. The second interaction, O3-H5···O3, has an overall distance of 3.033(6)Å. As the direction of the motif is the same as is observed with the other peroxyacids, forming a $C_1^1(5)$ chain (O3-H5-O1-C5-O2), it may be the case that this second interaction with the basic oxygen occurs in other cases where the hydrogen position is not determined in those published structures.

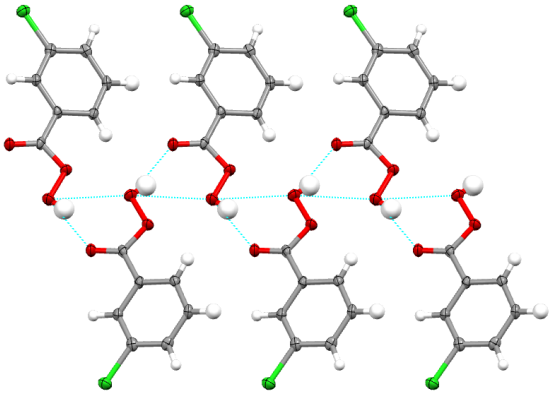

Figure 151 - Chains of MCPBA as viewed down the *a*-axis.

The hydrogen bonded chains are aligned along the *b*-axis of the structure, which can be seen clearly from the view down the *a*-axis (Figure 151), forming hydrogen bonded peroxyacid channels, enclosed by aromatic groups and ultimately chlorine atoms. This gives an overall distance between the chlorine atoms of successive molecules of 5.920(3)Å.

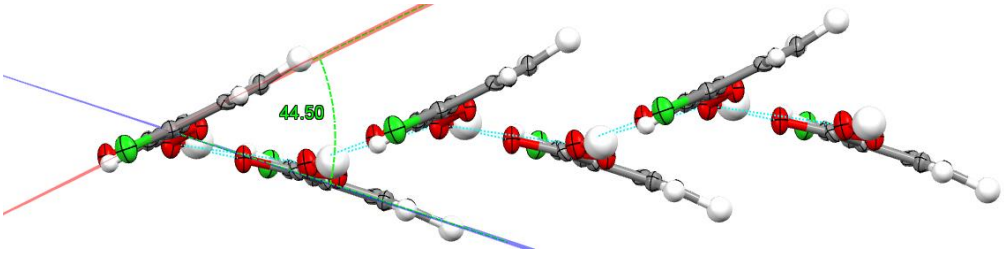

Figure 152 - MCPBA with planes generated by aromatic rings of hydrogen bonded molecules.

When the structure is rotated 90°, it can be observed that the planes generated by the aromatic rings are not parallel, but each alternating molecule is orientated at ~44.5° to the next molecule.

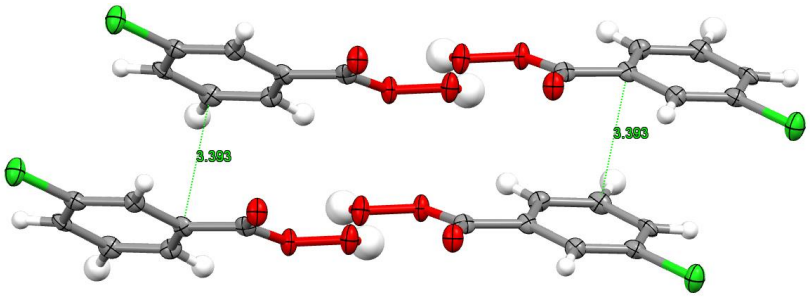

Figure 153 – π-π stacking present in the crystal structure of MCPBA.

The structure is stacked along the *a*-axis, producing skewed π-π stacking at a distance of 3.393(7)Å between the rings and subsequently generated planes of molecules, measured from the closest atom contacts between two neighbouring planes.

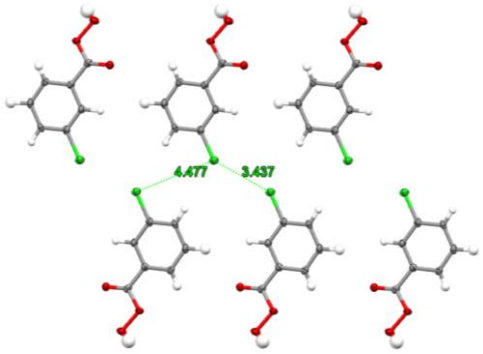

Figure 154 - Chlorine interactions in MCPBA.

The chlorine interactions form a chlorine channel with a distance of 3.437(2)Å, within the distance of the sum of the Van der Waals radii, and 4.477(2)Å (Figure 154).

This furthers the evidence that in the solid state, Swern's proposed dimerisation of peroxyacid molecules is contradicted, with the structure following the pattern of interactions of the basic oxygen and terminal hydrogen to carbonyl oxygen atoms of other peroxyacid molecules, forming a catemeric structure. There is also no evidence of intramolecular interaction within the molecule.

4.4 Crystal structure of 6-phthalimidoperoxyhexanoic acid

The crystal structure of 6-phthalimidoperoxyhexanoic acid (PAP) was obtained from a recrystallisation of the supplied material, marked with 71% purity, in acetone. The crystals were obtained by slow evaporation at a constant controlled temperature of 30°C using a temperature controlled hot plate and exist as very small, clear, colourless plate-like crystals. The data was of sufficient quality to model all H atoms from a Fourier difference map and the positions and thermal parameters were subsequently refined. This allowed for the refinement of all non-hydrogen atoms anisotropically, and all hydrogen atoms

isotropically, including the terminal hydrogen on the peroxyacid functional group, resolving the previous ambiguities in its location.

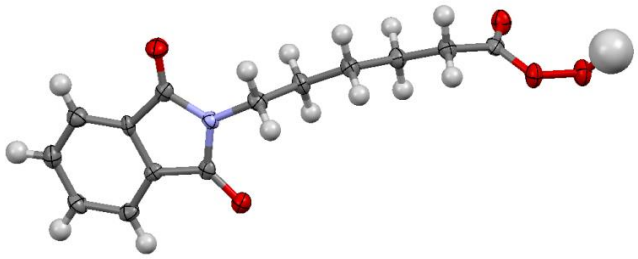

Figure 155 - The asymmetric unit of the crystal structure of 6-phthalimidoperoxyhexanoic acid.

4.4.1 Summary of diffraction experiment and data

Data were collected on a Bruker AXS, APEX II diffractometer at a collection temperature of 100K, but also subsequently repeated and confirmed on a Rigaku RAPID image plate diffractometer. The APEX-determined structure was solved to a final R-factor of 3.34%.

Table 17 - Crystal structure collection data for 6-phthalimidoperoxyhexanoic acid

Compound	6-Phthalimidoperoxyhexanoic acid
Formula	$C_{14}H_{15}N_1O_5$
Crystallisation Conditions	Evaporative crystallisation from acetone at 30°C
Molecular weight / gmol-1	277.28
Temperature (K)	100
Space Group	$P2_1/c$
a (Å)	18.814(4)
b (Å)	4.5065(10)
c (Å)	15.508(4)
α (°)	90
β (°)	90.959(9)
γ (°)	90
Volume ($Å^3$)	1314.7(5)
Z	4
θ range(˚)	1.082-18.981
Reflections Collected	13414
Independent	1050
Refln (obs.I>2theta(I))	849
Rint	0.057
Parameters	186
GooF on F^2	1.0683
R_1 (Observed)	0.0334
R_1 (all)	0.0464
wR_2 (all)	0.0837

4.4.2 Analysis of the structure and interactions of 6-phthalimidoperoxyhexanoic acid

It is immediately clear from the structure that the OH hydrogen position is not as well defined as the others. This could either be a result of bifurcation of the hydrogen bond, or

simply the inherent flexibility of the terminal OH compared to the other atoms. However a Fourier difference map only shows evidence of a single, slightly diffuse, peak when the residual electron density is viewed, with the assigned hydrogen removed.

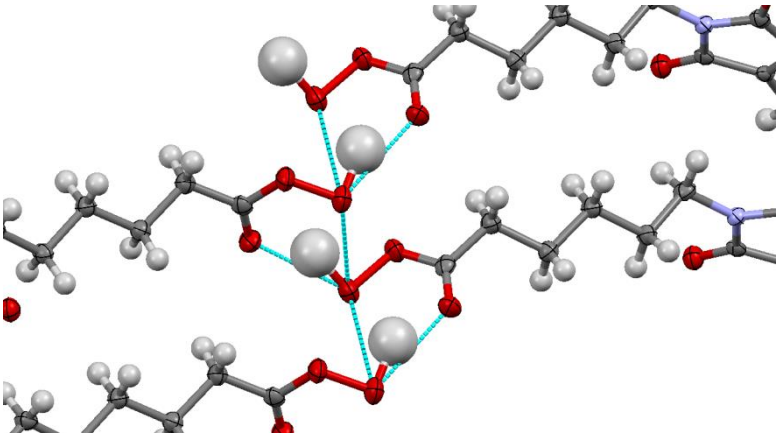

Figure 156 – Hydrogen bonding of peroxyacid groups in 6-phthalimidoperoxyhexanoic acid.

The hydrogen of the peroxyacid group is directed between the terminal oxygen and the carbonyl of a neighbouring peroxyacid group, forming a hydrogen bond with an O–H···O distance of 2.713(4)Å forming a familiar $C_1^1(5)$ chain (Figure 156). There is also a second, weaker interaction, similar to that observed with MCPBA, between the peroxy hydrogen and the terminal peroxy oxygen of the neighbouring molecule, with a O···H-O distance of 2.937(4)Å. The hydrogen is directed more towards carbonyl due to the stronger hydrogen bond, indicated by its shorter distance, however the moderate strength hydrogen bonding interaction with the neighbouring terminal oxygen in this bifurcated interaction reduces the bind angle at oxygen to 97(2)° as opposed to a standard angle of 104.45° as predicted by VSEPR theory. Statistical analysis of known crystal structures of peroxide oxygen, not limited to peroxy acids, indicates that this reduction in angle is not uncommon. It is, however, outside the known range for peroxyacids (99.7° – 112.2°), of which there are only five. The second interaction is significant and at least partially directing the hydrogen bond, which is echoed by the Fourier difference map, which shows only one electron density peak corresponding to the hydrogen.

The angling of the neighbouring phthalimido rings allows C-H···O interactions from the phthalimido carbonyl to an aromatic hydrogen and from the carbonyl on the other side of the molecule to an aliphatic hydrogen on carbon 3 of the chain, illustrated in Figure 157.

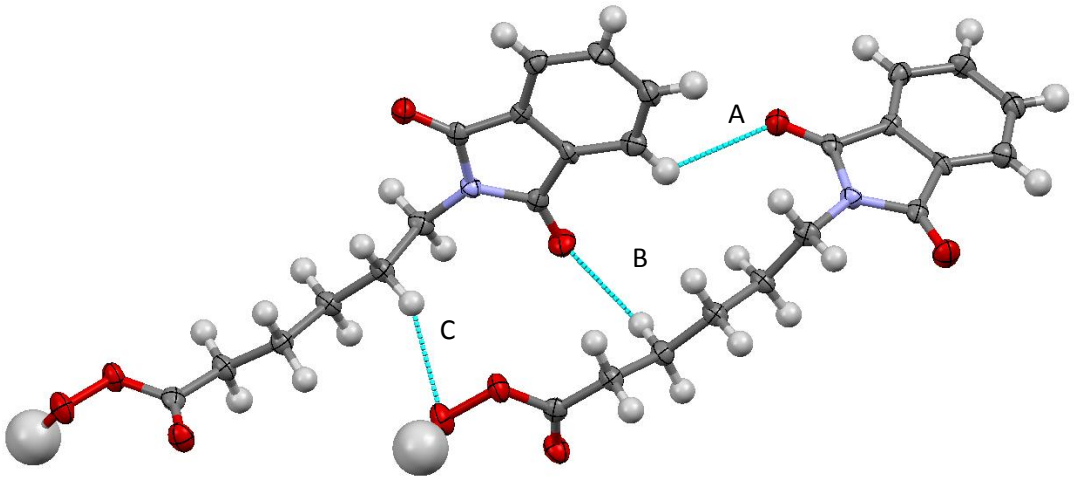

Figure 157 - Intermolecular interactions between 6-phthalimidoperoxyhexanoic acid molecules.

The C···O distances corresponding to these interactions (Figure 157, A and B), are 3.306(5)Å and 3.492(4)Å respectively and these are therefore relatively weak hydrogen bonds. Also shown in Figure 157 as C, is an oxygen - aliphatic hydrogen bond between carbon 5 of the chain and the terminal oxygen of the peroxy group. This is also a relatively weak hydrogen bond with an oxygen to carbon distance of 3.461(4)Å.

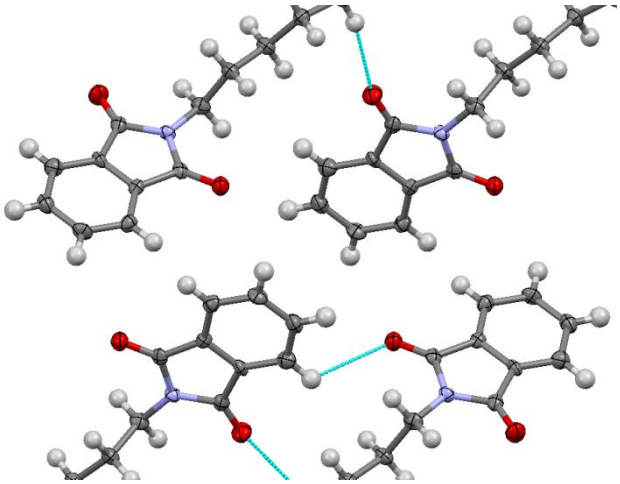

Figure 158 - Phthalimido packing arrangement in 6-phthalimidoperoxyhexanoic acid.

The phthalimido arrangement is such that the aromatic planes of adjacent molecules are at a distance greater than 3.8Å and are therefore defined to be too distant for the $\pi - \pi$ stacking to be significant. The intermolecular interactions are thus predominantly from the strong hydrogen bonding interactions observed around the peroxy acid group and the weaker hydrogen bonding between the carbonyls and the aliphatic hydrogens.

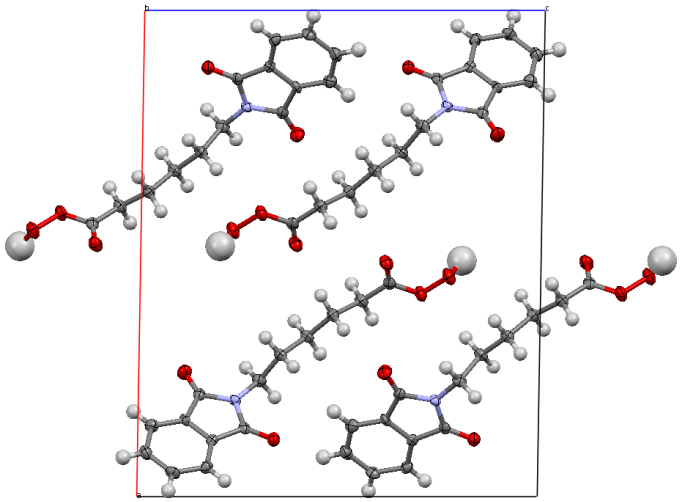

Figure 159 - Unit cell of PAP viewed along the *b*-axis.

As can be observed from viewing the structure along the *b*-axis, Figure 159, PAP molecules pack in rows of phthalimido groups interacting with each other, defined here as being at the top and bottom of the shown unit cell, with the peroxy acid groups interacting only with other peroxy acid groups, at the centre of the cell. This has the effect of creating rows of aromatic interactions separated by the aliphatic chain from conventional hydrogen bonding channels at the functional oxidising end of the molecule.

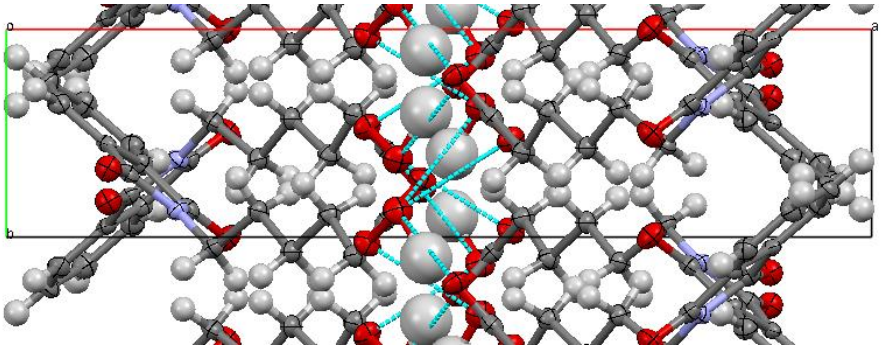

Figure 160 - 6-phthalimidoperoxyhexanoic acid oriented to view interactions between stacked molecules on the *a*-*b*-axis.

It can also be observed from Figure 160, further shown in Figure 161, that the phthalimido groups are not all stacked in the same direction. Neighbouring 6-phthalimidoperoxyhexanoic acid molecules lie with the planar phthalimido rings almost perpendicular to each other, at approximately averaged 80°, creating a saw tooth effect on the aromatic stacking motif. The flexibility of the number 6 carbon on the aliphatic chain allows the rest of the molecule to lie in an almost parallel alignment in the intersecting plane between the two rings. This allows for the reactive end of the molecules to lie relatively close to each other, within interacting distance, despite their mirrored translation.

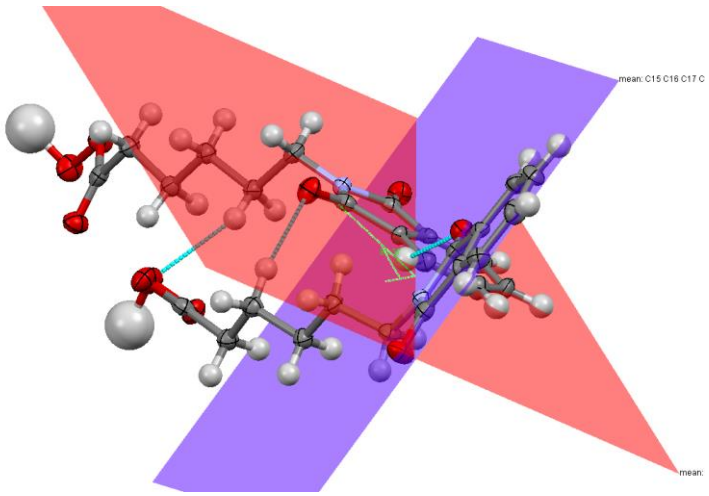

Figure 161 - Planes generated from phthalimido groups on neighbouring 6-phthalimidoperoxyhexanoic acid molecules.

4.5 Summary

From the evidence collected, it is clear that the molecules under study are indeed highly unstable, reacting under normally inert crystallisation conditions such as with standard laboratory solvents. Solvent selection has a major part to play in the retention of the peroxyacid character and production of crystals of these reactive materials. The solvent that offered the greatest success with recrystallisation of the target materials was acetone. However, as can be seen in the production of TATP, even the solvents in which the materials are relatively stable, reactions can take place that can be potentially hazardous. Attempts to use more extreme conditions to stabilise these reactive materials were unsuccessful. The use of strong acids and bases as additives in crystallisation environments that already proved to be unstable had only a negative effect, producing more side products.

From the crystallographic data collected, it has been confirmed that the peroxyacid group has propensity to interact through hydrogen bonding to carbonyl groups, and is stable in their presence. As such, any motif designed to interact with the peroxyacid functional group itself should include a strong hydrogen bond acceptor such as, or similar to, a carbonyl, or instead should be designed to react with other functionalities of the target molecule, such as the aromatic or phthalimido rings. The aliphatic chain of the PAP molecule allows for greater conformational flexibility than with *meta*-chloroperbenzoic acid, and this could perhaps be utilised for selective interaction with only one part of the molecule, such as only one end of the molecule, the phthalimido group or the peroxyacid group.

5. Multicomponent Molecular Complexes of Reactive Materials

Introducing a secondary material into the crystallisation process, as outlined in the introduction, could serve as a viable way of bringing together the target reactive material with a second component, potentially reducing its reactivity. The principle is similar to that adopted in other co-crystallisation approaches to physical property tuning – for example it is used to enhance the solubility of an insoluble active ingredient by coupling with a co-component with inherent solubility in the solvent used. The parallel here is that the inherent stability of the co-component offers stability to the reactive material when the complex is formed. The results outlined in this chapter represent the collected data from such attempts, assessing the suitability of each secondary component.

5.1 Carboxylic acids and peroxyacids

Given observed common interactions in the pure peroxyacid functionalised molecules, providing a strongly electron donating carbonyl with which the terminal peroxy hydrogen can interact seems a logical design strategy for creating a multi-component material. The fully oxidised carbonyl group is inherently stable in the presence of peroxyacids and could be a main feature in any synthons designed. The peroxyacid group itself has similarity with the carboxylic acid group, in terms of size and hydrogen bonding capability, a factor that tends to favour the formation of a hydrogen bonded co-crystal. In addition the weaker organic acids will be less likely to decompose the peroxyacids and their similarity to the decomposition products, the parent acids, could also potentially help maintain the equilibrium of the decomposition reaction in favour of the retention of the peroxyacid. A series of carboxylic acid molecules were thus selected as possible secondary components, as described below .

5.1.1 Peroxyacetic acid and carboxylic acids

Peroxyacetic acid (Figure 162), a liquid at room temperature, was added to carboxylic acid solutions in attempts to create a solid phase crystalline product.

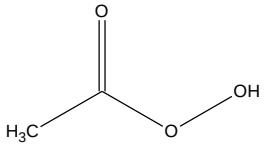

Figure 162 - Peroxyacetic acid - PAA

In all experiments, the acid was dissolved in the selected solvents with the addition of the peroxyacetic acid, from a 39% peroxyacetic acid solution, in a 1:1 molar ratio to attempt to grow a 1:1 molecular complex. The method of preparation was that of temperature

controlled evaporative crystallisation. The full XRPD patterns for each resulting product can be found in Appendix 2.

2-Chlorobenzoic acid

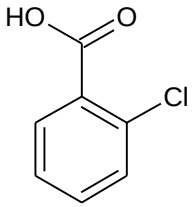

Figure 163 - 2-Chlorobenzoic acid

Peroxyacetic acid was crystallised with 2-chlorobenzoic acid (Figure 163) in acetone, methanol, ethanol, isopropanol and chloroform at 4°C and room temperature (Table 18).

Table 18 - Crystallisation conditions of peroxyacetic acid (PAA) and 2-chlorobenzoic acid

Sample ID	Component A	Component B	Solvent	Temperature	PolySNAP ID
AM01_01	PAA	2-chlorobenzoic acid	Acetone	4°C	8
AM01_03	PAA	2-chlorobenzoic acid	Methanol	4°C	7
AM01_04	PAA	2-chlorobenzoic acid	Methanol	Room temperature	6
AM01_05	PAA	2-chlorobenzoic acid	Ethanol	4°C	5
AM01_06	PAA	2-chlorobenzoic acid	Ethanol	Room temperature	4
AM01_07	PAA	2-chlorobenzoic acid	Isopropanol	4°C	3
AM01_08	PAA	2-chlorobenzoic acid	Isopropanol	Room temperature	2
AM01_09	PAA	2-chlorobenzoic acid	Chloroform	4°C	1

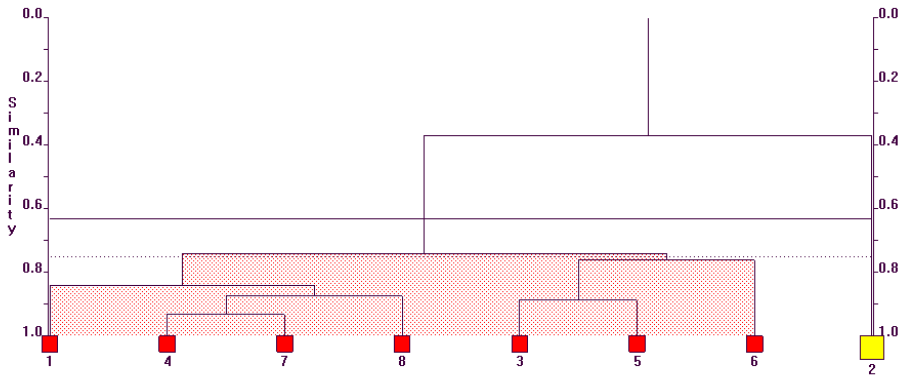

Figure 164 - Dendrogram of similarity of XRPD patterns collected from samples isolated from crystallisations of PAA and 2-chlorobenzoic acid.

All XRPD patterns of samples collected from the crystallisations have a greater than 75% similarity with the only exception being AM02_08 (Figure 164 – Sample 2 (yellow)). This represents a crystallisation of the two components in isopropanol at room temperature, and although its pattern has all the same major peaks, it is substantially more amorphous.

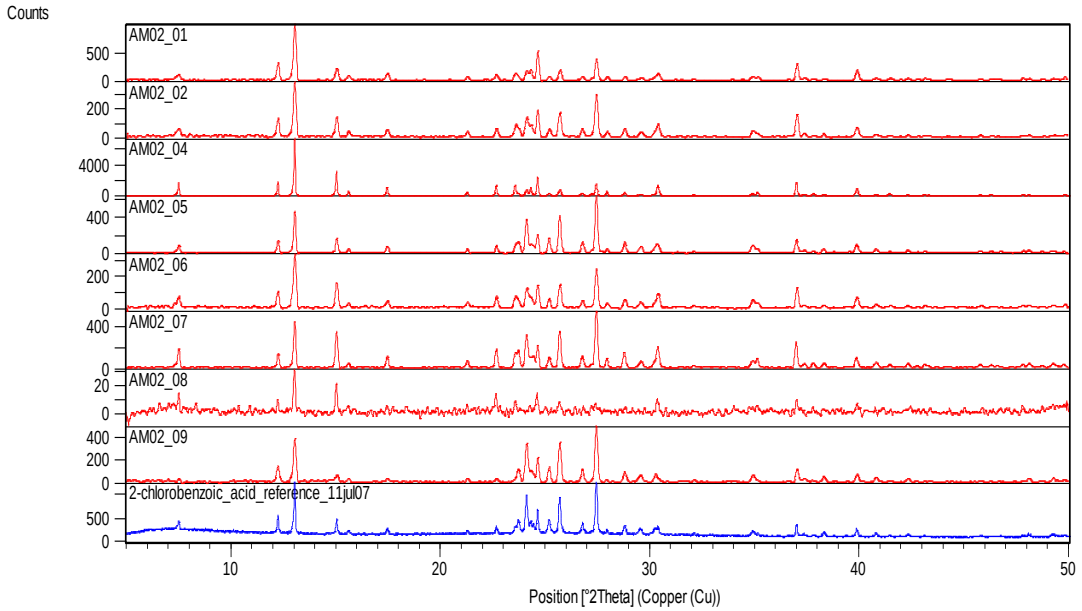

Figure 165 - XRPD patterns collected from crystallisations of PAA and 2-chlorobenzoic acid (red) compared with a reference pattern for 2-chlorobenzoic acid (blue).

On visual comparison, the collected XRPD patterns all show excellent correlation to the reference pattern for 2-chlorobenzoic acid with all peaks assigned. The peroxyacid has thus not formed a complex with the 2-chlorobenzoic acid.

3-Chlorobenzoic acid

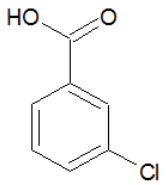

Figure 166 - 3-chlorobenzoic acid

A similar experiment was performed with 3-chlorobenzoic acid (Figure 166). The acid was dissolved in acetone, methanol, ethanol and isopropanol, to which peroxyacetic acid was added in a 1:1 acid to peroxyacid molar ratio and crystallised in a controlled temperature environment at both room temperature and 4°C (Table 19).

Table 19 - Crystallisation conditions of peroxyacetic acid (PAA) and 3-chlorobenzoic acid

Sample ID	Component A	Component B	Solvent	Temperature	PolySNAP ID
AM03_01	PAA	3-chlorobenzoic acid	Acetone	4°C	1
AM03_02	PAA	3-chlorobenzoic acid	Acetone	4°C	
AM03_03	PAA	3-chlorobenzoic acid	Methanol	4°C	2
AM03_04	PAA	3-chlorobenzoic acid	Methanol	Room temperature	3
AM03_05	PAA	3-chlorobenzoic acid	Ethanol	4°C	4
AM03_06	PAA	3-chlorobenzoic acid	Ethanol	Room temperature	5
AM03_07	PAA	3-chlorobenzoic acid	Isopropanol	4°C	6

The dendrogram representation of the statistical analysis from the XRPD patterns of the products shows that all patterns match at a minimum 60% correlation (Figure 167). The choice of a lower correlation level allows inclusion of those samples which upon visual identification contain the same Bragg peaks but have a larger amorphous background, reducing the correlation calculated in PolySNAP-3.

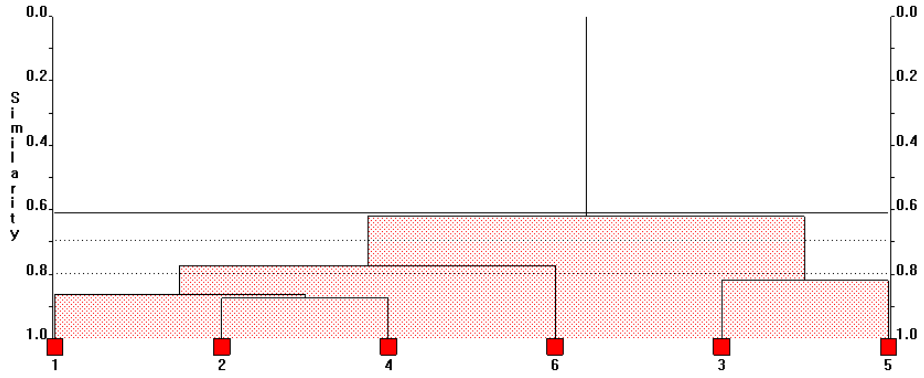

Figure 167 - Dendrogram of similarity of XRPD patterns collected from samples isolated of crystallisation of PAA and 3-chlorobenzoic acid.

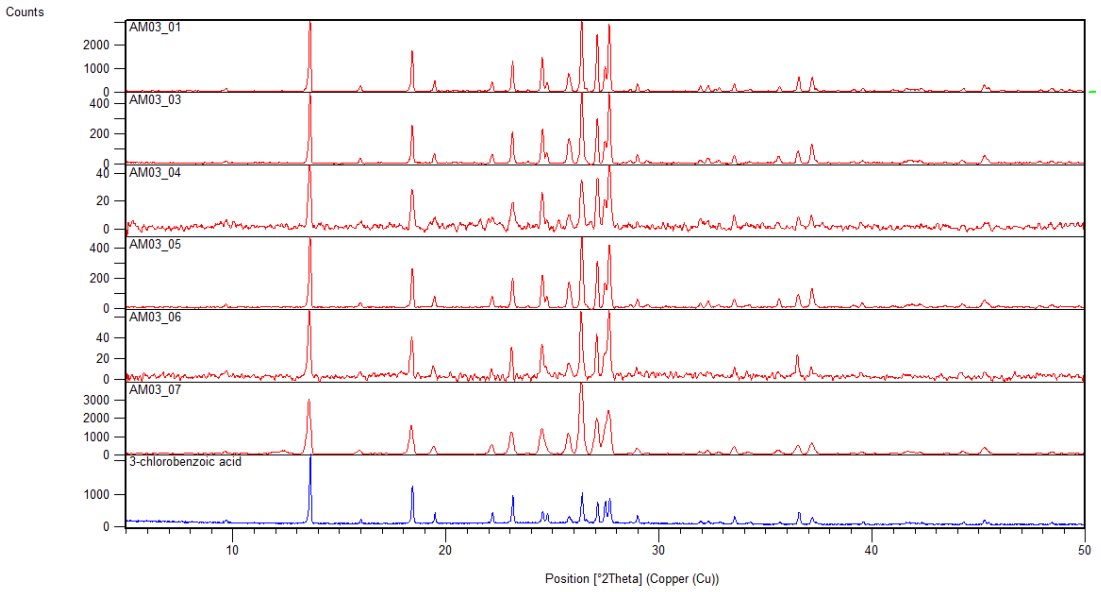

Figure 168 - XRPD patterns collected from crystallisations of PAA and 3-chlorobenzoic acid (red) compared with a reference pattern of 3-chlorobenzoic acid (blue).

All collected XRPD samples are an excellent match to the reference XRPD pattern of 3-chlorobenzoic acid (Figure 168) and thus no new crystalline forms are present in the samples. AM03_02 was confirmed as 3-chlorobenzoic acid by single crystal X-ray diffraction.

4-Chlorobenzoic acid

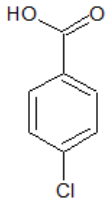

Figure 169 - 4-chlorobenzoic acid

In a similar manner to the previous experiments, 4-chlorobenzoic acid (Figure 169) was used under the crystallisation conditions outlined in Table 20.

Table 20 - Crystallisation conditions of peroxyacetic acid (PAA) and 4-chlorobenzoic acid

Sample ID	Component A	Component B	Solvent	Temperature	PolySNAP ID
AM04_01	PAA	4-chlorobenzoic acid	Acetone	4°C	1
AM04_02	PAA	4-chlorobenzoic acid	Acetone	Room temperature	2
AM04_03	PAA	4-chlorobenzoic acid	Methanol	4°C	3
AM04_04	PAA	4-chlorobenzoic acid	Methanol	Room temperature	4
AM04_06	PAA	4-chlorobenzoic acid	Ethanol	Room temperature	5
AM04_07	PAA	4-chlorobenzoic acid	Isopropanol	4°C	6
AM04_08	PAA	4-chlorobenzoic acid	Isopropanol	Room temperature	7

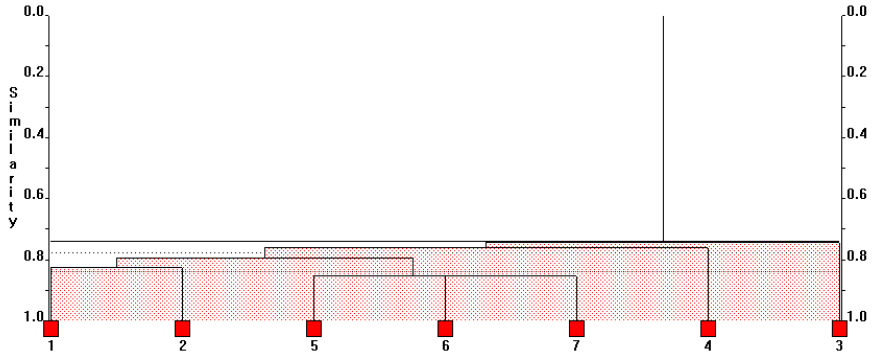

Figure 170 - Dendrogram of similarity of XRPD patterns collected from samples isolated from crystallisations of PAA and 4-chlorobenzoic acid.

As for 2 and 3-chlorobenzoic acid, the recrystallization attempts of 4-chlorobenzoic acid with peroxyacetic acid yield the same product in each crystallisation environment. The XRPD pattern show >74% similarity (Figure 170). By comparison of the patterns to the reference pattern of 4-chlorobenzoic acid (Figure 171), it can be seen that there are no additional crystalline forms present.

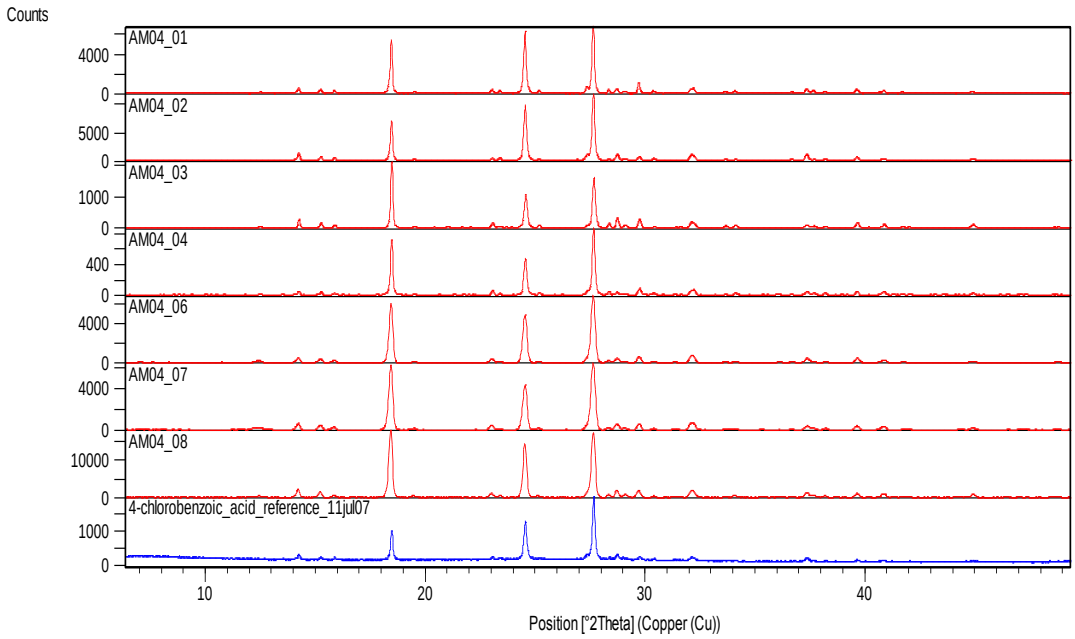

Figure 171 - XRPD patterns collected from crystallisations of PAA and 4-chlorobenzoic acid (red) compared with a reference pattern of 4-chlorobenzoic acid (blue).

2-Picolinic acid

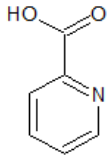

Figure 172 - 2-picolinic acid

Peroxyacetic acid and 2-picolinic acid (Figure 172) were mixed in 1:1 molar solution, which then underwent slow evaporation. The introduction of a second electron rich group was proposed to provide a second site for interaction with the terminal hydrogen of the peroxyacid group, providing the opportunity for a stronger, possibly bifurcated synthon. The crystallisation conditions which produced solid products suitable for XRPD analysis are detailed in Table 21.

Table 21 - Crystallisation conditions of peroxyacetic acid (PAA) and 2-picolinic acid

Sample ID	Component A	Component B	Solvent	Temperature	PolySNAP ID
AM05_01	PAA	2-picolinic acid	Acetone	4°C	1
AM05_02	PAA	2-picolinic acid	Acetone	Room temperature	2
AM05_03	PAA	2-picolinic acid	Chloroform	4°C	3
AM05_04	PAA	2-picolinic acid	Chloroform	Room temperature	4
AM05_06	PAA	2-picolinic acid	Ethyl Acetate	Room temperature	5

From the XRPD patterns, it is evident that formation of a new crystalline material has taken place, and the statistical analysis identified four distinct powder pattern types (Figure 173).

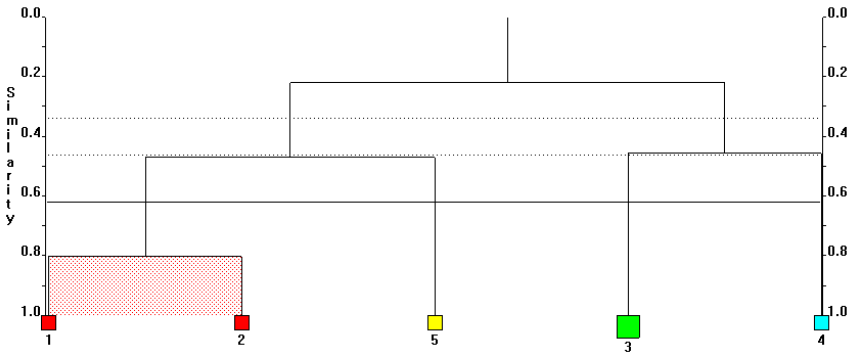

Figure 173 - Statistical analysis dendrogram of the crystallisation products of PAA and 2-picolinic acid.

The samples crystallised from acetone (red) can be identified by XRPD comparison to be mainly composed of 2-picolinic acid (Figure 174).

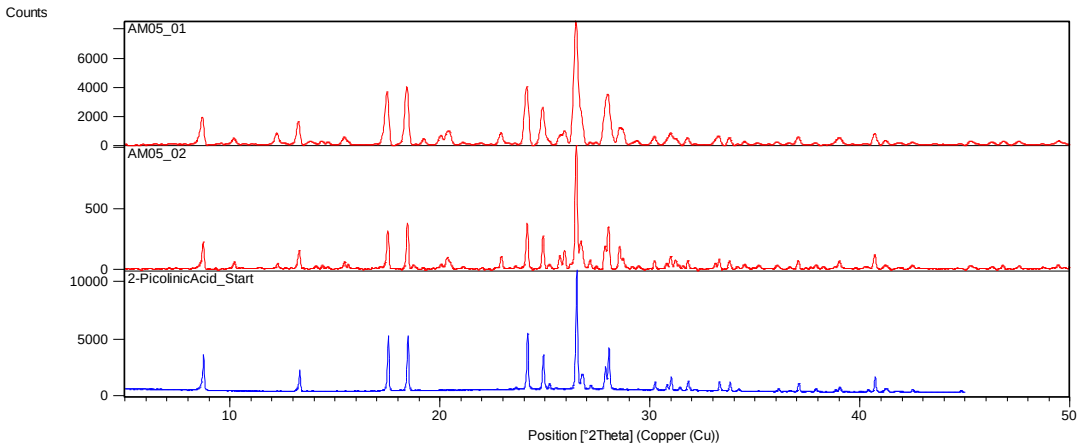

Figure 174 - XRPD patterns of PAA and 2-picolinic acid crystallised in acetone at 4°C (top) and room temperature (middle) compared to the reference XRPD pattern of 2-picolinic acid (bottom).

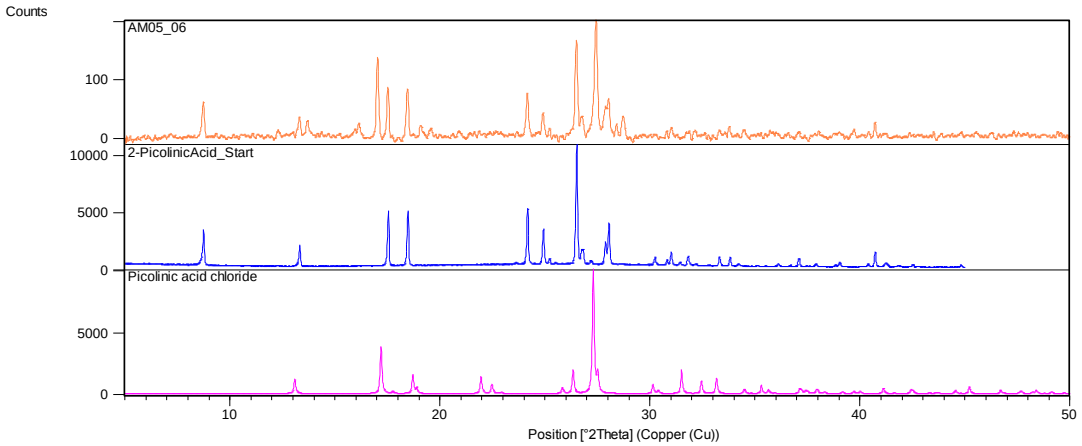

Figure 175 - XRPD of PAA crystallised with 2-picolinic acid in ethyl acetate (AM05_06; top) compared with reference patterns for 2-picolinic acid (middle) and 2-picolinic acid chloride (bottom).

The sample identified as 5 in the dendrogram (Figure 173) corresponds to the crystallisation from ethyl acetate at room temperature. As evidenced in Figure 175, this

sample comprises a mixture of the 2-picolinic acid starting material, with a chlorinated salt of the picolinic acid. The source of the chlorine in the formation of this material is proposed to be from contamination of the sample.

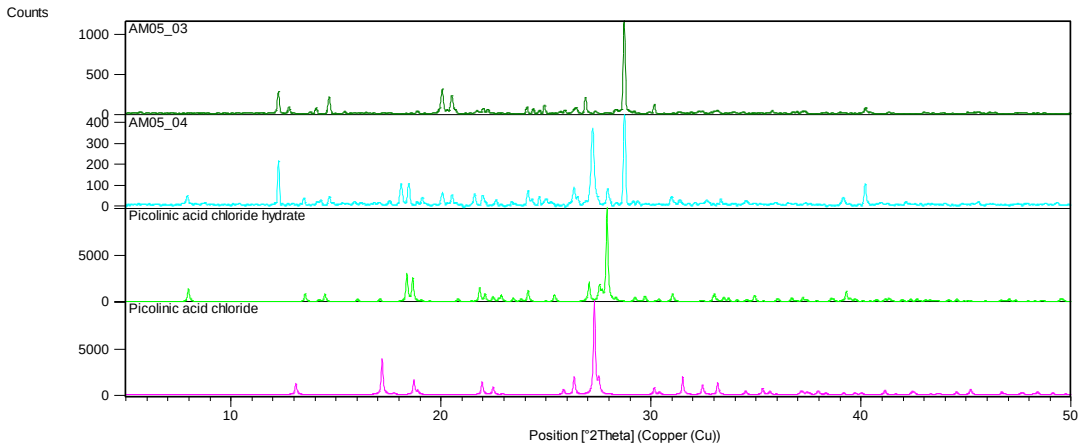

Figure 176 - XRPD patterns of PAA and 2-picolinic acid crystallised in chloroform at 4°C (black) and room temperature (light blue) compared to the reference XRPD pattern of 2-picolinic acid chloride (magenta), and a hydrated form (green).

The remaining samples were isolated from chloroform solution, which appears to have reacted to evolve chlorine which has then complexed with the picolinic acid in both the anhydrous form, as seen in the room temperature crystallisation, and the hydrated chloride, which is present almost exclusively in the 4°C sample and as a component in the room temperature sample. The shift in expected peak positions is due to the difference in the temperature of data acquisition between the 100K 2-picolinic acid hydrated chloride salt, and the room temperature XRPD patterns of the two samples.

No molecular complex of the peroxyacetic acid is formed under the chosen conditions.

1-Naphthaleneacetic acid

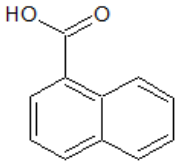

Figure 177 - 1-naphthaleneacetic acid

To bring a larger molecule into the crystallisation attempts, as well as a more developed π structure, 1-naphthaleneacetic acid was used in the cocrystallisation environment in the same equimolar approach as for the previous samples. The crystallisation conditions chosen for these cocrystallisations are detailed in Table 22.

Table 22 - Crystallisation conditions of peroxyacetic acid (PAA) and 1-naphthaleneacetic acid

Sample ID	Component A	Component B	Solvent	Temperature	PolySNAP ID
AM06_01	PAA	1-Naphthaleneacetic acid	Acetone	4°C	1
AM06_02	PAA	1-Naphthaleneacetic acid	Acetone	Room temperature	2
AM06_03	PAA	1-Naphthaleneacetic acid	Chloroform	4°C	3
AM06_05	PAA	1-Naphthaleneacetic acid	Diethyl ether	4°C	4
AM06_07	PAA	1-Naphthaleneacetic acid	Ethyl acetate	4°C	5
AM06_08	PAA	1-Naphthaleneacetic acid	Ethyl Acetate	Room temperature	6
AM06_09	PAA	1-Naphthaleneacetic acid	Acetonitrile	4°C	7

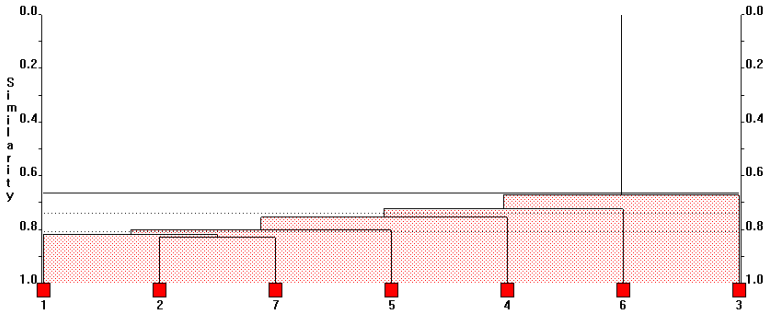

Figure 178 - Statistical analysis dendrogram of the crystallisation products of PAA and 1-naphthaleneacetic acid.

As shown by the statistical analysis, the samples analysed by XRPD all show a high correlation, at similarity of >65%, with the only differences resulting from gradual differences in the background levels of the scans.

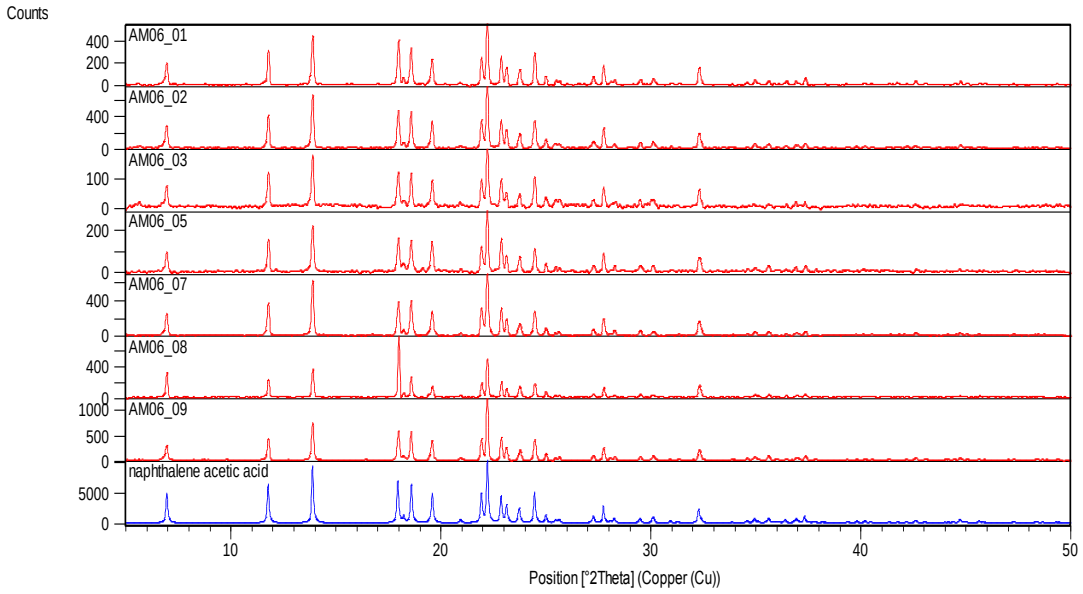

Figure 179 - XRPD patterns collected from crystallisations of PAA and 1-naphthaleneacetic acid (red) compared with a reference pattern of 1-naphthaleneacetic acid (blue).

When compared to the reference pattern of the 1-napthalene acetic acid starting material, the XRPD patterns show an excellent match with all Bragg peaks accounted for. The peroxyacetic acid has thus not formed a complex with the 1-napthalene acetic acid.

2-Hydroxybenzoic acid (salicylic acid)

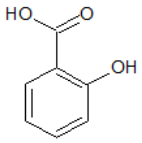

Figure 180 - Salicylic acid

Peroxyacetic acid was cocrystallised using the above procedure with salicylic acid (Figure 180), a secondary component with two hydrogen bond donors present which can provide a double donor motif on one side of the molecule, or a donor and acceptor within close proximity. This capability offers the opportunity for interaction through the terminal peroxyacid hydrogen, one of the two available peroxyacid oxygen atoms, or the peroxyacid carbonyl. This would provide a two hydrogen bond synthon with additional interaction strength. The crystallisation conditions chosen are outlined in Table 23.

Table 23 - Crystallisation conditions of peroxyacetic acid (PAA) and salicylic acid

Sample ID	Component A	Component B	Solvent	Temperature	PolySNAP ID
AM08_01	PAA	Salicylic acid	Acetone	4°C	1
AM08_02	PAA	Salicylic acid	Acetone	Room temperature	2
AM08_03	PAA	Salicylic acid	Chloroform	4°C	3
AM08_04	PAA	Salicylic acid	Chloroform	Room temperature	4
AM08_05	PAA	Salicylic acid	Diethyl Ether	4°C	5
AM08_06	PAA	Salicylic acid	Diethyl Ether	Room temperature	6
AM08_07	PAA	Salicylic acid	Ethyl Acetate	4°C	7
AM08_08	PAA	Salicylic acid	Ethyl Acetate	Room temperature	8
AM08_09	PAA	Salicylic acid	Acetonitrile	4°C	9
AM08_10	PAA	Salicylic acid	Acetonitrile	Room temperature	10

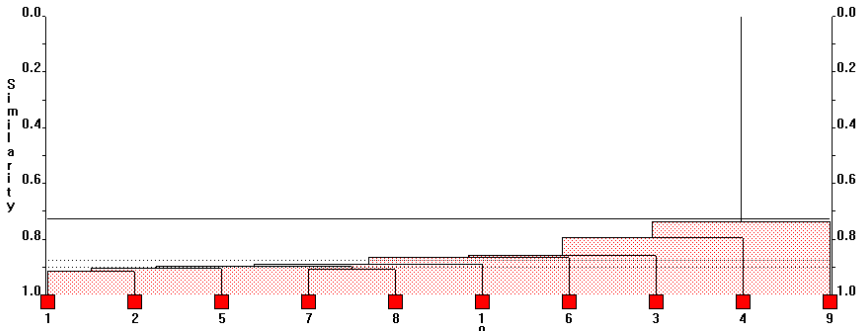

Figure 181 - Statistical analysis dendrogram of the crystallisation products of PAA and salicylic acid.

As shown in Figure 181, all XRPD patterns are well correlated, at a similarity of >72%.

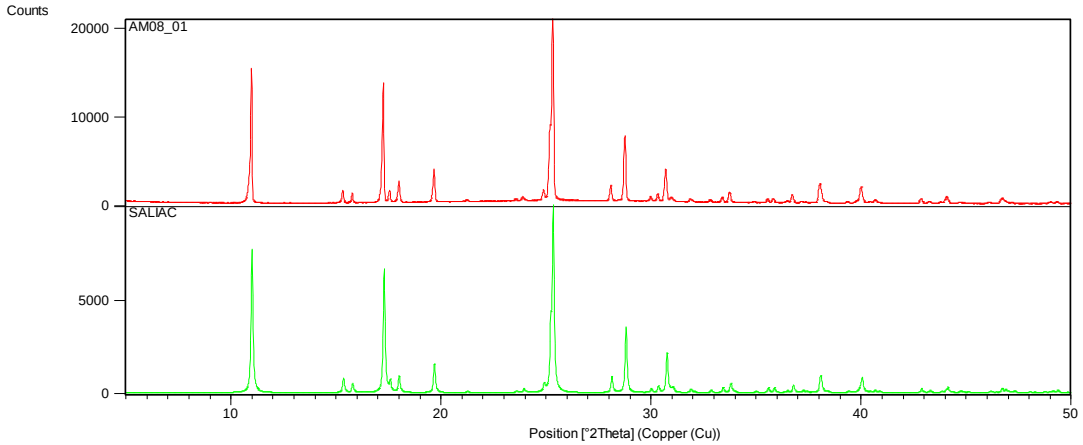

Figure 182 - Comparison of a representative sample of the XRPD patterns collected from the crystallisation of PAA with salicylic acid (red) with the reference XRPD pattern of the salicylic acid starting material (green).

As shown by the comparison of the XRPD pattern of a sample from the crystallisation experiments with a reference pattern of salicylic acid, it can be seen that no new crystalline materials have formed in any of the crystallisations.

3-hydroxybenzoic acid

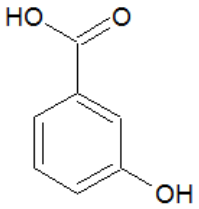

Figure 183 - 3-hydroxybenzoic acid

Following on from the methodology set out with salicylic acid of introducing a second hydrogen bond donor, 3-hydroxybenzoic acid (Figure 183) was also introduced with peroxyacetic acid, under the crystallisation conditions outlined in Table 24.

Table 24 - Crystallisation conditions of peroxyacetic acid (PAA) and 3-hydroxybenzoic acid

Sample ID	Component A	Component B	Solvent	Temperature	PolySNAP ID
AM09_01	PAA	3-hydroxybenzoic acid	Acetone	4°C	1
AM09_02	PAA	3-hydroxybenzoic acid	Acetone	Room temperature	2
AM09_05	PAA	3-hydroxybenzoic acid	Diethyl Ether	4°C	3
AM09_06	PAA	3-hydroxybenzoic acid	Diethyl Ether	Room temperature	4
AM09_07	PAA	3-hydroxybenzoic acid	Ethyl Acetate	4°C	5
AM09_08	PAA	3-hydroxybenzoic acid	Ethyl Acetate	Room temperature	6
AM09_09	PAA	3-hydroxybenzoic acid	Acetonitrile	4°C	7
AM09_10	PAA	3-hydroxybenzoic acid	Acetonitrile	Room temperature	8

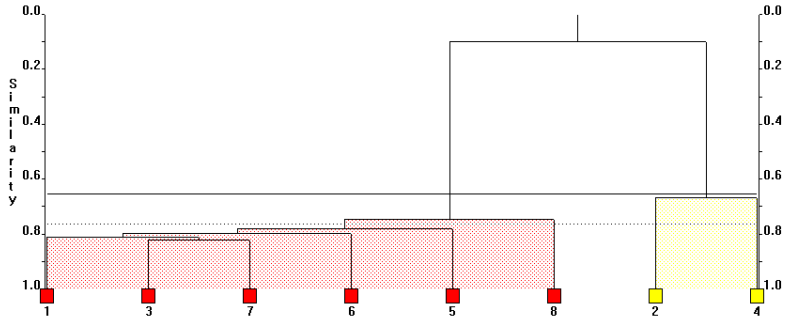

Figure 184 - Statistical analysis dendrogram of the crystallisation products of PAA and 3-hydroxybenzoic acid.

The statistical analysis of the XRPD patterns indicated that there are two distinct crystalline forms. The patterns for the most common form, Figure 184 (red), have >75% similarity. Examination of the XRPD patterns of the samples in this cluster identify them to be 3-hydroxybenzoic acid Form I with a high degree of purity (Figure 185).

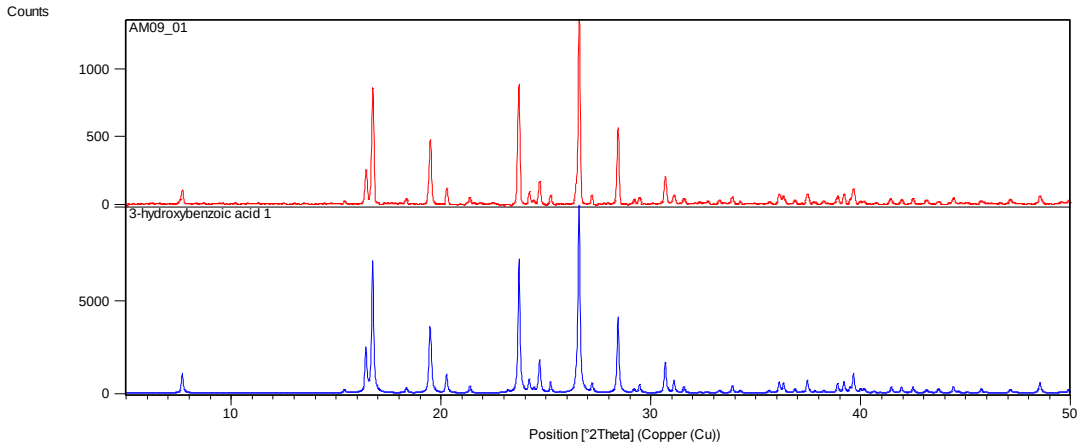

Figure 185 - XRPD patterns of a representative sample of the red main cluster of the crystallisation of PAA and 3-hydroxybenzoic acid (red) compared to the reference XRPD pattern of 3-hydroxybenzoic acid Form I (blue).

The second cluster consists of two samples, both room temperature crystallisations, AM09_02 and AM09_06, from acetone and diethyl ether respectively. These samples are confirmed to be predominantly 3-hydroxybenzoic acid Form II, as confirmed by XRPD analysis and comparison to the reference (Figure 186). Only starting materials have thus recrystallized.

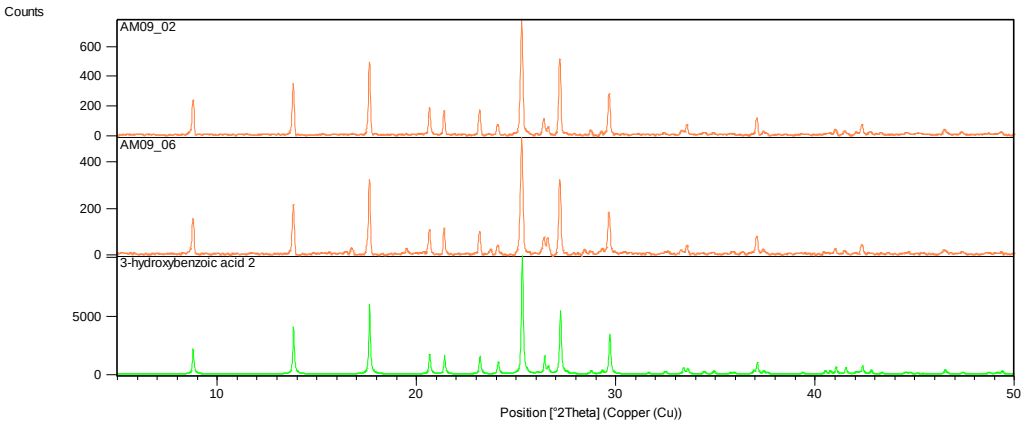

Figure 186 - XRPD patterns of a representative sample of the yellow cluster of the crystallisation of PAA and 3-hydroxybenzoic acid (red) compared to the reference XRPD pattern of 3-hydroxybenzoic acid Form II (green).

Malonic acid

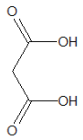

Figure 187 - Malonic acid

With two hydrogen bond donors and two acceptors and the added flexibility of the three carbon single bonded backbone of the molecule providing rotation, malonic acid (Figure 187) is an extremely versatile hydrogen bonding material, providing the opportunity for several hydrogen bonding motifs. Malonic acid was thus brought into a cocrystallisation environment with peroxyacetic acid in the conditions shown in

Table 25.

Table 25 - Crystallisation conditions of peroxyacetic acid (PAA) and malonic acid

Sample ID	Component A	Component B	Solvent	Temperature	PolySNAP ID
AM18_01	PAA	Malonic acid	Acetone	4°C	1
AM18_02	PAA	Malonic acid	Acetone	Room temperature	2
AM18_03	PAA	Malonic acid	Chloroform	4°C	3
AM18_04	PAA	Malonic acid	Chloroform	Room temperature	4
AM18_05	PAA	Malonic acid	Diethyl Ether	4°C	5
AM18_06	PAA	Malonic acid	Diethyl Ether	Room temperature	6
AM18_07	PAA	Malonic acid	Ethyl Acetate	4°C	7
AM18_08	PAA	Malonic acid	Ethyl Acetate	Room temperature	8

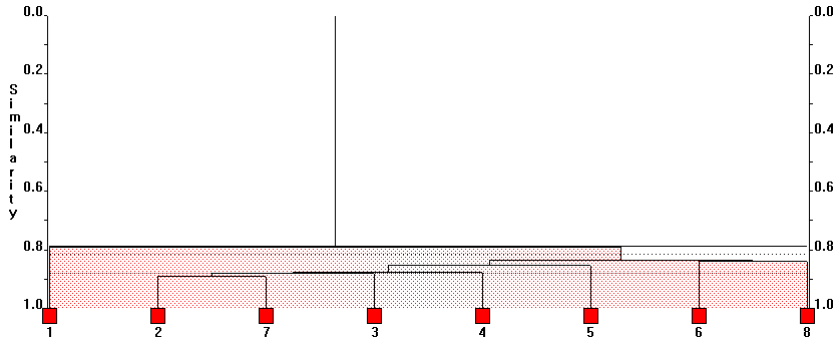

Figure 188 - Statistical analysis dendrogram of the crystallisation products of PAA and malonic acid.

As can be seen from the dendrogram in Figure 188, all the scans of the resultant materials show excellent correlation to each other with similarity >79%. As observed with all previous results using this methodology, all samples matched the co-component starting material (Figure 189).

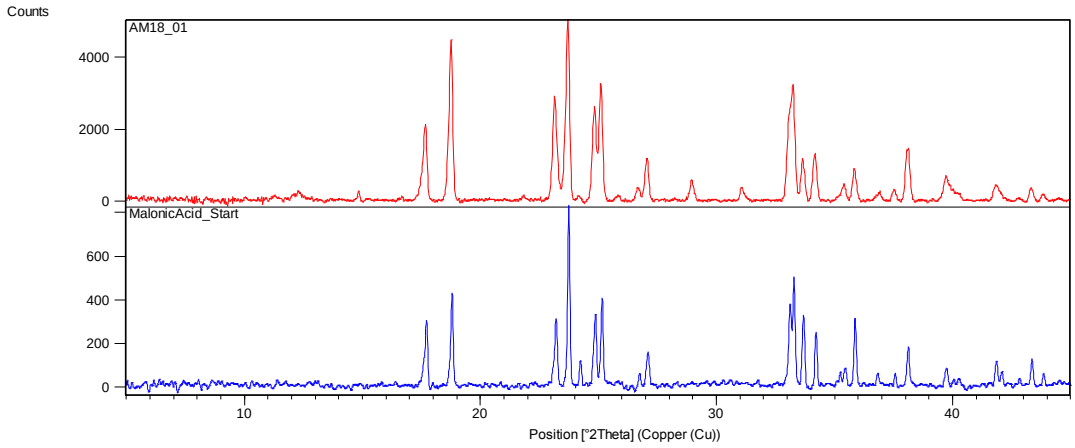

Figure 189 - XRPD pattern of a sample representative of all crystallisation products from PAA and malonic acid (red) compared to the reference pattern for malonic acid (blue).

Oxalic acid

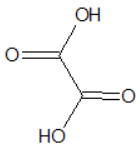

Figure 190 - Oxalic acid

Oxalic acid (Figure 190) has similar conformational flexibility to malonic acid and was thus also used as a secondary component for crystallisation with peroxyacetic acid, under the conditions shown in Table 26.

Table 26 - Crystallisation conditions of peroxyacetic acid (PAA) and oxalic acid

Sample ID	Component A	Component B	Solvent	Temperature	PolySNAP ID
AM19_01	PAA	Oxalic acid	Acetone	Room temperature	1
AM19_02	PAA	Oxalic acid	Acetone	4°C	2
AM19_05	PAA	Oxalic acid	Diethyl Ether	Room temperature	3
AM19_06	PAA	Oxalic acid	Diethyl Ether	4°C	4
AM19_07	PAA	Oxalic acid	Ethyl Acetate	Room temperature	5

These materials showed >60% similarity in correlation of their XRPD patterns, not particularly high for a PolySNAP 3 analysis. Manual analysis, however, confirmed that all samples are the same crystalline material, which matches pure oxalic acid dihydrate (Figure 191).

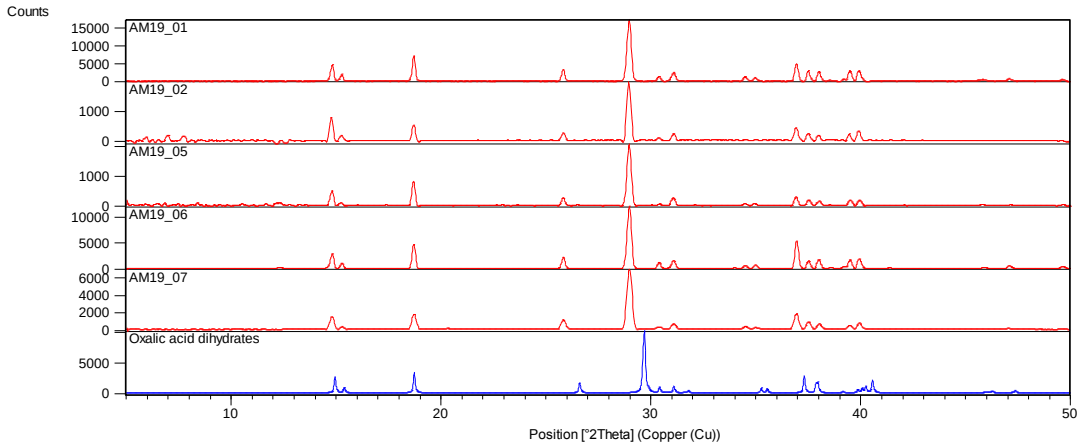

Figure 191 - XRPD patterns of all samples collected from the crystallisation of PAA and oxalic acid (red) compared to the reference pattern for oxalic acid dihydrate (blue).

5.1.2 *Meta*-chloroperbenzoic acid and carboxylic acids

The second peroxyacid to be subjected to this method is the larger solid molecule, *meta*-chloroperbenzoic acid (MCPBA). Expected solid products could thus include mixtures of MCPBA, 3-chlorobenzoic acid and residual secondary component starting materials, ras well as possible molecular complexes of the MCPBA or 3-chlorobenzoic acid and the secondary material. As with peroxyacetic acid, consideration of molecular recognition led to the choice of carboxylic acids as candidates for interaction with the MCPBA. Compared with peroxyacetic acid, MCPBA is of a more similar size to the secondary materials chosen and thus may be more likely to form molecular complexes.

The experiments were carried out by self-assembly through small scale evaporative crystallisation in temperature controlled environments and in a 1:1 peroxyacid to carboxylic acid ratio, to promote generation of 1:1 molecular complexes.

With so many possible outcomes from these experiments, and the high proportion of samples that resulted in a mixture of several crystalline materials, unambiguous statistical analysis proved difficult. Manual analysis by comparison to reference data proved more reliable in some cases. This is reflected in the results of the experiments detailed in this section.

2-chlorobenzoic acid, 3-chlorobenzoic acid, 4-chlorobenzoic acid and MCPBA are very similar molecules, providing similar packing and stacking interactivity and well matched hydrogen bond capabilities. They should thus provide a good basis for interaction between the two molecules in the cocrystallisations.

2-Chlorobenzoic acid

2-chlorobenzoic acid and MCPBA were combined in 1:1 molar ratio and dissolved in the solvent and temperature controlled environment as outlined in Table 27.

Table 27 - Crystallisation conditions of MCPBA and 2-chlorobenzoic acid

Sample ID	Component A	Component B	Solvent	Temperature	Analysis Group
AM10_01	MCPBA	2-chlorobenzoic acid	Acetone	Room temperature	A
AM10_02	MCPBA	2-chlorobenzoic acid	Acetone	4°C	amorphous
AM10_03	MCPBA	2-chlorobenzoic acid	Chloroform	Room temperature	A
AM10_04	MCPBA	2-chlorobenzoic acid	Chloroform	4°C	A
AM10_05	MCPBA	2-chlorobenzoic acid	Diethyl ether	Room temperature	B
AM10_06	MCPBA	2-chlorobenzoic acid	Diethyl ether	4°C	B
AM10_07	MCPBA	2-chlorobenzoic acid	Ethyl acetate	Room temperature	A
AM10_08	MCPBA	2-chlorobenzoic acid	Ethyl acetate	4°C	A

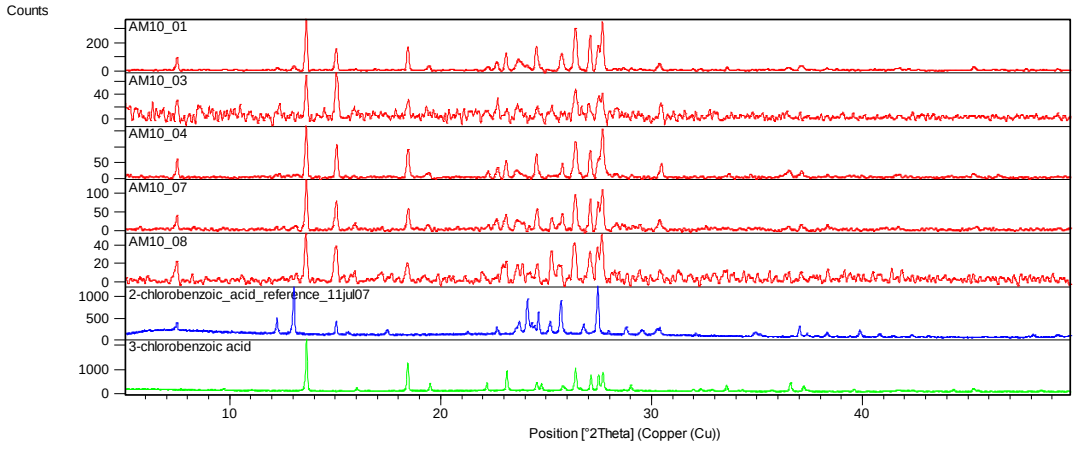

Figure 192 - XRPD patterns of samples crystallised from MCPBA and 2-chlorobenzoic acid defined as group A (red), compared to the reference patterns of 2-chlorobenzoic acid (blue) and 3-chlorobenzoic acid (green).

The samples from the crystallisation conditions defined in Table 27 as analysis group A, consist of all samples crystallised from acetone, chloroform and ethyl acetate at both room

temperature and 4°C, with the exception of the cocrystallisation in acetone at 4°C which is amorphous. As seen in Figure 192, these samples show good correlation to a combination of the Bragg peaks of the secondary starting material 2-chlorobenzoic acid and the decomposition product 3-chlorobenzoic acid, the parent acid of MCPBA. No other peaks are noticeably present in these samples and thus no recrystallised MCPBA remains. All crystalline MCPBA has been decomposed to the parent acid 3-chlorobenzoic acid and no new molecular complex formed.

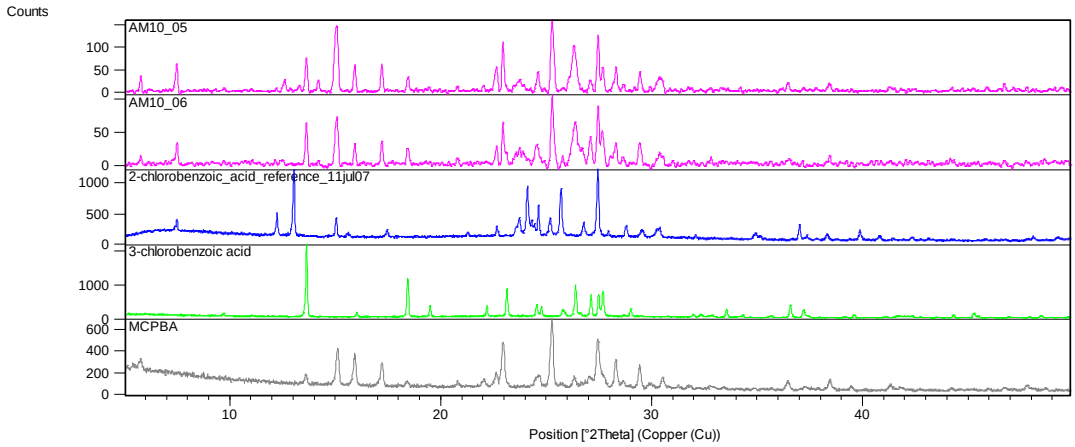

Figure 193 - XRPD patterns of samples crystallised from MCPBA and 2-chlorobenzoic acid defined as group B (purple), compared to the reference patterns of 2-chlorobenzoic acid (blue), 3-chlorobenzoic acid (green) and MCPBA (grey).

The remaining two samples, crystallised from diethyl ether at room temperature and 4°C, produce a second composition of materials. The XRPD patterns collected from these materials show the same peak profile as a combination of the three crystalline materials 2-chlorobenzoic acid, 3-chlorobenzoic acid and MCPBA (Figure 193), indicating that although some decomposition has taken place, a large proportion of crystalline MCPBA remains. As all peaks can be assigned, it can be taken that there have been no new materials formed.

3-Chlorobenzoic acid

3-Chlorobenzoic acid was cocrystallised with MCPBA in a 1:1 molar ratio under the same crystallisation environments as the experiment with 2-chlorobenzoic acid, as outlined in Table 28. The cocrystallisation of these materials is slightly different from the other chlorobenzoic acids in the fact that the secondary material is itself the decomposition product of the peroxyacid. This could aid retention of the peroxyacid within the equilibrium between the peroxyacid and the parent acid. The large excess of the parent acid should push the equilibrium in the direction of the formation of the peroxyacid, thus limiting its decomposition.

Table 28 - Crystallisation conditions of MCPBA and 3-chlorobenzoic acid

Sample ID	Component A	Component B	Solvent	Temperature
AM11_01	MCPBA	3-chlorobenzoic acid	Acetone	Room temperature
AM11_02	MCPBA	3-chlorobenzoic acid	Acetone	4°C
AM11_03	MCPBA	3-chlorobenzoic acid	Chloroform	Room temperature
AM11_04	MCPBA	3-chlorobenzoic acid	Chloroform	4°C
AM11_05	MCPBA	3-chlorobenzoic acid	Diethyl ether	Room temperature
AM11_06	MCPBA	3-chlorobenzoic acid	Diethyl ether	4°C
AM11_07	MCPBA	3-chlorobenzoic acid	Ethyl acetate	Room temperature
AM11_08	MCPBA	3-chlorobenzoic acid	Ethyl acetate	4°C

From the collected XRPD data of the resultant compounds, with the exception of AM11_03 – crystallisation of the two components in chloroform at room temperature – which is amorphous, it can be seen that all samples contain large amounts of 3-chlorobenzoic acid, as would be expected, with the presence of varying amounts of MCPBA. Crystalline MCPBA is present in small quantities in the acetone and chloroform samples but it is present in greater quantities in those samples crystallised from diethyl ether and ethyl acetate (Figure 194).

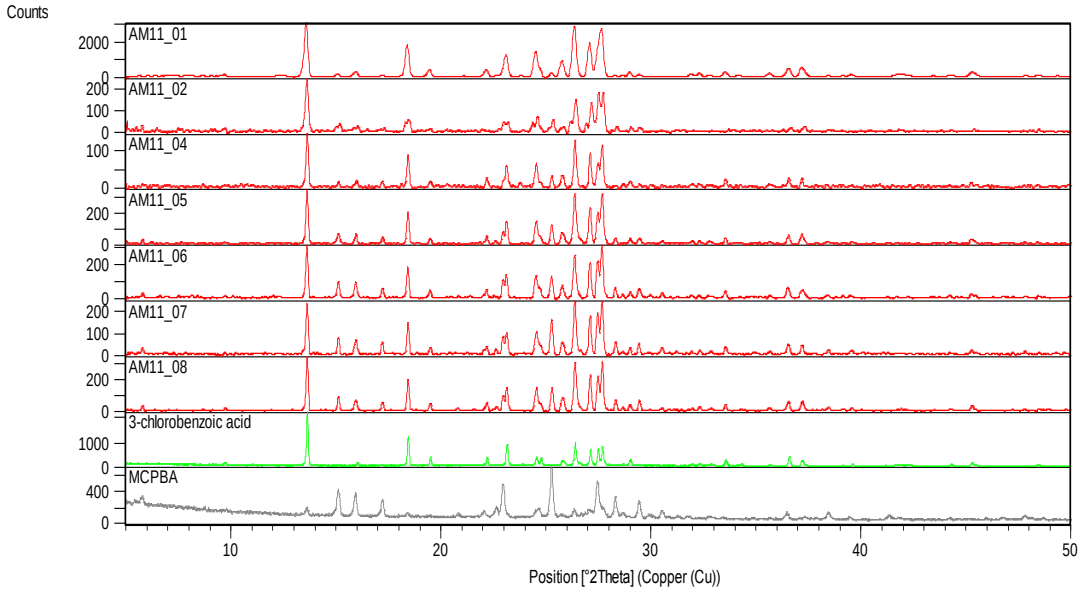

Figure 194 - XRPD patterns of samples crystallised from MCPBA and 3-chlorobenzoic acid (red) compared to the reference patterns of 3-chlorobenzoic acid (green) and MCPBA (grey).

4-Chlorobenzoic acid

Following the series of chlorobenzoic acids, 4-chlorobenzoic acid was cocrystallised under the same conditions with MCPBA (

Table 29).

Table 29 - Crystallisation conditions of MCPBA and 4-chlorobenzoic acid

Sample ID	Component A	Component B	Solvent	Temperature
AM12_01	MCPBA	3-chlorobenzoic acid	Acetone	Room temperature
AM12_02	MCPBA	3-chlorobenzoic acid	Acetone	4°C
AM12_03	MCPBA	3-chlorobenzoic acid	Chloroform	Room temperature
AM12_04	MCPBA	3-chlorobenzoic acid	Chloroform	4°C
AM12_05	MCPBA	3-chlorobenzoic acid	Diethyl ether	Room temperature
AM12_06	MCPBA	3-chlorobenzoic acid	Diethyl ether	4°C
AM12_07	MCPBA	3-chlorobenzoic acid	Ethyl acetate	Room temperature
AM12_08	MCPBA	3-chlorobenzoic acid	Ethyl acetate	4°C

Cocrystallisation with 4-chlorobenzoic acid results in the recrystallisation of the 4-chlorobenzoic acid in all cases, together with the MCPBA decomposition product 3-chlorobenzoic acid, with all scans showing the characteristic 3-chlorobenzoic acid Bragg peak at 13.6° in 2θ (Figure 195). The samples show only trace amounts of MCPBA, while recrystallisation in ethyl acetate at 4°C produced a sample that was significantly more amorphous than the other samples.

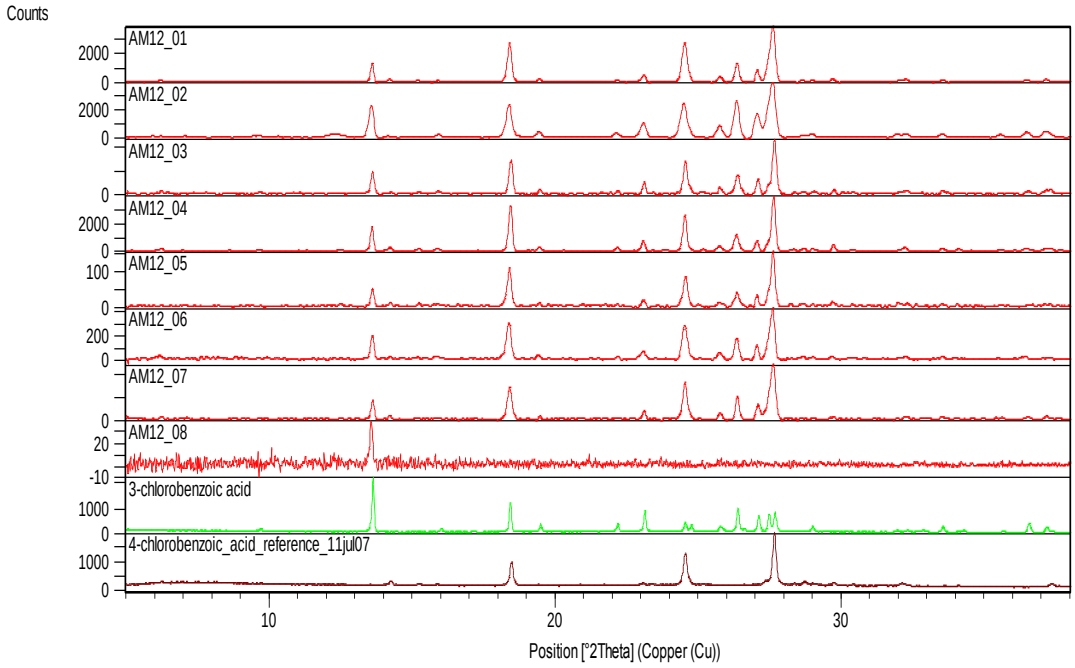

Figure 195 - XRPD patterns of samples crystallised from MCPBA and 4-chlorobenzoic acid (red), compared to the reference patterns of 3-chlorobenzoic acid (green) and 4-chlorobenzoic acid (brown).

None of the chlorobenzoic acids have proven to be effective in cocrystallising with MCPBA to produce a new solid phase material.

1-Naphthaleneacetic acid

As with the peroxyacetic acid experiments, 1-naphthaleneacetic acid was cocrystallised with MCPBA in a 1:1 molar ratio under controlled temperature conditions with selected solvents as outlined in Table 30.

Table 30 - Crystallisation conditions of MCPBA and 1-naphthaleneacetic acid

Sample ID	Component A	Component B	Solvent	Temperature
AM13_01	MCPBA	1-naphthaleneacetic acid	Acetone	Room temperature
AM13_02	MCPBA	1-naphthaleneacetic acid	Acetone	4°C
AM13_03	MCPBA	1-naphthaleneacetic acid	Chloroform	Room temperature
AM13_04	MCPBA	1-naphthaleneacetic acid	Chloroform	4°C
AM13_05	MCPBA	1-naphthaleneacetic acid	Diethyl ether	Room temperature
AM13_06	MCPBA	1-naphthaleneacetic acid	Diethyl ether	4°C
AM13_07	MCPBA	1-naphthaleneacetic acid	Ethyl acetate	Room temperature
AM13_08	MCPBA	1-naphthaleneacetic acid	Ethyl acetate	4°C

All crystallisations analysed with XRPD are shown in Figure 196 with the reference patterns for 3-chlorobenzoic acid and 1-naphthaleneacetic acid for comparison. It is clear that all features in XRPD patterns, which are identical for all crystallisations, are a combination of the powder patterns of the decomposed material, 3-chlorobenzoic acid, and 1-naphthaleneacetic acid. The results suggest complete decomposition of the peroxyacid and conversion to the parent acid and neither MCPBA nor its parent acid has interacted with the 1-naphthaleneacetic acid to form a new crystalline material.

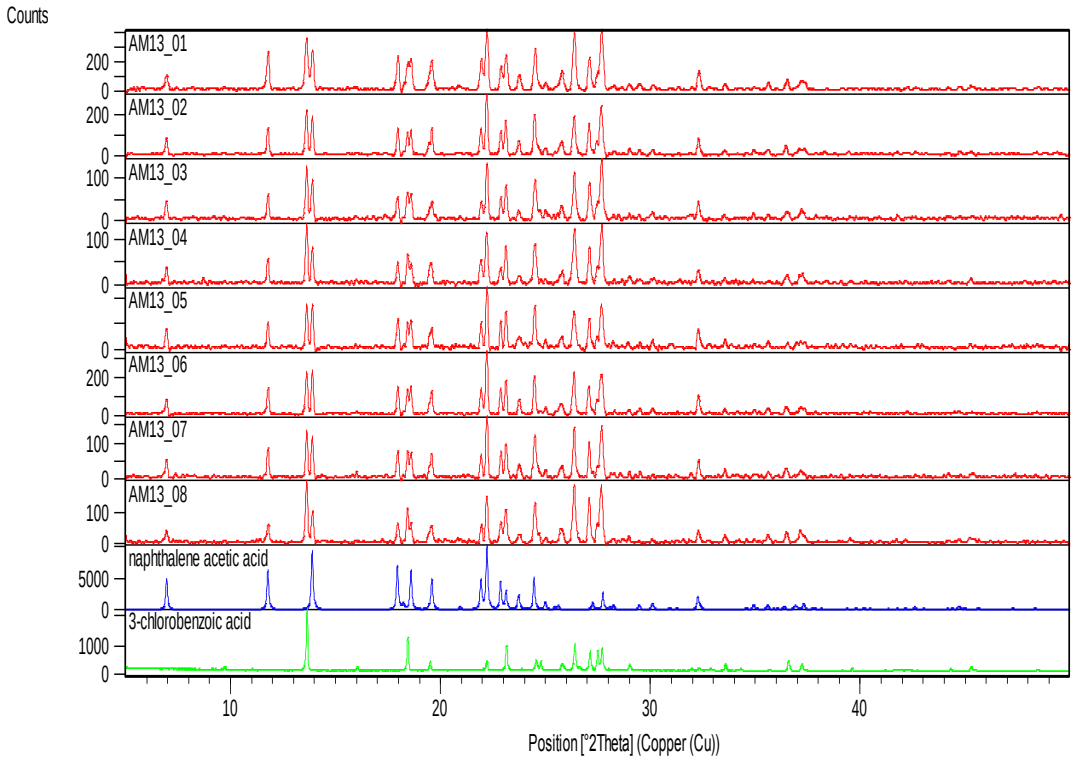

Figure 196 - XRPD patterns of samples crystallised from MCPBA and 1-naphthaleneacetic acid (red), compared to the reference patterns of 1-naphthaleneacetic acid (blue) and 3-chlorobenzoic acid (green).

2-Hydroxybenzoic acid (salicylic acid)

Following the methodology proposed for peroxyacetic acid, salicylic acid was introduced into cocrystallisations with MCPBA in order to take advantage of its hydrogen bond donor and acceptor features. The salicylic acid was dissolved in a 1:1 equimolar ratio with MCPBA, despite its multiple hydrogen bonding capabilities, and crystallised using the same slow evaporative crystallisation technique. The solvent and temperature parameters for these crystallisations are outlined in Table 31.

Table 31 - Crystallisation conditions of MCPBA and 2-hydroxybenzoic acid

Sample ID	Component A	Component B	Solvent	Temperature
AM14_01	MCPBA	2-hydroxybenzoic acid	Acetone	Room temperature
AM14_02	MCPBA	2-hydroxybenzoic acid	Acetone	4°C
AM14_03	MCPBA	2-hydroxybenzoic acid	Chloroform	Room temperature
AM14_04	MCPBA	2-hydroxybenzoic acid	Chloroform	4°C
AM14_05	MCPBA	2-hydroxybenzoic acid	Diethyl ether	Room temperature
AM14_06	MCPBA	2-hydroxybenzoic acid	Diethyl ether	4°C
AM14_07	MCPBA	2-hydroxybenzoic acid	Ethyl acetate	Room temperature
AM14_08	MCPBA	2-hydroxybenzoic acid	Ethyl acetate	4°C

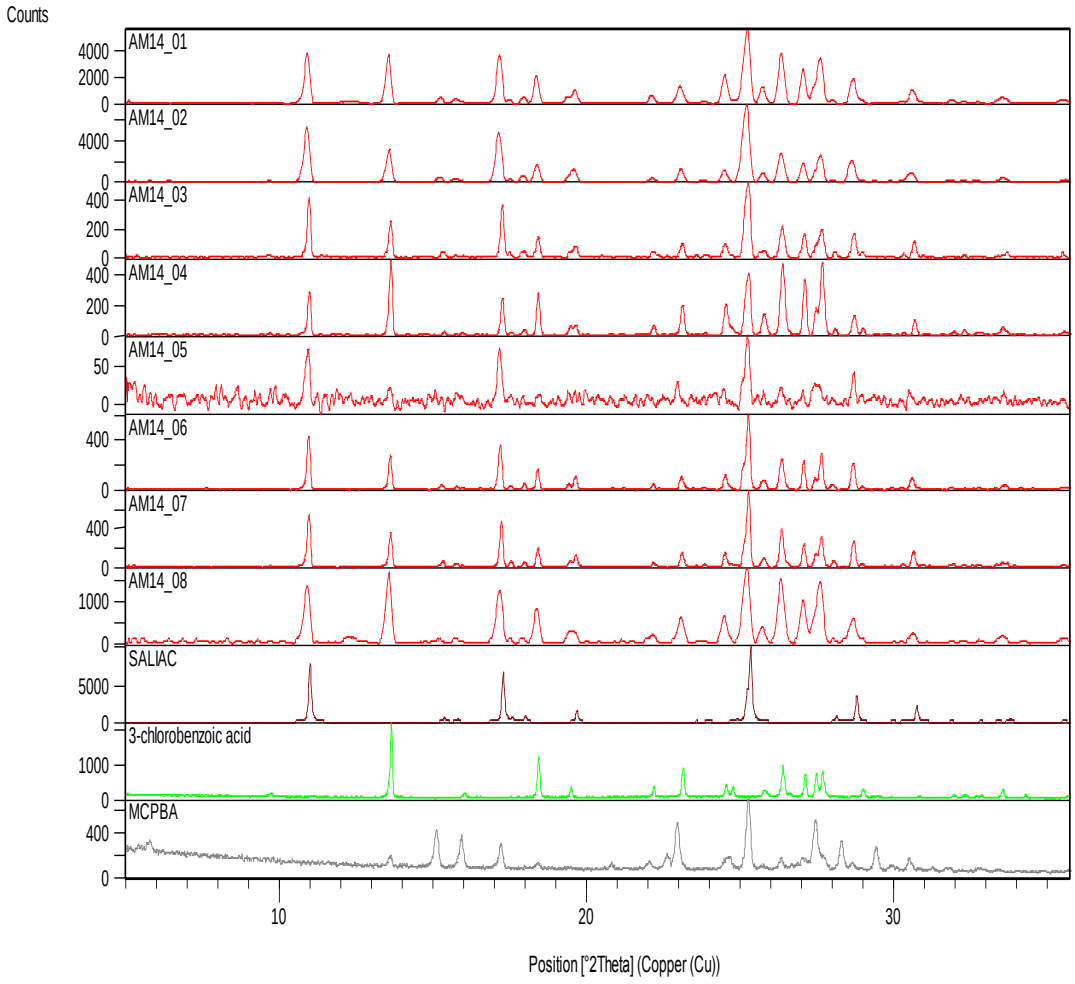

Figure 197 - XRPD patterns of samples crystallised from MCPBA and 2-hydroxybenzoic acid (red), compared to the reference patterns of 2-hydroxybenzoic acid (brown), 3-chlorobenzoic acid (green) and MCPBA (grey).

The collected XRPD patterns of this cocrystallisation screening result in patterns that consist only of a combination of salicylic acid and 3-chlorobenzoic acid (Figure 197). Trace amounts of MCPBA can possibly be found particularly in the region around 15° 2θ, however this area is also characteristic of peaks corresponding to salicylic acid. It is not possible to completely confirm that all MCPBA has been decomposed in the cocrystallisations. The cocrystallisation product from diethyl ether at room temperature is significantly more amorphous than the other samples, with no 3-chlorobenzoic acid present. It is possible in this case that the 3-chlorobenzoic acid did not crystallise in these conditions and is present as an amorphous background.

3-Hydroxybenzoic acid

3-Hydroxybenzoic acid was also crystallised with MCPBA in the same crystallisation solvent and temperature conditions as 2-hydroxybenzoic acid. The crystallisation parameters are outlined in Table 32.

Table 32 - Crystallisation conditions of MCPBA and 3-hydroxybenzoic acid

Sample ID	Component A	Component B	Solvent	Temperature	Analysis group
AM15_01	MCPBA	3-hydroxybenzoic acid	Acetone	Room temperature	A
AM15_02	MCPBA	3-hydroxybenzoic acid	Acetone	4°C	A
AM15_03	MCPBA	3-hydroxybenzoic acid	Chloroform	Room temperature	B
AM15_04	MCPBA	3-hydroxybenzoic acid	Chloroform	4°C	B
AM15_05	MCPBA	3-hydroxybenzoic acid	Diethyl ether	Room temperature	A
AM15_06	MCPBA	3-hydroxybenzoic acid	Diethyl ether	4°C	A
AM15_07	MCPBA	3-hydroxybenzoic acid	Ethyl acetate	Room temperature	A
AM15_08	MCPBA	3-hydroxybenzoic acid	Ethyl acetate	4°C	A

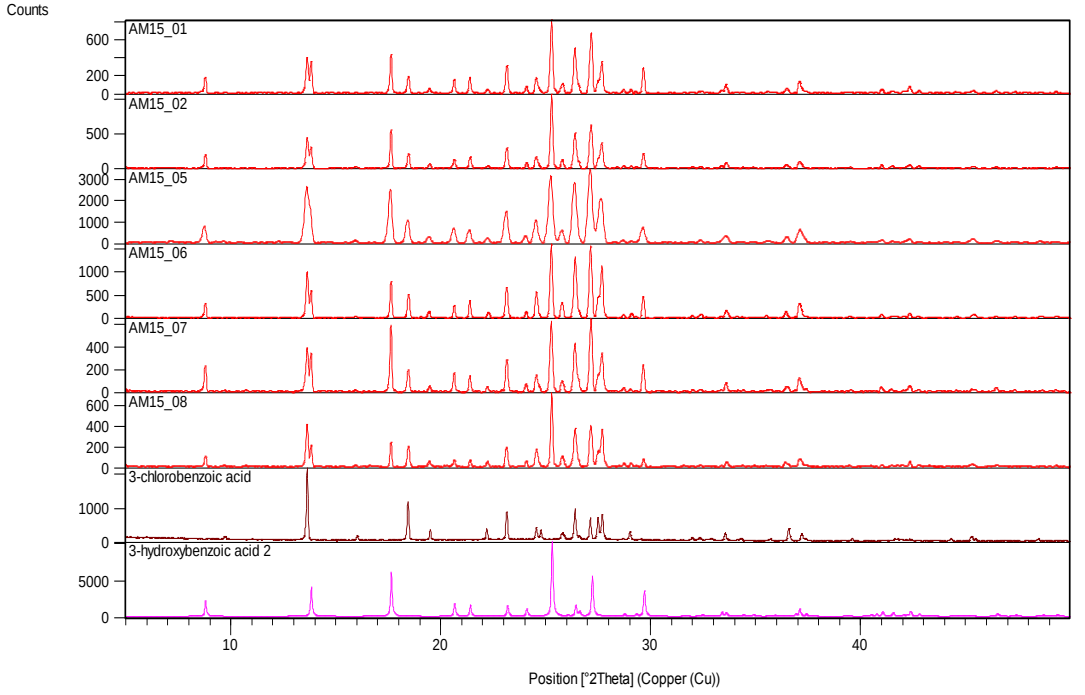

Figure 198 - XRPD patterns of samples crystallised from MCPBA and 3-hydroxybenzoic acid defined as group A (red), compared to the reference powder patterns of 3-chlorobenzoic acid (brown) and 3-hydroxybenzoic acid form II (purple).

The results collected from the XRPD patterns suggest two distinct pattern types, analysis groups A and B. Analysis group A consists of all samples crystallised from acetone, diethyl ether and ethyl acetate. By comparison to the reference patterns (Figure 198), it can be determined that group A corresponds to a mixed component sample containing 3-chlorobenzoic acid and 3-hydroxybenzoic acid form II. No MCPBA is present in the patterns and it can be taken that it has all converted to 3-chlorobenzoic acid.

The remaining samples, crystallised from chloroform at 4°C and room temperature, contain the same mixture of components, but with the additional presence of a large amount of crystalline MCPBA (Figure 199). It appears that with 3-hydroxybenzoic acid in chloroform, MCPBA does not decompose to its parent acid; however there is still no indication of any molecular complex formation, with no new peaks corresponding to unknown crystalline products.

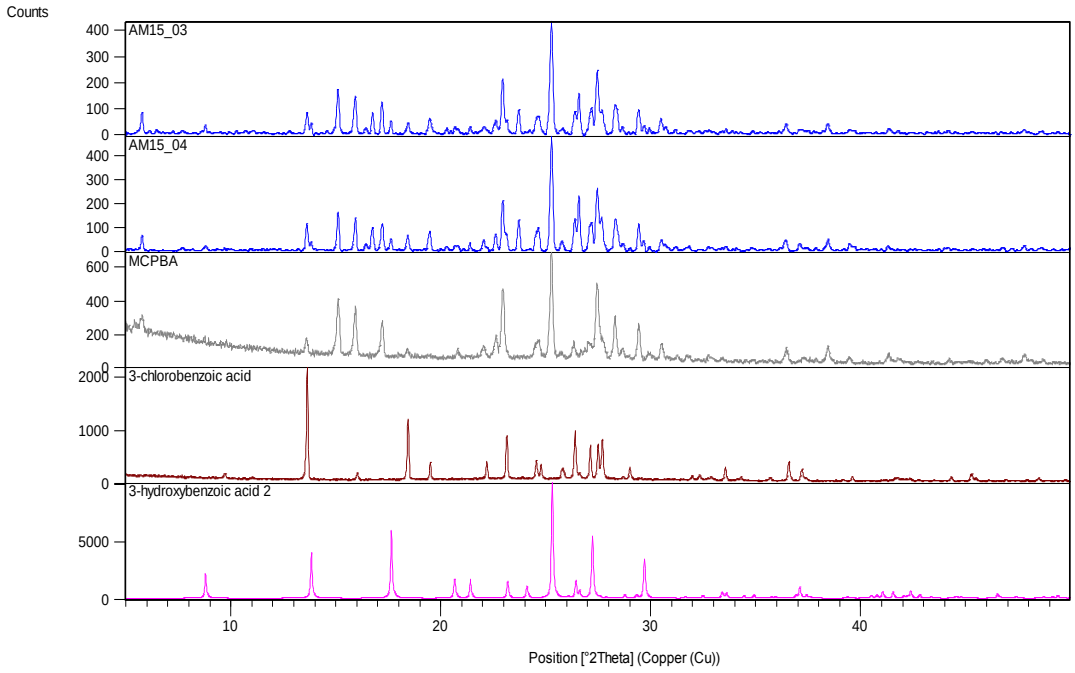

Figure 199 - XRPD patterns of samples crystallised from MCPBA and 3-hydroxybenzoic acid defined as group B (blue), compared to the reference powder patterns of MCPBA (grey), 3-chlorobenzoic acid (brown) and 3-hydroxybenzoic acid form II (purple).

None of the recrystallisation experiments with MCPBA and 3-hydroxybenzoic acid show the presence of Form I of 3-hydroxybenzoic acid.

Malonic Acid

MCPBA was crystallised in a 1:1 molar ratio with malonic acid in order to take advantage of its flexibility of geometry and hydrogen bonding motifs. The crystallisation conditions for these experiments which yielded solid materials suitable for study are outlined in Table 33.

Table 33 - Crystallisation conditions of MCPBA and malonic acid

Sample ID	Component A	Component B	Solvent	Temperature
AM22_01	MCPBA	Malonic acid	Acetone	Room temperature
AM22_02	MCPBA	Malonic acid	Acetone	4°C
AM22_03	MCPBA	Malonic acid	Chloroform	Room temperature
AM22_04	MCPBA	Malonic acid	Chloroform	4°C
AM22_05	MCPBA	Malonic acid	Diethyl ether	Room temperature
AM22_06	MCPBA	Malonic acid	Diethyl ether	4°C
AM22_07	MCPBA	Malonic acid	Ethyl acetate	Room temperature
AM22_08	MCPBA	Malonic acid	Ethyl acetate	4°C

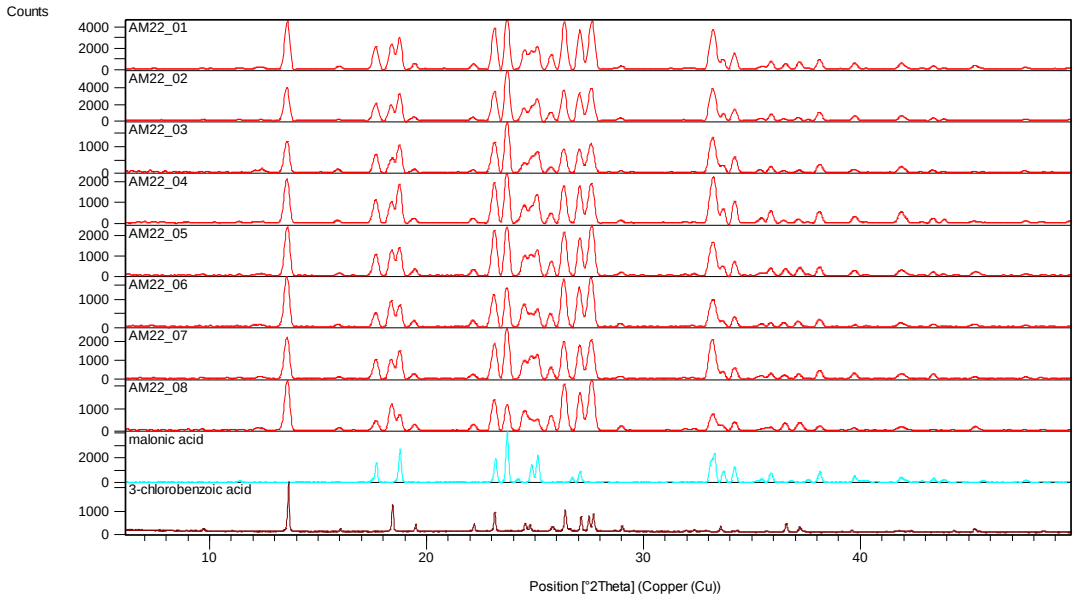

Figure 200 - XRPD patterns of samples crystallised from MCPBA and malonic acid (red), compared to the reference patterns of malonic acid (blue) and 3-chlorobenzoic acid (brown).

All XRPD patterns represent a mixed composition of malonic acid and the parent acid 3-chlorobenzoic acid, from decomposition of MCPBA (Figure 200).

Oxalic Acid

As a natural progression from the use of malonic acid, oxalic acid was cocrystallised with MCPBA under the same crystallisation conditions and parameters, detailed in Table 34.

Table 34 - Crystallisation conditions of MCPBA and oxalic acid

Sample ID	Component A	Component B	Solvent	Temperature
AM23_01	MCPBA	Oxalic acid	Acetone	Room temperature
AM23_02	MCPBA	Oxalic acid	Acetone	4°C
AM23_03	MCPBA	Oxalic acid	Chloroform	Room temperature
AM23_04	MCPBA	Oxalic acid	Chloroform	4°C
AM23_05	MCPBA	Oxalic acid	Diethyl ether	Room temperature
AM23_06	MCPBA	Oxalic acid	Diethyl ether	4°C
AM23_08	MCPBA	Oxalic acid	Ethyl acetate	4°C

The XRPD patterns collected from these crystallisation experiments show presence of primarily oxalic acid dihydrate with smaller amounts of the decomposition product 3-chlorobenzoic acid; no crystalline MCPBA is present. It is worthy of note that the sample

AM23_08, crystallisation from ethyl acetate at 4°C, has produced significantly more crystalline 3-chlorobenzoic acid than oxalic acid dehydrate (Figure 201). Either more decomposition of MCPBA has occurred in these conditions, or the oxalic acid dihydrate does not crystallise well in such an environment. There is no indication of molecular complex formation.

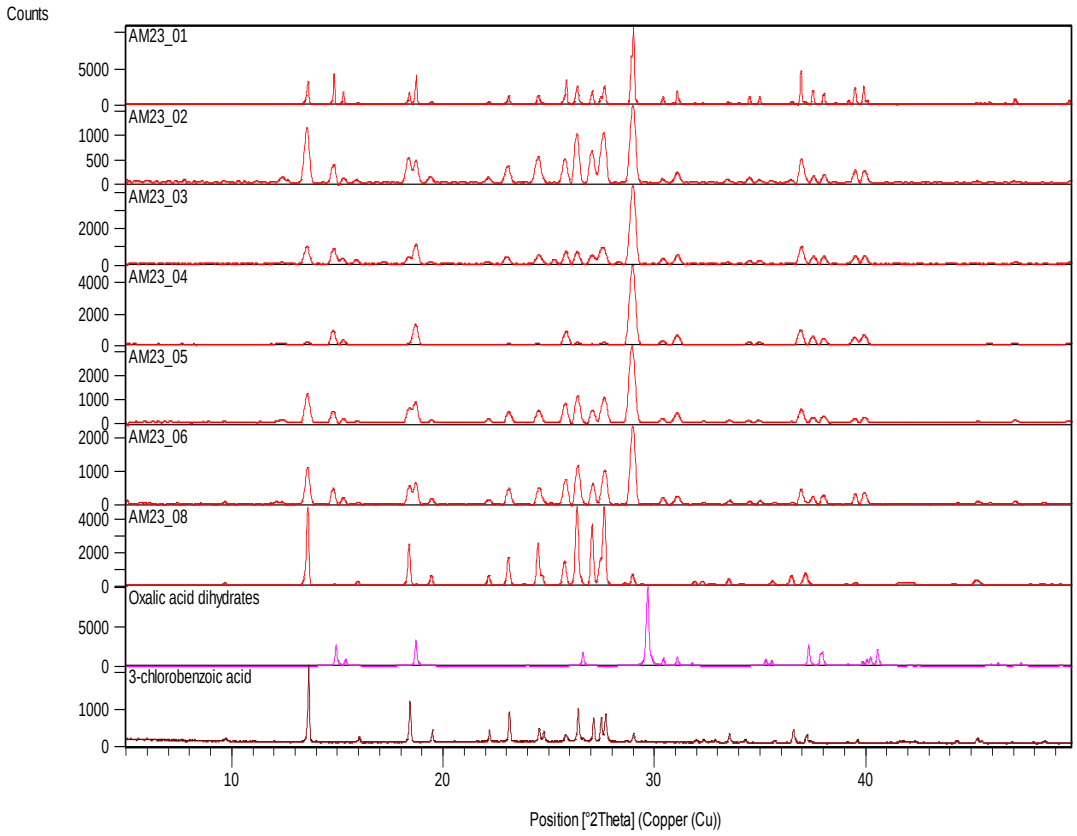

Figure 201 - XRPD patterns of samples crystallised from MCPBA and oxalic acid (red), compared to the reference patterns of oxalic acid dihydrate (purple) and 3-chlorobenzoic acid (brown).

Chloranilic acid

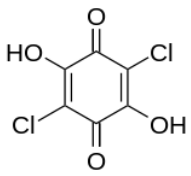

Figure 202 - Chloranilic acid

Although not a carboxylic acid, 2,5-dichloro-3,6-dihydroxybenzoquinone (chloranilic acid) shares many of the characteristics of a carboxylic acid, including a carbonyl and a hydroxyl group in relatively close proximity. It therefore shows complementarities with MCPBA that could possibly be utilised for hydrogen bond interactions. In particular the carbonyl

oxygen, which is deshielded by the aromaticity of the ring, may prove to be more attractive to the peroxy hydrogen, making a hydrogen bond between the two more likely.

Chloranilic acid, despite its two sets of hydrogen bond donors and acceptors, was crystallised in a 1:1 ratio with MCPBA under the solvent and controlled temperature conditions set out in Table 35. Only samples for which the preparation led to materials suitable for powder diffraction have been included.

Table 35 - Crystallisation conditions of MCPBA and chloranilic acid

Sample ID	Component A	Component B	Solvent	Temperature
AM64_01	MCPBA	Chloranilic acid	Acetone	4°C
AM64_02	MCPBA	Chloranilic acid	Acetone	Room temperature
AM64_04	MCPBA	Chloranilic acid	Methyl acetate	Room temperature
AM64_05	MCPBA	Chloranilic acid	Ethyl acetate	4°C
AM64_07	MCPBA	Chloranilic acid	Diethyl ether	4°C

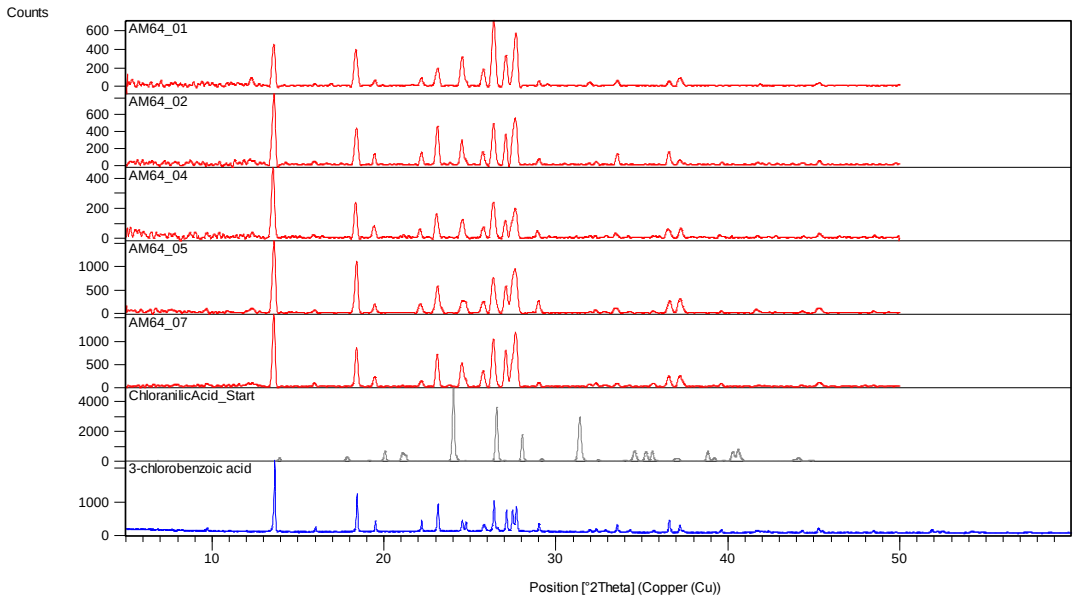

Figure 203 - XRPD patterns of collected materials from the cocrystallisations of MCPBA and chloranilic acid (red) compared with reference patterns of chloranilic acid (grey) and 3-chlorobenzoic acid (blue).

From the XRPD data (Figure 203), all samples contain high amounts of 3-chlorobenzoic acid with no indications of any MCPBA or chloranilic acid present. It is likely that all the MCPBA has decomposed to the parent acid. The lack of crystalline chloranilic acid may suggest a further reaction has taken place as, in general, chloranilic acid crystallises well in many conditions and is usually a reliable co-component for the formation of co-crystals with carboxylic acids.

Bromanilic acid

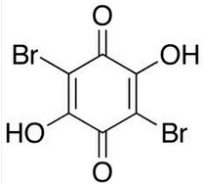

Figure 204 - Bromanilic acid

Complexes of bromanilic acid are typically isostructural to those of chloranilic acid and it can in some cases be substituted as a molecular complex component in a cocrystallisation experiment. It has the same interaction capabilities and was thus used for cocrystallisation with MCPBA in the same conditions as chloranilic acid.

Table 36 - Crystallisation conditions of MCPBA and bromanilic acid

Sample ID	Component A	Component B	Solvent	Temperature
AM65_01	MCPBA	Bromanilic acid	Acetone	4°C
AM65_02	MCPBA	Bromanilic acid	Acetone	Room temperature
AM65_03	MCPBA	Bromanilic acid	Methyl acetate	4°C
AM65_04	MCPBA	Bromanilic acid	Methyl acetate	Room temperature
AM65_05	MCPBA	Bromanilic acid	Ethyl acetate	4°C
AM65_06	MCPBA	Bromanilic acid	Ethyl acetate	Room temperature
AM65_07	MCPBA	Bromanilic acid	Diethyl ether	4°C
AM64_08	MCPBA	Bromanilic acid	Diethyl ether	Room temperature

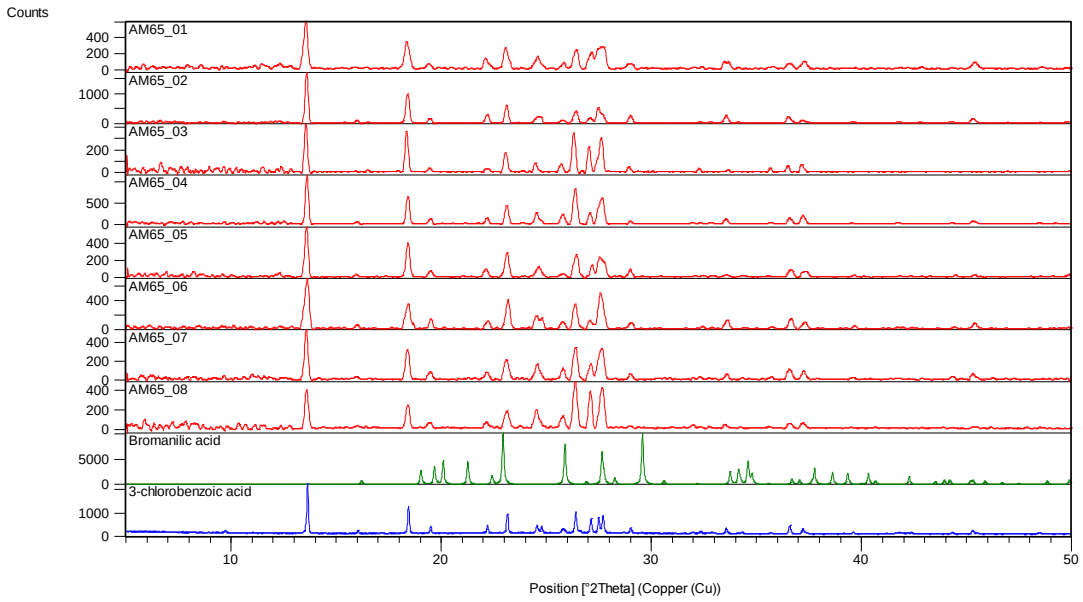

Figure 205 - XRPD patterns of collected materials from the cocrystallisations of MCPBA and bromanilic acid (red) compared with reference patterns of bromanilic acid (green) and 3-chlorobenzoic acid (blue).

As can be seen from the collected XRPD patterns of the materials (Figure 205), there is no indication of any bromanilic acid present in the cocrystallisation products. All the MCPBA has decomposed to the parent 3-chlorobenzoic acid, with no other Bragg peaks present.

5.1.3 6-Phthalimidoperoxyhexanoic acid and carboxylic acids

Following from the MCPBA experiments, the largest target peroxyacid studied, 6-phthalimidoperoxyhexanoic acid (PAP) was subjected to the same cocrystallisation conditions as the other peroxyacids, with the same choices of co-molecules selected. The π-π interacting character of the phthalimido group present in PAP offers additional interaction possibilities to those of the peroxyacid group of the molecule. It is therefore possible that PAP, may take on some of the characteristics of both a π-π stacking molecule those of the other peroxyacids studied. The aliphatic chain separates these two components, and thus they can be targeted for interaction separately. The carboxylic acids cocrystallised with PAP were specifically targeted at the peroxyacid end of the molecule in keeping with the aims of the other two peroxyacid cocrystallisations.

2-Chlorobenzoic acid

PAP was cocrystallised in a 1:1 equimolar ratio with 2-chlorobenzoic acid by the same evaporative crystallisation method as used for the other solid peroxyacid, MCPBA, with the aim to generating molecular complexes through interaction between the peroxyacid functional group and the carboxylic acid. The solvents chosen for crystallisation were methanol, ethanol, acetone and ethyl acetate, solvents in which PAP has demonstrated stability. The crystallisation parameters for each sample are detailed in Table 37.

Table 37 - Crystallisation conditions of PAP and 2-chlorobenzoic acid

Sample ID	Component A	Component B	Solvent	Temperature	Analysis Group
AM26_01	PAP	2-Chlorobenzoic acid	Methanol	4°C	A
AM26_02	PAP	2-Chlorobenzoic acid	Methanol	Room temperature	A
AM26_03	PAP	2-Chlorobenzoic acid	Methanol	30°C	B
AM26_04	PAP	2-Chlorobenzoic acid	Ethanol	4°C	C
AM26_05	PAP	2-Chlorobenzoic acid	Ethanol	Room temperature	D
AM26_06	PAP	2-Chlorobenzoic acid	Ethanol	30°C	D
AM26_07	PAP	2-Chlorobenzoic acid	Acetone	4°C	E
AM26_08	PAP	2-Chlorobenzoic acid	Acetone	Room temperature	E
AM26_09	PAP	2-Chlorobenzoic acid	Acetone	30°C	E
AM26_11	PAP	2-Chlorobenzoic acid	Ethyl Acetate	Room temperature	E
AM26_12	PAP	2-Chlorobenzoic acid	Ethyl Acetate	30°C	E

The collected XRPD patterns of the resultant materials show high amounts of amorphous background leading to difficulty in isolating which compositions of materials are present in each sample. From the powder patterns however, five distinct mixtures have been identified and their composition identified. For convenience these have been grouped, as shown in Table 37, and can be analysed as follows.

Group A consist of two samples crystallised from methanol at 4°C and room temperature, with XRPD patterns shown in Figure 206.

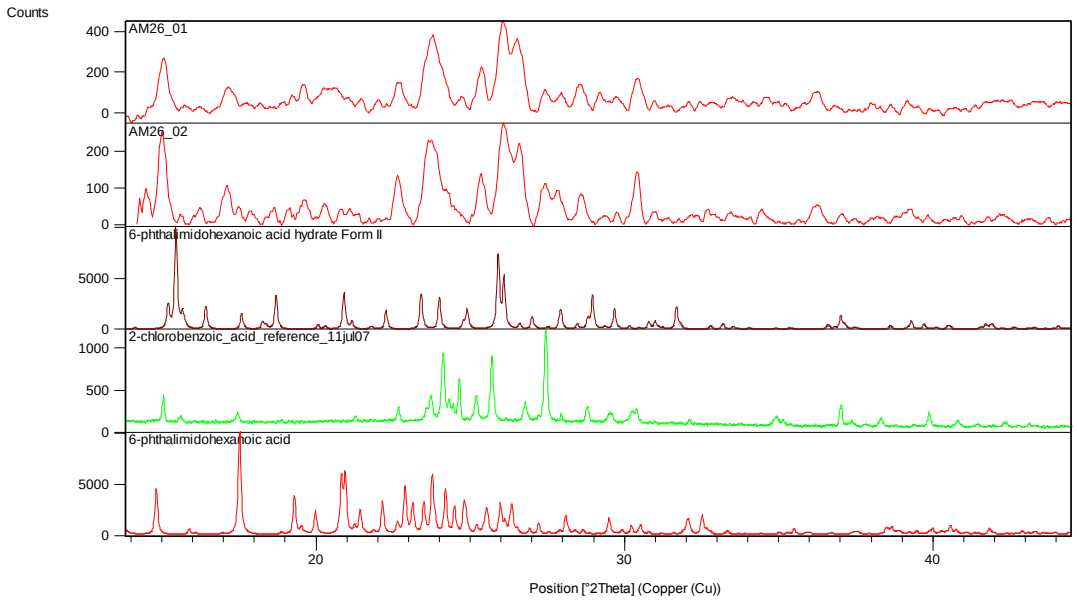

Figure 206 - XRPD patterns of collected materials from the cocrystallisations of PAP and 2-chlorobenzoic acid from analysis group A (red) compared with reference patterns of 6-phthalimidohexanoic acid hydrate Form II (brown), 2-chlorobenzoic acid (green) and 6-phthalimidohexanoic acid (red).

Samples in group A consist of a mixture of the parent acid of PAP, its newly found hydrated form (Form II) and 2-chlorobenzoic acid. The PAP has thus decomposed and has not interacted with the secondary component.

Group B, consists of a single pattern AM26_03, crystallised from methanol at 30°C. Although this is also highly amorphous, it can be identified by XRPD (Figure 207) to consist of a mixture of the Form II hydrate of the parent acid, and PAP itself, with no other crystalline materials present.

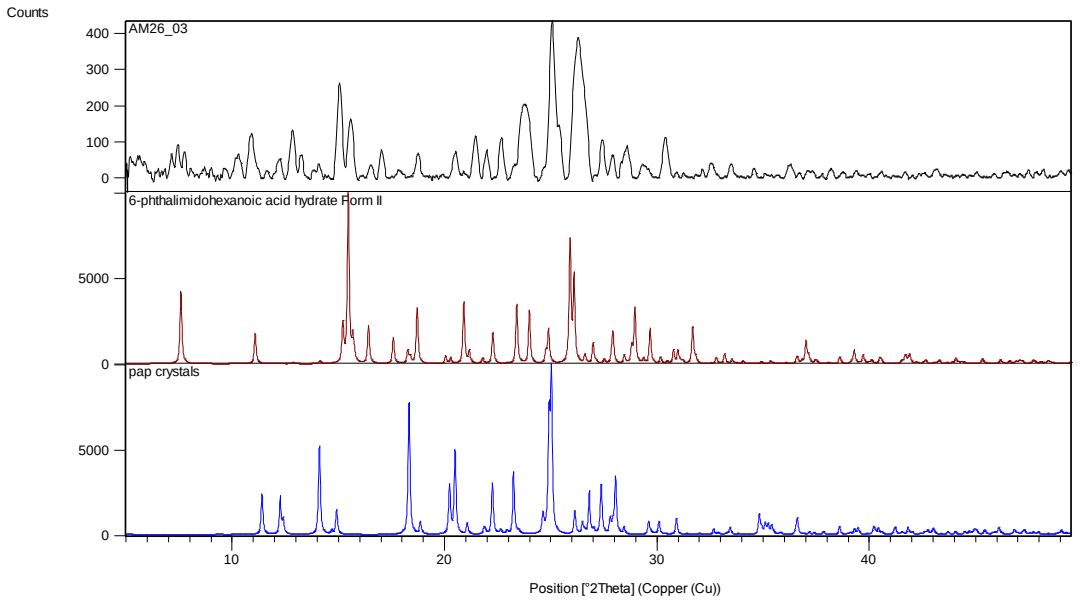

Figure 207 - XRPD patterns of collected materials from the cocrystallisations of PAP and 2-chlorobenzoic acid from analysis group B (black) compared with reference patterns of 6-phthalimidohexanoic acid hydrate Form II (brown) and PAP (blue).

Analysis group C, another single sample, is from the crystallisation from ethanol at 4°C. It consists primarily of the Form II hydrate of decomposed PAP, and 2-chlorobenzoic acid (Figure 208).

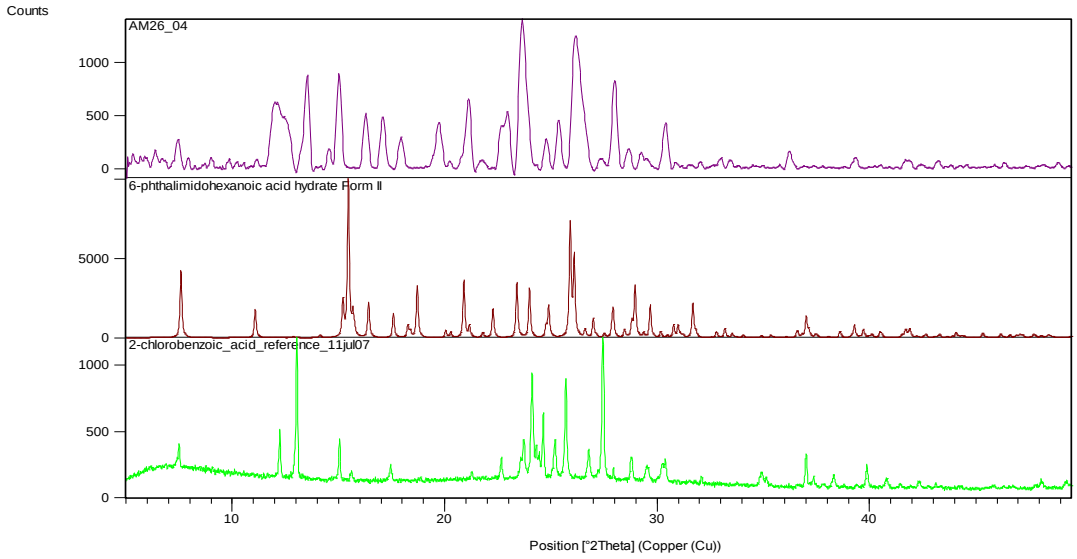

Figure 208 - XRPD patterns of collected materials from the cocrystallisations of PAP and 2-chlorobenzoic acid from analysis group C (purple) compared with reference patterns of 6-phthalimidohexanoic acid hydrate Form II (brown) and 2-chlorobenzoic acid (green).

Group D, representing the samples crystallised from ethanol at room temperature and 30°C, show a similar composition to one another. They both appear to be comprised of a mixture of decomposed PAP – 6-phthalimidohexanoic acid – and Form I of its hydrate

(Figure 209). There appears to be no crystalline 2-chlorobenzoic acid present in these samples.

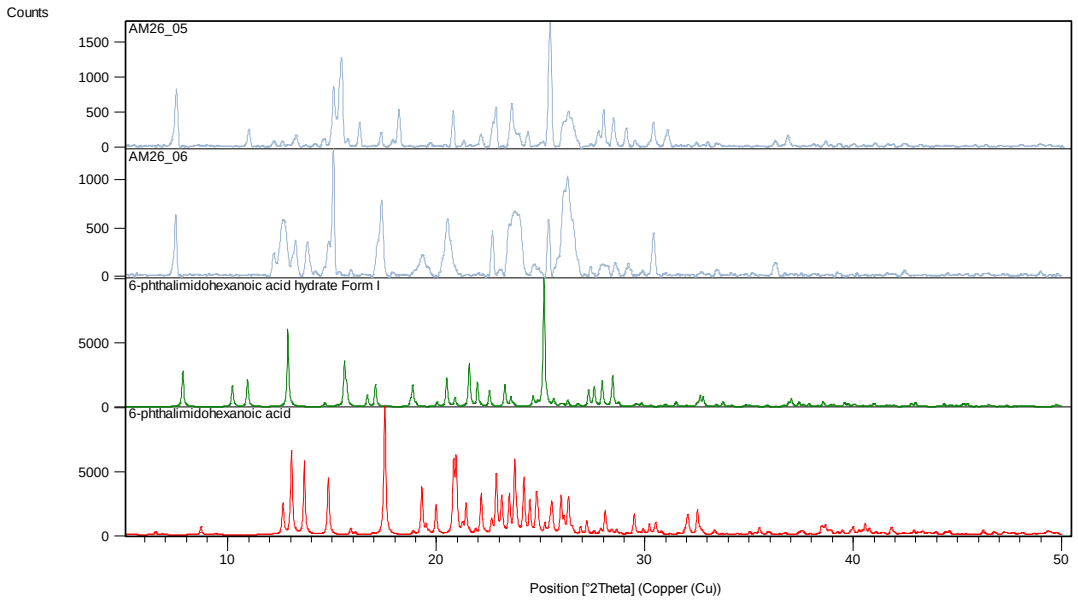

Figure 209 - XRPD patterns of collected materials from the cocrystallisations of PAP and 2-chlorobenzoic acid from analysis group D (violet) compared with reference patterns of 6-phthalimidohexanoic acid hydrate Form I (green) and 6-phthalimidohexanoic acid (red).

Finally the remaining samples, all from acetone and ethyl acetate solution, are show clearly by XRPD to be comprised entirely of recrystallised PAP peroxyacid and 2-chlorobenzoic acid (Figure 210). Although the PAP has been retained in these crystallisations, there is no indication of the formaionof a molecular complex.

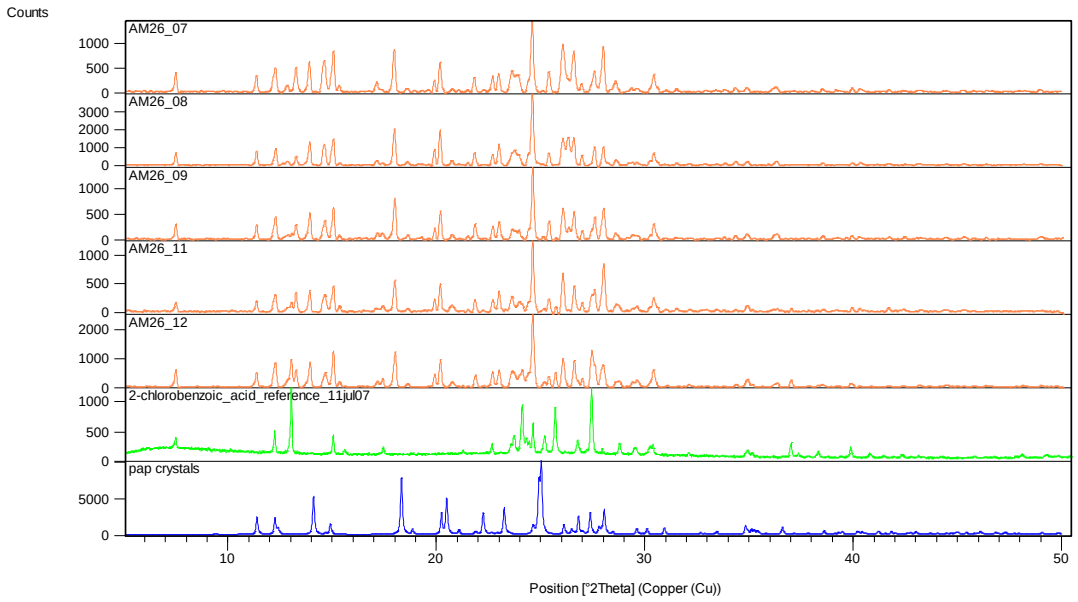

Figure 210 - XRPD patterns of collected materials from the cocrystallisations of PAP and 2-chlorobenzoic acid from analysis group E (violet) compared with reference patterns of 2-chlorobenzoic acid (green) and PAP (blue).

3-Chlorobenzoic acid

3-chlorobenzoic acid was crystallised with PAP under the same conditions as for as 2-chlorobenzoic acid (Table 38).

Table 38 - Crystallisation conditions of PAP and 3-chlorobenzoic acid

Sample ID	Component A	Component B	Solvent	Temperature	Analysis Group
AM25_01	PAP	3-Chlorobenzoic acid	Methanol	4°C	A
AM25_02	PAP	3-Chlorobenzoic acid	Methanol	Room temperature	amorphous
AM25_03	PAP	3-Chlorobenzoic acid	Methanol	30°C	A
AM25_05	PAP	3-Chlorobenzoic acid	Ethanol	Room temperature	A
AM25_06	PAP	3-Chlorobenzoic acid	Ethanol	30°C	A
AM25_07	PAP	3-Chlorobenzoic acid	Acetone	4°C	A
AM25_08	PAP	3-Chlorobenzoic acid	Acetone	Room temperature	A
AM25_09	PAP	3-Chlorobenzoic acid	Acetone	30°C	A
AM25_10	PAP	3-Chlorobenzoic acid	Ethyl Acetate	4°C	A
AM25_11	PAP	3-Chlorobenzoic acid	Ethyl Acetate	Room temperature	A
AM25_12	PAP	3-Chlorobenzoic acid	Ethyl Acetate	30°C	A

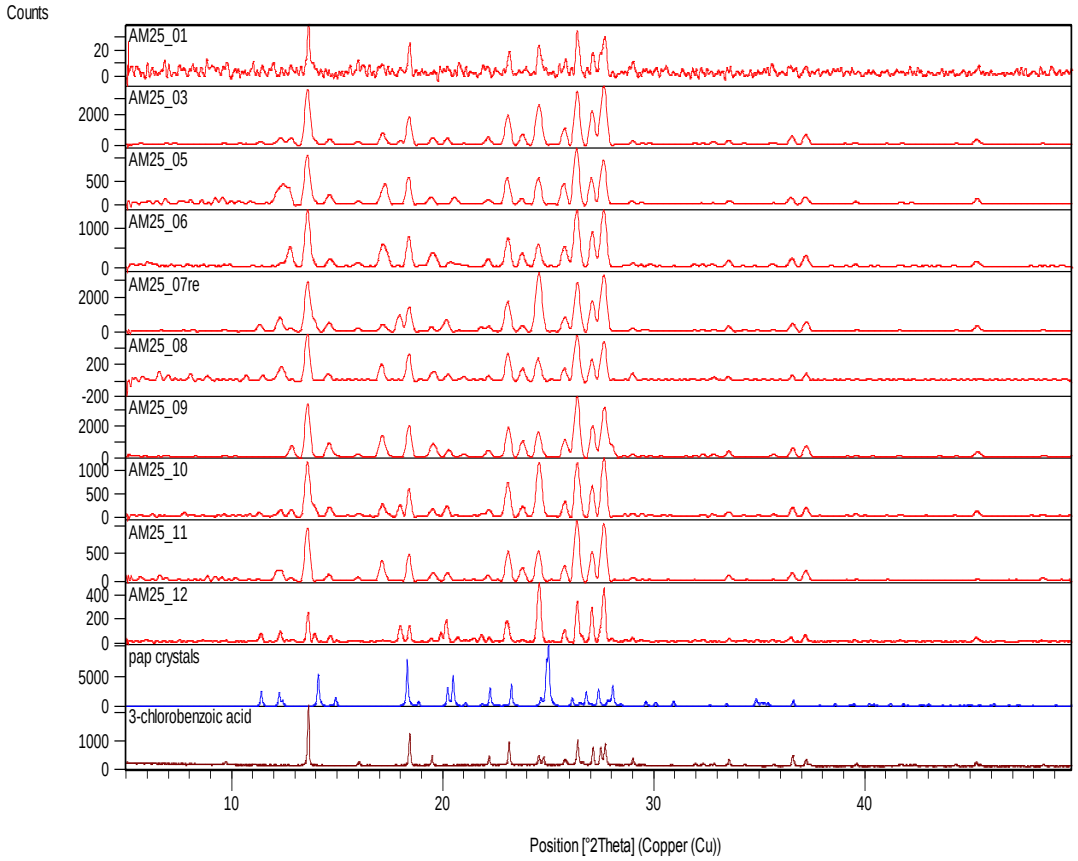

Figure 211 - XRPD patterns of collected materials from the cocrystallisations of PAP and 3-chlorobenzoic acid (red) compared with reference patterns of 6-phthalimidoperoxyhexanoic acid - PAP (blue) and 3-chlorobenzoic acid (brown).

The resulting samples were analysed by XRPD (Figure 211) and, with the exception of the sample from methanol at room temperature which appears to be completely amorphous,

all appear to be comprised of recrystallised 6-phthalimidoperoxyhexanoic acid and 3-chlorobenzoic acid only. There are no indications of any other materials present.

4-Chlorobenzoic acid

4-chlorobenzoic acid was cocrystallised with PAP under the same conditions. From the XRPD analysis of the collected materials, they can be categorised into three groups as defined by their analysis group in Table 39.

Table 39 - Crystallisation conditions of PAP and 4-chlorobenzoic acid

Sample ID	Component A	Component B	Solvent	Temperature	Analysis Group
AM27_01	PAP	4-Chlorobenzoic acid	Methanol	4°C	A
AM27_02	PAP	4-Chlorobenzoic acid	Methanol	Room temperature	A
AM27_03	PAP	4-Chlorobenzoic acid	Methanol	30°C	B
AM27_04	PAP	4-Chlorobenzoic acid	Ethanol	4°C	C
AM27_05	PAP	4-Chlorobenzoic acid	Ethanol	Room temperature	B
AM27_06	PAP	4-Chlorobenzoic acid	Ethanol	30°C	B
AM27_07	PAP	4-Chlorobenzoic acid	Acetone	4°C	C
AM27_08	PAP	4-Chlorobenzoic acid	Acetone	Room temperature	B
AM27_10	PAP	4-Chlorobenzoic acid	Ethyl Acetate	4°C	B
AM27_11	PAP	4-Chlorobenzoic acid	Ethyl Acetate	Room temperature	B
AM27_12	PAP	4-Chlorobenzoic acid	Ethyl Acetate	30°C	B

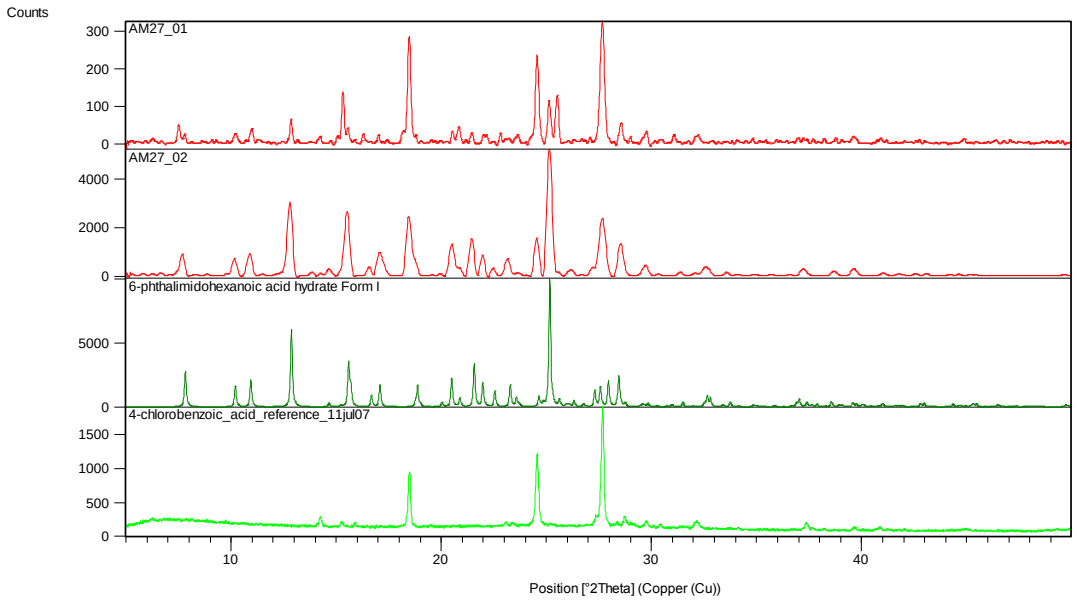

Figure 212 – XRPD patterns of collected materials from the cocrystallisations of PAP and 4-chlorobenzoic acid from analysis group A (red) compared with reference patterns of 4-chlorobenzoic acid (green) and 6-phthalimidohexanoic acid monohydrate Form I (dark green)

Analysis group A, samples AM27_01 and AM27_02, crystallised from methanol consist of a combination of crystalline 4-chlorobenzoic acid and 6-phthalimidohexanoic acid monohydrate Form I (Figure 212). It is worth noting that Form II was also found, from analysis of single crystals extracted from AM27_01, however they are not representative of the bulk of the sample.

Group B, as defined in Table 39, contains the majority of samples in the screening. From comparison of the XRPD data with reference patterns, these samples consist of a mixture of 4-chlorobenzoic acid and 6-phthalimidohexanoic acid only (Figure 213).

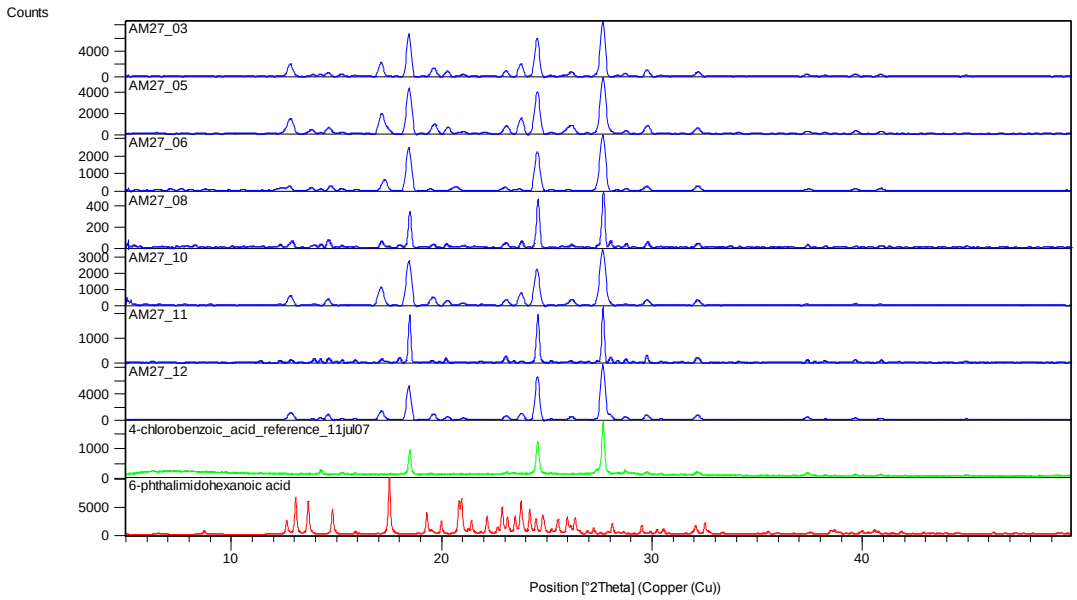

Figure 213 – XRPD patterns of collected materials from the cocrystallisations of PAP and 4-chlorobenzoic acid from analysis group B (blue) compared with reference pattern of 4-chlorobenzoic acid (green) and 6-phthalimidohexanoic acid (red).

The final two samples, defined as group C, crystallisations in ethanol and acetone at 4°C can be seen from the XRPD data (Figure 214) to be recrystallised 4-chlorobenzoic acid only.

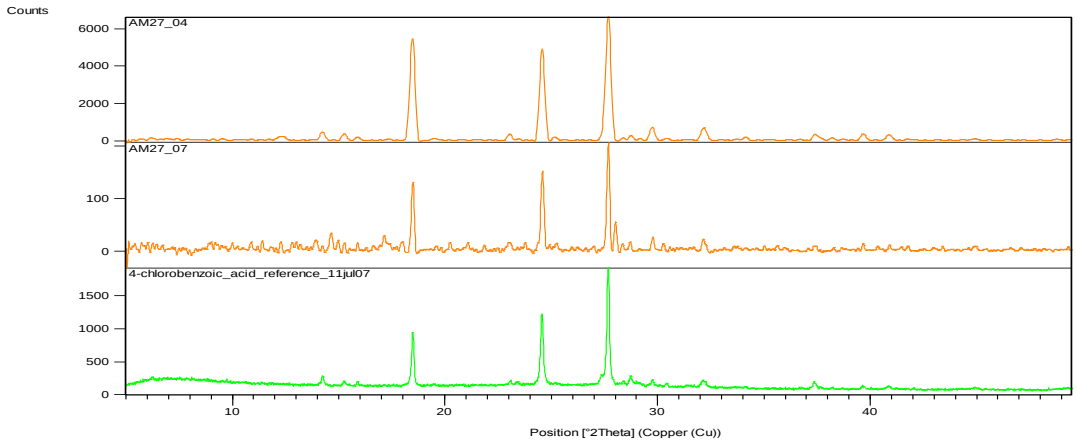

Figure 214 - XRPD patterns of collected materials from the cocrystallisations of PAP and 4-chlorobenzoic acid from analysis group C (orange) compared with reference patterns of 4-chlorobenzoic acid (green) and 6-phthalimidohexanoic acid monohydrate Form I (dark green).

1-Naphthaleneacetic acid

PAP and 1-naphthaleneacetic acid have similar sized π conjugated systems as well as the peroxyacid and carboxylic acid similarities previously discussed. Being closer in size and

features to PAP, there may be more likelihood of 1-naphthaleneacetic acid producing a molecular complex. The crystallisation conditions chosen for the 1:1 equimolar cocrystallisations are outlined in Table 40.

Table 40 - Crystallisation conditions of PAP and 1-naphthaleneacetic acid

Sample ID	Component A	Component B	Solvent	Temperature
AM28_01	PAP	1-Naphthaleneacetic acid	Methanol	4°C
AM28_03	PAP	1-Naphthaleneacetic acid	Methanol	30°C
AM28_04	PAP	1-Naphthaleneacetic acid	Ethanol	4°C
AM28_05	PAP	1-Naphthaleneacetic acid	Ethanol	Room temperature
AM28_06	PAP	1-Naphthaleneacetic acid	Ethanol	30°C
AM28_07	PAP	1-Naphthaleneacetic acid	Acetone	4°C
AM28_08	PAP	1-Naphthaleneacetic acid	Acetone	Room temperature
AM28_08	PAP	1-Naphthaleneacetic acid	Acetone	30°C
AM28_10	PAP	1-Naphthaleneacetic acid	Ethyl Acetate	4°C
AM28_11	PAP	1-Naphthaleneacetic acid	Ethyl Acetate	Room temperature
AM28_12	PAP	1-Naphthaleneacetic acid	Ethyl Acetate	30°C
AM28_13	PAP	1-Naphthaleneacetic acid	Diethyl Ether	4°C
AM28_14	PAP	1-Naphthaleneacetic acid	Diethyl Ether	Room temperature
AM28_15	PAP	1-Naphthaleneacetic acid	Diethyl Ether	30°C

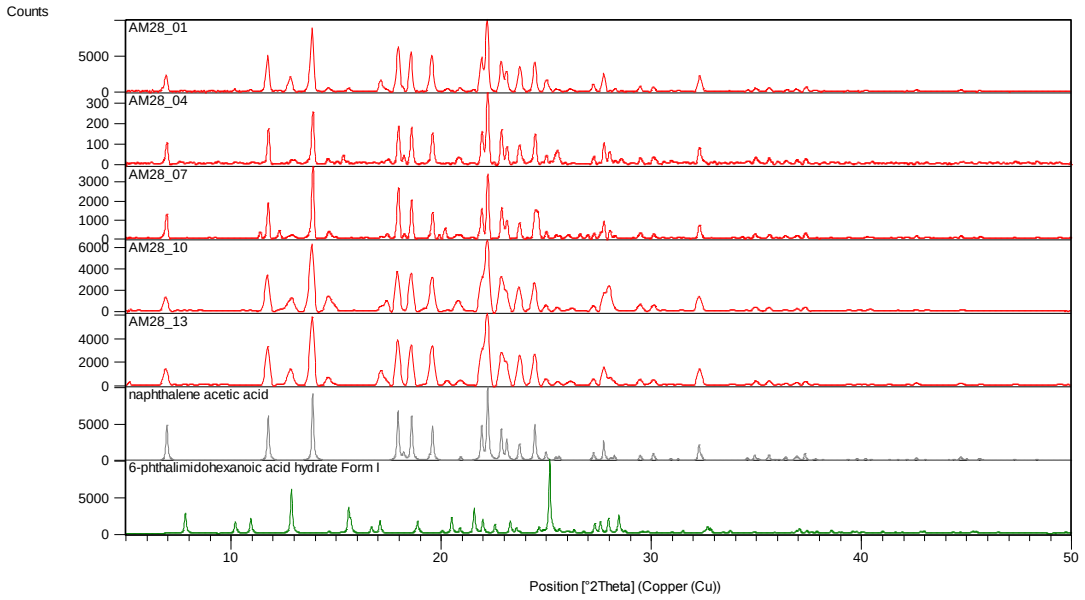

Figure 215 - XRPD patterns of collected materials from each solvent in the cocrystallisations of PAP and 1-naphthaleneacetic acid compared with reference patterns of 1-naphthaleneacetic acid (grey) and 6-phthalimidohexanoic acid monohydrate Form I (dark green)

From the collected XRPD data, it can be seen that all samples have created a mixed material of similar compositions containing only 1-naphthaleneacetic acid crystals and decomposed PAP in the form of its monohydrate (Form I) (Figure 215). A representative sample from each solvent environment is shown. Some small traces of PAP may be present in some of the samples by indication of the most intense Bragg peaks; however with such a

high background, most of which is removed in processing along with the hidden signal, it cannot be verified.

2-Hydroxybenzoic acid (Salicylic acid)

PAP was also crystallised with salicylic acid under the conditions outlined in Table 41, with a 1:1 molar ratio of peroxyacid to carboxylic acid. As with the other peroxyacids, it is possible that the additional hydrogen bond donor might aid in the formation of motifs creating a molecular complex with the peroxyacid functional group. However, with the additional carbonyls present in the phthalimido group of PAP providing two additional hydrogen bond acceptors, an interaction could also be generated at the other end of the molecule.

Table 41 - Crystallisation conditions of PAP and salicylic acid

Sample ID	Component A	Component B	Solvent	Temperature
AM29_01	PAP	2-Hydroxybenzoic acid	Methanol	4°C
AM29_02	PAP	2-Hydroxybenzoic acid	Methanol	Room Temperature
AM29_03	PAP	2-Hydroxybenzoic acid	Methanol	30°C
AM29_04	PAP	2-Hydroxybenzoic acid	Ethanol	4°C
AM29_05	PAP	2-Hydroxybenzoic acid	Ethanol	Room temperature
AM29_06	PAP	2-Hydroxybenzoic acid	Ethanol	30°C
AM29_07	PAP	2-Hydroxybenzoic acid	Acetone	4°C
AM29_08	PAP	2-Hydroxybenzoic acid	Acetone	Room temperature
AM29_08	PAP	2-Hydroxybenzoic acid	Acetone	30°C
AM29_10	PAP	2-Hydroxybenzoic acid	Ethyl Acetate	4°C
AM29_11	PAP	2-Hydroxybenzoic acid	Ethyl Acetate	Room temperature
AM29_12	PAP	2-Hydroxybenzoic acid	Ethyl Acetate	30°C
AM29_13	PAP	2-Hydroxybenzoic acid	Diethyl Ether	4°C
AM29_14	PAP	2-Hydroxybenzoic acid	Diethyl Ether	Room temperature
AM29_15	PAP	2-Hydroxybenzoic acid	Diethyl Ether	30°C

The PAP has again decomposed and recrystallised as the hydrated parent acid (Form I), as shown by XRPD comparison to the reference patterns of the starting material and the decomposed PAP products (Figure 216). From analysis of the pattern profiles, there appears to be little or no PAP remaining in any samples.

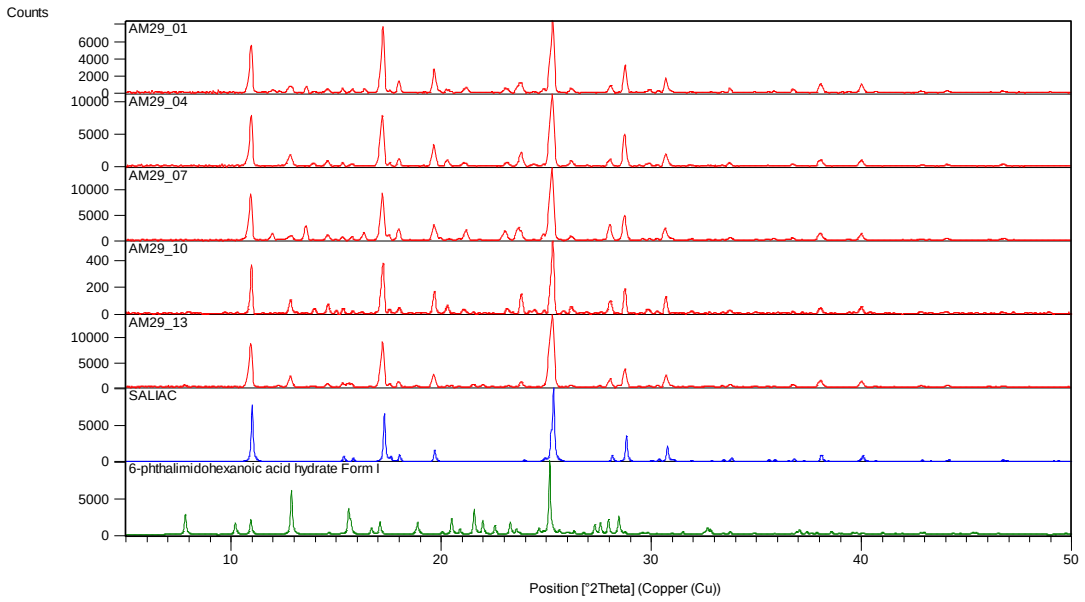

Figure 216 - XRPD patterns of selected materials from the cocrystallisations of PAP and salicylic acid (red) compared with reference patterns of salicylic acid (blue) and 6-phthalimidohexanoic acid monohydrate Form I (dark green).

3-Hydroxybenzoic acid

PAP was also cocrystallised with the salicylic acid isomer 3-hydroxybenzoic acid. As with MCPBA, it is expected that the two hydrogen bond donors are fully available for interaction with the acceptors of the peroxyacid. 3-hydroxybenzoic acid was cocrystallised with PAP in a 1:1 equimolar ratio with crystallisation environments as shown in Table 42.

From the collected XRPD data of the resulting materials, the patterns can be categorised into 4 distinct analysis groups, as defined in the table. The contents of each group are discussed below.

Table 42 - Crystallisation conditions of PAP and 3-hydroxybenzoic acid

Sample ID	Component A	Component B	Solvent	Temperature	Analysis Group
AM30_01	PAP	3-Hydroxybenzoic acid	Methanol	4°C	A
AM30_02	PAP	3-Hydroxybenzoic acid	Methanol	Room Temperature	B
AM30_03	PAP	3-Hydroxybenzoic acid	Methanol	30°C	C
AM30_04	PAP	3-Hydroxybenzoic acid	Ethanol	4°C	B
AM30_05	PAP	3-Hydroxybenzoic acid	Ethanol	Room temperature	B
AM30_06	PAP	3-Hydroxybenzoic acid	Ethanol	30°C	C
AM30_07	PAP	3-Hydroxybenzoic acid	Acetone	4°C	D
AM30_08	PAP	3-Hydroxybenzoic acid	Acetone	Room temperature	C
AM30_09	PAP	3-Hydroxybenzoic acid	Acetone	30°C	D
AM30_10	PAP	3-Hydroxybenzoic acid	Ethyl Acetate	4°C	A
AM30_11	PAP	3-Hydroxybenzoic acid	Ethyl Acetate	Room temperature	A
AM30_12	PAP	3-Hydroxybenzoic acid	Ethyl Acetate	30°C	A
AM30_13	PAP	3-Hydroxybenzoic acid	Diethyl Ether	4°C	A
AM30_14	PAP	3-Hydroxybenzoic acid	Diethyl Ether	Room temperature	A
AM30_15	PAP	3-Hydroxybenzoic acid	Diethyl Ether	30°C	A

The samples in group A, primarily samples from ethyl acetate and diethyl ether, but also methanol at 4°C, contain recrystallised form II of 3-hydroxybenzoic acid and recrystallised PAP. There is no indication of molecular complex formation in the XRPD patterns (Figure 217).

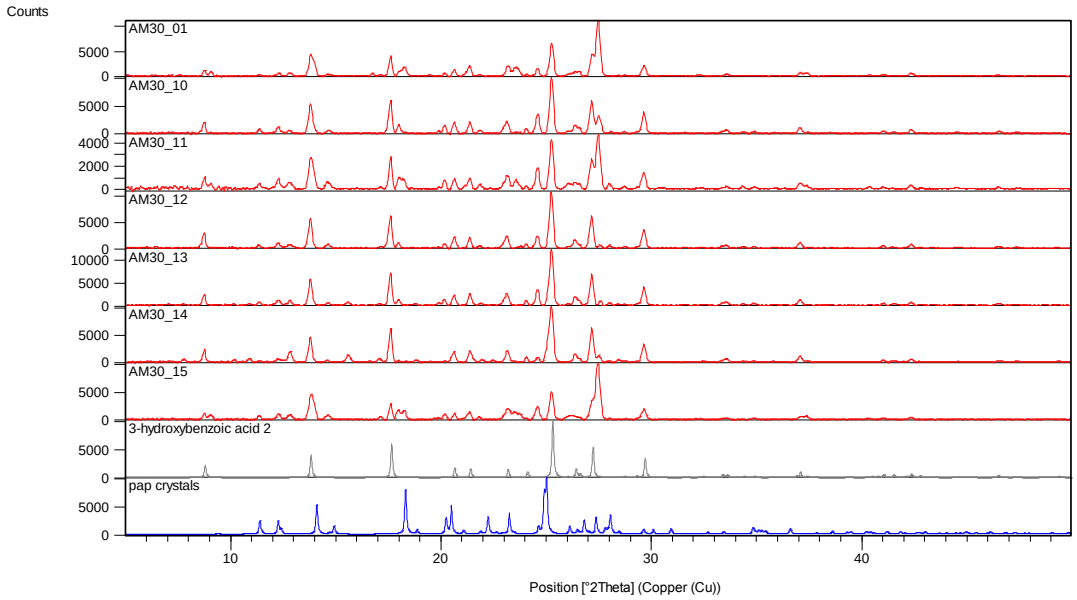

Figure 217 – XRPD patterns of collected materials from the cocrystallisations of PAP and 3-hydroxybenzoic acid from analysis group A (red) compared with reference patterns of 3-hydroxybenzoic acid Form II (grey) and PAP (blue).

Group B, indicated in orange, crystallised from methanol at room temperature and ethanol at 4°C and room temperature is represented by the XRPD patterns in Figure 218. The products peaks can be attributed to the presence of both polymorphs of 3-hydroxybenzoic acid, as well as recrystallised PAP. Again, however, all peaks can be assigned and no new crystalline complexes have been formed.

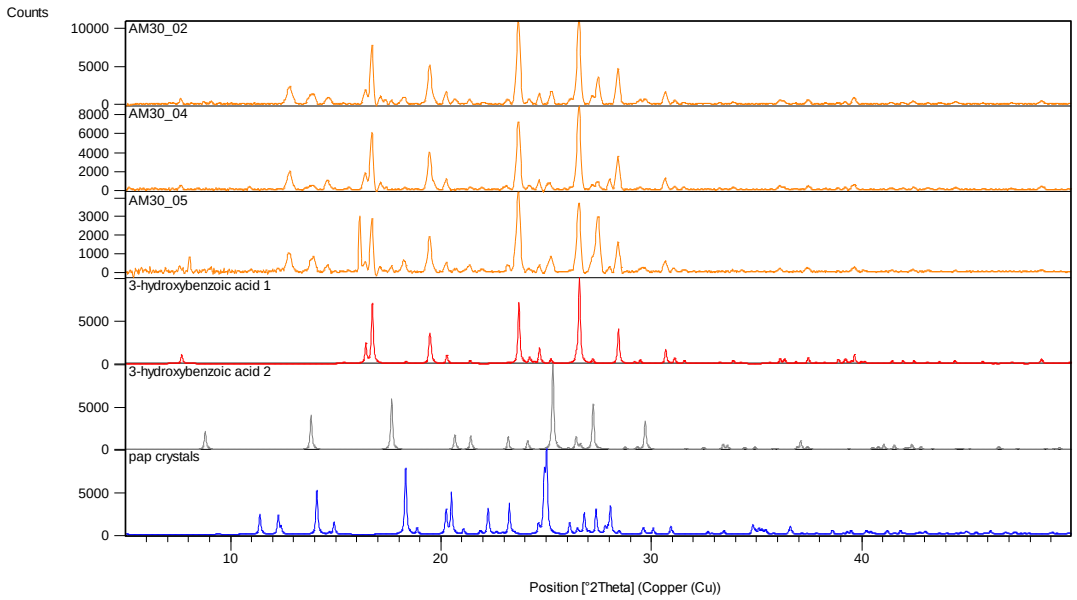

Figure 218 – XRPD patterns of collected materials from the cocrystallisations of PAP and 3-hydroxybenzoic acid from analysis group B (orange) compared with reference patterns of 3-hydroxybenzoic acid Form I (red), 3-hydroxybenzoic acid form II (grey) and PAP (blue).

The cocrystallisation products identified as analysis group C, from methanol and ethanol solutions at 30°C, and also acetone at room temperature, have a high degree of amorphous content and only weak XRPD scans could be obtained. After removal of the large background, few features remain, and caution is required in their interpretation. The smaller of the peaks observed in these samples appear to correspond to the strongest peaks of 3-hydroxybenzoic acid form II and recrystallised PAP. The major feature in these three scans, however, is the high intensity peak at 27.5° in 2θ (Figure 219). Aside from a large preferred orientation peak arising from 3-hydroxybenzoic acid form II, there are no known materials from the decomposition of PAP or the crystallisation of 3-hydroxybenzoic acid that would explain the presence of this very large peak in relation to the intensities of the other components present. Further analysis would be required to determine the origin of this significant peak.

The final two samples, group D (purple), contain the same combination of materials as group C, but with different proportions of the crystalline materials 3-hydroxybenzoic acid form II and PAP. They also contain the anomalous peak at 27.5° in 2θ (Figure 220), but it is less prominent in group D, possibly as this material is more crystalline or there is a lesser content of the unknown component attributed to this peak. The similarity with group C products is consistent with the fact that both sets of samples are crystallised from acetone.

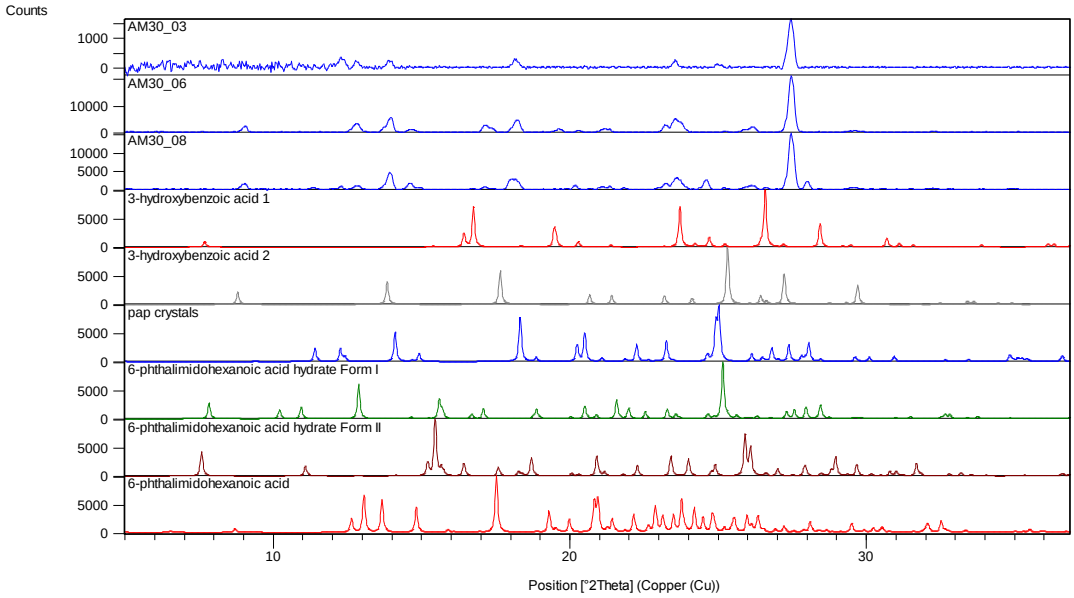

Figure 219 - XRPD patterns of collected materials from the cocrystallisations of PAP and 3-hydroxybenzoic acid from analysis group C (blue) compared with reference patterns of all known crystal forms of the starting materials and their known decomposition products.

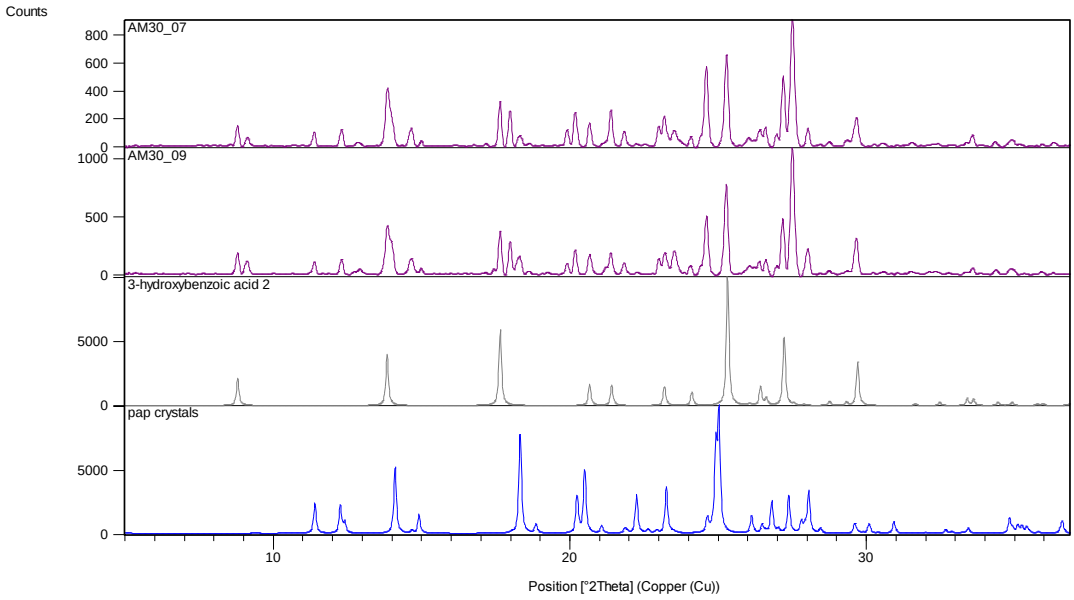

Figure 220 - XRPD patterns of collected materials from the cocrystallisations of PAP and 3-hydroxybenzoic acid from analysis group D (purple) compared with reference patterns 3-hydroxybenzoic acid form II (grey) and PAP (blue).

Malonic acid

PAP was also cocrystallised in a 1:1 molar ratio with malonic acid from acetone at 4°C and room temperature (AM38_14 and AM38_15) with the addition of a small amount, around 5 drops, of hydrogen peroxide in an attempt to buffer the decomposition of the peroxyacid. The crystallisation setup was otherwise similar to the previous experiments. The resulting

materials were analysed by XRPD (Figure 221). The collected XRPD data shows the presence of a high amorphous background in the samples; subtraction of this reveals the peaks shown. These show the presence of malonic acid and the decomposed PAP parent acid. The sample crystallised at 4°C shows the presence of an additional peak at 28° 2θ, but with such high background samples, this could be from a mis-correction of the data. There is no evidence of an unknown crystalline product.

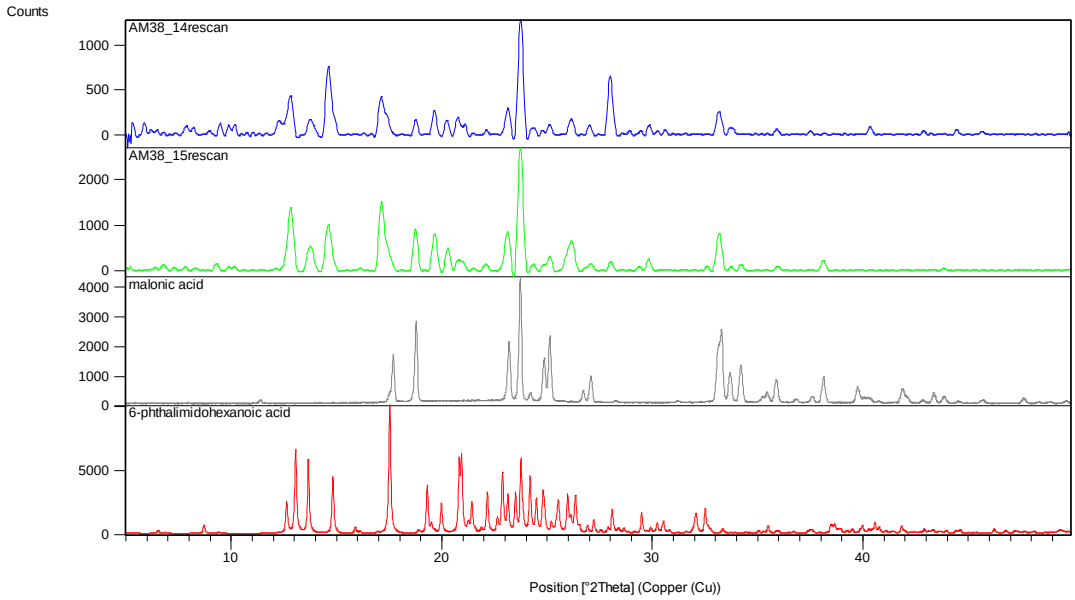

Figure 221 - AM38_14 (blue) and AM38_15 (green), XRPD patterns of resultant materials from the cocrystallisation of malonic acid and PAP with HOOH, compared to the reference patterns for malonic acid (grey) and 6-phthalimidohexanoic acid (red).

Oxalic acid

Oxalic acid was also cocrystallised with PAP in a 1:1 molar ratio with malonic acid from acetone at 4°C and room temperature (AM38_16 and AM38_17) with the addition of a small amount, around 5 drops, of hydrogen peroxide in an attempt to buffer the decomposition of the peroxyacid under otherwise the same crystallisation procedure. The resulting materials were analysed by XRPD.

The XRPD patterns from these two samples again contained high levels of amorphous background scattering which had to be subtracted. The resulting peaks were compared to those of known decomposition products and starting materials (Figure 222), indicating that the product contains the β form of oxalic acid, traces of PAP and a larger amount of 6-phthalimidohexanoic acid monohydrate Form I. The majority of the PAP has thus decomposed with no molecular complex formation indicated.

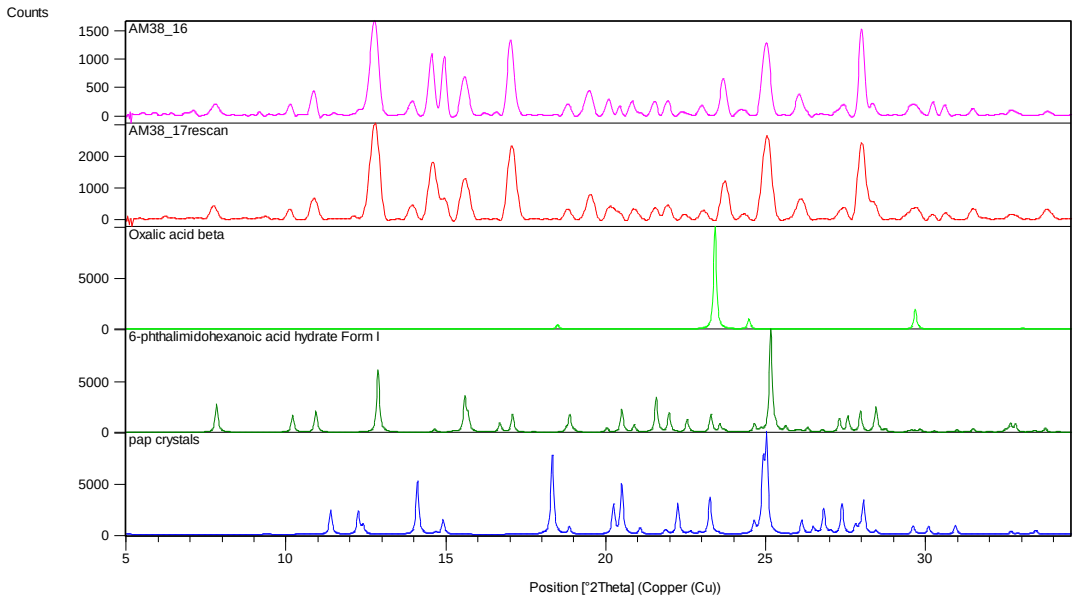

Figure 222 - XRPD patterns of resultant materials from the cocrystallisation of oxalic acid and PAP with HOOH, AM38_16 (purple) and AM38_17 (red), compared to the reference patterns for oxalic acid β form (green), 6-phthalimidohexanoic acid monohydrate form I (olive) and PAP (blue).

Chloranilic acid

Chloranilic acid was cocrystallised with PAP in a 1:1 equimolar ratio with the addition of 5 drops of HOOH as an anti-decomposition buffer. The crystallisation conditions, solvent and controlled crystallisation temperature, from which solid products were obtained, are given in Table 43.

Table 43 - Crystallisation conditions of PAP and chloranilic acid

Sample ID	Component A	Component B	Solvent	Temperature	Analysis Group
AM66_02	PAP	Chloranilic acid	Acetone	Room temperature	A
AM66_03	PAP	Chloranilic acid	Methyl acetate	4°C	B
AM66_05	PAP	Chloranilic acid	Ethyl acetate	4°C	A
AM66_06	PAP	Chloranilic acid	Ethyl acetate	Room temperature	A

The resulting materials were analysed by XRPD and found to fall into two groups defined in Table 43 as A and B. Analysis group A, consisting of both of the samples crystallised in ethyl acetate at 4°C and room temperature, as well as the sample crystallised from acetone at room temperature, share many similar features in their XRPD patterns (Figure 223). The majority of these features correspond well and indicate a strong presence of the parent acid – 6-phthalimidohexanoic acid. Chloranilic acid also may be present in these samples but in a much smaller quantity. The peak at 28° in 2θ could only be assigned, however, by assuming a high degree of preferred orientation in the samples; it could also correspond to an unidentified component.

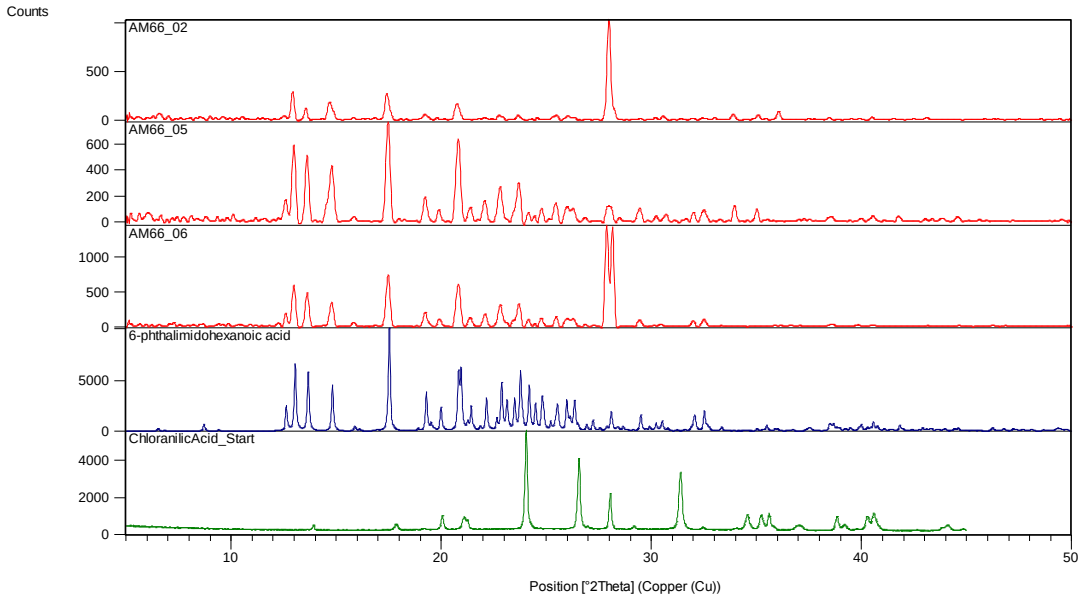

Figure 223 - XRPD patterns of collected materials from the cocrystallisations of PAP and chloranilic acid from analysis group A (red) compared with reference patterns of 6-phthalimidohexanoic acid (navy) and chloranilic acid (green).

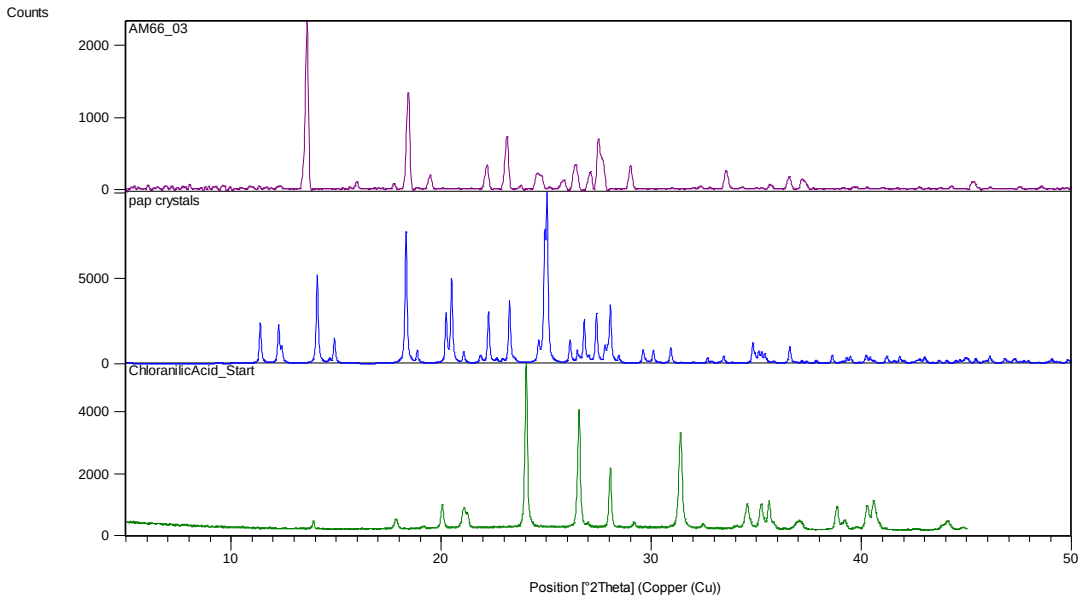

Figure 224 - XRPD patterns of collected material from the cocrystallisation of PAP and chloranilic acid from analysis group B (purple) compared with reference patterns of PAP (blue) and chloranilic acid (green).

Group B is obtained from the cocrystallisation in methyl acetate at 4°C. This sample had a high background content and the constituents of the sample are not particularly clear. Most peaks can be assigned by contributions from recrystallised PAP and the chloranilic

acid starting materials (Figure 224),but further study would be required on the cocrystallisations of PAP and chloranilic acid with HOOH added.

Bromanilic acid

Bromanilic acid was similarly crystallised with PAP in a 1:1 equimolar ratio in acetone at a constant temperature of 4°C (AM67_01) and room temperature (AM67_02) with the addition of 5 drops of hydrogen peroxide. Both samples when analysed by XRPD proved to contain high quantities of amorphous material as seen in the background, leading to a limited amount of the information in the patterns.

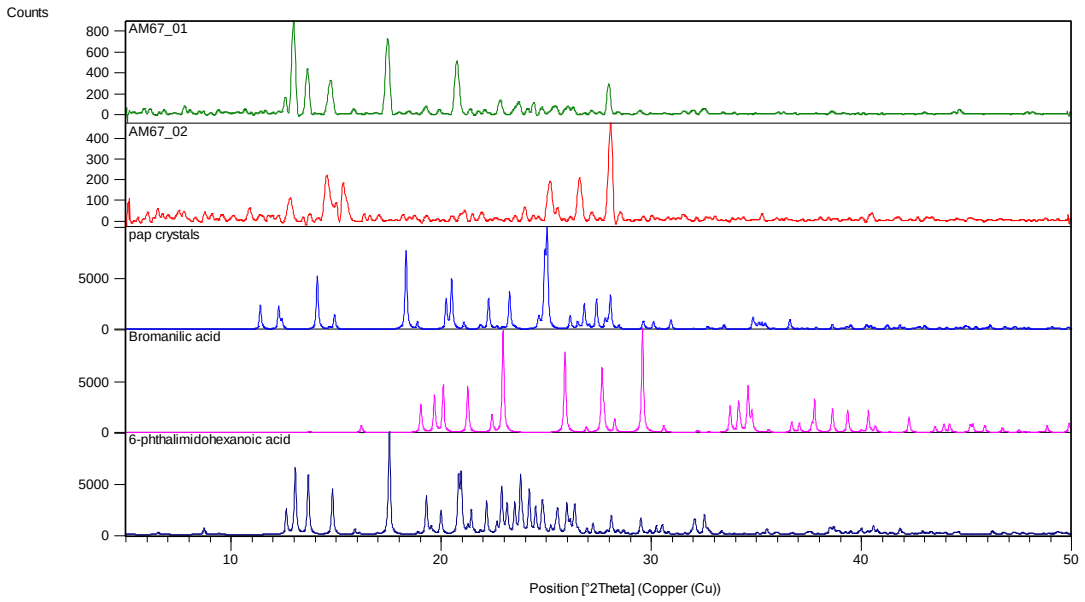

Figure 225 – XRPD patterns of collected materials from the cocrystallisation of PAP and bromanilic acid with the addition of HOOH in acetone at 4°C (green) and room temperature (red) compared to the reference patterns for PAP (blue), bromanilic acid (purple) and 6-phthalimidohexanoic acid (navy).

The remaining peaks (Figure 225) indicate that the sample recrystallized at 4°C contains primarily the decomposed PAP parent acid (6-phthalimidohexanoic acid) and some bromanilic acid. The sample crystallised at room temperature contains greater quantities of bromanilic acid and there may be some indication of PAP in the lower angle peaks.

5.1.4 Unresolved materials

Cocrystallisations were also performed between the following materials, all at 1:1 ratio:

- Meta-chloroperbenzoic acid and picolinic acid
- Meta-chloroperbenzoic acid and dipicolinic acid
- 6-phthalimidoperoxyhexanoic acid and picolinic acid
- 6-phthalimidoperoxyhexanoic acid and dipicolinic acid

Unit cell screening of single crystals extracted from the samples yielded only starting materials, which may or may not be representative of the bulk of the sample. These crystallisation experiments have yet to be fully assessed along with the remaining materials from the noted acid cocrystallisations.

5.2 π-π interacting materials, proton sponges and peroxyacids

Through targeting the π bonded region of the target molecules, the secondary components within this section were brought together in a crystallisation environment in a 1:1 ratio with the target materials with the aim of forming π-π interactions, creating molecular complexes of a stacked nature. This methodology was designed specifically not to interact with the peroxyacid functional group itself, as the peroxyacid functionality was too unstable to be a primary point of interaction in a cocrystallisation experiment. Although the proton sponges used have the additional capability of inducing proton transfer from the target material, they are robust π bond containing aromatic materials and may be considered within this category as their π-π stacking interactions often form a major directing factor in their crystal structures.

As with the carboxylic acid cocrystallisations, the experiments were carried out in a range of solvents under temperature controlled evaporative crystallisation, as will be described for each experiment set.

5.2.1 Meta-chloroperbenzoic acid and π-π interacting materials

With its aromatic ring, MCPBA is a prime candidate for π-π stacking interactions and as such was cocrystallised with second components of a similar molecular shape and size. On addition to π stacking capacity, each of the selected co-molecules had hydrogen bond donor or acceptor capability, to take advantage of any possible interactions with the peroxyacid group.

1,4-Dihydroxybenzene (Hydroquinone)

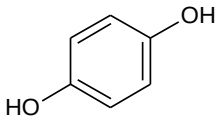

Figure 226 - 1,4-Dihydroxybenzene (hydroquinone)

Hydroquinone (Figure 226), with its aromatic ring and two hydrogen bond donors in the form of hydroxyl groups, was chosen primarily for its π-π stacking interaction potential with MCPBA. It was crystallised with MCPBA in a 1:1 equimolar ratio in a series of crystallisations. A representative result of these experiments is shown in the XRPD pattern

in Figure 227, from AM68_02 – cocrystallisation in acetone at room temperature with the addition of a few drops of hydrogen peroxide.

This indicates the presence of 3-chlorobenzoic acid only, with no or very little other crystalline materials present. The majority of the crystalline MCPBA has thus been decomposed to the parent acid.

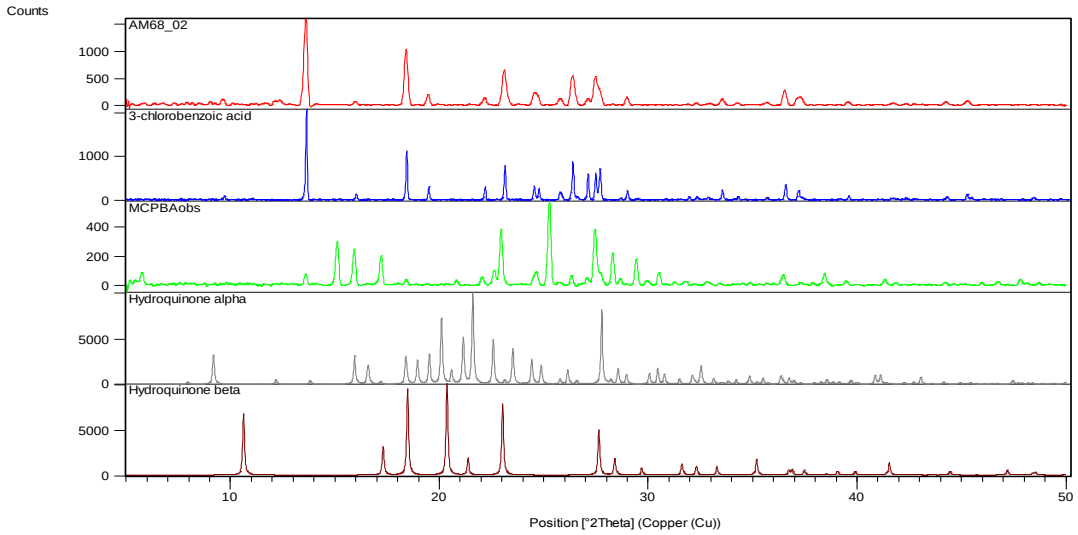

Figure 227 - XRPD pattern of collected material from cocrystallisation of MCPBA and hydroquinone in acetone at room temperature (red) compared with the reference patterns of 3-chlorobenzoic acid (blue), MCPBA (green), and hydroquinone alpha form (grey) and beta form (brown).

2-Hydroxybenzophenone

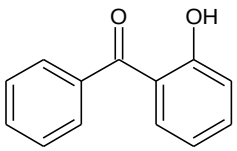

Figure 228 - 2-hydroxybenzophenone

With its twin aromatic ring arrangement and hydrogen bond donor and acceptor available, 2-hydroxybenzophenone (Figure 228) was selected as a material with potential to stack with MCPBA or form hydrogen bonds to the peroxyacid group. It was utilised in 1:1 equimolar cocrystallisation experiments, similar solvents with hydrogen peroxide addition as for previous experiments at controlled temperatures of 4°C and room temperature. Those experiments for which XRPD data were collected are displayed in Table 44.

Table 44 - Crystallisation conditions of MCPBA and 2-hydroxybenzophenone

Sample ID	Component A	Component B	Solvent	Temperature
AM80_01	MCPBA	2-Hydroxybenzophenone	Acetone	4°C
AM80_03	MCPBA	2-Hydroxybenzophenone	Methyl acetate	4°C
AM80_07	MCPBA	2-Hydroxybenzophenone	Diethyl ether	4°C

As can be seen from the XRPD data (Figure 229), all patterns show distinctive peaks corresponding to 3-chlorobenzoic acid, particularly in the sample collected from acetone at 4°C, in which all peaks can be attributed to 3-chlorobenzoic acid. The samples crystallised from methyl acetate and diethyl ether at 4°C also show a large content of 3-chlorobenzoic acid, along with 2-hydroxybenzophenone. Once again the MCPBA appears to have decomposed to the parent acid in all recorded samples.

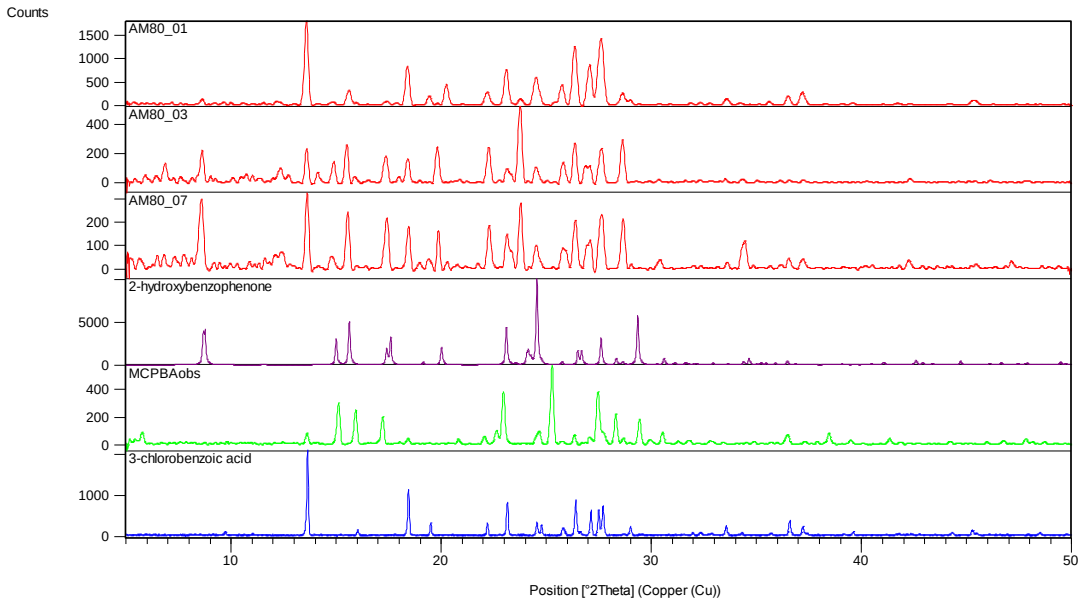

Figure 229 - XRPD patterns of collected materials from the cocrystallisation of PAP and 2-hydroxybenzophenone with the addition of HOOH in acetone at 4°C (top red), methyl acetate at 4°C (middle red) and diethyl ether at 4°C (bottom red) compared to the reference patterns for 2-hydroxybenzophenone (purple), MCPBA (green) and 3-chlorobenzoic acid (blue).

3-Hydroxybenzophenone

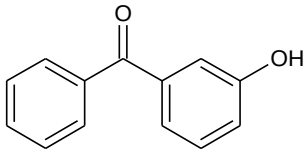

Figure 230 – 3-hydroxybenzophenone

3-hydroxybenzophenone (Figure 230) is a more attractive hydrogen bonding co-material for MCPBA, as the 3-hydroxyl group is unable to form an intramolecular hydrogen bond. This co-molecule was screened under the same 1:1 conditions as 2-hydroxybenzophenone. The crystallisation conditions for which XRPD data were obtained from the products are detailed in Table 45. As with the previous experiments, a small amount of hydrogen

peroxide was added to the crystallisation to aid in the prevention of decomposition to the parent acid. The resulting XRPD patterns were compared to those of the starting materials and known decomposition products (Figure 231).

Table 45 - Crystallisation conditions of MCPBA and 3-hydroxybenzophenone

Sample ID	Component A	Component B	Solvent	Temperature
AM82_01	MCPBA	3-Hydroxybenzophenone	Acetone	4°C
AM82_03	MCPBA	3-Hydroxybenzophenone	Methyl acetate	4°C
AM82_05	MCPBA	3-Hydroxybenzophenone	Ethyl acetate	4°C
AM82_07	MCPBA	3-Hydroxybenzophenone	Diethyl ether	4°C

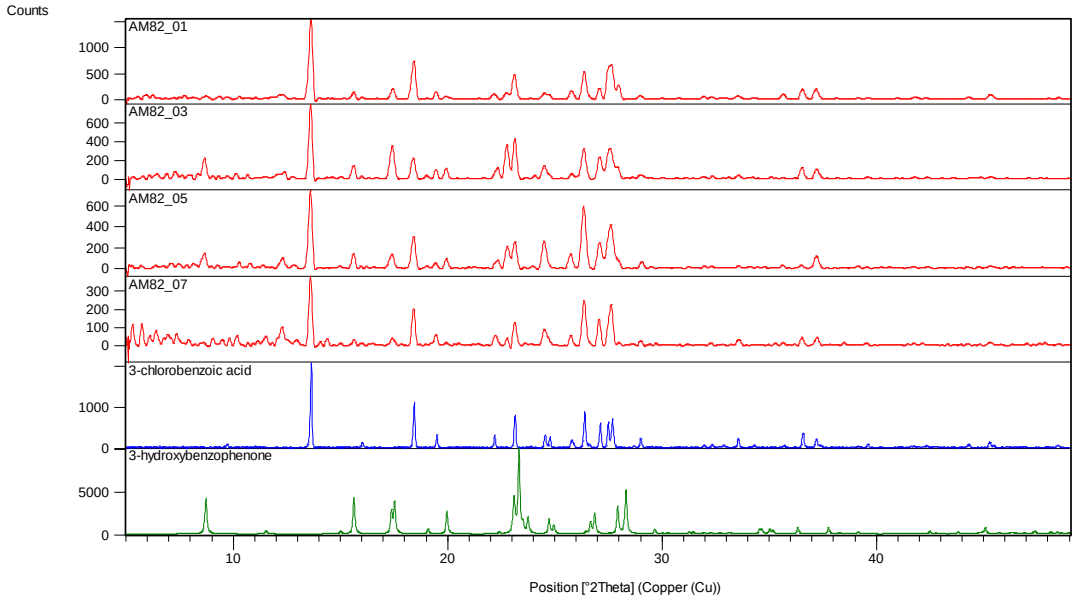

Figure 231 - XRPD patterns of collected materials from the cocrystallisation of MCPBA and 3-hydroxybenzophenone with the addition of HOOH in acetone at 4°C (top red), methyl acetate at 4°C (2nd red), methyl acetate at 4°C (3rd red) and diethyl ether at 4°C (bottom red) compared to the reference patterns of 3-chlorobenzoic acid (blue) and 3-hydroxybenzophenone (green).

From the XRPD pattern comparison it can be observed that the samples resulting from acetone and diethyl ether solution contain only crystalline 3-chlorobenzoic acid. Any other materials present must be amorphous. The samples from methyl acetate and ethyl acetate also show a strong presence of 3-chlorobenzoic acid but also recrystallised 3-hydroxybenzophenone in trace amounts. In all samples the MCPBA has decomposed to the parent acid without generation of a new molecular complex.

2-Chlorobenzophenone

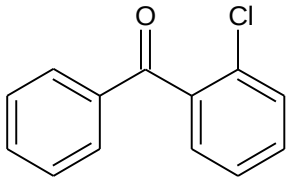

Figure 232 - 2-chlorobenzophenone

The cocrystallisation of MCPBA and 2-chlorobenzophenone (Figure 232) with the addition of hydrogen peroxide crystallised in a 1:1 equimolar ratio from methyl acetate at room temperature produced a material that from XRPD analysis appears poorly crystalline (Figure 233).

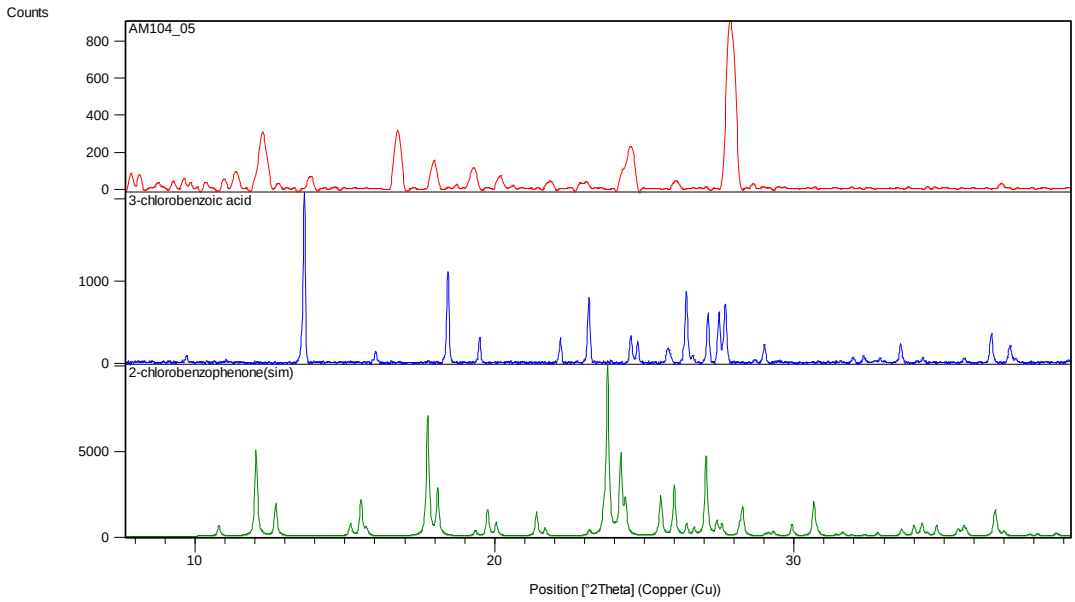

Figure 233 - XRPD pattern of material collected from the cocrystallisation of MCPBA and 2-chlorobenzophenone crystallised from methyl acetate at room temperature compared with the reference patterns of 3-chlorobenzoic acid (blue) and 2-chlorobenzophenone (green)

From the XRPD pattern comparison to starting materials and known decomposition products, the peaks present after removal of the background, can be attributed to a combination of 3-chlorobenzoic acid and 2-chlorobenzophenone. It is thus likely that the MCPBA has decomposed to the parent acid.

5.2.2 6-Phthalimidoperoxyhexanoic acid and π-π interacting materials

When dealing with π-π interacting materials and PAP, the focus of the candidate interactions is primarily upon the phthalimido end of the molecule. The planar phthalimido group can stack readily and has great conformational flexibility with respect to the hydrogen bonding head of the molecule as a result of the long aliphatic chain. This should

allow it to pack effectively between molecules whilst separating the peroxyacid head from the area of π interaction; this is seen in the crystal structures of 6-phthalimidohexanoic acid and its family. Introducing a second π-π stacking material into the crystallisation could thus create a new molecular complex with the peroxyacid through solely π interactions, removing the need to interact with the unstable peroxyacid functional group.

To this end, PAP was cocrystallised with a range of selected aromatic materials, including those with hydrogen bonding potential and proton sponges.

2-Hydroxybenzophenone

2-Hydroxybenzophenone was cocrystallised with 6-phthalimidoperoxyhexanoic acid in a 1:1 equimolar ratio in a selected range of solvents and crystallisation temperatures as set out in Table 46. The resultant materials were analysed by XRPD for assessment of crystalline material content and indication of the formation of any new components in the crystallisation process. The crystallisation was aided by the addition of 5 drops of hydrogen peroxide to buffer the equilibrium of the decomposition reaction of the peroxyacid.

Table 46 - Crystallisation conditions of PAP and 2-hydroxybenzophenone

Sample ID	Component A	Component B	Solvent	Temperature
AM81_01	PAP	2-Hydroxybenzophenone	Acetone	4°C
AM81_03	PAP	2-Hydroxybenzophenone	Methyl acetate	4°C

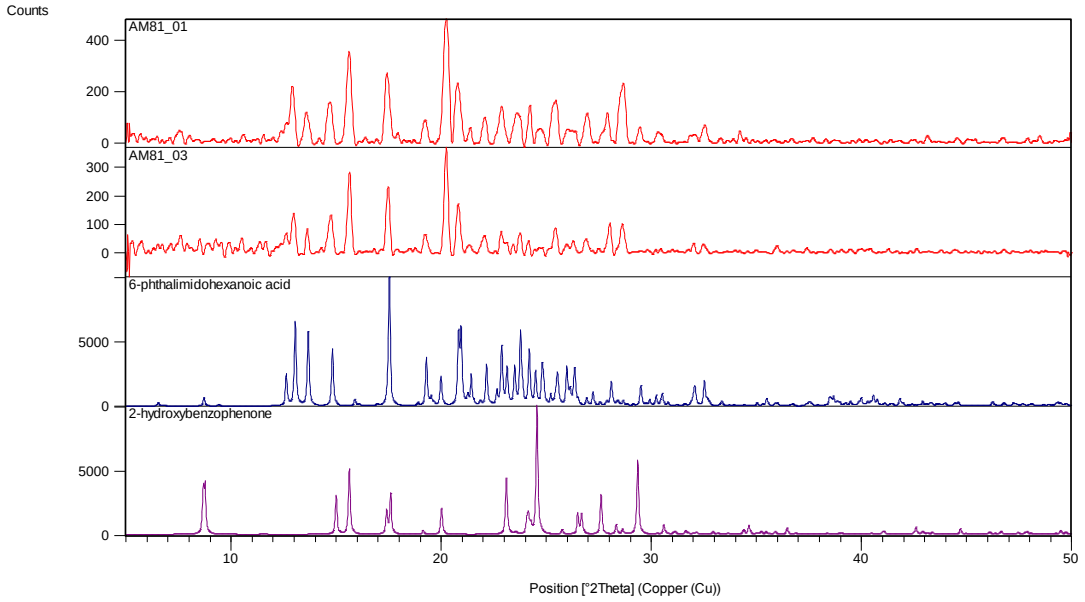

Figure 234 - XRPD patterns of materials collected from the cocrystallisation of PAP and 2-hydroxybenophenone (red) compared with the reference patterns of 6-phthalimidohexanoic acid (blue) and 2-hydroxybenzophenone (purple)

From the two samples for which XRPD data could be collected (Figure 234, Table 46), it can be clearly determined that the resulting materials from both experiments are a combination of 2-hydroxybenzophenone and the PAP decomposition product 6-phthalimidohexanoic acid. The peroxyacid is thus decomposed to the parent acid under these conditions, with no indication of molecular complex formation.

3-Hydroxybenzophenone

PAP was also cocrystallised with 3-hydroxybenzophenone, under the same condition under an equimolar ratio and within a temperature controlled environment. The crystallisation conditions for each experiment that resulted in a material that was analysed by XRPD are outlined in Table 47.

Table 47 - Crystallisation conditions of PAP and 3-hydroxybenzophenone

Sample ID	Component A	Component B	Solvent	Temperature	Analysis Group
AM83_01	PAP	3-Hydroxybenzophenone	Acetone	4°C	A
AM83_02	PAP	3-Hydroxybenzophenone	Acetone	Room temperature	B
AM83_03	PAP	3-Hydroxybenzophenone	Methyl Acetate	4°C	A
AM83_05	PAP	3-Hydroxybenzophenone	Ethyl acetate	4°C	B
AM83_07	PAP	3-Hydroxybenzophenone	Diethyl ether	4°C	B

From analysis of the collected XRPD data, the samples can be split into two categories, defined in the table as analysis groups A and B.

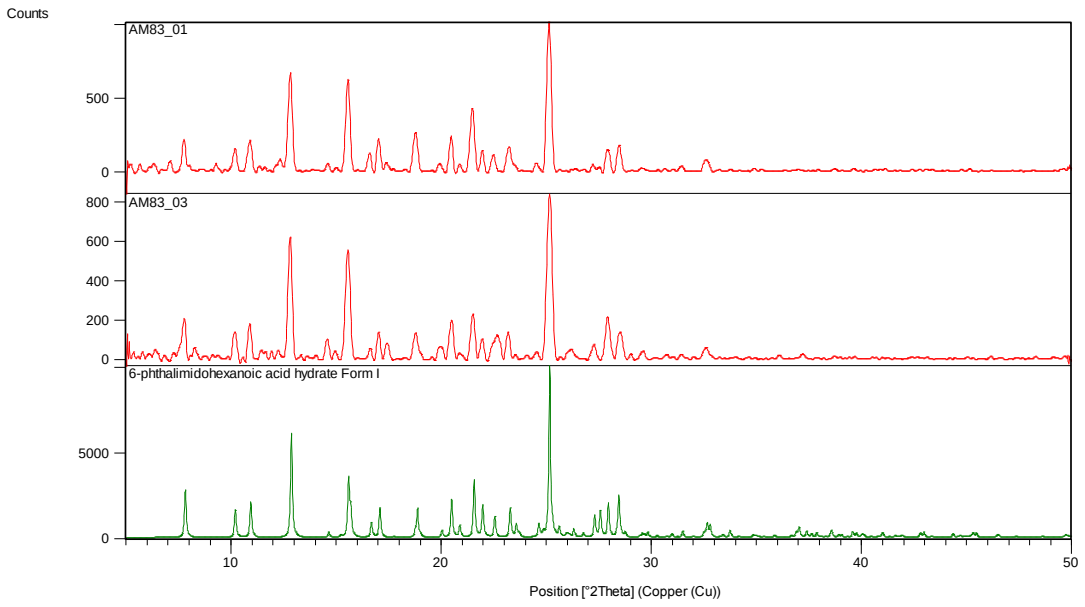

Figure 235 - XRPD patterns from the cocrystallisation of PAP and 3-hydroxybenzophenone defined as analysis group A (red) compared to a reference pattern of 6-phthalimidohexanoic acid monohydrate Form I (green).

The samples in analysis group A (Figure 235), from acetone and methyl acetate at 4°C, resulted in recrystallisation of 6-phthalimidohexanoic acid monohydrate (Form I), with no

unidentified Bragg peaks present. The secondary component material, 3-hydroxybenzophenone cannot be seen and is assumed to be amorphous. The PAP in these crystallisations has decomposed to the parent acid.

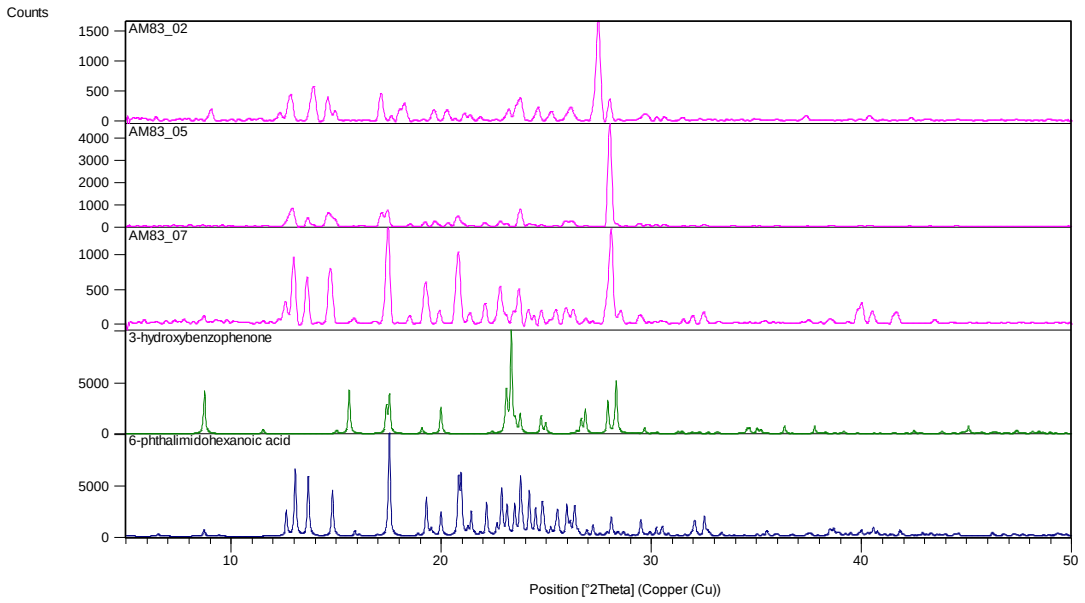

Figure 236 - XRPD patterns from the cocrystallisation of PAP and 3-hydroxybenzophenone defined as analysis group B (magenta) compared to a reference pattern of 3-hydroxybenzophenone (olive) and 6-phthalimidohexanoic acid (navy)

The remaining samples for which data were collected are defined as analysis group B. These materials all have peaks indicative of a composition containing both 6-phthalimidohexanoic acid and 3-hydroxybenzoic acid (Figure 236). All samples in this crystallisation set for which data were collected resulted in decomposition of the peroxyacid.

4-Hydroxybenzophenone

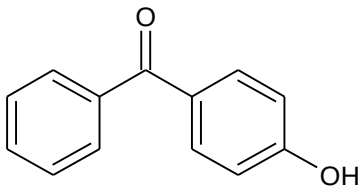

Figure 237 - 4-hydroxybenzophenone

PAP was crystallised with 4-hydroxybenzophenone (Figure 237) in a 1:1 equimolar evaporative crystallisation under the same conditions as the previous two hyroxybenzophenones. Although no XRPD data was collected from these materials, single crystal analysis of selected samples from the cocrystallisation from methanol at 30°C

revealed the presence of a reaction product, benzoic acid (Figure 238), an oxidation product of the 4-hydroxybenzophenone.

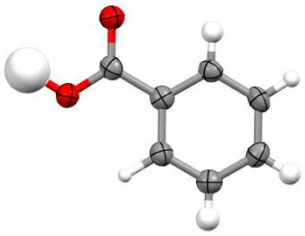

Figure 238 - Benzoic acid

The oxidising agents, either the PAP or the hydrogen peroxide, must therefore have oxidised the 4-hydroxybenzophenone molecule at the carbonyl, suggesting that the corresponding leaving group, 1-hydroxy-4-methylbenzene or a further oxidised material must also be present. A crystal structure of this material was collected, however the data is not of higher quality to that of this molecule as recorded in the CSD[46, 156].

From analysis of the simulated XRPD pattern of this crystal structure with those of the products from the other hydroxybenzophenone cocrystallisations, no similarity is evident between the peak profiles and therefore this decomposition product cannot be a major component in the product materials.

Benzimidazole

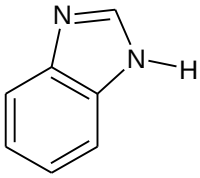

Figure 239 - Benzimidazole

Benzimidazole (Figure 239) is a planar molecule with an aromatic ring and an available electron rich nitrogen site for interaction. This was selected cocrystallisation attempts, not only for its π-π interactions, but also for its ability to deprotonate co-components by forming a strong hydrogen bond by proton transfer to the heterocyclic nitrogen. It could thus potentially strip the peroxyacid hydrogen from the basic oxygen forming a salt, completely changing the electronic nature of the peroxide chain of the peroxyacid and its resulting reactivity. With respect to the characteristics of PAP, it shares a common size and shape with the phthalimido group, potentially aiding molecular recognition. Benzimidazole was therefore crystallised with PAP in a 1:1 molar ratio under the conditions outlined in Table 48, and allowed to crystallise by slow evaporation.

Table 48 - Crystallisation conditions of PAP and Benzimidazole

Sample ID	Component A	Component B	Solvent	Temperature
AM31_02	PAP	Benzimidazole	Methanol	Room temperature
AM31_05	PAP	Benzimidazole	Ethanol	Room temperature
AM31_06	PAP	Benzimidazole	Ethanol	30°C
AM31_07	PAP	Benzimidazole	Acetone	4°C
AM31_08	PAP	Benzimidazole	Acetone	Room temperature
AM31_09	PAP	Benzimidazole	Acetone	30°C
AM31_10	PAP	Benzimidazole	Ethyl acetate	4°C
AM31_11	PAP	Benzimidazole	Ethyl acetate	Room temperature
AM31_12	PAP	Benzimidazole	Ethyl acetate	30°C
AM31_13	PAP	Benzimidazole	Diethyl Ether	4°C
AM31_14	PAP	Benzimidazole	Diethyl Ether	Room temperature
AM31_15	PAP	Benzimidazole	Diethyl Ether	30°C

All XRPD patterns of the materials collected from the cocrystallisation experiments show a high degree of similarity, but they do not correspond to benzimidazole, PAP, or any of the known PAP decomposition products (Figure 240 Figure 162). These products thus warranted further study.

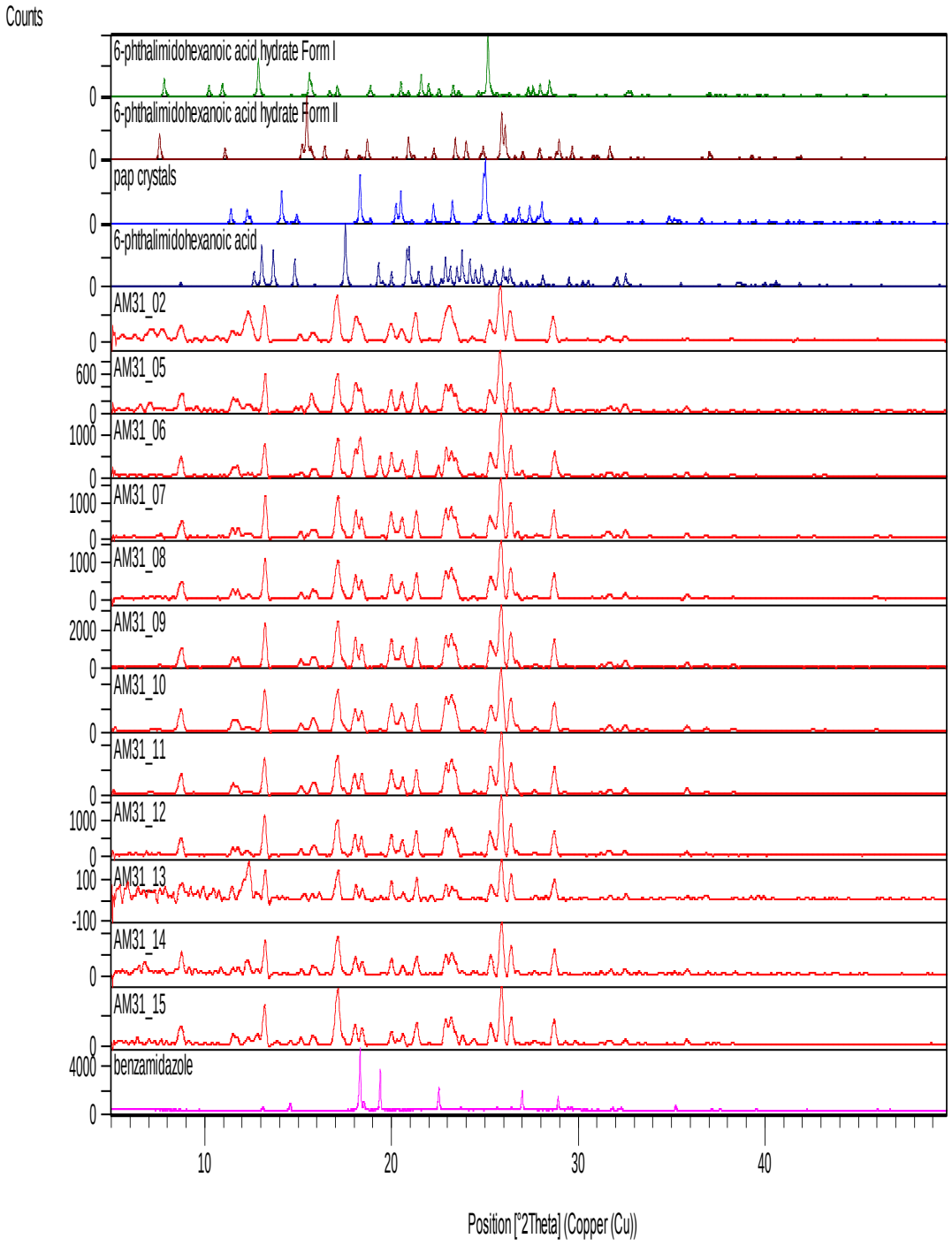

Figure 240 - Collected materials from the cocrystallisation of PAP and benzimidazole (red) compared to the reference patterns of 6-phthalimidohexanoic acid monohydrate Forms I (green) and II (brown), PAP (blue), 6-phthalimidohexanoic acid (Navy) and benzimidazole (magenta).

Suitable crystals for single crystal X-ray diffraction were extracted from sample AM31_11, crystallisation from ethyl acetate at room temperature, and were subsequently measured on the Rigaku R-Axis diffractometer at 100K. The data collection details are shown in Table 49.

Table 49 - Crystal structure collection data for 6-phthalimidohexanoic acid benzimidazole benzimidazol-1-ol (1:1:1) molecular complex

Compound	6-phthalimidohexanoic acid benzimidazole benzimidazol-1-ol (1:1:1) molecular complex
Formula	$C_{28}H_{27}O_{4.4}N_5$
Crystallisation Conditions	Reaction product from cocrystallisation of 6-phthalimidoperoxyhexanoic acid and benzimidazole in ethyl acetate at room temperature
Molecular weight / $gmol^{-1}$	503.95
Temperature (K)	100
Space Group	P-1
a (Å)	5.3091(9)
b (Å)	11.754(2)
c (Å)	20.033(3)
α (°)	87.840(6)
β (°)	85.105(6)
γ (°)	76.980(5)
Volume ($Å^3$)	1213.3(4)
Z	2
Z'	1
θ range/˚	3.1-27.6
Reflections Collected	26030
Independent	5515
Refln (obs.I>2theta(I))	3786
R_{int}	0.0514
Parameters	458
GooF on F^2	1.042
R_1 (Observed)	0.0563
R_1 (all)	0.0877
wR_2 (all)	0.1368

The determined structure is a molecular complex of the decomposed PAP parent acid (6-phthalimidohexanoic acid) and benzimidazole. There are three molecular species present, of which there are two chemically different moieties related to benzimidazole.

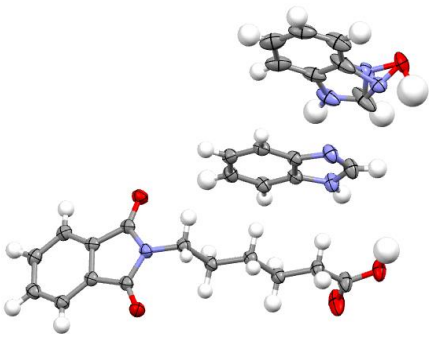

Figure 241 - Asymmetric unit of benzimidazole, benzimidazol-1-ol and 6-phthalimidohexanoic acid.

As can be seen in Figure 241, the asymmetric unit not only contains a molecule of decomposed PAP, and a molecule of benzimidazole, but a partially oxidised benzimidazole derivative. The cocrystallisation conditions have led to oxidisation of the available nitrogen on the benzimidazole molecule by the peroxyacid, producing benzimidizol-1-ol.

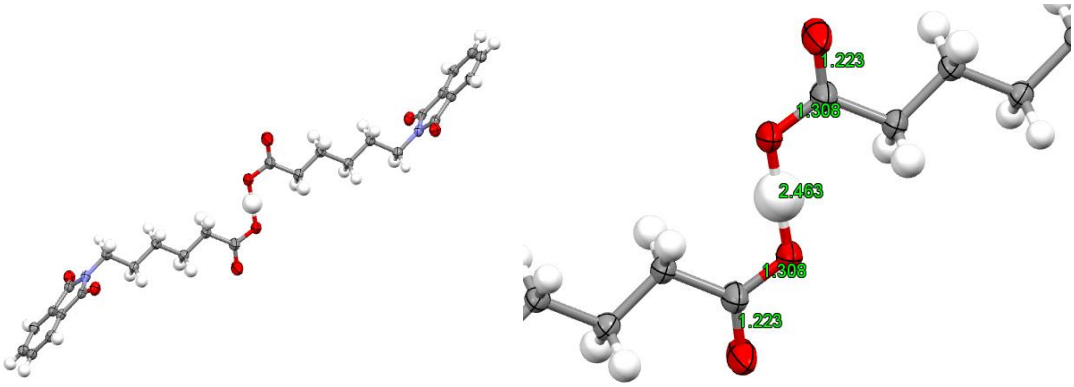

Figure 242 - 6-phthalimidohexanoic acid dimer formed over the inversion centre (left), bond length measurements of short strong hydrogen bond between the two carboxylic acid functional groups (right)

The peroxyacid itself is lost in the process, with its decomposition product 6-phthalimidohexanoic acid retained in the structure as part of the molecular complex. The decomposed PAP molecules are dimerised via a single short strong hydrogen bond between the carboxylic acid groups, with O···H-O distance 2.463(3)Å (Figure 242). The hydrogen atom is situated on an inversion centre between the two molecules.

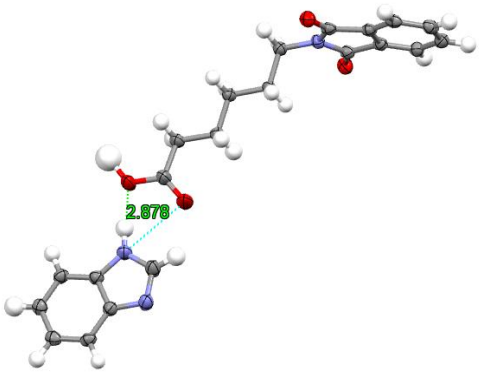

Figure 243 - Moderate strength hydrogen bond between carboxylic acid and benzimidazole directed towards the hydroxyl oxygen of the group.

The carboxylic acid of the decomposed PAP is also involved in a second, moderate strength, hydrogen bond of N-H···O distance 2.878(3)Å (170(2)°) between the unreacted benzimidazole molecule and the hydroxyl oxygen of the carboxylic acid group (Figure 243). The unreacted benzimidazole is further hydrogen bonded to the oxidized benzimidazole via a second moderate strength hydrogen bond with the oxidised benzimidazole amine with a N-H···N distance of 2.737(3)Å (173(3)°) (Figure 244).

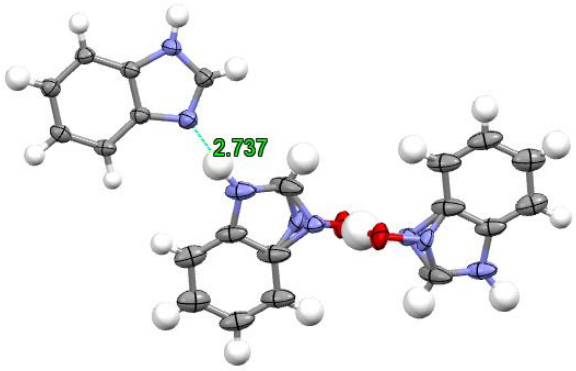

Figure 244 - The moderate strength hydrogen bond between the lone pair of the nitrogen on the unreacted benzimidazole molecule and the amine hydrogen of the reacted benzimidazole

The final molecule in the asymmetric unit is the partially oxidised benzimidazole molecule. The X-ray diffraction data suggest that the nitrogen of the benzimidazole molecule (N5) is disordered over two positions corresponding to an oxidised and non-oxidised form (Figure 245). The oxygen atom (O5) has 40% occupancy which corresponds to N5 at the N5B position; the hydroxyl group is thus associated with this nitrogen. N5A is the un-oxidised nitrogen.

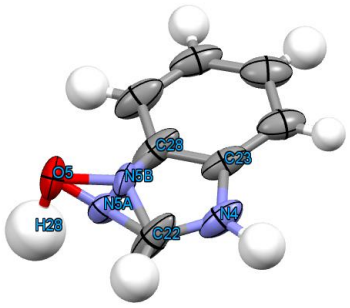

Figure 245 - Partially oxidised benzimidazole / benzimidazol-1-ol molecule

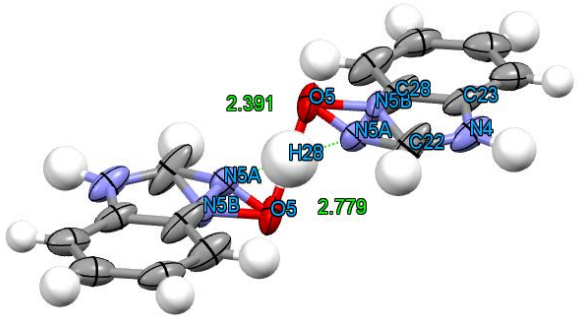

Figure 246 - Two alternative hydrogen bond arrangements over the inversion centre between the two partially oxidised benzimidazole molecules.

The hydrogen H28 sits over the inversion centre and two hydrogen bonding arrangements are possible, depending on the disorder configuration. If the molecules are oxidised, there is a short, strong O5···H28···O5 hydrogen bond at a distance of 2.391(6)Å, while if they are not oxidised, there is a N5A···H28··N5A moderate strength hydrogen bond of distance 2.779(6)Å. This alternating hydrogen bonding motif affects the atomic displacement parameters of the remaining non hydrogen atoms on the benzimidazole molecule, but only N5 can be fully split to two positions in the disorder model.

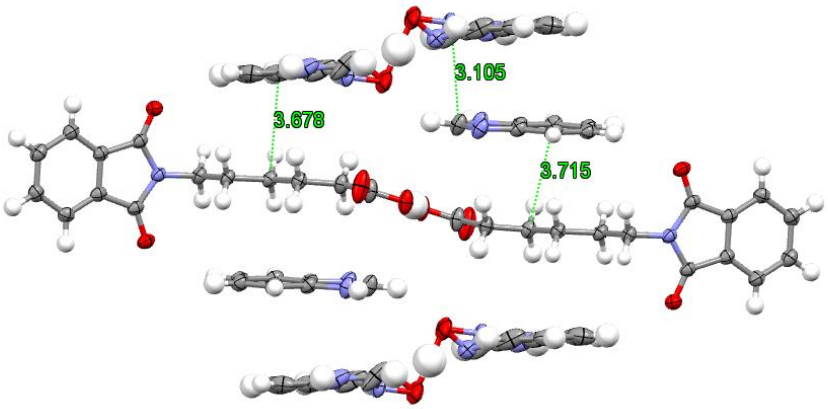

Figure 247 - Stacking of benzimidazole molecules over the aliphatic chain and carboxylic acid dimer.

The benzimidazole molecules stack directly over the aliphatic chains of the decomposed PAP hydrogen bonded dimer forming aliphatic C-H···π interactions at distances of 3.678(3)Å and 3.715(3)Å, packing between the closest atoms of the phthalimido groups of the two decomposed PAP molecules (Figure 247). The non-oxidised benzimidazole further stacks in a skewed overlap with the oxidised benzimidazole molecule at a distance of 3.105(4)Å.

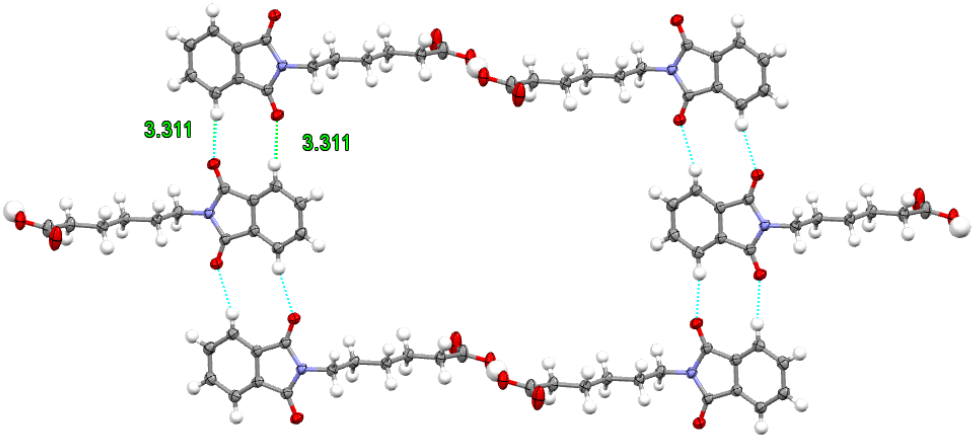

Figure 248 - Alternating phthalimido groups forming hydrogen bonded squares. The benzimidazole molecules contained within this square arrangement are omitted for clarity.

The phthalimido groups adopt an alternate arrangement creating two carbonyl to aromatic C-H···O hydrogen bonds at a distance of 3.311(2)Å (172(2)°) forming a hydrogen bonded square arrangement (Figure 248) around the benzimidazole molecules.

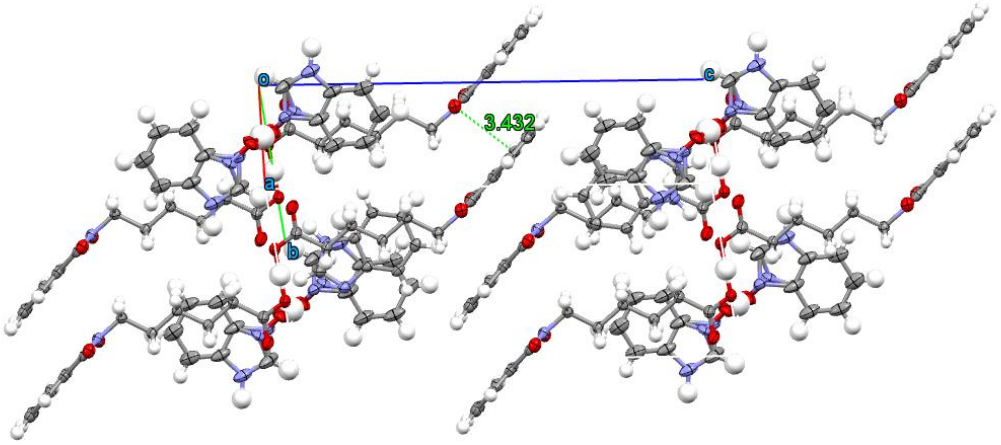

Figure 249 - Skewed stack arrangement of phthalimido groups perpendicular to the stacking of the benzimidazole molecules

Finally, the phthalimido groups also stack with each other in a skewed arrangement along the *ab* diagonal, with a π-π interaction distance of 3.432(3)Å forming an overlapping zigzag arrangement (Figure 249).

The simulated XRPD pattern generated by this structure is an excellent match to the patterns observed from all of the cocrystallisations in this experiment set and is thus fully representative of the bulk sample product (Figure 250).

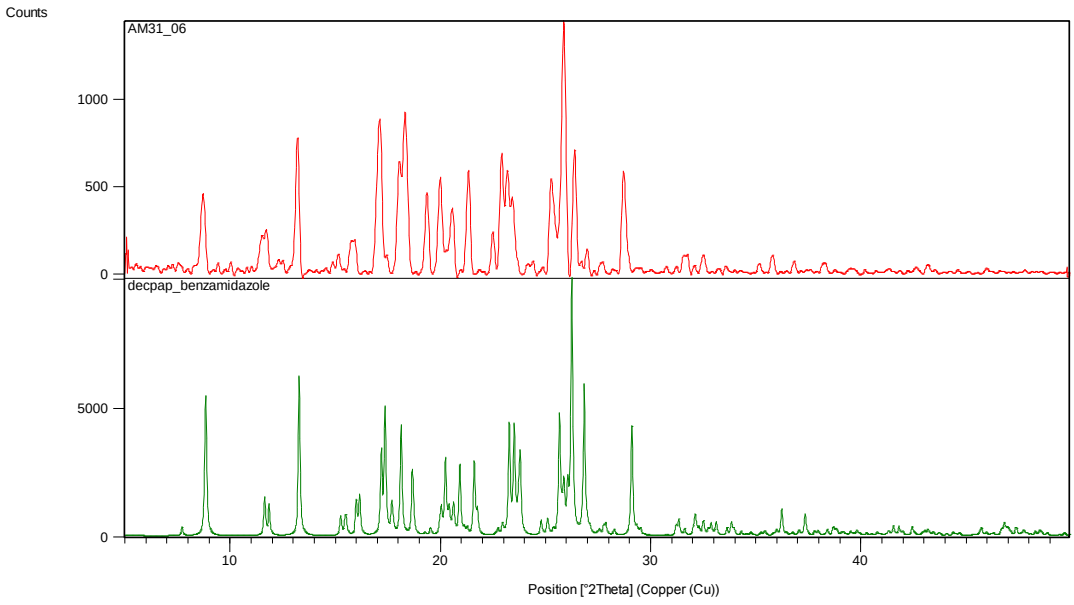

Figure 250 - XRPD pattern representative of all samples collected from the cocrystallisation of PAP and benzimidazole (red) compared to the simulated structure of the 6-phthalimidohexanoic acid benzimidazole benzimidizol-1-ol molecular complex (green).

5.2.3 Unresolved materials

Cocrystallisations were also performed between the following materials, all in a 1:1 ratio:

- Meta-chloroperbenzoic acid and Benzimidazole
- Meta-chloroperbenzoic acid and DMAN “Proton Sponge”
- Meta-chloroperbenzoic acid and 1,3-Dihydroxybenzene (Resorcinol)
- Meta-chloroperbenzoic acid and 1,2-Dihydroxybenzene (Catechol)
- Meta-chloroperbenzoic acid and 1-Chloro-2-nitrobenzene
- Meta-chloroperbenzoic acid and 1-Chloro-3-nitrobenzene
- Meta-chloroperbenzoic acid and 4,4-Bipyridine
- Meta-chloroperbenzoic acid and 4-Hydroxybenzophenone
- Meta-chloroperbenzoic acid and Naphthazerin
- Meta-chloroperbenzoic acid and Tetrahydroxyquinone
- 6-phthalimidoperoxyhexanoic acid and 1,4-Dihydroxybenzene (Hydroquinone)
- 6-phthalimidoperoxyhexanoic acid and 1,3-Dihydroxybenzene (Resorcinol)
- 6-phthalimidoperoxyhexanoic acid and 1,2-Dihydroxybenzene (Catechol)
- 6-phthalimidoperoxyhexanoic acid and 1-Chloro-2-nitrobenzene
- 6-phthalimidoperoxyhexanoic acid and 1-Chloro-3-nitrobenzene
- 6-phthalimidoperoxyhexanoic acid and 4,4-Bipyridine
- 6-phthalimidoperoxyhexanoic acid and 2-Chlorobenzophenone
- 6-phthalimidoperoxyhexanoic acid and Tetrahydroxyquinone
- 6-phthalimidoperoxyhexanoic acid and Naphthazarin
- 6-phthalimidoperoxyhexanoic acid and DMAN “Proton sponge”

Unit cell screening of single crystals extracted from the samples yielded only starting materials, which may or may not be representative of the bulk of the sample. These crystallisation experiments have yet to be fully assessed along with the remaining unscreened materials from the noted π –π stacking directed cocrystallisations.

5.3 Metals and peroxyacids

The combination of the target peroxyacids with metal salts was also explored. Using the same technique as with other cocrystallisation experiments the aim was to form either coordinated metal complexes with the peroxyacid as ligand, or crystalline salts with an altered reactivity. The reactions with a metal centre, however, have the risk that

association may be a highly reactive process, or possibly irreversible, with no way to recover the peroxyacid after complex formation.

This method was therefore explored in a limited way, allowing for a cautious approach. As for the carboxylic acids and the π-π associating materials, the components were brought together for evaporative crystallisation in equimolar ratios, to favour a 1:1 association of the materials upon crystallisation in a series of solvents in temperature controlled environments as detailed for each experiment.

5.3.1 *Meta*-chloroperbenzoic acid and metals

MCPBA was crystallised in a 1:1 molar ratio with a range of acid salts in the presence of a small amount of hydrogen peroxide to buffer the retention of the peroxyacid. The solvent and temperature was varied in order to maximise the chances of producing a complex containing the MCPBA.

Magnesium Chloride

The crystallisation conditions used are given in Table 50

Table 50 - Crystallisation conditions of MCPBA and magnesium chloride

Sample ID	Component A	Component B	Solvent	Temperature
AM50_01	MCPBA	Magnesium chloride	Ethyl acetate	4°C
AM50_04	MCPBA	Magnesium chloride	Chloroform	4°C
AM50_08	MCPBA	Magnesium chloride	Acetone	Room temperature
AM50_10	MCPBA	Magnesium chloride	Diethyl ether	4°C
AM50_13	MCPBA	Magnesium chloride	Dichloromethane	4°C
AM50_14	MCPBA	Magnesium chloride	Dichloromethane	Room temperature
AM50_16	MCPBA	Magnesium chloride	Methanol	4°C
AM50_20	MCPBA	Magnesium chloride	Methyl acetate	Room temperature
AM50_22	MCPBA	Magnesium chloride	Isopropanol	4°C
AM50_25	MCPBA	Magnesium chloride	Ethanol	4°C
AM50_26	MCPBA	Magnesium chloride	ethanol	Room temperature

From the XRPD data of the analysed samples, 3-chlorobenzoic acid is present in all samples that showed significant crystallinity (Figure 251). All samples were very weakly diffracting, making further analysis very difficult and unreliable. The crystallisations from acetone, methyl acetate and ethanol at room temperature all support the conclusion that the peroxyacid has decomposed and not formed a complex, through identification of 3-chlorobenzoic acid crystals from these products by single crystal unit cell screening.

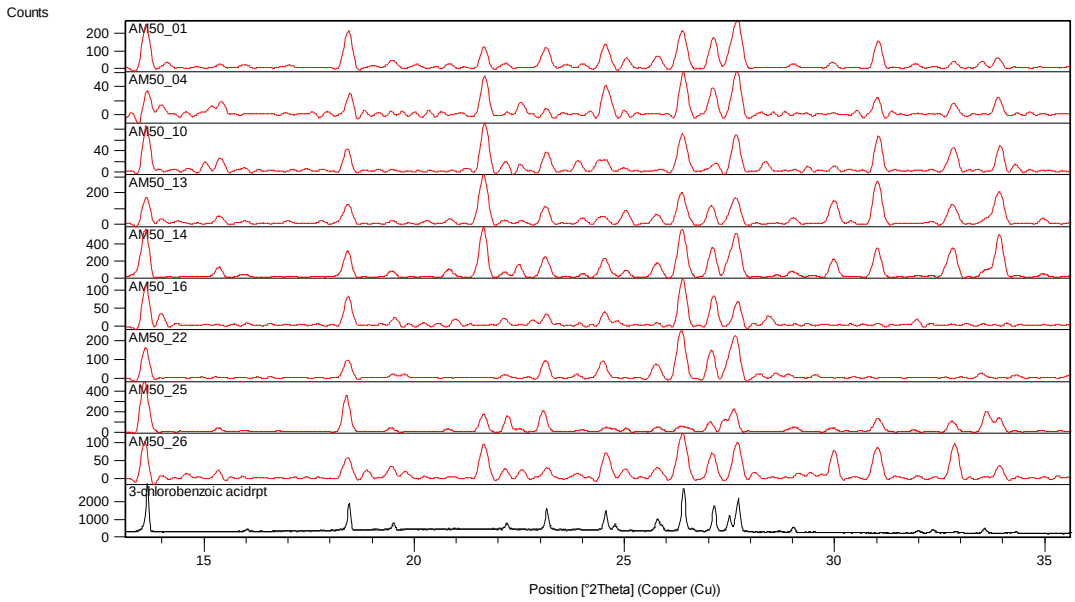

Figure 251 - XRPD patterns of the products of cocrystallisation of MCPBA and magnesium chloride (red) compared with the reference pattern from 3-chlorobenzoic acid (black).

Calcium Chloride

The crystallisation conditions used are given in Table 51

Table 51 - Crystallisation conditions of MCPBA and calcium chloride

Sample ID	Component A	Component B	Solvent	Temperature
AM53_01	MCPBA	Calcium chloride	Ethyl acetate	4°C
AM53_02	MCPBA	Calcium chloride	Ethyl acetate	Room temperature
AM53_13	MCPBA	Calcium chloride	dichloromethane	4°C
AM53_19	MCPBA	Calcium chloride	Methyl acetate	4°C
AM53_22	MCPBA	Calcium chloride	isopropanol	4°C

As with magnesium chloride, all samples analysed showed 3-chlorobenzoic acid as the only significant crystalline component present (Figure 252). The peroxyacid has again decomposed to the parent acid without interaction with the metal.

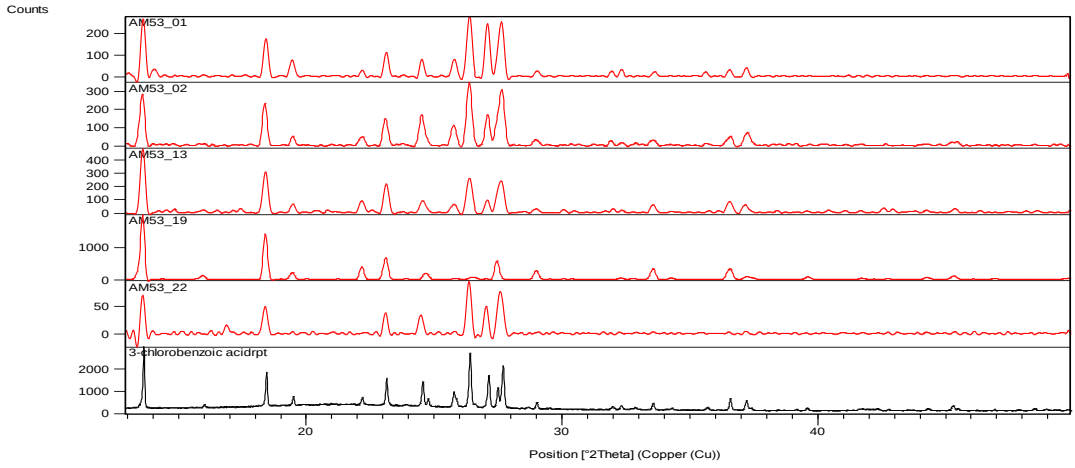

Figure 252 - XRPD patterns of the products of cocrystallisation of MCPBA and calcium chloride (red) compared with the reference pattern of 3-chlorobenzoic acid (black).

Copper Chloride

The crystallisation conditions used are given in Table 52.

Table 52 - Crystallisation conditions of MCPBA and copper chloride

Sample ID	Component A	Component B	Solvent	Temperature
AM86_03	MCPBA	Copper chloride	Methyl acetate	4°C
AM86_05	MCPBA	Copper chloride	Ethyl acetate	4°C
AM86_07	MCPBA	Copper chloride	Diethyl ether	4°C

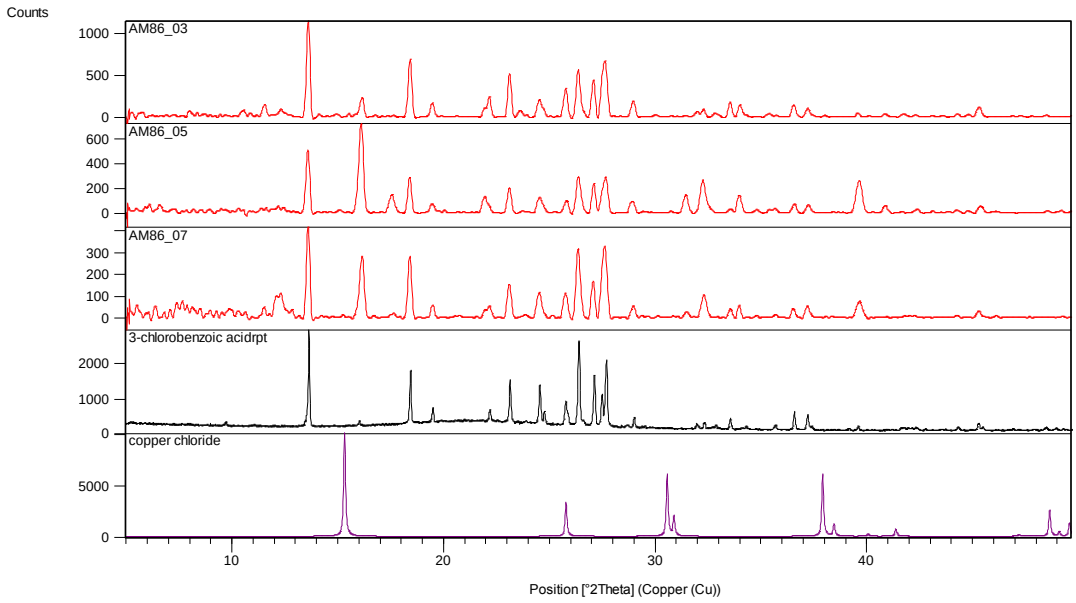

Figure 253 - XRPD patterns of the products cocrystallisation of MCPBA and copper chloride (red) compared with 3-chlorobenzoic acid (black) and copper chloride (purple) reference patterns.

The patterns from this series of experiments indicate the presence of 3-chlorobenzoic acid and copper chloride in the final materials (Figure 253). The MCPBA has decomposed to the parent acid and no interaction is observed with the metal in the solid state.

Copper Sulfate

The crystallisation conditions used are given in Table 53

Table 53 - Crystallisation conditions of MCPBA and copper sulfate

Sample ID	Component A	Component B	Solvent	Temperature
AM87_03	MCPBA	Copper sulfate	Methyl acetate	4°C
AM87_05	MCPBA	Copper sulfate	Ethyl acetate	4°C
AM87_07	MCPBA	Copper sulfate	Diethyl ether	4°C

The samples collected from the crystallisation of MCPBA and copper sulfate that were analysed by XRPD all contain varying amounts of 3-chlorobenzoic acid (Figure 254). The poorest match to the reference pattern is found for AM87_05, the material from ethyl acetate at 4°C. The remaining peaks in the samples, however, do not correspond to any of the starting materials or decomposition products. Further investigation is required the

origin of the unaccounted significant peaks, which could be achieved by future single crystal analysis.

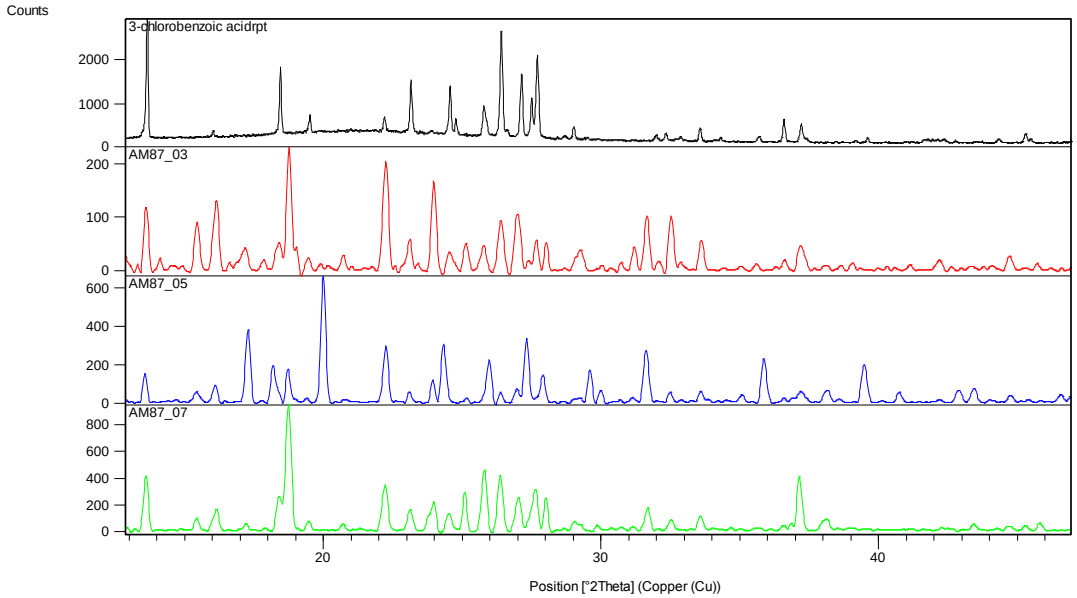

Figure 254 - XRPD patterns of the products of cocrystallisation of MCPBA and copper sulfate in methyl acetate (red), ethyl acetate (blue) and diethyl ether (green) all at 4°C compared with the reference pattern for 3-chlorobenzoic acid (black).

5.3.2 6-Phthalimidoperoxyhexanoic acid and metals

PAP was crystallised in a 1:1 molar ratio with the following acid salts in the presence of a small amount of hydrogen peroxide to buffer the retention of the peroxyacid, as for MCPBA. The solvent and temperature was varied in order to achieve the maximum possibility of creating a new material that included the peroxyacid.

Magnesium Chloride

The crystallisation conditions used are given in Table 54.

Table 54 - Crystallisation conditions of PAP and magnesium chloride

Sample ID	Component A	Component B	Solvent	Temperature	Scan Group/s
AM51_01	PAP	Magnesium chloride	Ethyl acetate	4°C	A
AM51_02	PAP	Magnesium chloride	Ethyl acetate	Room temperature	A
AM51_04	PAP	Magnesium chloride	Chloroform	4°C	A
AM51_07	PAP	Magnesium chloride	Acetone	4°C	B
AM51_08	PAP	Magnesium chloride	Acetone	Room temperature	A
AM51_10	PAP	Magnesium chloride	Diethyl ether	4°C	A & B
AM51_11	PAP	Magnesium chloride	Diethyl ether	Room temperature	A
AM51_14	PAP	Magnesium chloride	Dichloromethane	Room temperature	A
AM51_19	PAP	Magnesium chloride	Methyl acetate	4°C	A
AM51_25	PAP	Magnesium chloride	Ethanol	4°C	B
AM51_26	PAP	Magnesium chloride	Ethanol	Room temperature	A

From the analysed XRPD data, two product groups have been recognised, as defined in Table 54.

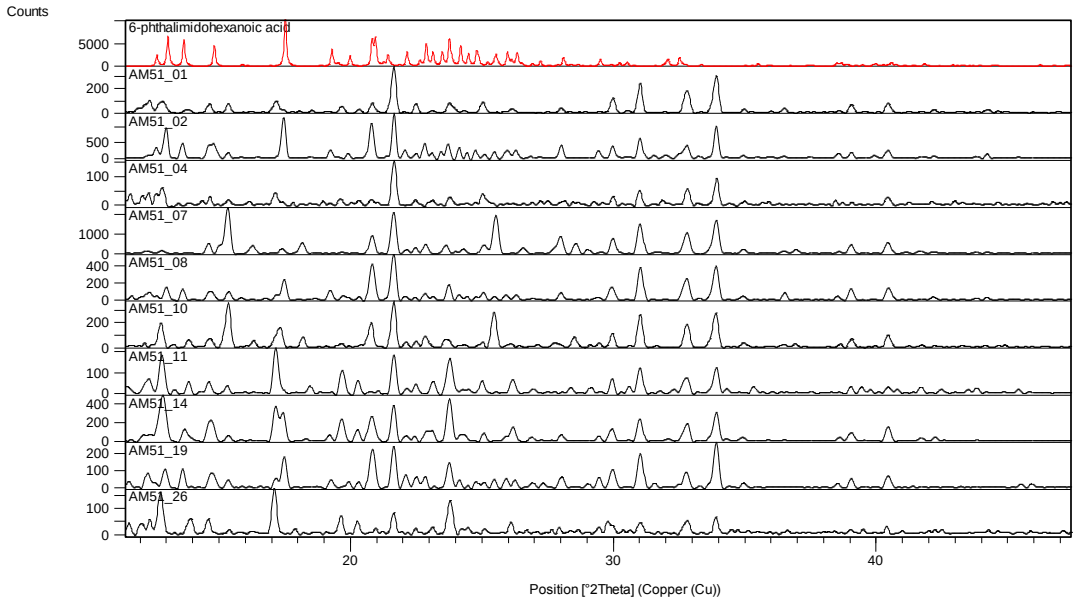

Figure 255 – XRPD patterns of collected scans categorised as group A from the crystallisation of PAP with magnesium chloride and hydrogen peroxide (black), compared with the reference pattern of 6-phthalimidohexanoic acid (red).

Samples falling into category A, are those in which 6-phthtlaimidohexanoic acid is present in the pattern in differing proportions. In some of these samples they are not the main component, however the pattern profiles indicate that that the strongest peaks are present. This is particularly noted at around 17.5° in 2θ and in the region between 12° and 15° 2θ where the characteristic peak profile can be seen (Figure 255).

In samples categorised as group B, distinctive peaks originating from the profile of 6-phthalimidohexanoic acid monohydrate Form I can be found; this is most evident at around 25° 2θ (Figure 256). These reference patterns account for some of the Bragg peaks found in the experimental patterns, however many are unaccounted for – in particular the peaks between 30° and 34° 2θ found in all of the samples cannot be assigned by any known pattern. More study, particularly single crystal analysis, is needed on this material to attempt to find a structure of a known unit cell corresponding to these peaks.

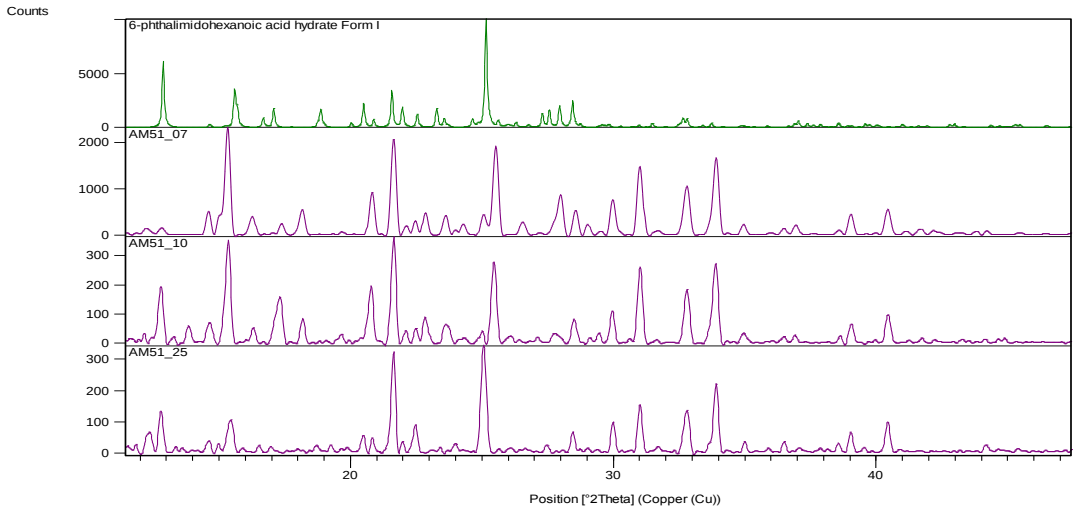

Figure 256 - XRPD patterns of collected scans categorised as group B from the crystallisation of PAP with magnesium chloride and hydrogen peroxide (purple), compared with the reference pattern of 6-phthalimidohexanoic acid monohydrate form I (black).

Calcium Chloride

The crystallisation conditions used are given in Table 55

Table 55 - Crystallisation conditions of PAP and calcium chloride

Sample ID	Component A	Component B	Solvent	Temperature	Scan Group/s
AM54_01	PAP	Calcium chloride	Ethyl acetate	4°C	A
AM54_02	PAP	Calcium chloride	Ethyl acetate	Room temperature	Amorphous
AM54_04	PAP	Calcium chloride	Chloroform	4°C	Amorphous
AM54_05	PAP	Calcium chloride	Chloroform	Room temperature	Amorphous
AM54_07	PAP	Calcium chloride	Acetone	4°C	B
AM54_10	PAP	Calcium chloride	Diethyl ether	4°C	B
AM54_13	PAP	Calcium chloride	Dichloromethane	Room temperature	Amorphous
AM54_14	PAP	Calcium chloride	Dichloromethane	4°C	Amorphous
AM54_19	PAP	Calcium chloride	Methyl acetate	4°C	C
AM54_20	PAP	Calcium chloride	Methyl acetate	Room temperature	C
AM54_22	PAP	Calcium chloride	Isopropanol	4°C	Amorphous
AM54_23	PAP	Calcium chloride	isopropanol	Room temperature	Amorphous

Analysis of the resultant materials by XRPD proved to be very difficult as the samples were poorly crystalline, some showing no reflections at all. These samples are marked on Table 55 as amorphous. The remaining samples were categorised into 3 groups, A, B and C.

Group A is from ethyl acetate at 4°C, which by powder pattern comparison clearly indicates the presence of triacetone-triperoxide form I in the sample along with unidentified secondary materials (Figure 257 red). This can only be from oxidation of the methyl acetate by the PAP or the hydrogen peroxide and subsequent formation of TATP crystals.

Group B, from acetone and diethyl ether at 4°C, shows similarity with the primary peaks of the decomposed PAP product 6-phthalimidohexanoic acid, however the patterns are very weak so only the presence of the strongest reflections is observed (Figure 257 black).

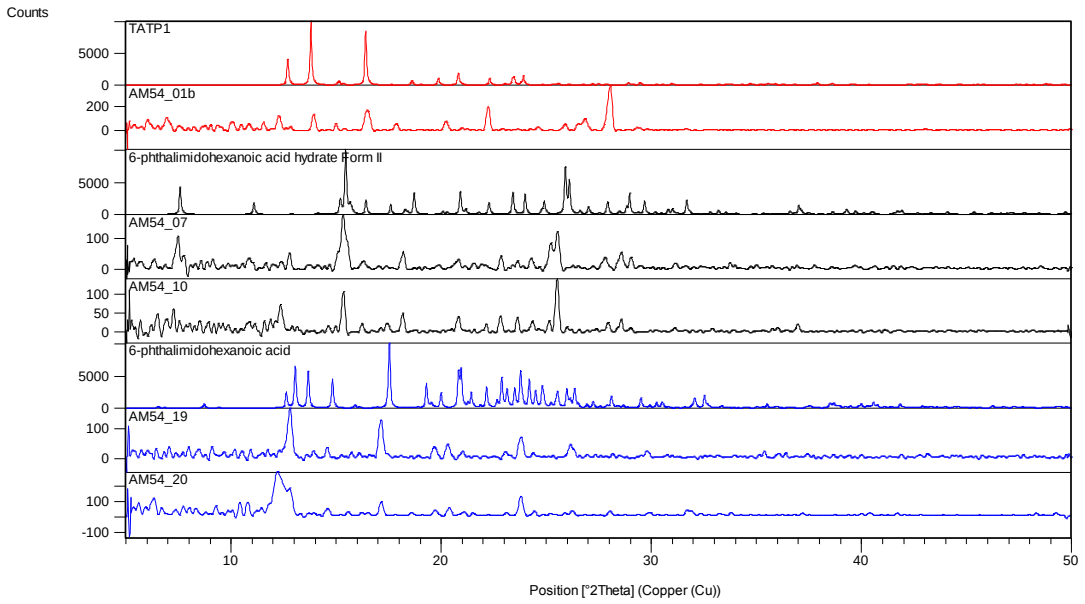

Figure 257 - XRPD patterns of materials from crystallisation of PAP with calcium chloride and hydrogen peroxide compared to matching reference patterns. Analysis group A (red) with reference TATP (top red), analysis group B (black) with reference 6-phthalimidohexanoic acid monohydrate form II (top black) and analysis group C (blue) with reference 6-phthalimidohexanoic acid (top blue).

The final group C again are represented by extremely weak patterns, but they do show some similarity to the strongest features in the pattern profile of the decomposed PAP product 6-phthalimidohexanoic acid (Figure 257 blue).

There is no clear indication in any of the samples analysed that would suggest that PAP has been retained or that a new complex has formed, other than the reaction product TATP.

Copper Chloride

The crystallisation conditions used are given in Table 56

Table 56 - Crystallisation conditions of PAP and copper chloride

Sample ID	Component A	Component B	Solvent	Temperature
AM88_01	PAP	Copper chloride	Acetone	4°C
AM88_03	PAP	Copper chloride	Methyl acetate	4°C
AM88_05	PAP	Copper chloride	Ethyl acetate	4°C

From the collected XRPD data of the samples, it can be seen by comparison to the reference materials powder patterns that the composition of all three of the samples is a mixture of copper chloride and the decomposed PAP parent acid – 6-phthalimidohexanoic acid monohydrate (form I) as is shown in Figure 258. There is no indication of PAP in the samples or that any new complexes have formed.

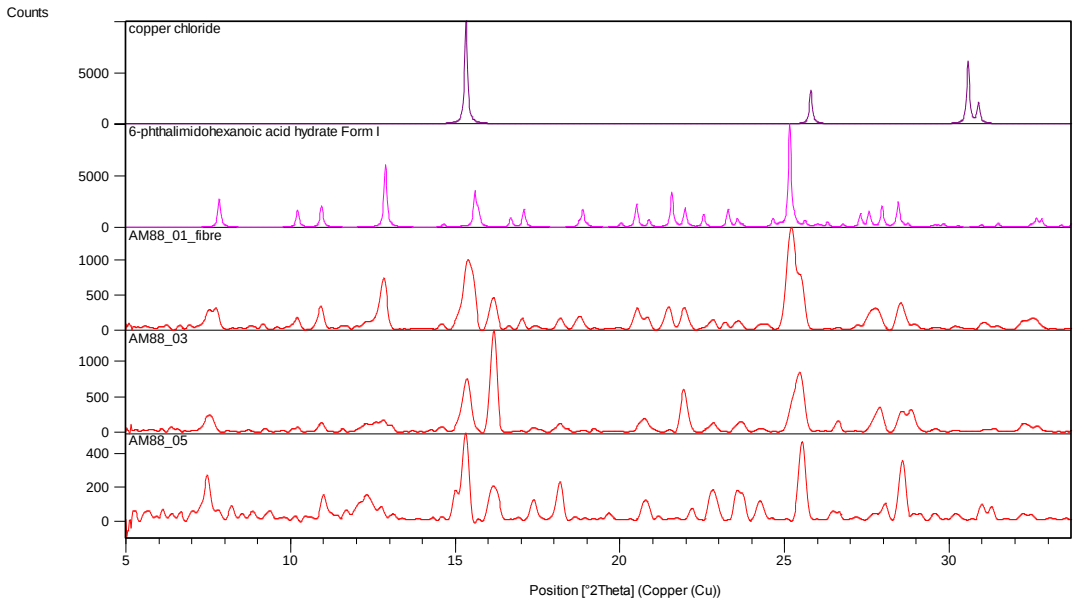

Figure 258 - XRPD patterns of materials collected from the crystallisation of PAP and copper chloride with hydrogen peroxide (red) compared to reference patterns of copper chloride (purple) and 6-phthalimidohexanoic acid monohydrate form I (magenta).

Copper Sulfate

6-phthalimidoperoxyhexanoic acid was also crystallised with copper sulfate with the addition of hydrogen peroxide under similar conditions, however at the time of writing, no results have been obtained for analysis.

5.4 Conclusions

Utilising carboxylic acids as secondary materials for cocrystallisation conditions has yielded no positive results in terms of complex formation with the target peroxyacids. Addition of many of the carboxylic acids has led to the complete decomposition of the peroxyacids and recrystallization of the co-component, favouring self-association rather than molecular association with the target material or its decomposition products. It is unexpected that there is no evidence of complex formation between the parent acids and the carboxylic acid secondary materials. This could possibly be a result of the equilibrium reaction in play throughout the crystallisation preventing molecular recognition as a result of constantly interchanging functionality between a carboxylic acid and peroxyacid group. It seems however that the carboxylic acid functionality is incompatible for interaction with the peroxyacid group, and no new materials have been formed.

With the non-carboxylic acid functionalised materials, such as the π-π interacting materials there also has been little to no success in creating a new material complex. In the majority of cases, decomposition to the parent acid of the peroxyacid is the normal outcome, with

few exceptions to the rule. The new molecular complex between the parent acid and benzimidazole leads to a supposition that molecular similarity to the largest part of the molecule could be a potential route to reliably creating molecular complexes with PAP, but this requires more investigation. A possible future direction would be to use a non-functionalised, or fully oxidised functionality within phthalimido molecules, where no chemical reactions can take place during the crystallisation process.

The crystallisation with metals has yielded no new complexes. If this approach is to work more effectively, a more directed synthesis methodology would perhaps be better suited rather than soft molecular recognition and salt formation.

Addition of hydrogen peroxide to crystallisation experiments throughout the research seems to have had the effect of producing fewer crystalline or more amorphous materials. This could possibly be explained by the effect of the equilibrium reaction and subsequent functional group changes in disturbing the molecular recognition step in the crystallisation process. This could be equally the case for the secondary material, as the presence of hydrogen peroxide may instigate an oxidation of any carboxylic acid group present in these materials, again potentially disrupting molecular recognition possibilities.

6. Hosting Reactive materials

This Chapter discusses a different approach to stabilising the target reactive materials which focusses upon trying to design systems in which the highly reactive and unstable target molecules would interact in molecular complexes with selected co-components using the principles of crystal engineering and molecular recognition. The technique discussed here instead involves bringing the material into a larger, more stable structure, which could lead to protection of the molecules within a hosted environment and an overall reduction in their reactivity.

As described in the introduction, there are several ways in which this could be achieved: through assembly of a host structure around the molecules, such as with urea complexes, or by utilising pre-assembled hosts, such as the large and highly stable cyclodextrins, to host the target reactive materials within their structure.

Another area explored is that of potential hosting within layered materials. In particular the montmorillonite clay Bentonite was used in an attempt to allow the inclusion of the target reactive material 6-phthalimidoperoxyhexanoic acid (PAP) within its layered arrangement.

6.1 Urea based hosting

The ability of urea to create channelled networks around secondary guest materials[90] proposed a possible strategy for molecularly encapsulating reactive peroxyacids into a larger structure that may possibly add stability to the guest material. Both urea and thiourea, which has larger structural footprint and porosity as noted earlier, were studied as a way of enclosing the target peroxyacid molecules within a protective molecular shell.

Both materials, urea and thiourea, were first tested with hydrogen peroxide in a range of typical crystallisation conditions to determine if the channelled structures could first be created under such reactive conditions. As noted in the previous chapter, inclusion of hydrogen peroxide into the crystallisation environment has in general decreased crystallinity in the final sample but as the urea based molecules are not directly interacting with the functional group of the target molecules, this may not pose an issue in this case.

6.1.1 Urea and hydrogen peroxide

Urea was crystallised an a range of solvents at 4°C and room temperature as detailed in Table 57, and the collected crystalline materials analysed by XRPD and single crystal unit cell analysis.

Table 57 - Crystallisation of Urea in selected solvents with hydrogen peroxide

Sample	HOOH	Solvent	Temperature	Analysis group
AM39_01	5 Drops	Methanol	4°C	A
AM39_02	5 Drops	Methanol	Room temperature	A
AM39_03	5 Drops	Ethanol	4°C	B
AM39_04	5 Drops	Ethanol	Room temperature	A
AM39_05	5 Drops	Acetone	4°C	A
AM39_06	5 Drops	Acetone	Room temperature	B
AM39_07	5 Drops	Methyl Acetate	4°C	A
AM39_08	5 Drops	Methyl Acetate	Room temperature	A
AM39_09	5 Drops	Ethyl Acetate	4°C	A
AM39_10	5 Drops	Ethyl Acetate	Room temperature	A
AM39_11	5 Drops	Chloroform	4°C	A
AM39_12	5 Drops	Chloroform	Room temperature	A
AM39_13	5 Drops	Dichloromethane	4°C	A
AM39_14	5 Drops	Dichloromethane	Room temperature	A

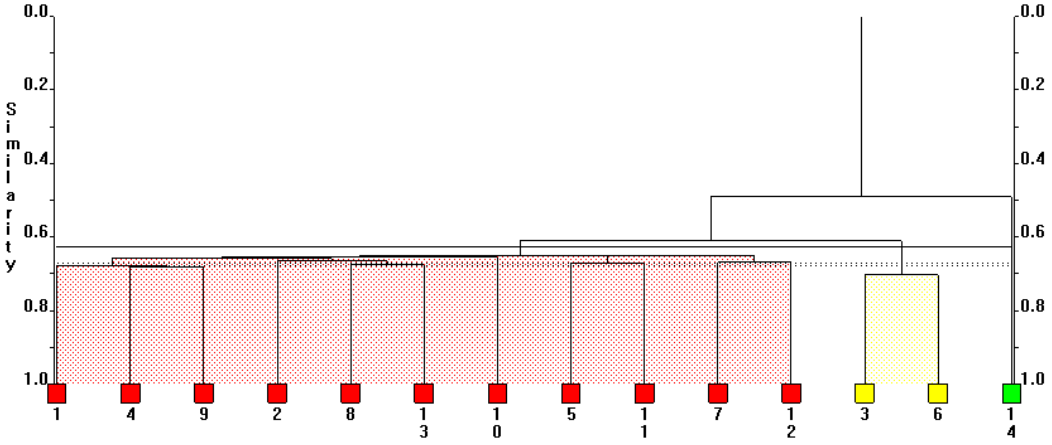

Figure 259 - XRPD clustering dendrogram showing three pattern types present.

The XRPD data was clustered using PolySNAP3[123] and found to contain three clustered pattern types. The largest of the three clusters, defined as group A and shown as red in Figure 259, corresponds to the recrystallisation of the starting material urea on its own, as shown by pattern comparison of a representative sample (Figure 260).

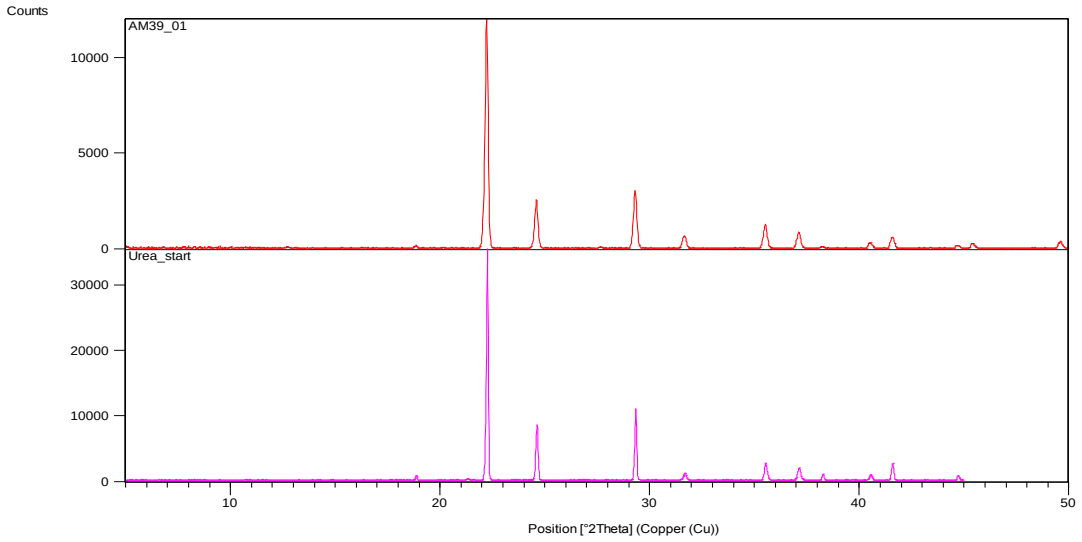

Figure 260 - XRPD pattern representative of group A (red) compared to the reference pattern of the urea starting material (magenta).

XRPD pattern comparison for the second cluster, denoted B and shown as yellow in Figure 259, shows the presence of the same recrystallised starting material as shown in group A but with the addition of a second material. This is a hydrogen peroxide:urea complex (Figure 261) previously determined and recorded in the CSD[157].

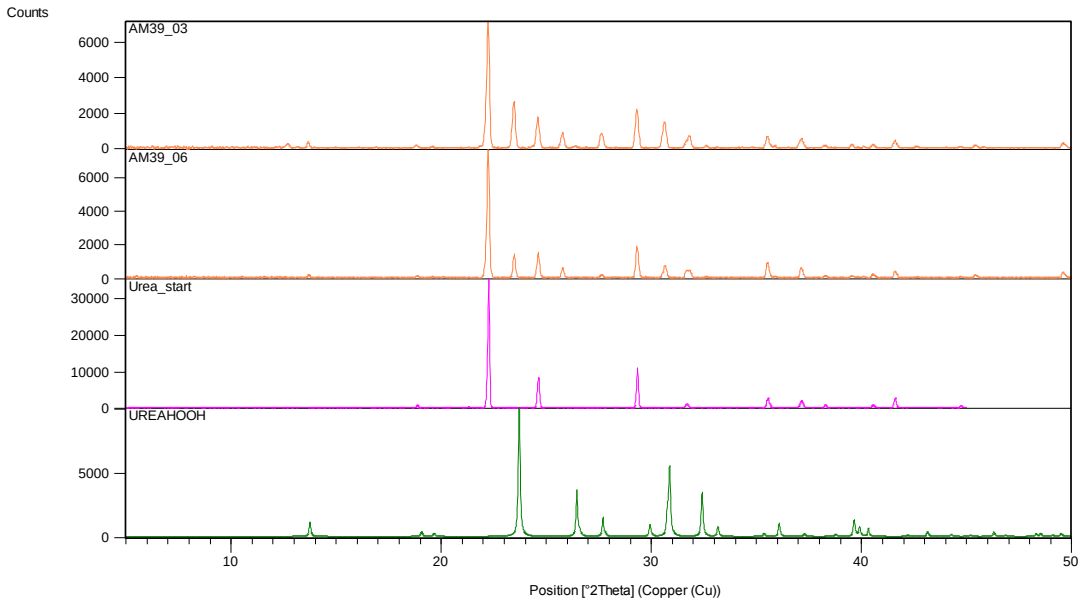

Figure 261 - XRPD patterns of group B (orange) compared to the reference patterns of the urea starting material (magenta) and the urea:hydrogen peroxide complex (olive).

The third cluster denoted C and shown as yellow in the dendrogram (Figure 259) is a good match for group A by manual analysis of the XRPD pattern. However a much higher background and poorer crystallinity results in a less good match, leading to a separate clustering of this group.

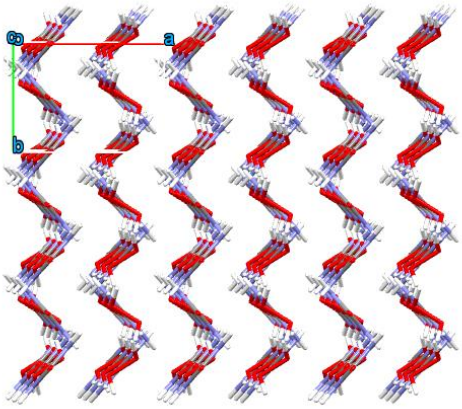

Figure 262 - Urea:HOOH cocrystal structure as viewed down the c-axis

Thy hydrogen peroxide:urea 1:1 complex structure[157] is not a tunnelled complex but a 1:1 structure featuring a zigzag motif (Figure 262). However it is stable and proves urea to be unreactive in the presence of strong oxidising agents. This complex was also proved to be present in samples from both methyl acetate and ethyl acetate solution at room temperature as confirmed by single crystal analysis. However these crystals are not sufficiently abundant to form the bulk of the sample as determined by XRPD.

6.1.2 Thiourea and hydrogen peroxide

The same experimental procedure was performed with thiourea. In this case, however, upon addition of the oxidising agent, the thiourea reacted violently, likely a result of the strong sulfur-oxygen affinity. Any recrystallisations of peroxyacids in thiourea would likely result in a similar reaction and consequently this direction was not pursued.

6.1.3 Urea and 6-phthalimidoperoxyhexanoic acid

With urea proving to be stable in the presence of peroxyacids, 6-phthalimidoperoxyhexanoic acid (PAP) was added to urea in the presence of a small amount of hydrogen peroxide with the aim of creating either a hosted material or a molecular complex between the two. They were prepared in equimolar quantities and cocrystallised in a selected range of solvents at both 4°C and room temperature. Those for which XRPD data were collected for are shown, along with their crystallisation conditions, in Table 58.

Table 58 - Crystallisation of urea with PAP in selected solvents with hydrogen peroxide

Sample	Component A	Component B	HOOH	Solvent	Temperature
AM41_01	Urea	PAP	5 Drops	Methanol	4°C
AM41_03	Urea	PAP	5 Drops	Ethanol	4°C
AM41_05	Urea	PAP	5 Drops	Acetone	4°C
AM41_07	Urea	PAP	5 Drops	Methyl Acetate	4°C
AM41_08	Urea	PAP	5 Drops	Methyl acetate	4°C
AM41_09	Urea	PAP	5 Drops	Ethyl Acetate	4°C
AM41_11	Urea	PAP	5 Drops	Chloroform	4°C

These samples that were analysed by XRPD indicated that the urea had recrystallised in all cases with the decomposed PAP parent acid 6-phthalimidoperoxyhexanoic acid present in trace amounts in all samples. The sample produced from methanol, however, shows a significantly increased amount of the parent acid as can be seen in Figure 263.

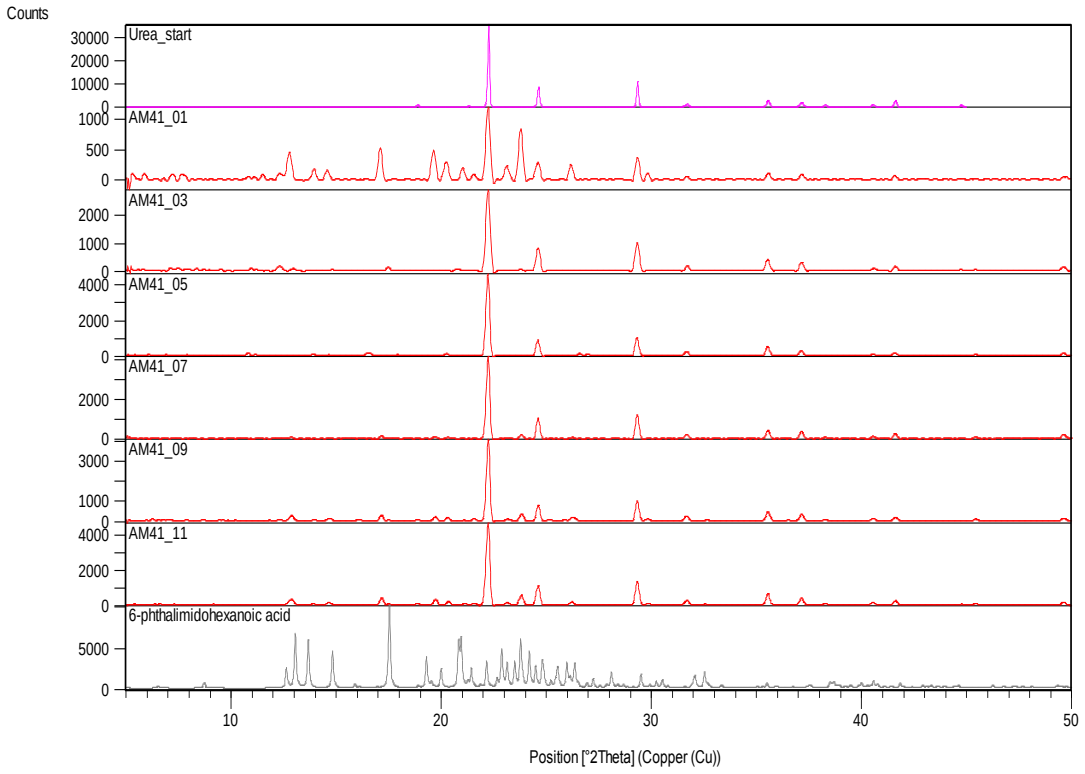

Figure 263 - XRPD patterns of resultant material from cocrystallisations of urea and PAP with hydrogen peroxide (red) compared to the reference structure of urea (magenta) and 6-phthalimidohexanoic acid (grey).

Suitable crystals from AM41_08 were analysed by single crystal XRD and found to consist of the urea:HOOH cocrystal described above.

The combination of these results would seem to suggest that the PAP molecule has decomposed to a significant extent, and partially recrystallised as the parent acid, irrespective of the recrystallisation behaviour of the urea. A small percentage of the HOOH

present in the crystallisation or resulting of the decomposition of the PAP, crystallises with the urea to create a known molecular complex.

6.1.4 Urea and *meta*-Chloroperbenzoic acid

Following the experiments with urea and PAP, MCPBA was crystallised under the same conditions. In this case, hydrogen peroxide was excluded from the crystallisation in order not to compete with the peroxyacid as a target for the urea. The crystallisation conditions for which XRPD data were obtained are detailed in Table 59.

Table 59 - Crystallisation of urea with MCPBA in selected solvents with hydrogen peroxide

Sample	Component A	Component B	Solvent	Temperature
AM41_01	Urea	MCPBA	Acetone	4°C
AM41_03	Urea	MCPBA	Methyl Acetate	4°C
AM41_05	Urea	MCPBA	Ethyl Acetate	4°C
AM41_07	Urea	MCPBA	Diethyl Ether	4°C

The resultant materials were analysed by XRPD and found to be comprised of the urea starting material and the urea:hydrogen peroxide complex in smaller amounts (Figure 264). This confirms decomposition of the peroxyacid to supply the urea with hydrogen peroxide that must be available to form the complex.

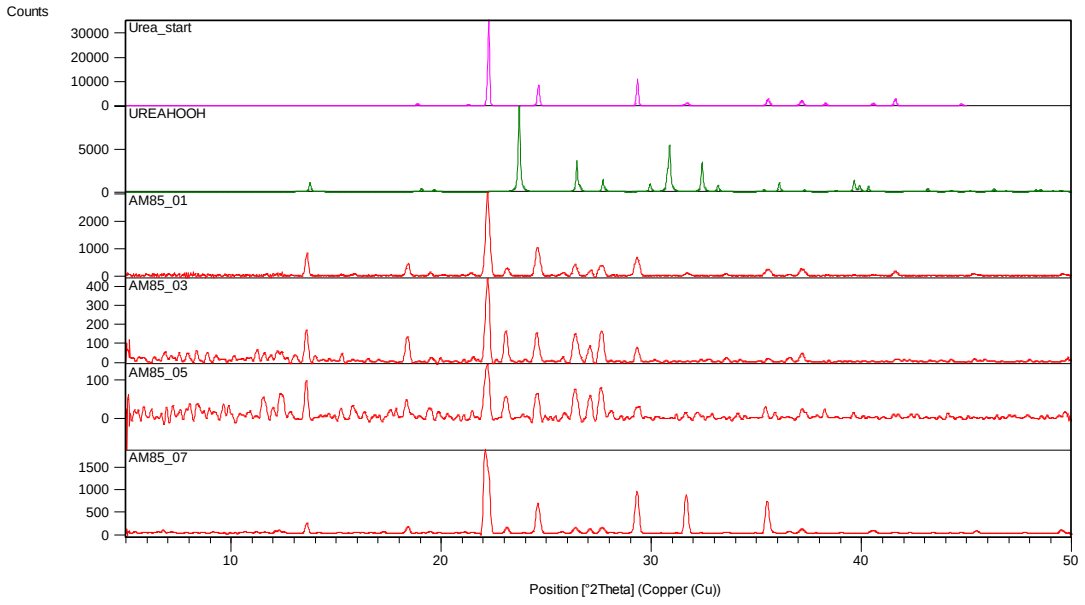

Figure 264 - XRPD patterns of crystallisation products of urea and MCPBA (red) compared with reference patterns of the urea starting material (magenta) and the urea:HOOH complex (green).

6.1.5 Summary

Crystallisation with urea and thiourea has failed to produce a channelled complex around the peroxyacid molecules, with thiourea reacting quite violently with the strongly oxidising

materials making it wholly incompatible with them. Urea did form a molecular complex with hydrogen peroxide in several systems and proves to be stable in the presence of the reactive materials. However it may be aiding in the decomposition of the peroxyacid group by removing liberated hydrogen peroxide from the environment, thus accelerating the decomposition equilibrium.

Finding the correct conditions for producing a channelled structure around the peroxyacids without decomposition of the functional group could still potentially lead to the formation of a clathrate structure hosting a peroxyacid. More success may be achieved with the aliphatic peroxyacids, such as peroxypelagonic acid, which would better suit hosting of the peroxyacid in the relatively small dimensions of the channels.

6.2 Hosting within cyclodextrins

Hosting with cyclodextrins and cyclodextrin derived molecules is a potential way of creating a robust cage structure around guest molecules that physically encapsulates them. This could prevent them from reacting readily with molecules external to the structure. Cyclodextrins are stable molecules and as such were not expected to react with the oxidising peroxyacids and offered a potential route for stabilisation. Crystallisations were prepared of α-, β- and triacetyl-β-cyclodextrin with the peroxyacids under study. Some of these crystallisations were carried out with the addition of hydrogen peroxide, and bases such as sodium and potassium hydroxide. This follows the work on "edible MOF's" by Smaldone[96] as a synthesis methodology for trapping molecules.

Prior to experiments with the peroxyacids, it was confirmed that recrystallisation of the cyclodextrins was possible, with formation of the β-cyclodextrin metal frameworks successfully achieved in the absence of peroxyacid as confirmed by single crystal diffraction and unit cell determination.

6.2.1 *meta*-chloroperbenzoic acid and β-cyclodextrin potassium framework

A cocrystallisation experiment using MCPBA and β-cyclodextrin with the addition of potassium hydroxide in water produced single crystal samples. These were confirmed to be an unknown crystal structure by evaluation of the unit cell parameters against those in the CSD[136]. Single crystal X-ray data from these crystals were therefore collected on the Rigaku R-axis image plate diffractometer to determine the structure of the new material formed. The experiment details and crystal structure parameters are shown in Table 60.

Table 60 - Crystal structure collection data for potassium β-cyclodextrin 3-chlorobenzoic acid clathrate

Compound	**3-Chlorobenzoic acid potassium-β-cyclodextrin clathrate**
Formula	$C_{105}H_{141}O_{98}Cl_3K_3$
Crystallisation Conditions	MCPBA, β-cyclodextrin and potassium hydroxide in water at 30°C
Molecular weight / $gmol^{-1}$	3194.9
Temperature (K)	100
Space Group	P1
a (Å)	14.9575(17)
b (Å)	15.7246(18)
c (Å)	15.7755(18)
α (°)	89.733(4)
β (°)	75.565(4)
γ (°)	76.220(4)
Volume ($Å^3$)	3483.94(55)
Z	1
Z'	1
θ range/˚	3.06 – 27.48
Reflections Collected	44410
Independent	28565
Refln (obs.I>2theta(I))	18336
R_{int}	0.0531
Parameters	1889
GooF on F^2	1.077
R_1 (Observed)	0.0978
R_1 (all)	0.1337
wR_2 (all)	0.3057
Flack Parameter	0.04(7)

From the determined crystal structure, it can be seen that the cocrystallisation experiment has resulted in the formation of a cyclodextrin/potassium host structure with a 3-chlorobenzoic acid guest. The latter is decomposed from the MCPBA peroxy-acid starting material and subsequently included in the structure (Figure 265).

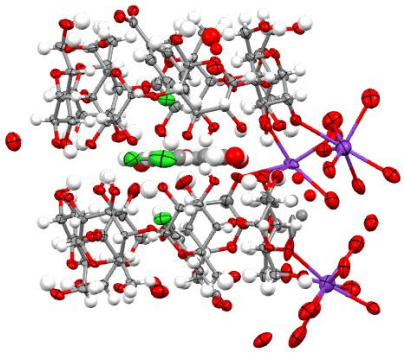

Figure 265 - Asymmetric unit of the beta-cyclodextrin potassium 3-chlorobenzoic acid clathrate.

The crystal structure may be dissected into three constituent parts, the cyclodextrin/potassium frame, the intercalated 3-chlorobenzoic acid molecules, and the

crystallised solvent water molecules throughout the structure. The latter is a consequence of crystallisation in water as a solvent and is common for cyclodextrin structures. The number of water molecules in the structure is not always well defined as they are freely situated within voids generated by the large and inefficiently packed structure. The included water molecules are hydrogen bonded to the abundant hydroxyl groups on the external side of the cyclodextrin rings. There are nine independent oxygen atoms determined in the structure and each of these is assumed to be water molecules. However the size of the structure and the disorder present precludes determination of the solvent water hydrogen atoms (Figure 266).

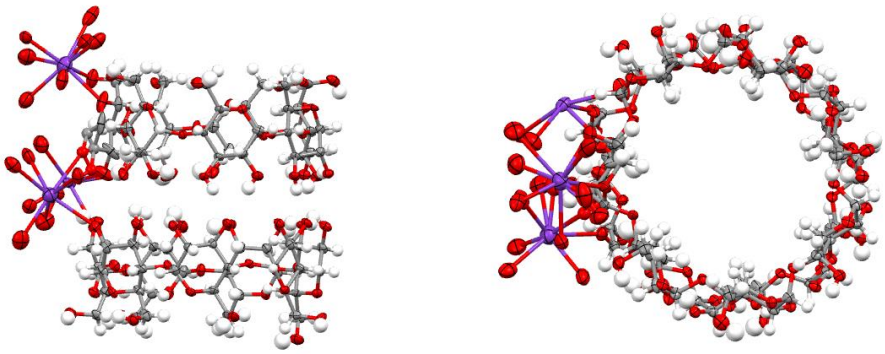

Figure 266 - The asymmetric unit of the K-β-cyclodextrin framework only as viewed from side on and top down orientations showing external facing hydroxyl groups available for hydrogen bonding to H_2O.

The cyclodextrin framework is the largest component of the structure and directs the structure with its connectivity. The β-cyclodextrin molecules, as observed regularly in the literature[85, 96], form the familiar barrel arrangement (Figure 267 left), creating a hollow in which large guest materials may be hosted, with an approximately 3Å average separation between the oxygen atoms of the two molecules. This has the effect of creating a void that is approximately 12Å wide at the centre point of the barrel and 10Å at either end, measured from atom centre points. In this structure however, the β-cyclodextrin molecules are bridged by two potassium ions, one forming three short contacts and the other forming one ordered contact and a two-position disordered contact, resulting in changes in the conformation of the glucose molecule the cyclodextrin ring (Figure 267 right).

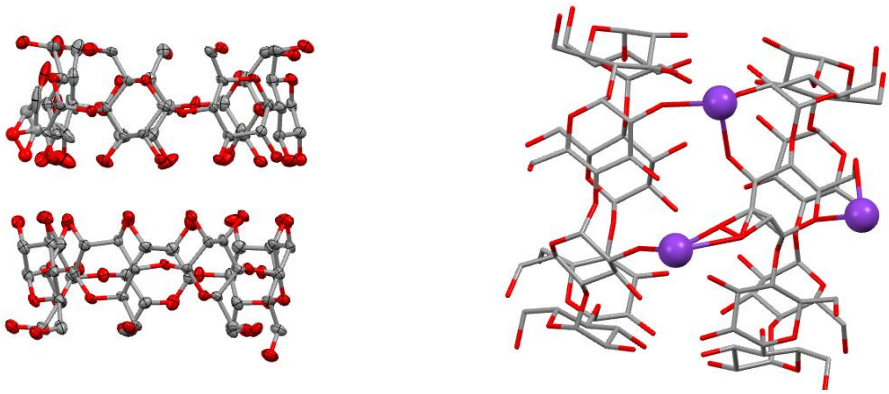

Figure 267 - Common barrel arrangement of β-cyclodextrin molecules within the framework (left). Two bridging potassium ions and one top mounted potassium ion in the structure (right)

The β-cyclodextrin molecules are then further connected through the potassium ions to water molecules, which bridge the gap via hydrogen bonding at the widest points between the molecules. The molecules are also further connected with extensive hydrogen bonding networks between the barrels themselves, aligning all the molecules on the same axis, creating channels of pores (Figure 268 left).

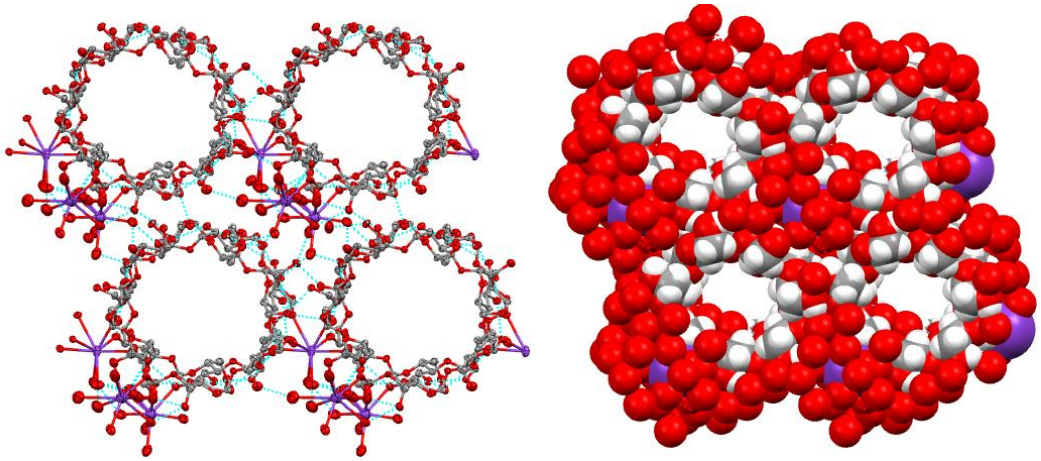

Figure 268 – the β-cyclodextrin framework is linked together with ionic interactions and extensive hydrogen bonding (left). The cyclodextrin molecules overlap leaving only internal voids in the framework (right).

The hydrogen bonded molecules are in sufficiently close proximity to overlap the van der Waals radii of the neighbouring barrels, leaving only the internal voids available for secondary molecules (Figure 268 right). Inside the voids of the barrels, there are three 3-chlorobenzoic acid molecules (Figure 269 left), two of which are ordered and orientated inside the cyclodextrin rings, in plane with the length of the void, and a third molecule located in the gap between the two sides of the barrel arrangement, disordered between two positions (Figure 269 right).

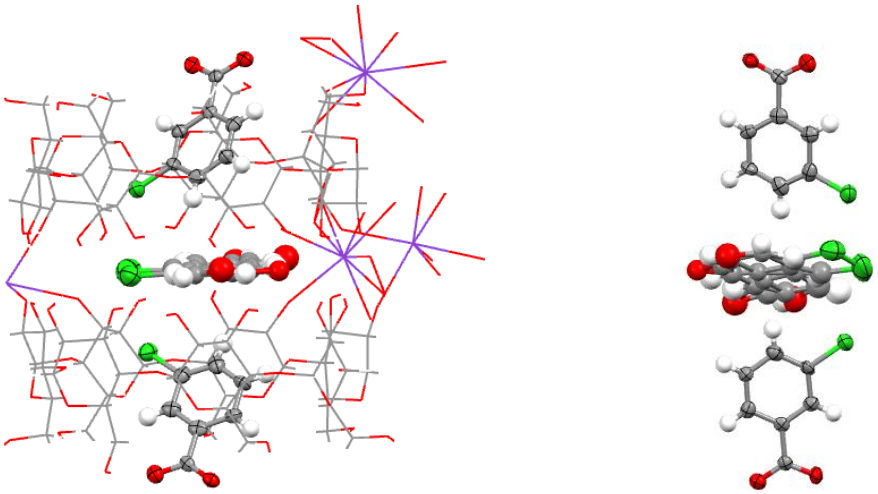

Figure 269 - Three 3-chlorobenzoic acid molecules located inside the core of the barrel arrangement of -cyclodextrin (left). The three 3-chlorobenzoic acid molecules, two are static, one is disordered (right).

The two ordered molecules are at an aromatic C-H···π stacking distances of 3.82(1)Å and 4.04(2)Å to the disordered centre molecule, with their chlorine atoms clustered around a single area with Cl···Cl distances between 3.111(9)Å and 4.657(6)Å depending on which site is assigned to the disordered molecule.

The disordered molecule itself is situated over two positions, each at about 50% occupancy. The molecules can be separated from each other, as shown in Figure 270, with the atom positions and hydrogen locations assigned for each molecule. In the disordered configuration, the molecule flips orientation, moving the position of the chlorine atom by 2.10(2)Å , with rotation of the carboxylic acid group about 120° around the centre point of the two molecules. This disorder either induces or is induced by the disorder in the bridging potassium ions between the cyclodextrins.

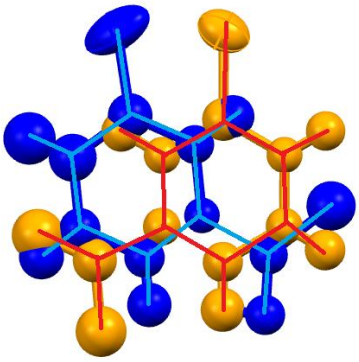

Figure 270 - 50/50% disordered 3-chlorobenzoic acid molecule at the centre of the cyclodextrin barrel, with connectivity of individual disordered components highlighted in blue and orange for clarity.

The resulting material can therefore be described as a 3:2:3 potassium : cyclodextrin L 3-chlorobenzoic acid complex.

Given the ability of this complex to host the peroxy-acid decomposition product 3-chlorobenzoic acid, it may be possible either to crystallise MCPBA into the structure if the correct conditions are found for retention, or to re-functionalise the peroxyacid after formation of the complex by reacting with hydrogen peroxide. Hydrogen peroxide itself, as a result of its small size, may be able to enter into the pore along with the 3-chlorobenzoic acid and re-functionalise the acid group.

6.2.2 Summary

More of the materials set up and crystallised in this area need to be studied in more detail, particularly those containing MCPBA, to assess whether a condition has been isolated in which the peroxyacid has been crystallised into the clathrate with the peroxyacid functionality retained. The host framework may also be compatible with inclusion of the larger PAP molecule. The probability of this being possible appears high, with a cyclodextrin based PAP already on the market and sold as Cavamax® W7/Eureco®[158], with no crystal structure recorded. However, due to time constraints it was not possible to pursue this further in this project.

6.3 Hosting within clays

Montmorillonite based materials such as Bentonite are known to have a semi-stable layered structure in which the pore sizes are constant throughout the material. They have a general composition of $[Al_2(OH)_2(Si_2O_5)_2]$[13] [159] and their texture properties are dependent on the contents of the layers, the charge of the intercalated material and any mechanical working of the layered material itself. However, the porosity is not yet fully understood[159]. The pore sizes of the materials are known to change as a result of saturation and hydration, and it has been shown to be possible to place a desired material into the intercalant pores in literature precedents[160].

The proposed and generally accepted mechanism of intercalation is that with the hydration of the layered material, the pores or layers separate, allowing inclusion of the solvent, and thus any material present in the solvent (Figure 271). As the material is dehydrated, the pore or layer returns to a smaller dimension, with the deposition of the solvated target material into the enlarged spacing, entrapping the molecule into the structure of the clay itself.

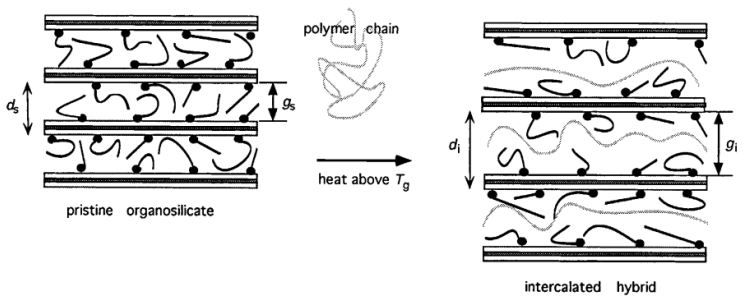

Figure 271 - intercalation of a material into a layered montmorillonite[161].

The effect of this upon the montmorillonite structure is an observed increase in the size of the spacing between the layers, termed the "basal" spacing, corresponding to the increase in space needed for the intercalant to be hosted within the material. This can be measured from powder X-ray diffraction data as a low angle peak which can give a direct measurement as to the average physical size of the spacing throughout the material as shown in Figure 272.

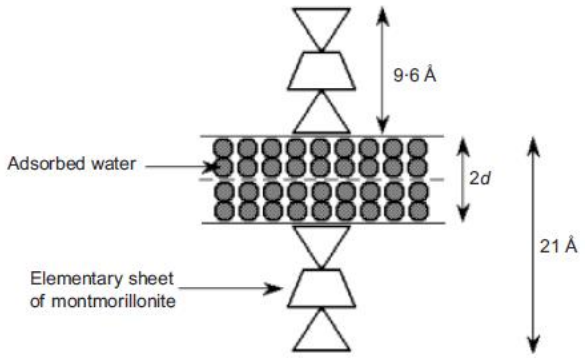

Figure 272 - Schematic of intercalation layer distances in a Montmorillonite clay[160]

6.3.1 Intercalation of materials into clays by solid grinding

To investigate the use of this material as a potential host for the target peroxy-acids, solvent free grinding of the reactive component with the bentonite clay was achieved by manually grinding the bentonite clay and PAP together in initial weight per weight measurements under completely dry conditions. This led to the formation of unremarkable dry powders as could be expected. This was repeated for acetic acid, peroxyacetic acid and *meta*-chloroperobenzoic acid. These samples were analysed by XRPD and the patterns collected showed no change in the position of the basal peak in all samples except that prepared with PAP (Figure 273) where a significant shift of this characteristic peak to a lower angle in 2θ was observed. All patterns are given in Appendix 3.

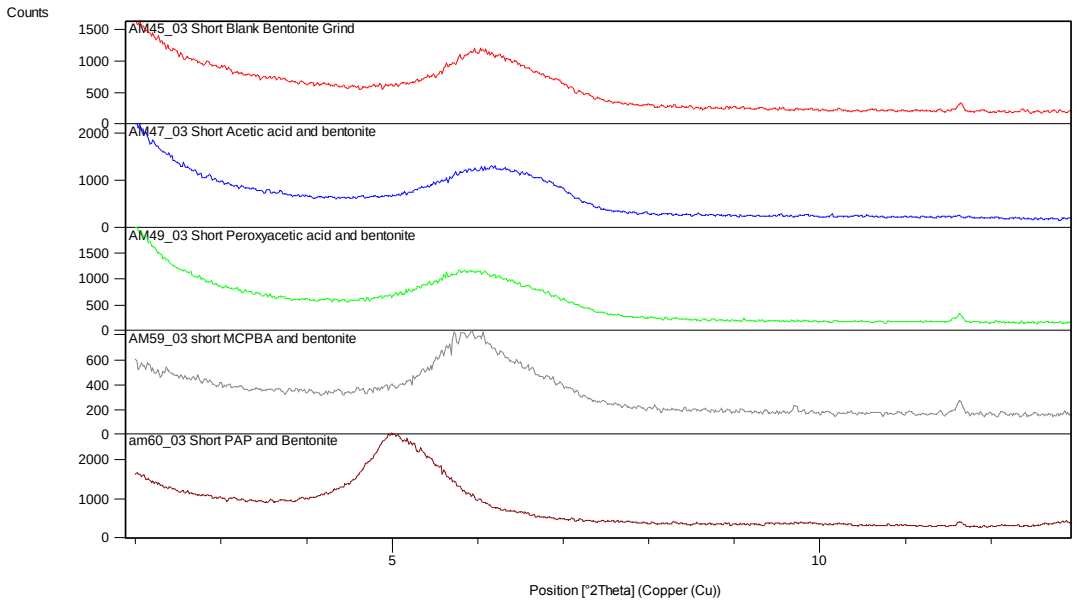

Figure 273 - Basal spacing change measured in XRPD patterns of Bentonite-intercalate grinding with solely Bentonite (red), acetic acid (blue), peroxyacetic acid (green) *meta*-chloroperbenzoic acid (grey) and 6-phthalimidoperoxyhexanoic acid (PAP; brown).

To confirm and characterise further this result observed with PAP, the experiment was repeated and the pattern of the resulting material was analysed immediately by XRPD. This initial pattern showed no difference to that of the recorded powder pattern of the clay alone. However, when the sample was left for a period of a week to a month and analysed for a second time, a significant change in position of the the broad peak was observed. This shift correspnds to the previously observed shift in basal spacing between a blank grind and a grind with the PAP present (Figure 274). In addition to the structural effects, there is thus a kinetic effect evident, with a significant structural change in the clay structure as a function of time.

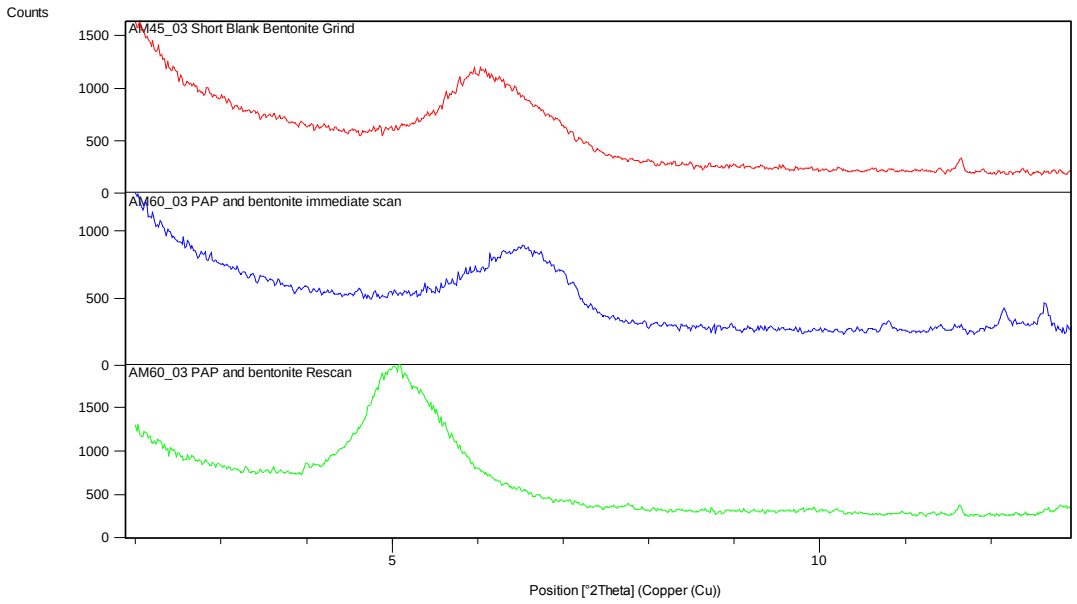

Figure 274 - Bentonite and PAP XRPD patterns: blank Bentonite (red); that resulting from a pattern determined immediately following the grinding of Bentonite and PAP (blue) and a later re-scan of the same system (green).

With the initial rough volume for volume experiment, there was an increase in basal spacing from 14.7Å to 17.7Å, as can be seen in the XRPD (Figure 273). This is consistent with the possibility of intercalation of a guest (possibly PAP) into the host clay material by slow solvation which could be aided by hygroscopic solvation of PAP by atmospheric water. The change in basal spacing corresponds to an inter-layer spacing increase in 3Å, more than sufficient to incorporate a PAP molecule oriented along the plane of the spacing. As such the material and this preparation method was further investigated.

The initial observation was shown to be repeatable by a second experiment via solvent drop grinding. A manual grinding technique was utilised, with a mortar and pestle, and grinding the material for no longer than three minutes in the presence of a catalytic amount of acetone (several drops, enough to wet the material out). Acetone was chosen as the solvent catalyst due to the believed balance of stability and solubility displayed by PAP in this solvent. This was also repeated with MCPBA to assess if direct solvation-assisted grinding would have the same effect upon that peroxyacid. As can be noted from Figure 275, the solvent drop sample with MCPBA did not initiate an increase in the basal spacing.

The repeat PAP grinding experiment upon near immediate analysis by XRPD of the resulting dry material, it was noted that the clay had once again expressed a shift in the basal spacing observed upon immediate analysis and as such a solvating effect was confirmed to be a requirement of the process. The proposed mechanism is that the target material is dissolved on the microscopic scale and forced into the layers or pores of the hosting material, depositing itself, and remaining after the solvent has been removed, thus forcing the layers to remain open as determined by the spacing increase.

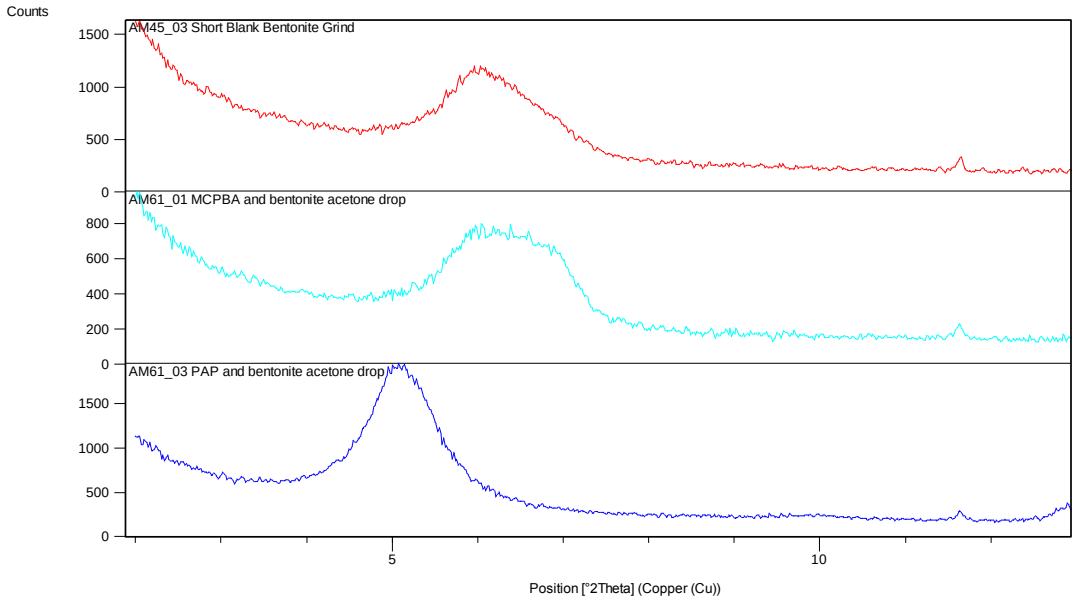

Figure 275 - Bentonite three-minute grind blank (red) compared with MCPBA solvent drop grind (light blue) and PAP solvent drop grind (dark blue).

In order to achieve a better understanding of the physical changes in these materials, SEM images were taken of the resulting products.

In the first set of images (Figure 276) it can be seen that dry grinding of Bentonite and PAP has resulted in the production of small crystallites and non-crystalline features appearing throughout the material. These non-crystalline features were measured to be up to 10 microns in diameter.

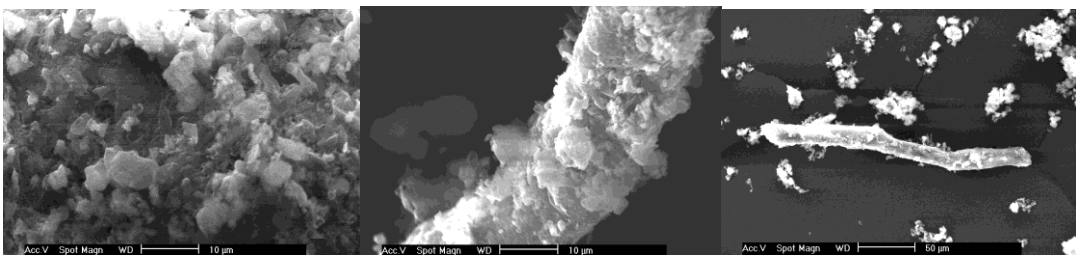

Figure 276 – SEM images of dry ground Bentonite with PAP showing distinct crystalline and non-crystalline features within the sample.

However, if a sample is dry ground and analysed within 1 hour, a completely different set of images is observed (Figure 277). In these images, taken at similar magnifactions, no crystallites or substantial non-crystalline features are observed.

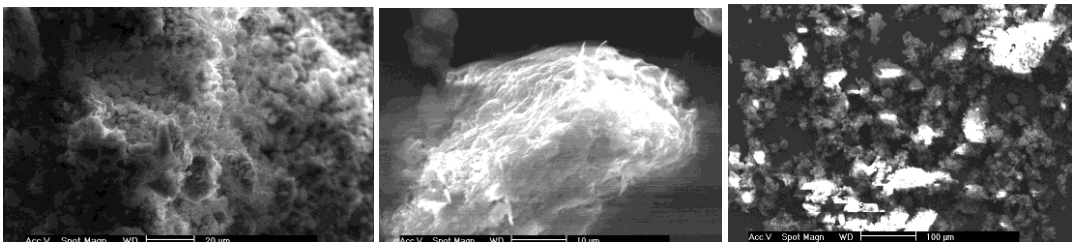

Figure 277 – SEM images of dry ground Bentonite and PAP observed within one hour of grinding.

When solvent drop grinding is used, again the crystallites and substantial non-crystalline features are observed within the structure of the intercalating material immediately (Figure 278).

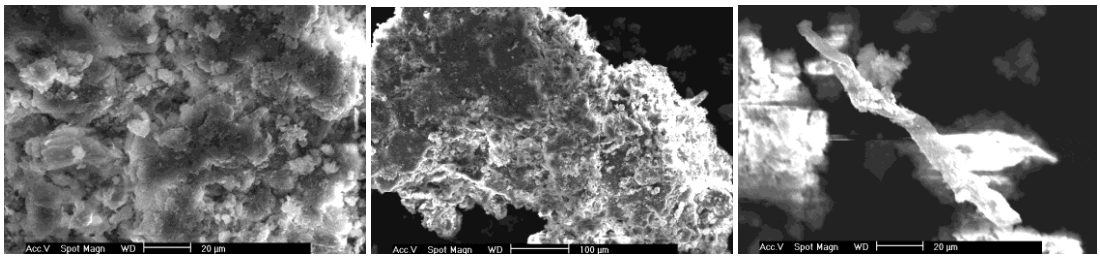

Figure 278 - SEM images of solvent drop ground Bentonite and PAP.

This mirrors the XRPD analysis of the ground materials, where the developed dry-ground and solvent drop-ground resultant materials show a change in basal spacing, whereas the dry-ground samples analysed immediately, do not.

In order to assess the effect that the quantity of PAP ground with the Bentonite would have on the basal spacing, measured quantities of the clay and the PAP were manually ground together with acetone drops added, for 3 minutes each. Details of the ratios used are listed in Table 61 and varied from 10:1 to 1:2 Bentonite:peroxyacid ratio, in 0.01g steps. The basal spacing was calculated by first smoothing the peak and then peak picking using

X'pert Highscore Plus[148] to determine the maximum in 2θ, which was subsequently converted to a d-spacing.

Table 61 - Bentonite and PAP measurements added to grinding experiments with corresponding basal spacing

Sample	Bentonite (g)	PAP (g)	Grind time (s)	Basal Spacing (Å)
AM102_01	0.10	0.01	180	15.92
AM102_02	0.10	0.02	180	16.25
AM102_03	0.10	0.03	180	16.47
AM102_04	0.10	0.04	180	16.64
AM102_05	0.10	0.05	180	17.21
AM102_06	0.10	0.06	180	17.02
AM102_07	0.10	0.07	180	17.63
AM102_08	0.10	0.08	180	17.60
AM102_09	0.10	0.09	180	17.55
AM102_10	0.10	0.10	180	17.80
AM102_11	0.10	0.11	180	17.18
AM102_12	0.10	0.12	180	17.35
AM102_13	0.10	0.13	180	17.50
AM102_14	0.10	0.14	180	17.32
AM102_15	0.10	0.15	180	17.32
AM102_16	0.10	0.16	180	17.33
AM102_17	0.10	0.17	180	17.49
AM102_18	0.10	0.18	180	17.72
AM102_19	0.10	0.19	180	17.60
AM102_20	0.10	0.20	180	17.87
Blank	0.10	0.00	180	14.93

Visually from the powder patterns (Figure 280), the increase in d-spacing appears to follow a linear trend, levelling off at around a 1:1 wt./wt. ratio of PAP to Bentonite. The peak fitting results, although showing a more irregular peak position, bear out the overall trend of increase until the spacing of approximately 17.5Å is achieved. There is a noticeable with a change in gradient from 0.7g of PAP onwards. Samples corresponding to 0.07g, 0.10g and 0.18g of PAP were analysed by XRPD scans to 50° 2θ. These were chosen as representative of the start of gradient change, maximum shift of basal spacing, and beyond the maximum shift (Figure 279).

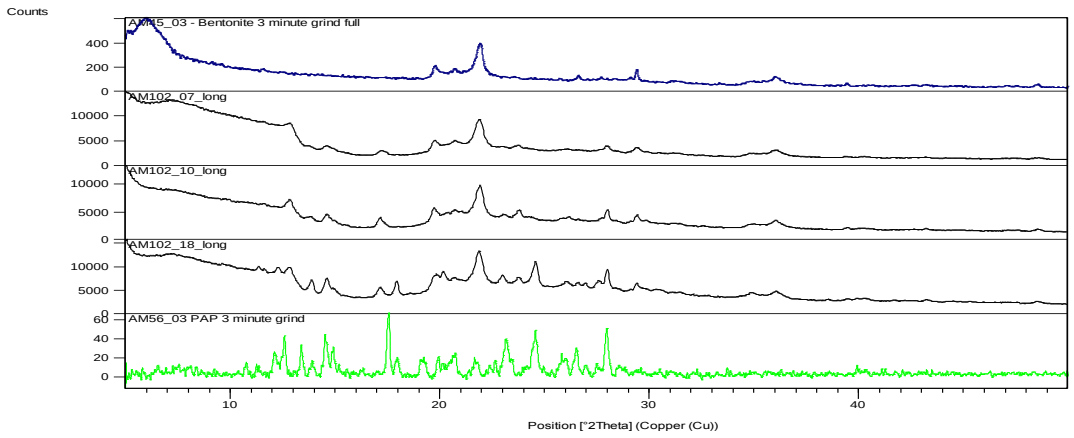

Figure 279 – Full XRPD patterns of Bentonite ground for three minutes (navy), Bentonite and PAP grinds with acetone samples AM102_07, AM102_10 and AM102_18 respectively (black top, middle and bottom) and of PAP ground for three minutes (green).

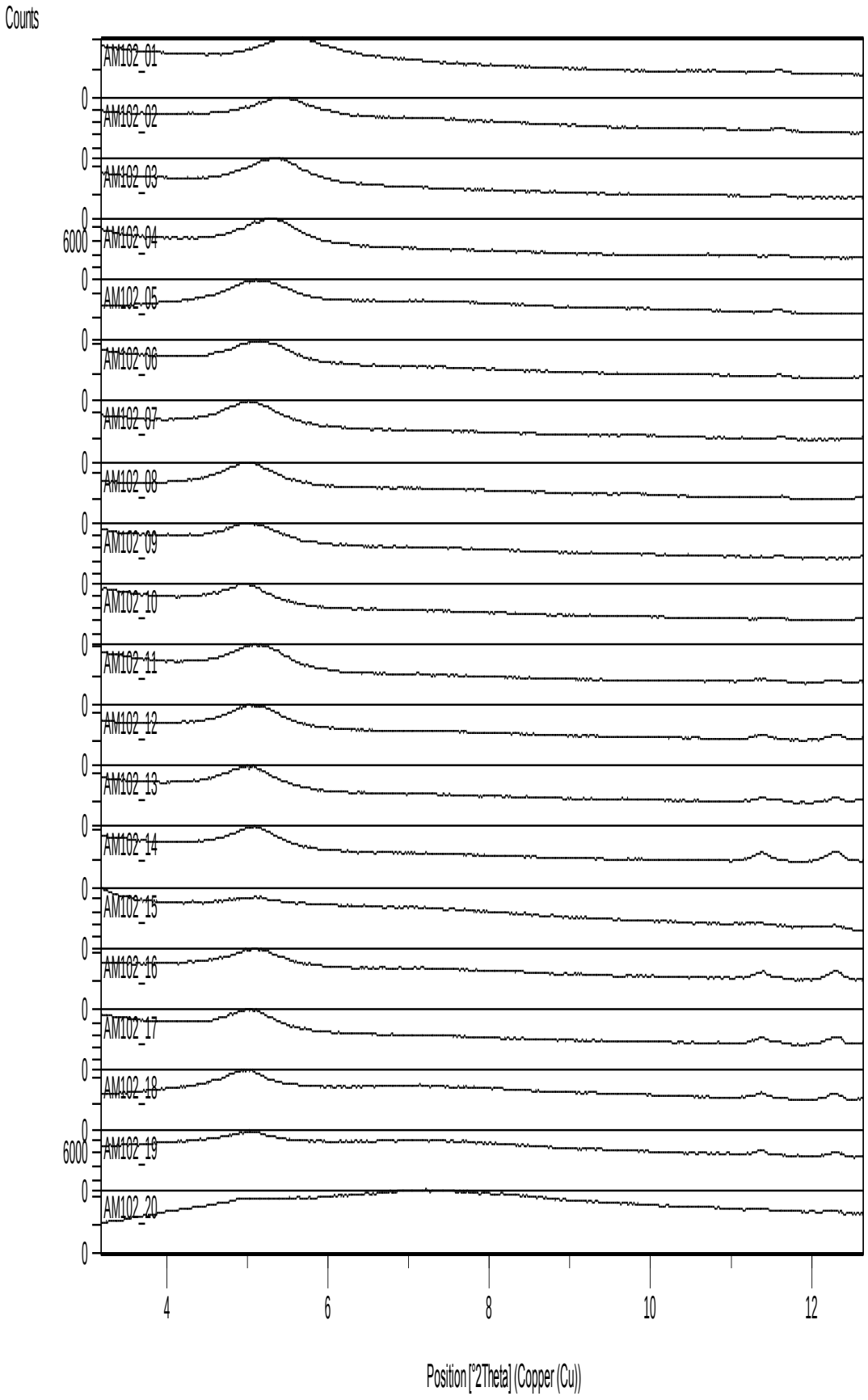

Figure 280 - XRPD patterns of collected samples from weight/weight incrementing solvent drop grind of Bentonite and PAP with acetone. The increase in PAP added proceeds downwards from AM102_01 being the smallest amount to AM102_20 being the largest.

The XRPD (Figure 279) shows, in comparison to the reference patterns for PAP and Bentonite ground individually for three minutes that almost no crystalline PAP is observed with the 0.07g addition. Upon reaching the maximum d-spacing change, small traces of PAP may be observed, and by the addition of 0.18g, PAP is clearly visible in its crystalline state. These results may be suggestive that the PAP is being intercalated until the point where maximum d-spacing shift has occurred (approx. 1:1 wt./wt.), and after that point, excess PAP is crystallised alongside the formed material. This suggests a limit to the quantity of PAP able to be intercalated into the spacings. Patterns beyond this point are essentially meaningless as the quantity of PAP prevents precise determination of the basal spacing.

A plot of the data is seen to plateau, at a point where the basal spacing no longer increases with an increase in PAP (Figure 281). As noted above, some of the data points deviate from the indicated trend – this is probably the result of the manual and therefore incomplete grinding technique employed, which may leave excess material not intercalated.

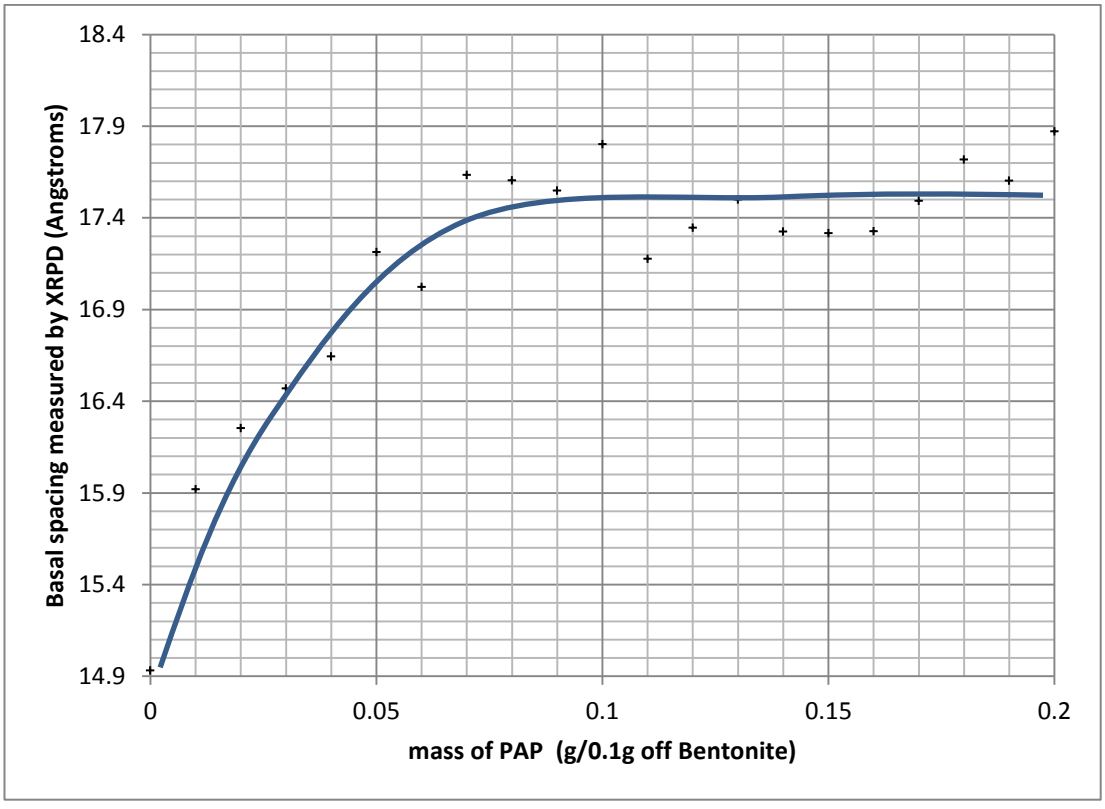

Figure 281 - Plot of basal spacing with respect to the mass of PAP added to the solvent assisted grind with a guide line drawn to indicate the trend.

This experiment was repeated with decomposed PAP ground into Bentonite clay. Samples were measured accurately to four decimal places and the measurements are shown in

Table 62 below. Mass has been corrected for the altered molecular weights of the decomposed PAP used to correspond to the same molar ratio with respect to the 0.1g of clay used as used for the PAP-clay grinding experiments.

Table 62 - 6-Phthalimidohexanoic acid and Bentonite solvent drop grind with acetone,

Sample	Bentonite (g)	Decomposed PAP (g)	Time (s)	Corrected mass(g)	d spacing (Å)
AM115_01	0.1030	0.0022	180	0.0021	15.15
AM115_02	0.1012	0.0111	180	0.0109	16.19
AM115_03	0.1063	0.0254	180	0.0238	16.46
AM115_04	0.1021	0.0333	180	0.0326	16.38
AM115_05	0.1007	0.0426	180	0.0423	16.78
AM115_06	0.1021	0.0555	180	0.0543	16.84
AM115_07	0.1006	0.0633	180	0.0629	16.96
AM115_08	0.1006	0.0715	180	0.0710	16.68
AM115_09	0.1032	0.0821	180	0.0795	17.36
AM115_10	0.1020	0.0933	180	0.0914	17.40
AM115_11	0.1027	0.1059	180	0.1031	17.58
AM115_12	0.1055	0.1137	180	0.1077	17.31
AM115_13	0.1008	0.1243	180	0.1233	17.40
AM115_14	0.1001	0.1341	180	0.1339	17.53
AM115_15	0.1000	0.1437	180	0.1437	17.27
AM115_16	0.1010	0.1565	180	0.1549	17.85
AM115_17	0.1040	0.1665	180	0.1600	17.78

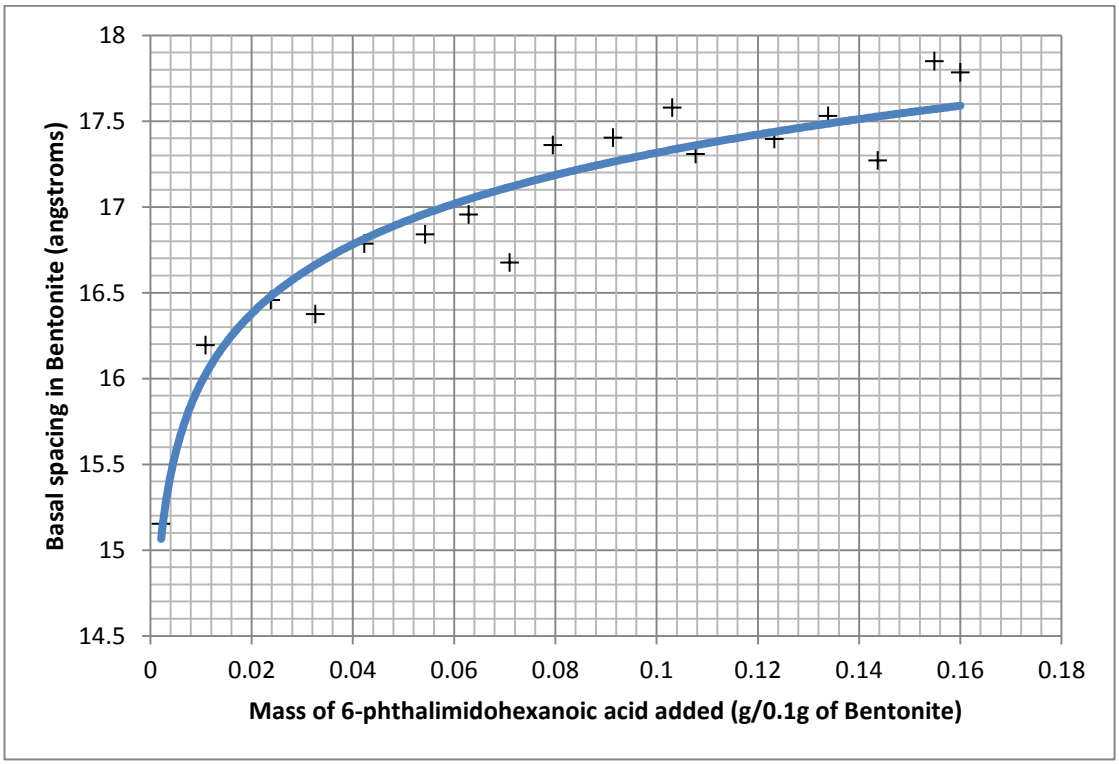

Figure 282 - Plot of basal spacing with respect to the mass of 6-phthalimidohexanoic acid added to the solvent assisted grind with acetone, with logarithmic line of best fit.

The results give a better logarithmic fit and show the same or similar characteristic curve that is observed with PAP where the trend plateaus. The points on the graph fit better to a trend than the less accurately measured PAP results. Again, however, the scatter in the points likely stems from inconsistencies in the grinding method. Localised areas of the sample with less material worked into it than others could lead to an uneven distribution of basal spacing throughout the sample.

The fact that 6-phthalimidohexanoic acid added in the same way to the grinding process has a similar effect on the spacing as the PAP indicates that it is not the peroxyacid itself reacting with the clay to chemically change it, but the whole molecule that is having a physical effect on the Bentonite spacing. This is supported by the previous findings of a lack of change in samples ground with MCPBA or peroxyacetic acid, which may be too small to have significant effect on the basal spacing even if intervalated.

This does not, however, confirm that the material inside the spacing is in fact a peroxyacid or whether it has decomposed. It is known from the full length XRPD scans that in the presence of PAP in excess of the mass required to reach the plateauing effect on the clay basal spacing, further addition of PAP is crystallised around the material. However there is no indication from these structural measurements that the functionality has been retained inside the clay host material.

When the Bentonite and PAP grind samples are analysed by Raman spectroscopy, using the Horiba spectrometer, there is no similarity between the final sample and the spectrum collected for PAP alone (Figure 283). The presence of the clay prevents the analysis of the intercalated material and only a background signal is seen, matching that of the pure clay itself. Comparison of the IR spectra does indicate the presence of the molecule (Figure 284), however the limitation on the technique itself prevents the explicit detection of the O-O peroxide bond due to the lack of a dipole in the bond. Thus, the IR results would be consistent with the presence of the peroxyacid or of the parent acid.

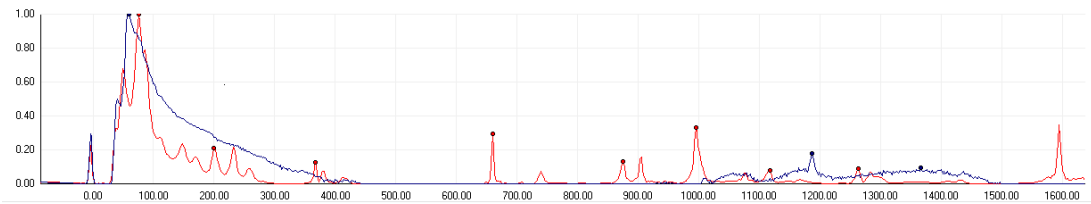

Figure 283 - Raman spectra overlay of PAP (red) and the ground sample of Bentonite with PAP (blue).

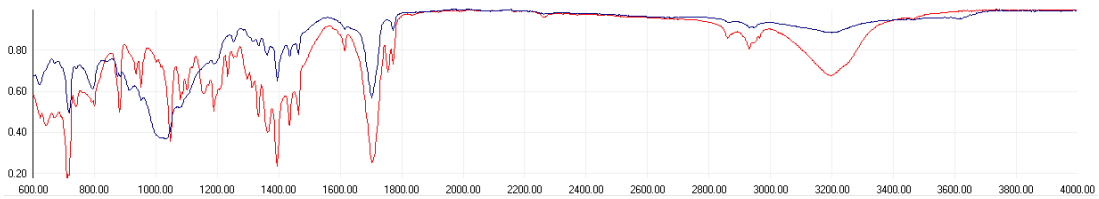

Figure 284 - IR spectra overlay of PAP (red) and the ground sample of Bentonite with PAP (blue)

The use of spectroscopy to determine the contents of the clay is hindered by the presence of both the clay itself, and by the remaining PAP external to the clay, which could give a false indication of what is inside the host-guest material of interest. An alternative testing method therefore had to be sought.

6.3.2 Reactivity testing

Upon advice given by the industrial collaborator, it was learned that certain dyes within household products discolour in the presence of PAP. In particular "Ariel Excel Gel" (Procter and Gamble), a blue coloured liquid laundry detergent, will turn green on reaction with PAP.

Testing of the materials created by the first Bentonite grind of PAP was therefore undertaken with the gel. Before the addition of materials., the gel is seen to be blue and translucent (Figure 285).

Figure 285 - Testing gel before addition of materials in wells I, II and III (left to right).

To well I was added de-ionised water only. Unground PAP and a small amount of water were added to well II, while sample AM102_09 (90% PAP / 100% clay), a sample from before clay saturation, plus some water was added to well III. No immediate change was observed but when left overnight, the PAP on its own in well II had changed the colour of the mixture to green, indicating oxidation had occurred (Figure 286).

Figure 286 - Testing gel after 24 hours of materials added in wells I, II and III (left to right).

The sample in well III of Bentonite with intercalated PAP has shown no colour change, indicating that the material is not oxidising the gel. This could be a result of the clay locking the reactivity of PAP in the mixture, or that the material has decomposed prior to addition into the clay or during the process.

Figure 287 - Testing gel after 24 hours of materials added in wells IV, V and VI (left to right).

Three more samples in the series of experiments were tested, corresponding to 20% PAP to Bentonite, 110% PAP to Bentonite and 190% PAP to Bentonite. Testing reveals the 20% sample does not oxidise the gel, however the other two show signs of darkening indicating that PAP is present and free to react with the indicator, either from residual un-intercalated material, or from the re-introduced PAP from the intercalated spacings.

6.3.3 Summary

It is clear that PAP or its decomposed product the parent 6-phthalimidohexanoic acid, interacts with Bentonite to increase the pore size in the clay, removing the ability of the added peroxy-acid to oxidise secondary materials, up to a point where the quantity of PAP is greater than the point at which the Bentonite basal spacing will no longer expand. Below this point there is no oxidation of secondary materials from the intercalated sample and this method may therefore have achieved the goal of stabilisation of the reactive PAP peroxy-acid. Further investigation into defining the nature of the material intercalated is needed, as well as further testing of reactivity to define a condition at which the intercalated material is released.

7. Molecular complexes of agrichemicals

One of the aims of this research was to forming new molecular complexes involving agrichemicals (also sometimes known as Active Agrichemical Ingredients, or AAIs) as a way of changing the physical properties of the materials, for better dispersion, a change in solubility, modified melting point, and better stability. The latter is of particular relevance in the context of the related work on reactive peroxyacids presented earlier, and many agrochemical materials have a high degree of intrinsically reactivity to aid their function. To this end the two agrichemicals, 2,4-dichlorophenoxyacetic acid - 2,4-D (Figure 10) and 3,4-dichlorophenoxyacetic acid – 3,4-D (Figure 11) were cocrystallised with a range of secondary components with the aim of creating new molecular complexes in which the interactions of the agrichemical could be studied for a better understanding of their molecular interactions, and the effect they have on the physical properties of the material.

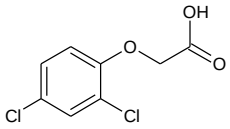

Figure 288 – Molecular structure of 2,4-Dichlorophenoxyacetic acid (2,4-D).

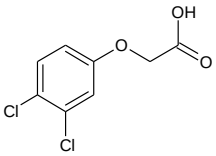

Figure 289 – Molecular structure of 3,4-Dichlorophenoxyacetic acid (3,4-D).

The two molecules 2,4-D and 3,4-D have a near identical molecular structure, with only a rearrangement of one chlorine position on the benzene ring and they share the same primary hydrogen bonding interactions. Both molecules should therefore be able to form similar motifs with secondary materials introduced into the crystallisation environment as potential co-components in molecular complexes.

The primary potential hydrogen bond interaction point on 2,4-D and 3,4-D is focussed around the carboxylic acid group, which in previous studies has been shown not to dimerise, but instead dissociate, particularly in the presence of a strong electron rich donor site on the co-molecule[106, 107]. As such, the present research on these molecules focussed on interaction between these molecules and secondary components containing amine groups, primarily imidazole based molecules.

7.1 Chlorophenoxyacetic acids and Imidazole

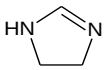

Figure 290 – Molecular structure of imidazole

2,4-D and 3,4-D were cocrystallised with imidazole (Figure 290) in a 1:1 equimolar ratio in methanol, ethanol, acetone, ethyl acetate and diethyl ether, both at room temperature and 30°C in the attempt to create molecular complexes for study by X-ray diffraction. The experiments were successful in growing crystals from both sets of cocrystallisations suitable for study by single crystal X-ray diffraction on the Rigaku R-axis image plate diffractometer.

7.1.1 2,4-Dichlorophenoxyacetic acid and Imidazole

Slow evaporation of 2-4-dichlorophenoxyacetic acid and imidazole dissolved in methanol and held at a constant crystallisation temperature of 30°C yielded a new material, as identified by a previously undetermined unit cell from single crystal X-ray diffraction. The unit cell did not correspond to either of the starting materials, and was thus subjected to a full data collection, detailed in

Table 4.

Table 63 - Crystal structure collection data for 2,4-Dichlorophenoxyacetate imidazolium complex.

Compound	**2,4-Dichlorophenoxyacetate imidazolium complex**
Formula	$C_8H_5O_3Cl_2$: $C_3H_5N_2$
Crystallisation Conditions	Cocrystallisation of 2,4-D and imidazole in methanol at 30°C
Molecular weight / $gmol^{-1}$	289.114
Temperature (K)	100
Space Group	$P2_1/c$
a (Å)	4.897(3)
b (Å)	12.641(7)
c (Å)	19.725(11)
α (°)	90
β (°)	90.626(10)
γ (°)	90
Volume ($Å^3$)	1221.0(12)
Z	4
Z'	1
θ range/°	7.58-53.70
Reflections Collected	16436
Independent	2810
Refln (obs.I>2theta(I))	2154
R_{int}	0.0673
Parameters	203
GooF on F^2	1.121
R_1 (Observed)	0.0509
R_1 (all)	0.0689
wR_2 (all)	0.1346

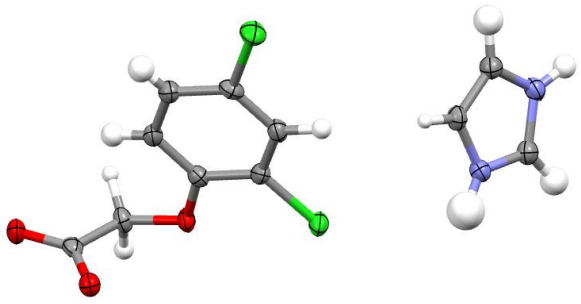

Figure 291 - Asymmetric unit of 2,4-D Imidazolium complex consisting of one acetate ion and one amide.

Analysis of the crystal structure reveals that in the asymmetric unit (Figure 291), there is a 1:1 composition of 2,4-D and imidazole. The 2,4-D has been deprotonated at the carboxylic acid, forming an acetate ion, with the hydrogen atom transferred to the available lone pair on the amine of the imidazole molecule, forming an imidazolium ion, thus preserving the charge balance.

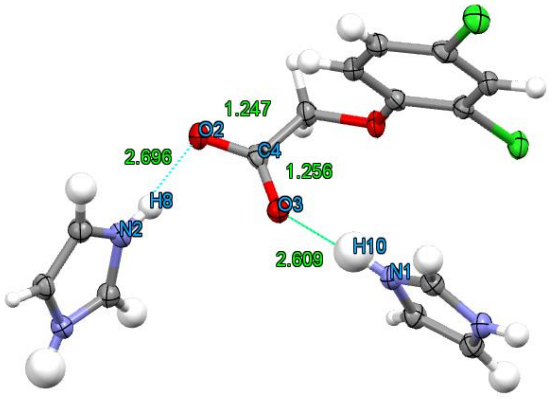

Figure 292 - Primary moderate strength hydrogen bonds situated between the amide and acetate functional groups N2-H8···O2 and N1-H10···O3.

The primary hydrogen bonds between the molecules are located between the acetate functional group and the amide group, N2-H8···O2, at an overall distance of 2.696(4)Å (166(4)°), and N1-H10···O3, at a distance of 2.609(4)Å (171(6)°), making them both moderate strength hydrogen bonds as defined by Jeffrey[21] (Figure 292). The C4-O2 covalent bond is slightly shorter than the C4-O3 covalent bond at respective distances of 1.247(4)Å and 1.256(4)Å. The hydrogens are clearly located from the Fourier peaks on the axis of the bonds, bonded to the nitrogen atoms. This creates a $C^2_2(8)$ chain motif along the *b*-axis of the structure, alternating between imidazolium and phenoxyacetate molecules (Figure 293).

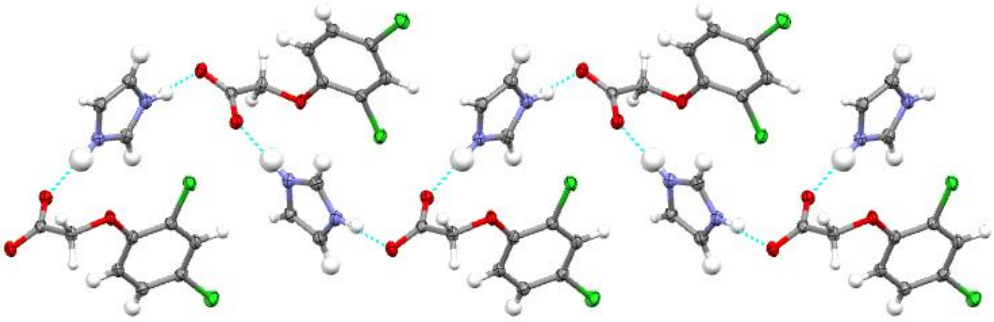

Figure 293 - Phenoxyacetate - imidazolium $C^2_2(8)$ motif along *b*-axis of the crystal structure.

The acetate group is further associated via O3 to Cl1 via a interaction of distance 3.067(3)Å, generating a $C^1_1(8)$ motif through the 2,4-D molecule along the *b*-axis also (Figure 294).

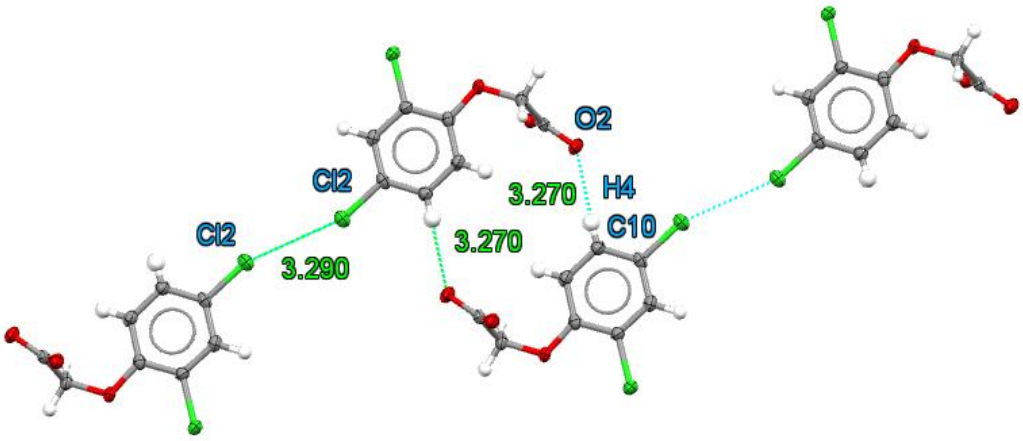

Figure 294 - View of 2,4-D molecules only along the b-axis showing the Cl2···Cl2 interaction and the C10-H4···O2 interactions.

Also along the *b*-axis is a chlorine···chlorine interaction at a distance of 3.290(2)Å and a $R^2_2(16)$ ring motif generated by the C10-H4···O2 aromatic hydrogen bond at a C···O distance of 3.270(5)Å.

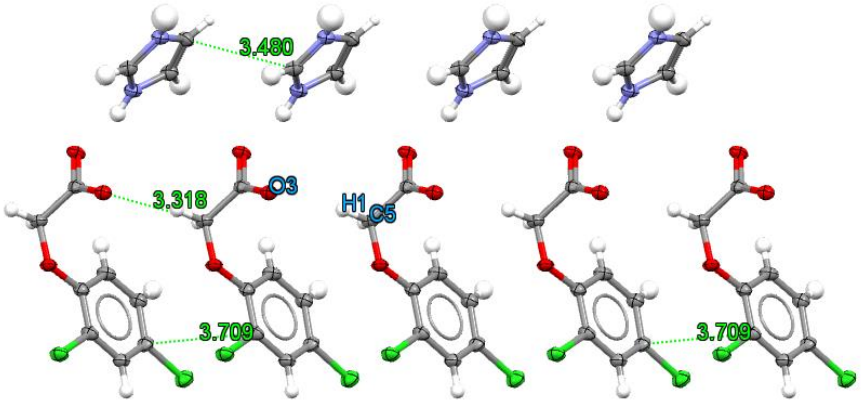

Figure 295 – packing of aromatic rings in 2,5-D imidazolium complex as viewed down the c-axis.

Finally, there is an an aliphatic C-H···O hydrogen bond between C5 and acetate oxygen O3 (Figure 295), at an overall C···O distance of 3.318(5)Å, linking the parallel packed 2,4-D molecules along the direction of the *a*-axis. Neither the 2,4-D nor the the imidazolium ion show direct π-π stacking arrangements as they do not sit over each other. At their closest non hydrogen distances, the 2,4-D molecules are 3.709(4)Å apart, while imidazolim molecules are slightly closer to each other, at 3.480(6)Å.

7.1.2 3,4-Dichlorophenoxyacetic acid and Imidazole

3,4-D and imidazole cocrystallised in acetone at room temperature also produced crystals of a new material suitable for study by single crystal X-ray diffraction and therefore received a full data collection. The details of the data collection and the crystal structure parameters are outlined in Table 64.

Table 64 - Crystal structure collection data for 2,4-Dichlorophenoxyacetate imidazolium complex

Compound	**3,4-Dichlorophenoxyacetate imidazolium complex**
Formula	$C_8H_5O_3Cl_2$: $C_3H_5N_2$
Crystallisation Conditions	Cocrystallisation of 3,4-D and imidazole in acetone at room temperature
Molecular weight / $gmol^{-1}$	289.114
Temperature (K)	100
Space Group	P-1
a (Å)	9.207(3)
b (Å)	11.157(3)
c (Å)	12.699(4)
α (°)	89.135(8)
β (°)	73.247(10)
γ (°)	89.237(8)
Volume ($Å^3$)	1248.9(6)
Z	4
Z'	2
θ range/˚	3.02 – 27.47
Reflections Collected	28129
Independent	5639
Refln (obs.I>2theta(I))	5120
R_{int}	0.0211
Parameters	405
GooF on F^2	1.070
R_1 (Observed)	0.0271
R_1 (all)	0.0302
wR_2 (all)	0.0713

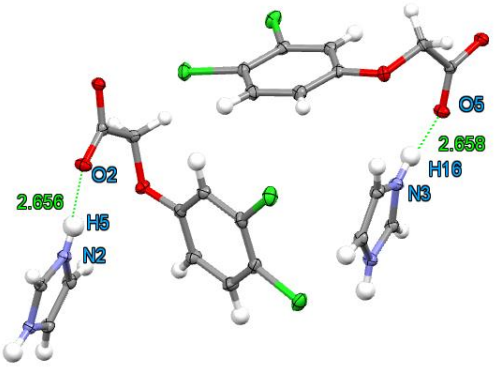

Figure 296 - Asymmetric unit of the 3,4-D Imidazolium complex showing the hydrogen bond interactions between the two ion pairs.

The collected structure was identified to be a 1:1 3,4-dichlorophenoxyacetate imidazolium complex, comprising of two pairs of ions within the asymmetric unit, paired by hydrogen bonds originating from the amine groups of the imidazolium ions to the acetate groups of

the 3,4-D molecules. The distances of the interactions are 2.658(2)Å (N3-H16···O5) (167(2)°) and 2.656(2)Å (N2-H5···O2) (167(2)°), making them both moderate strength interactions (Figure 296). These interactions are continued through the imidazolium molecules to the next acetate group of the symmetrically equivalent molecule of the next cell, with the hydrogen bonds originating from the opposite sides of the imidazole molecules generating a further two slightly weaker hydrogen bonds at a distance of 2.665(2)Å (176(2)°) (N4-H19···O6) and 2.683(2)Å (176(2)°) (N1-H3···O3) as highlighted in Figure 297.

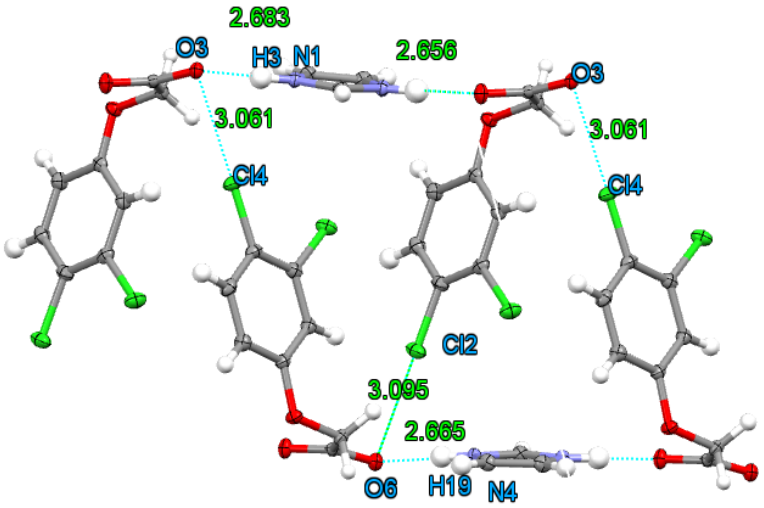

Figure 297 - 3,4D and imidazolium ion chains generated along the a-axis.

As seen along the *a*-axis there are two distinct chlorine-oxygen interactions, Cl4···O3 and Cl2···O6, at similar distances of 3.061(1)Å and 3.092(1)Å, respectively (Figure 297). This has the effect of generating two $C^2_2(8)$ chains, (N1···O3---O2···N1; Figure 298) and (N4···O6---O5···N3; Figure 299), with interweaving aromatic groups. This results in the formation of columns along the *a*-axis with an end to face zig-zag orientation of the aromatic groups. The symmetry equivalent aromatic groups are distant from each other at over 7Å and do not form stacking interactions.

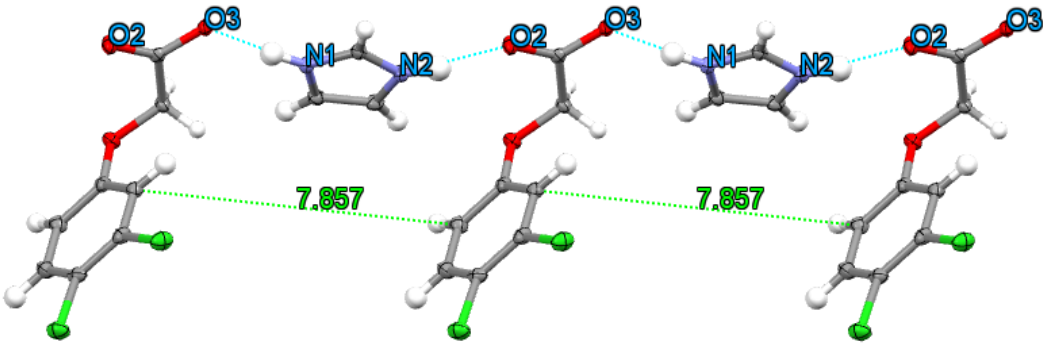

Figure 298 - 3,4-D and imidazolium (N1···O3---O2···N1) chains.

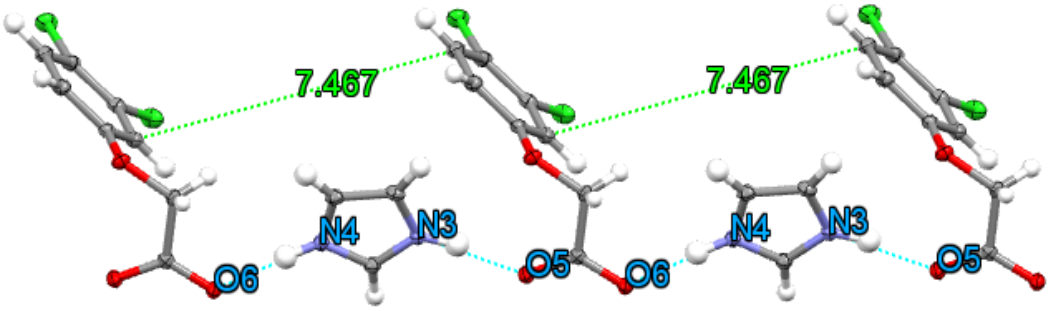

Figure 299 - 3,4-D and imidazolium (N1···O3---O2···N1) chains.

The end to face stacked aromatic rings are further connected via an aromatic hydrogen to chlorine and an aromatic hydrogen to oxygen interaction, at the overall distances, 3.632(2)Å (C14···O5), 3.767(1)Å (C13···Cl1), 3.634(2)Å (C22···O2) and 3.835(2)Å (C21···Cl3). These interactions are highlighted in Figure 300.

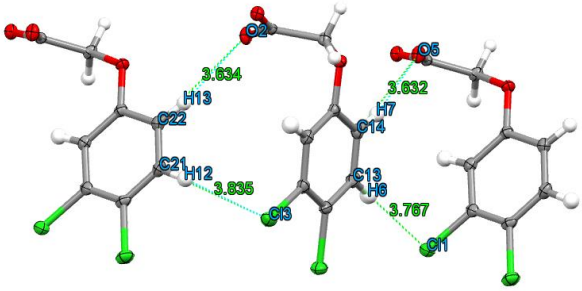

Figure 300 - End to face stacking interactions and consequent contacts in the crystal structure of 3,4-D imidazolium complex.

The chains of imidazolium molecules stack in a skewed arrangement on top of each other in the direction of the *c*-axis, parallel with the *ab* plane, creating channels of stacked aromatic and chlorine sandwich layers, at a stacking distance of 3.231(2)Å (Figure 301).

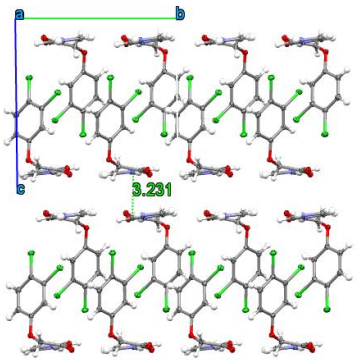

Figure 301 - Sandwiched aromatic sheets present in 3,4-D imidazolium complex on the ab plane.

7.1.3 Thermal analysis of 2,4-D and 3,4-D imidazolium complexes

The new 2,4-D and 3,4-D imidazolium complexes were analysed by DSC and compared to the scans of their respective starting materials to assess whether the new forms offer this aspect of modified physical properties as set out in the project aims.

In the 2,4-dichlorophenoxyacetate imidazolium complex, only one thermal event can be seen in the sample scan, at 130-137 °C (Figure 302), corresponding to a product melting transition. This event does not correspond to any of the starting materials and is a 6°C decrease from that observed in pure 2,4-D. This molecular complex is thus less thermally stable than the starting material.

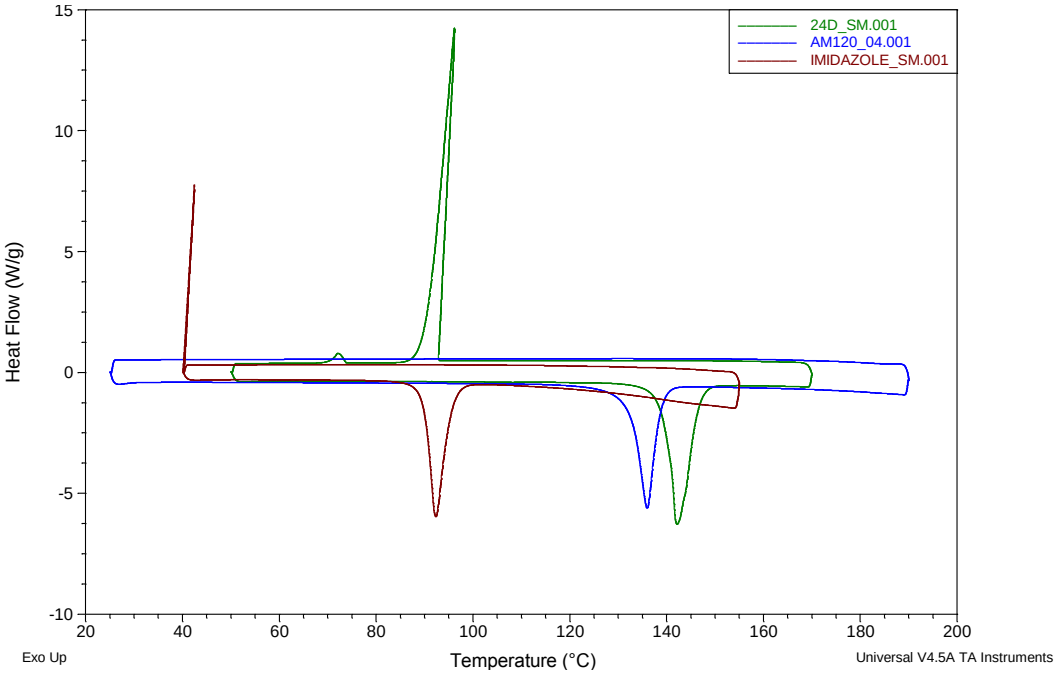

Figure 302 - DSC scans of 2,4-Dichlorophenoxyacetic acid (green), imidazole (brown) and the 2,4-D imidazolium complex (blue).

The DSC scan of the 3,4-dichlorophenoxyacetate imidazolium complex (Figure 303) has resulted in a more complex result. Three endothermic events can be noticed at 57-66 °C, a

very broad event at 98-103 °C and a smaller event at 116-118 °C, none of which correspond to either of the starting materials, and one exothermic event from 60-57 °C. This possibly suggests that this material may be polymorphic, with several forms which are transitioned through the heating cycle, reaching a final melting point, and then recrystallizing on the cooling cycle at the original crystal form. These other forms should be investigated, ideally by higher temperature single crystal X-ray diffraction to determine if a change in the crystal structure is observed. All exothermic transitions, however, are at a much lower temperature than the 3,4-D melting point at 140-142 °C, and this complex is therefore also less thermally stable.

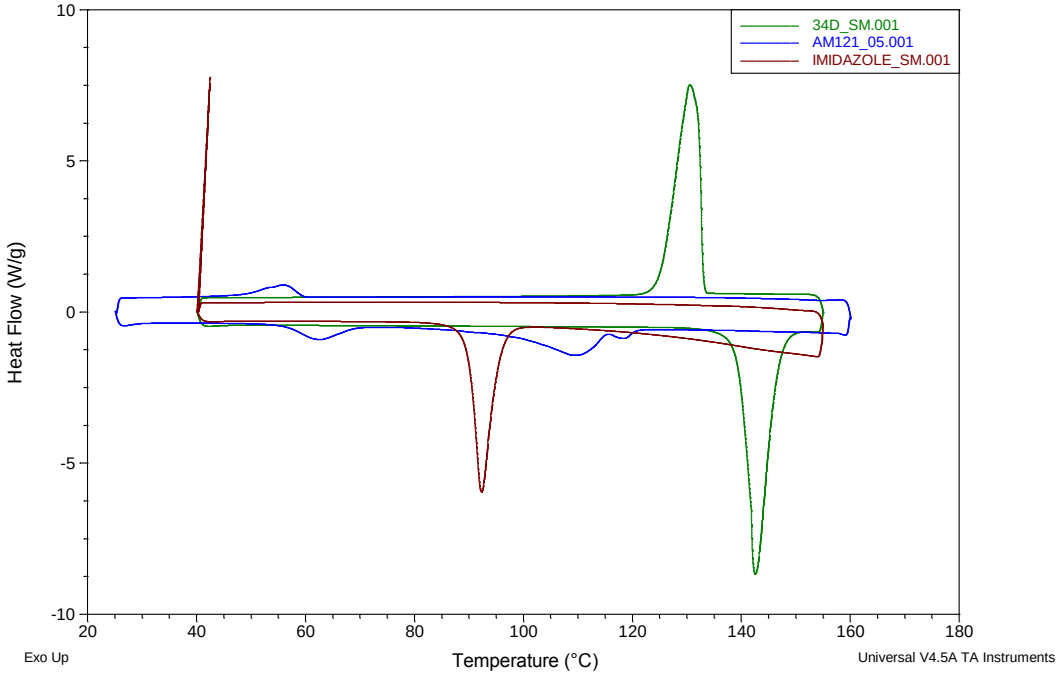

Figure 303 - DSC scans of 3,4-Dichlorophenoxyacetic acid (green), imidazole (brown) and the 3,4-D imidazolium complex (blue).

7.2 Chlorophenoxyacetic acids and 4(5)-methylimidazole

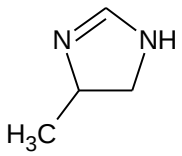

Figure 304 - Molecular structure of 4(5)-methylimidazole.

Both 2,4-D and 3,4-D were further studied by cocrystallising with a slightly larger methyl substituted analogue of imidazole, 4(5)-methylimidazole (Figure 304). Under the same slow evaporative crystallisation method, crystallisations were performed in methanol, ethanol, acetone, ethyl acetate and diethyl ether, both at room temperature and 30°C. As

with the imidazole crystallisations, suitable crystals for study by single crystal X-ray diffraction were found amongst both sets of experiments.

7.2.1 2,4-Dichlorophenoxyacetic acid and 4(5)-methylimidazole

Slow evaporative crystallisation of 2-4-dichlorophenoxyacetic acid and 4(5)-methylimidazole dissolved in ethyl acetate and held at a constant crystallisation temperature of 30°C yielded a new material which was subjected to a full data collection, detailed in Table 65.

Table 65 - Crystal structure collection data for 2,4-Dichlorophenoxyacetate 4(5)-methylimidazolium monohydrate

Compound	**2,4-Dichlorophenoxyacetate 4(5)-methylimidazolium monohydrate**
Formula	$C_8H_5O_3Cl_2$: $C_4H_7N_2$:H_2O
Crystallisation Conditions	2,4-D and 4(5)-methylimidazole crystallised in ethyl acetate at 30°C
Molecular weight / gmol^{-1}	321.15
Temperature (K)	100
Space Group	$P2_12_12_1$
a (Å)	4.7865(5)
b (Å)	12.7296(14)
c (Å)	23.727(3)
α (^{o})	90
β (^{o})	90
γ (^{o})	90
Volume (*Å^3*)	1445.7(3)
Z	4
Z'	1
θ range/°	3.03 – 27.48
Reflections Collected	19031
Independent	3309
Refln (obs.I>2theta(I))	3039
R_{int}	0.0517
Parameters	237
GooF on F^2	1.059
R_1 (Observed)	0.0321
R_1 (all)	0.0368
wR_2 (all)	0.0723
Flack Parameter	-0.02(5)

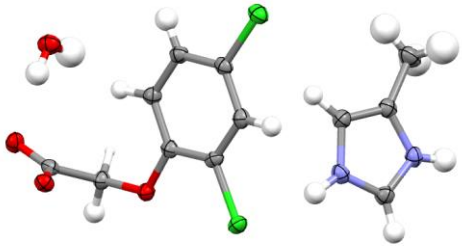

Figure 305 - Asymmetric unit of 2,4-D 4(5)-methylimidazole monohydrate.

The asymmetric unit of the 2,4-D 4(5)-methylimidazole monohydrate structure contains one of each of the three components with the proton of the 2,4-D relocated to the available nitrogen of the methylimidazolium molecule (Figure 305).

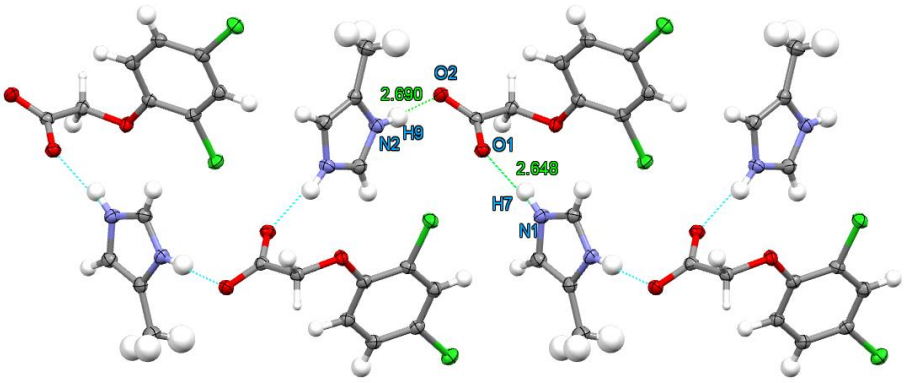

Figure 306 - Hydrogen bonding network forming a chain flowing through 2,4-D back to 4(5)-methylimidazolium molecules.

The two larger molecules form a chain of acetate to amine hydrogen bonds, all of moderate strength, originating from either side of the methylimidazolium ion at distances 2.690(2)Å (175(3)°) (N2-H9···O2) and 2.648(2)Å (164(2)°) (N1-H7···O1) creating an entirely moderate strength $C^2_2(8)$ chain motif (Figure 306).

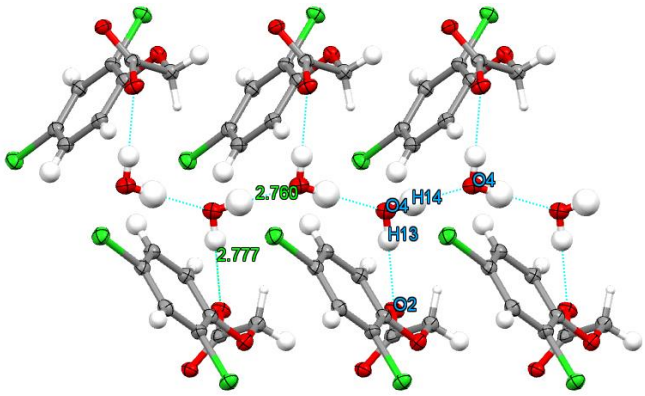

Figure 307 - 2,4-D molecules hydrogen boned to linear chain of alternating water molecules in the structure.

Also hydrogen bonded to the acetate functional group are the water molecules at a distance of 2.777(2)Å (175(3)°) (O4-H13···O2), bound with moderated strength interactions to themselves forming an alternating orientation one dimensional chain of water molecules running throughout the structure with a 2.760(3)Å (176(3)°) hydrogen bond linking the chain (O4-H14···O4; Figure 307).

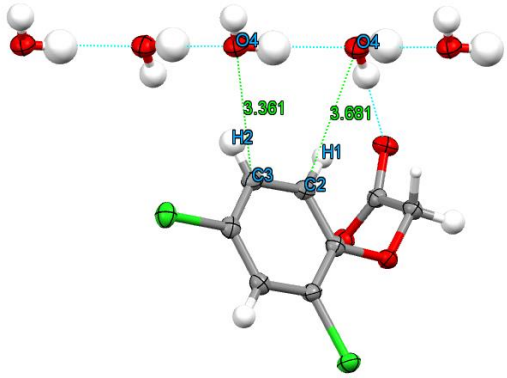

Figure 308 - Weaker aromatic hydrogen bonds from 2,4-D molecule to chain water molecules.

The water molecules are further held in place by much weaker aromatic C-H···O interactions originating from the aromatic 5 and 6 positions, with respective distances of 3.361(3)Å and 3.681(3)Å. These contacts are at the limit of a hydrogen bond interaction, however they are directed towards the oxygen atom of the water molecules and thus probably have a weak stabilising effect (Figure 308).

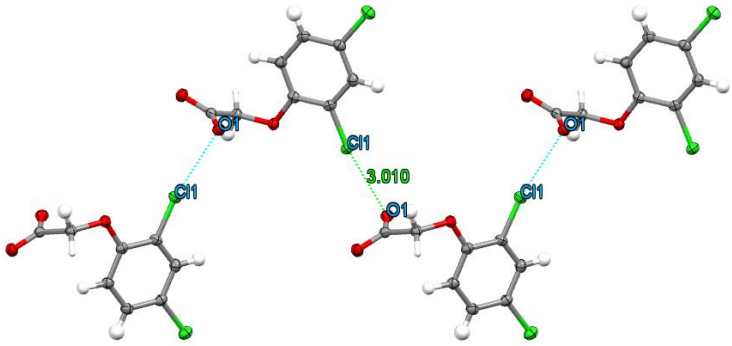

Figure 309 - 2,4-D with 4(5)-methylimidazolium hidden showing chlorine oxygen interaction chain.

The chlorine atoms on the 2,4-D molecule interact with the neighbouring 2,4D molecule with a Cl···Cl distance of 3.1010(1)Å; these are the only interactions between the molecules that are not part of the methylimidazolium chain (Figure 309).

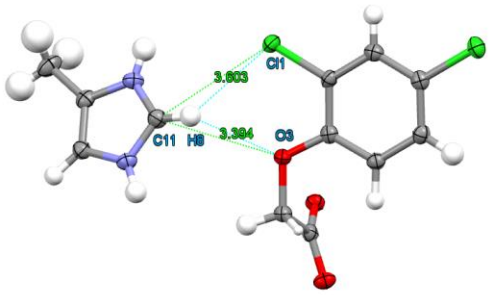

Figure 310 - C-H···O and C-H···Cl interactions from 4(5)-methylimidazolium ion to chlorine and oxygen on 2,4-D.

The methylimidazolium ion also has C-H···O and C-H···Cl interactions with the 2,4-D molecule, as shown in Figure 310. The chlorine interaction is the weaker of the two, and as a result the C-H bond is directed more towards the lone pair of O3, the chain oxygen with a C11···O3 distance of 3.394(2)Å; this is still a very weak interaction.

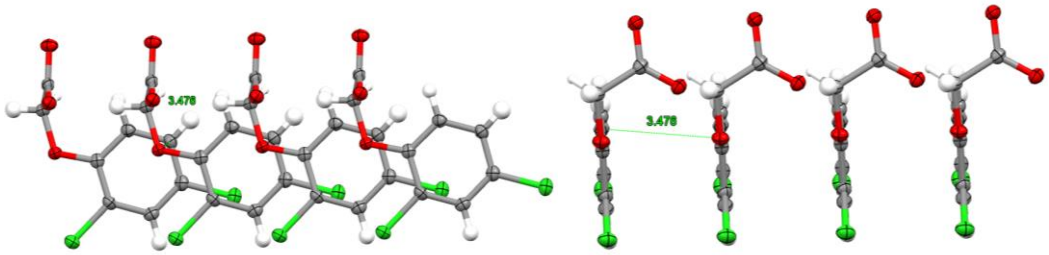

Figure 311 - packing of 2,4-D aromatic rings viewed perpendicular from the plane of the ring (left) and looking down the planes of the rings (right).

Finally, the 3,4-D molecules pack on top of each other at a closest interatomic distance of 3.476(3)Å (Figure 311; right). This is within the range of π-π stacking interaction with the molecules stacked in a skewed arrangement. The chain oxygen with its lone pairs sit above the π cloud (Figure 312; left) reinforcing the structure through π-σ interactions.

7.2.2 3,4-Dichlorophenoxyacetic acid and 4(5)-methylimidazole

Cocrystallisation of 3-4-dichlorophenoxyacetic acid and 4(5)-methylimidazole dissolved in acetone and held at a constant crystallisation temperature of 30°C yielded a new material which was subjected to a full data collection, detailed in

Table 66.

Table 66 - Crystal structure collection data for 3,4-Dichlorophenoxyacetate 4(5)-methylimidazolium molecular complex

Compound	**3,4-Dichlorophenoxyacetate 4(5)-methylimidazolium complex**
Formula	$C_8H_5O_3Cl_2$: $C_4H_7N_2$
Crystallisation Conditions	3,4-D crystallised with 4(5)-methylimidazole in acetone at 30°C
Molecular weight / gmol^{-1}	303.14
Temperature (K)	100
Space Group	$P2_1/c$
a (Å)	6.9895(6)
b (Å)	24.7289(17)
c (Å)	7.5806(5)
α (°)	90
β (°)	100.125(7)
γ (°)	90
Volume (*Å^3*)	1289.85(17)
Z	4
Z'	1
θ range/°	3.07 – 27.48
Reflections Collected	154.01
Independent	2947
Refln (obs.I>2theta(I))	2358
R_{int}	0.0391
Parameters	220
GooF on F^2	1.100
R_1 (Observed)	0.0376
R_1 (all)	0.0505
wR_2 (all)	0.1074

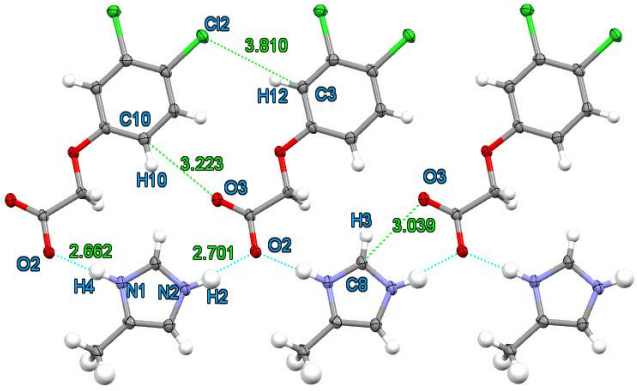

Figure 312 – Planar hydrogen bonding network of the 3,4-D 4(5)-methylimidazolium structure.

The structure of the 3,4-D methylimidazolium complex is predominantly planar, with all aromatic molecules lying in a sheet, with only the methyl hydrogens and CH_2 hydrogens protruding from this. Similar to the other structures with imidazole based co-molecules, the two protonated amine groups propagate a hydrogen bonded chain throughout the structure (Figure 312). The two main interactions are both associated with O2 – one of the acetate oxygens – with distances 2.662(2)Å (174(2)°) and 2.702(2)Å (167(3)°) from N1 and

N2, respectively. Yet again these are moderate strength hydrogen bonds, with a similar distance as seen in the previous structures.

The second acetate oxygen, O3 is directed towards H10, with an overall C10···O3 distance of 3.223(3)Å forming a very weak aromatic hydrogen bond. This is further supported by the 5 position aromatic hydrogen directed with a very weak interaction towards the chain oxygen, and the 3.810(2)Å Cl2···H12-C3 interaction. O3 also forms a second interaction with H3 at an overall distance (O3···C8) of 3.039(2)Å (132(7)°).

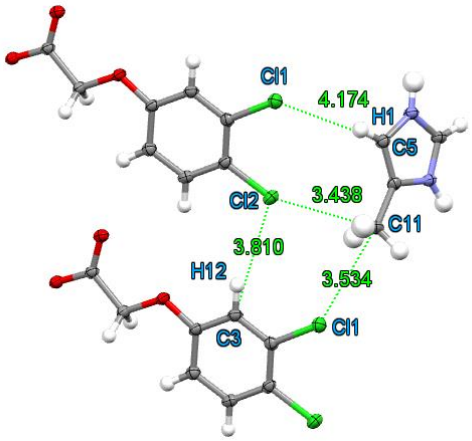

Figure 313 - C-H to chlorine interactions observed between 3,4-D and 4(5)-methylimidazolium ions.

The 3,4-D molecules have several chlorine interactions with the methylimidazolium molecule and the neighbouring 3,4-D molecule (Figure 313). Cl1 and Cl2 both interact with the bulky methyl group at distances of 3.534(2)Å and 3.438(2)Å respectively, whilst Cl2 also is very close to interaction range, at 3.810(2)Å to H12 (measured distance from Cl2···C3), an aromatic hydrogen, The C-H contact with Cl1 is more distant, at 4.174(2)Å, and less likely to make a significant contribution to the packing.

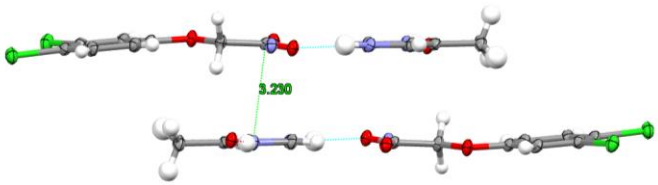

Figure 314 - Planes of molecules of alternating orientation 2,4-D and methylimidazolium ions.

Finally, the planes stack at a measured distance of 3.230(2)Å (Figure 314) forming a zig-zag arrangement of alternating units along the *b*-axis, creating ribbons with chlorine and methyl hydrogen edges traversing the *a*-axis (Figure 315).

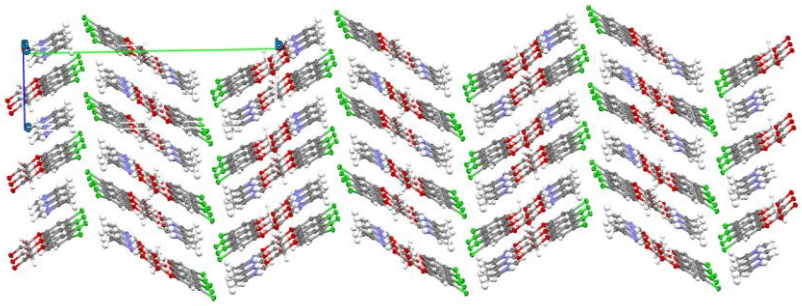

Figure 315 - Planes forming narrow ribbons down *a*-axis edged by chlorine atoms and methyl groups.

7.2.3 Thermal analysis of 2,4-D and 3,4-D 4(5)-methylimidazolium complexes

The 2,4-D and 3,4-D 4(5)-methylimidazolium molecular complexes were analysed by DSC and compared to their respective reference scans to assess physical property modification.

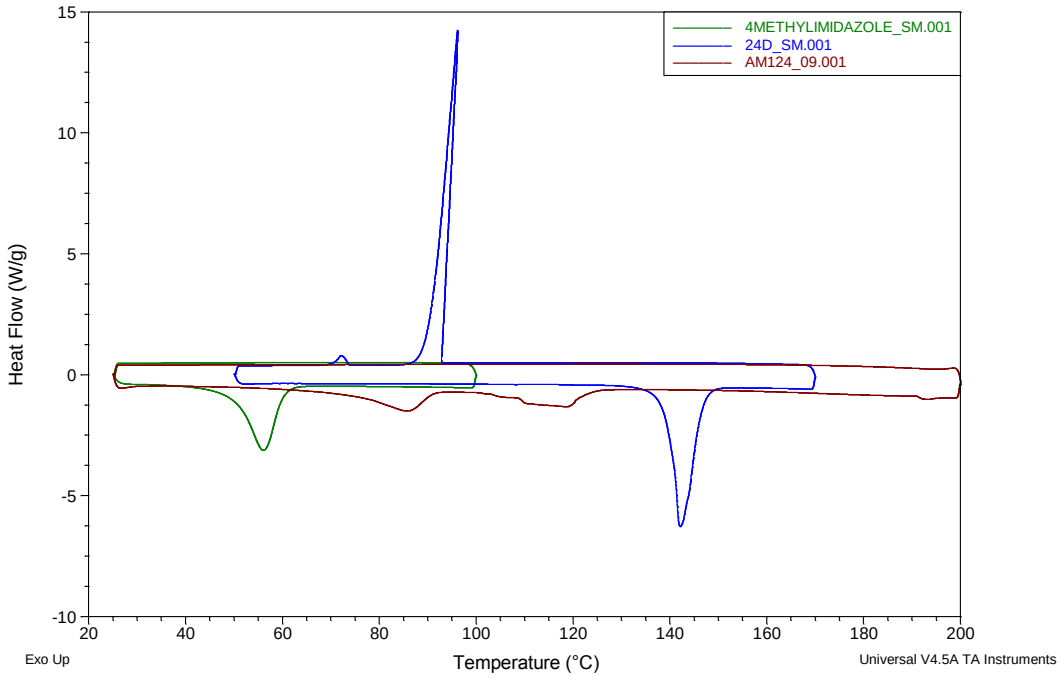

Figure 316 - DSC scans of 2,4-Dichlorophenoxyacetic acid (blue), 4(5)-methylimidazole (green) and the 2,4-D 4(5)-methylimidazolium complex (brown).

The DSC scan of the 2,4-D complex, which was recognised to be a hydrated structure, showed multiple thermal events upon heating (Figure 316). Two broad events at 70-85 °C and 110-120°C are evident that do not correspond to either of the starting materials. It could be the case that the first of these events, is from the evolution of the water from the structure, and the second is the melting point of the structure. Both of these events however are below the point at which the 2,4-D shows its melting peak, and thus the complex is less thermally stable than the starting material.

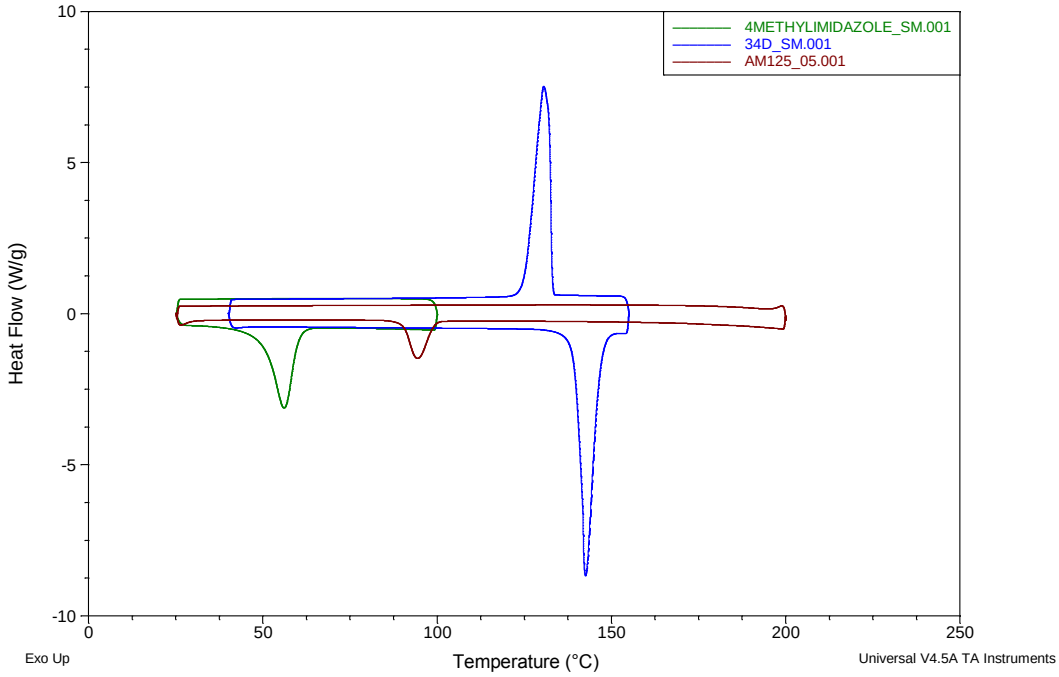

Figure 317 - DSC scans of 3,4-dichlorophenoxyacetic acid (blue), 4(5)-methylimidazole (green) and the 3,4-D 4(5)-methylimidazolium complex (brown).

The DSC scan of the 3,4-D complex is much sharper. The new complex (Figure 317; brown) is clearly experiencing one melting transition, which is situated between the melting points of the two starting materials at about 97-100 °C. Both new molecular complexes discussed in this section are thus less thermally stable than their agrichemical component in the pure form.

7.3 Chlorophenoxyacetic acids and benzimidazole

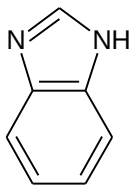

Figure 318 - Molecular structure of benzimidazole.

With a similar behaviour and functionality to that of the imidazoles, benzimidazole (Figure 318) was the next material to be crystallised with 2,4-D and 3,4-D with the aim of creating a more stable molecular complex. Benzimidazole itself has a significantly higher thermal stability than imidazole, and it was hoped than it would lend itself to the molecular complexes formed. This touched on work previously explored by Liu[106] in which a 2,4-D benzimidazolium monohydrate complex was studied, and therefore the potential for

interaction was known, however the crystallisation was screened to see if an anhydrous form could be found. As such, slow evaporative cocrystallisation experiments were performed as before with methanol, ethanol, acetone, ethyl acetate and diethyl ether as solvents, both at room temperature and 30°C. This yielded two more new materials, one from the 2,4-D experiments, and one from 3,4-D.

7.3.1 2,4-Dichlorophenoxyacetic acid and benzimidazole

Crystallisation of 2-4-dichlorophenoxyacetic acid and benzimidazole dissolved in acetone and held at room temperature for crystallisation yielded a new material which was subjected to a full data collection, detailed in Table 67.

Table 67 - Crystal structure collection data for 2,4-Dichlorophenoxyacetate benzimidazolium complex

Compound	**2,4-Dichlorophenoxyacetate benzimidazolium complex**
Formula	$C_8H_5O_3Cl_2$: $C_7 7_5N_2$
Crystallisation Conditions	2,4-D crystallised with benzimidazole in acetone at room temperature
Molecular weight / gmol^{-1}	339.17
Temperature (K)	100
Space Group	Pbca
a (Å)	30.342(2)
b (Å)	11.3122(4)
c (Å)	8.4753(4)
α (^{o})	90
β (^{o})	90
γ (^{o})	90
Volume (*Å^3*)	2909.0(3)
Z	8
Z'	1
θ range/˚	3.08 – 27.48
Reflections Collected	32095
Independent	3324
Refln (obs.I>2theta(I))	2914
R_{int}	0.0267
Parameters	247
GooF on F^2	1.053
R_1 (Observed)	0.0283
R_1 (all)	0.0333
wR_2 (all)	0.0715

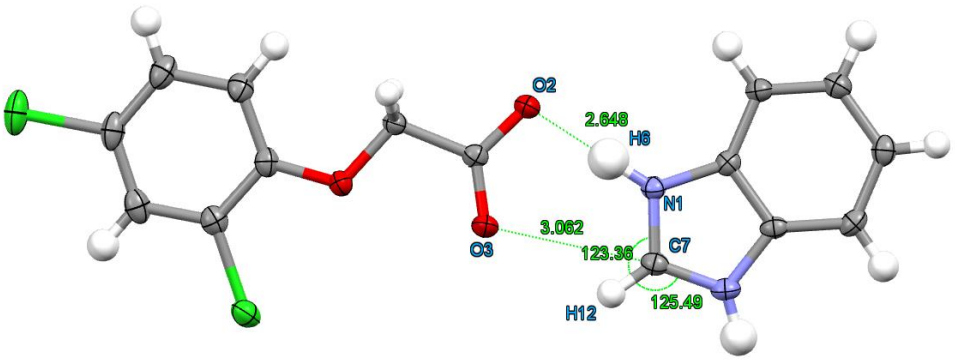

Figure 319 - Asymmetric unit of 2,4-D and benzimidazolium ions forming $R^2_2(7)$ motif.

The asymmetric unit of the 2,4-D benzimidazolium structure collected contains one of each molecule, interacting in an $R^2_2(7)$ motif between one side of the amine head of the benzimidazolium molecule and the acetate group of the 2,4-D (Figure 319). The motif is formed by a moderate strength hydrogen bond originating from the amine group with a distance of 2.648(1)Å (179(2)°) between N1···O2. This is supported by a weaker interaction from the benzimidazole head hydrogen to O3, with a measured distance from the head carbon to O3 of 3.062(2)Å. This is confirmed to be a weak interaction by a very slight bending of the C-H electron density towards O3.

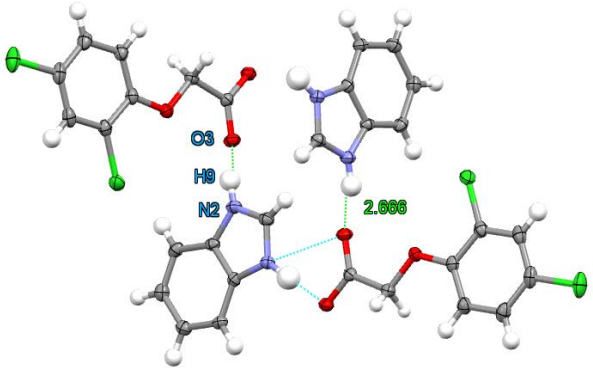

Figure 320 - Larger 2(2,4-D) 2(benzimidazolium) $R^4_4(16)$ motif.

As with the other imidazole based molecules, the other side of the benzimidazolium forms hydrogen bonds through a second interaction to acetate oxygen O3, with another moderate strength distance of 2.666(1)Å (149(2)°) (N2···O3). This has the effect of generating a larger $R^4_4(16)$ ring motif (Figure 320).

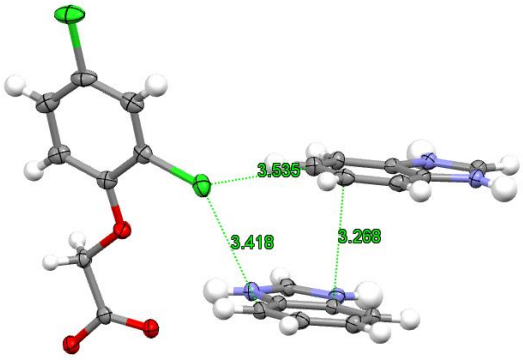

Figure 321 - Position 2 chlorine on 2,4-D has two short contacts with aromatic hydrogens on two benzimidazolium molecules.

The 2-position chlorine on the 2,4-D (Figure 321) makes two contacts with different benzimidazolium molecules at distances of 3.535(1)Å (Cl···H-C) and 3.418(1)Å (Cl···N), aiding the stacking of the molecules, which is at 3.268(2)Å planar separation measure between the distance of the closest atoms in the planes.

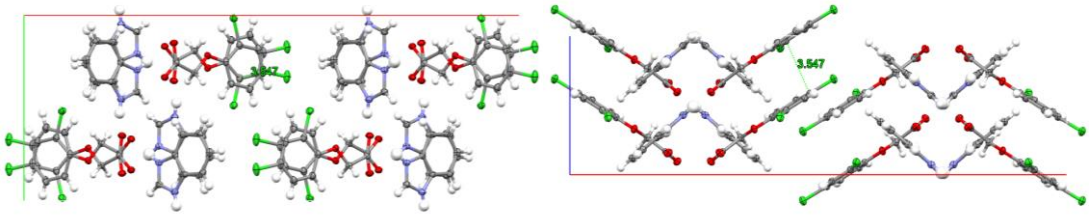

Figure 322 – Packed molecules sit indirectly over each other (left), forming echelon arrangements (right).

The skewed stacking of the molecules again prevents π interaction, with distances between stacking molecules between 3.41-3.54 Å for 2,4-D molecules and 3.25-3.55 Å for imidazolium molecules. The indirect stacking forms an inverting echelon pattern as can be seen in Figure 322 (right).

7.3.2 3,4-Dichlorophenoxyacetic acid and benzimidazole

2-4-dichlorophenoxyacetic acid and benzimidazole were dissolved in ethyl acetate and held at 30°C for crystallisation yielded a new material which was subjected to a full data collection, detailed in

Table 68.

Table 68 - Crystal structure collection data for 3,4-Dichlorophenoxyacetate benzimidazolium molecular complex

Compound	**3,4-Dichlorophenoxyacetate benzimidazolium complex**
Formula	$C_8H_5O_3Cl_2$: $C_7H_5N_2$
Crystallisation Conditions	3,4-D crystallised with benzimidazole in ethyl acetate at 30°C
Molecular weight / $gmol^{-1}$	339.17
Temperature (K)	100
Space Group	Pc
a (Å)	13.8047(7)
b (Å)	4.8070(3)
c (Å)	33.829(2)
α (°)	90
β (°)	90.490(6)
γ (°)	90
Volume ($Å^3$)	2244.8(2)
Z	6
Z'	3
θ range/°	3.18 – 27.48
Reflections Collected	21677
Independent	9813
Refln (obs.I>2theta(I))	7131
R_{int}	0.0447
Parameters	739
GooF on F^2	1.066
R_1 (Observed)	0.0346
R_1 (all)	0.0637
wR_2 (all)	0.0886
Flack parameter	-0.01(4)

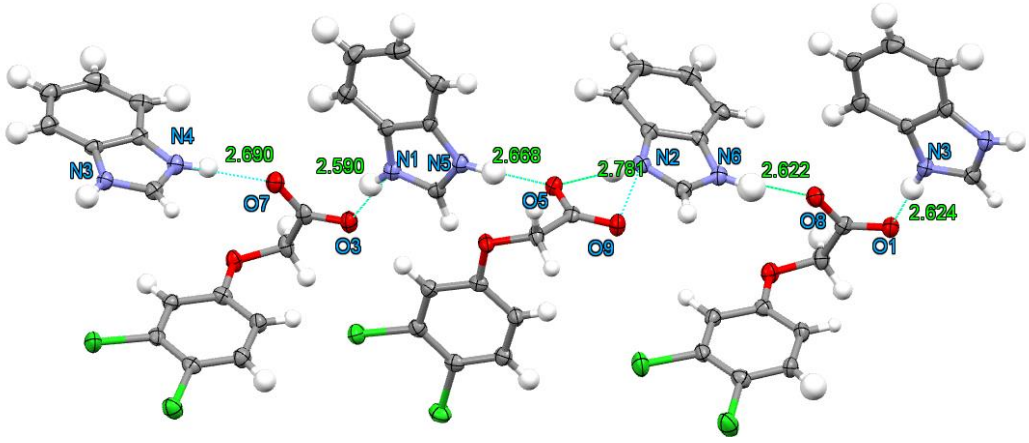

Figure 323 - Symmetry inequivalent molecules in the 3,4-D benzimidazolium structure, showing the extended hydrogen bonding network.

The 3,4-D and benzimidazolium structure is more irregular than the other structures. It follows the same imidazolium hydrogen bonding chain motif, however the molecules are slightly out of arrangement, seen most prominently at the shared acetate oxygen O5, which is hydrogen bonded from both N2 and N5 (Figure 323). As can be seen in Table 69,

the N-H···O hydrogen bonding distances are all of moderate strength, which has come to be expected from the other structures.

Table 69 – hydrogen bond distances in the 3,4-D benzimidazolium structure

Atom 1	Atom 2	Length	Angle
N1	O3	2.590(3)	161(3)°
N4	O7	2.690(3)	161(3)°
N5	O5	2.668(3)	172(3)°
N2	O5	2.781(3)	176(3)°
N6	O8	2.622(3)	169(4)°
N3	O1	2.624(3)	171(4)°

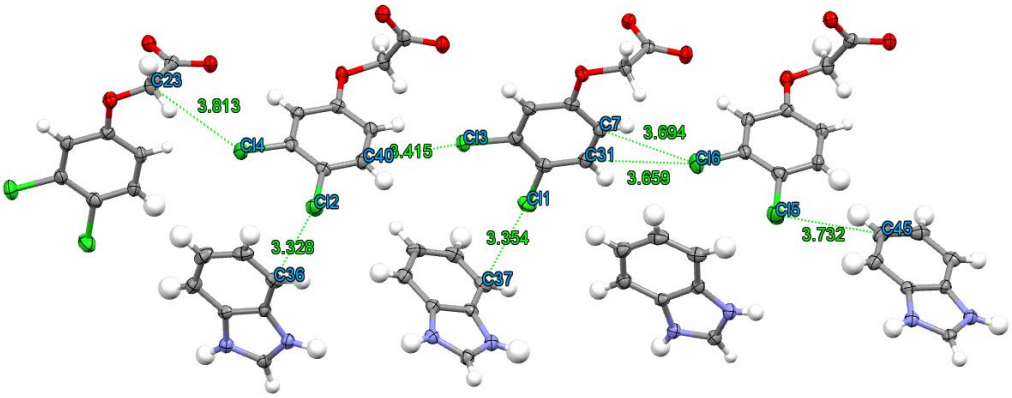

Figure 324 - Aromatic hydrogen to chlorine interactions in the 3,4-D benzimidazolium structure.

On the other sides of the molecules, the chlorine atoms experience a similar skewing of their average bond lengths, as seen in Figure 324, and shown in Table 70.

Table 70 – chlorine interaction distances in the 3,4-D benzimidazolium structure

Atom 1	Atom 2	Length
Cl2	C36	3.328(3)
Cl3	C40	3.415(3)
Cl1	C37	3.354(3)
Cl5	C45	3.732(4)
Cl6	C31	3.659(3)
Cl6	C7	3.694(3)
Cl4	C23	3.813(3)

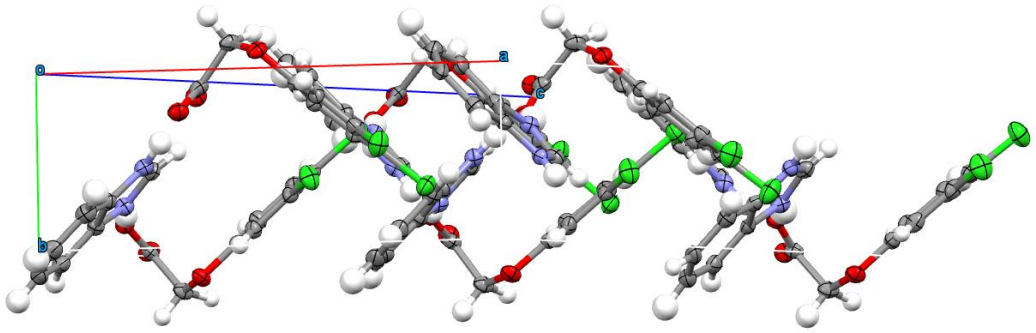

Figure 325 - Irregular packing in 3,4-D benzimidazolium structure.

Together, this creates an irregular packing pattern (Figure 325). This may not be the most stable form of the structure, as it does not conform with the normal arrangements through the rest of the more regularly arranged structural motifs in the series. This molecular complex should be screened for possible polymorphism.

7.3.3 Thermal analysis of 2,4-D and 3,4-D benzimidazolium complexes

The thermal analysis of the 2,4-D and 3,4-D benzimidazolium complexes is very clear. Both materials show only one endothermic transition that does not correspond to either starting material.

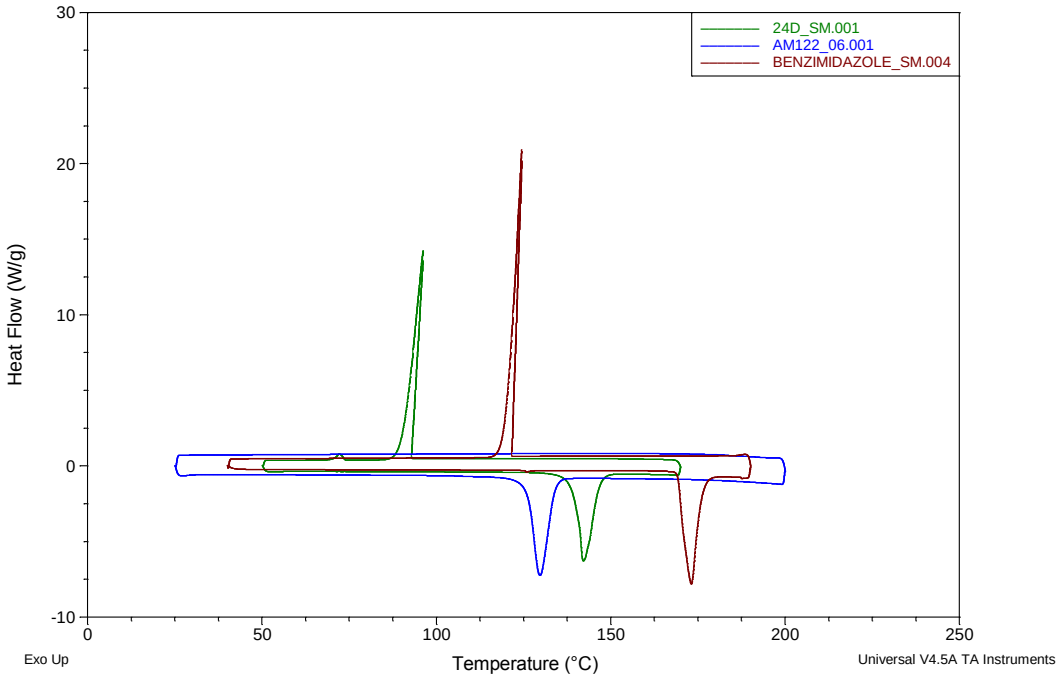

Figure 326 - DSC scans of 2,4-Dichlorophenoxyacetic acid (green), benzimidazole (brown) and the 2,4-D benzimidazolium complex (blue).

The 2-4-D sample shows an endothermic event at 131-134 °C (Figure 326; blue) that appears before the melting points of the starting materials. The new molecular complex is therefore less thermally stable than either of the starting materials.

The 3,4-D complex shows only one transition peak (Figure 327) but at a much lower temperature (about 30° lower). This is likely a result of the much poorer ordering of the structure than its 2,4-D isomer. The endothermic peak observed for the complex is at 98-102 °C and is also significantly lower than the melting points of either of its starting materials.

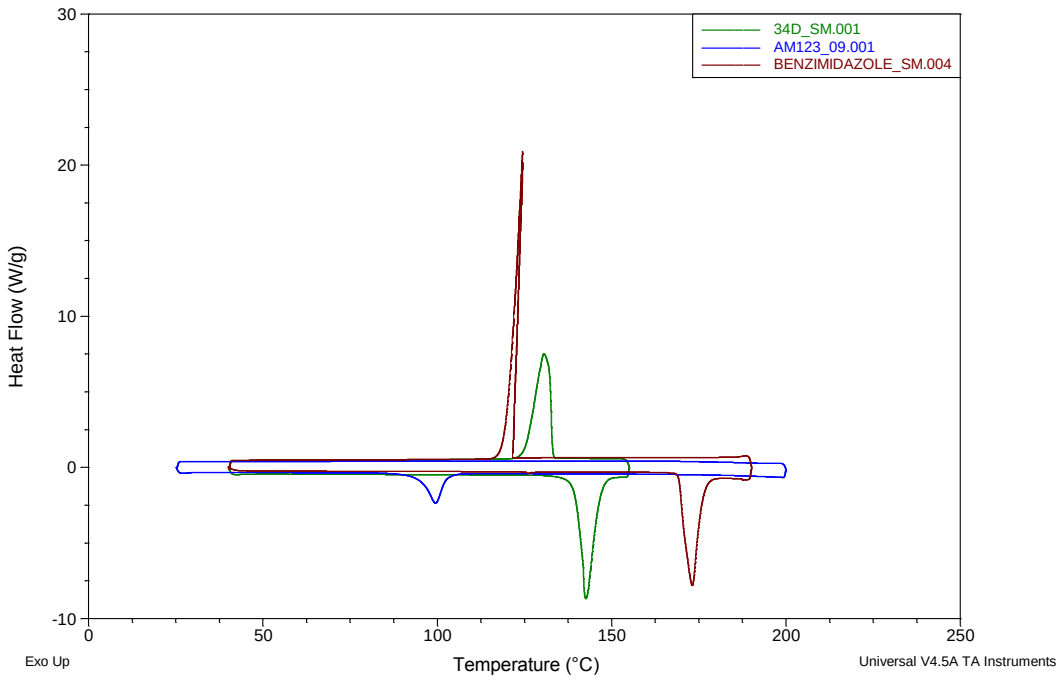

Figure 327 - DSC scans of 3,4-Dichlorophenoxyacetic acid (green), benzimidazole (brown) and the 3,4-D benzimidazolium complex (blue).

7.4 Chlorophenoxyacetic acids and 1-methylbenzimidazole

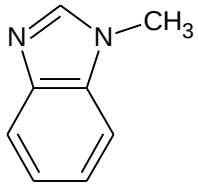

Figure 328 - Molecular structure of 1-methylbenzimidazole

1-methylbenzimidazole (Figure 328), with one of its available hydrogen bonding sites essentially blocked off entirely by the methyl group, should offer the potential for significantly different hydrogen bonding motifs to those found for benzimidazole. It was therefore studied under equimolar cocrystallisation conditions with 2,4-D and 3,4-D in methanol, ethanol, acetone, ethyl acetate and diethyl ether at both room temperature and

30°C, with the aim to generate molecular complexes for study. Single crystals suitable for study were found from the 2,4-D experiments and studied by single crystal X-ray diffraction:

7.4.1 2,4-Dichlorophenoxyacetic acid and1-methylbenzimidazole

Single crystals were recovered from the crystallisation of 2,4-D and 1-methylbenzimidazole and upon identification that a new material had been formed, were subjected to a full data collection on the image plate diffractometer. The details of the collection and subsequent crystal structure solution are outlined in Table 71.

Table 71 - Crystal structure collection data for 2,4-Dichlorphenoxyacetate 1-methylbenzimidazolium molecular complex

Compound	**2,4-Dichlorphenoxyacetic acid 1-methylbenzimidazole complex**
Formula	$C_8H_6O_3Cl_2:C_8H_8N_2$
Crystallisation Conditions	2,4-D crystallised with 1-methylbenzimidazole in acetone at room temperature
Molecular weight / $gmol^{-1}$	353.19
Temperature (K)	100
Space Group	$P2_1/c$
a (Å)	14.495(4)
b (Å)	11.082(3)
c (Å)	10.772(3)
α (°)	90
β (°)	110.318(8)
γ (°)	90
Volume ($Å^3$)	1622.1(8)
Z	4
Z'	1
θ range/˚	3.44 – 27.48
Reflections Collected	8946
Independent	3669
Refln (obs.I>2theta(I))	1968
R_{int}	0.0799
Parameters	264
GooF on F^2	1.006
R_1 (Observed)	0.0882
R_1 (all)	0.153
wR_2 (all)	0.2613

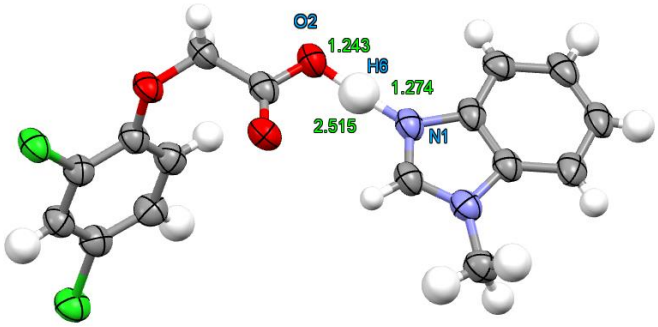

Figure 329 - Asymmetric unit of the 2,4-D 1-methylbenzimidazole structure featuring the short strong N-H···O hydrogen bond.

With the removal of one of the hydrogen bonding sites from the benzimidazole molecule the hydrogen bond strength of the main hydrogen bonding interaction, as seen in the asymmetric unit of the 2,4-D 1-methylnezimidazole (Figure 329), is seen to increase making the N1-H6-O2 interaction a short, strong hydrogen bond at an N···O distance of 2.515(6)Å (176(6)°). With the electron density associated with the hydrogen modelled at distances of 1.24(7)Å (H6-O2) and 1.27(7)Å (H6-N1), the error on the distance makes the association of the hydrogen to either of the molecules indeterminate, being close to centre within error. However, it is slightly closer to the oxygen and for convenience the complex will be discussed in non-deprotonated terms.

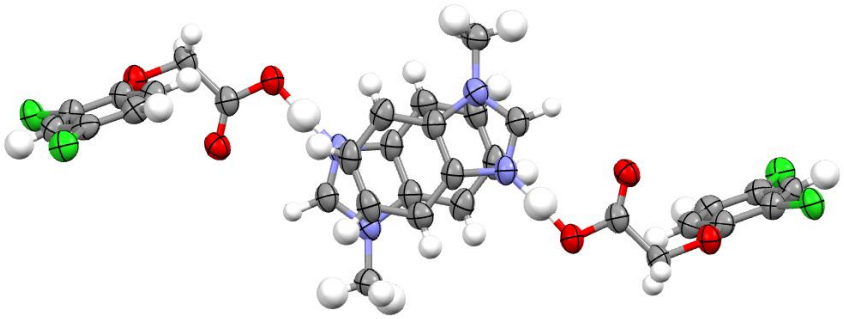

Figure 330 – 1-methylbenzimidazole stacking forming asymmetric unit dimers.

The 1-methylbenzimidazole molecules stack with a medium strength π-π stacking interaction at 3.457(7)Å, with overlapping 5 and 6 membered rings (Figure 330). This has the effect of producing a π-π bonded dimer of the molecules that are hydrogen bonded in the asymmetric unit to two 2,4-D molecules. The "asymmetric unit dimer" thus orientates the 2,4-D molecules perpendicular to the plane of the methylbenzimidazole molecules, forming in directions favourable to the available π-π interaction. This feature is utilised

further in the structure, with π-π interactions forming between 2,4-D groups at a distance of 3.463(8)Å, with the appearance of creating a π-π stacked chain of asymmetric unit dimers (Figure 331).

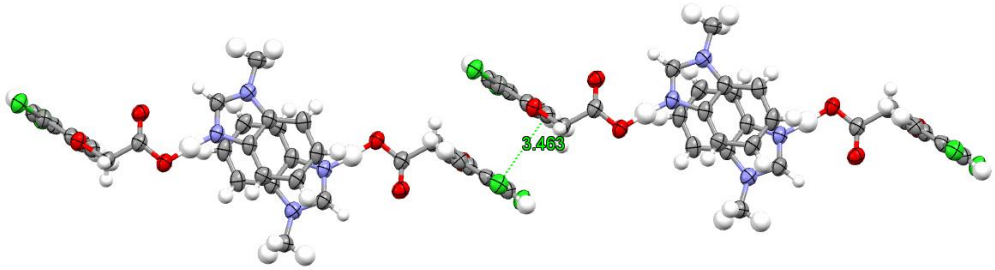

Figure 331 - stacking of 2,4-D molecules forming a π-π stacking chain.

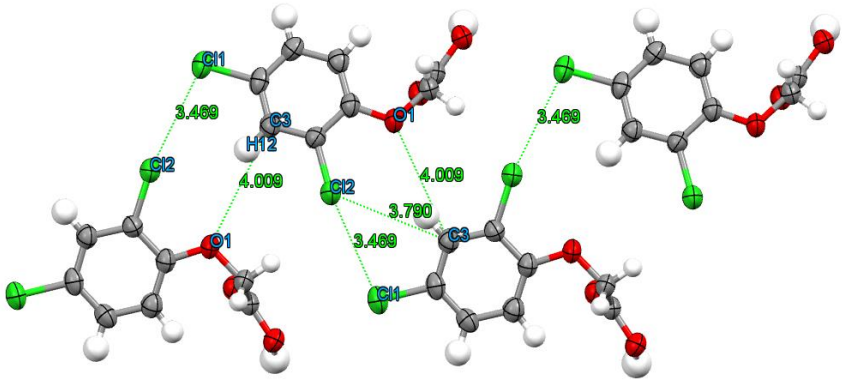

Figure 332 - 2,4-D molecules in the complex, with 1-methylbenzimidazole molecules hidden, showing chlorine and aromatic hydrogen interactions.

The dimers are further supported by a network of chlorine interactions between the 2,4-D molecules along the plane of their aromatic rings (Figure 332) with a Cl1···Cl2 distance measured at 3.469(2)Å and an additional contact to the aromatic C-H on the 3 position of the benzene ring with Cl2···C3 distance. There is also a very weak C-H···O interaction involving the chain oxygen O1 with C3···O1 distance of 4.009(7)Å.

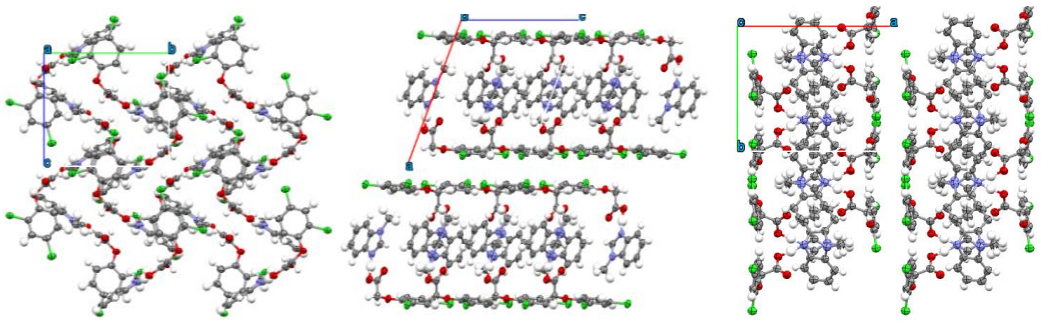

Figure 333 - 2,4-D 1-methylbenzimidazole structure viewed down the *a*, *b* and *c* axes (left, centre and right).

The overall motif of the packed structure is well ordered, with a tight zig-zag arrangement visible viewed down the *a*-axis (Figure 333; left) and sandwich planes with 3,4-D edges and 1-methylbenzimidazole centres seen when viewed down the *b* and *c* axes (Figure 333; middle and right).

7.4.2 3,4-Dichlorophenoxyacetic acid and 1-methybenzimidazole

Crystallisations of 3,4-dichlorophenoxyacetic acid and 1-methylbenzimidazole have produced no crystals suitable for single crystal X-ray diffraction purposes at the time of writing. However, samples were isolated which were suitable for DSC analysis, the results of which may be found in the following thermal analysis section.

7.3.3 Thermal analysis of 2,4-D and possible 3,4-D 1-methylbenzimidazole complexes

The final 2,4-D complex studied, that with benzimidazole, was analysed by DSC and found to contain two thermal events, one of which corresponds to the melting point of the 1-methylbenzimidazole, while the other is at 100-102°C (Figure 334; brown). This would suggest that the new complex co-exists with some residual methylbenzimidazole present in the product. The melting transition of the new complex is again found to be less than that of 2,4-D and therefore less thermally stable than the parent agrichemical.

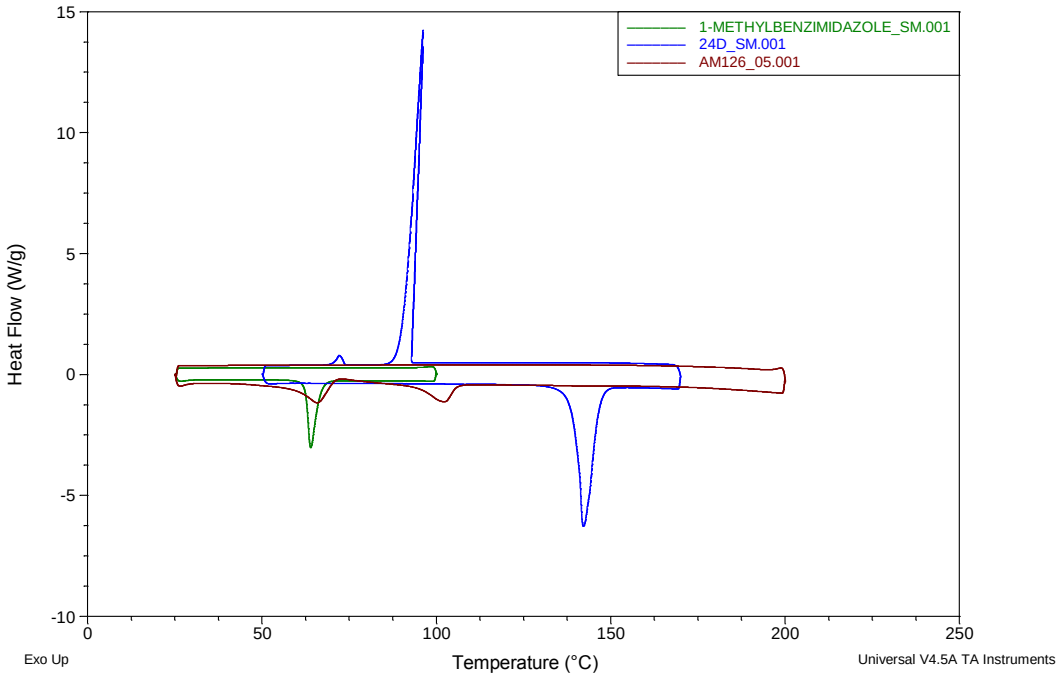

Figure 334 - DSC scans of 2,4-Dichlorophenoxyacetic acid (blue), 1-methylbenzimidazole (green) and the 2,4-D 1-methylbenzimidazolium complex (brown).

The DSC of the material collected from the crystallisation experiment of 3,4-D and 1-methylimidazole has produced a similar result with a melting transition again

corresponding to the 1-methylbenzimidazole starting material, and a further melt at around 78-81 °C (Figure 335; brown). This would suggest that this material too has formed a new complex, which should be analysed by single crystal X-ray diffraction when suitable crystals are found.

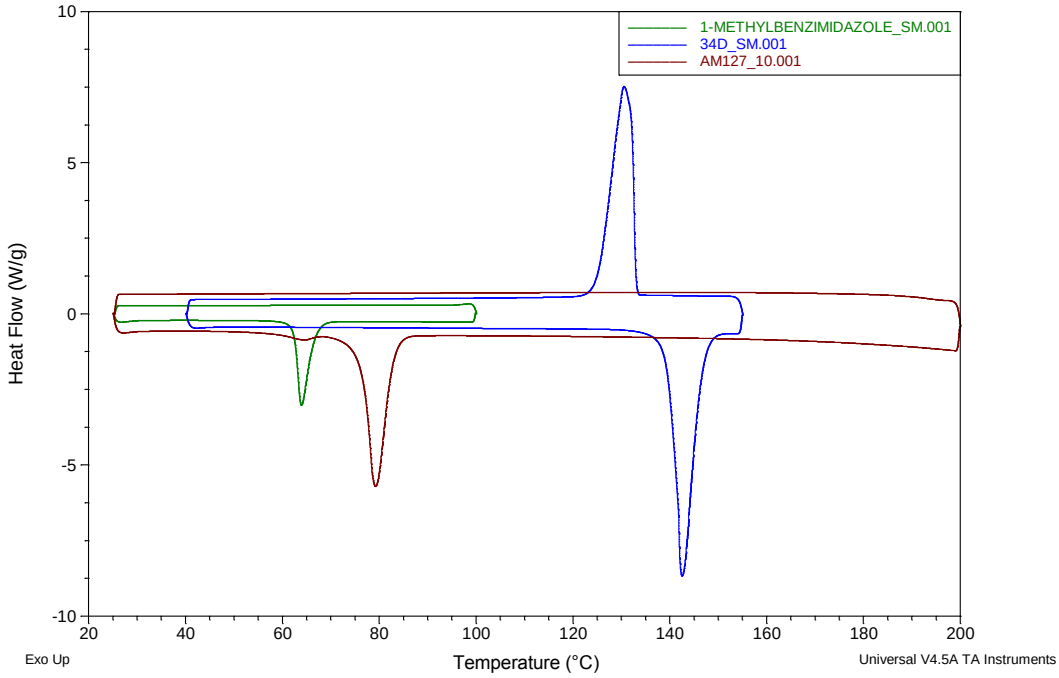

Figure 335 - DSC scans of 3,4-Dichlorophenoxyacetic acid (blue), 1-methylbenzimidazole (green) and the unresolved sample from the crystallisation of 3,4-D and 1-methylbenzimidazole (brown).

7.5 Unresolved materials

Several other crystallisations of 2,4-D and 3,4-D were initiated, but due to time constraints, have not as yet been analysed. These were as follows:

- 2,4D and DMAN
- 2,4-D and α-cyclodextrin
- 2,4-D and β-cyclodextrin
- 2,4-D and tri-acetyl-β-cyclodextrin
- 2,4-D and Hydroxyethyl-β-cyclodextrin

7.6 Summary

New structures were produced with 2,4-D and 3,4-D with several imidazole based molecules, the majority of which showed similar imidazolium – N-H double hydrogen bond motifs to deprotonated carboxylic acid functional groups, forming chains throughout the structures of moderate hydrogen bond strength. This motif was lost however when one of the nitrogen molecules was further substituted with a methyl group.

All molecular complexes formed were showed to be less thermally stable than the component agrichemical when analysed by DSC. This is likely to mean that they would be more soluble as a result, based on the frequent correlation between these two parameters; dissolution testing of these materials is planned within the group in future.

The resultant product from the cocrystallisation of 3-4-D and 1-methylbenzimidazole has been identified as a new material by DSC and should be further characterised to determine its content and structure, along with the analysis of the materials that have not yet been studied by structural methods.

8. Conclusions

8.1 Reactive materials

Working with reactive materials has proven to be very challenging. Their high degree of reactivity resulting from the energetics of their molecular structures leads to a high degree of incompatibility with a wide range of secondary components normally exploited in molecular complex formation. This drastically limits the available conditions in which the target materials can be used, with respect to solvent, additives, atmospheric considerations and consequently storage and application. However, as reactive materials form some of the most useful and important chemicals for vital functions in many industries, finding a way to control them effectively is an area which merits research. With this in view, the research outlined in this work into finding new methods of working with these materials, and finding new ways to add stability to them in a reliable and functional way that does not prevent them for from being used in their desired application, has driven the multi-faceted approach used to try and achieve the goal of a stabilised reactive material.

The use of crystallography as a tool for this goal is a valid approach, with due time and diligence given to screening desired targets for a more complete understanding of their individual reactivities, compatibilities and incompatibilities, with different types of materials. This is targeted at the design of a method for stabilising them to suit the individual needs of the chemical or series of chemicals through targeting individual reactive sites on the concerned molecule itself. The use of a crystal engineering methodology to achieve this is well suited to the aim, as it too requires understanding and targeting of molecular features in order to achieve desired material of multiple components, and creating a new material in the solid state, with its own characteristic features and physical properties, which may be more suitable for potential application.

In some cases crystallising the target reactive materials in single component form has even proved to be a delicate procedure, requiring extensive screening with an array of many different conditions to find one that best suits the reactive material under study. Where databases exist with detailed information on the likely reactivity and compatibility of these reactive materials, this can be achieved easily through identification of patterns. However, this is seldom the case for highly reactive materials, and empirical research must be performed in order to provide a full understanding of the target reactive compound that is to be stabilised.

8.2 Organic peroxyacids

Working with organic peroxyacids is an extremely delicate procedure, and throughout this research there have been many pitfalls whilst trying to find a reliable way to stabilise these materials. Being the most reactive of all the organic peroxides, they are notoriously incompatible with a wide range of materials, forming equally if not more hazardous energetic outcomes if not treated carefully. Successfully working with these materials is possible, however, and a range of studies of the target materials used as a basis for this research have been successful.

8.2.1 Screening and crystallisation of organic peroxyacids

8.2.1.1 Solvents for peroxyacids

The screening process for finding optimal conditions for crystallisation of reactive peroxides has involved trialling a medium to wide range of solvents, many of which resulted in the decomposition of the peroxyacids to the parent acids. This occurred either through absorption of water into the solvent and thus making it available for use in the decomposition reaction below (Figure 336), or by directly reacting with the solvent itself to form new materials.

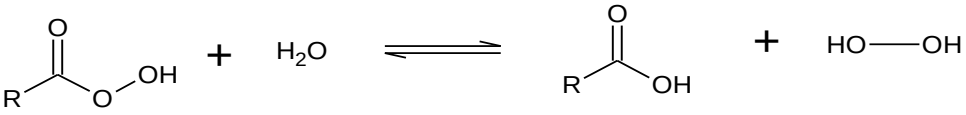

Figure 336 - Reversed reaction of formation of a peroxyacid, or the "decomposition reaction".

Recrystallisation attempts of the peroxyacid *meta*-chloroperbenzoic acid, led to decomposition that reliably formed its parent acid, 3-chlorobenzoic acid (Figure 101), which although very structurally similar to the peroxyacid from which it decomposes, shows no evidence of interacting with the peroxyacid in the solid state.

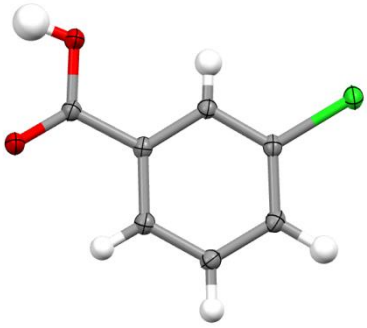

Figure 337 - Crystal structure asymmetric unit of 3-chlorobenzoic acid.

Also, reaction of the peroxyacid MCPBA or its other decomposition product, hydrogen peroxide, with acetone readily forms the unstable energetic material triacetone triperoxide, TATP (Figure 110).

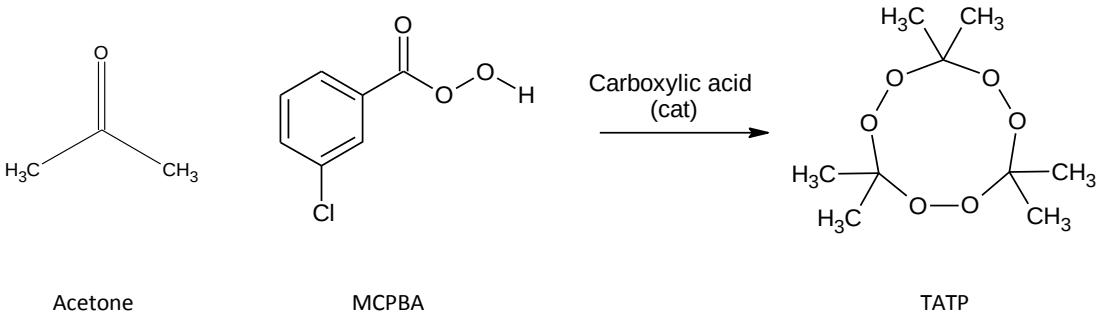

Acetone MCPBA TATP

Figure 338 - Synthesis of TATP under crystallisation conditions for MCPBA.

Production of the TATP material in this manner is not the standard approach, and the crystal structure was collected and solved for completeness (Figure 115).

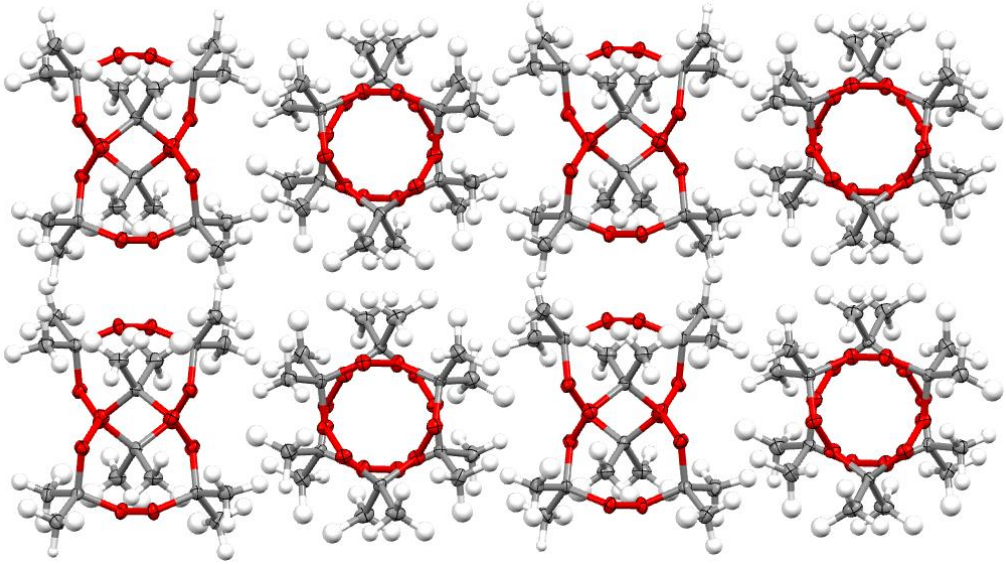

Figure 339 - 3 layers of TATP chains viewed down the b-axis of the collected TATP structure

What was unexpectedly encountered however is that the solvent that so readily reacts with peroxides to form TATP – acetone – was the one in which MCPBA was most stable, as determined at both 4°C and room temperature, and a crystal structure of the MCPBA reactive material was achieved from these conditions.

With the second, larger, peroxyacid, 6-phthalimidoperoxyhexanoic acid (PSP), a similar outcome was encountered with decomposition to the parent acid – 6-phthalimidohexanoic acid, and to its hydrate, a new polymorph of which was discovered (Figure 134).

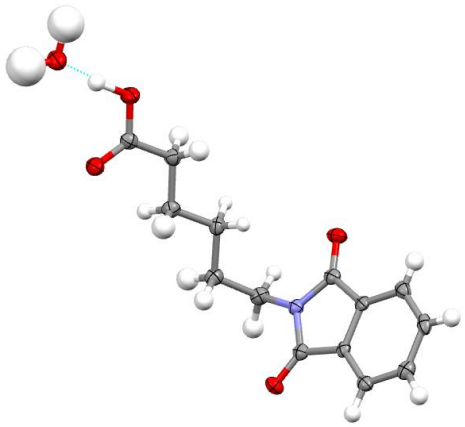

Figure 340 - Asymmetric unit of 6-phthalimidohexanoic acid monohydrate Form II.

A selection of solvent conditions were found in which PAP could crystallise without decomposing, and this was taken forward to the succeeding crystallisations (Table 72).

Table 72 - Solvent conditions from which PAP was successfully recrystallised

Sample ID	Recrystallisation solvent	Temperature
AM24_01	Methanol	4°C
AM24_10	Acetone	Room temperature
AM24_11	Diethyl Ether	4°C
AM32_03	Acetone	4°C
AM32_04	Acetone	4°C
AM32_05	Acetone	Room temperature
AM32_06	Acetone	Room temperature
AM32_07	Acetone	30°C
AM32_09	Methyl Acetate	4°C
AM32_10	Methyl Acetate	Room temperature
AM32_11	Methyl Acetate	30°C

8.2.1.2 Additiives in peroxyacid recrystallisations

Adding components to the crystallisation process, in particular hydrochloric acid and sodium hydroxide to change the acidity and basicity of the crystallisation, as well as hydrogen peroxide proved to be unsuccessful in retaining the peroxyacid functionality.

The addition of hydrochloric acid to crystallisations of peroxyacids seems to expedite the decomposition of the peroxyacid in all cases. The hydrogen ion reacts readily with the peroxyacid group to create a water molecule, decomposing the peroxyacid to its parent carboxylic acid.

Crystallisation with the addition of sodium hydroxide resulted in the crystallisation of "soda ash" or sodium carbonate heptahydrate, a common material in which the peroxyacid oxidises a solvent to produce a carbonate for the salt to be formed with.

The addition of hydrogen peroxide, with the aim of reversing the decomposition equilibrium, had the more curious effect of preventing recrystallisation, making resulting materials more amorphous. It is suggested that this may be a result of the functional group exchanging back and forward from carboxylic acid to peroxyacid, preventing its use in molecular association with the primary or secondary materials.

8.2.1.3 Crystal structures of target materials

The crystal structure of MCPBA was obtained from acetone recrystallisations and proved to have a similar hydrogen bonding motif in its functional group as the known peroxyacids. With the determination of the presence of the hydrogen atom, the pairing relationship between two peroxyacids could be properly defined as a catemeric arrangement, and not the previously proposed dimeric arrangement[11, 12] (Figure 150).

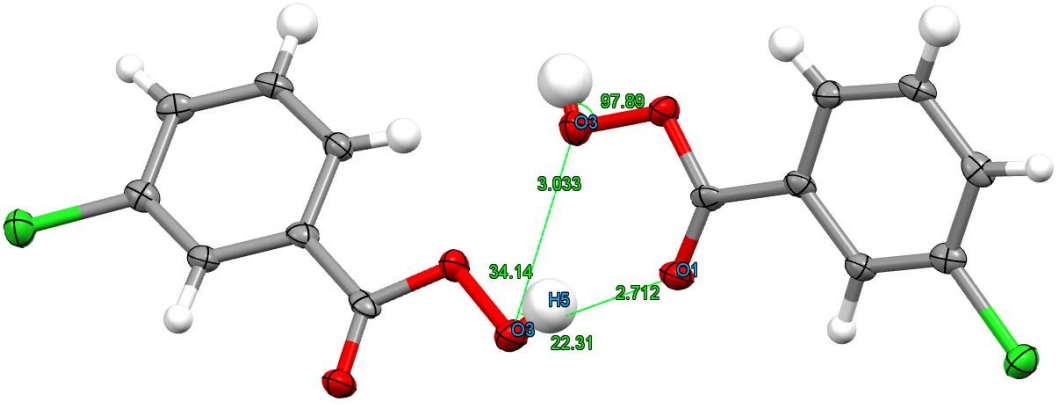

Figure 341 - Hydrogen bonding of peroxyacid group in MCPBA viewed along *a*-axis.

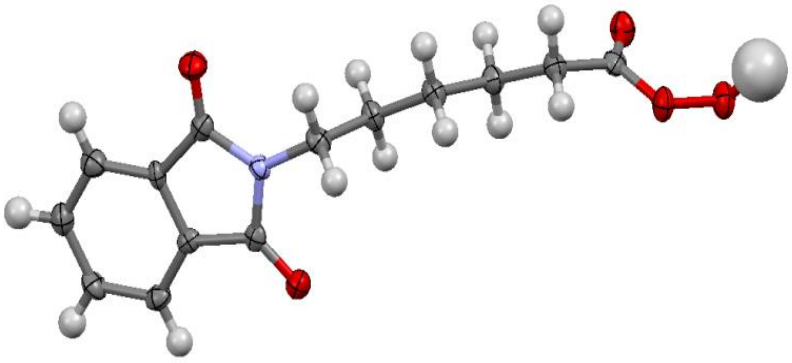

Figure 342 - Asymmetric unit of the crystal structure of 6-phthalimidoperoxyhexanoic acid (PAP).

This was further confirmed by the determination of the structure of 6-phthalimidoperoxyhexanoic acid, PAP (Figure 342), in which the peroxyacid functional group head also showed the same catemeric motif (Figure 156).

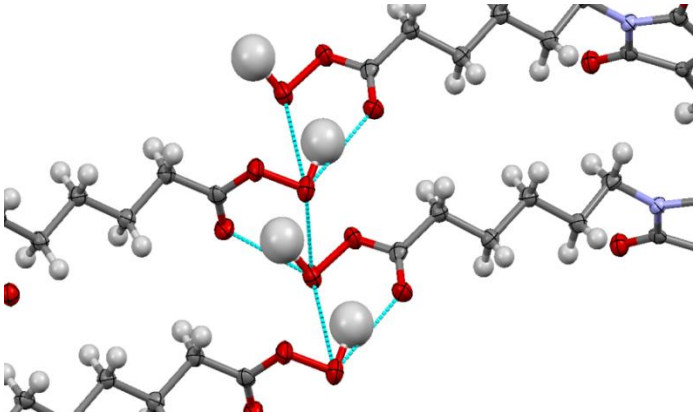

Figure 343 – Hydrogen bonding of peroxyacid groups in 6-phthalimidoperoxyhexanoic acid.

8.2.2 Using carboxylic acids for cocrystallisation with peroxyacids

Crystallisation of peroxyacids with carboxylic acids proved unsuccessful, not only leading to decomposition of the peroxyacids to the parent acids, but even the resulting parent acids did not undergo molecular complex formation with the secondary acid components in the crystallisation. The peroxyacids were not only incompatible chemically with then explored conditions, but some unknown factor is preventing association of the carboxylic acid group.

No new complexes were formed with peroxyacids and carboxylic acids.

8.2.3 Using π-π interacting materials for crystallisation with peroxyacids

Cocrystallisation with larger molecules with a strong π-interacting character also proved unsuccessful in producing peroxy-acid molecular complexes, with decomposition of both the peroxyacids and the secondary materials evident. For example, 4-

hydroxybenzophenone was oxidised by the peroxyacid to form a crystalline structure of benzoic acid.

Crystallisation of PAP with benzimidazole formed a new crystalline material, which was found to be a partially oxidised/nonoxidised benzimidazole – 6-phthalimidohexanoic acid complex, in which one of the two benzimidazole molecules in the asymmetric unit has been oxidised at 40% occurrence to form a hydroxyl group on the available amine (Figure 241).

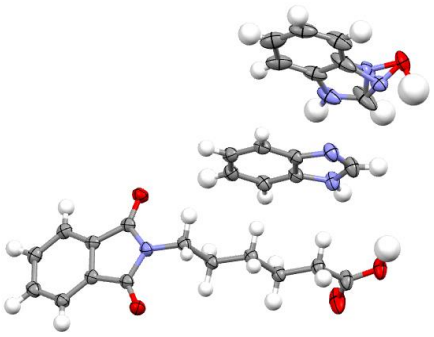

Figure 344 - Asymmetric unit of oxidised benzimidazole, benzimidazole and 6-phthalimidohexanoic acid

8.2.4 Crystallising reactive materials with metals

Crystallisation of reactive peroxyacids with metals resulted in decomposition in the majority of cases, to form the parent acids with no other new materials formed. However the analysis of these materials is by no means complete and the collected samples await further analytical investigations in future.

8.2.5 Hosting reactive materials

The concept of locking the reactive material inside a larger, more stable, structure led to the investigation of several host-guest combination methodologies, including urea channelling, the use of cyclodextrins and layered materials such as montmorillonite clays.

8.2.5.1 Hosting in Urea based structures

Hosting with urea based structures, that is urea channels and thiourea, proved to be unsuccessful. Thiourea was violently reactive with the organic peroxides and thus entirely excluded from consideration. Urea tended to recrystallise on its own as the starting material, or in the presence of hydrogen peroxide, forming a known hydrogen peroxide urea 1:1 cocrystal, as determined by single crystal XRD – unit cell analysis and X-ray powder diffraction methods. No new materials aside from this previously known cocrystal were found for analysis.

8.2.5.2 Hosting in cyclodextrins

Hosting materials within cyclodextrins proved to be more successful. A crystalline host structure with organic peroxyacid contained inside was not obtained, however a structure of a β-cyclodextrin potassium framework with the MCPBA parent acid (3-chlorobenzoic acid) intercalated into its barrel shaped structure was achieved, with two ordered and one disordered guest molecules (Figure 269).

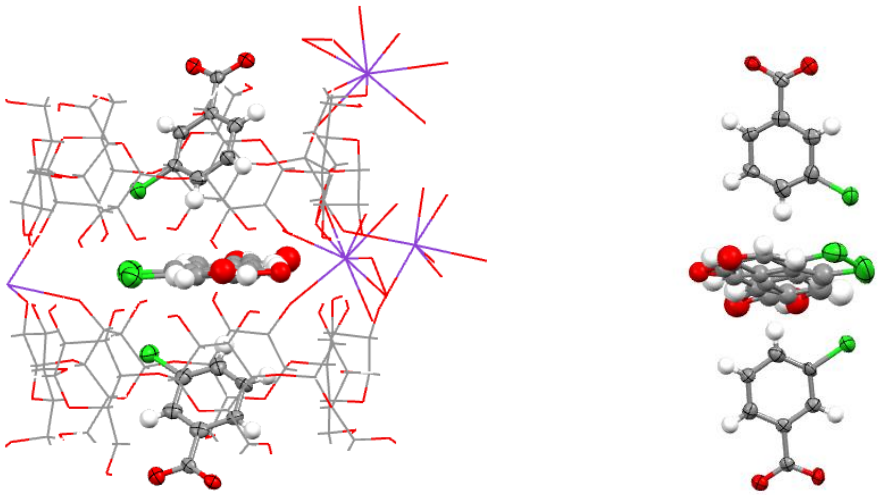

Figure 345 - Three 3-chlorobenzoic acid molecules located inside the core of the barrel arrangement of -cyclodextrin (left). Of the three 3-chlorobenzoic acid molecules, two are ordered, one is disordered (right).

It is proposed that with additional research, this could prove to be a possible solution to the hosting approach of a peroxyacid, given the correct conditions for retaining the peroxyacid are found, in which this structural arrangement also assembles.

8.2.5.3 Hosting within layered materials

Hosting the peroxyacids within the montmorillonite clay Bentonite proved to be unsuccessful for smaller molecules and MCPBA, however with PAP a significant change in the structure of the hosting material was observed. This corresponded to an increase in the interlayer spacing by more than 3Å upon application of the peroxyacid through solvent assisted grinding techniques. This was quantified and found to be scalable to a point at which the clay can no longer accept any more of the material. Determination of the contents of the material once the spacing increase (and the intercalation of the guest) had occurred proved difficult. The same effect is observed with the PAP parent acid and as such the effect is not limited to the peroxyacid functionalised material. Testing of the intercalated material revealed limited oxidising ability on a test material up to the point of saturation of the pores in the clay. After that point the testing material is strongly oxidised, possibly due to the present of remaining peroxyacid outside the clay. It is clear that under

these intercalation conditions the peroxyacid is encouraged not to decompose, a positive outcome that can be pursued in future work.

8.3 Agrochemicals

Cocrystallisation with agrochemicals was another direction focussed in this research in an attempt to change their physical properties to better suit the need of the end application. The high reactivity of many active agrichemical ingredients (AAIs) provides a clear link to the work on reactive materials. To this end the target materials 2,4-dichlorophenoxyacetic acid (2,4-D) and 3,4-dichlorophenoxyacetic acid (3,4-D) were cocrystallised with imidazole based materials with a good degree of success.

8.3.1 Cocrystallising with imidazole based components

New molecular complexes were formed between 2,4-D and imidazole, 4(5)-methylimidazole, benzimidazole and 1-methylbenzimidazole, and between 3,4-D and imidazole, 4(5)-methylimidazole and benzimidazole. A common recurring motif throughout the crystallisations and the resulting molecular complexes was the generation of an imidazolium based ion with two of the nitrogen atoms on the molecules protonated. This then generated moderate strength hydrogen bonds to the acetate groups created on the chlorophenoxyacetic acid molecules as a result of the deprotonation (Figure 299).

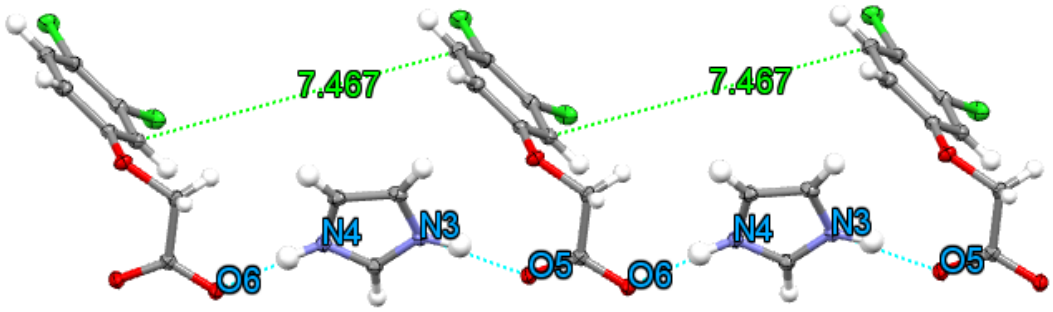

Figure 346 - 3,4-D and imidazolium (N1···O3-O2···N1) chains.

The 1-methyl benzimidazole complex, however, did not generate this motif due to the occupation of one of the nitrogen sites by the methyl group. Instead an interesting π-stacking driven structure was formed (Figure 331), with only one hydrogen bond existing between the 2,4-D and the 1-methylbenzimidazole nitrogen atom which, as a short, strong N-H-O hydrogen bond, is significantly stronger than the moderate strength chain interactions in the primary motif.

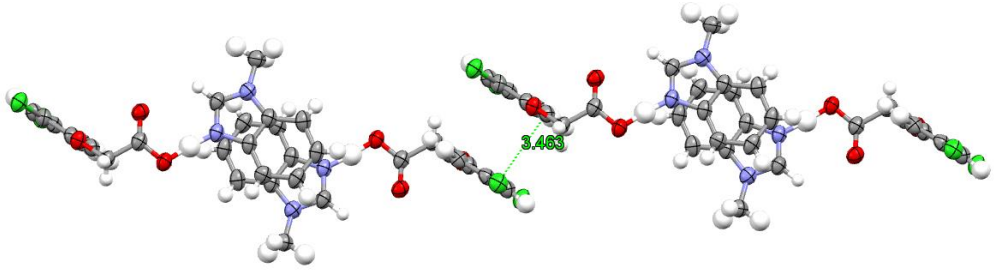

Figure 347 - stacking of 2,4-D molecules with 1-methylbenzimidazole forming a π-π stacking chain.

8.3.2 Thermal analysis of crystal structures

The thermal analysis of these new materials all showed that the melting points of the generated molecular complexes were at a lower temperature than those of the agrichemical used in synthesis of the complex. The new materials were therefore less thermally stable than the original compounds.

The thermal analysis also revealed one sample for which a new material has likely formed but for which no crystal structure exists. This is the result of crystallisation between 3,4-dichlorophenoxyacetic acid and 1-methylbenzimidazole. This should be investigated and fully characterised to complete the series of molecules investigated.

8.4 Forward look

Although the outcome of many of the experiments was unsuccessful in creating a stabilised molecular complex, a lot of new information was gathered about the target materials which may be used to further understand the interactions and limitations of these. As such further investigation of these materials will be aided by this information, and finding a hosting method or a crystal engineering strategy which will perform the task needed for stabilisation is just a process of tuning the conditions and materials until the correct method is found.

The solvent selection for crystallisation needs to be widened to find more possible environments for crystallisation of the peroxyacids as well as more in depth temperature screening, with more low temperature experiments to reduce available free energy in the systems.

The crystallisation in host materials showed the most promise, with the cyclodextrin cage structures stable in presence of peroxyacids, and able to incorporate molecules of the correct size. Further investigation needs to be carried out on these with greatly expanded

experimental conditions tested for inclusion of the materials with retention of the peroxyacid. Again, finding the correct conditions for this to be achieved should be a process of elimination and then fine tuning until the target is achieved.

The positive results on clays also propose a very promising direction for further work. The intercalation of reactive materials into the pores of the material cannot only be limited to one target reactive molecule and this method may be applicable to reactive materials other than PAP.

The agrichemical studies yielded many new structures clearly offers a rich vein for producing molecular complexes. It was noted during the research into the chlorophenoxyacetic acids that no crystals exist with these materials in their protonated state, which in the work proved to create a much stronger hydrogen bond. As such efforts should be made to direct the crystallisations towards retention of the carboxylic acid functionality of these materials for assessment of the change in physical properties.

The most lacking feature in this research was time. Given enough time, more complete investigations of the materials formed could be achieved, with many crystallisations and samples still requiring analysis. One of the most important things to realise is that in this type of exploratory research every sample was a different experiment, with each of them are as important as the next; complete analysis of all samples is required for the full understanding to be achieved. The answer may already be in a vial of crystals that hasn't been opened yet!

References

1. Ibne-Rasa, K. M.; Edwards, J. O., The Mechanism of the Oxidation of Some Aromatic Amines by Peroxyacetic Acid. *J. Am. Chem. Soc.* **1962,** *84* (5), 763-768.
2. Curci, R.; Diprete, R. A.; Modena, G., Experimental Bearing on Role of Solvent in Oxidation of Some Organic Compounds by Peroxy Acids. *Journal of Organic Chemistry* **1970,** *35* (3), 740 - 745.
3. Klaas, M. R. G.; Warwel, S., Lipase-catalyzed preparation of peroxy acids and their use for epoxidation. *Journal of Molecular Catalysis a-Chemical* **1997,** *117* (1-3), 311-319; Liu, B.; Meng, X.-G.; Li, W.-Y.; Zhou, L.-C.; Hu, C.-W., Theoretical and Experimental Studies on Selective Oxidation of Aromatic Ketone by Performic Acid. *The Journal of Physical Chemistry A* **2012,** *116* (11), 2920-2926.
4. Yusuf, Z.; Luckman, J. A.; Wright, T.; Kaeding, J. M.; Aykroyd, T. N.; Hendrickson, M. S.; Doyle, C. M.; Riehle, R. D., Control and wash cycle for activation and deactivation of chemistry in the wash bath of anautomatic washer. US Patent 20,120,011,662: 2012.
5. Dykstra, R. R. W. C., OH, US), Pancheri, Eugene Joseph (Montgomery, OH, US) Liquid laundry detergent composition comprising a source of peracid and having a pH profile that is controlled with respect to the pKa of the source of peracid. 2011.
6. Dias, L. C.; Pullan, R. J. F.; Sanger, A. J., Oxidative hair coloring compositions which contain a preformed organic peroxyacid oxidizing agent. US Patent 6,022,381: 2000; Church, J. A.; Prencipe, M.; Lewin, M., Oral composition having improved tooth whitening effect. US Patent 5,279,816: 1994.
7. Gao, Y.; Cranston, R., Recent advances in antimicrobial treatments of textiles. *Textile Research Journal* **2008,** *78* (1), 60-72; Devenyns, J., A process for delignifying pulp with organic peroxyacid in the presence of phosphonic acids and their salts. US Patent 5,552,018: 1996.
8. Knowles, A., Recent developments of safer formulations of agrochemicals. *The Environmentalist* **2008,** *28* (1), 35-44.
9. Buzzaccarini, F.; Delplancke, P. F.; Scialla, S.; Todini, O.; Gagliardini, A., Bleaching compositions. EP Patent 1,010,751: 2005.
10. Johnston, J. P., Peroxyacid bleach compositions having increased solubility. US Patent 4,126,573: 1978.
11. Swern, D., Organic Peracids. *Chemical Reviews* **1949,** *45* (1), 1-68.
12. Swern, D., *Organic peroxides*. Wiley: 1961.
13. Xia, J.; Matyjaszewski, K., Homogeneous reverse atom transfer radical polymerization of styrene initiated by peroxides. *Macromolecules* **1999,** *32* (16), 5199-5202.
14. Feeder, N.; Jones, W., Four omega-phthalimidoaliphatic peracids. *Acta Crystallographica Section C-Crystal Structure Communications* **1996,** *52*, 1516-1520.
15. Sagel, J. A.; Schulz, C. A.; Merz, R. J.; Nicholson, A. E., Laundry compositions containing peroxyacid bleach and perfume particles. EP Patent 0,332,259: 1997.
16. Clayden, J.; Greeves, N.; Warren, S.; Wothers, P., *Organic Chemistry*. 2nd ed.; Oxford University Press: New York, 2001; p 1512.
17. Kavcic, R.; Plesnicar, B., The Effect of Solvents with Basic Oxygen in Epoxidation with Organic Peroxy Acids. *Journal of Organic Chemistry* **1969,** *35* (6), 2033-2035.
18. Weaver, R. J.; Minarik, C. E.; Boyd, F. T., Influence of Rainfall on the Effectiveness of 2,4-Dichlorophenoxyacetic Acid Sprayed for Herbicidal Purposes. *Botanical Gazette* **1946,** *107* (4), 540-544.
19. Katritzky, A. R.; Jain, R.; Lomaka, A.; Petrukhin, R.; Maran, U.; Karelson, M., Perspective on the Relationship between Melting Points and Chemical Structure. *Crystal Growth & Design* **2001,** *1* (4), 261-265.
20. Desiraju, G. R., Crystal engineering: A holistic view. *Angewandte Chemie-International Edition* **2007,** *46* (44), 8342-8356.

21. Jeffrey, G. A., *An Introduction to Hydrogen Bonding*. 1997.
22. Adam, M. S.; Parkin, A.; Thomas, L. H.; Wilson, C. C., Bifurcated hydrogen-bonded synthons in molecular complexes of picolines with chloranilic acid. *CrystEngComm* **2010,** *12* (3), 917-924.
23. Etter, M. C., Encoding and decoding hydrogen-bond patterns of organic compounds. *Accounts of Chemical Research* **1990,** *23* (4), 120-126.
24. Janiak, C., A critical account on π–π stacking in metal complexes with aromatic nitrogen-containing ligands. *Journal of the Chemical Society, Dalton Transactions* **2000,** (21), 3885-3896.
25. Dorn, T.; Janiak, C.; Abu-Shandi, K., Hydrogen-bonding, pi-stacking and Cl-anioninteractions of linear bipyridinium cations with phosphate, chloride and [CoCl4](2-) anions. *CrystEngComm* **2005,** *7* (106), 633-641.
26. Pedireddi, V.; Reddy, D. S.; Goud, B. S.; Craig, D. C.; Rae, A. D.; Desiraju, G. R., The nature of halogen halogen interactions and the crystal structure of 1, 3, 5, 7-tetraiodoadamantane. *Journal of the Chemical Society, Perkin Transactions 2* **1994,** (11), 2353-2360.
27. Desiraju, G. R.; Parthasarathy, R., The nature of halogen...halogen interactions: are short halogen contacts due to specific attractive forces or due to close packing of nonspherical atoms? *J. Am. Chem. Soc.* **1989,** *111* (23), 8725-8726.
28. Metrangolo, P.; Neukirch, H.; Pilati, T.; Resnati, G., Halogen bonding based recognition processes: a world parallel to hydrogen bonding. *Accounts of Chemical Research* **2005,** *38* (5), 386-395.
29. Cheney, M. L.; Weyna, D. R.; Shan, N.; Hanna, M.; Wojtas, L.; Zaworotko, M. J., Coformer selection in pharmaceutical cocrystal development: A case study of a meloxicam aspirin cocrystal that exhibits enhanced solubility and pharmacokinetics. *Journal of Pharmaceutical Sciences* **2011,** *100* (6), 2172-2181; Chen, J.; Sarma, B.; Evans, J. M. B.; Myerson, A. S., Pharmaceutical crystallization. *Crystal Growth & Design* **2011**.
30. Mura, P.; Faucci, M.; Manderioli, A.; Bramanti, G.; Ceccarelli, L., Compatibility study between ibuproxam and pharmaceutical excipients using differential scanning calorimetry, hot-stage microscopy and scanning electron microscopy. *Journal of pharmaceutical and biomedical analysis* **1998,** *18* (1), 151-163.
31. Blagden, N.; De Matas, M.; Gavan, P.; York, P., Crystal engineering of active pharmaceutical ingredients to improve solubility and dissolution rates. *Advanced Drug Delivery Reviews* **2007,** *59* (7), 617-630.
32. Walsh, R. B.; Bradner, M.; Fleischman, S.; Morales, L.; Moulton, B.; Rodriguez-Hornedo, N.; Zaworotko, M., Crystal engineering of the composition of pharmaceutical phases. *Chem. Commun.* **2003,** (2), 186-187.
33. Blagden, N.; Berry, D. J.; Parkin, A.; Javed, H.; Ibrahim, A.; Gavan, P. T.; De Matos, L. L.; Seaton, C. C., Current directions in co-crystal growth. *New Journal of Chemistry* **2008,** *32* (10), 1659-1672.
34. Schultheiss, N.; Newman, A., Pharmaceutical Cocrystals and Their Physicochemical Properties. *Crystal Growth & Design* **2009,** *9* (6), 2950-2967.
35. Shan, N.; Zaworotko, M. J., The role of cocrystals in pharmaceutical science. *Drug Discovery Today* **2008,** *13* (9), 440-446.
36. Cheney, M. L.; Shan, N.; Healey, E. R.; Hanna, M.; Wojtas, L.; Zaworotko, M. J.; Sava, V.; Song, S.; Sanchez-Ramos, J. R., Effects of crystal form on solubility and pharmacokinetics: a crystal engineering case study of lamotrigine. *Crystal Growth & Design* **2009,** *10* (1), 394-405; Aakeröy, C. B.; Forbes, S.; Desper, J., Using cocrystals to systematically modulate aqueous solubility and melting behavior of an anticancer drug. *J. Am. Chem. Soc.* **2009,** *131* (47), 17048-17049.
37. McNamara, D. P.; Childs, S. L.; Giordano, J.; Iarriccio, A.; Cassidy, J.; Shet, M. S.; Mannion, R.; O'Donnell, E.; Park, A., Use of a glutaric acid cocrystal to improve oral bioavailability of a low solubility API. *Pharmaceutical research* **2006,** *23* (8), 1888-1897.

38. Braga, D.; Grepioni, F., *Making crystals by design*. John Wiley & Sons: 2007.
39. Zhang, J.; Gembicky, M.; Messerschmidt, M.; Coppens, P., Hydrogen-bond quenching of photodecarbonylation in the solid state and recovery of reactivity by co-crystallization. *Chem. Commun.* **2007,** (23), 2399-2401.
40. Caronna, T.; Liantonio, R.; Logothetis, T. A.; Metrangolo, P.; Pilati, T.; Resnati, G., Halogen Bonding and π-π Stacking Control Reactivity in the Solid State. *J. Am. Chem. Soc.* **2004,** *126* (14), 4500-4501.
41. Braga, D.; Brammer, L.; Champness, N. R., New trends in crystal engineering. *CrystEngComm* **2005,** *7*, 1-19.
42. Desiraju, G. R., Supramolecular synthons in crystal engineering—a new organic synthesis. *Angewandte Chemie International Edition in English* **1995,** *34* (21), 2311-2327.
43. Hagler, A.; Dauber, P.; Lifson, S., Consistent force field studies of intermolecular forces in hydrogen-bonded crystals. 3. The C: O. cntdot.. cntdot.. cntdot. HO hydrogen bond and the analysis of the energetics and packing of carboxylic acids. *J. Am. Chem. Soc.* **1979,** *101* (18), 5131-5141; Saha, B. K.; Nangia, A.; Jaskolski, M., Crystal engineering with hydrogen bonds and halogen bonds. *Crystengcomm* **2005,** *7*, 355-358; Barooah, N.; Singh, W. M.; Baruah, J. B., Preferential deprotonation and conformational stability of dicarboxylic acids: A packing effect. *Journal of Molecular Structure* **2008,** *875* (1-3), 329-338.
44. Aakeroy, C. B.; Salmon, D. J., Building co-crystals with molecular sense and supramolecular sensibility. *Crystengcomm* **2005,** *7*, 439-448.
45. Levilain, G.; Coquerel, G., Pitfalls and rewards of preferential crystallization. *CrystEngComm* **2010,** *12* (7), 1983-1992.
46. Allen, F., The Cambridge Structural Database: a quarter of a million crystal structures and rising. *Acta Crystallographica Section B* **2002,** *58* (3 Part 1), 380-388.
47. Galek, P. T.; Fabian, L.; Allen, F. H., Universal prediction of intramolecular hydrogen bonds in organic crystals. *Acta Crystallographica Section B: Structural Science* **2010,** *66* (2), 237-252.
48. Lommerse, J. P.; Motherwell, W. S.; Ammon, H. L.; Dunitz, J. D.; Gavezzotti, A.; Hofmann, D. W.; Leusen, F. J.; Mooij, W. T.; Price, S. L.; Schweizer, B., A test of crystal structure prediction of small organic molecules. *Acta Crystallographica Section B: Structural Science* **2000,** *56* (4), 697-714; Bardwell, D. A.; Adjiman, C. S.; Arnautova, Y. A.; Bartashevich, E.; Boerrigter, S. X.; Braun, D. E.; Cruz-Cabeza, A. J.; Day, G. M.; Della Valle, R. G.; Desiraju, G. R., Towards crystal structure prediction of complex organic compounds-a report on the fifth blind test. *Acta Crystallographica Section B: Structural Science* **2011,** *67* (6), 535-551.
49. Bernstein, J., Polymorphism − A Perspective. *Crystal Growth & Design* **2011,** *11* (3), 632-650.
50. Price, S. L., Computed crystal energy landscapes for understanding and predicting organic crystal structures and polymorphism. *Accounts of Chemical Research* **2008,** *42* (1), 117-126.
51. Bernstein, J., *Polymorphism in Molecular Crystals*. 2002; Vol. 14.
52. McCrone, W., Physics and Chemistry of the Organic Solid State, Vol. 2, edited by D. *Fox, MM Labes & A. Weissberger* **1965**, 725-767.
53. Karpinski, P. H., Polymorphism of active pharmaceutical ingredients. *Chemical Engineering & Technology* **2006,** *29* (2), 233-237.
54. Bauer, J.; Spanton, S.; Henry, R.; Quick, J.; Dziki, W.; Porter, W.; Morris, J., Ritonavir: An extraordinary example of conformational polymorphism. *Pharmaceutical Research* **2001,** *18* (6), 859-866.
55. Clarke, H. D.; Arora, K. K.; Bass, H.; Kavuru, P.; Ong, T. T.; Pujari, T.; Wojtas, L.; Zaworotko, M. J., Structure Stability Relationships in Cocrystal Hydrates: Does the Promiscuity of Water Make Crystalline Hydrates the Nemesis of Crystal Engineering? *Crystal Growth & Design 10* (5), 2152-2167.

56. Bingham, A. L.; Hughes, D. S.; Hursthouse, M. B.; Lancaster, R. W.; Tavener, S.; Threlfall, T. L., Over one hundred solvates of sulfathiazole. *Chem. Commun.* **2001,** (7), 603-604.
57. Vishweshwar, P.; Mcmahon, J. A.; Bis, J. A.; Zaworotko, M. J., Pharmaceutical co-crystals. *Journal of Pharmaceutical Sciences* **2006,** *95* (3), 499-516.
58. Aakeroy, C. B.; Champness, N. R.; Janiak, C., Recent advances in crystal engineering. *Crystengcomm 12* (1), 22-43.
59. Price, C. P.; Glick, G. D.; Matzger, A. J., Dissecting the behavior of a promiscuous solvate former. *Angewandte Chemie International Edition* **2006,** *45* (13), 2062-2066.
60. Guo, M.-J.; Diao, C.-H.; Jing, Z.-L.; Dong, B.; Fan, Z.; Wang, M., The structure of inclusion complex of β-cyclodextrin with p-nitrophenoxyacetic acid in solution and the solid state. *J. Incl. Phenom. Macrocycl. Chem.* **2010,** *67* (3), 393-398.
61. Van der Sluis, P.; Spek, A., BYPASS: an effective method for the refinement of crystal structures containing disordered solvent regions. *Acta Crystallographica Section A: Foundations of Crystallography* **1990,** *46* (3), 194-201.
62. Aakeroy, C. B.; Desper, J.; Fasulo, M.; Hussain, I.; Levin, B.; Schultheiss, N., Ten years of co-crystal synthesis; the good, the bad, and the ugly. *Crystengcomm* **2008,** *10* (12), 1816-1821.
63. Bond, A. D., What is a co-crystal? *Crystengcomm* **2007,** *9* (9), 833-834; Desiraju, G. R., Crystal and co-crystal. *Crystengcomm* **2003,** *5*, 466-467; Dunitz, J. D., Crystal and co-crystal: a second opinion. *CrystEngComm* **2003,** *5* (91), 506-506.
64. Herbstein, F. H., 5-Oxatricyclo [5.1. 0.01, 3] octan-4-one, containing an enantiomorph and a racemate and not two polymorphs, is another example of a composite crystal. *Acta Crystallographica Section B: Structural Science* **2003,** *59* (2), 303-304.
65. FrisÌŒcÌŒicÌ, T.; Jones, W., Recent Advances in Understanding the Mechanism of Cocrystal Formation via Grinding. *Crystal Growth & Design* **2009,** *9* (3), 1621-1637.
66. Friscic, T.; Childs, S. L.; Rizvi, S. A. A.; Jones, W., The role of solvent in mechanochemical and sonochemical cocrystal formation: a solubility-based approach for predicting cocrystallisation outcome. *Crystengcomm* **2009,** *11* (3), 418-426.
67. Trask, A. V.; Motherwell, W. D. S.; Jones, W., Solvent-drop grinding: green polymorph control of cocrystallisation. *Chem. Commun.* **2004,** (7), 890-891.
68. Aakeroy, C. B.; Forbes, S.; Desper, J., Using Cocrystals To Systematically Modulate Aqueous Solubility and Melting Behavior of an Anticancer Drug. *J. Am. Chem. Soc.* **2009,** *131* (47), 17048-17049.
69. Bhatt, P. M.; Azim, Y.; Thakur, T. S.; Desiraju, G. R., Co-crystals of the anti-HIV drugs lamivudine and zidovudine. *Crystal Growth and Design* **2008,** *9* (2), 951-957.
70. Vishweshwar, P.; McMahon, J. A.; Oliveira, M.; Peterson, M. L.; Zaworotko, M. J., The predictably elusive form II of aspirin. *J. Am. Chem. Soc.* **2005,** *127* (48), 16802-16803.
71. Urbanus, J.; Roelands, C. P. M.; Verdoes, D.; Jansens, P. J.; ter Horst, J. H., Co-Crystallization as a Separation Technology: Controlling Product Concentrations by Co-Crystals. *Crystal Growth & Design*.
72. Zeller, B. L.; Kaleda, W. W.; Saleeb, F. Z., Coffee extract decaffeination method. Google Patents: 1985.
73. George, N.; Forrest, J. O.; Burton, R. C.; Aakeroy, C. B., Co-crystals of pyrimethanil or cyprodinil. US Patent App. 13/696,180: 2011; Boghmans, C. P. L.; Meeus, L. M. F., Tabletting of Ervthritol. EP Patent 2,334,202: 2012; Boghmans, C. P. L.; Meeus, L. M. F., Tabletting of erythritol and isomalt. WO Patent App. PCT/EP2010/004,223: 2010.
74. Landenberger, K. B., Cocrystallization of Energetic Materials. **2013**; Bolton, O.; Simke, L. R.; Pagoria, P. F.; Matzger, A. J., High Power Explosive with Good Sensitivity: A 2: 1 Cocrystal of CL-20: HMX. *Crystal Growth & Design* **2012,** *12* (9), 4311-4314; Wei, C.; Huang, H.; Duan, X.; Pei, C., Structures and Properties Prediction of HMX/TATB Co-Crystal. *Propellants, Explosives, Pyrotechnics* **2011,** *36* (5), 416-423; Millar, D. I.; Maynard-Casely, H. E.; Allan, D. R.; Cumming, A. S.; Lennie, A. R.; Mackay, A. J.; Oswald, I. D.; Tang, C. C.;

Pulham, C. R., Crystal engineering of energetic materials: Co-crystals of CL-20. *CrystEngComm* **2012,** *14* (10), 3742-3749.
75. Childs, S. L.; Stahly, G. P.; Park, A., The salt-cocrystal continuum: the influence of crystal structure on ionization state. *Molecular Pharmaceutics* **2007,** *4* (3), 323-338.
76. Cruz-Cabeza, A. J., Acid-base crystalline complexes and the pKa rule. *CrystEngComm* **2012,** *14* (20), 6362-6365.
77. Amai, M.; Endo, T.; Nagase, H.; Ueda, H.; Nakagaki, M., 1 : 1 complex of octadecanoic acid and 3-pyridinecarboxamide. *Acta Crystallographica Section C-Crystal Structure Communications* **1998,** *54*, 1367-1369.
78. Kreimir Molanov, B. K.-P., Salts and co-crystals of chloranilic acid with organic bases: is it possible to predict a salt formation? *CrystEngComm* **2010,** *12*, 925-939.
79. Haynes, D. A.; Pietersen, L. K., Hydrogen bonding networks in ammonium carboxylate salts: the crystal structures of phenylethylammonium fumarate-fumaric acid, phenylethylammonium succinate-succinic acid and anilinium fumarate-fumaric acid. *CrystEngComm* **2008,** *10* (5), 518-524.
80. Mohamed, S.; Tocher, D. A.; Vickers, M.; Karamertzanis, P. G.; Price, S. L., Salt or cocrystal? A new series of crystal structures formed from simple pyridines and carboxylic acids. *Crystal Growth and Design* **2009,** *9* (6), 2881-2889.
81. Berge, S. M.; Bighley, L. D.; Monkhouse, D. C., Pharmaceutical salts. *Journal of Pharmaceutical Sciences* **1977,** *66* (1), 1-19; Aakeröy, C. B.; Fasulo, M. E.; Desper, J., Cocrystal or salt: Does it really matter? *Molecular Pharmaceutics* **2007,** *4* (3), 317-322; Wouters, J.; Quéré, L.; Thurston, D. E.; Martinez, A., *Pharmaceutical salts and co-crystals*. Royal Society of Chemistry: 2011; Vol. 16.
82. Uekama, K.; Hirayama, F.; Irie, T., Cyclodextrin Drug Carrier Systems. *Chemical Reviews* **1998,** *98* (5), 2045-2076; Faucci, M. T.; Melani, F.; Mura, P., 1H-NMR and molecular modelling techniques for the investigation of the inclusion complex of econazole with α-cyclodextrin in the presence of malic acid. *Journal of pharmaceutical and biomedical analysis* **2000,** *23* (1), 25-31; Puliti, R.; Mattia, C. A.; Paduano, L., Crystal structure of a new α-cyclodextrin hydrate form. Molecular geometry and packing features: disordered solvent contribution. *Carbohydrate Research* **1998,** *310* (1), 1-8; Rougier, N. M.; Cruickshank, D. L.; Vico, R. V.; Bourne, S. A.; Caira, M. R.; Buján, E. I.; de Rossi, R. H., Effect of cyclodextrins on the reactivity of fenitrothion. *Carbohydrate Research* **2011,** *346* (2), 322-327; Mino R. Caira, D. L. C. a. S. A. B., Solid-state structures and thermal properties of inclusion complexes of the phenylurea herbicide cycluron with permethylated cyclodextrins. *Ann Arbor, Michigan: MPublishing, University of Michigan Library, ARKIVOC* **2011,** *vii*, 103-115.
83. Hickey, M. B.; Peterson, M. L.; Scoppettuolo, L. A.; Morrisette, S. L.; Vetter, A.; Guzmán, H.; Remenar, J. F.; Zhang, Z.; Tawa, M. D.; Haley, S., Performance comparison of a co-crystal of carbamazepine with marketed product. *European journal of pharmaceutics and biopharmaceutics* **2007,** *67* (1), 112-119; Domanska, U.; Pelczarska, A.; Pobudkowska, A., Effect of 2-Hydroxypropyl-beta-cyclodextrin on Solubility of Sparingly Soluble Drug Derivatives of Anthranilic Acid. *International Journal of Molecular Sciences 12* (4), 2383-2394; Tsuchiya, Y.; Shiraki, T.; Matsumoto, T.; Sugikawa, K.; Sada, K.; Yamano, A.; Shinkai, S., Supramolecular Dye Inclusion Single Crystals Created from 2,3,6-Trimethyl-β-cyclodextrin and Porphyrins. *Chemistry – A European Journal* **2012,** *18* (2), 456-465.
84. Clark, D. L.; Keogh, D. W.; Palmer, P. D.; Scott, B. L.; Tait, C. D., Synthesis and Structure of the First Transuranium Crown Ether Inclusion Complex:[NpO2 ([18] Crown-6)] ClO4. *Angewandte Chemie International Edition* **1998,** *37* (1-2), 164-166.
85. Kamitori, S.; Hirotsu, K.; Higuchi, T., Crystal and molecular structures of double macrocyclic inclusion complexes composed of cyclodextrins, crown ethers, and cations. *J. Am. Chem. Soc.* **1987,** *109* (8), 2409-2414.
86. Zhao, Y.; Xue, S.; Zhu, Q.; Tao, Z.; Zhang, J.; Wei, Z.; Long, L.; Hu, M.; Xiao, H.; Day, A., Synthesis of a symmetrical tetrasubstituted cucurbit [6] uril and its host-guest inclusion complex with 2, 2′-bipyridine. *Chinese Science Bulletin* **2004,** *49* (11), 1111-1116; Mock, W.

L.; Shih, N. Y., Structure and selectivity in host-guest complexes of cucurbituril. *The Journal of Organic Chemistry* **1986,** *51* (23), 4440-4446.
87. Thakral, S.; Madan, A. K., Urea co-inclusion compounds of glipizide for the improvement of dissolution profile. *J. Incl. Phenom. Macrocycl. Chem.* **2008,** *60* (3-4), 203-209.
88. Radell, J.; Connolly, J., *Determination of relative stability of urea complexes from X-ray powder diffraction data*. Springer: 1961.
89. Smith, A., The crystal structure of the urea-hydrocarbon complexes. *Acta Crystallographica* **1952,** *5* (2), 224-235.
90. Harris, K. D., Meldola lecture: understanding the properties of urea and thiourea inclusion compounds. *Chem. Soc. Rev.* **1997,** *26* (4), 279-289.
91. Weber, E.; MacNicol, D.; Toda, F.; Bishop, R., Comprehensive supramolecular chemistry. Pergamon Press: Oxford: 1996; Vol. 6, pp 535-592.
92. Griffith, O. H., Electron Spin Resonance and Molecular Motion of the RCHĊHCOOR' Radicals in X-Irradiated Ester—Urea Inclusion Compounds. *The Journal of Chemical Physics* **1964,** *41*, 1093.
93. Shimizu, L. S.; Smith, M. D.; Hughes, A. D.; Shimizu, K. D., Self-assembly of a bis-urea macrocycle into a columnar nanotube. *Chem. Commun.* **2001,** (17), 1592-1593.
94. Shimizu, L. S.; Hughes, A. D.; Smith, M. D.; Davis, M. J.; Zhang, B. P.; zur Loye, H.-C.; Shimizu, K. D., Self-assembled nanotubes that reversibly bind acetic acid guests. *J. Am. Chem. Soc.* **2003,** *125* (49), 14972-14973.
95. Rowsell, J. L.; Yaghi, O. M., Metal–organic frameworks: a new class of porous materials. *Microporous and Mesoporous Materials* **2004,** *73* (1), 3-14.
96. Smaldone, R. A.; Forgan, R. S.; Furukawa, H.; Gassensmith, J. J.; Slawin, A. M. Z.; Yaghi, O. M.; Stoddart, J. F., Metal–Organic Frameworks from Edible Natural Products. *Angewandte Chemie International Edition* **2010,** *49* (46), 8630-8634.
97. Belitsku.D; Jeffrey, G. A., Crystal Structure of Peroxypelargonic Acid. *Acta Crystallographica* **1965,** *18*, 458-&.
98. Batsanov, A., 3-Fluoro-4-methylbenzoic acid. *Acta Crystallographica Section E* **2004,** *60* (11), o1948-o1949; Choudhury, A. R.; Guru Row, T. N., 5-Fluorosalicylic acid. *Acta Crystallographica Section E* **2004,** *60* (9), o1595-o1597; Chandrasekaran, A.; Day, R. O.; Holmes, R. R., Coordination of Carbonyl and Carboxyl Oxygen Atoms with Phosphorus in the Presence of Hydrogen Bonding. Pâˆ'O Donor Action. *Inorganic Chemistry* **2001,** *40* (24), 6229-6238; Odutola, J. A.; Dyke, T. R., Polarity of Hydrogen Bonded Complexes - Nitric acid and carboxylic acid dimers. *J. Chem. Phys.* **1978,** *68* (12), 5663-5665.
99. Feeder, N.; Jones, W., Comparative-Study of Crystal Packing in Amido-Benzoic and Amido-Perbenzoic Acids. *Molecular Crystals and Liquid Crystals Science and Technology Section a-Molecular Crystals and Liquid Crystals* **1994,** *240*, 231-239.
100. Bruno, I. J.; Cole, J. C.; Lommerse, J. P.; Rowland, R. S.; Taylor, R.; Verdonk, M. L., IsoStar: a library of information about nonbonded interactions. *Journal of computer-aided molecular design* **1997,** *11* (6), 525-537.
101. Griffith, W. P.; Skapski, A. C.; West, A. P., Crystal structure of the novel bleaching agent hexa-aquomagnesium(II) bis(2-carboxylato-monoperoxy-benzoic acid), [Mg(H2O)6](C8H5O5)2. *Inorganica Chimica Acta* **1982,** *65*, L249-L250.
102. Sieroń, L.; Kobyłecka, J.; Turek, A., Crystal Packing and Supramolecular Motifs in Four Phenoxyalkanoic Acid Herbicides—Low-Temperature Redeterminations. *Organic Chemistry International* **2011,** *2011*.
103. Smith, G.; Kennard, C. H. L.; White, A. H., (3,4-Dichlorophenoxy)acetic acid. *Acta Crystallographica Section B* **1981,** *37* (7), 1454-1455.
104. Byriel, K.; Kennard, C.; Lynch, D.; Smith, G.; Thompson, J., Molecular Cocrystals of Carboxylic Acids. IX. Carboxylic Acid Interactions With Organic Heterocyclic Bases. The Crystal Structures of the Adducts of (2, 4-Dichlorophenoxy) acetic Acid With 3-

Hydroxypyridine, 2, 4, 6-Trinitrobenzoic Acid With 2-Aminopyrimidine, and 4-Nitrobenzoic Acid With 3-Amino-1, 2, 4-triazole. *Australian Journal of Chemistry* **1992,** *45* (6), 969-981.
105. Kennard, C. H. L.; Smith, G.; O'Reilly, E. J., Metal-phenoxyalkanoic acid interactions. Part 11 Crystal structure of potassium 2, 4-dichlorophenoxy-acatate hemihydrate. *Inorganica Chimica Acta* **1983,** *77* (0), L181-L184; Ma, D.-Y.; Guo, H.-F.; Lu, K.; Pan, Y.; Qin, L., Syntheses and structural characterizations of three transition metal coordination complexes based on flexible 2,4-dichlorophenoxyacetate (2,4-DCP). *Journal of Coordination Chemistry* **2012,** *65* (9), 1610-1620.
106. Liu, H.-L.; Wang, Q.-Z.; Jian, F.-F., Benzimidazolium 2-(2,4-dichlorophenoxy)acetate monohydrate. *Acta Crystallographica Section E* **2009,** *65* (12), o3043.
107. Liu, H.-L.; Guo, S.-H.; Li, Y.-Y.; Jian, F.-F., Ammonium 2-(2,4-dichlorophenoxy)acetate hemihydrate. *Acta Crystallographica Section E* **2009,** *65* (8), o1905; Subramanian, R. R.; Anandan, S. S.; Kwek, K. H.; Low, K. S.; Shanmuga Sundara Raj, S.; Fun, H.-K.; Razak, I. A.; Hanna, J. V.; Ng, S. W., Dicyclohexylammonium 2,4-dichlorophenoxyacetate and (2,4-dichlorophenoxyacetato-O,O')bis(triphenylphosphine-P)silver(I). *Acta Crystallographica Section C* **2000,** *56* (7), e292-e294.
108. Tsorteki, F.; Bethanis, K.; Mentzafos, D., Structure of the inclusion complexes of heptakis(2,3,6-tri-O-methyl)-β-cyclodextrin with indole-3-butyric acid and 2,4-dichlorophenoxyacetic acid. *Carbohydrate Research* **2004,** *339* (2), 233-240; Tsorteki, F.; Mentzafos, D., Structure of the complex of heptakis(2,6-di-O-methyl)-β-cyclodextrin with (2,4-dichlorophenoxy)acetic acid. *Carbohydrate Research* **2002,** *337* (13), 1229-1233.
109. Lynch, D. E.; Smith, G.; Freney, D.; Byriel, K. A.; Kennard, C. H., Molecular Cocrystals of Carboxylic Acids. XV. Preparation and Characterization of Heterocyclic Base Adducts With a Series of Carboxylic Acids, and the Crystal Structures of the Adducts of 2-Aminopyrimidine With 2, 6-Dihydroxybenzoic Acid, 4-Aminobenzoic Acid, Phenoxyacetic Acid,(2, 4-Dichlorophenoxy) acetic Acid,(3, 4-Dichlorophenoxy)-acetic Acid and Salicylic Acid, and 2-Aminopyridine With 2, 6-Dihydroxybenzoic Acid. *Australian Journal of Chemistry* **1994,** *47* (6), 1097-1115.
110. Smith, G.; Cooper, C. J.; Chauhan, V.; Lynch, D. E.; Healy, P.; Parsons, S., Conformational comparisons between phenoxyacetic acid derivatives in adducts and in the free form. *Australian Journal of Chemistry* **1999,** *52* (7), 695-704.
111. Lynch, D. E.; Smith, G.; Byriel, K. A.; Kennard, C. H. L., Molecular co-crystals of carboxylic acids. 11. Structure of the 1:1 adduct of triphenylphosphine oxide with (3,4-dichlorophenoxy)acetic acid. *Acta Crystallographica Section C* **1993,** *49* (4), 718-721.
112. Lynch, D. E.; Daly, D.; Parsons, S., 2-Amino-5-chloro-1,3-benzoxazol-3-ium 2-(3,4-dichlorophenoxy)acetate. *Acta Crystallographica Section C* **2000,** *56* (12), 1478-1479.
113. Dinnebier, R. E., *Powder diffraction: theory and practice*. Royal Society of Chemistry: 2008.
114. Massa, W., *Crystal structure determination*. Springer: 2004.
115. Clegg, W., *Crystal Structure Determination*. Oxford University Press: Oxford, 1998; Vol. 60, p 86.
116. Oszlanyi, G.; Suto, A., The charge flipping algorithm. *Acta Crystallographica Section A: Foundations of Crystallography* **2007,** *64* (1), 123-134.
117. Elser, V., Solution of the crystallographic phase problem by iterated projections. *Acta Crystallographica Section A: Foundations of Crystallography* **2003,** *59* (3), 201-209.
118. Palatinus, L.; van der Lee, A., Symmetry determination following structure solution in P1. *Journal of Applied Crystallography* **2008,** *41* (6), 975-984.
119. Macrae, C. F.; Bruno, I. J.; Chisholm, J. A.; Edgington, P. R.; McCabe, P.; Pidcock, E.; Rodriguez-Monge, L.; Taylor, R.; Streek, J. v.; Wood, P. A., Mercury CSD 2.0-new features for the visualization and investigation of crystal structures. *Journal of Applied Crystallography* **2008,** *41* (2), 466-470.

120. Young, R. A.; Mackie, P. E.; von Dreele, R. B., Application of the pattern-fitting structure-refinement method of X-ray powder diffractometer patterns. *Journal of Applied Crystallography* **1977,** *10* (4), 262-269.
121. David, W. I. F.; Shankland, K.; Shankland, N., Routine determination of molecular crystal structures from powder diffraction data. *Chem. Commun.* **1998,** (8), 931-932.
122. David, W. I. F.; Shankland, K.; van de Streek, J.; Pidcock, E.; Motherwell, W. D. S.; Cole, J. C., DASH: a program for crystal structure determination from powder diffraction data. *Journal of Applied Crystallography* **2006,** *39*, 910-915.
123. Barr, G.; Dong, W.; Gilmore, C. J., PolySNAP3: a computer program for analysing and visualizing high-throughput data from diffraction and spectroscopic sources. *Journal of Applied Crystallography* **2009,** *42* (5), 965-974.
124. Williams, D. H.; Fleming, I., *Spectroscopic methods in organic chemistry*. McGraw-Hill London: 1980.
125. Brittain, H. G., Vibrational Spectroscopic Studies of Cocrystals and Salts. 2. The Benzylamine-Benzoic Acid System. *Crystal Growth & Design* **2009,** *9* (8), 3497-3503.
126. Young, H. D.; Freedman, R. A., Sears and Zemanski's University Physics: with modern Physics, 11th. Pearson Education Inc. published as Addison Wesley: 2003.
127. Clas, S.-D.; Dalton, C. R.; Hancock, B. C., Differential scanning calorimetry: applications in drug development. *Pharmaceutical science & technology today* **1999,** *2* (8), 311-320.
128. Lu, E.; Rodríguez-Hornedo, N.; Suryanarayanan, R., A rapid thermal method for cocrystal screening. *CrystEngComm* **2008,** *10* (6), 665-668.
129. Vitez, I. M.; Newman, A. W.; Davidovich, M.; Kiesnowski, C., The evolution of hot-stage microscopy to aid solid-state characterizations of pharmaceutical solids. *Thermochimica acta* **1998,** *324* (1), 187-196.
130. Cabeza, A. J. C.; Day, G. M.; Motherwell, W. S.; Jones, W., Solvent inclusion in form II carbamazepine. *Chem. Commun.* **2007,** (16), 1600-1602.
131. Berry, D. J.; Seaton, C. C.; Clegg, W.; Harrington, R. W.; Coles, S. J.; Horton, P. N.; Hursthouse, M. B.; Storey, R.; Jones, W.; Friscic, T., Applying hot-stage microscopy to co-crystal screening: a study of nicotinamide with seven active pharmaceutical ingredients. *Crystal Growth and Design* **2008,** *8* (5), 1697-1712.
132. Clegg, W.; Blake, A. J.; Cole, J. M., *Crystal structure analysis: principles and practice*. International Union of Crystallography: 2001.
133. Rastogi, R. P.; Bassi, P. S.; Chadha, S. L., Mechanism of Reaction between Hydrocarbons and Picric Acid in Solid State. *Journal of Physical Chemistry* **1963,** *67* (12), 2569-&.
134. Braga, D.; Grepioni, F., Making crystals from crystals: a green route to crystal engineering and polymorphism. *Chem. Commun.* **2005,** (29), 3635-3645.
135. Americas, R., Rigaku Corporation (2009) CrystalClear (Version 2.0). *Rigaku Americas 9009*, 77381-5209.
136. Allen, F. H., The Cambridge Structural Database: a quarter of a million crystal structures and rising. *Acta Crystallogr. Sect. B-Struct. Sci.* **2002,** *58*, 380-388.
137. Higashi, T., ABSCOR-An Empirical Absorption Correction Based on Fourier Coefficient Fitting. *Rigaku Corp., Tokyo* **1995**.
138. Bruker, A., APEX2—software suite for crystallographic programs. *Bruker AXS Inc., Madison* **2009**.
139. Sheldrick, G., sadabs. University of Göttingen, Germany: 1996.
140. Hooft, R., COLLECT Nonius BV. *Delft, The Netherlands* **1998**.
141. Otwinowski, Z.; Minor, W., Denzo and Scalepack. *Crystallography of Biological Macromolecules* **2001,** *2*.
142. Farrugia, L. J., WinGX Program System. *J. Appl. Cryst.* **1999,** *32*, 837-838.
143. Sheldrick, G., SHELXS-86: structure solving program. *University of Göttingen, Germany* **1986**.

144. Altomare, A.; Cascarano, G.; Giacovazzo, C.; Guargliardi, A.; Camalli, M.; Burla, M.; Polidori, G., SIR-92, A powerful direct methods package. *Acta Crystallogr. A* **1993,** *49*, 55.
145. Palatinus, L.; Chapuis, G., SUPERFLIP-a computer program for the solution of crystal structures by charge flipping in arbitrary dimensions. *Journal of Applied Crystallography* **2007,** *40* (4), 786-790.
146. Sheldrick, G., SHELXL-97, Program for crystal structure refinement; University of Göttingen: Göttingen, Germany, 1997. *There is no corresponding record for this reference* **2006**.
147. Kienle, M.; Jacob, M., DIFFRAC plus XRD Commander. Version: 2003.
148. X'Pert HighScore Plus, V., 2.2 b (2.2. 2)(Date: 01-11-2006): Produced by: PANalytical BV Alemo. *The Netherlands*.
149. OLYMPUS BTX Benchtop XRD. http://www.olympus-ims.com/en/xrf-xrd/mobile-benchtop-xrd/btx/ (accessed 31/07/2013).
150. *Universal Analysis 2000*, 4.5.0.5; TA Instruments - Waters LLC.
151. Reany, O.; Kapon, M.; Botoshansky, M.; Keinan, E., Rich Polymorphism in Triacetone-Triperoxide. *Crystal Growth & Design* **2009,** *9* (8), 3661-3670.
152. Feeder, N.; Jones, W., 2-Phthalimidoethanoic acid monohydrate (I) and 6-phthalimidohexanoic acid monohydrate (II). *Acta Crystallographica Section C* **1994,** *50* (5), 820-823.
153. Feeder, N.; Jones, W., Structures of Five [omega]-Phthalimidoaliphatic Carboxylic Acids. *Acta Crystallographica Section C* **1996,** *52* (4), 913-919.
154. Belsky, A.; Hellenbrandt, M.; Karen, V. L.; Luksch, P., New developments in the Inorganic Crystal Structure Database (ICSD): accessibility in support of materials research and design. *Acta Crystallographica Section B: Structural Science* **2002,** *58* (3), 364-369.
155. Oosterhof, H.; Witkamp, G. J.; van Rosmalen, G. M., Antisolvent crystallization of anhydrous sodium carbonate at atmospherical conditions. *AIChE journal* **2001,** *47* (3), 602-608.
156. Wilson, C. C.; Shankland, N.; Florence, A. J., A single-crystal neutron diffraction study of the temperature dependence of hydrogen-atom disorder in benzoic acid dimers. *Journal of the Chemical Society, Faraday Transactions* **1996,** *92* (24), 5051-5057.
157. Fritchie, C. J., Jnr; McMullan, R. K., Neutron diffraction study of the 1:1 urea:hydrogen peroxide complex at 81 K. *Acta Crystallographica Section B* **1981,** *37* (5), 1086-1091.
158. AG, W. C. CAVAMAX® W7/EURECO - Wacker Chemie AG. http://www.wacker.com/cms/en/products-markets/products/product.jsp?product=8957 (accessed 01/10/2013).
159. Segad, M.; Jonsson, B.; Ãkesson, T.; Cabane, B., Ca/Na Montmorillonite: Structure, Forces and Swelling Properties. *Langmuir* **2010,** *26* (8), 5782-5790.
160. Montes-H, G.; Geraud, Y.; Duplay, J.; Reuschlé, T., ESEM observations of compacted bentonite submitted to hydration/dehydration conditions. *Colloids and Surfaces A: Physicochemical and Engineering Aspects* **2005,** *262* (1-3), 14-22.
161. Sikka, M.; Cerini, L. N.; Ghosh, S. S.; Winey, K. I., Melt intercalation of polystyrene in layered silicates. *Journal of Polymer Science Part B: Polymer Physics* **1996,** *34* (8), 1443-1449.

APPENDICES – Experimental Data

Appendix 1 –Crystallisation of Reactive Materials

X-ray Powder Diffraction (XRPD) data

Meta-chloroperbenzoic acid (MCPBA)

AM01_01 – MCPBA + Methanol crystallised at room temperature

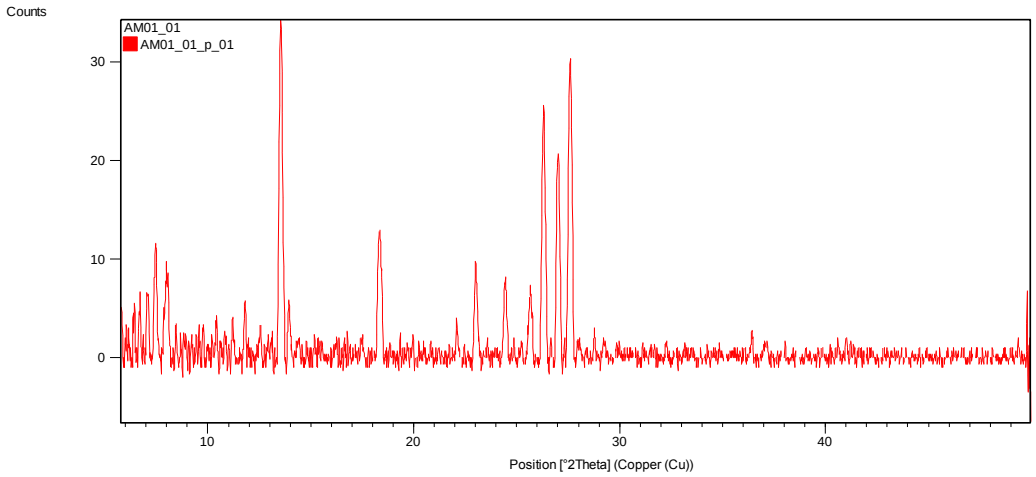

AM01_02 – MCPBA + Methanol crystallised at 4°C

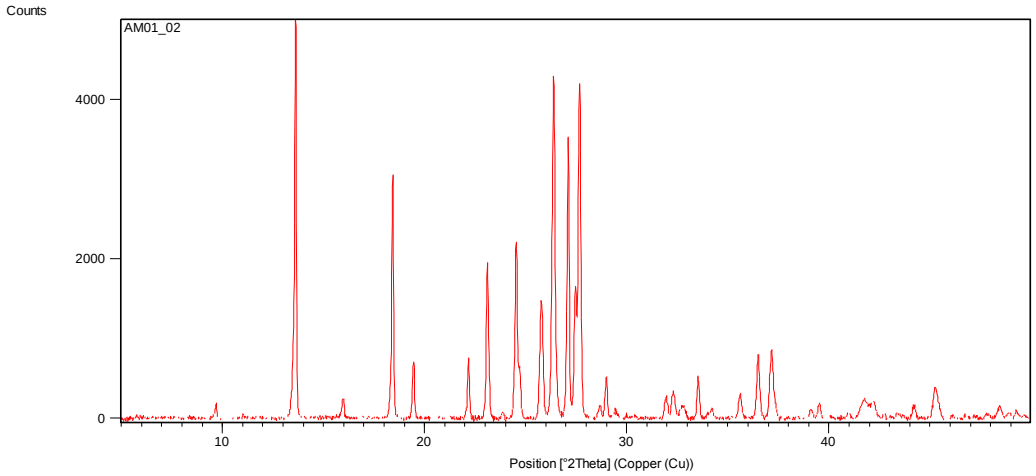

AM01_03 – MCPBA + Ethanol crystallised at room temperature

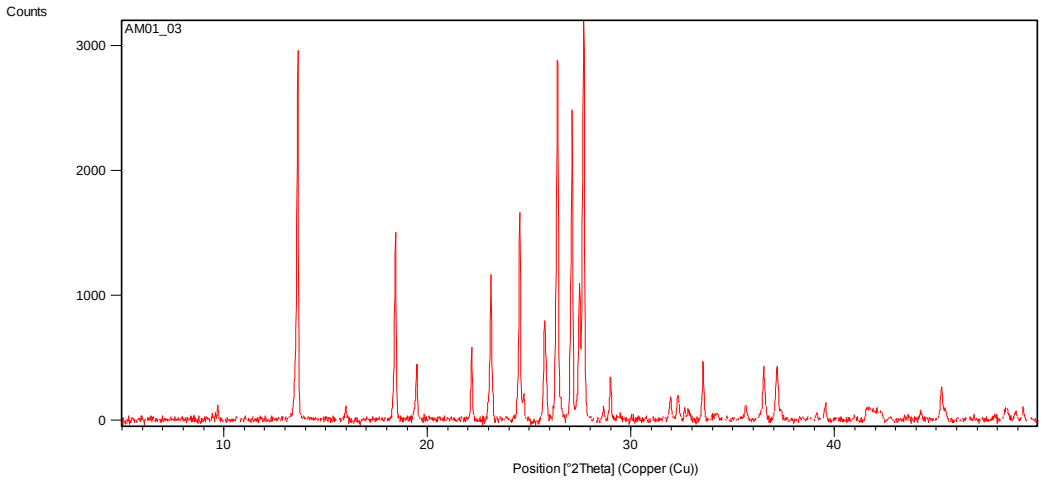

AM01_04 – MCPBA + Ethanol crystallised at 4°C

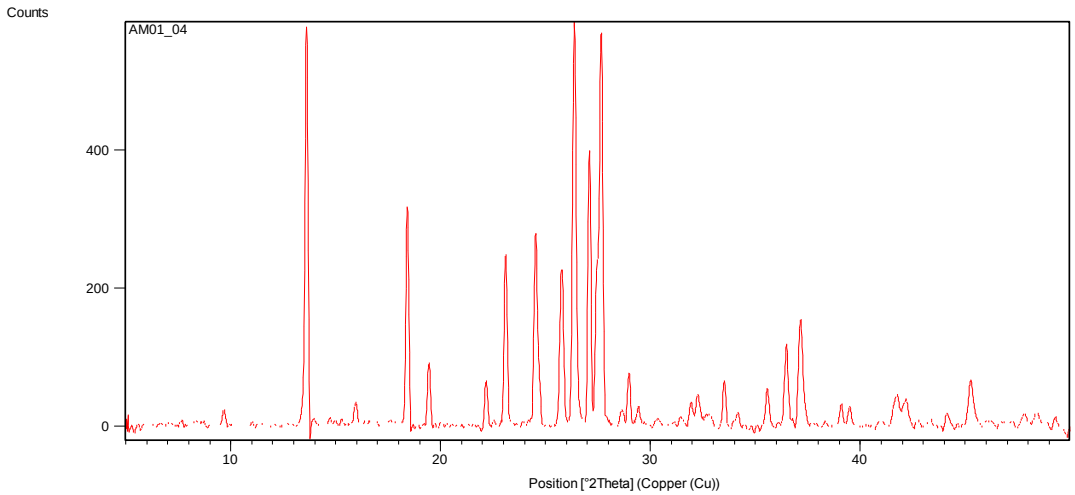

AM01_05 – MCPBA + Isopropanol crystallised at room temperature

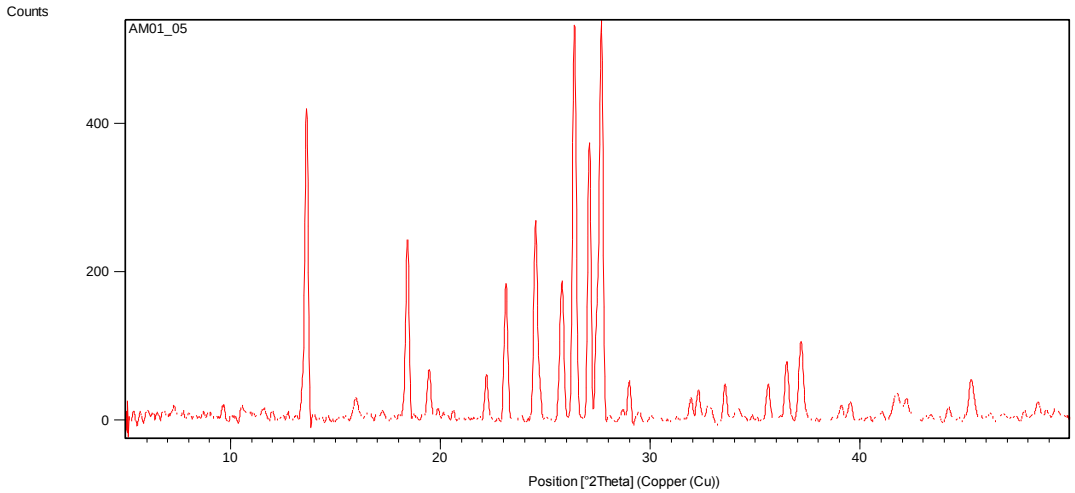

AM01_06 – MCPBA + Isopropanol crystallised at 4°C

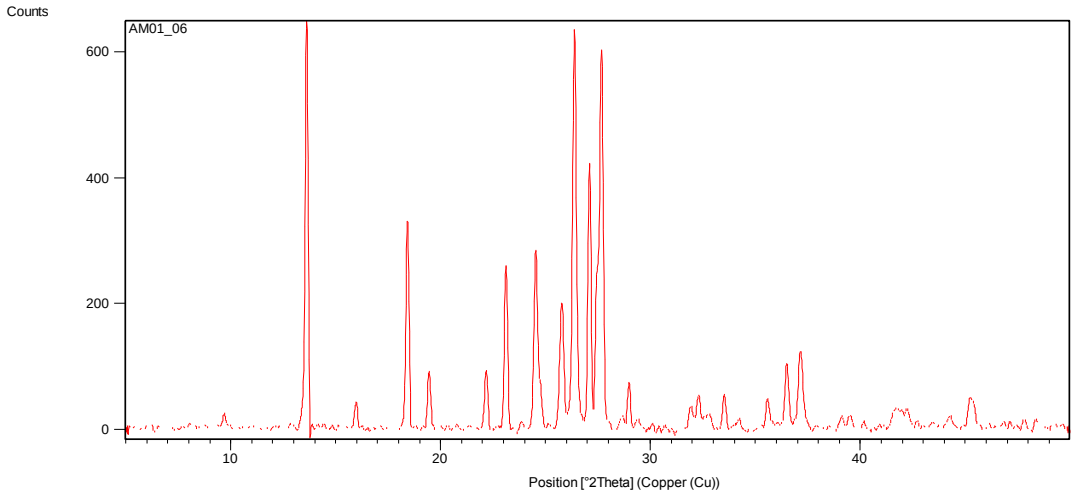

AM01_07 – MCPBA + Acetone crystallised at room temperature

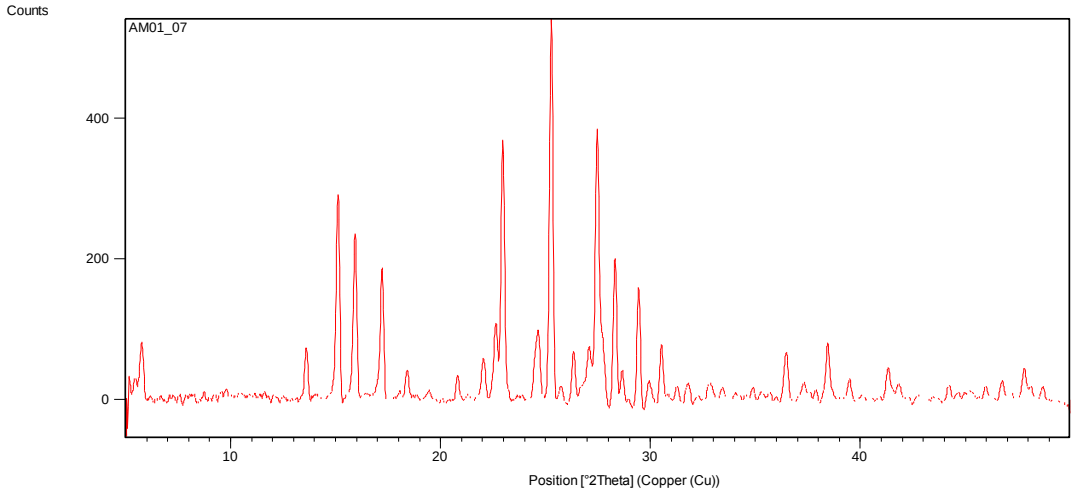

AM01_08 – MCPBA + Acetone crystallised at 4°C

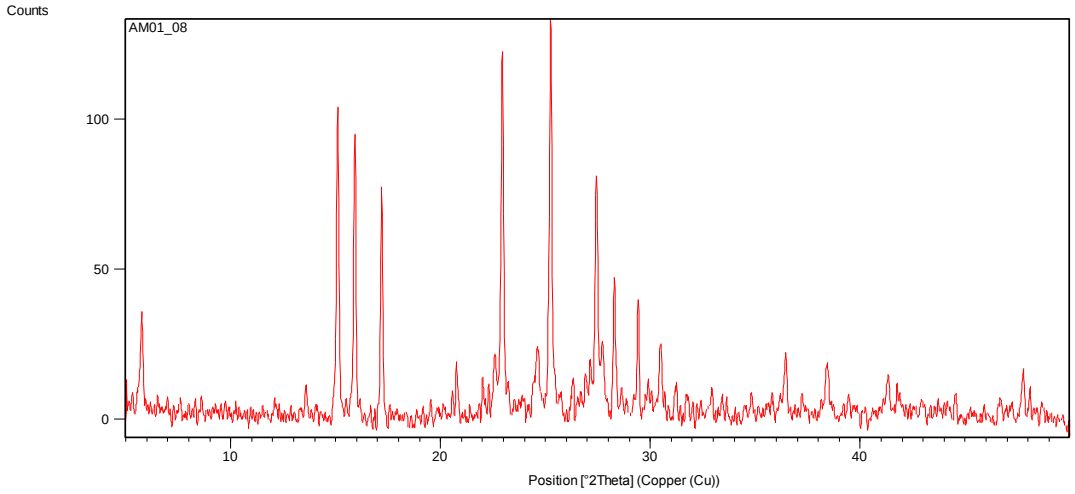

AM35_06 – MCPBA + Methanol with hydrogen peroxide crystallised at 4°C

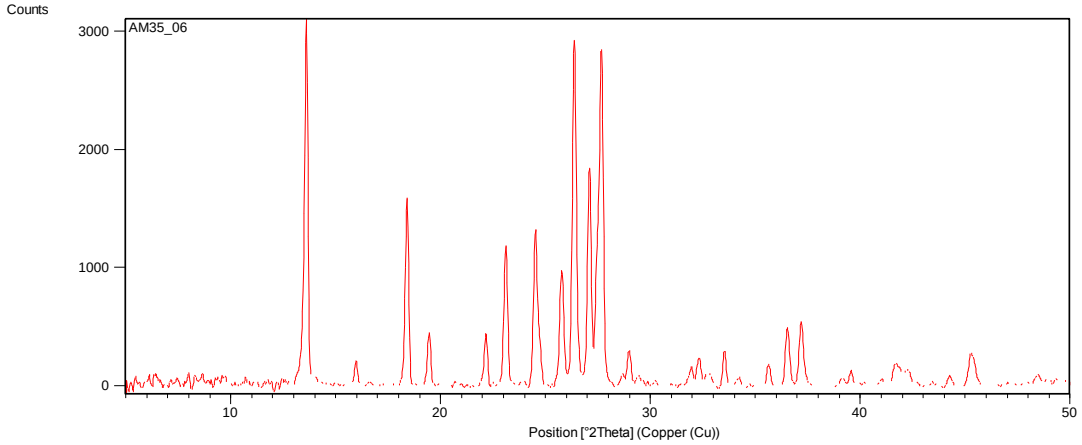

AM35_07 - MCPBA + Methanol with hydrogen peroxide crystallised at room temperature

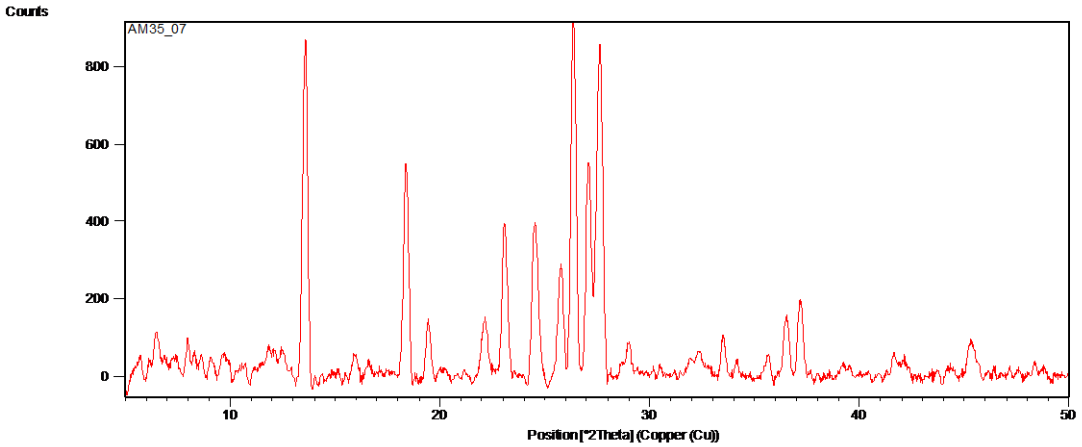

AM34_01 – MCPBA + Methanol with hydrochloric acid crystallised at 4°C

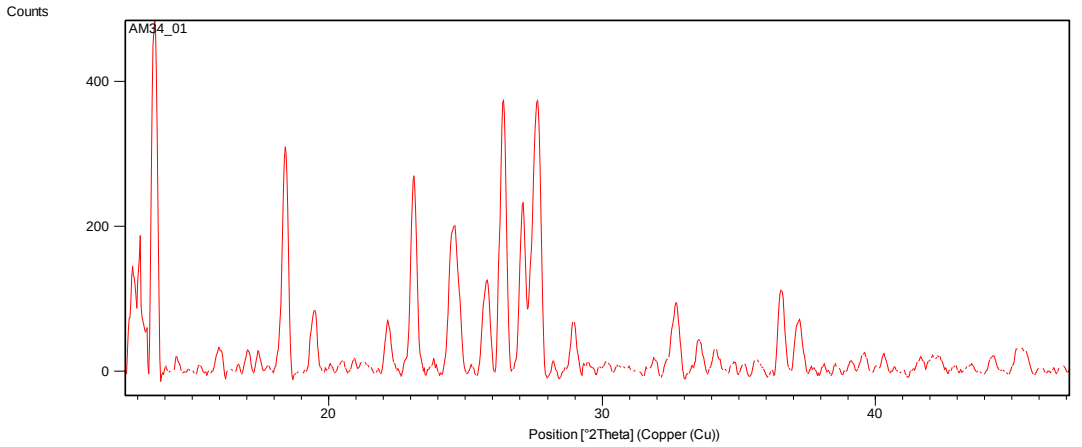

AM34_04 – MCPBA + methanol with sodium hydroxide crystallised at room temperature

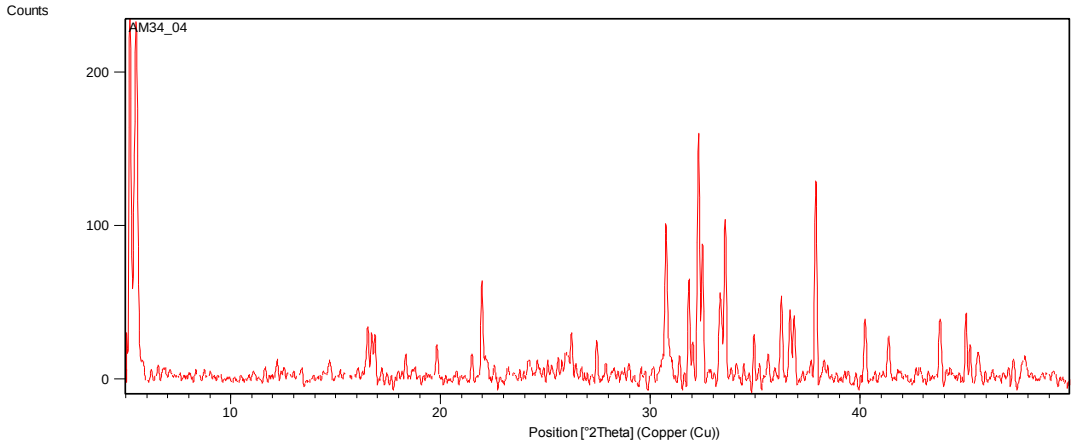

AM34_06 – MCPBA + ethanol with hydrochloric acid crystallised at room temperature

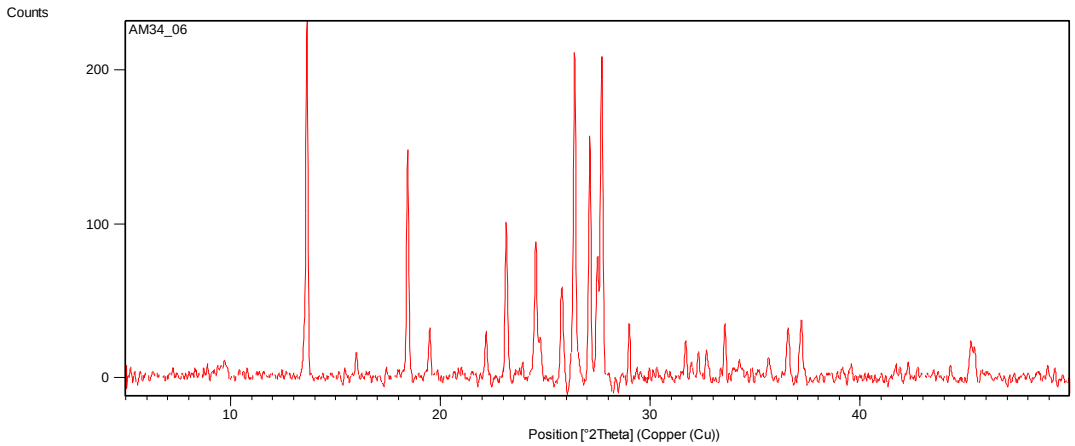

AM34_07 – MCPBA + ethanol with sodium hydroxide crystallised at 4°C

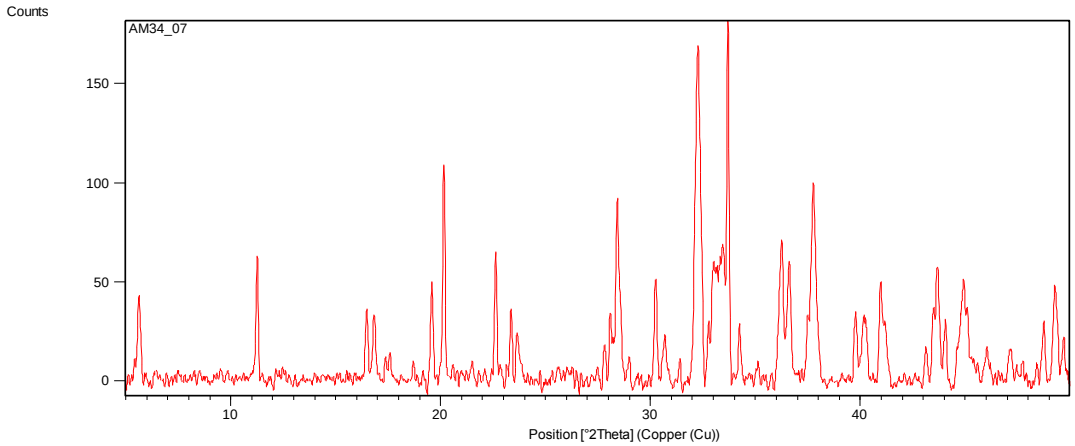

AM34_08 – MCPBA + ethanol with sodium hydroxide crystallised at room temperature

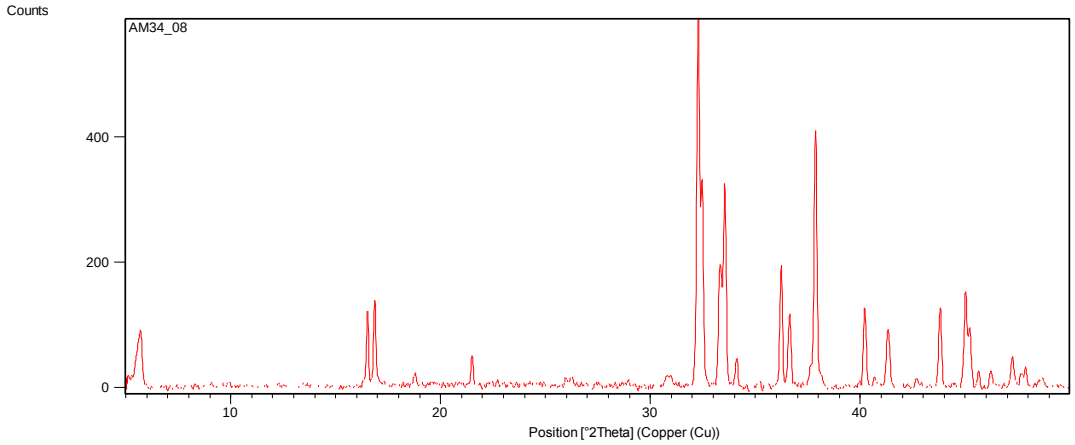

6-Phthalimidoperoxyhexanoic acid (PAP)

AM24_01 – 6-phthalimidoperoxyhexanoic acid + Methanol crystallised at 4°C

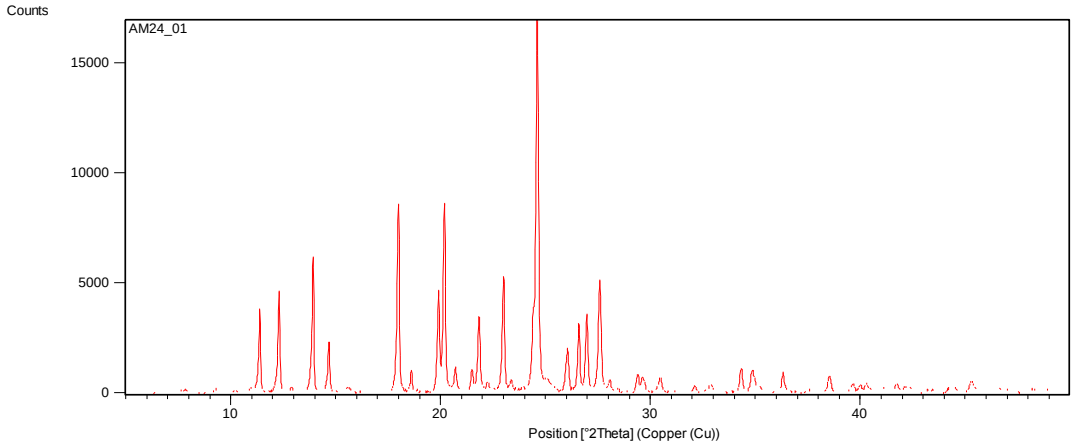

AM24_02 – 6-phthalimidoperoxyhexanoic acid + Methanol crystallised at room temperature

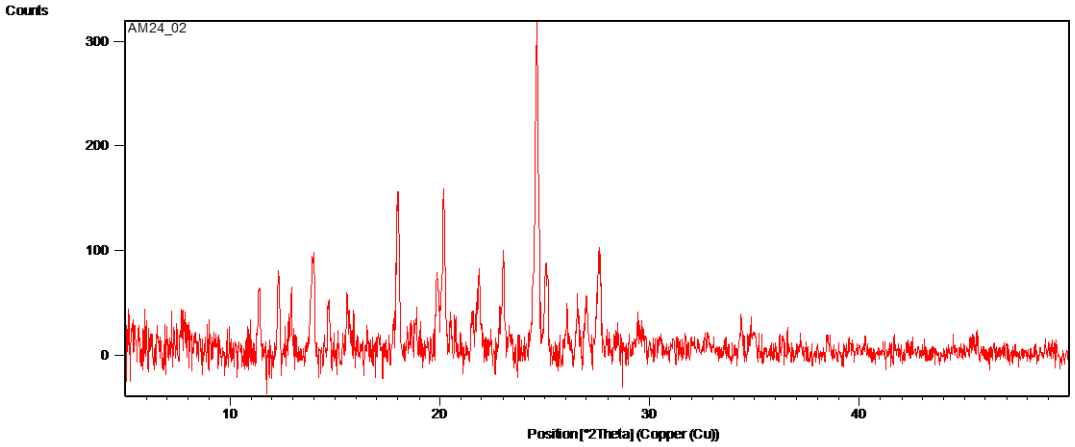

AM24_03 – 6-phthalimidoperoxyhexanoic acid +Ethanol crystallised at 4°C

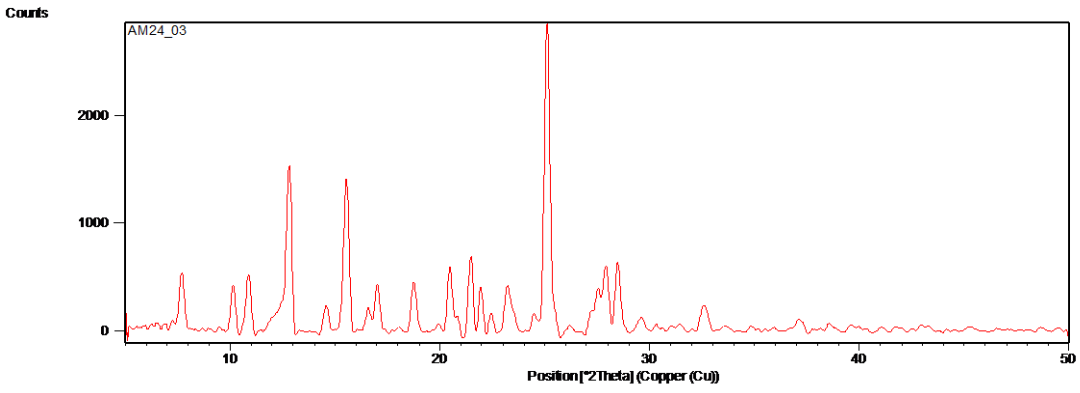

AM24_05 – 6-phthalimidoperoxyhexanoic acid + isopropanol crystallised at 4°C

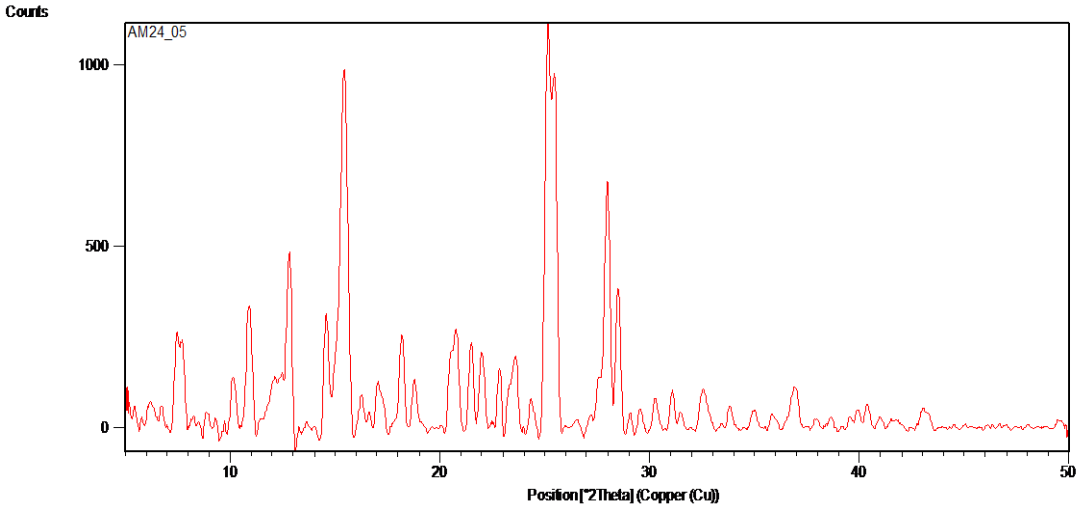

AM24_06 – 6-phthalimidoperoxyhexanoic acid + isopropanol crystallised at room temperature

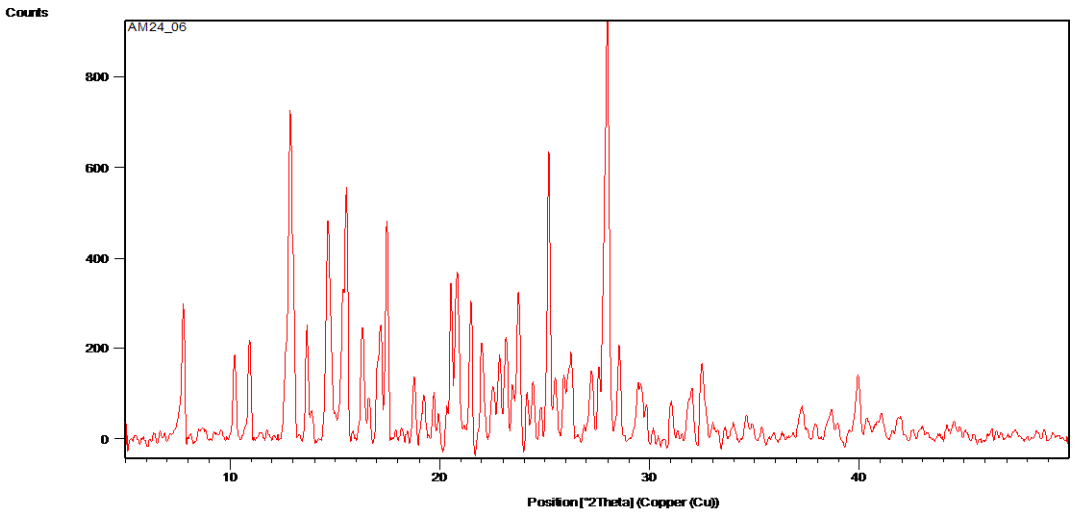

AM24_07 – 6-phthalimidoperoxyhexanoic acid + chloroform crystallised at 4°C

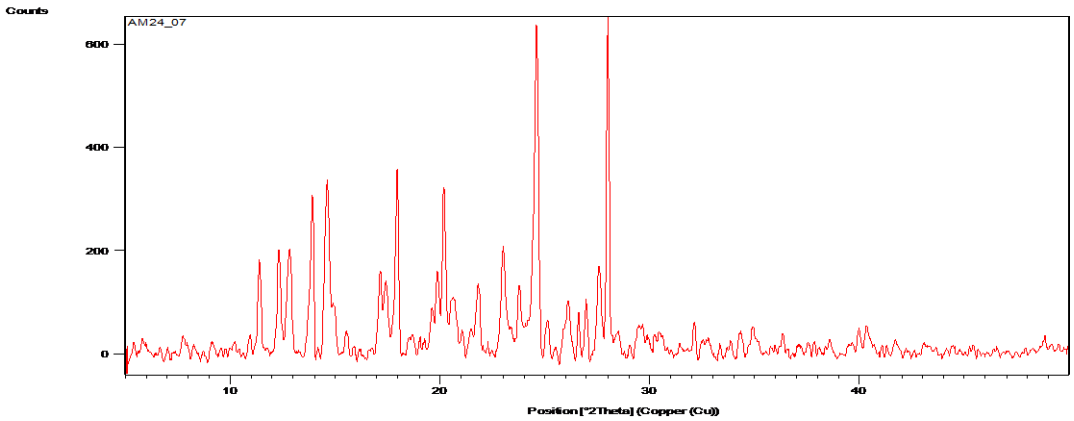

AM24_08 – 6-phthalimidoperoxyhexanoic acid + chloroform crystallised at room temperature

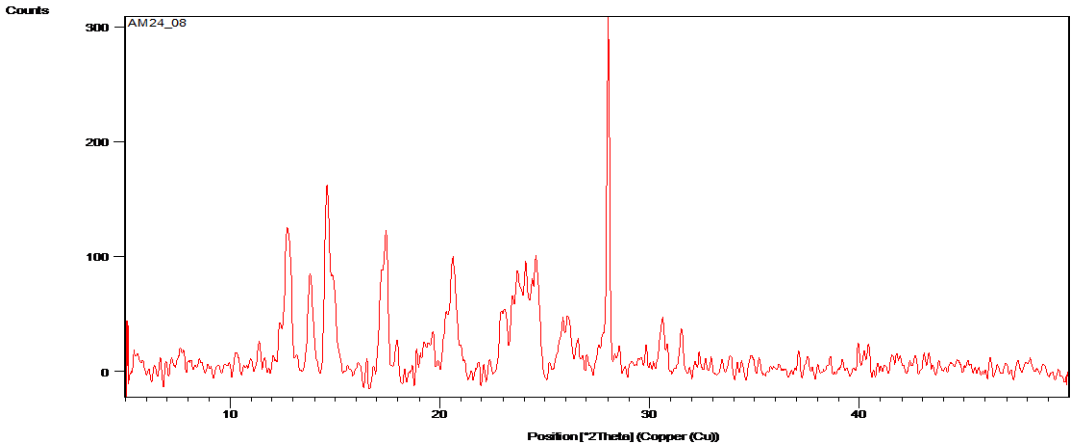

AM24_09 – 6-phthalimidoperoxyhexanoic acid + acetone crystallised at 4°C

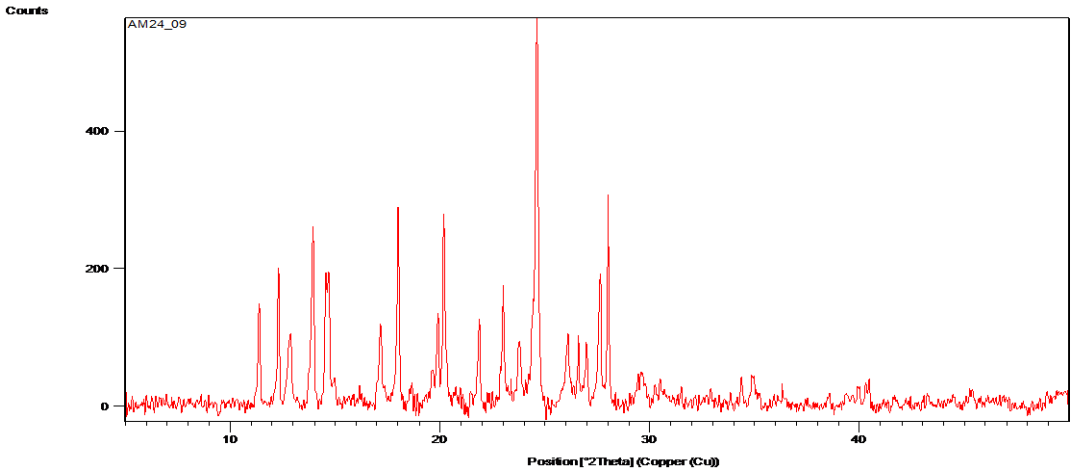

AM24_10 – 6-phthalimidoperoxyhexanoic acid + acetone crystallised at room temperature

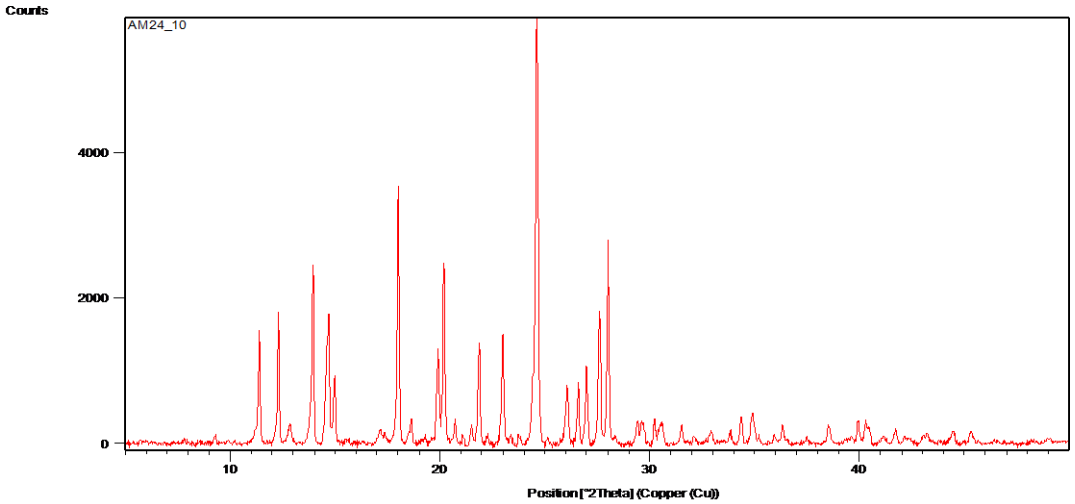

AM24_11 – 6-phthalimidoperoxyhexanoic acid + diethyl ether crystallised at 4°C

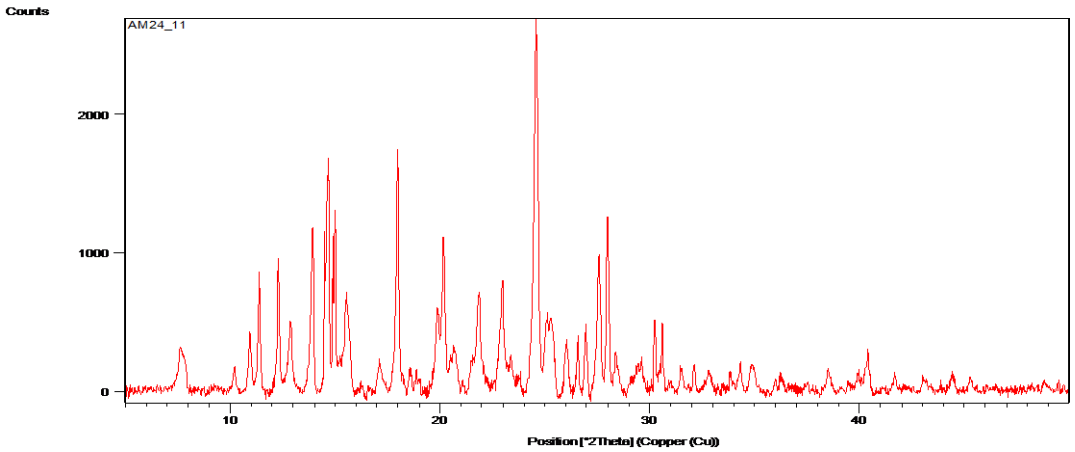

AM24_12 – 6-phthalimidoperoxyhexanoic acid + diethyl ether crystallised at room temperature

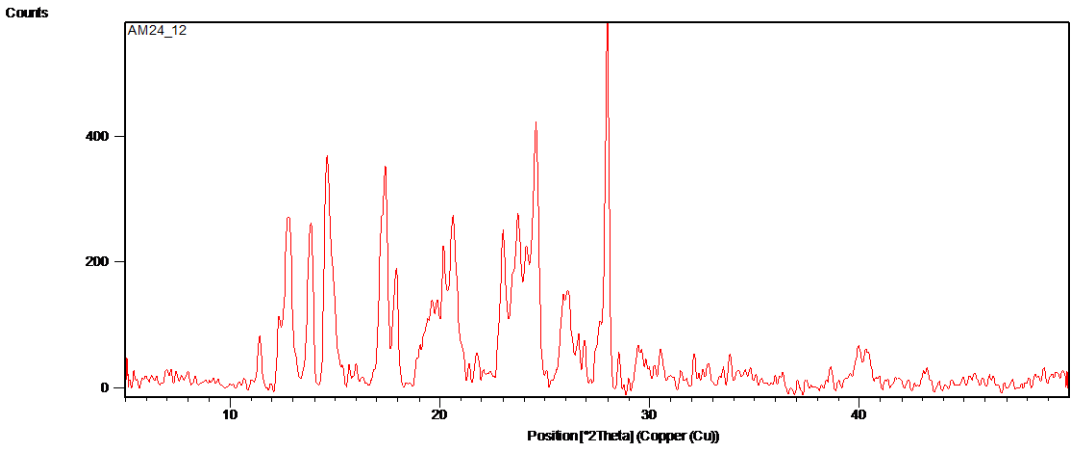

AM24_13 – 6-phthalimidoperoxyhexanoic acid + ethyl acetate crystallised at 4°C

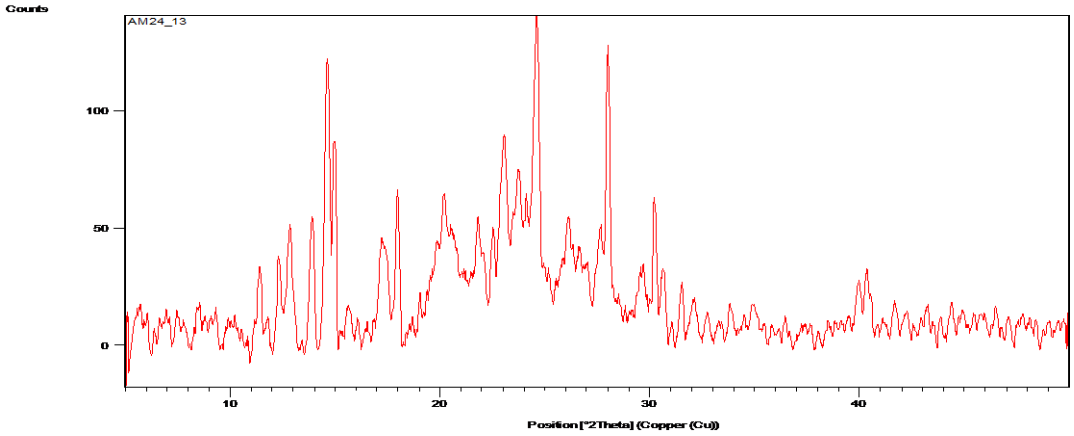

AM24_14 – 6-phthalimidoperoxyhexanoic acid + ethyl acetate crystallised at room temperature

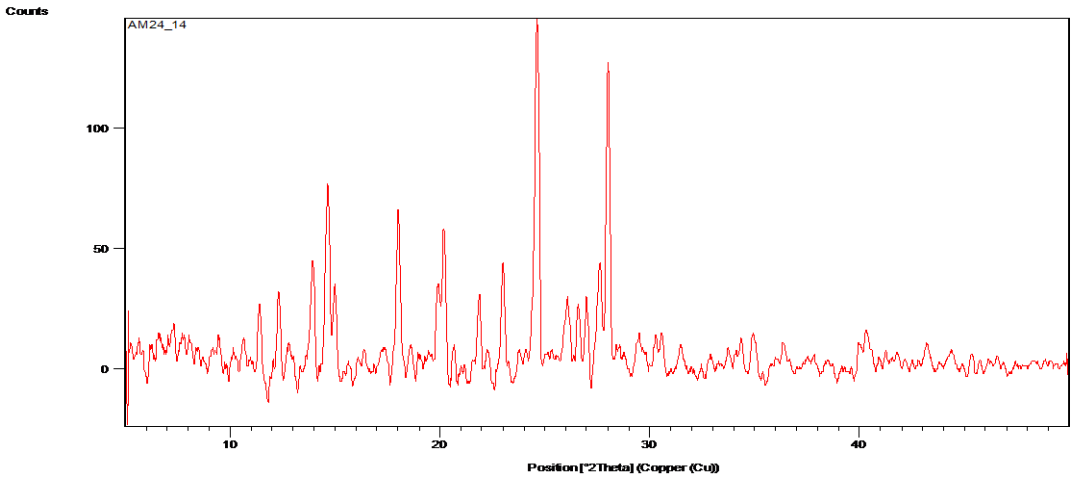

AM24_16 – 6-phthalimidoperoxyhexanoic acid + morpholine crystallised at room temperature

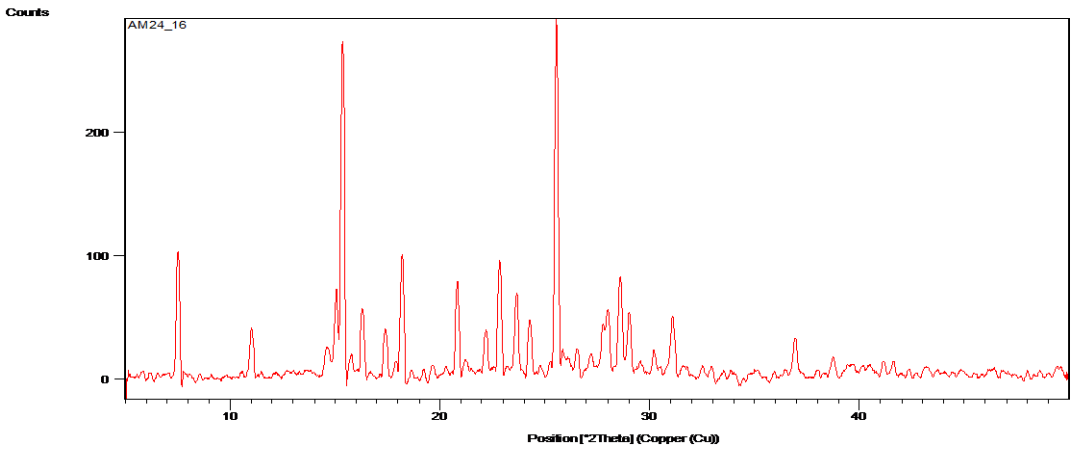

AM24_17 – 6-phthalimidoperoxyhexanoic acid + 1,4-dioxane crystallised at 4°C

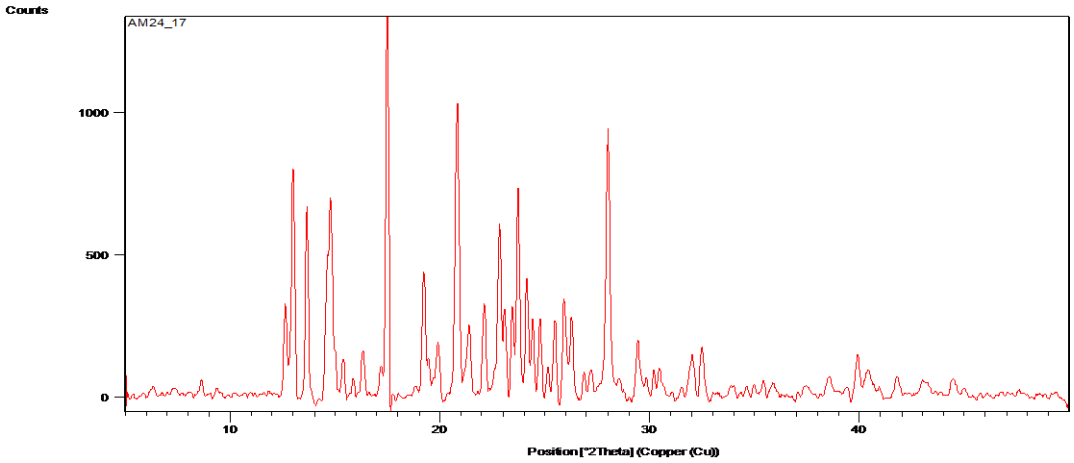

AM24_18 – 6-phthalimidoperoxyhexanoic acid + 1,4-dioxane crystallised at room temperature

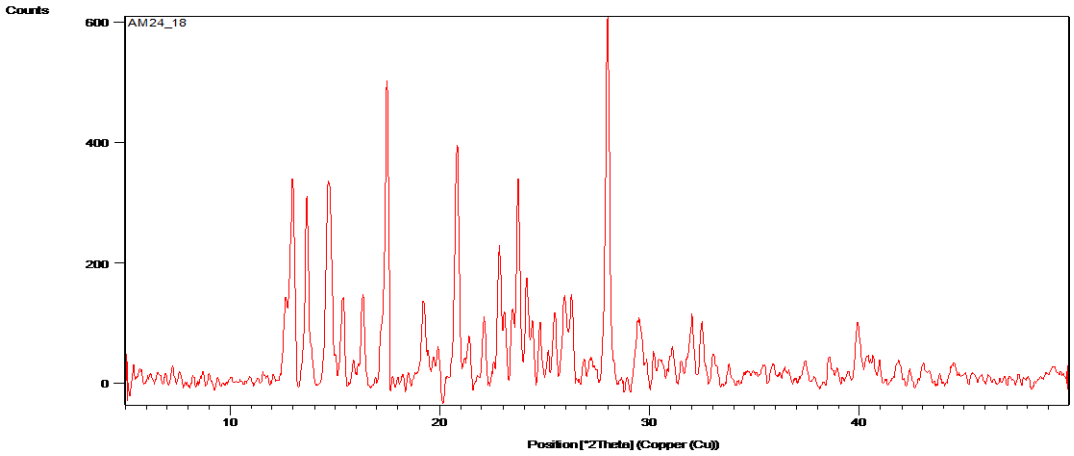

AM32_03 and AM32_04 – Repeat of 6-phthalimidoperoxyhexanoic acid + Acetone crystallised at 4°C

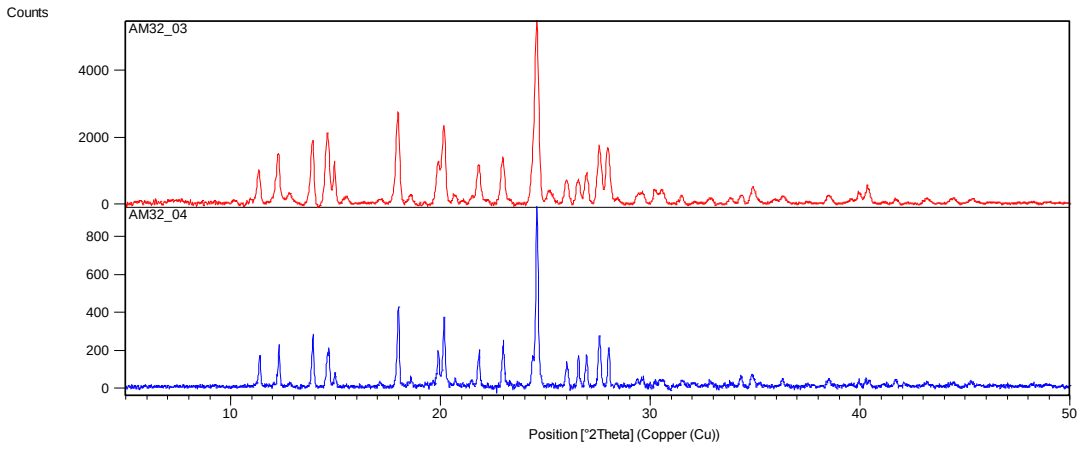

AM32_05 and AM32_06 – Repeat of 6-phthalimidoperoxyhexanoic acid + acetone crystallised at room temperature

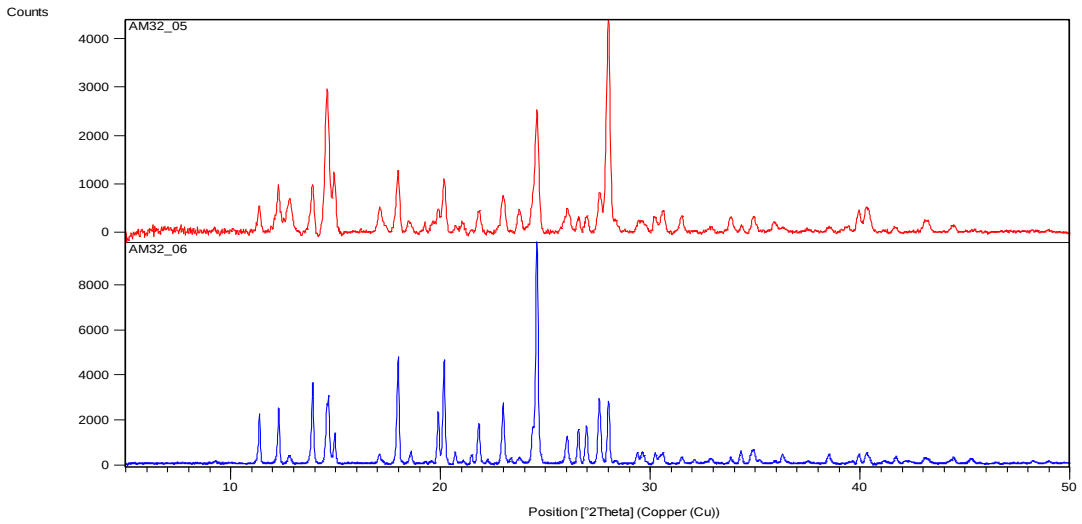

AM32_07 – 6-phthalimidoperoxyhexanoic acid + Acetone crystallised at 30°C

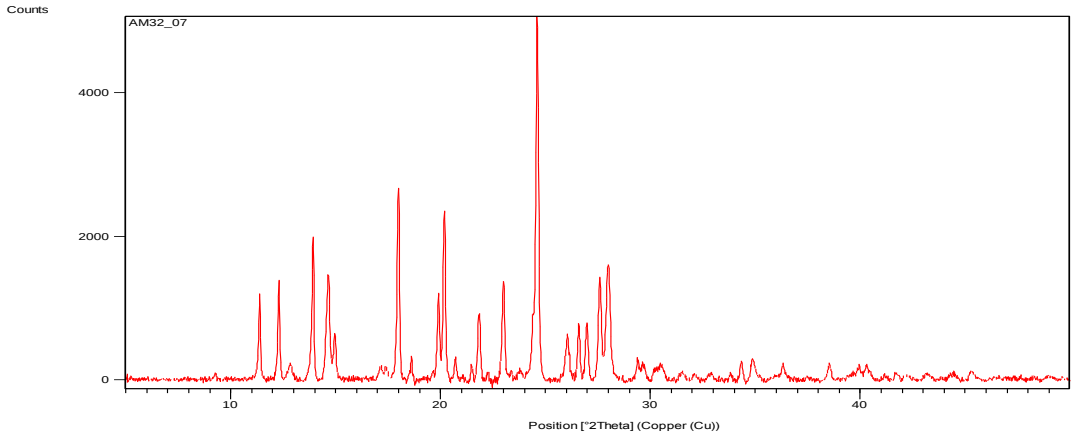

AM32_08 – 6-phthalimidoperoxyhexanoic acid +Acetone crystallised at 50°C

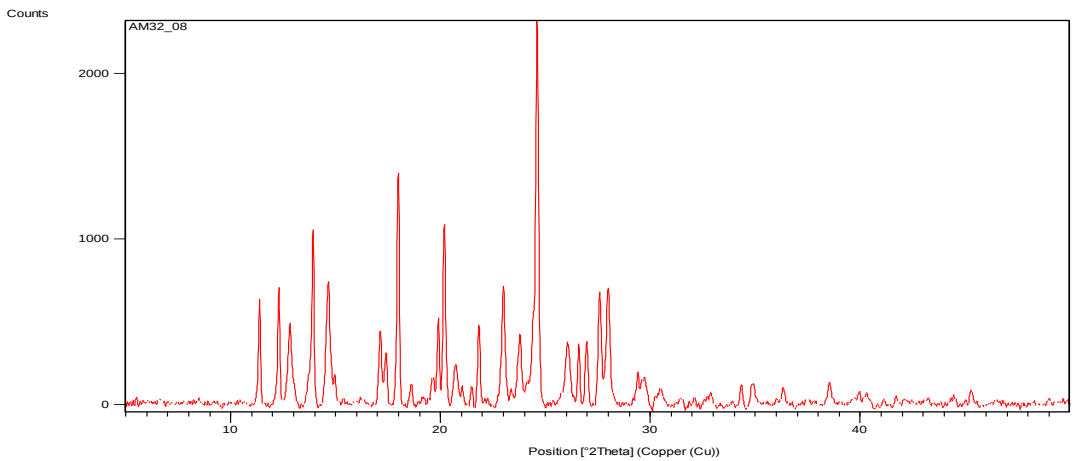

AM32_09 – 6-phthalimidoperoxyhexanoic acid + methyl acetate crystallised at 4°C

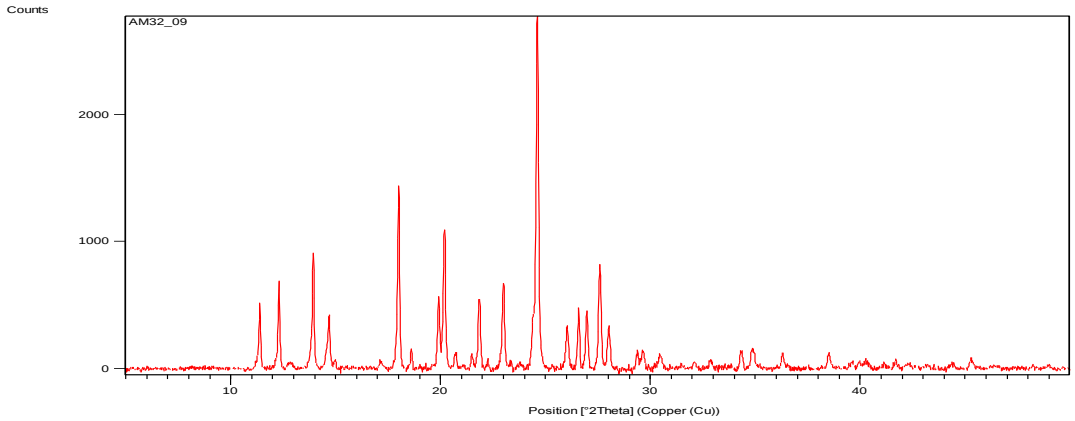

AM32_10 – 6-phthalimidoperoxyhexanoic acid + methyl acetate crystallised at room temperature

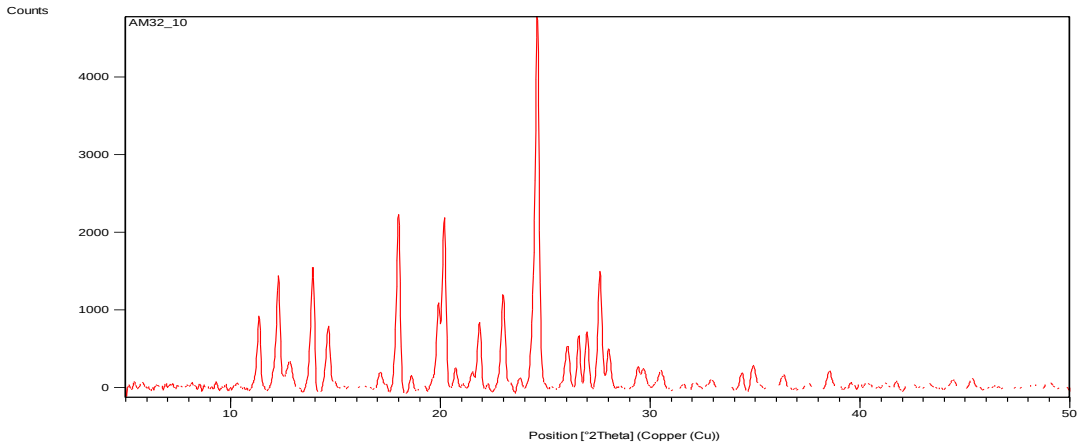

AM32_11 – 6-phthalimidoperoxyhexanoic acid + methyl acetate crystallised at 30°C

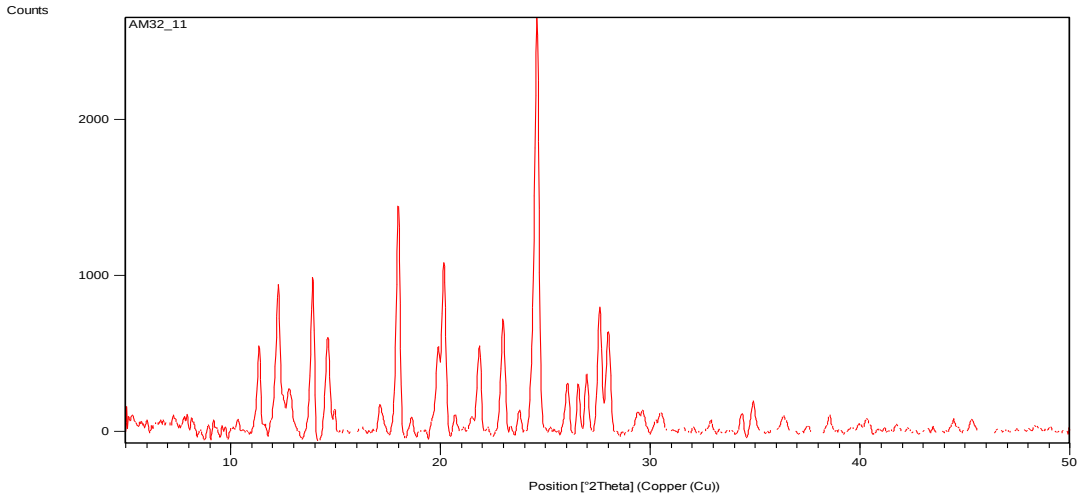

AM32_12 – 6-phthalimidoperoxyhexanoic acid + methanol with hydrogen peroxide crystallised at 4°C

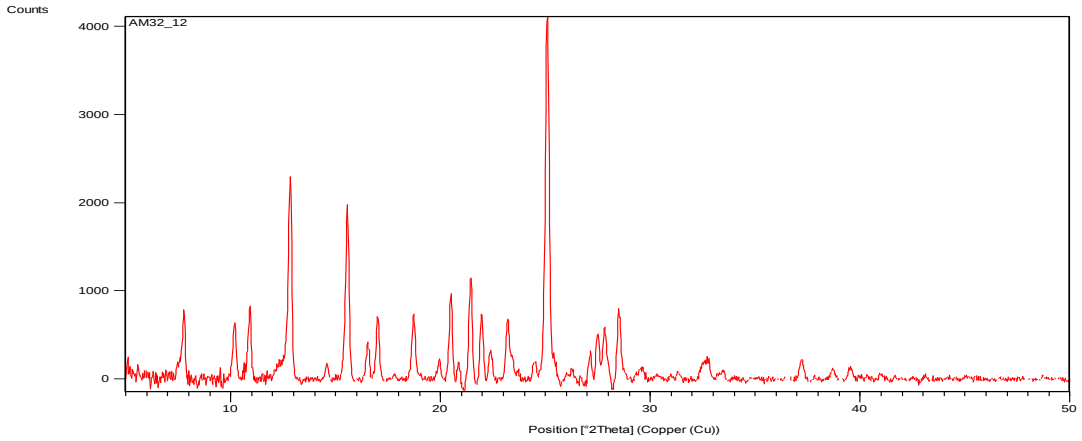

AM32_14 – 6-phthalimidoperoxyhexanoic acid + methanol with hydrogen peroxide crystallised at 30°C

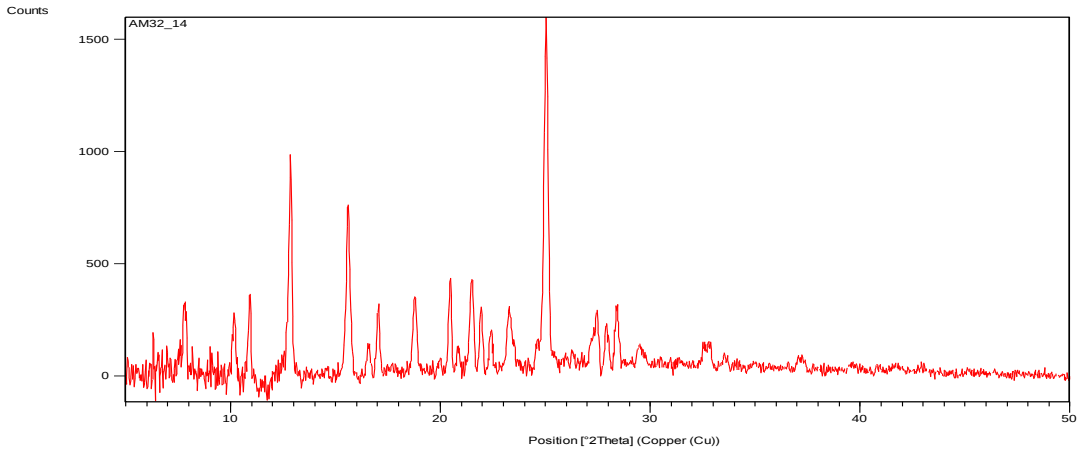

AM32_15 – 6-phthalimidoperoxyhexanoic acid + ethanol with hydrogen peroxide crystallised at 4°C

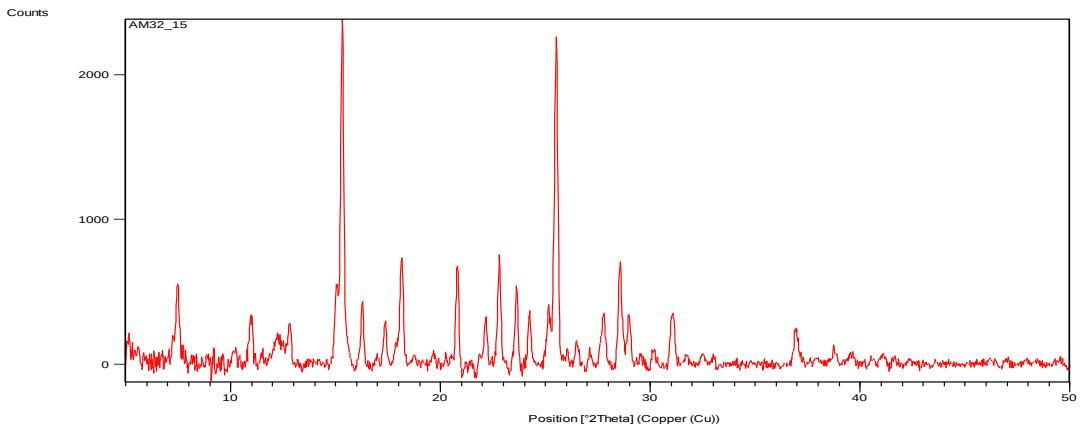

AM32_16 – 6-phthalimidoperoxyhexanoic acid + ethanol with hydrogen peroxide crystallised at room temperature

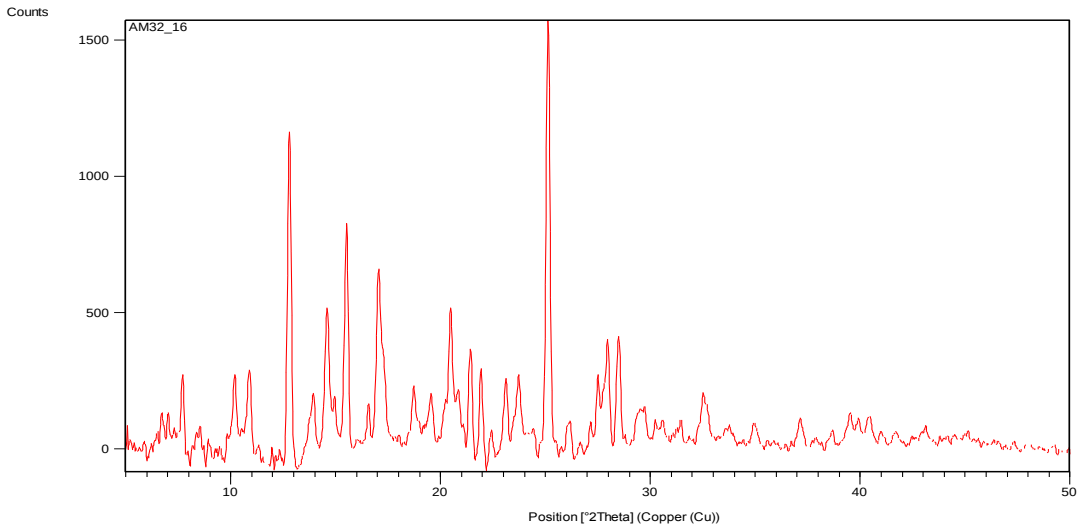

AM32_17 – 6-phthalimidoperoxyhexanoic acid + ethanol with hydrogen peroxide crystallised at 30°C

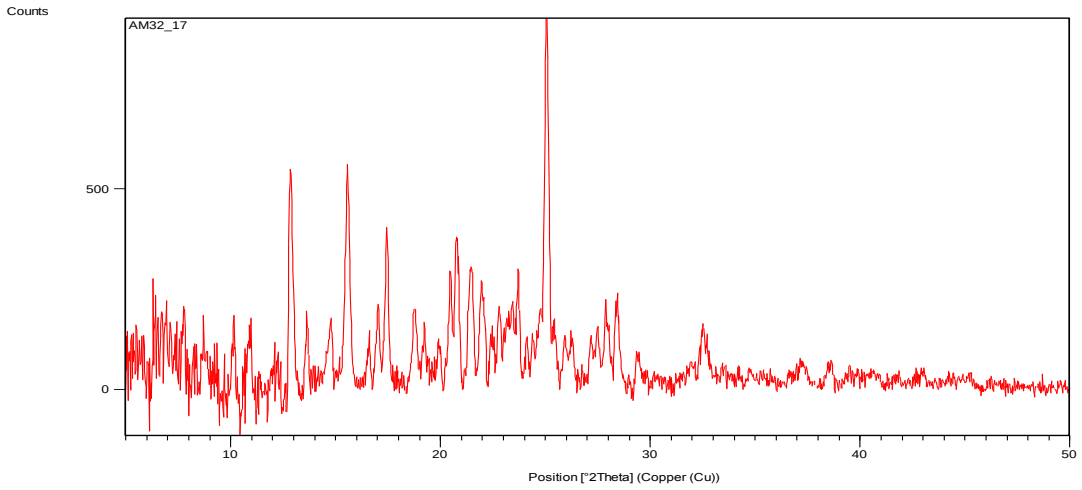

AM33_01 – 6-phthalimidoperoxyhexanoic acid + methanol with hydrochloric acid crystallised at 4°C

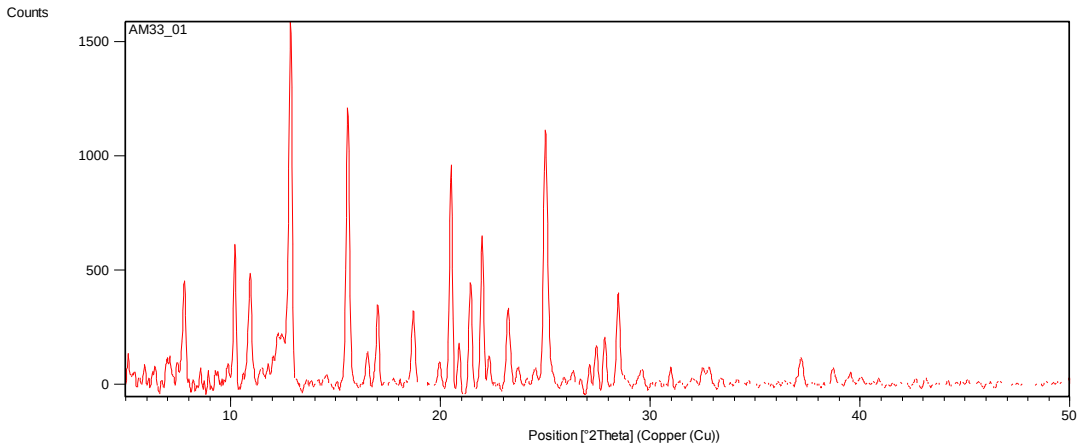

AM33_02 – 6-phthalimidoperoxyhexanoic acid + methanol with hydrochloric acid crystallised at room temperature

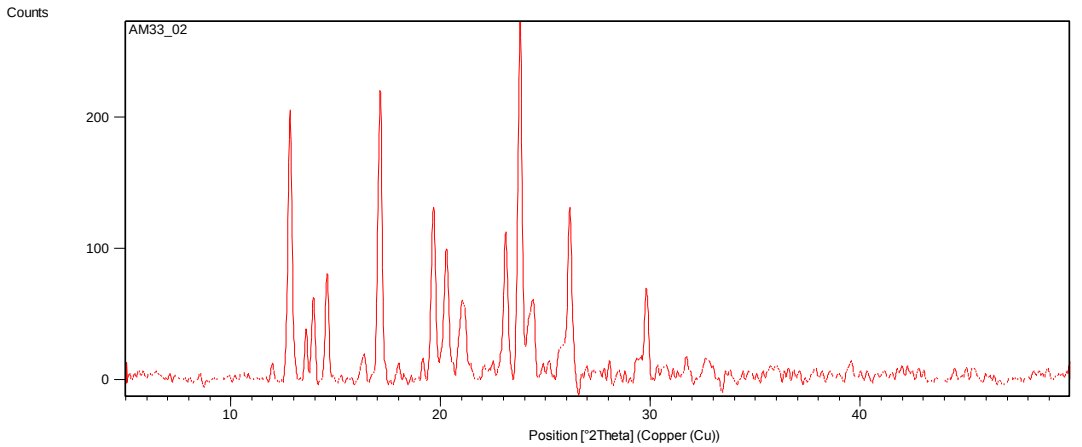

AM33_03 – 6-phthalimidoperoxyhexanoic acid + ethanol with hydrochloric acid crystallised at 4°C

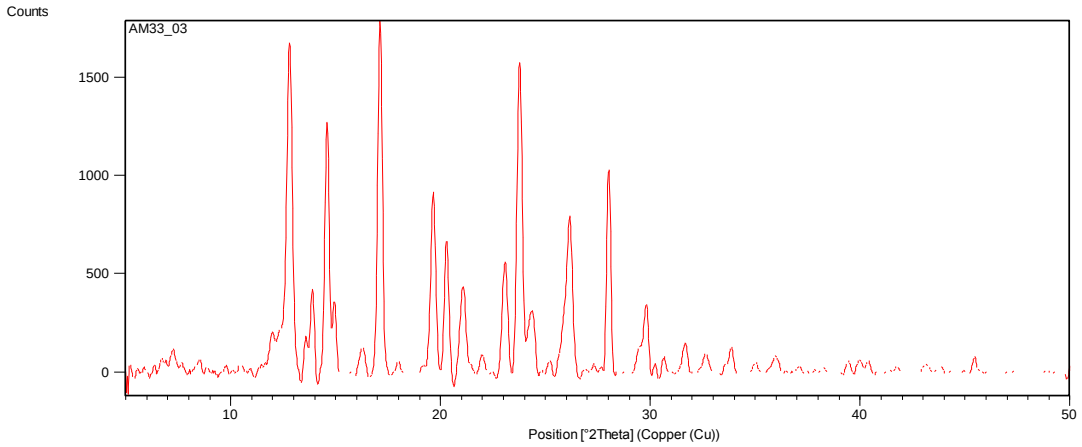

AM33_04 – 6-phthalimidoperoxyhexanoic acid + ethanol with hydrochloric acid crystallised at room temperature

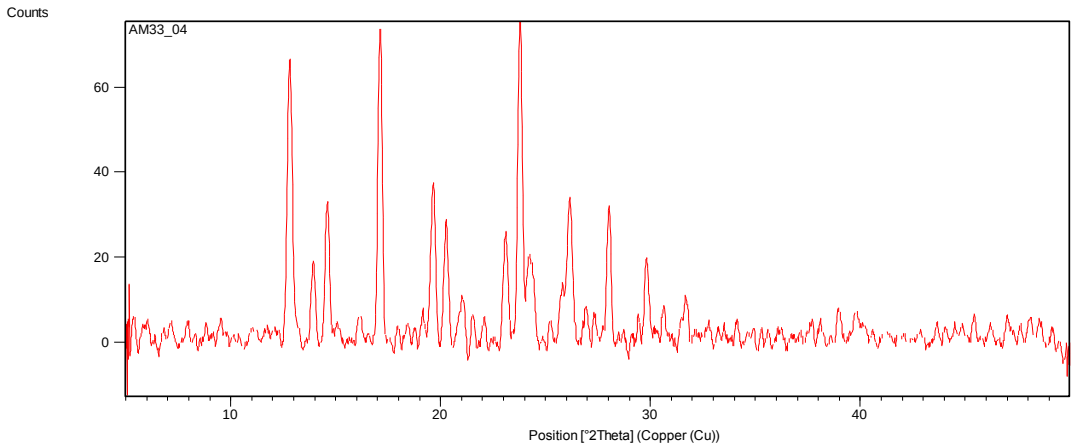

AM33_06 – 6-phthalimidoperoxyhexanoic acid + methanol with sodium hydroxide crystallised at room temperature

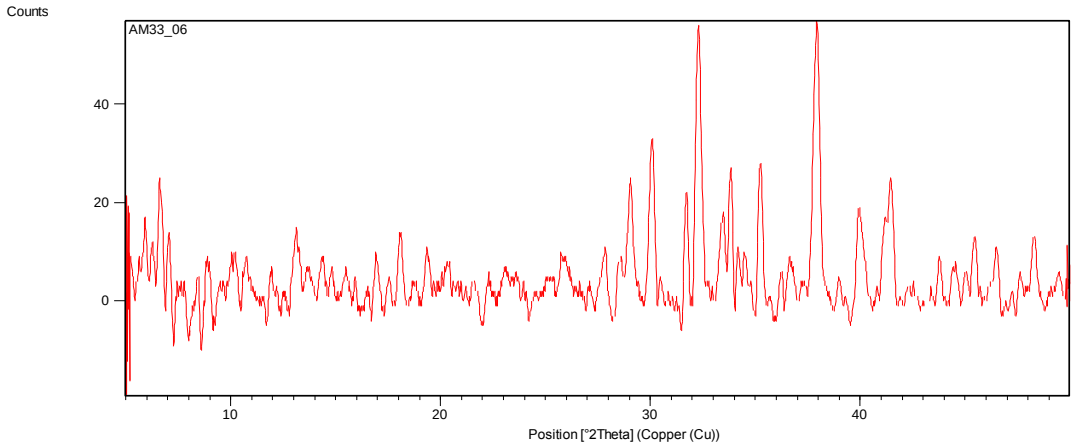

AM33_07 – 6-phthalimidoperoxyhexanoic acid + ethanol with sodium hydroxide crystallised at 4°C

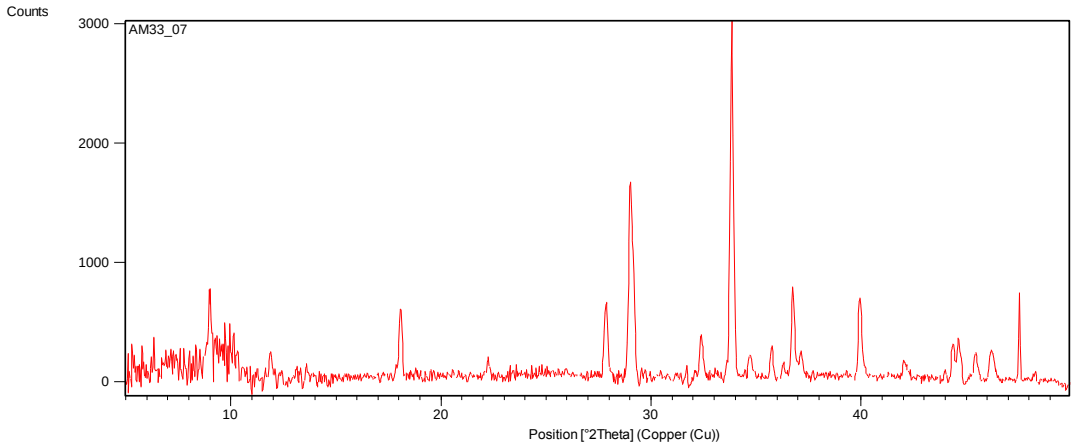

AM33_08 – 6-phthalimidoperoxyhexanoic acid + ethanol with sodium hydroxide crystallised at room temperature

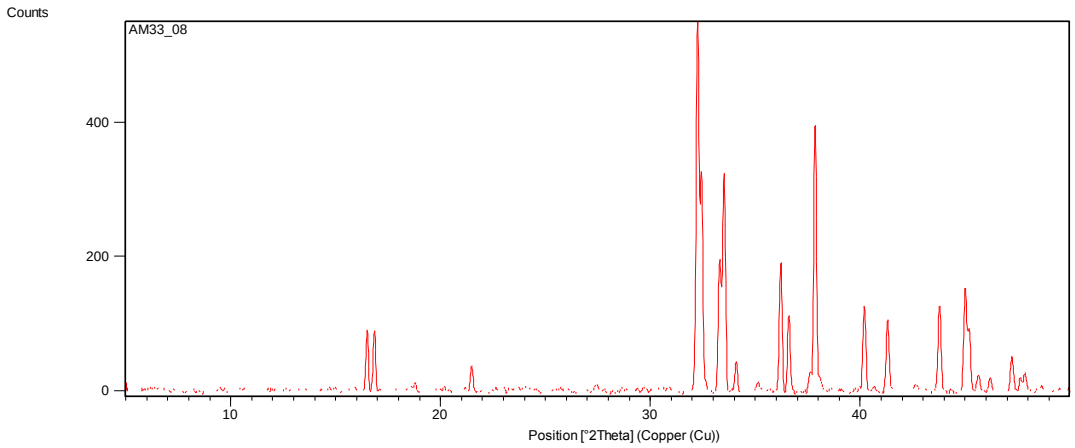

Appendix 2 –Multicomponent Molecular Complexes of Reactive Materials

XRPD Data

Cocrystallisations with carboxylic acids

Peroxyacetic acid and 2-chlorobenzoic acid

AM02_01 – PAA + 2-chlorobenzoic acid crystallised in acetone at 4°C

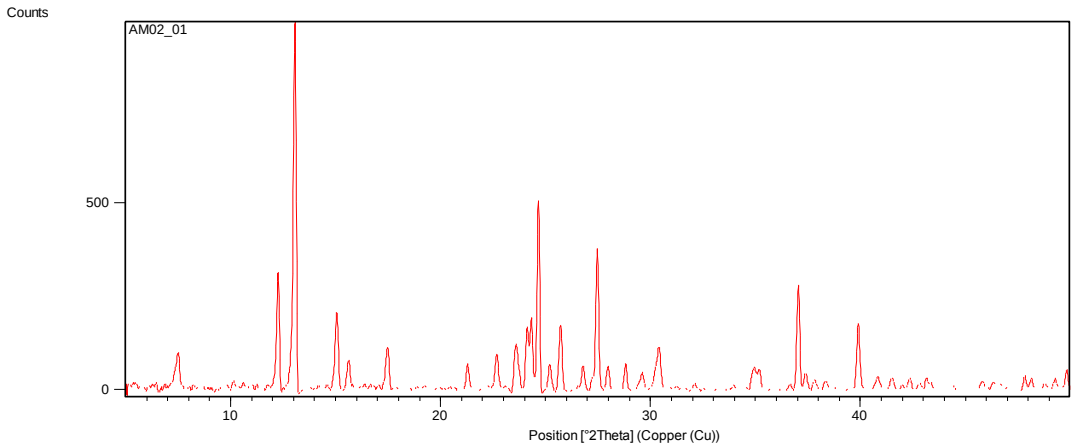

AM02_02 – PAA + 2-chlorobenzoic acid crystallised in acetone at room temperature

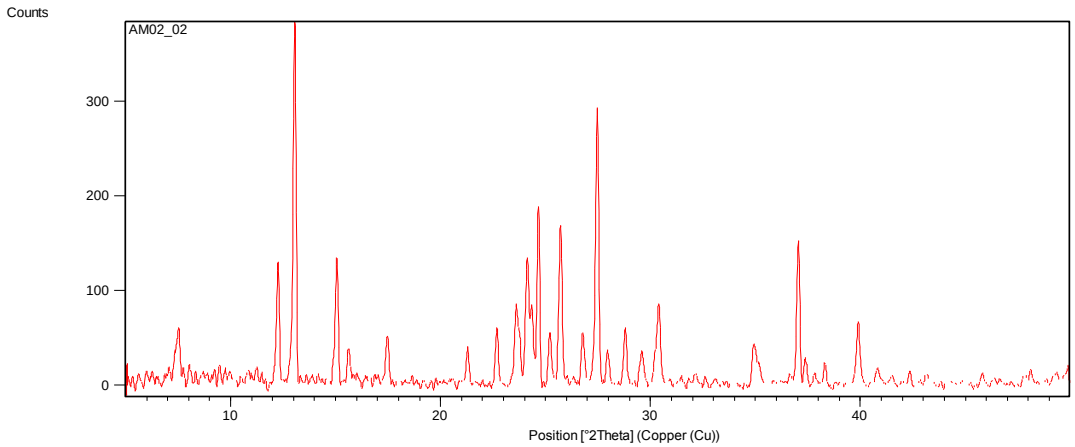

AM02_04 – PAA + 2-chlorobenzoic acid crystallised in methanol at room temperature

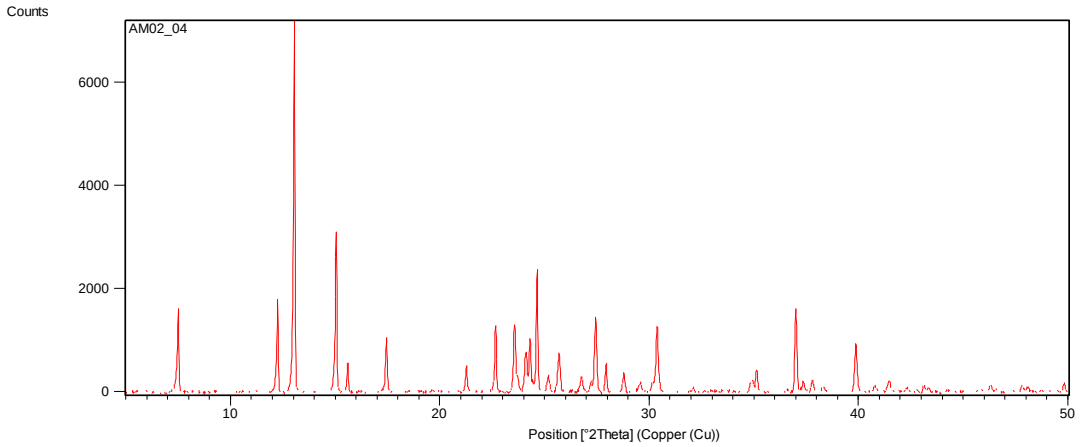

AM02_05 – PAA + 2-chlorobenzoic acid crystallised in ethanol at 4°C

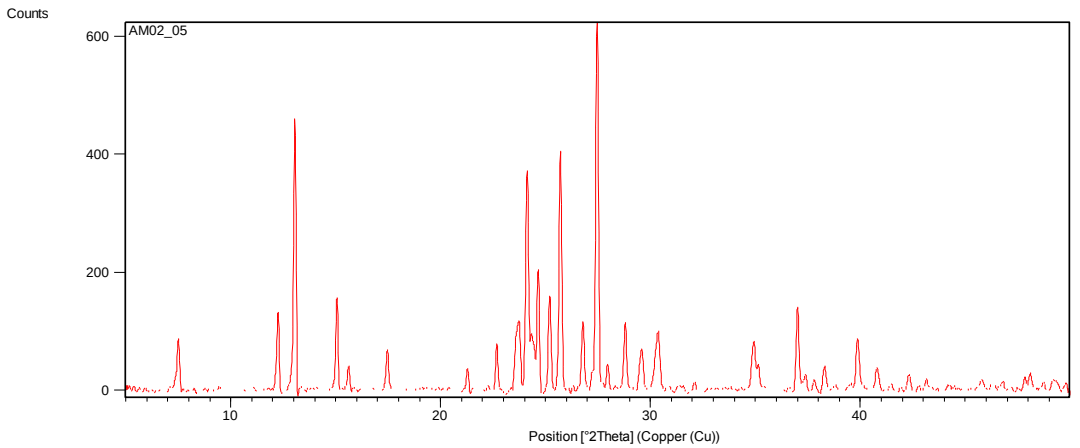

AM02_06 – PAA + 2-chlorobenzoic acid crystallised in ethanol at room temperature

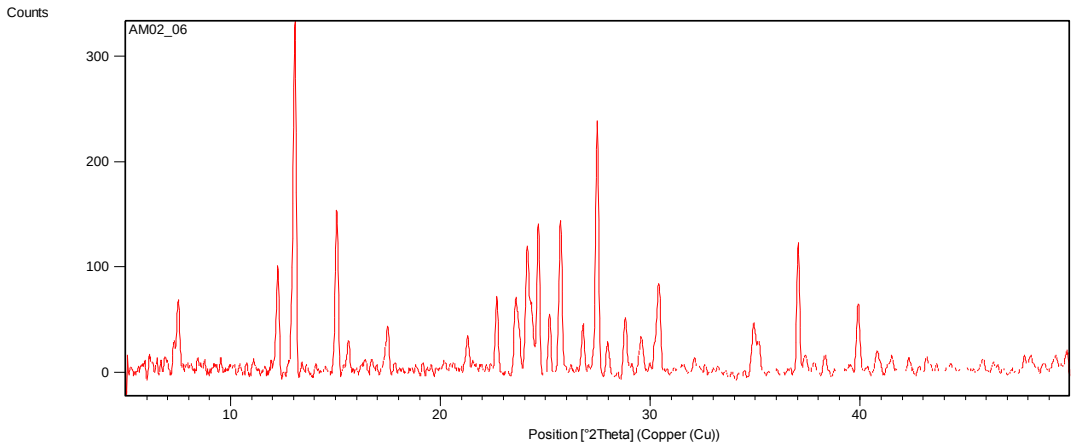

AM02_07 – PAA + 2-chlorobenzoic acid crystallised in isopropanol at 4°C

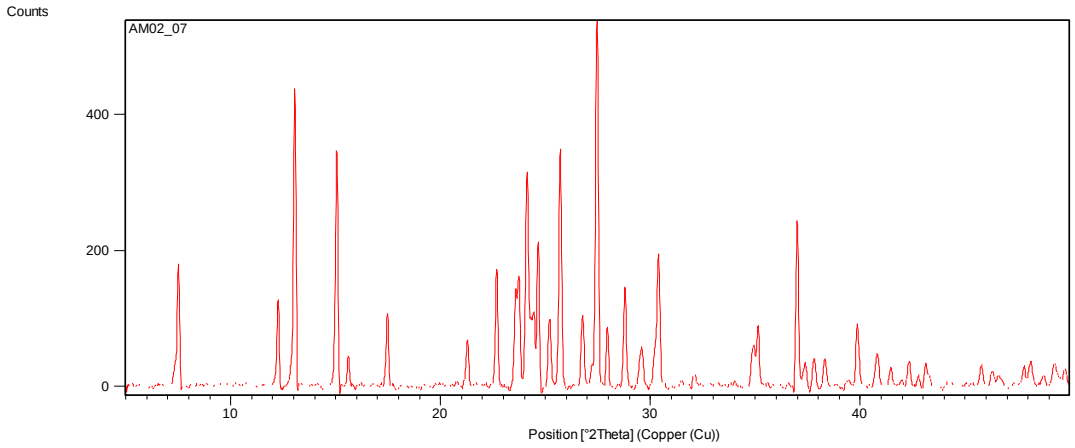

AM02_08 – PAA + 2-chlorobenzoic acid crystallised in isopropanol at room temperature

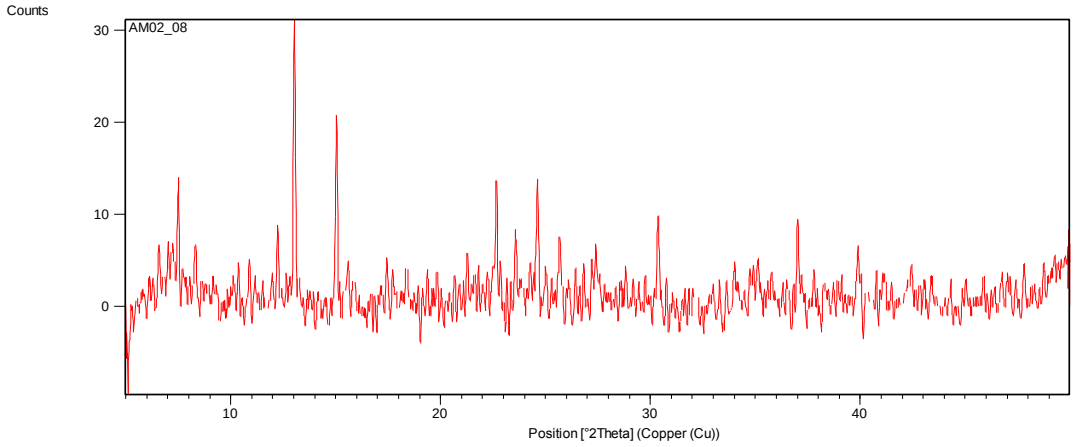

AM02_09 – PAA + 2-chlorobenzoic acid crystallised in chloroform at 4°C

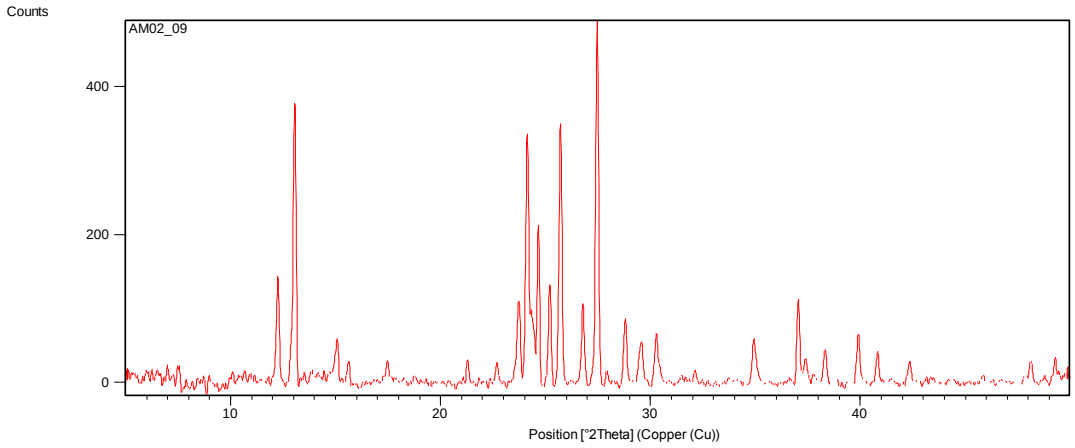

Peroxyacetic acid and 3-chlorobenzoic acid

AM03_01 PAA + 3-chlorobenzoic acid crystallised in acetone at 4°C

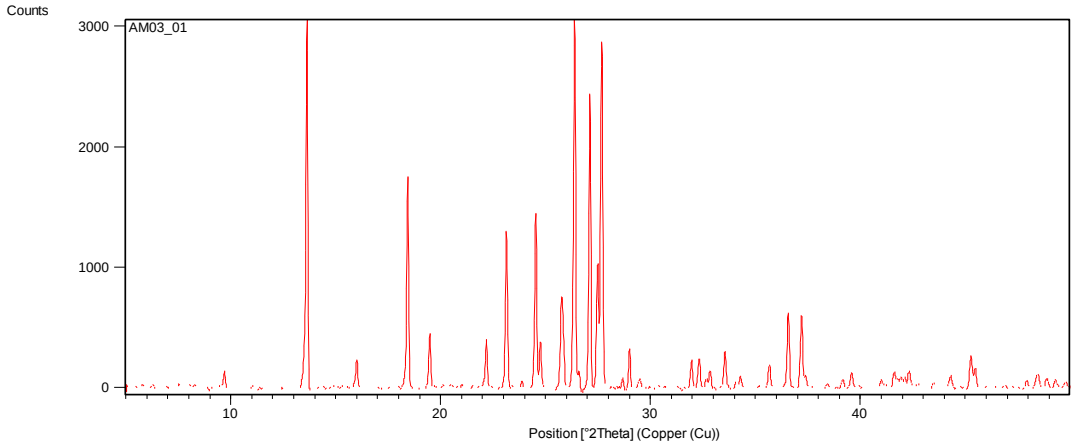

AM03_03 PAA + 3-chlorobenzoic acid crystallised in methanol at 4°C

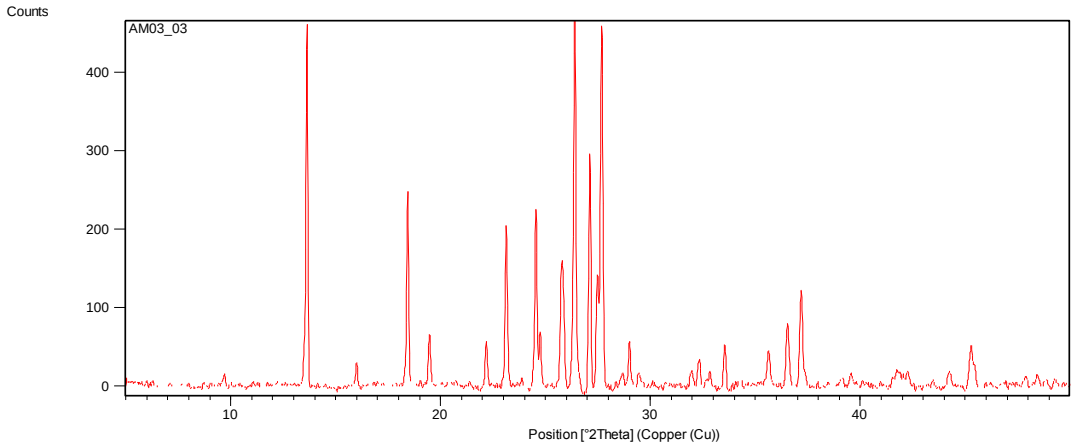

AM03_04 PAA + 3-chlorobenzoic acid crystallised in methanol at room temperature

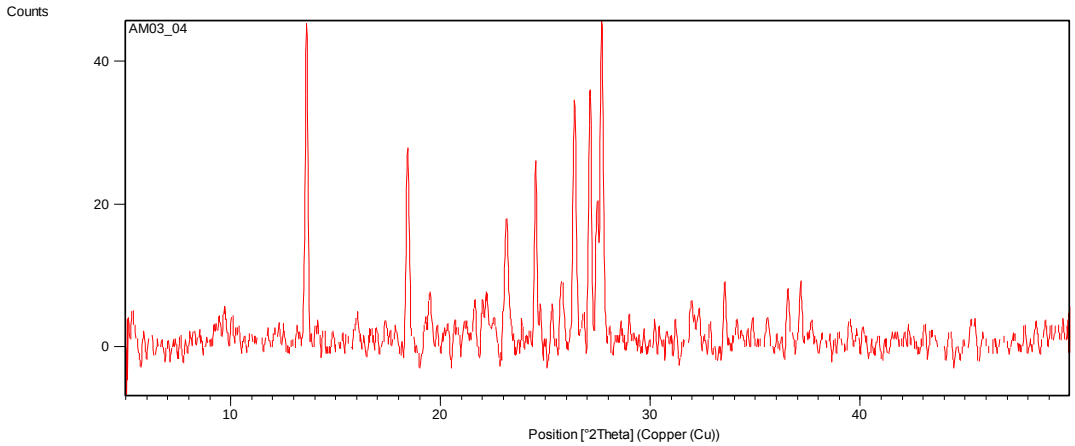

AM03_05 PAA + 3-chlorobenzoic acid crystallised in ethanol at 4°C

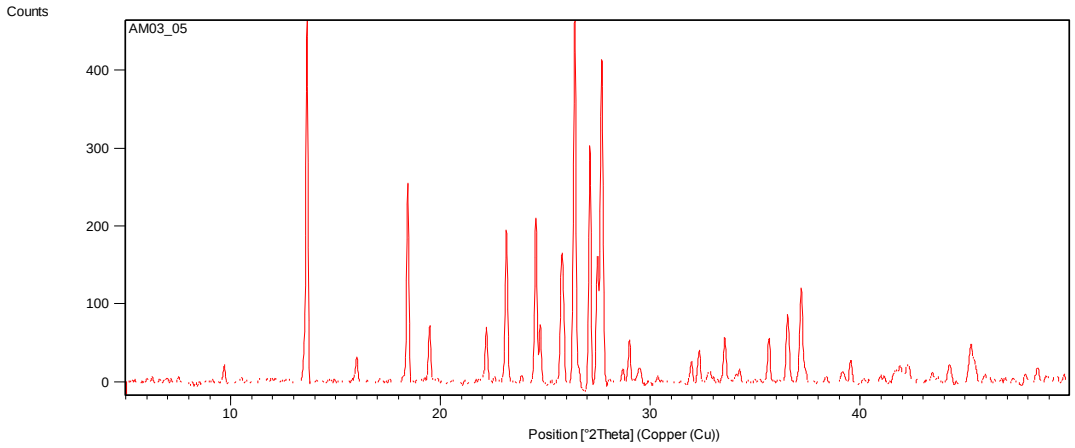

AM03_06 PAA + 3-chlorobenzoic acid crystallised in ethanol at room temperature

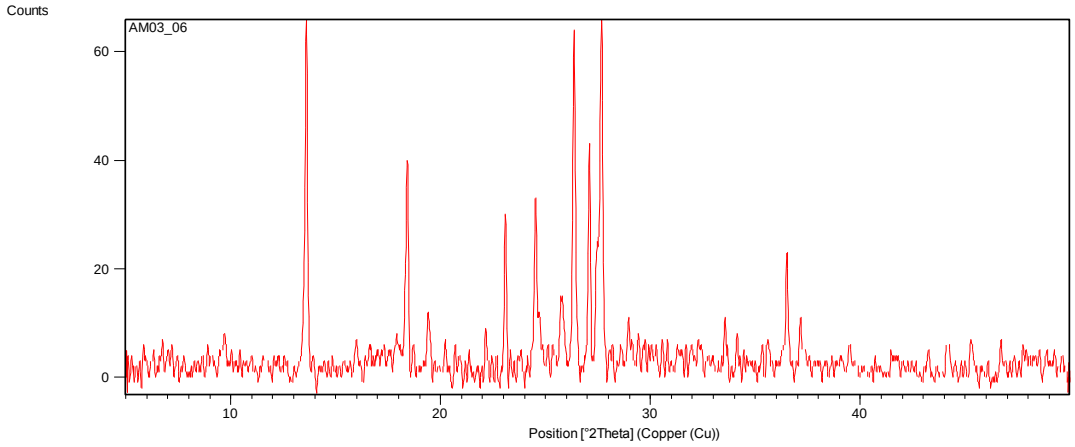

AM03_07 PAA + 3-chlorobenzoic acid crystallised in isopropanol at 4°C

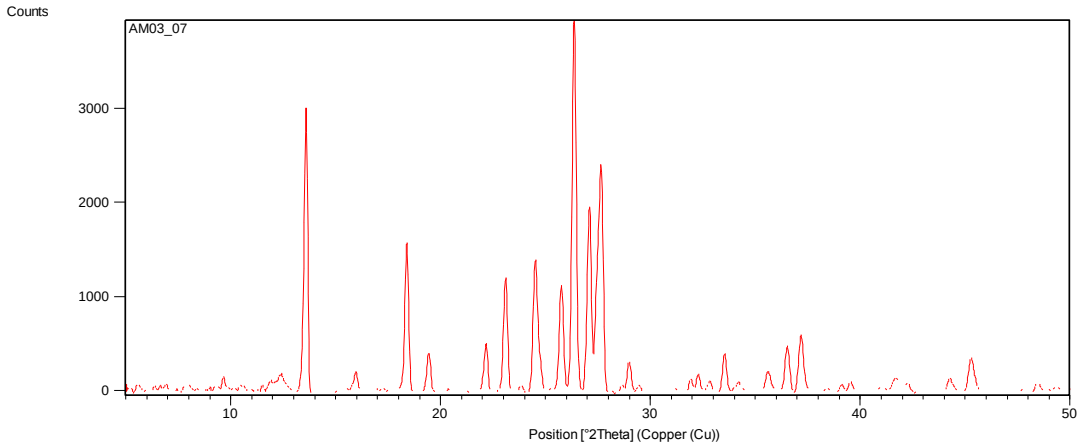

Peroxyacetic acid and 4-chlorobenzoic acid

AM04_01 PAA + 4-chlorobenzoic acid crystallised in acetone at 4°C

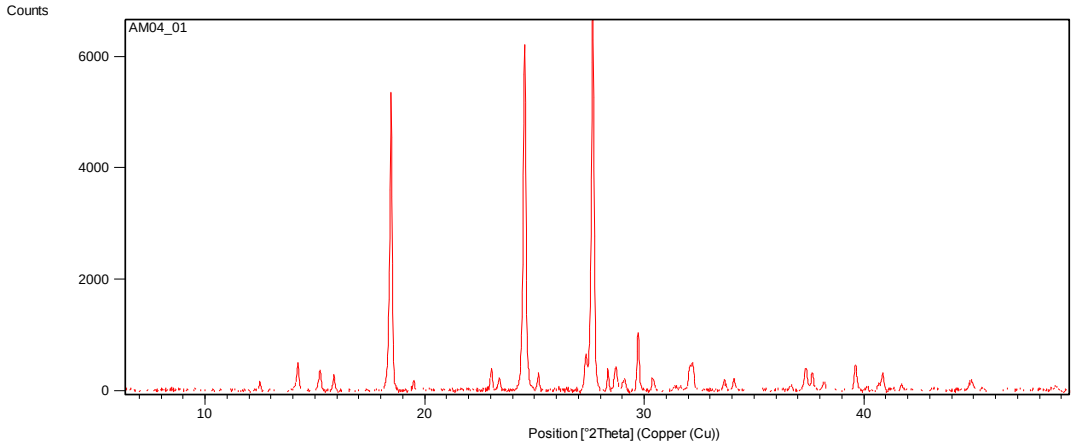

AM04_02 PAA + 4-chlorobenzoic acid crystallised in acetone at room temperature

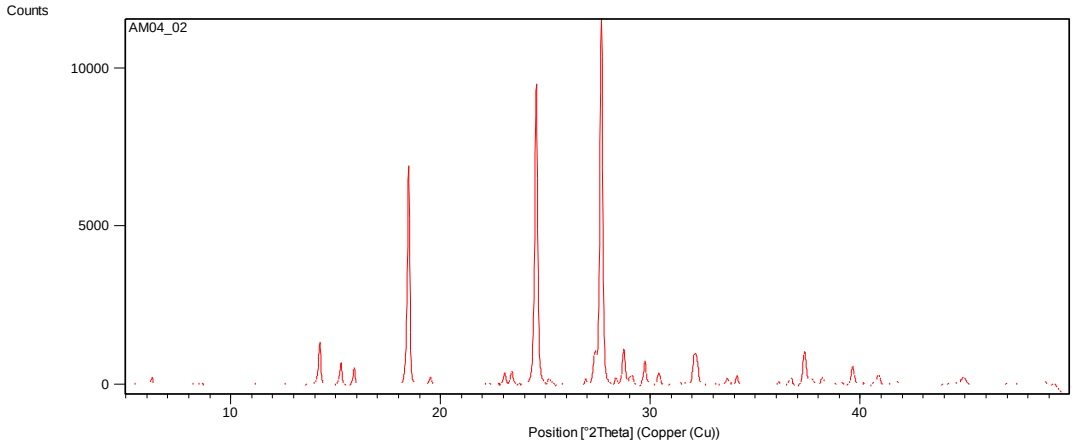

AM04_03 PAA + 4-chlorobenzoic acid crystallised in methanol at 4°C

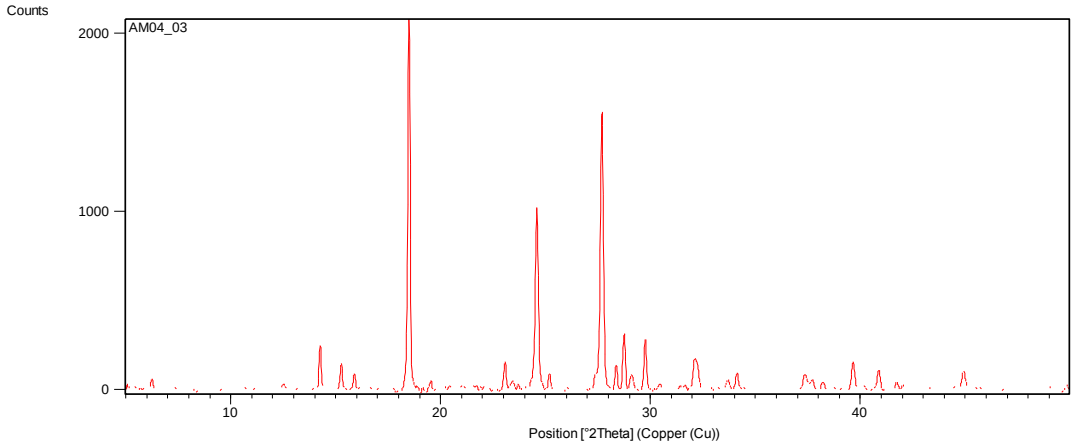

AM04_04 PAA + 4-chlorobenzoic acid crystallised in methanol at room temperature

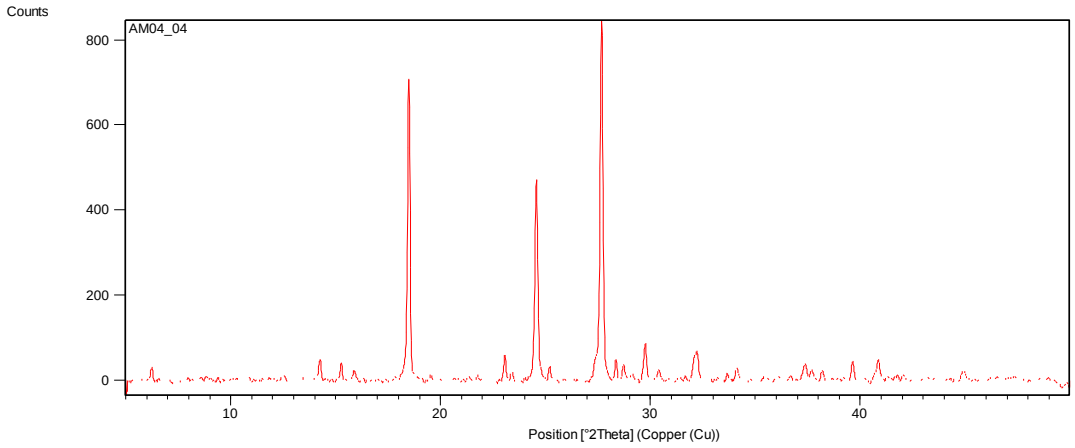

AM04_06 PAA + 4-chlorobenzoic acid crystallised in ethanol at room temperature

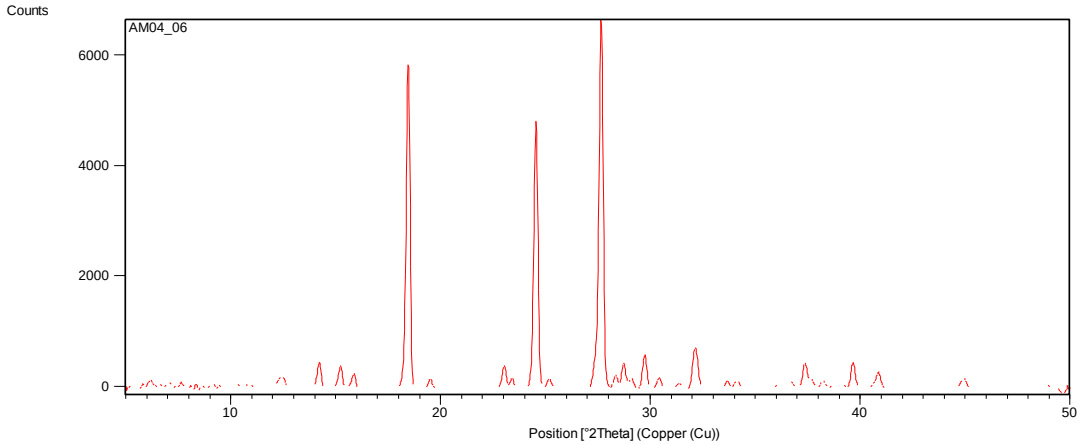

AM04_07 PAA + 4-chlorobenzoic acid crystallised in isopropanol at 4°C

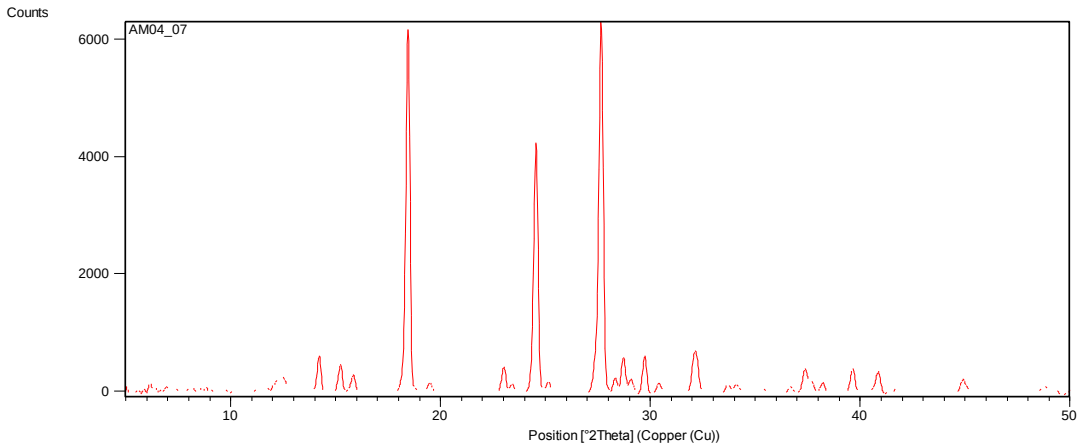

AM04_08 PAA + 4-chlorobenzoic acid crystallised in isopropanol at room temperature

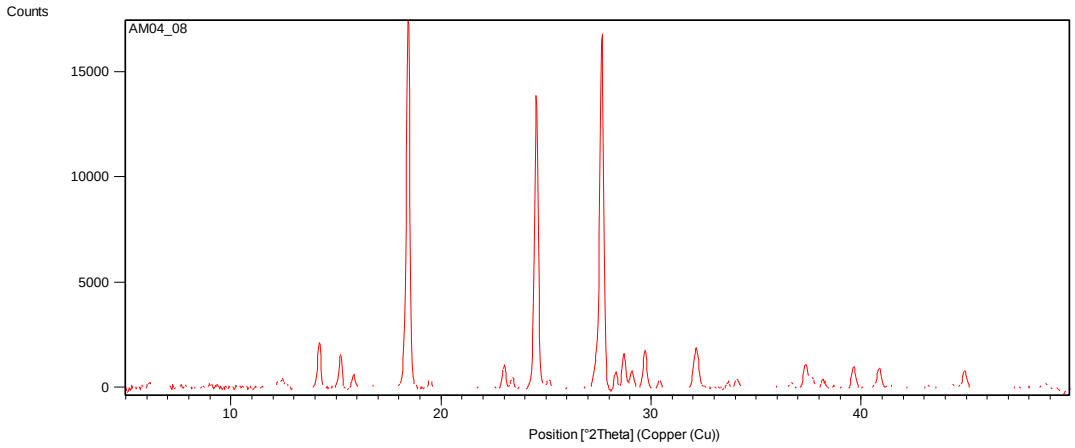

Peroxyacetic acid and 2-picolinic acid

AM05_01 PAA + 2-picolinic acid crystallised in acetone at 4°C

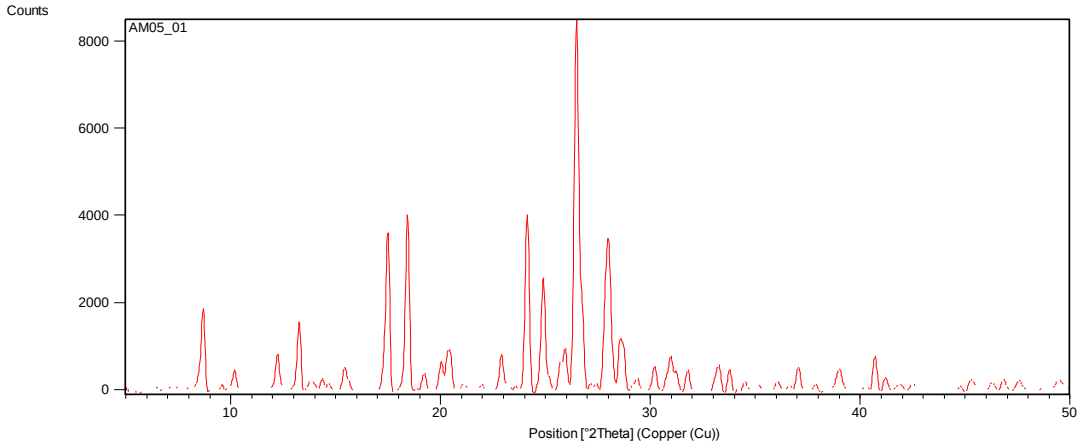

AM05_02 PAA + 2-picolinic acid crystallised in acetone at room temperature

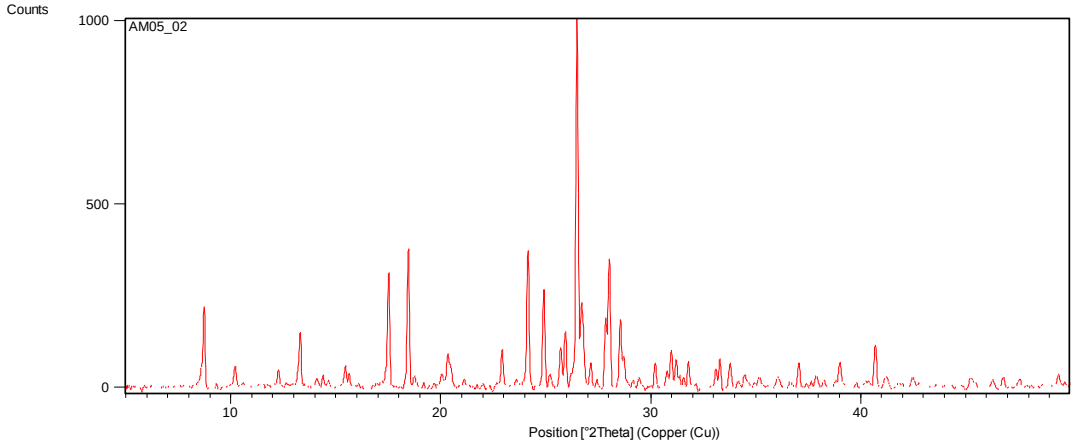

AM05_03 PAA + 2-picolinic acid crystallised in chloroform at 4°C

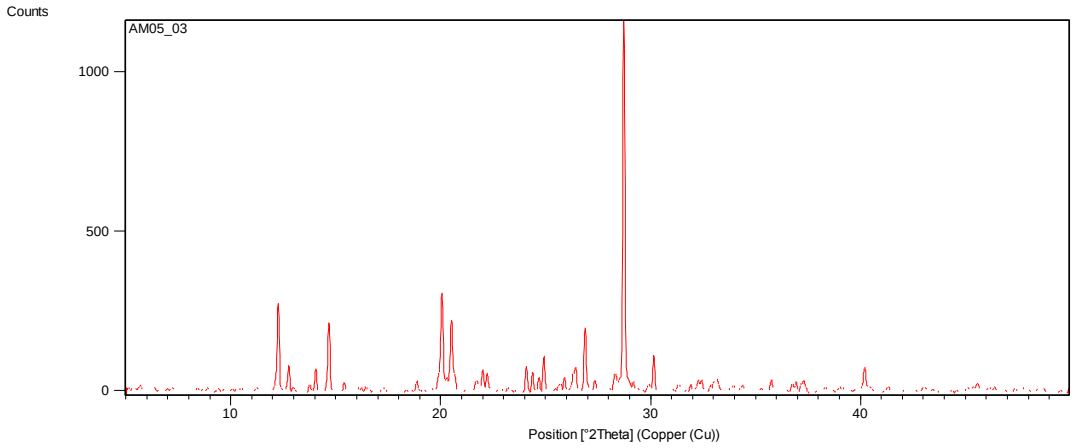

AM05_04 PAA + 2-picolinic acid crystallised in chloroform at room temperature

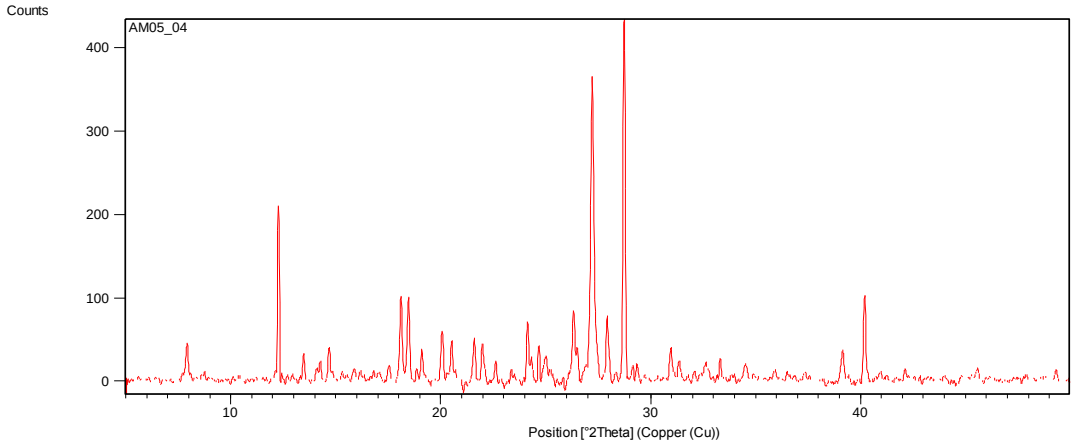

AM05_06 PAA + 2-picolinic acid crystallised in acetone at room temperature

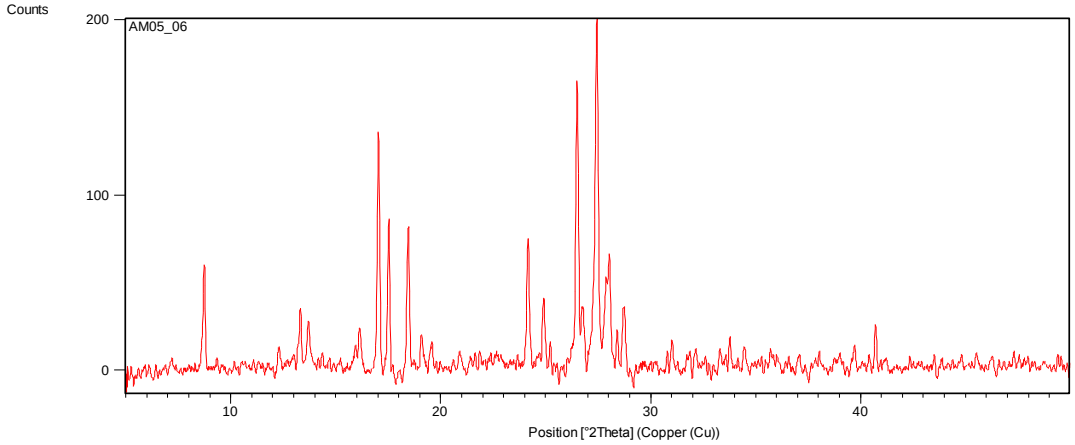

Peroxyacetic acid and 1-naphthaleneacetic acid

AM06_01 PAA + 1-Naphthaleneacetic acid crystallised in acetone at 4°C

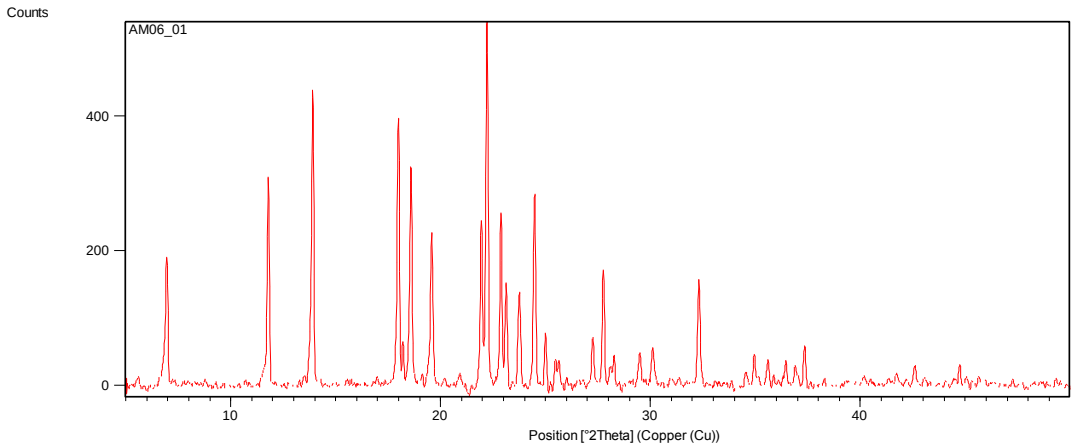

AM06_02 PAA + 1-Naphthaleneacetic acid crystallised in acetone at room temperature

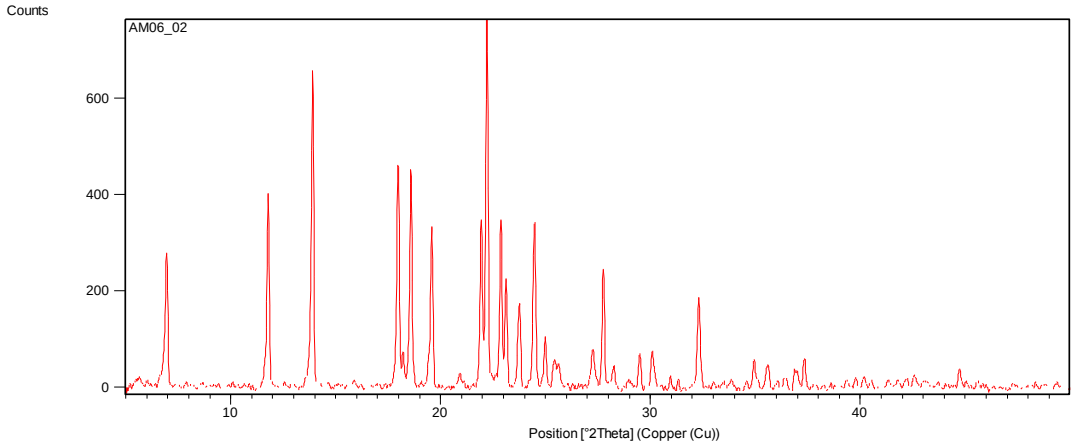

AM06_03 PAA + 1-Naphthaleneacetic acid crystallised in chloroform at 4°C

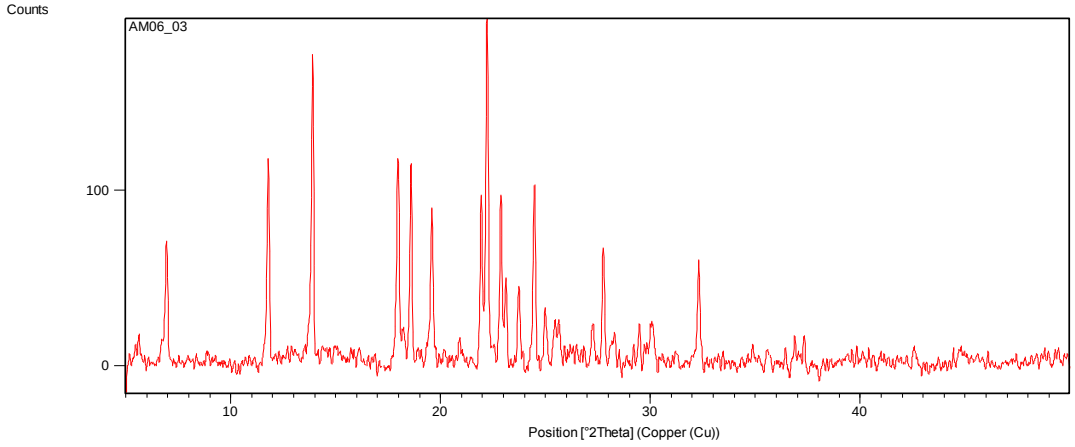

AM06_05 PAA + 1-Naphthaleneacetic acid crystallised in diethyl ether at 4°C

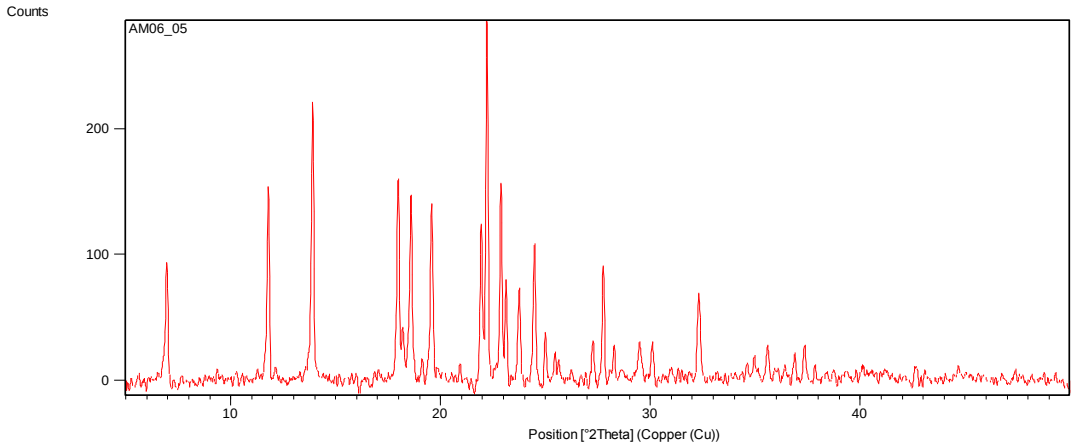

AM06_07 PAA + 1-Naphthaleneacetic acid crystallised in ethyl acetate at 4°C

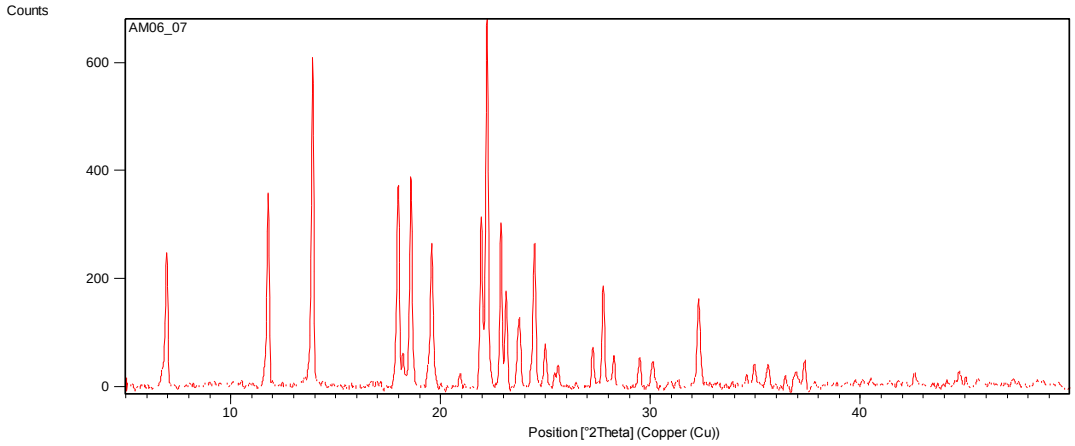

AM06_08 PAA + 1-Naphthaleneacetic acid crystallised in ethyl acetate at room temperature

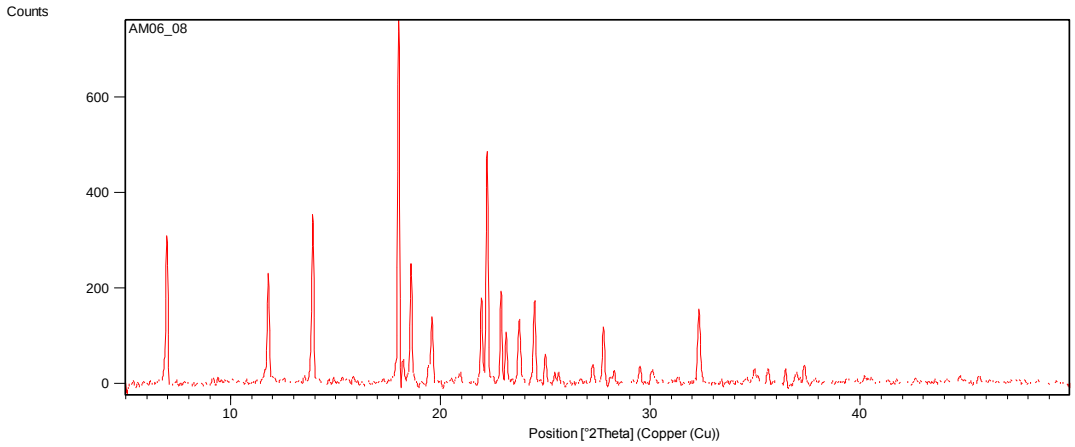

AM06_09 PAA + 1-Naphthaleneacetic acid crystallised in acetonitrile at 4°C

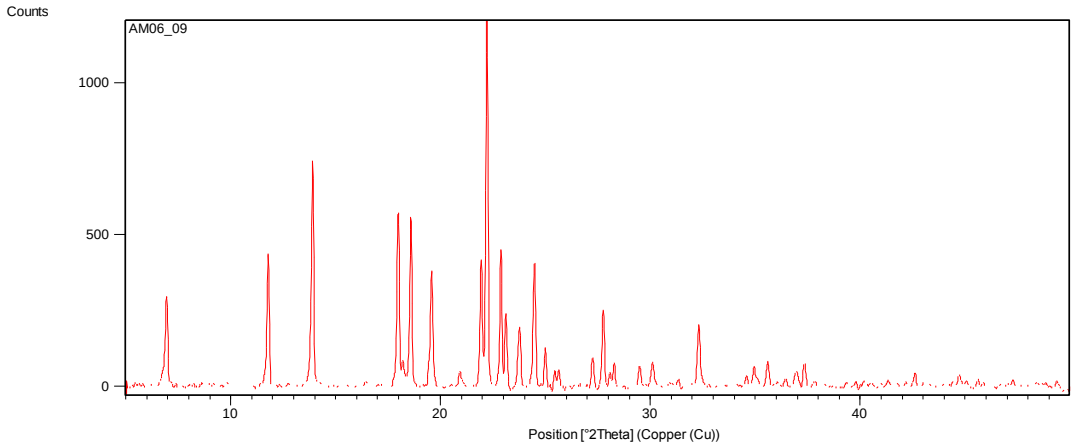

Peroxyacetic acid and Salicylic acid

AM08_01 PAA + Salicylic acid crystallised in acetone at 4°C

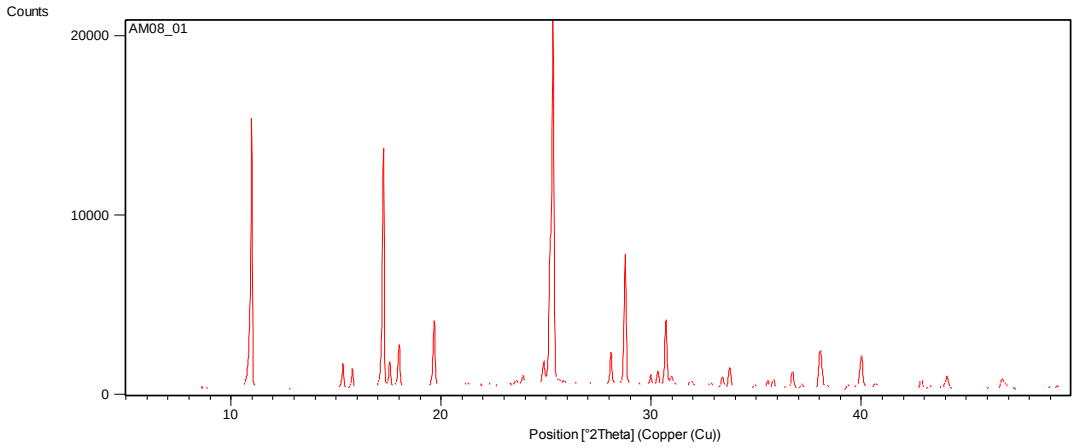

AM08_02 PAA + Salicylic acid crystallised in acetone at room temperature

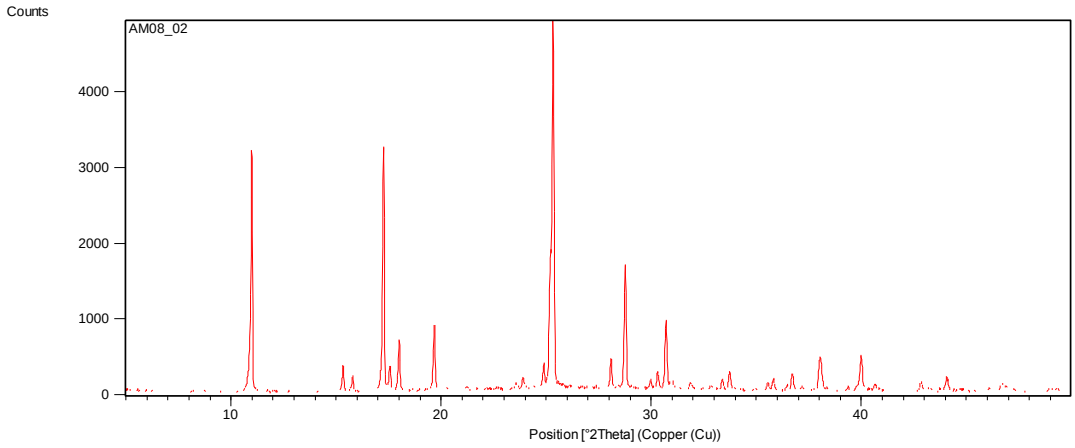

AM08_03 PAA + Salicylic acid crystallised in chloroform at 4°C

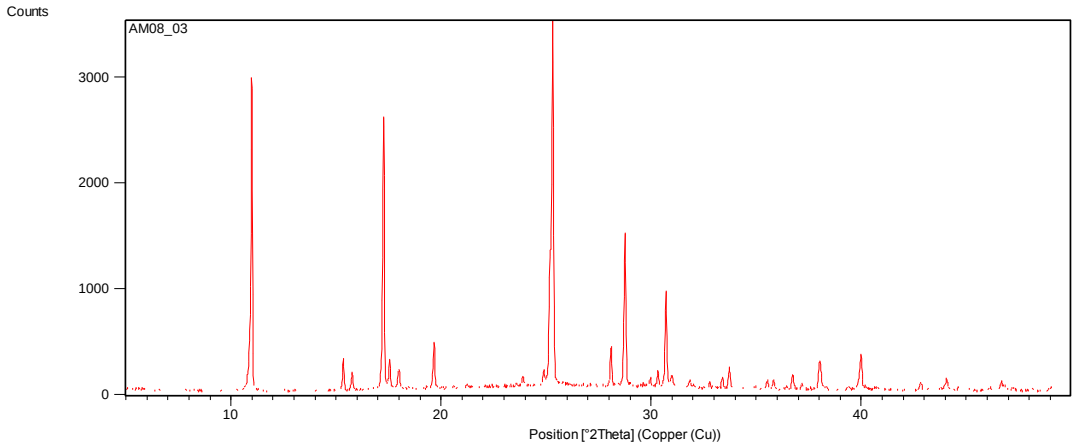

AM08_04 PAA + Salicylic acid crystallised in chloroform at room temperature

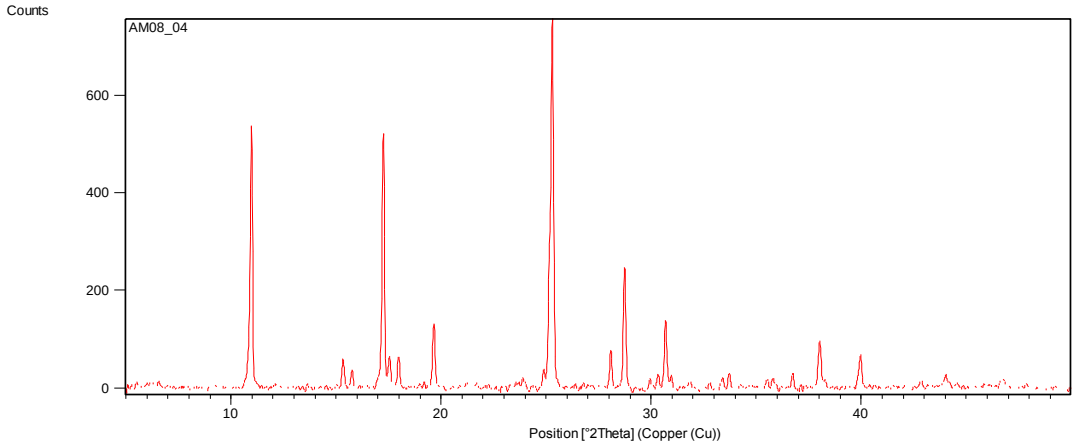

AM08_05 PAA + Salicylic acid crystallised in diethyl ether at 4°C

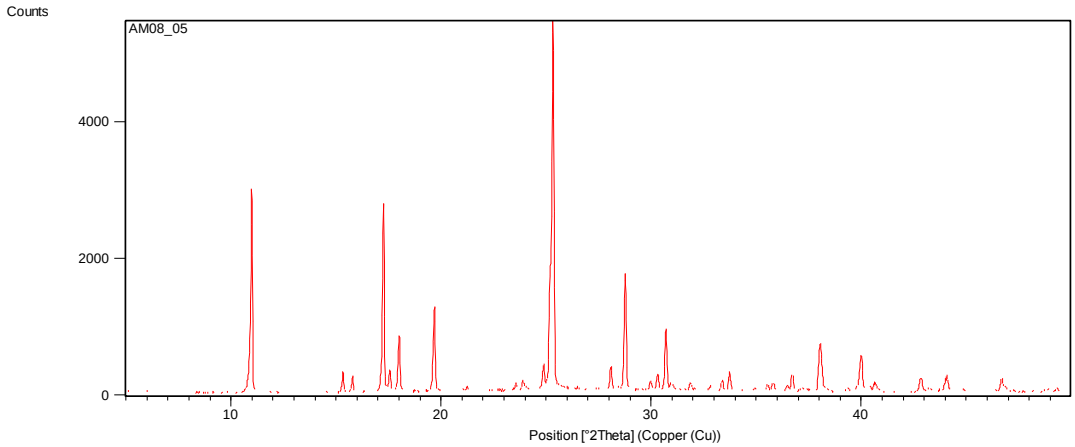

AM08_06 PAA + Salicylic acid crystallised in diethyl ether at room temperature

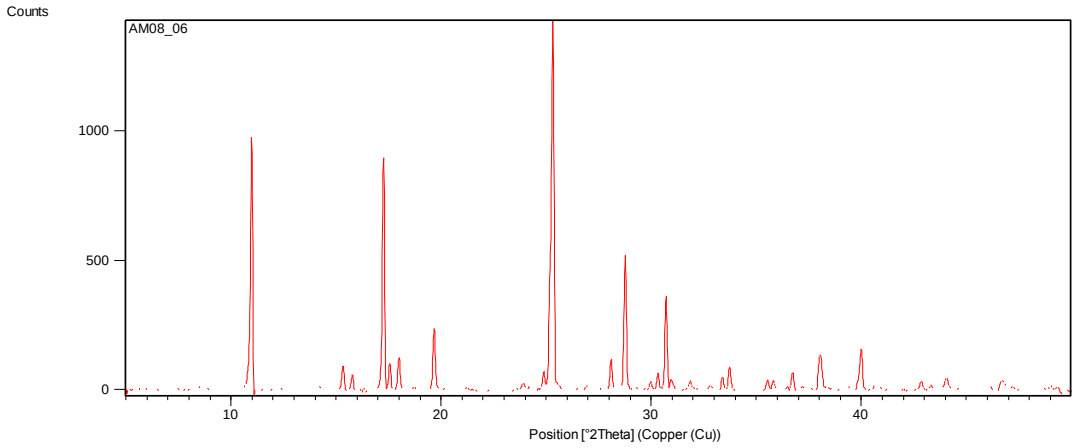

AM08_07 PAA + Salicylic acid crystallised in ethyl acetate at 4°C

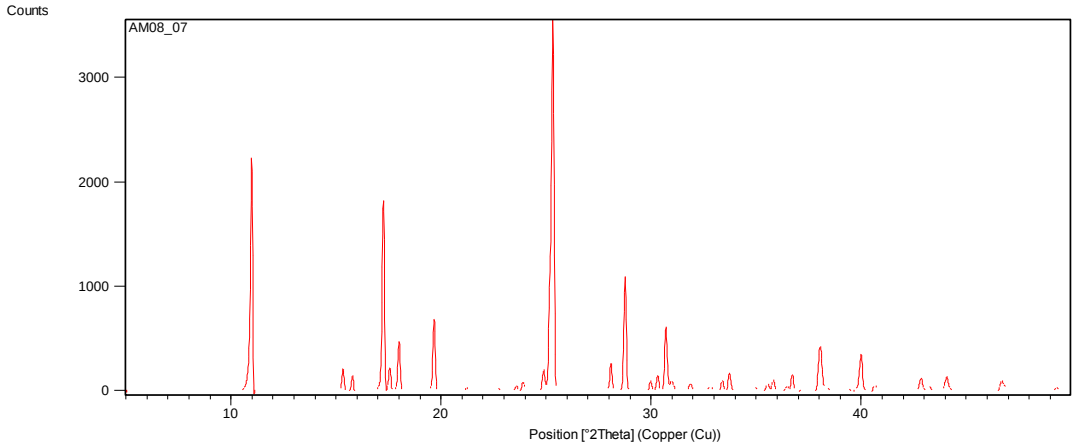

AM08_08 PAA + Salicylic acid crystallised in ethyl acetate at room temperature

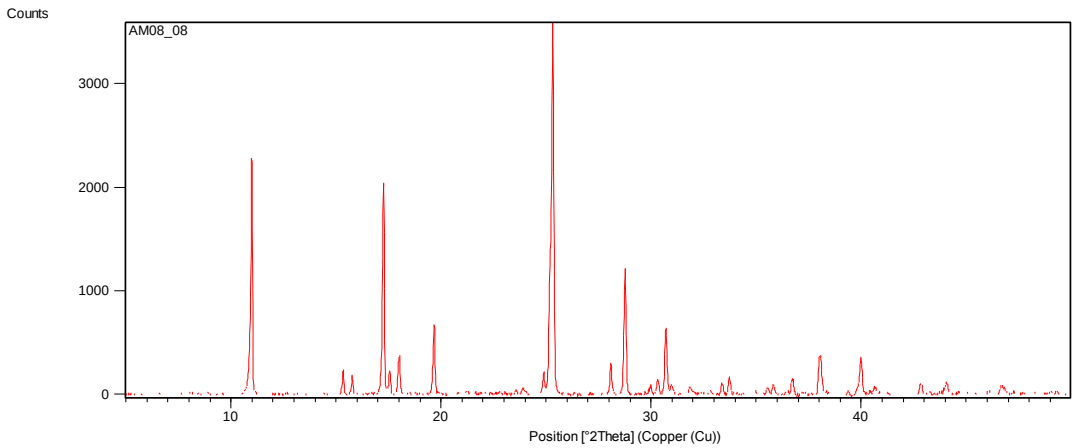

AM08_09 PAA + Salicylic acid crystallised in acetonitrile at 4°C

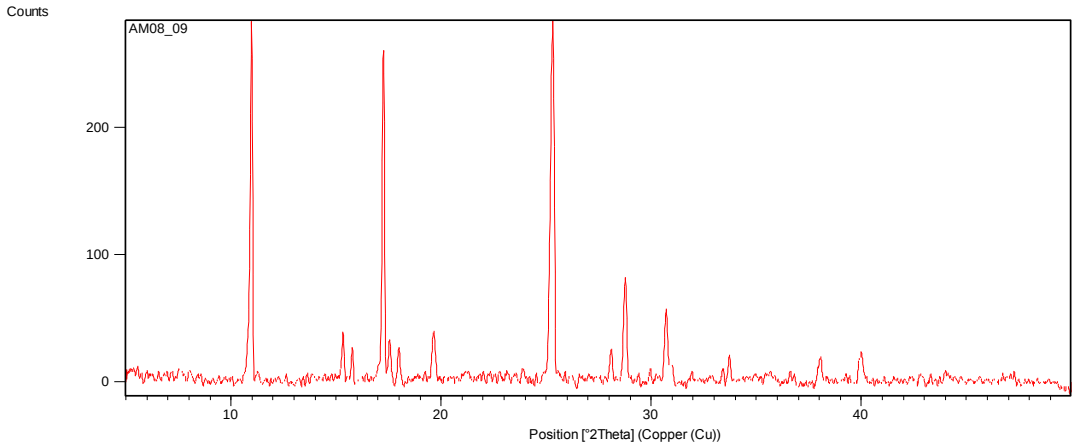

AM08_10 PAA + Salicylic acid crystallised in acetonitrile at room temperature

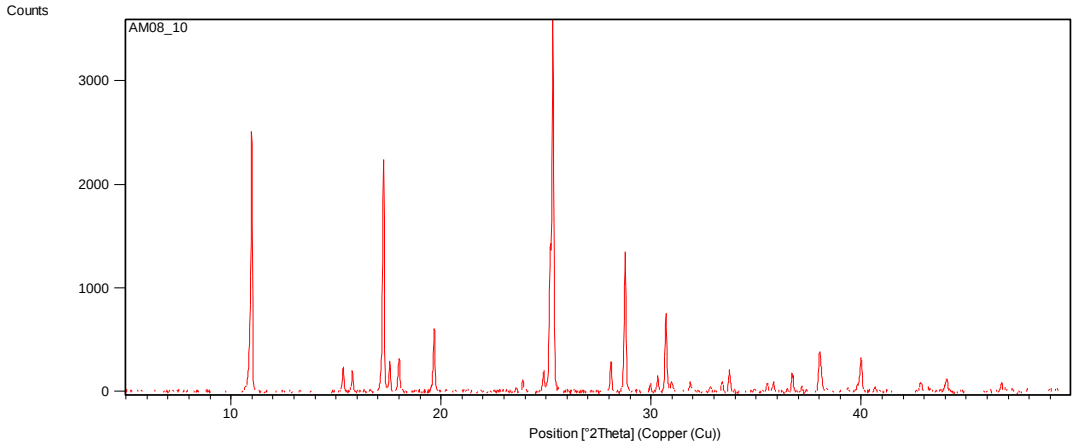

Peroxyacetic acid and 3-hydroxybenzoic acid

AM09_01 – PAA + 3-hydroxybenzoic acid crystallised in acetone at 4°C

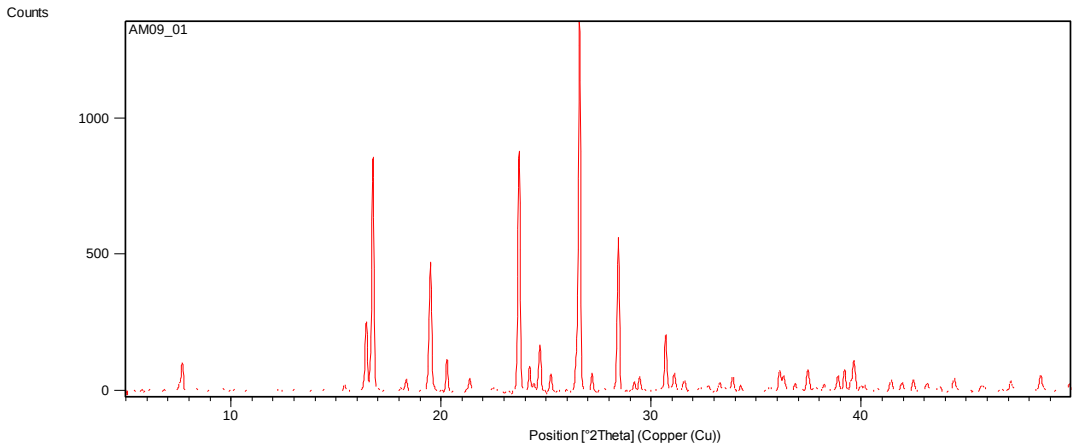

AM09_02 – PAA + 3-hydroxybenzoic acid crystallised in acetone at room temperature

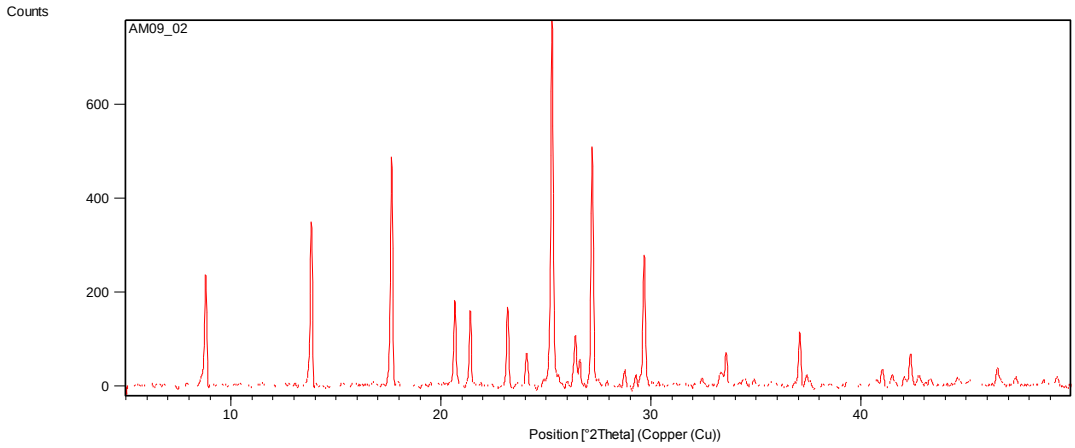

AM09_05 – PAA + 3-hydroxybenzoic acid crystallised in diethyl ether at 4°C

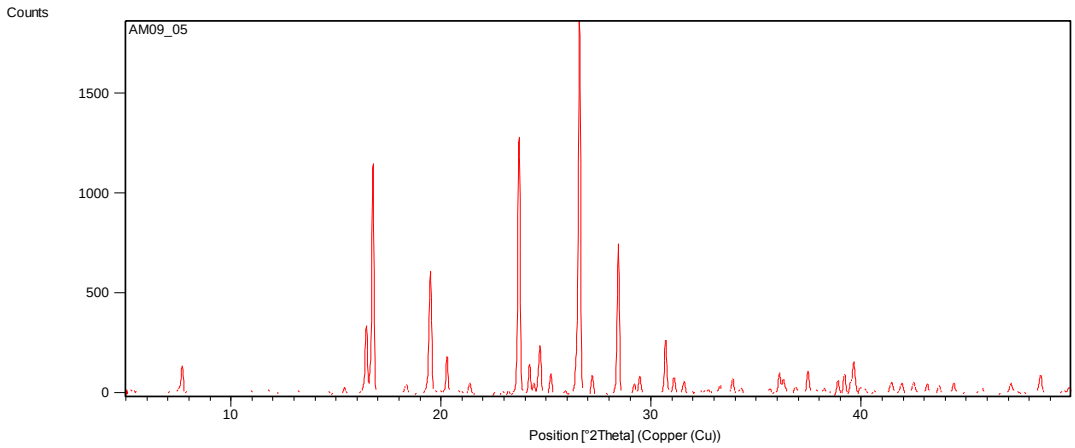

AM09_06 – PAA + 3-hydroxybenzoic acid crystallised in diethyl ether at room temperature

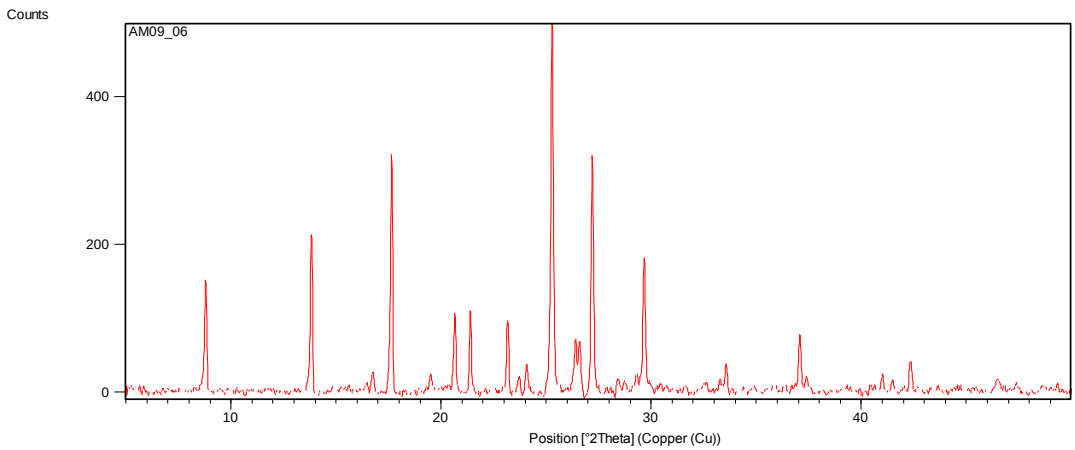

AM09_07 – PAA + 3-hydroxybenzoic acid crystallised in ethyl acetate at 4°C

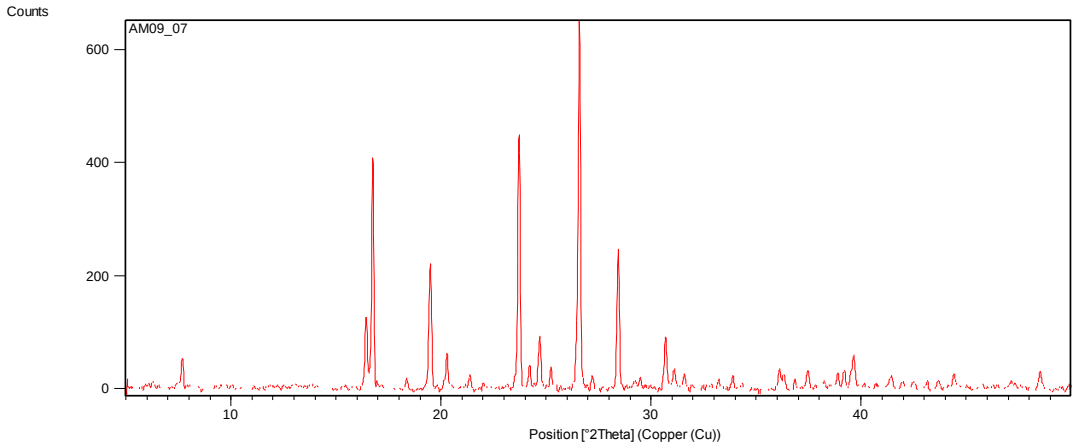

AM09_08 – PAA + 3-hydroxybenzoic acid crystallised in ethyl acetate at room temperature

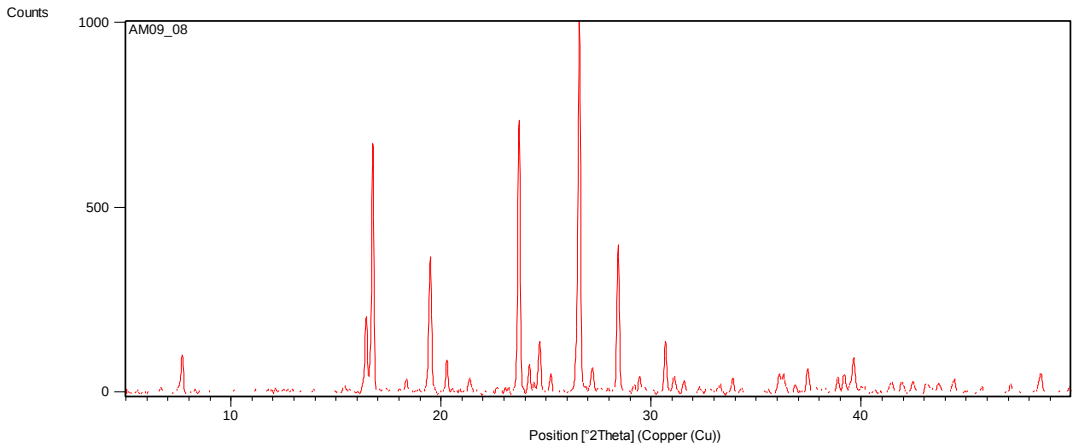

AM09_09 – PAA + 3-hydroxybenzoic acid crystallised in acetonitrile at 4°C

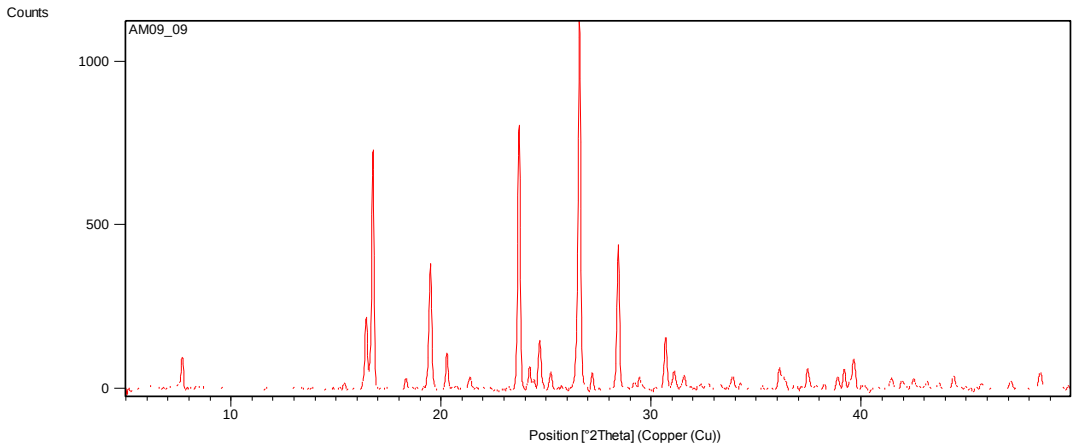

AM09_10 – PAA + 3-hydroxybenzoic acid crystallised in acetonitrile at room temperature

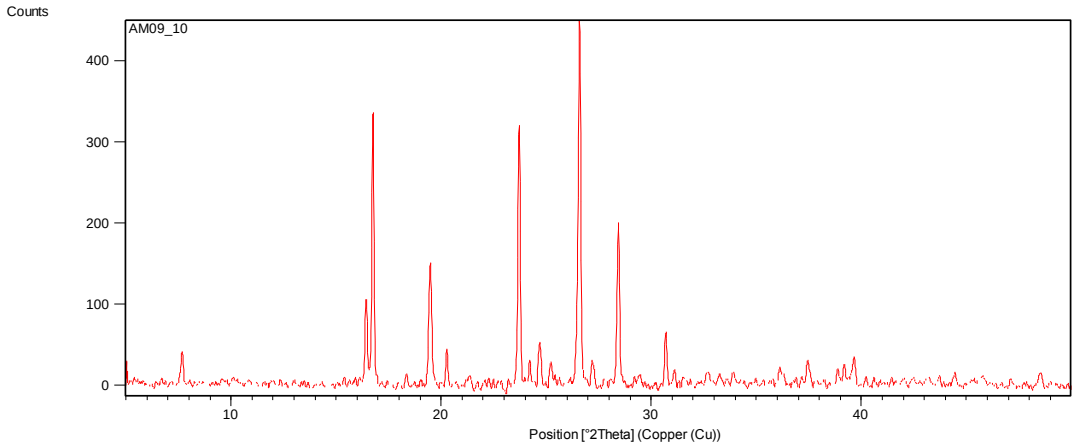

Peroxyacetic acid and Malonic acid

AM18_01 – PAA + Malonic acid crystallised in acetone at 4°C

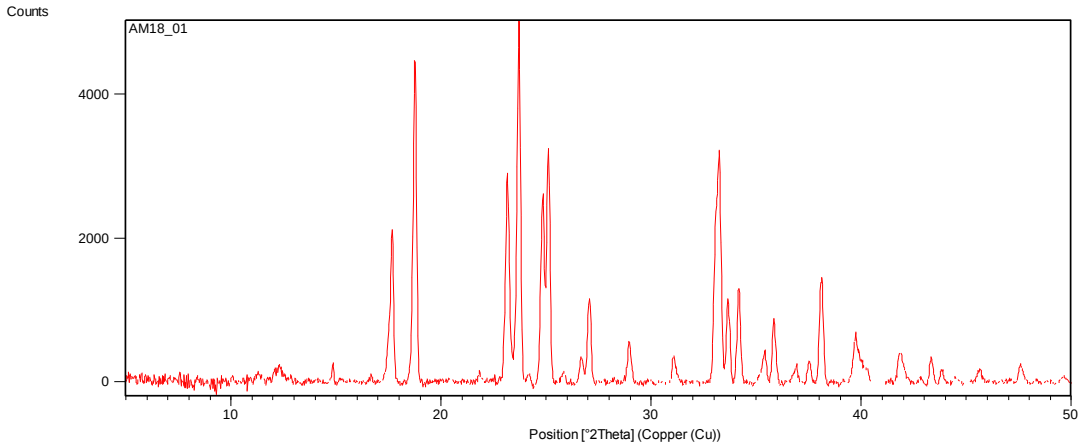

AM18_02 – PAA + Malonic acid crystallised in acetone at room temperature

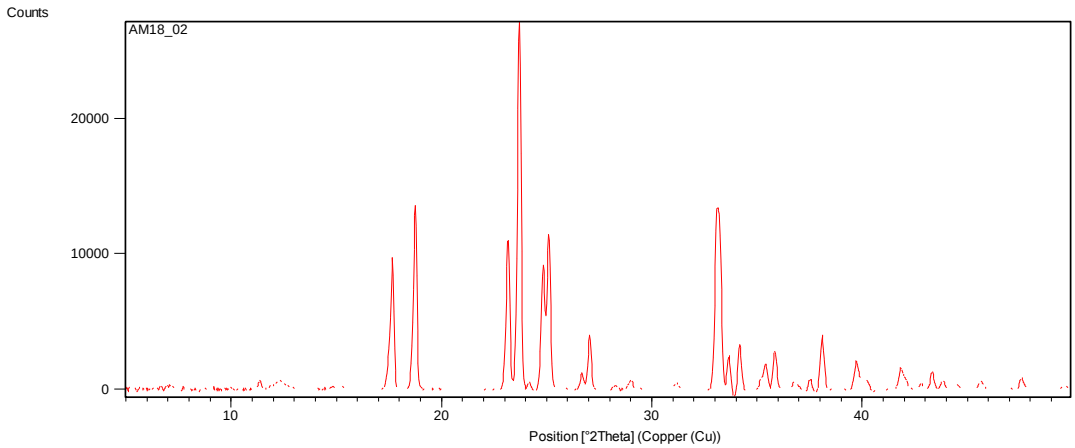

AM18_03 – PAA + Malonic acid crystallised in acetone at 4°C

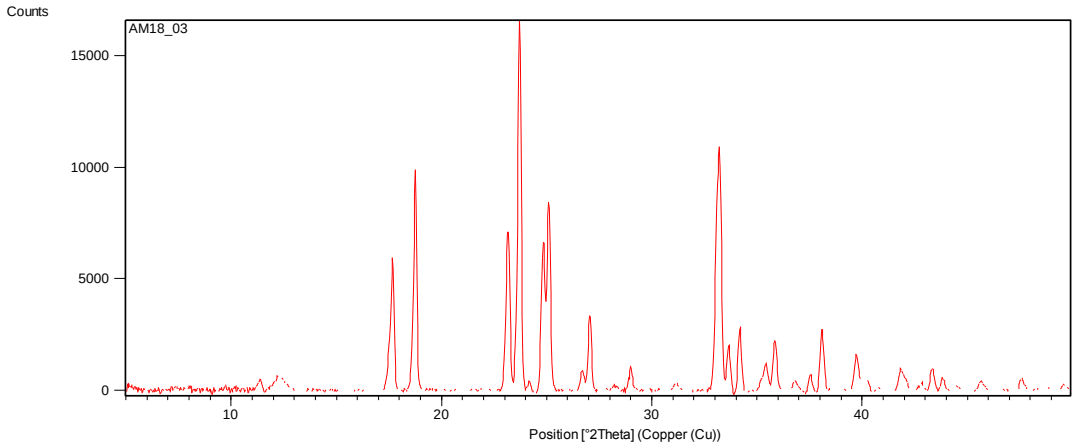

AM18_04 – PAA + Malonic acid crystallised in acetone at room temperature

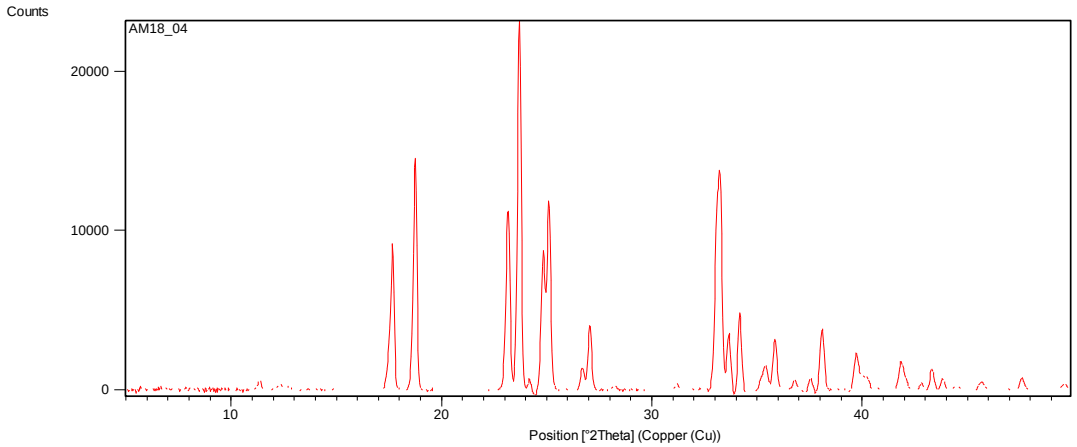

AM18_05 – PAA + Malonic acid crystallised in acetone at 4°C

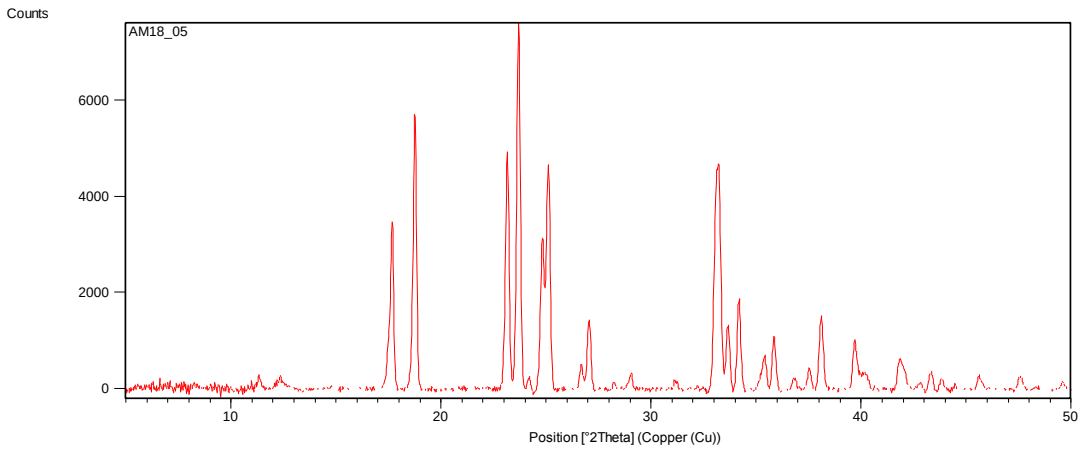

AM18_06 – PAA + Malonic acid crystallised in acetone at room temperature

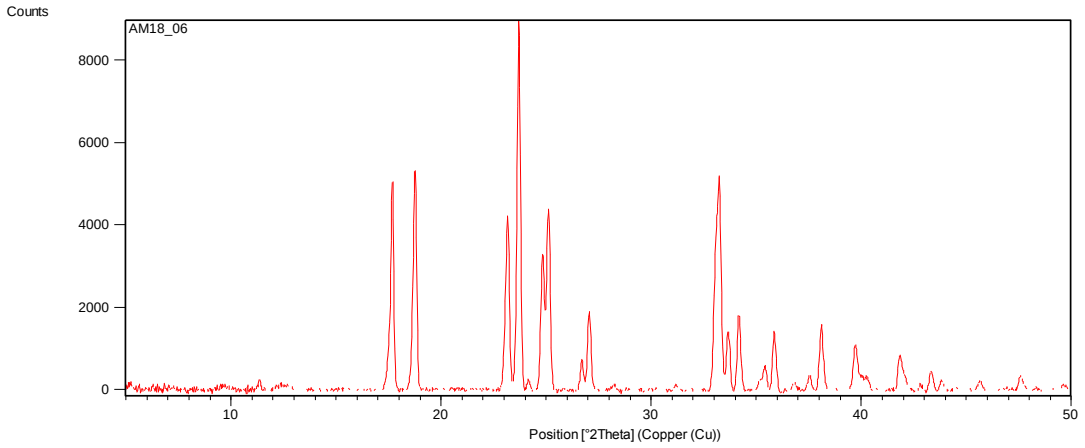

AM18_07 – PAA + Malonic acid crystallised in acetone at 4°C

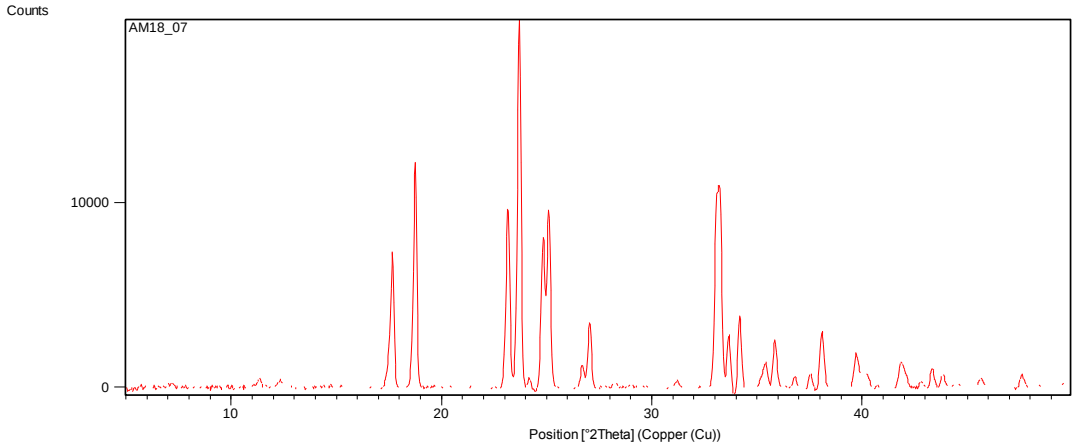

AM18_08 – PAA + Malonic acid crystallised in acetone at room temperature

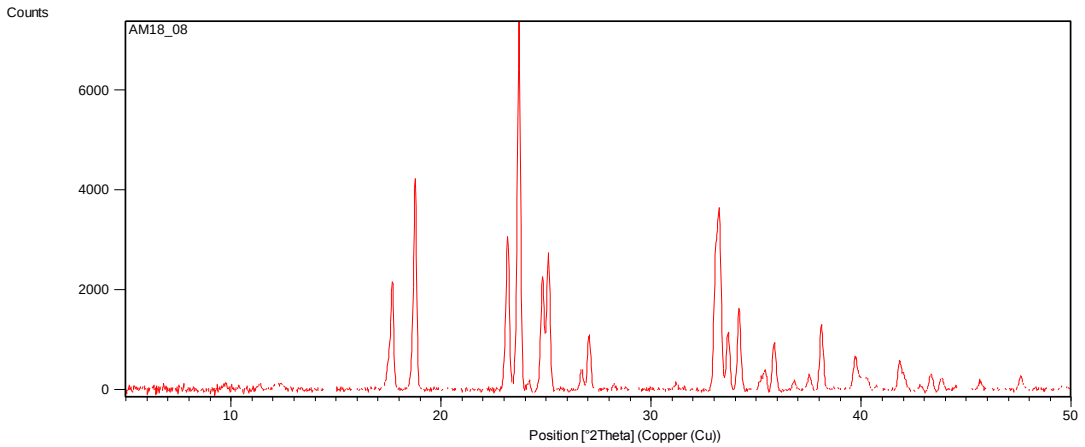

Peroxyacetic acid and oxalic acid

AM19_01 – PAA + oxalic acid crystallised in acetone at room temperature

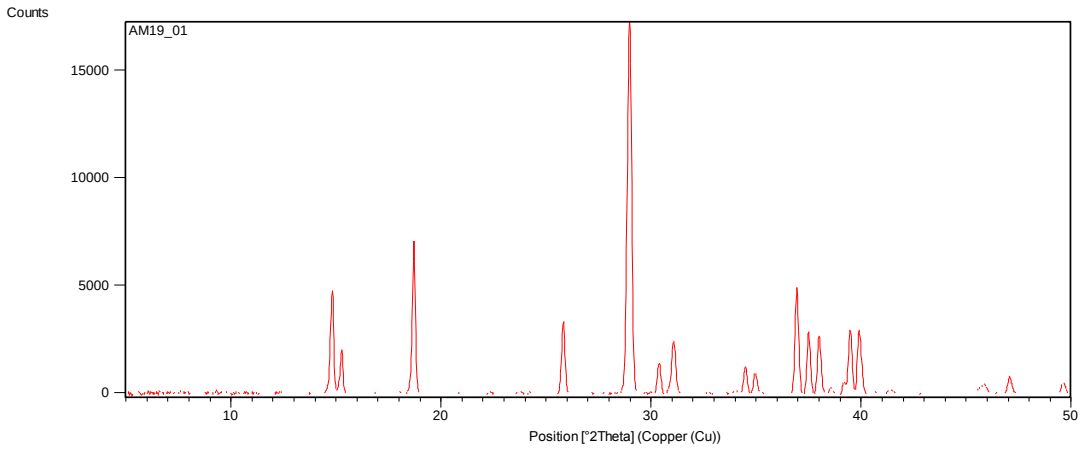

AM19_02 – PAA + oxalic acid crystallised in acetone at 4°C

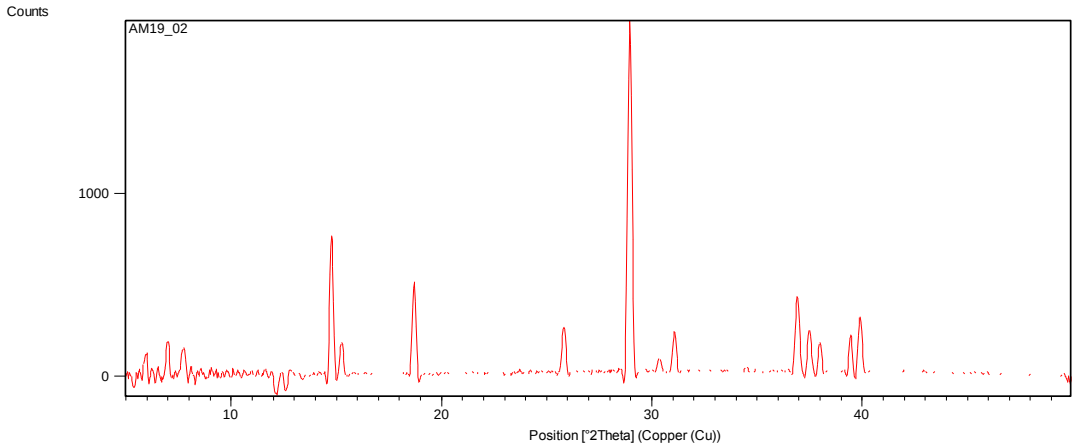

M19_05 – PAA + oxalic acid crystallised in diethyl ether at room temperature

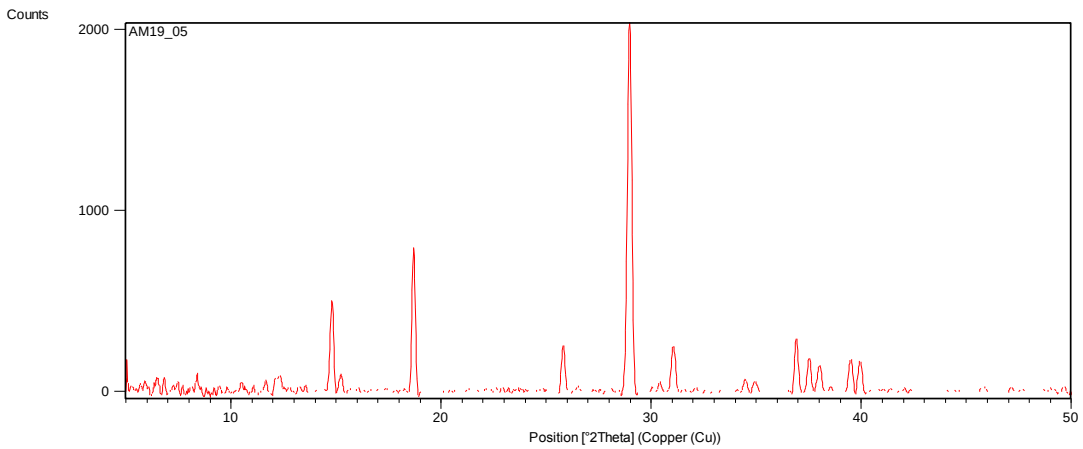

AM19_06 – PAA + oxalic acid crystallised in diethyl ether at 4°C

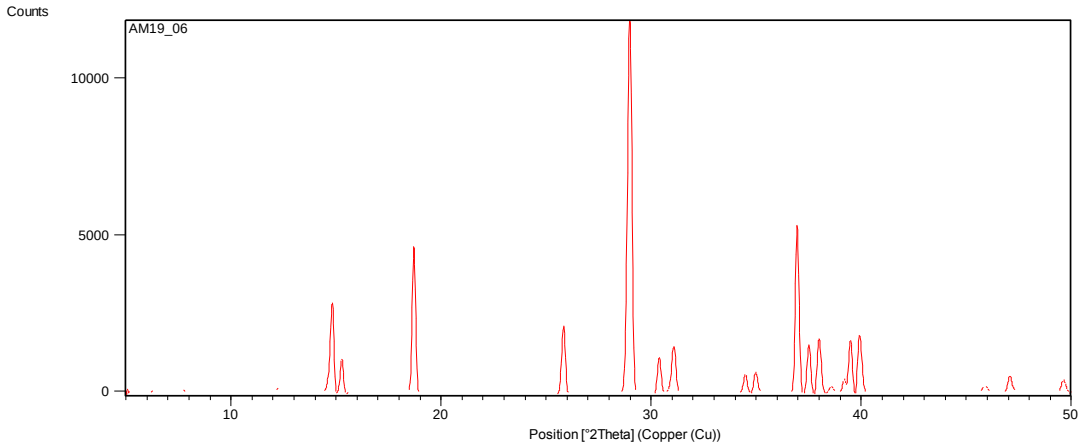

AM19_07 – PAA + oxalic acid crystallised in ethyl acetate at room temperature

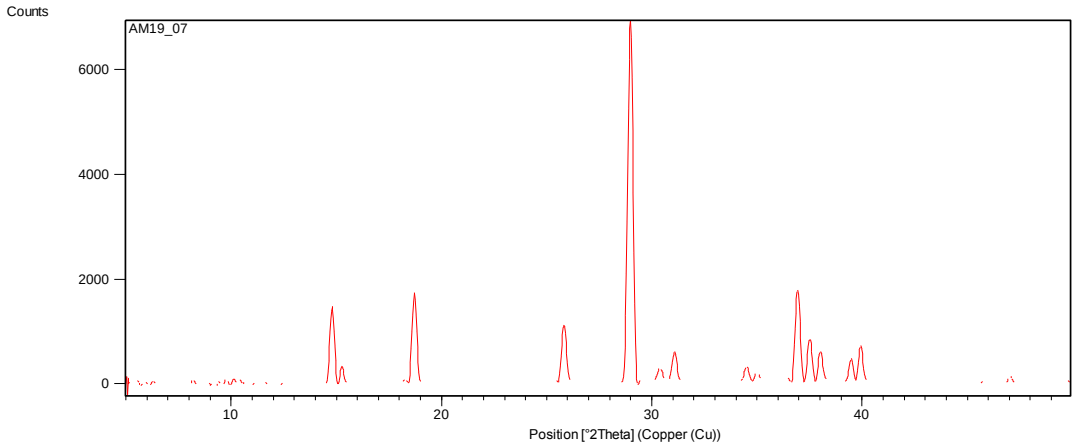

MCPBA and 2-chlorobenzoic acid

AM10_01 MCPBA + 2-chlorobenzoic acid crystallised in acetone at room temperature

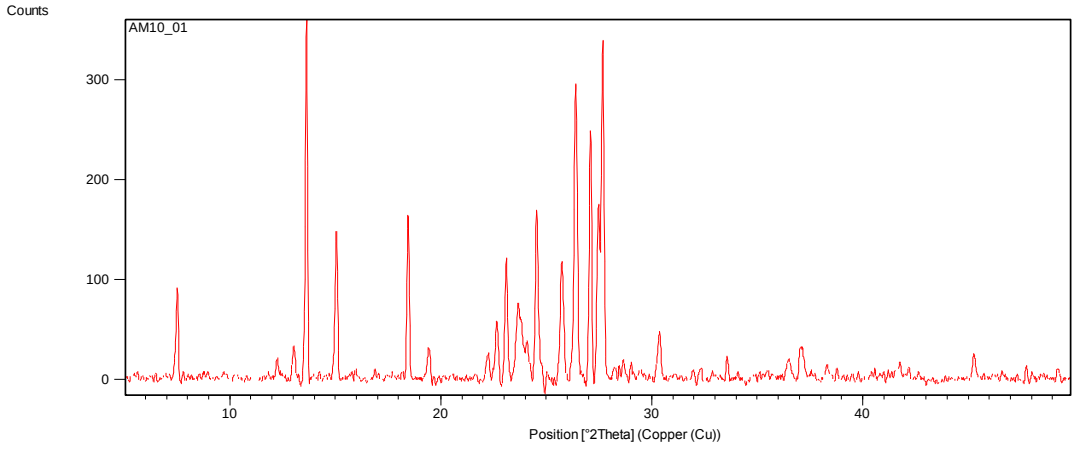

AM10_02 MCPBA + 2-chlorobenzoic acid crystallised in acetone at 4°C

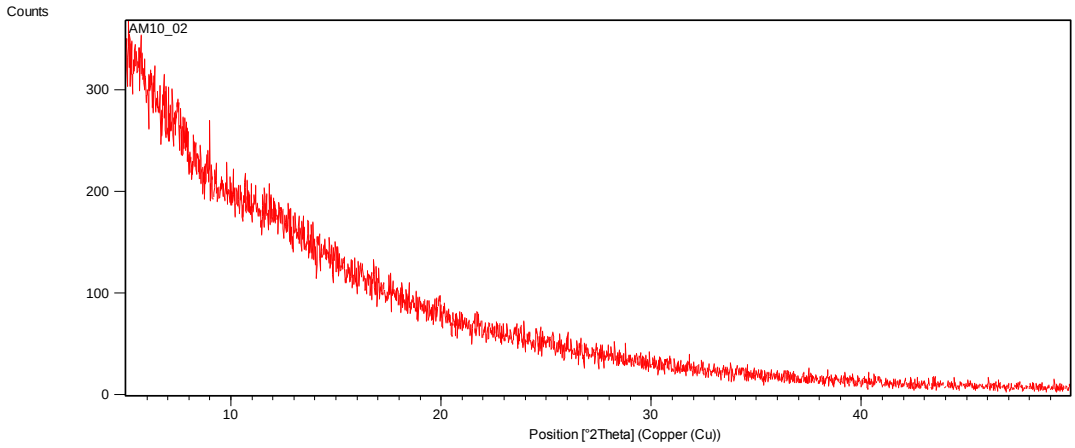

AM10_03 MCPBA + 2-chlorobenzoic acid crystallised in chloroform at room temperature

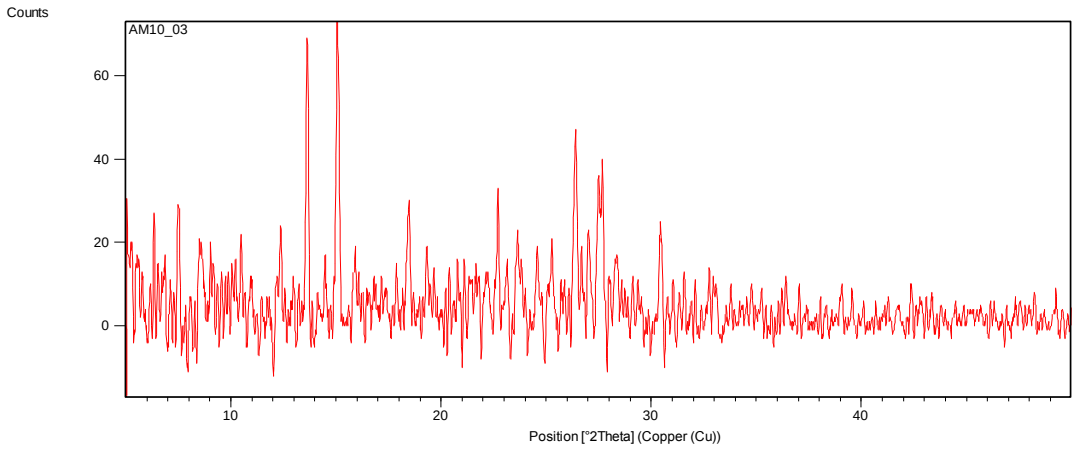

AM10_04 MCPBA + 2-chlorobenzoic acid crystallised in chloroform at 4°C

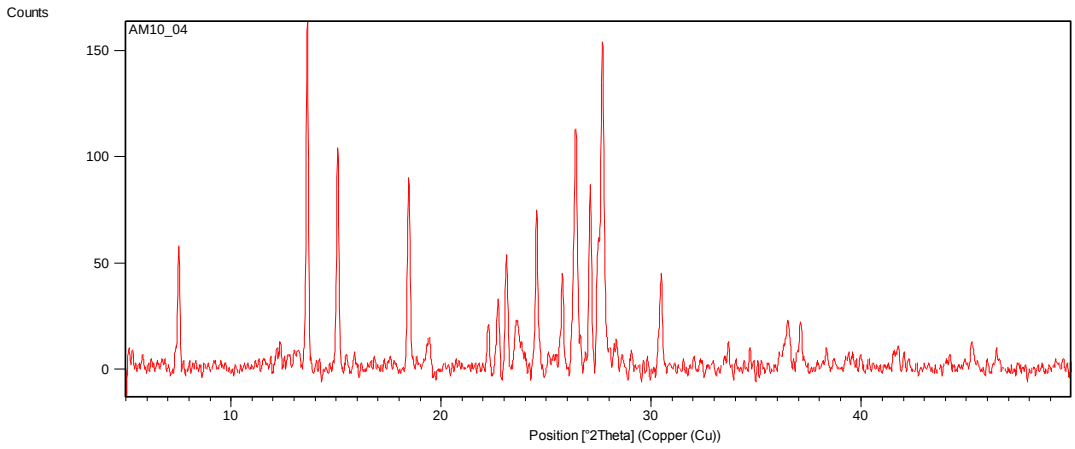

AM10_05 MCPBA + 2-chlorobenzoic acid crystallised in diethyl ether at room temperature

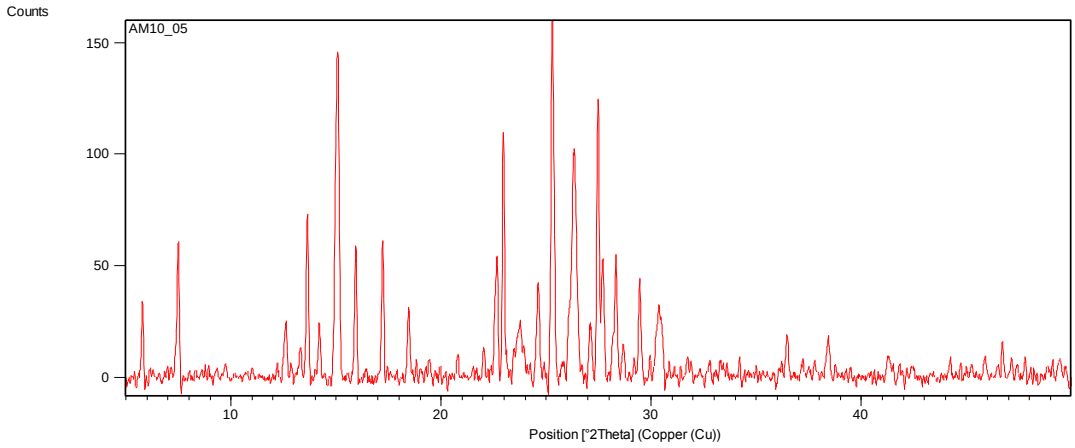

AM10_06 MCPBA + 2-chlorobenzoic acid crystallised in diethyl ether at 4°C

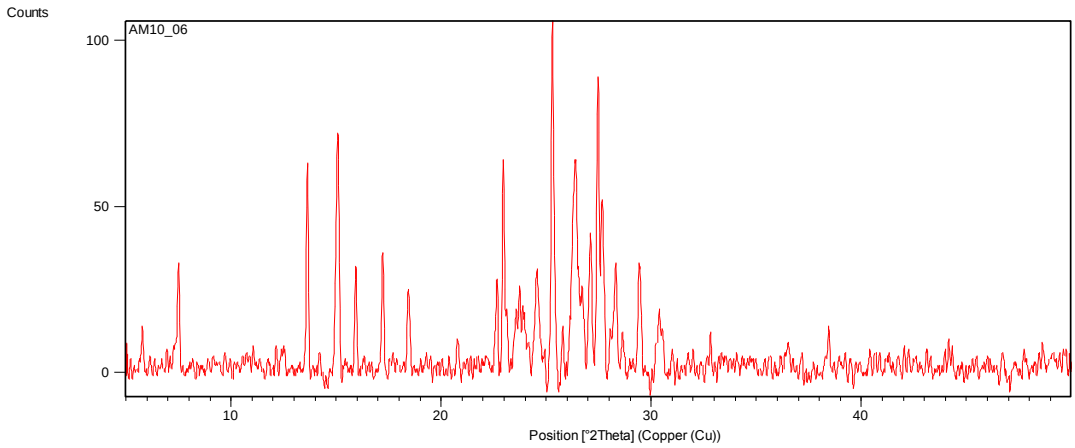

AM10_07 MCPBA + 2-chlorobenzoic acid crystallised in ethyl acetate at room temperature

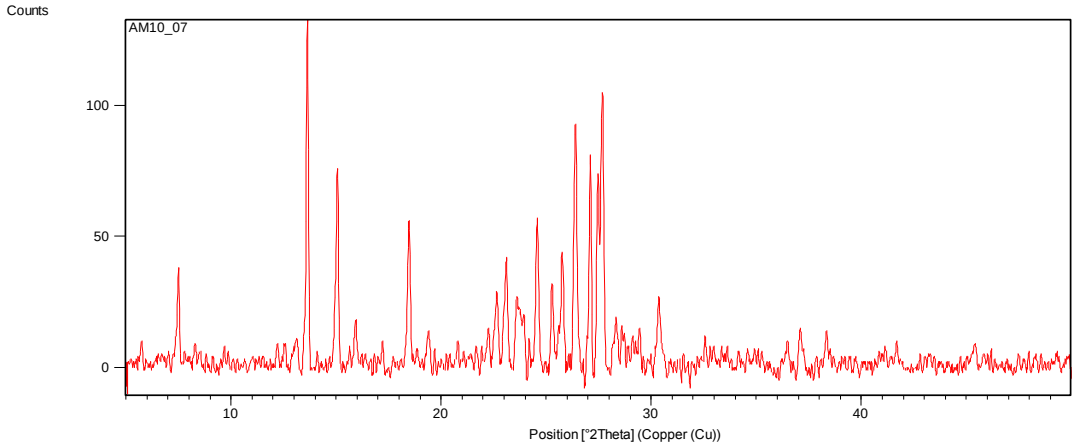

AM10_08 MCPBA + 2-chlorobenzoic acid crystallised in ethyl acetate at 4°C

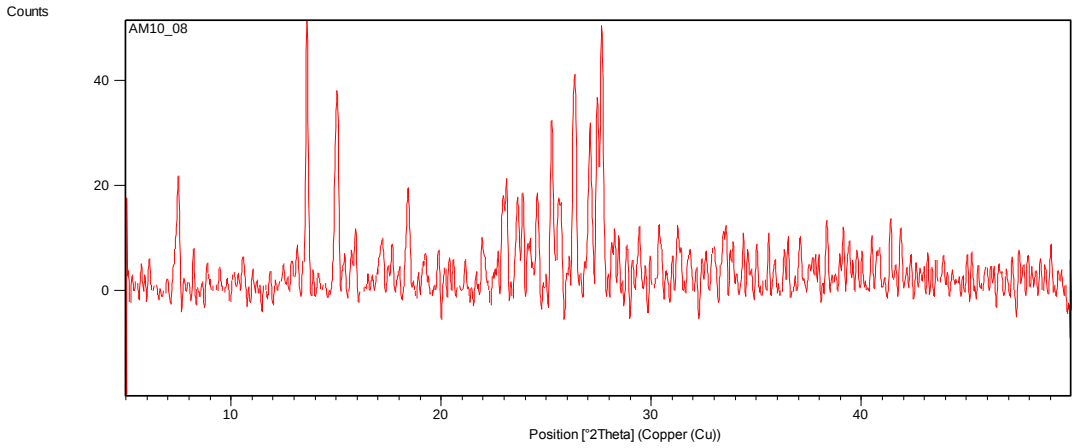

MCPBA and 3-chlorobenzoic acid

AM10_01 MCPBA + 2-chlorobenzoic acid crystallised in acetone at room temperature

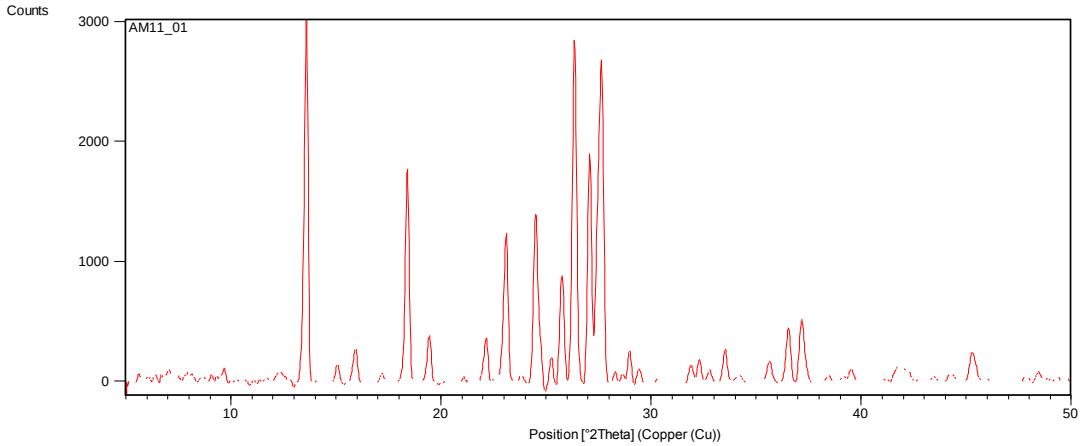

AM10_02 MCPBA + 2-chlorobenzoic acid crystallised in acetone at 4°C

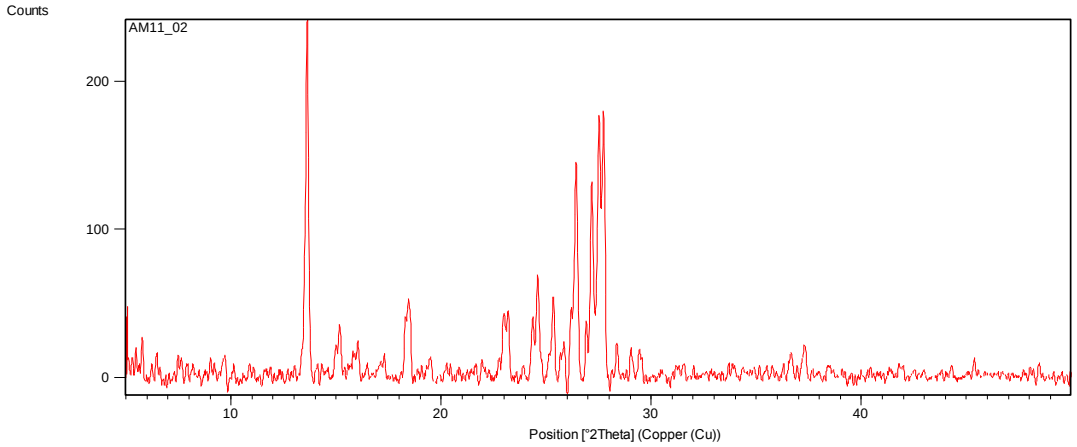

AM10_03 MCPBA + 2-chlorobenzoic acid crystallised in chloroform at room temperature

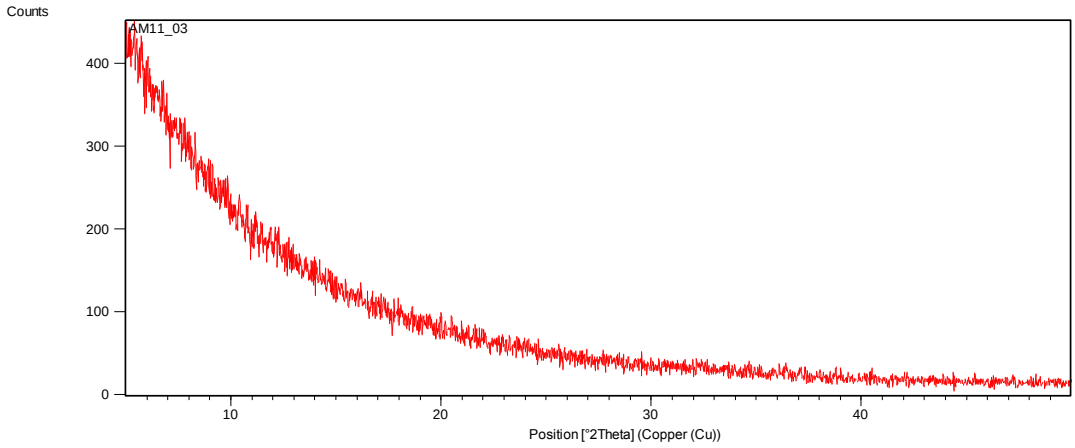

AM10_04 MCPBA + 2-chlorobenzoic acid crystallised in chloroform at 4°C

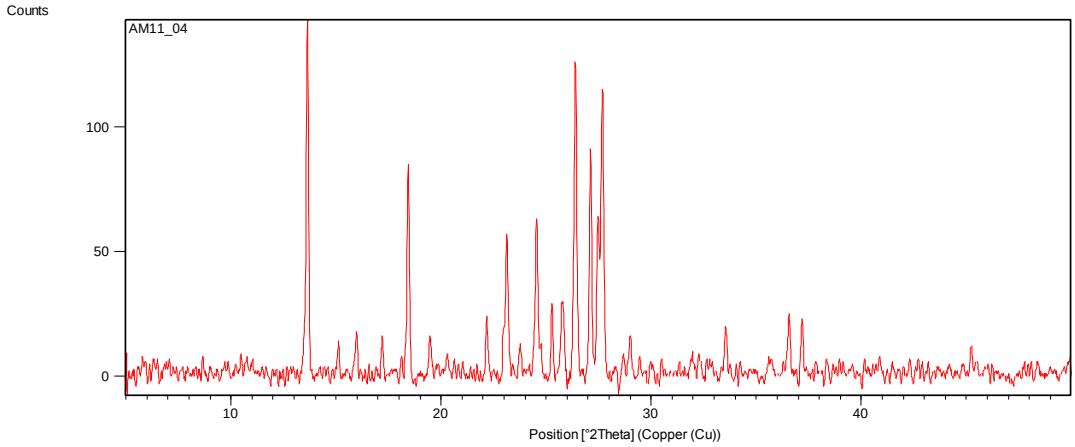

AM10_05 MCPBA + 2-chlorobenzoic acid crystallised in diethyl ether at room temperature

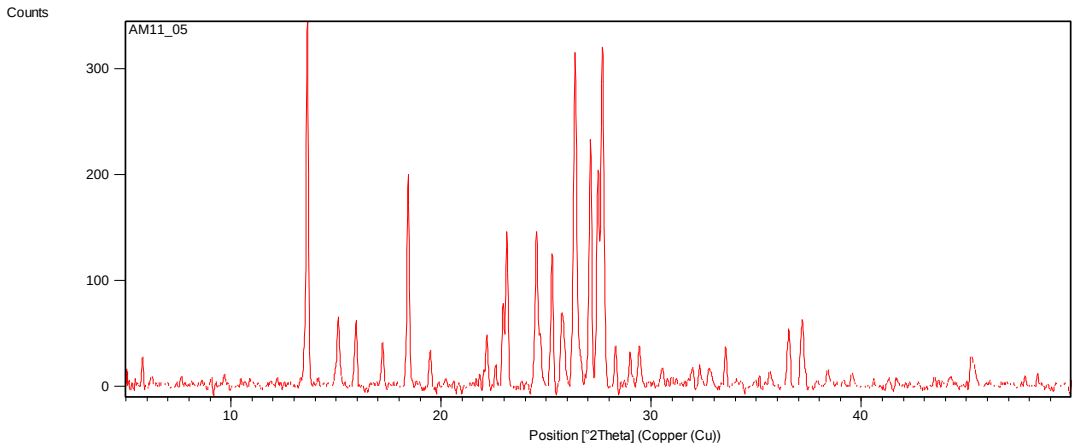

AM10_06 MCPBA + 2-chlorobenzoic acid crystallised in diethyl ether at 4°C

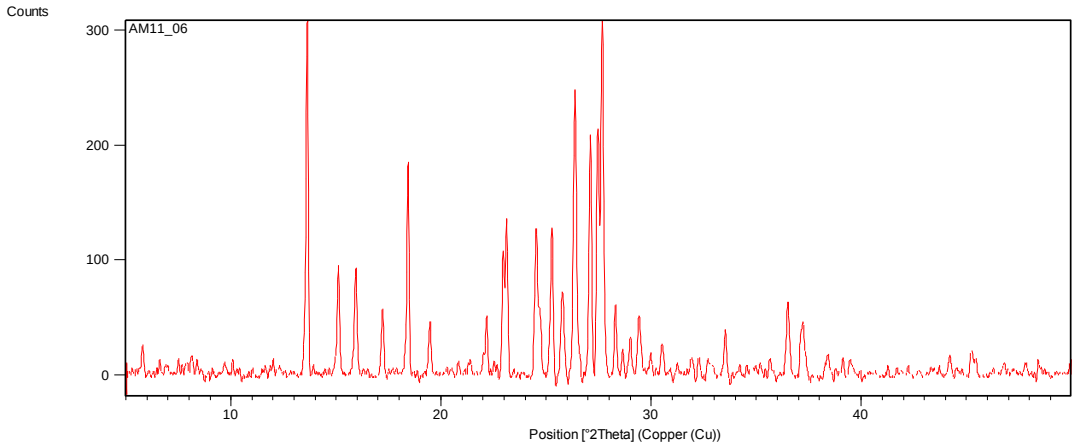

AM10_07 MCPBA + 2-chlorobenzoic acid crystallised in ethyl acetate at room temperature

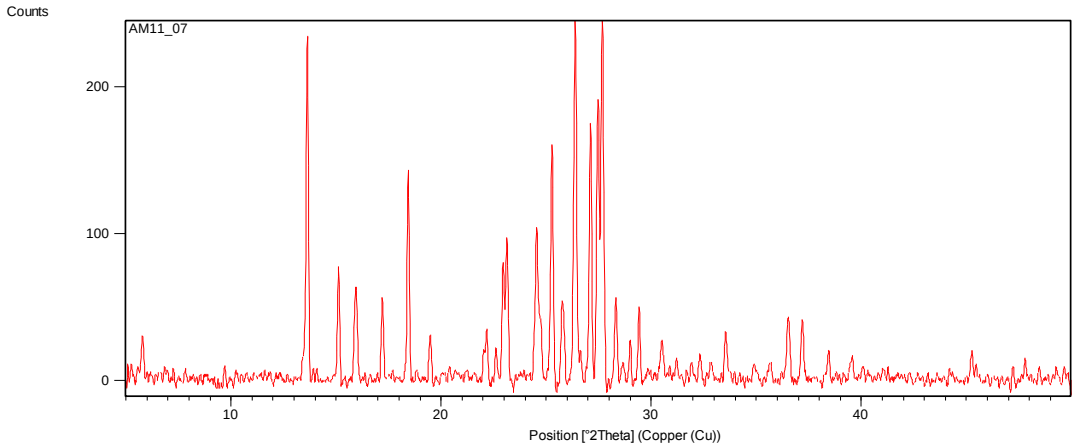

AM10_08 MCPBA + 2-chlorobenzoic acid crystallised in ethyl acetate at 4°C

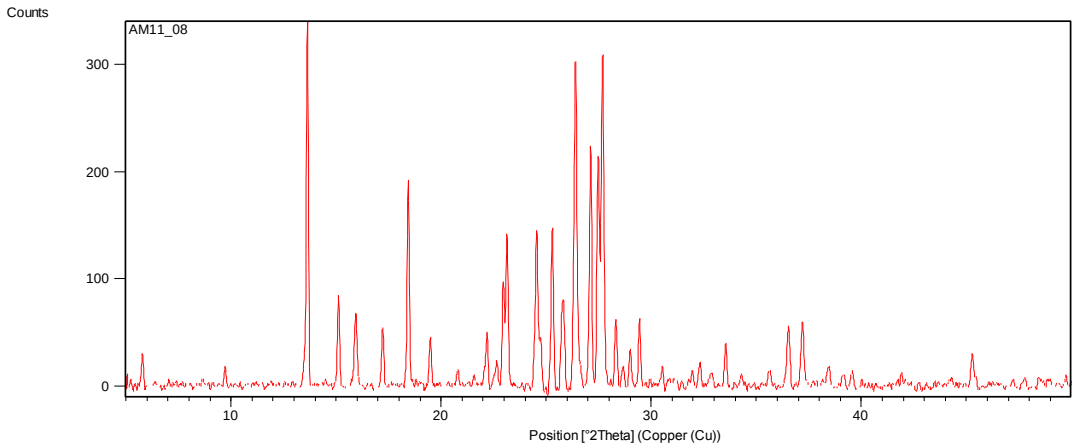

MCPBA and 4-chlorobenzoic acid

AM12_01 – MCPBA + 4-chlorobenzoic acid crystallised in acetone at room temperature

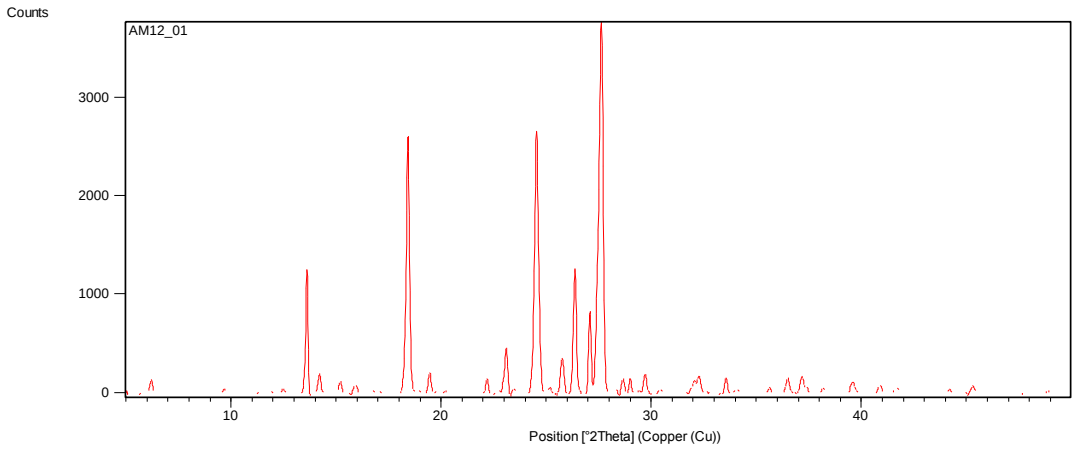

AM12_02 – MCPBA + 4-chlorobenzoic acid crystallised in acetone at 4°C

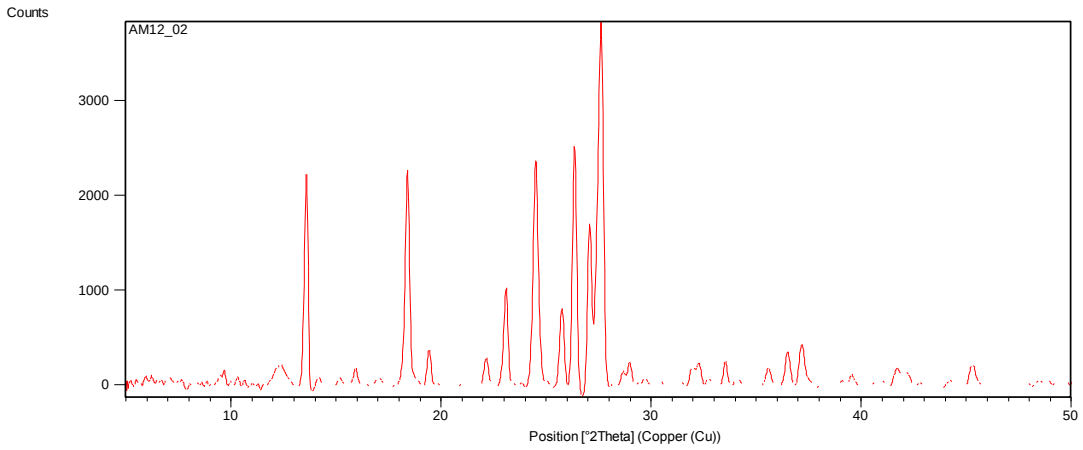

AM12_03 – MCPBA + 4-chlorobenzoic acid crystallised in chloroform at room temperature

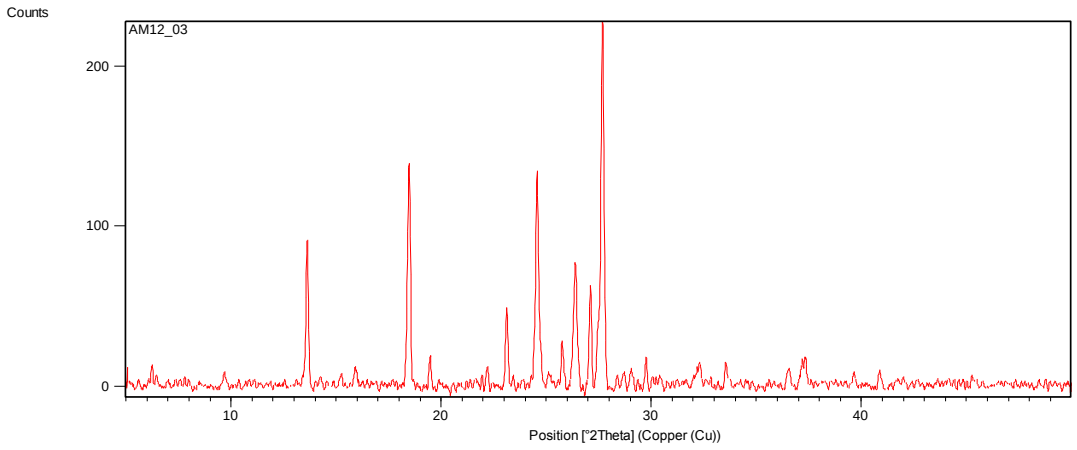

AM12_04 – MCPBA + 4-chlorobenzoic acid crystallised in chloroform at 4°C

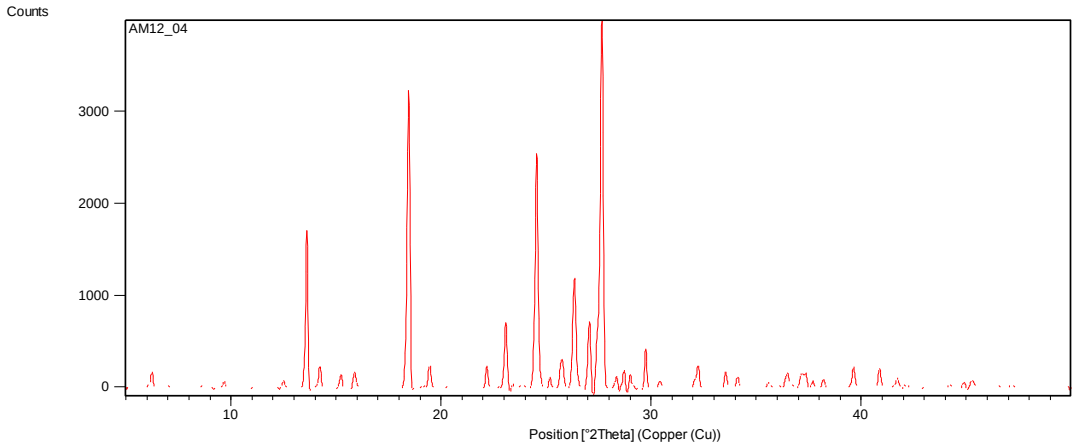

AM12_05 – MCPBA + 4-chlorobenzoic acid crystallised in diethyl ether at room temperature

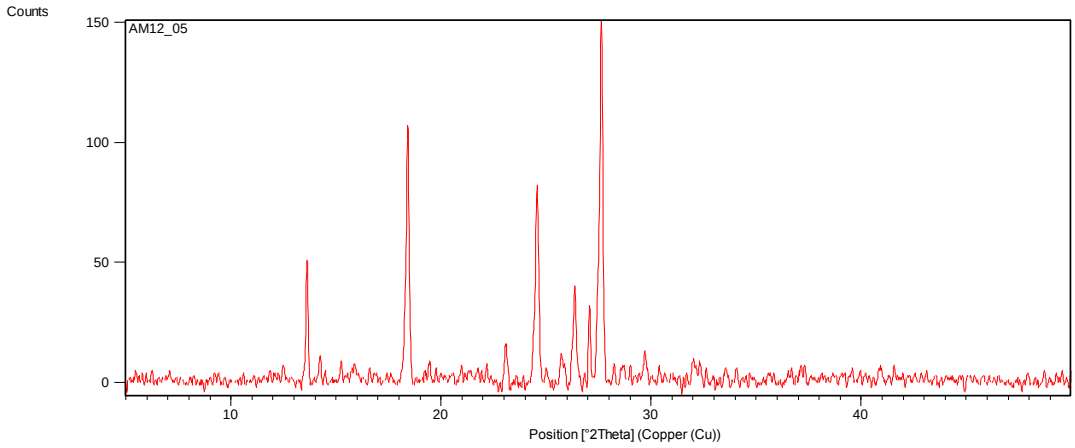

AM12_06 – MCPBA + 4-chlorobenzoic acid crystallised in diethyl ether at 4°C

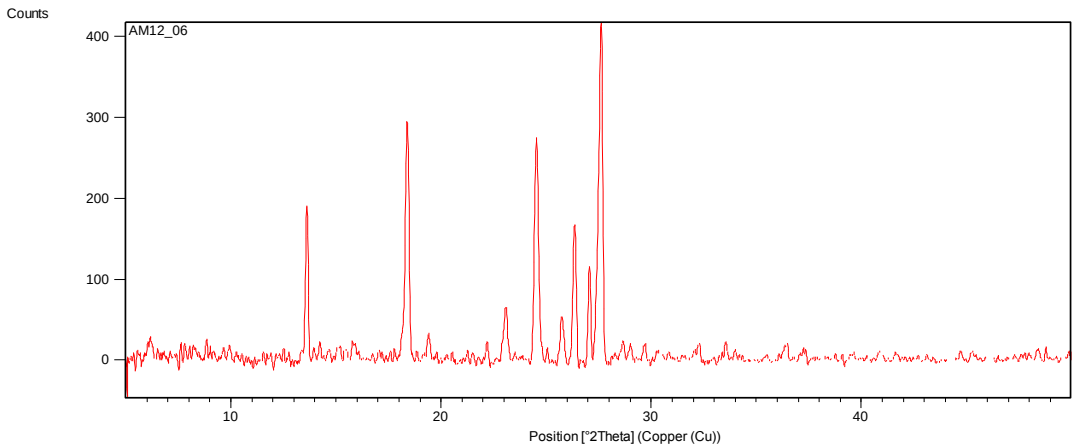

AM12_07 – MCPBA + 4-chlorobenzoic acid crystallised in ethyl acetate at room temperature

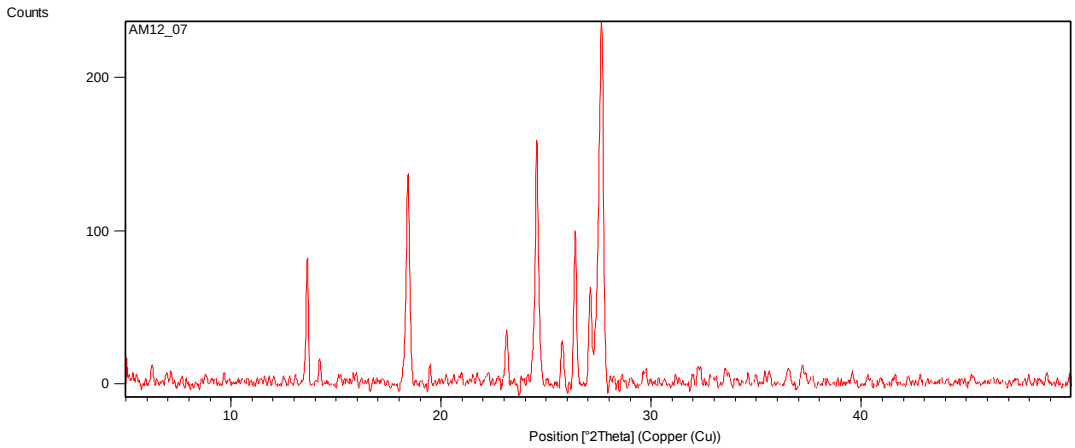

AM12_08 – MCPBA + 4-chlorobenzoic acid crystallised in ethyl acetate at 4°C

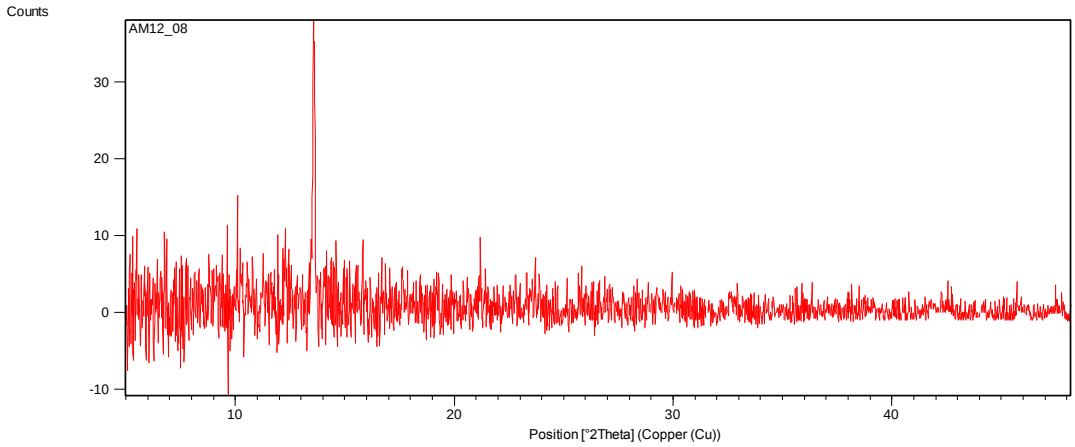

MCPBA and 1-napthaleneacetic acid

AM13_01 – MCPBA + 1-naphthaleneacetic acid crystallised in acetone at room temperature

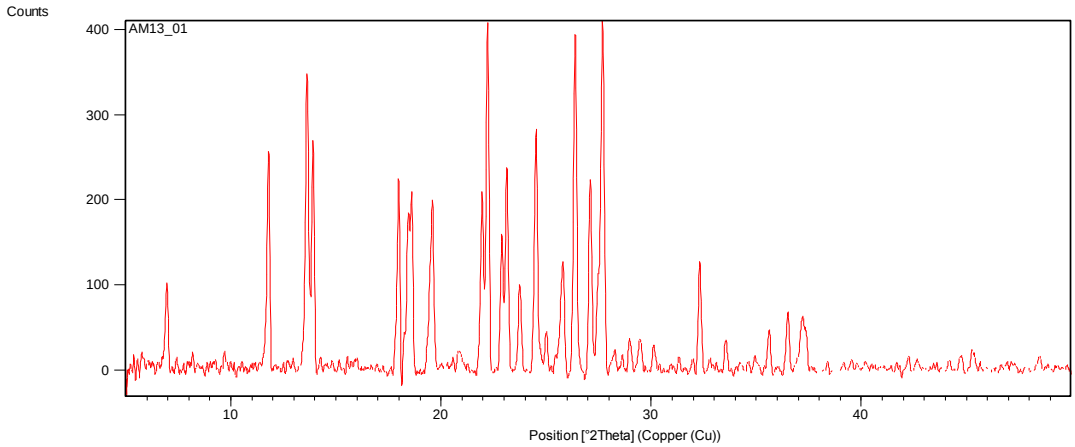

AM13_02 – MCPBA + 1-naphthaleneacetic acid crystallised in acetone at 4°C

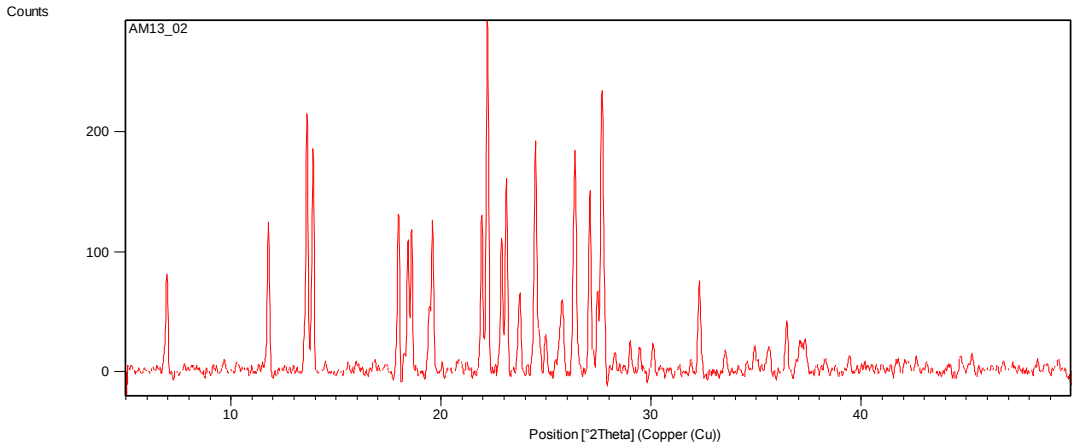

AM13_03 – MCPBA + 1-naphthaleneacetic acid crystallised in chloroform at room temperature

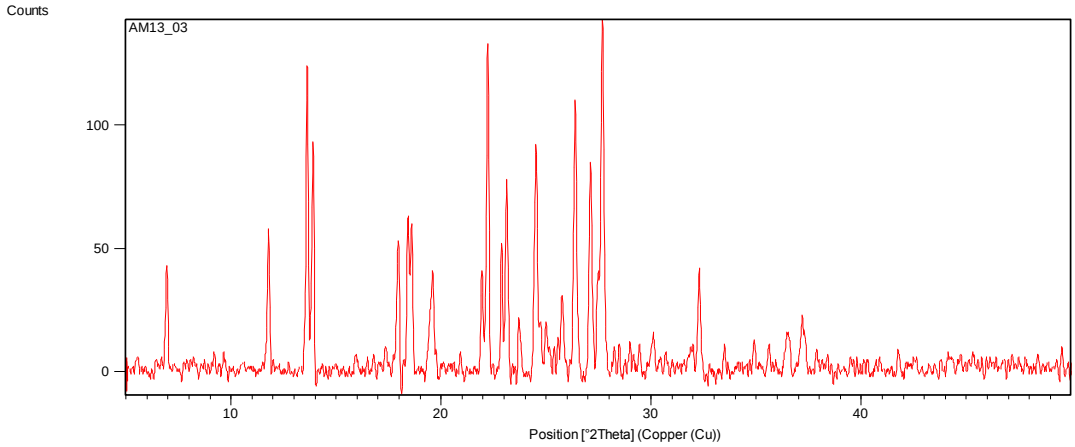

AM13_04 – MCPBA + 1-naphthaleneacetic acid crystallised in chloroform at 4°C

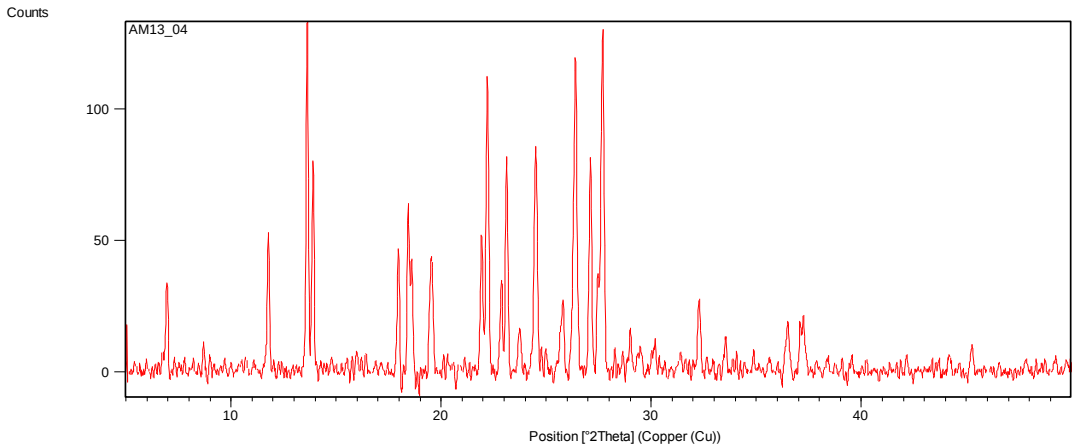

AM13_05 – MCPBA + 1-naphthaleneacetic acid crystallised in diethyl ether at room temperature

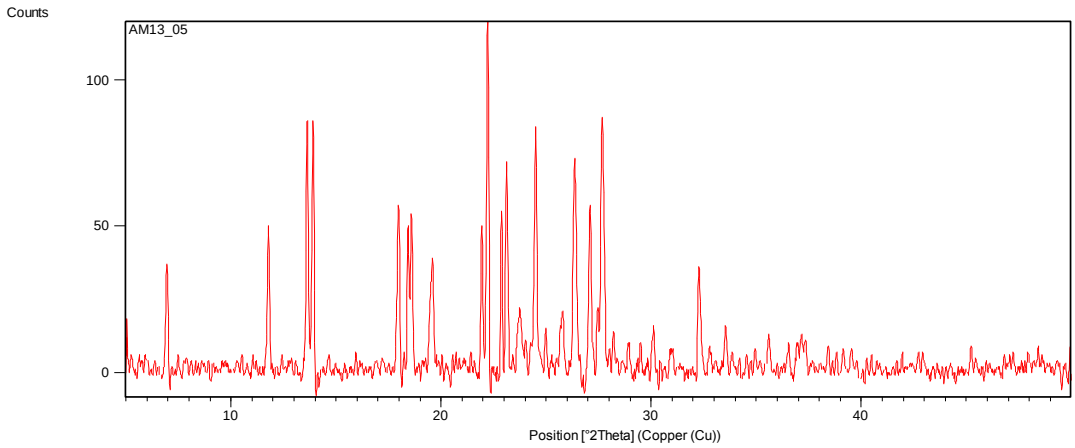

AM13_06 – MCPBA + 1-naphthaleneacetic acid crystallised in diethyl ether at 4°C

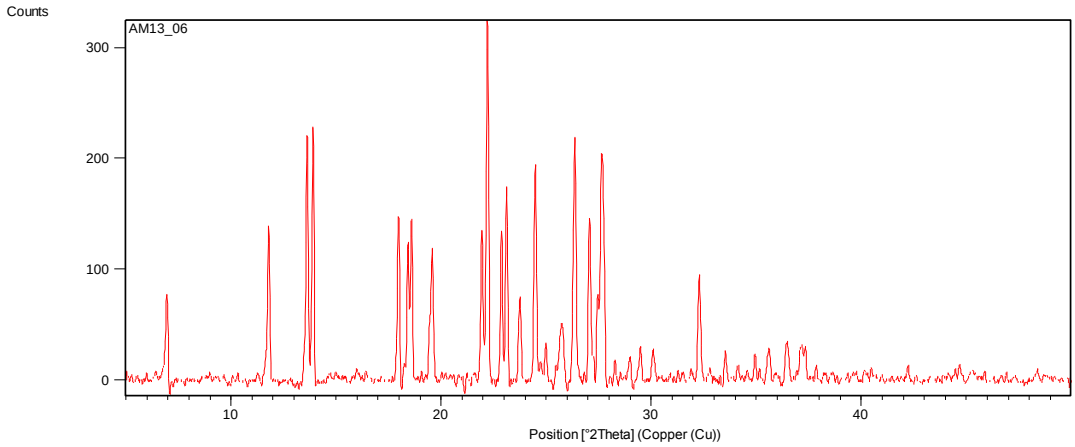

AM13_07 – MCPBA + 1-naphthaleneacetic acid crystallised in ethyl acetate at room temperature

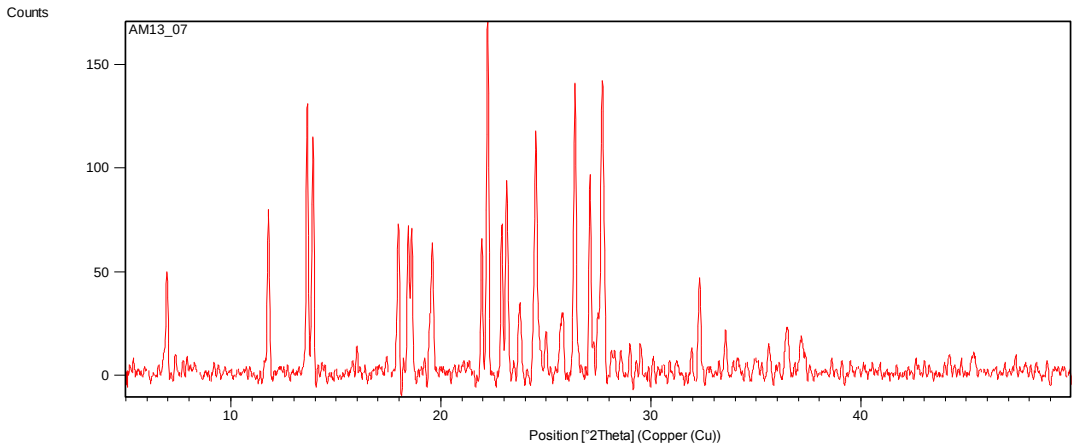

AM13_08 – MCPBA + 1-naphthaleneacetic acid crystallised in ethyl acetate at 4°C

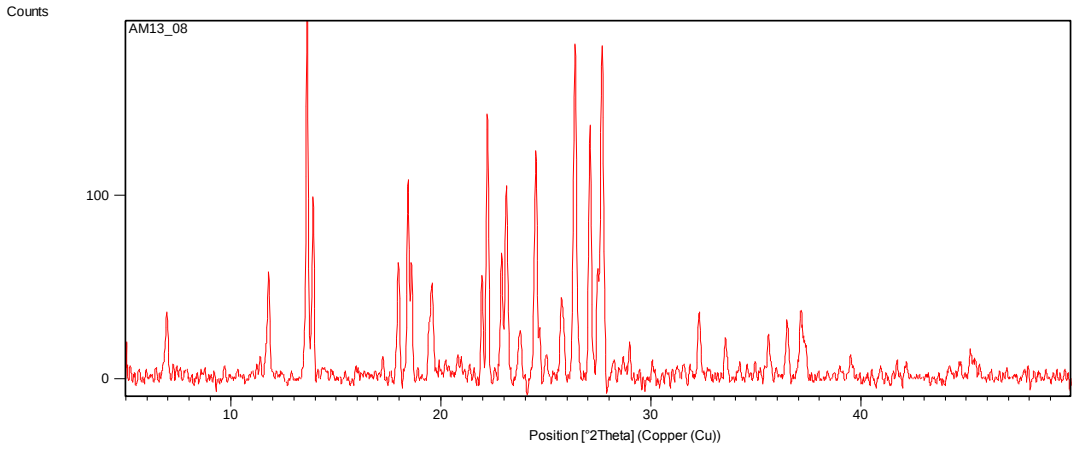

MCPBA and 2-hydroxybenzoic acid

AM14_01 – MCPBA + salicylic acid crystallised in acetone at room temperature

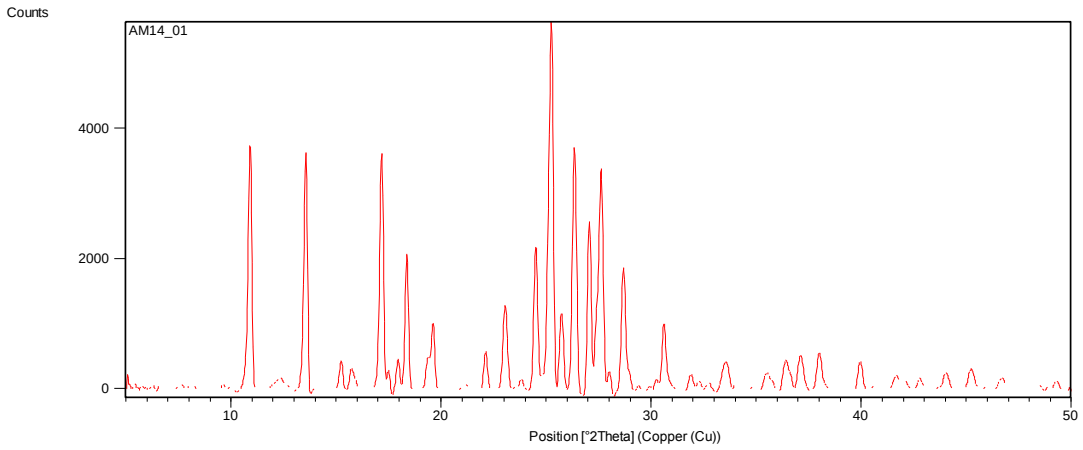

AM14_02 – MCPBA + salicylic acid crystallised in acetone at 4°C

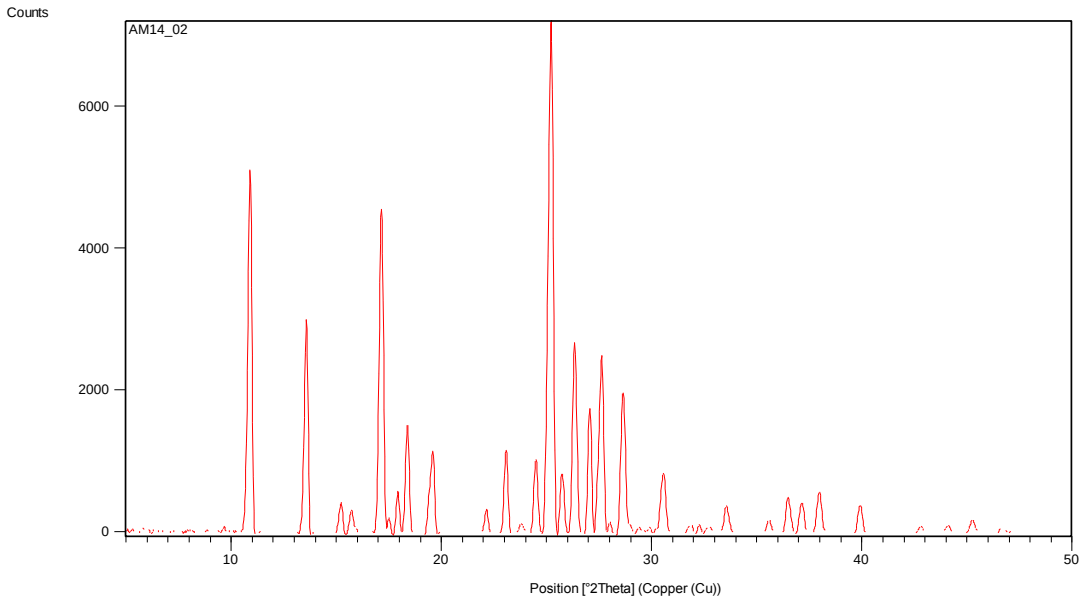

AM14_03 – MCPBA + salicylic acid crystallised in chloroform at room temperature

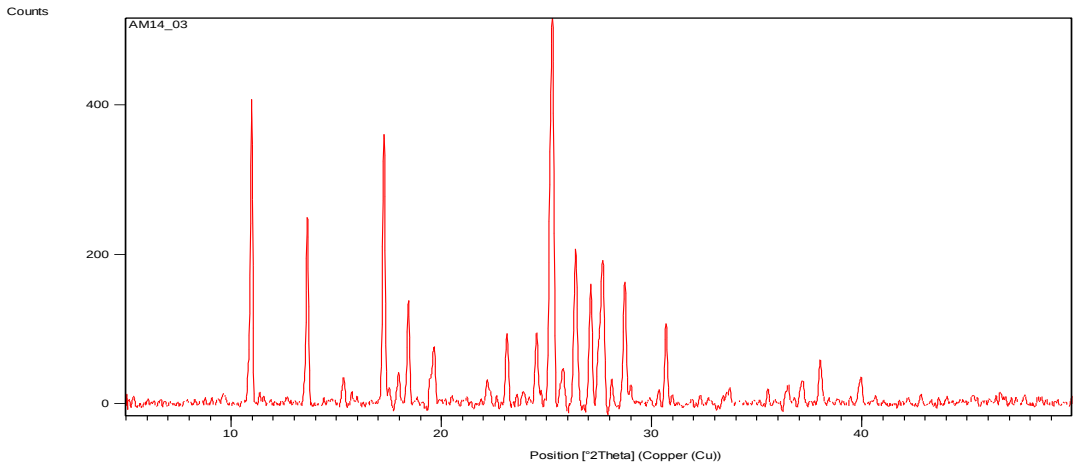

AM14_04 – MCPBA + salicylic acid crystallised in chloroform at 4°C

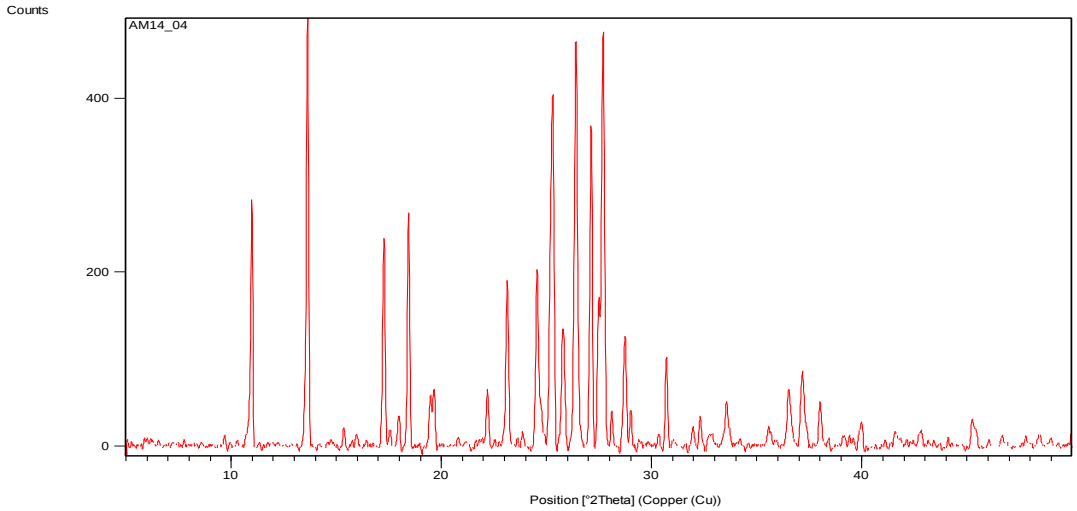

AM14_05 – MCPBA + salicylic acid crystallised in diethyl ether at room temperature

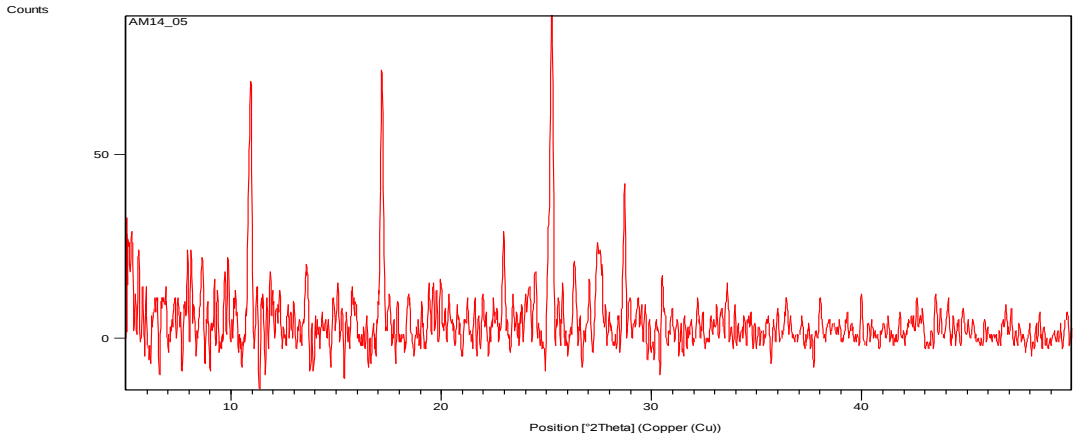

AM14_06 – MCPBA + salicylic acid crystallised in diethyl ether at 4°C

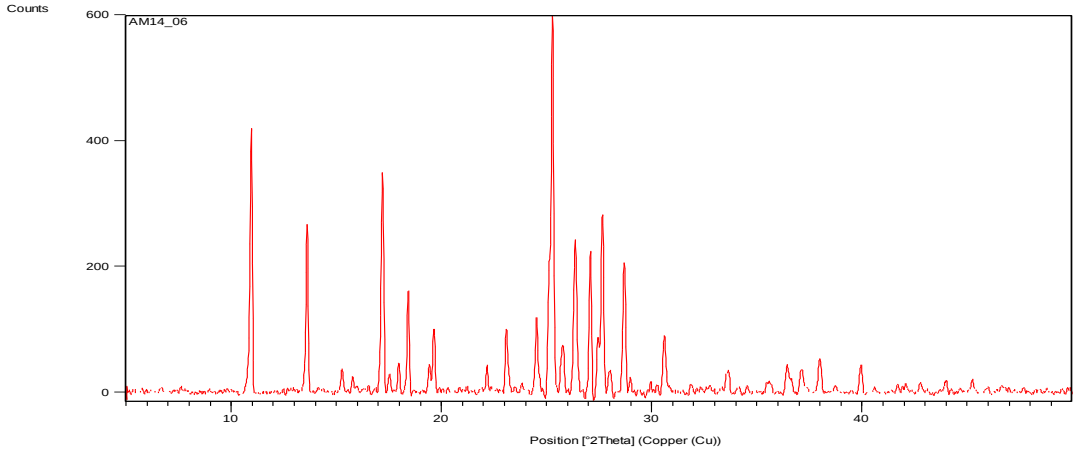

AM14_07 – MCPBA + salicylic acid crystallised in ethyl acetate at room temperature

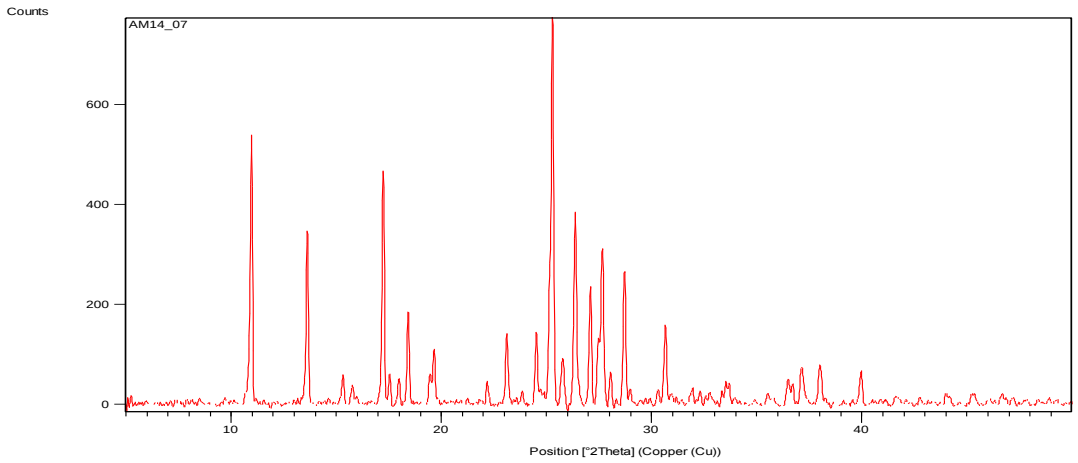

AM14_08 – MCPBA + salicylic acid crystallised in ethyl acetate at 4°C

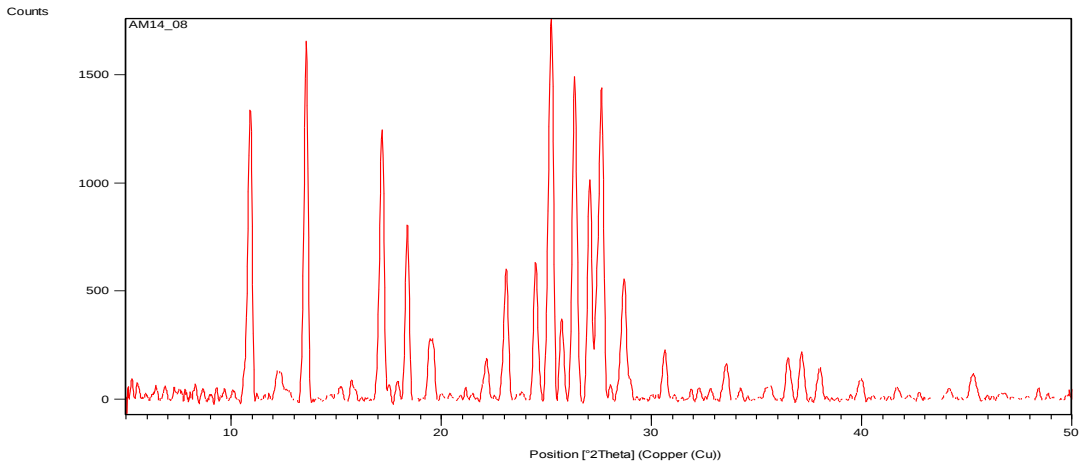

MCPBA and 3-hydroxybenzoic acid

AM15_01 – MCPBA + 3-hydroxybenzoic acid crystallised in acetone at room temperature

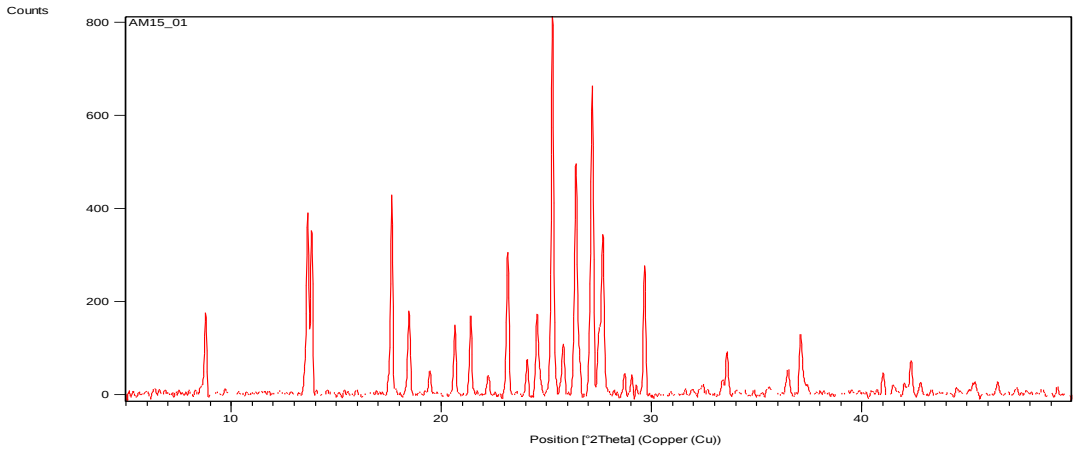

AM15_02 – MCPBA + 3-hydroxybenzoic acid crystallised in acetone at 4°C

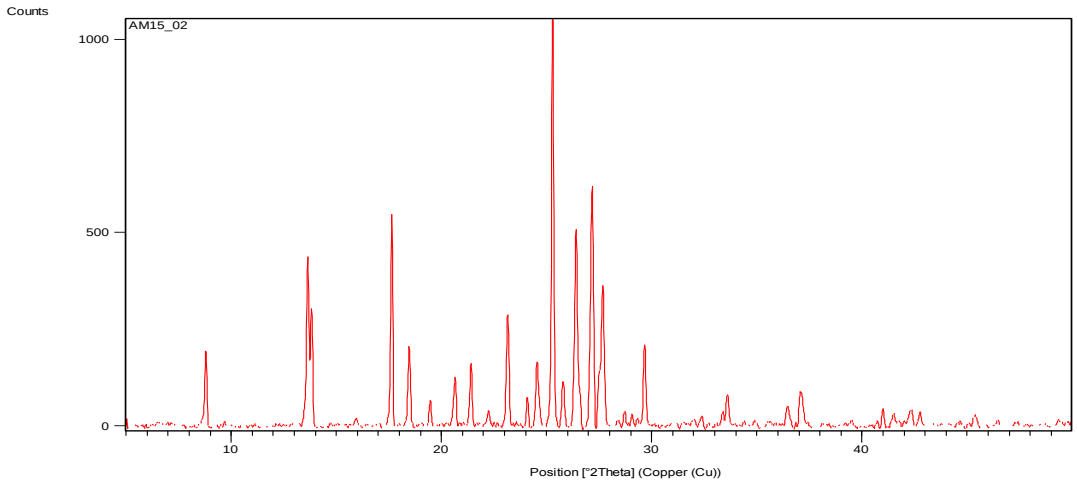

AM15_03 – MCPBA + 3-hydroxybenzoic acid crystallised in chloroform at room temperature

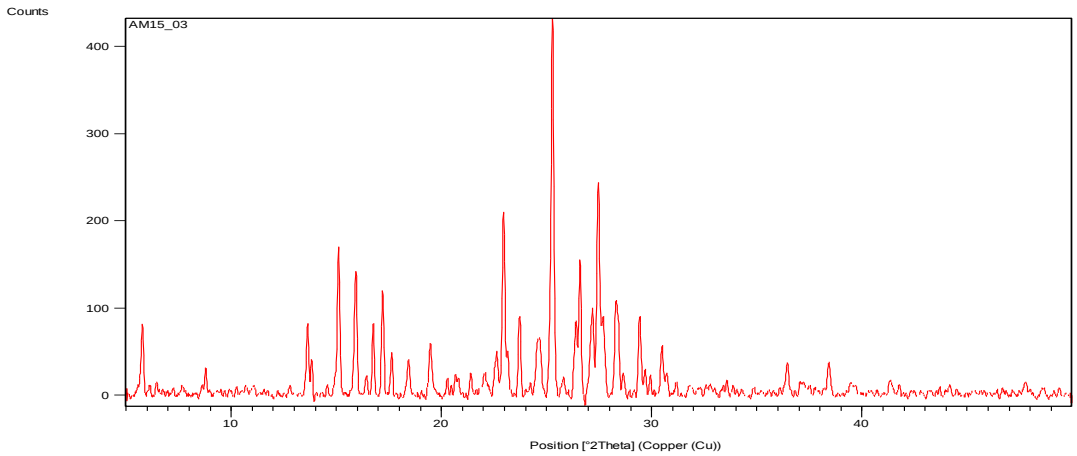

AM15_04 – MCPBA + 3-hydroxybenzoic acid crystallised in chloroform at 4°C

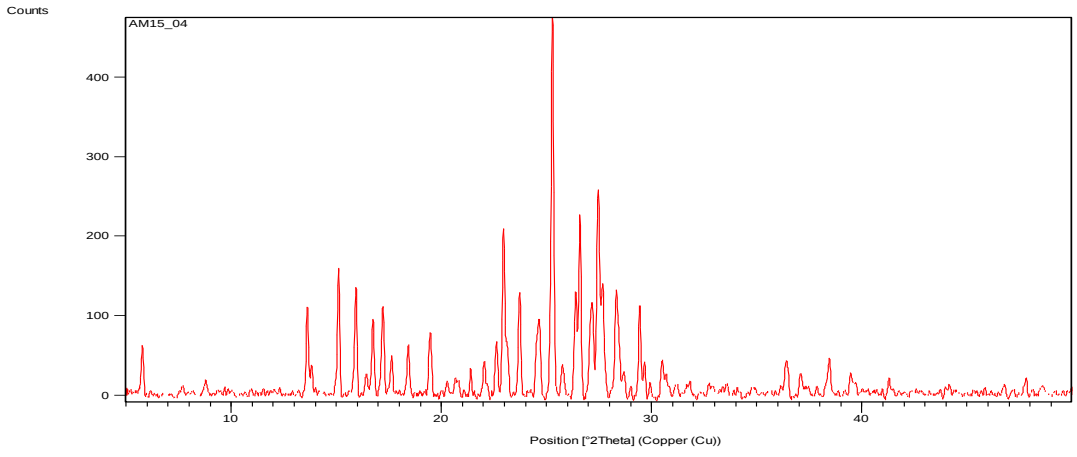

AM15_05 – MCPBA + 3-hydroxybenzoic acid crystallised in diethyl ether at room temperature

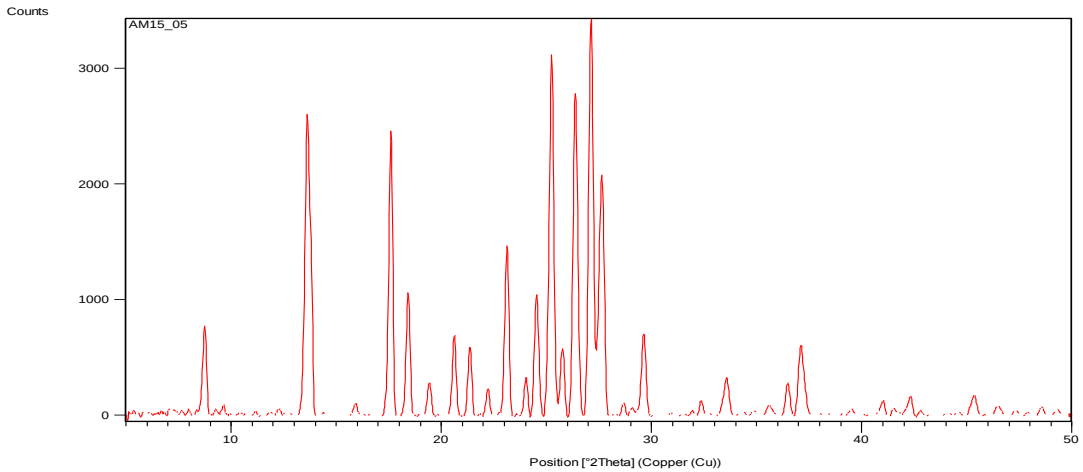

AM15_06 – MCPBA + 3-hydroxybenzoic acid crystallised in diethyl ether at 4°C

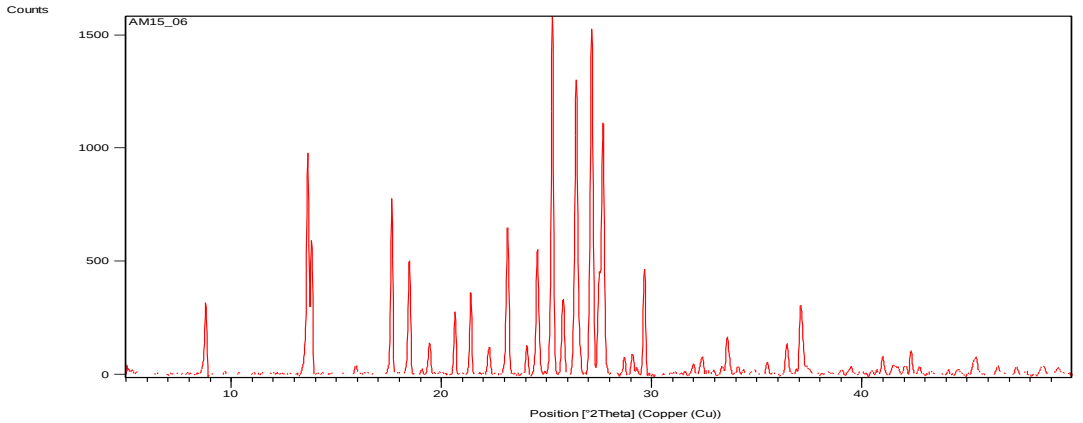

AM15_07 – MCPBA + 3-hydroxybenzoic acid crystallised in ethyl acetate at room temperature

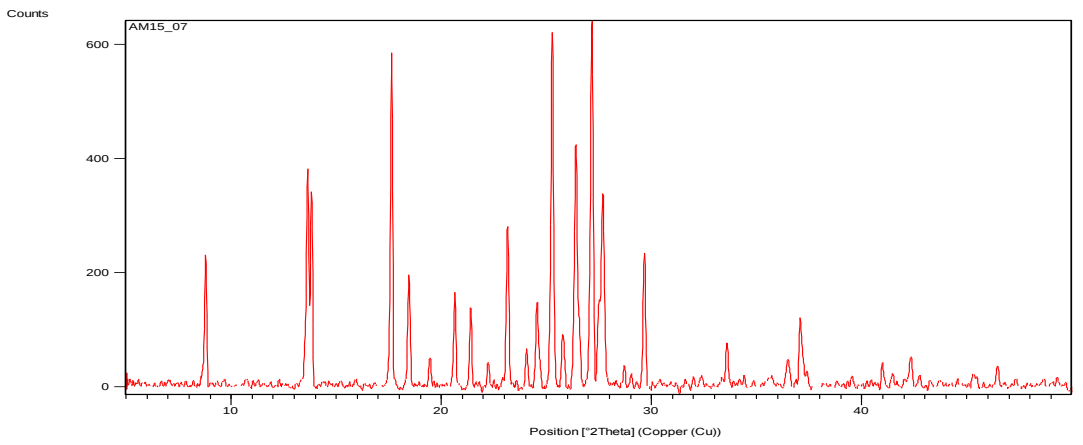

AM15_08 – MCPBA + 3-hydroxybenzoic acid crystallised in ethyl acetate at 4°C

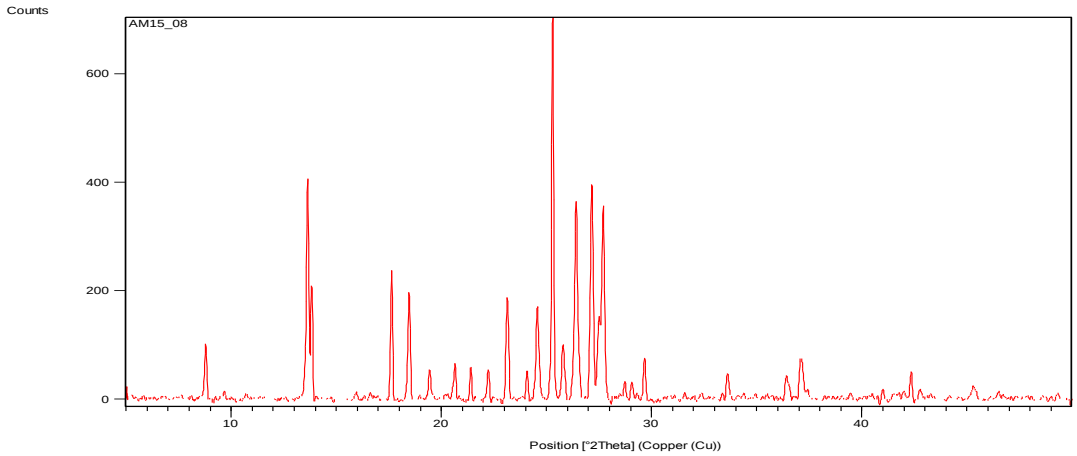

MCPBA and malonic acid

AM22_01 – MCPBA + malonic acid crystallised in acetone at room temperature

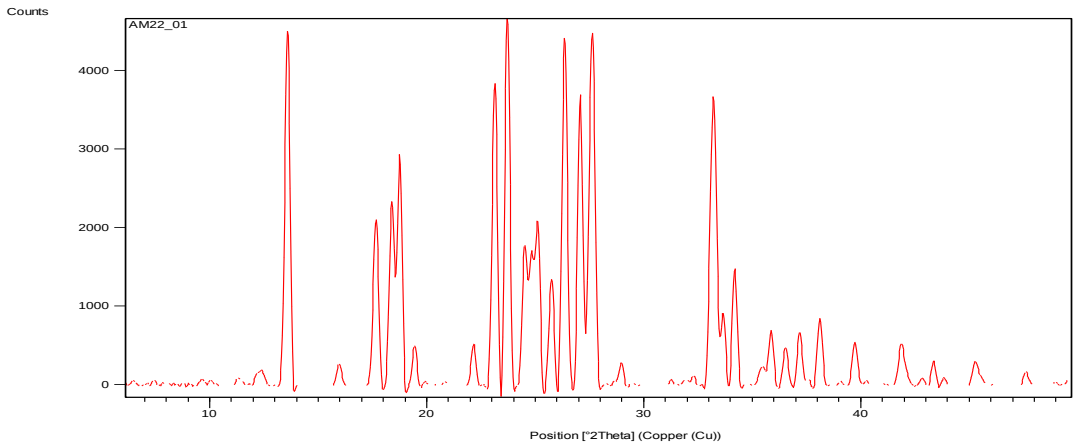

AM22_02 – MCPBA + malonic acid crystallised in acetone at 4°C

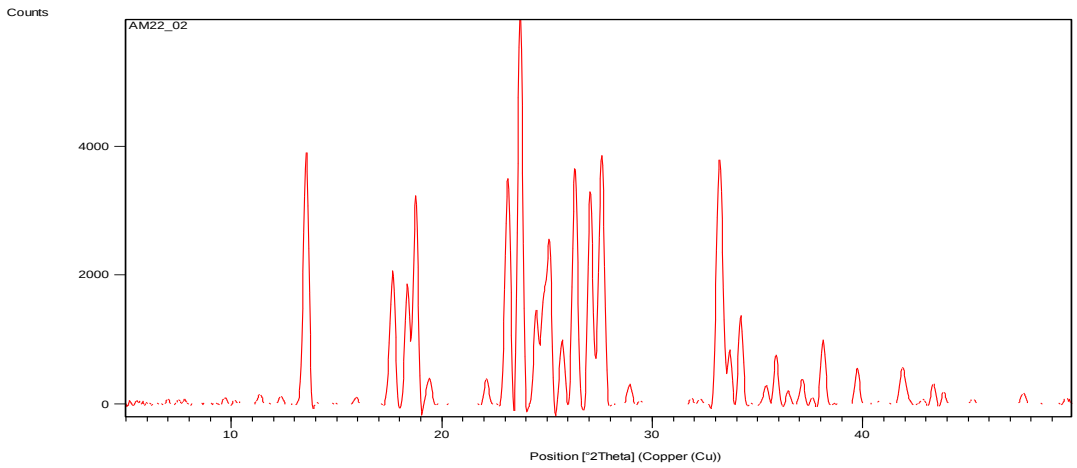

AM22_03 – MCPBA + malonic acid crystallised in chloroform at room temperature

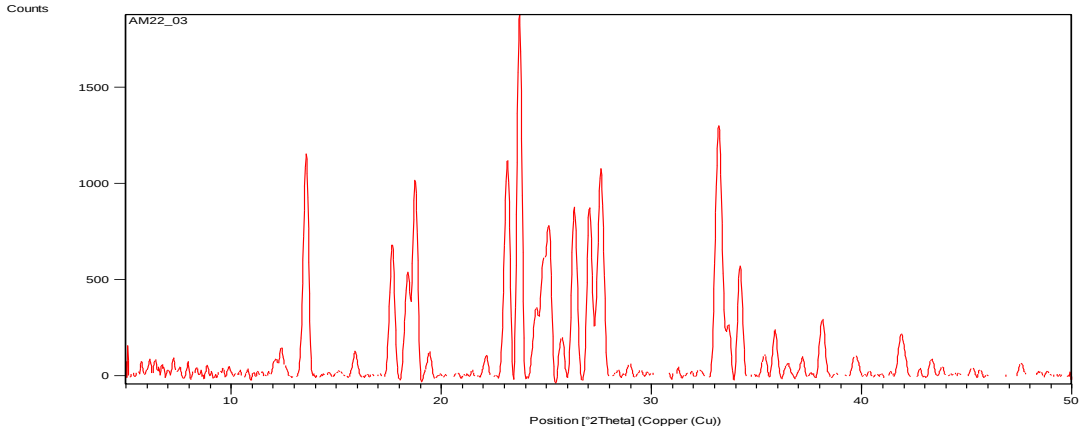

AM22_04 – MCPBA + malonic acid crystallised in chloroform at 4°C

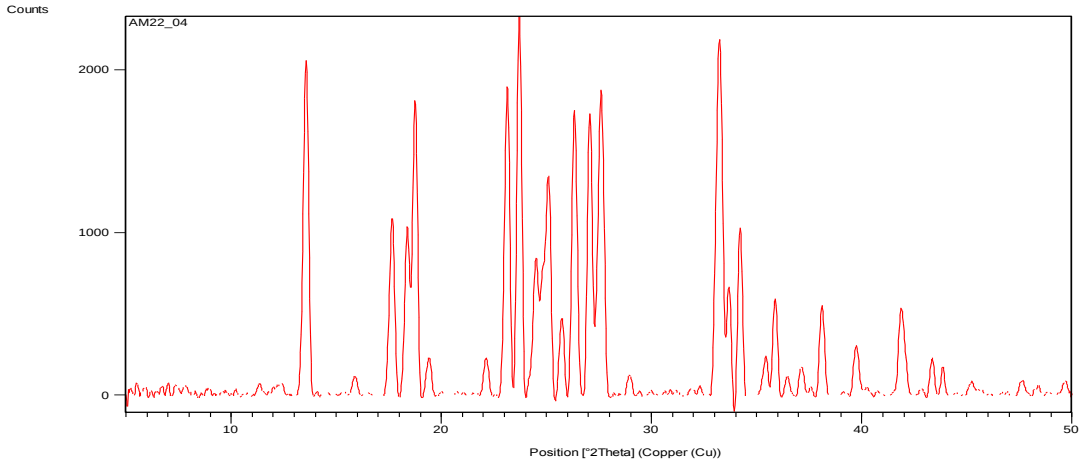

AM22_05 – MCPBA + malonic acid crystallised in diethyl ether at room temperature

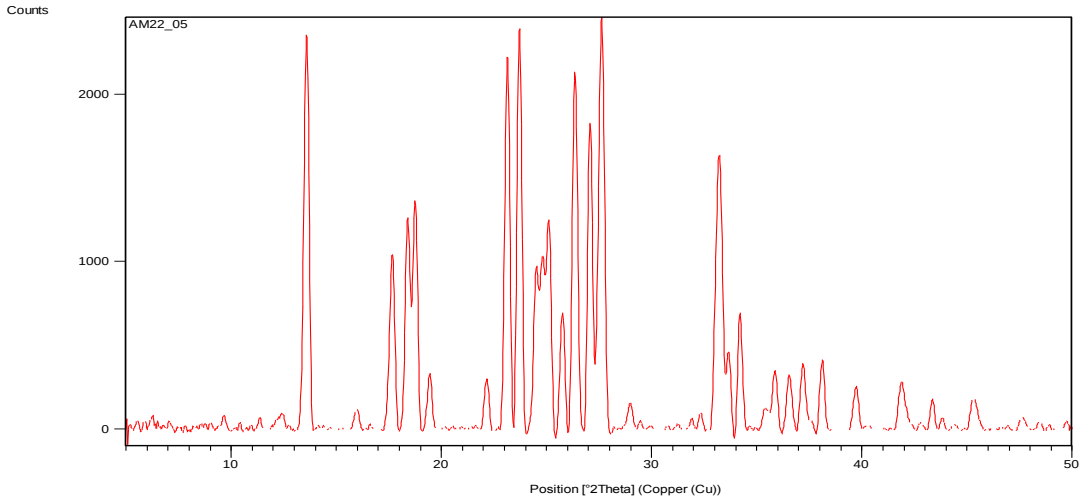

AM22_06 – MCPBA + malonic acid crystallised in diethyl ether at 4°C

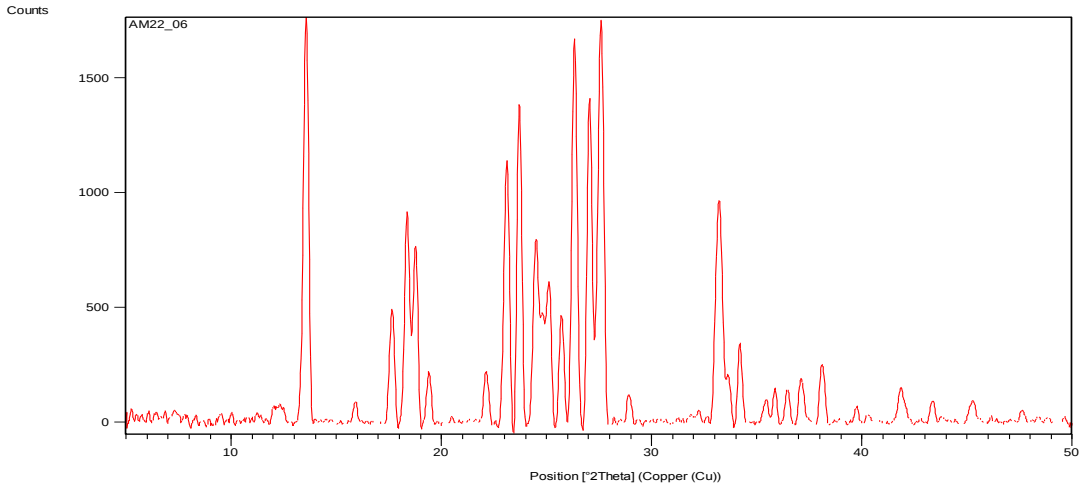

AM22_07 – MCPBA + malonic acid crystallised in ethyl acetate at room temperature

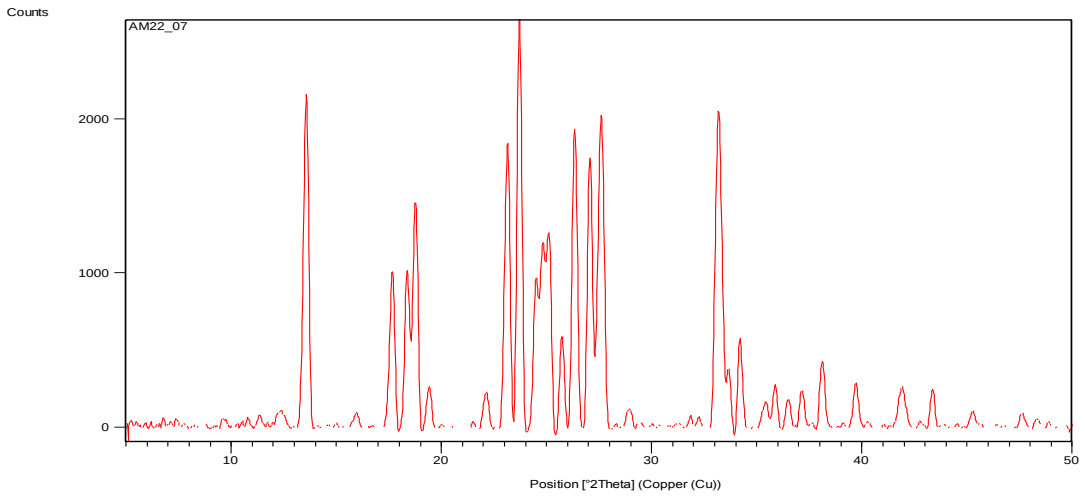

AM22_08 – MCPBA + salicylic acid crystallised in ethyl acetate at 4°C

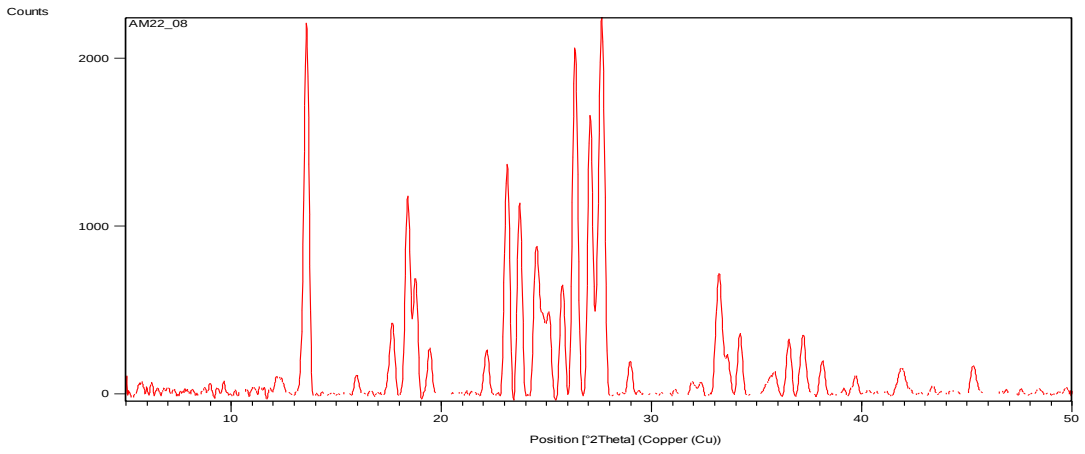

MCPBA and oxalic acid

AM23_01 – MCPBA + oxalic acid crystallised in acetone at room temperature

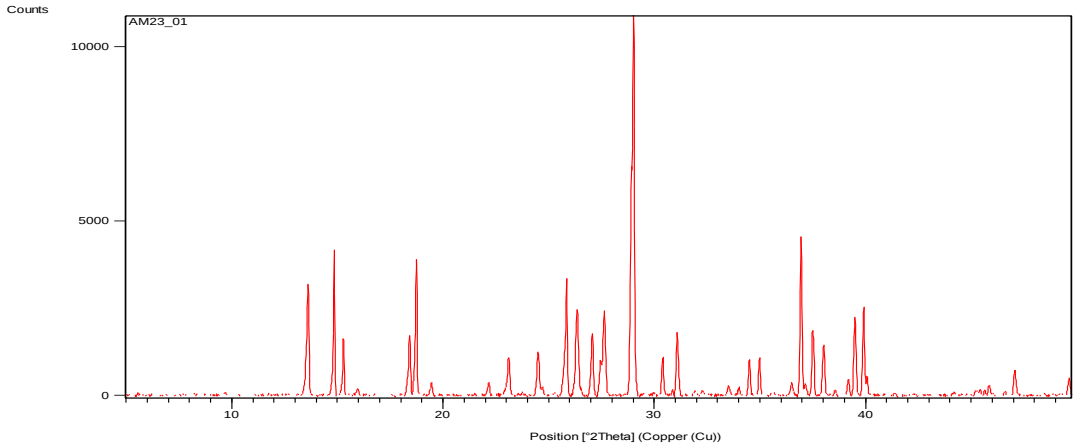

AM23_02 – MCPBA + oxalic acid crystallised in acetone at 4°C

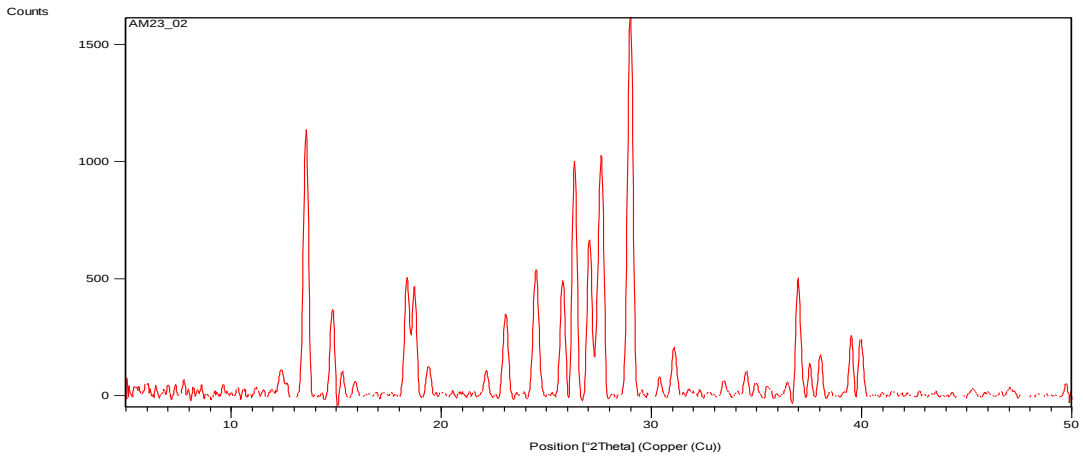

AM23_03 – MCPBA + oxalic acid crystallised in chloroform at room temperature

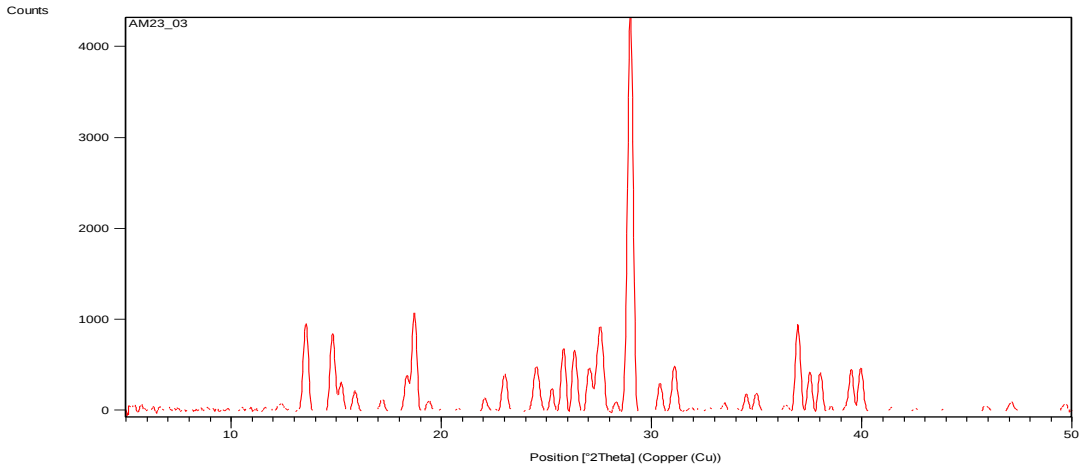

AM23_04 – MCPBA + oxalic acid crystallised in chloroform at 4°C

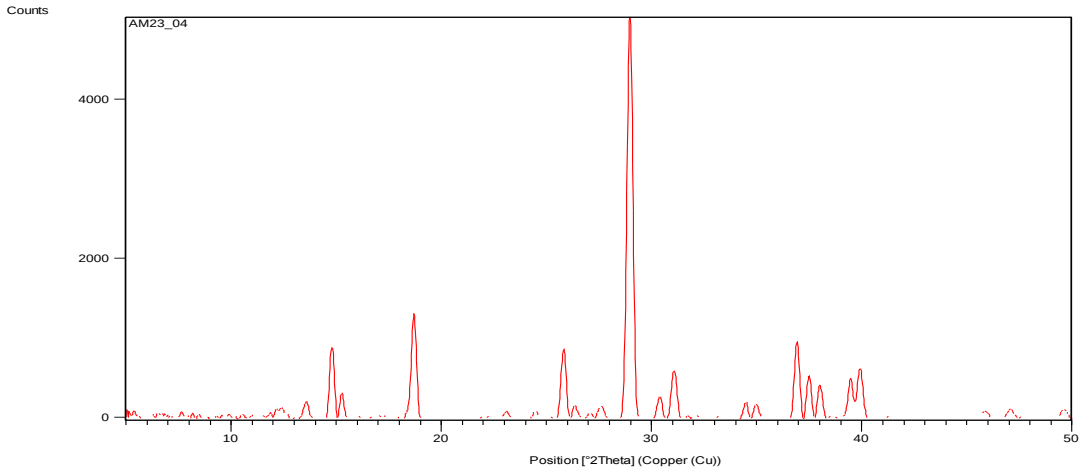

AM23_05 – MCPBA + oxalic acid crystallised in diethyl ether at room temperature

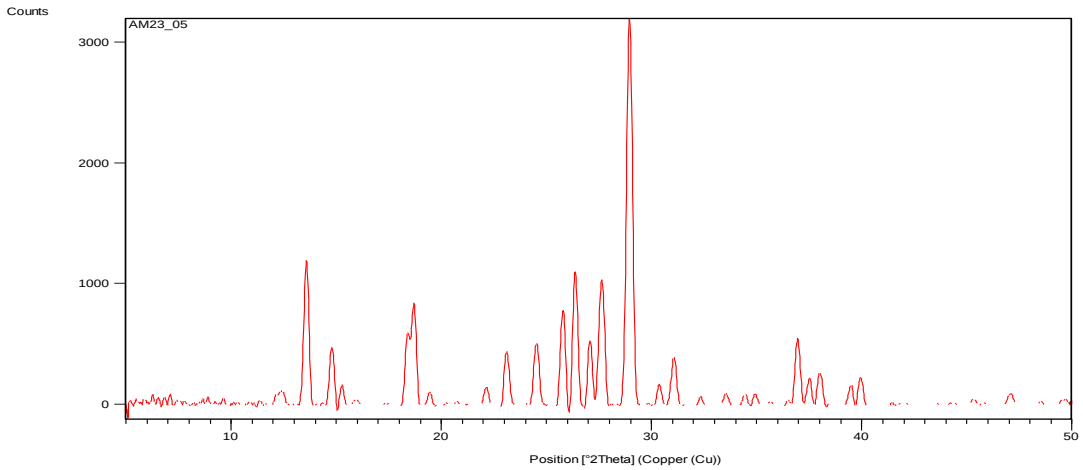

AM23_06 – MCPBA + oxalic acid crystallised in diethyl ether at 4°C

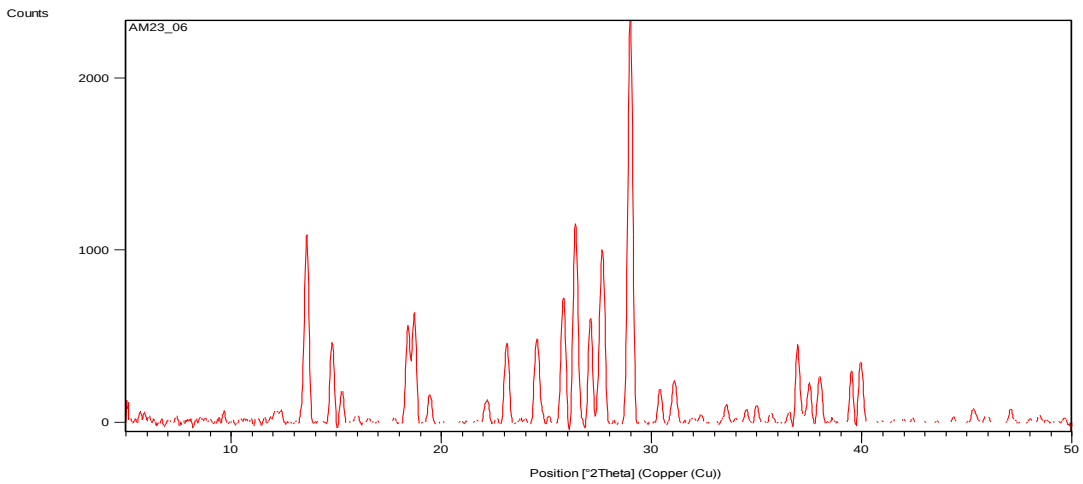

AM23_08 – MCPBA + oxalic acid crystallised in ethyl acetate at 4°C

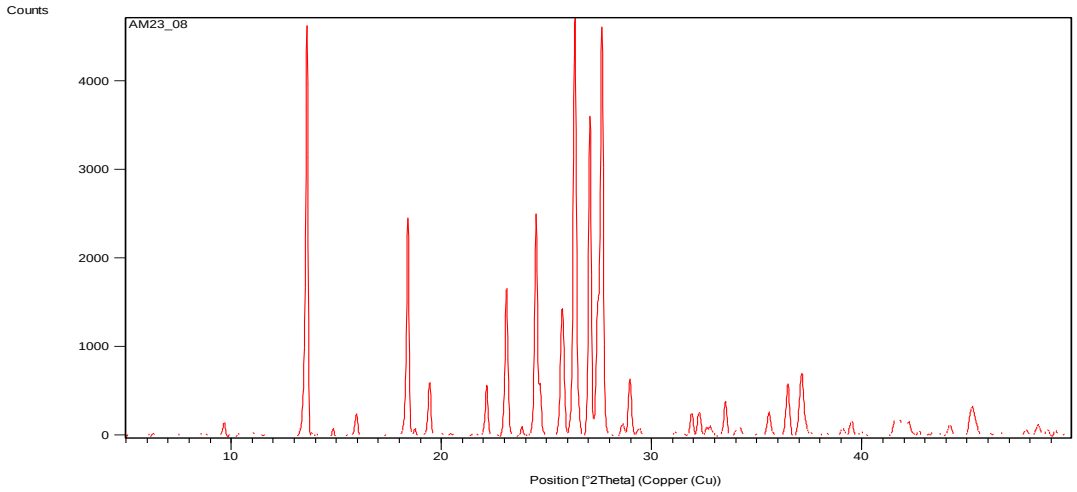

MCPBA and chloranilic acid

AM64_01 – MCPBA + chloranilic acid crystallised in acetone at 4°C

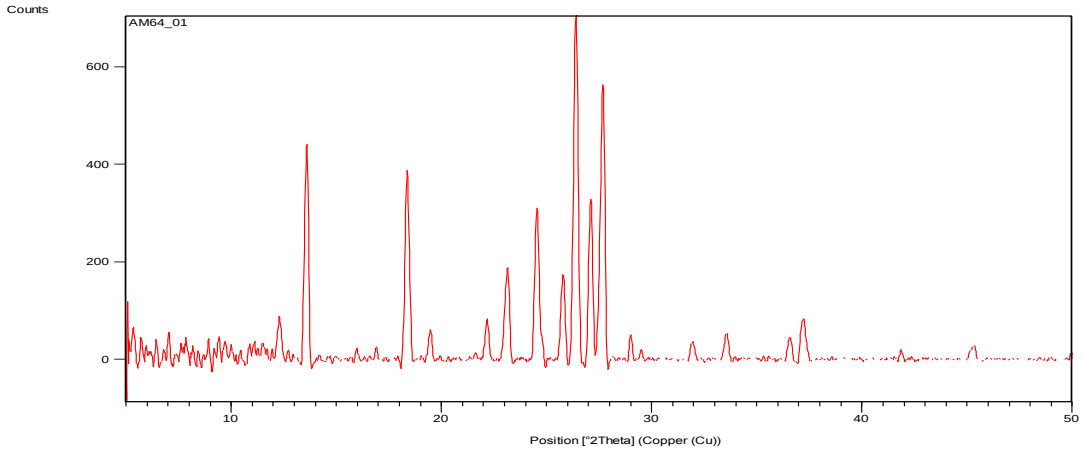

AM64_02 – MCPBA + chloranilic acid crystallised in acetone at room temperature

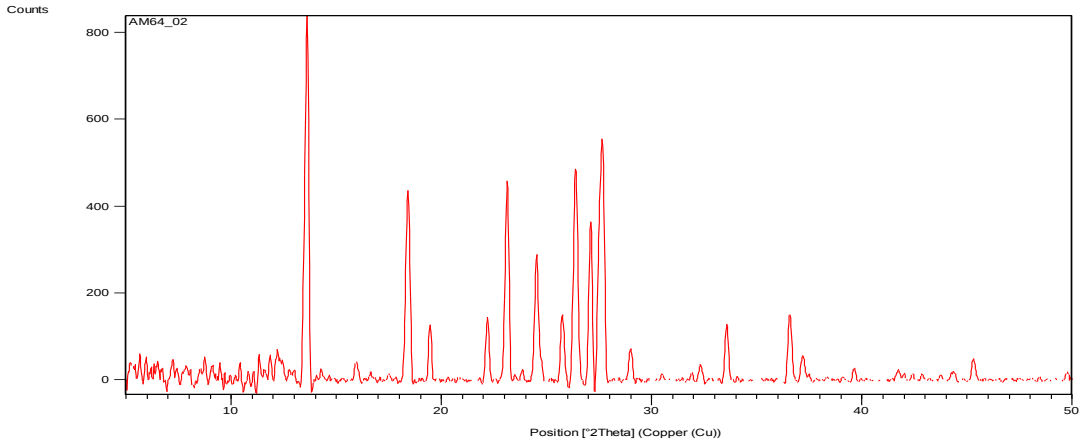

AM64_04 – MCPBA + chloranilic acid crystallised in methyl acetate at room temperature

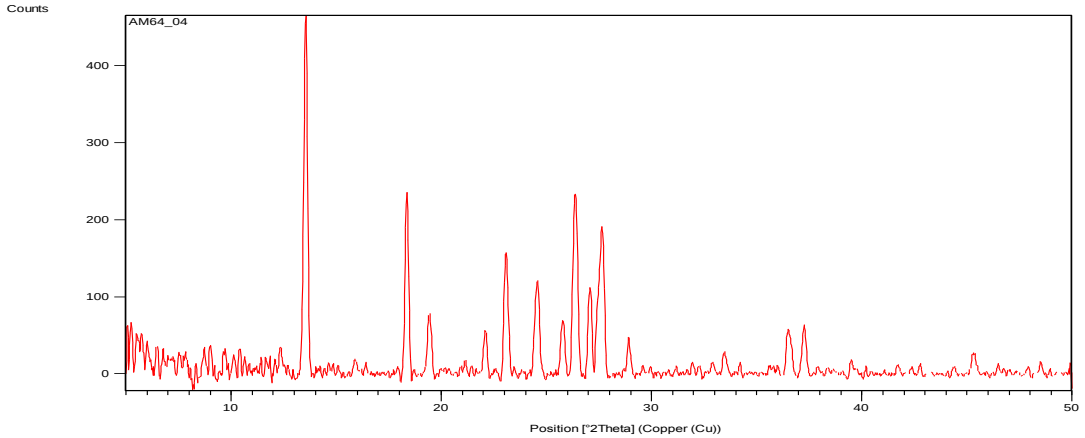

AM64_05 – MCPBA + chloranilic acid crystallised in ethyl acetate ether at 4°C

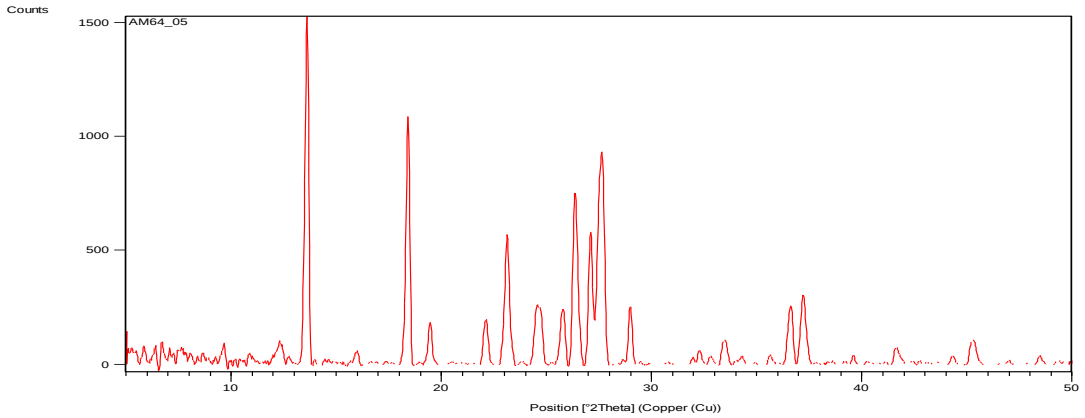

AM64_07 – MCPBA + chloranilic acid crystallised in diethyl ether at 4°C

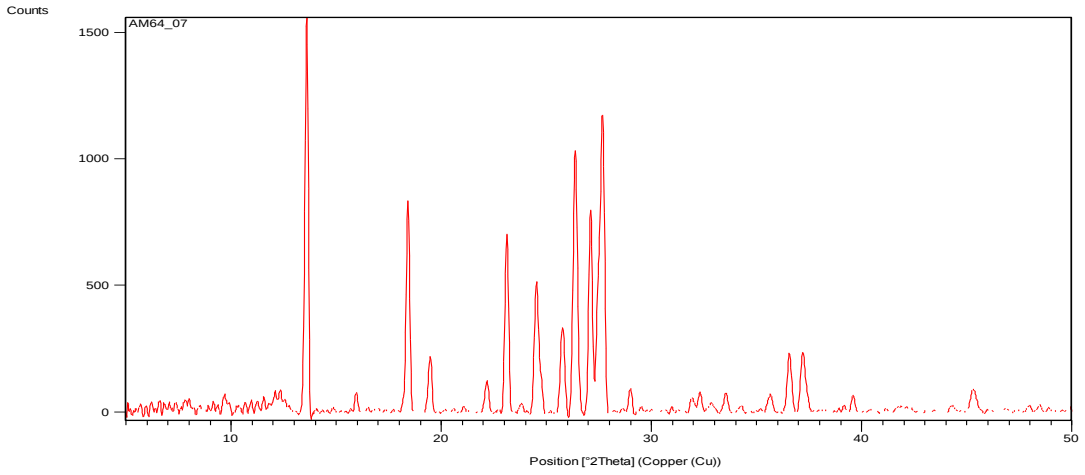

MCPBA and bromanilic acid

AM65_01 – MCPBA + bromanilic acid crystallised in acetone at 4°C

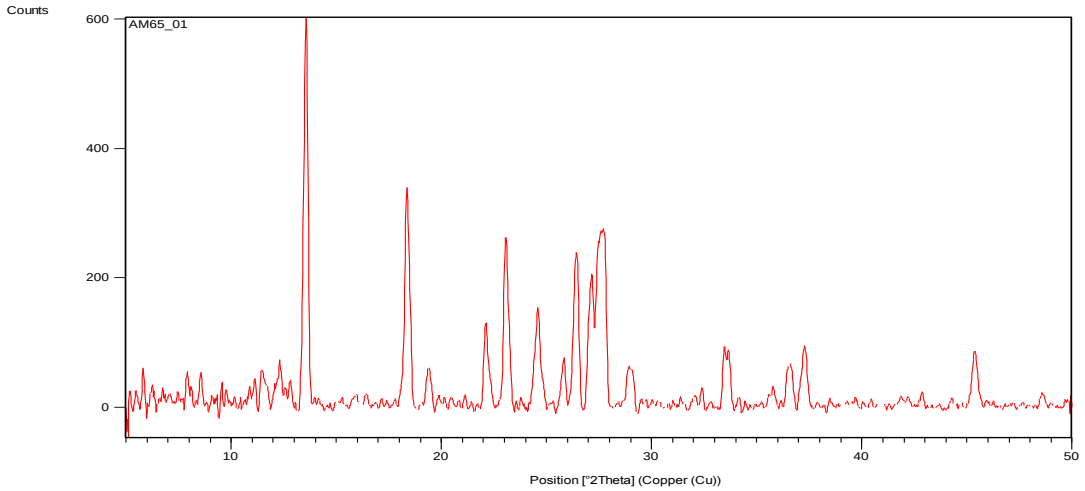

AM65_02 – MCPBA + bromanilic acid crystallised in acetone at room temperature

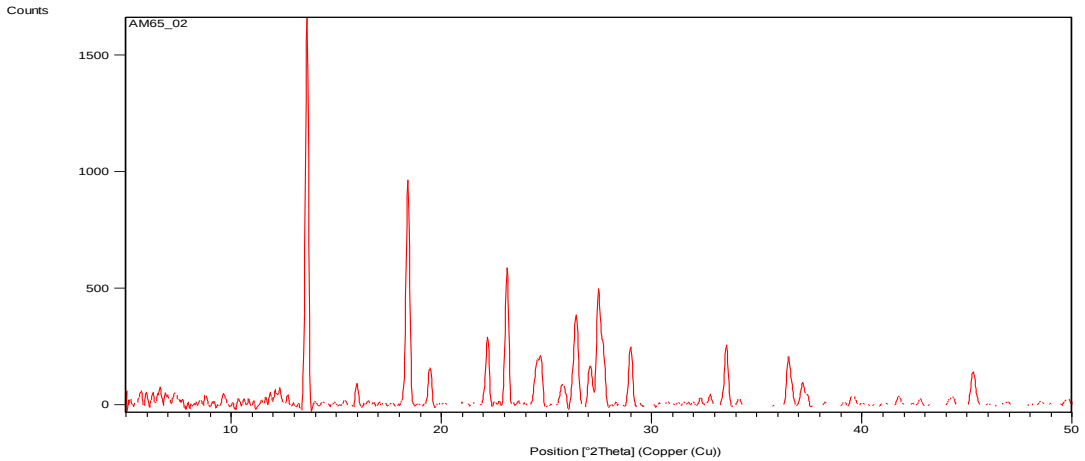

AM65_03 – MCPBA + bromanilic acid crystallised in methyl acetate at 4°C

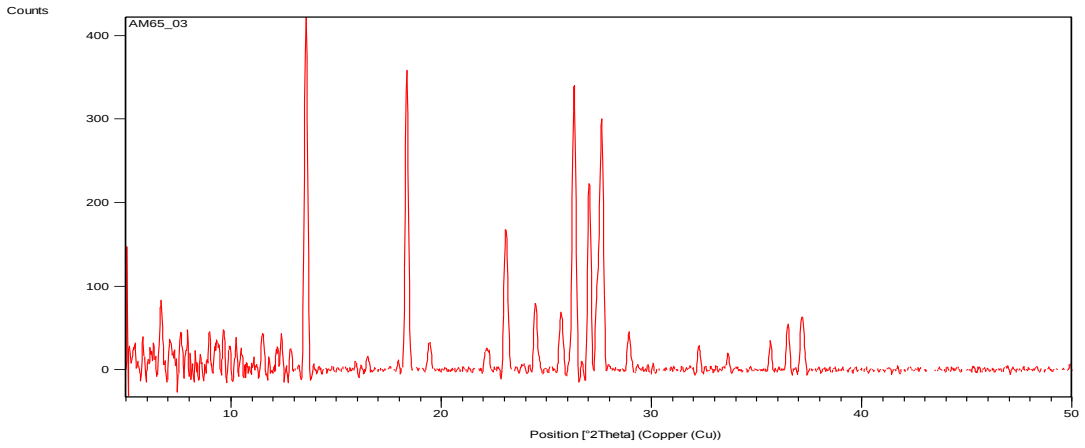

AM65_04 – MCPBA + bromanilic acid crystallised in methyl acetate at room temperature

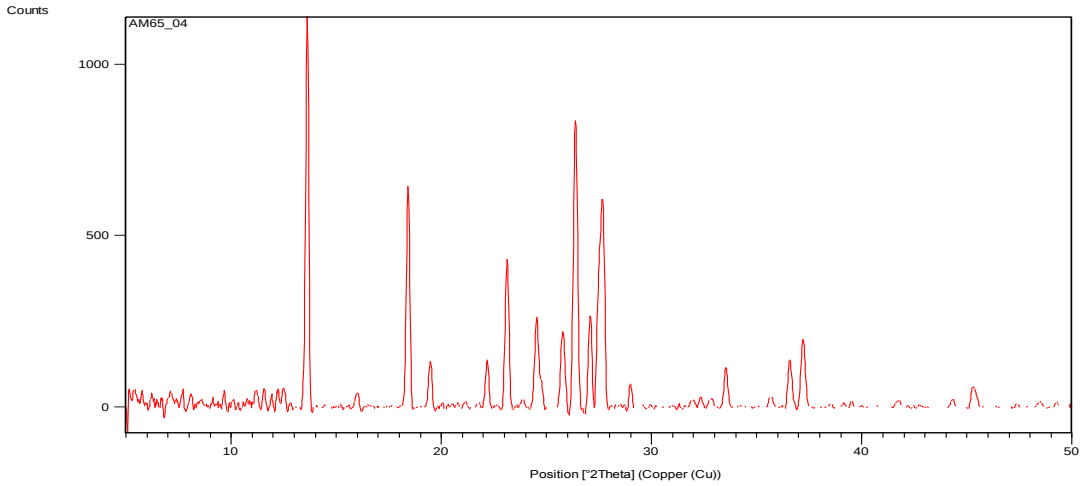

AM65_05 – MCPBA + bromanilic acid crystallised in ethyl acetate at 4°C

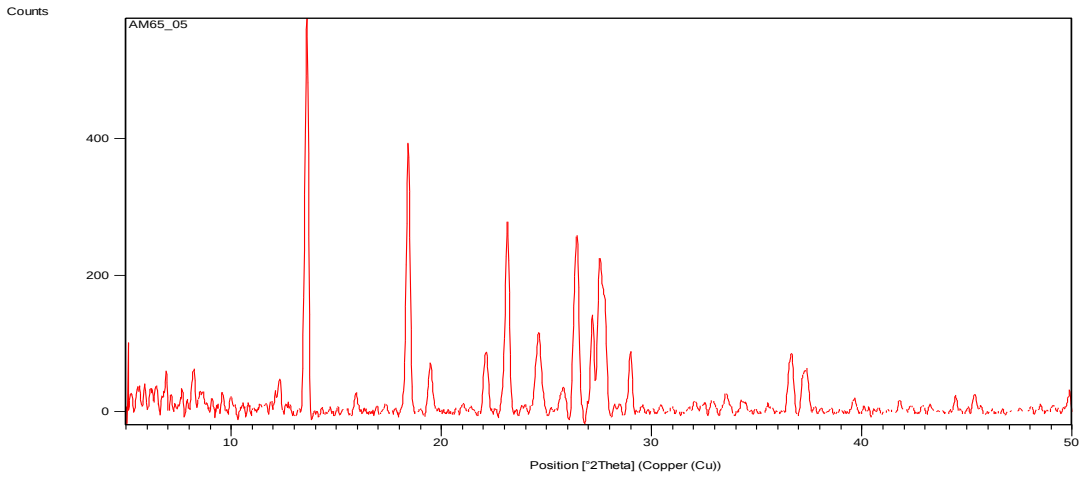

AM65_06 – MCPBA + bromanilic acid crystallised in ethyl acetate at room temperature

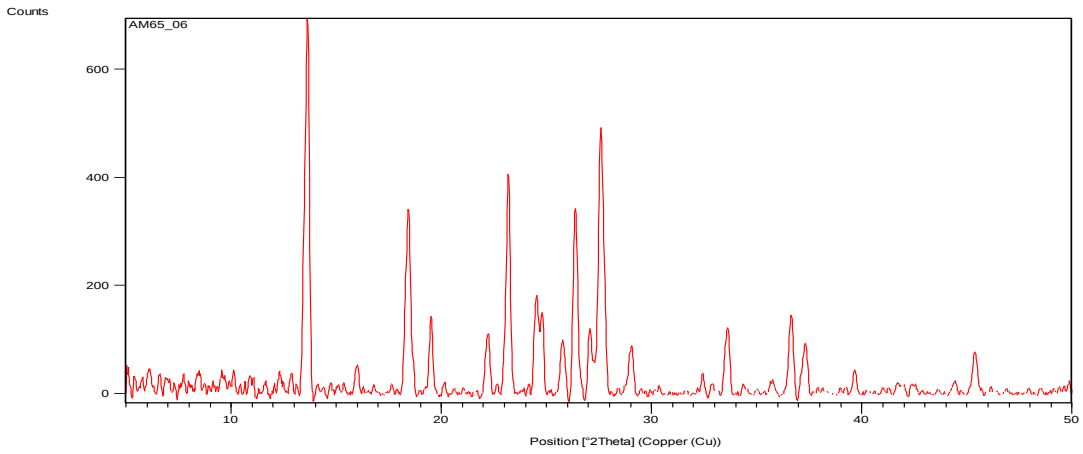

AM65_07 – MCPBA + bromanilic acid crystallised in diethyl ether at 4°C

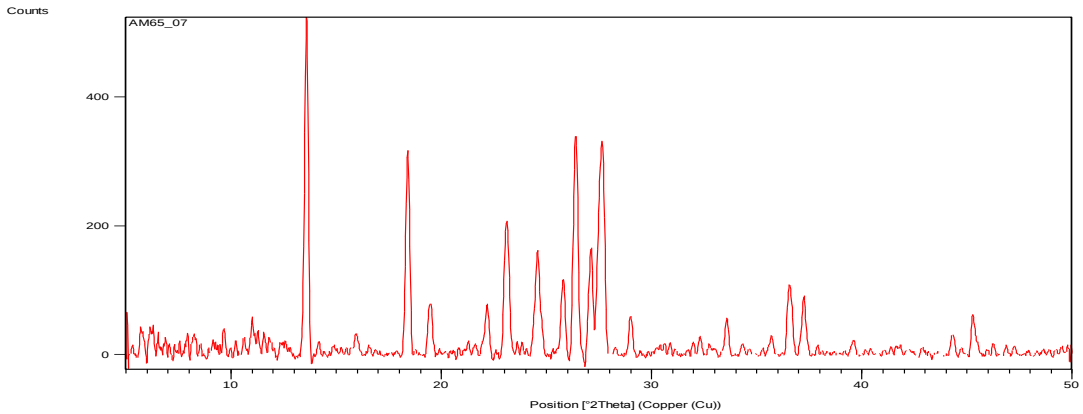

AM65_08 – MCPBA + bromanilic acid crystallised in diethyl ether at room temperature

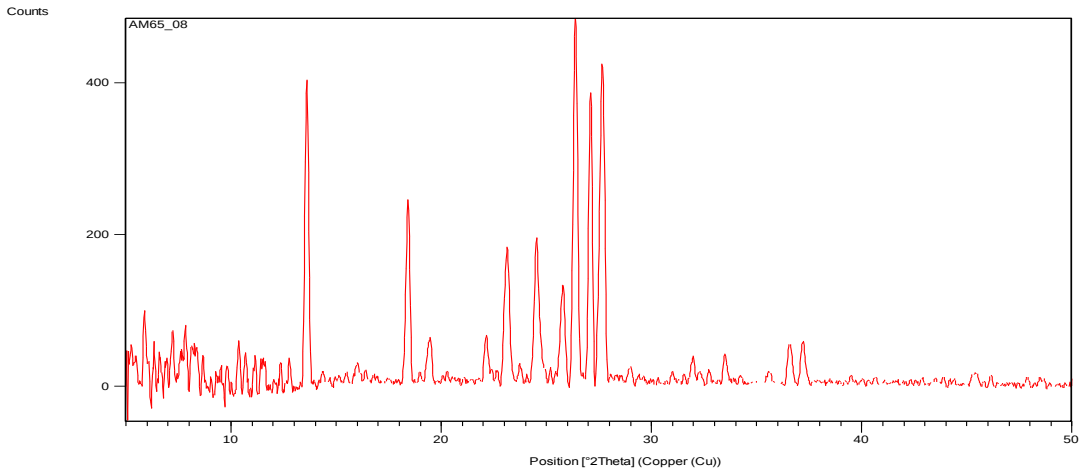

PAP and 2-chlorobenzoic acid

AM26_01 – PAP + 2-chlorobenzoic acid crystallised in methanol at 4°C

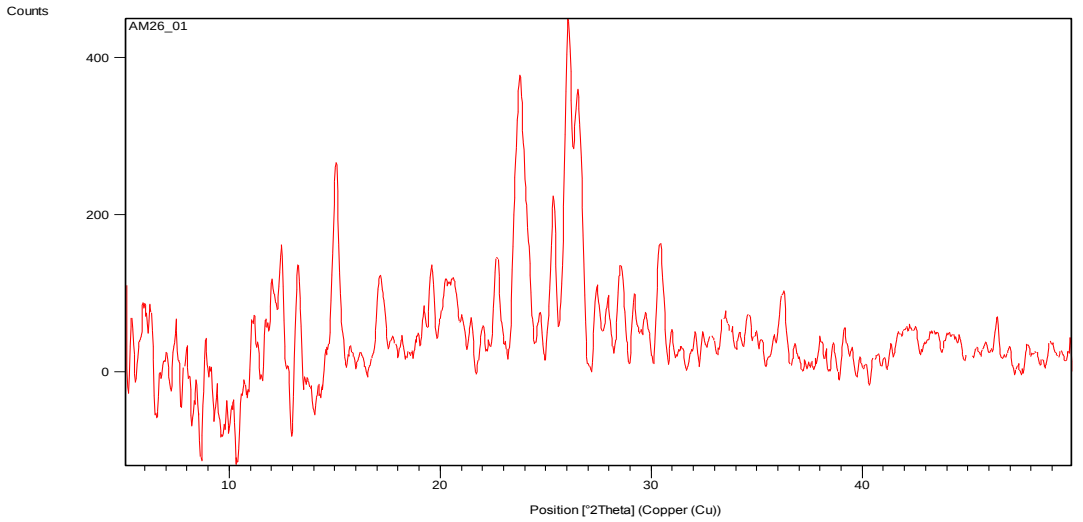

AM26_02 – PAP + 2-chlorobenzoic acid crystallised in methanol at room temperature

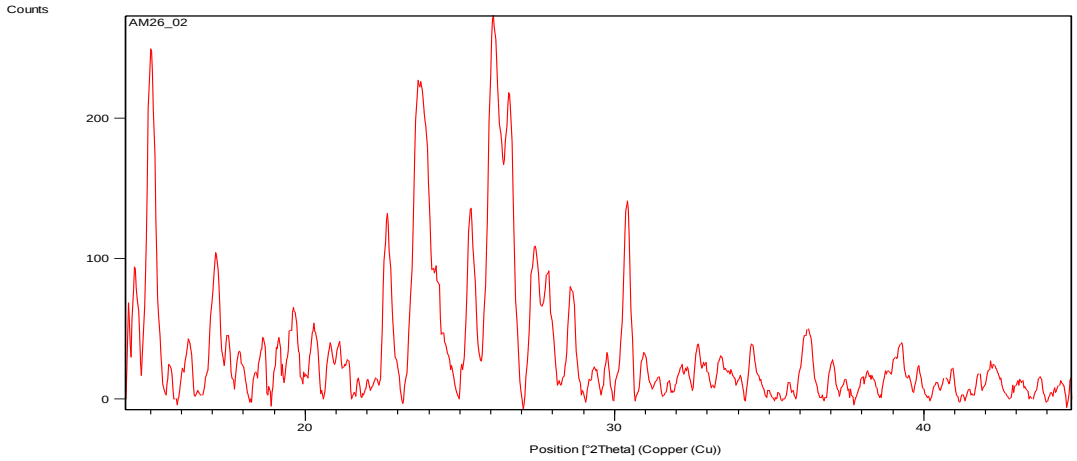

AM26_03 – PAP + 2-chlorobenzoic acid crystallised in methanol at 30°C

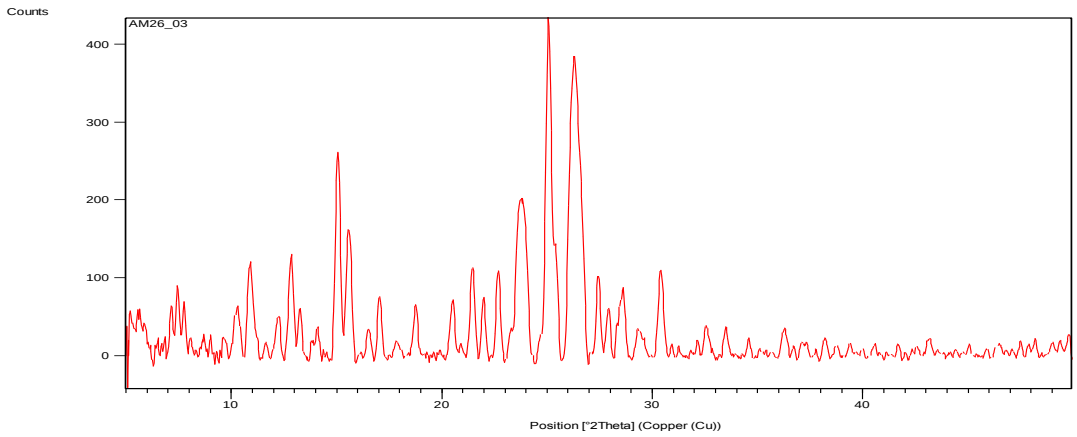

AM26_04 – PAP + 2-chlorobenzoic acid crystallised in ethanol at 4°C

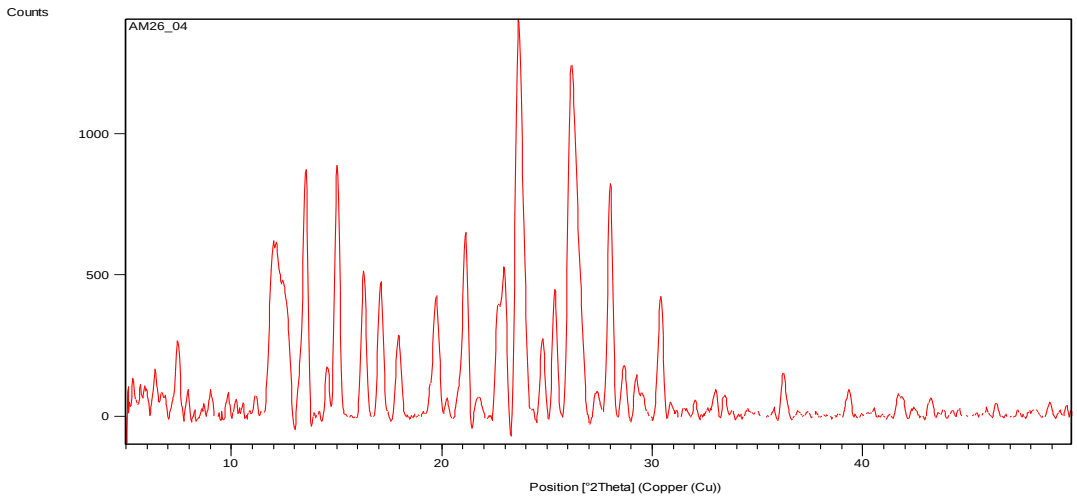

AM26_05 – PAP + 2-chlorobenzoic acid crystallised in ethanol at room temperature

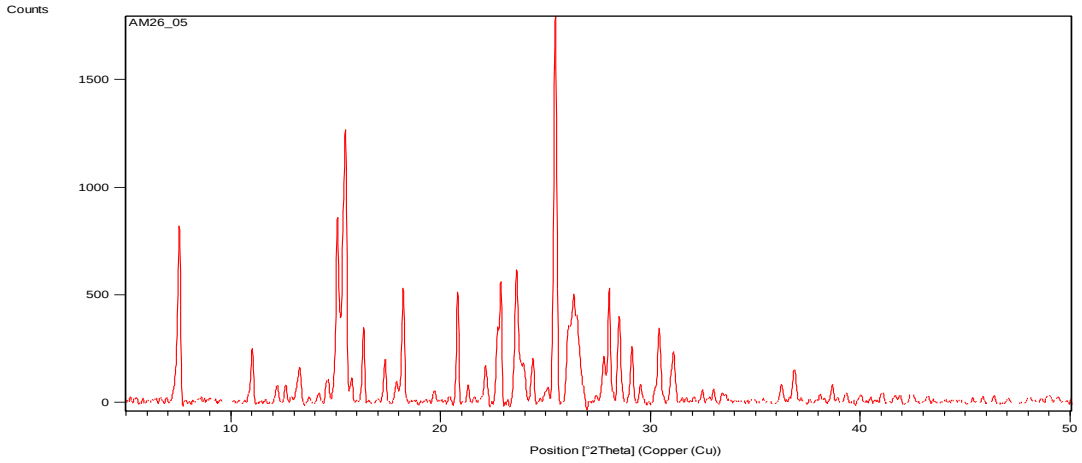

AM26_06 – PAP + 2-chlorobenzoic acid crystallised in ethanol at 30°C

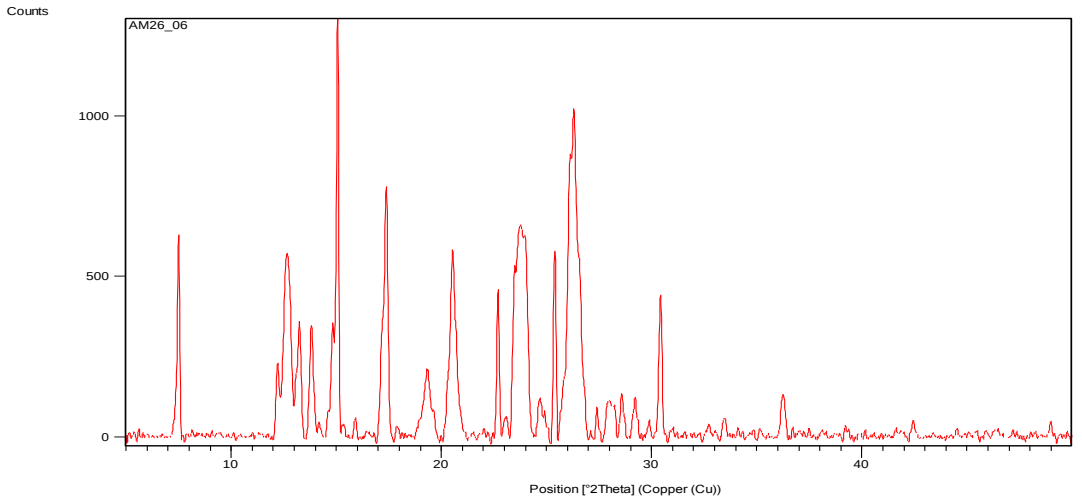

AM26_07 – PAP + 2-chlorobenzoic acid crystallised in acetone at 4°C

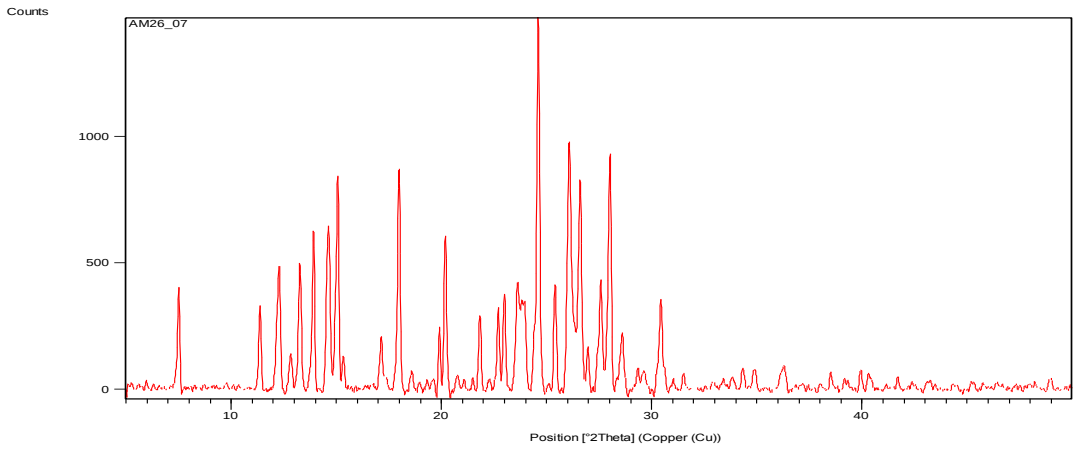

AM26_08 – PAP + 2-chlorobenzoic acid crystallised in acetone at room temperature

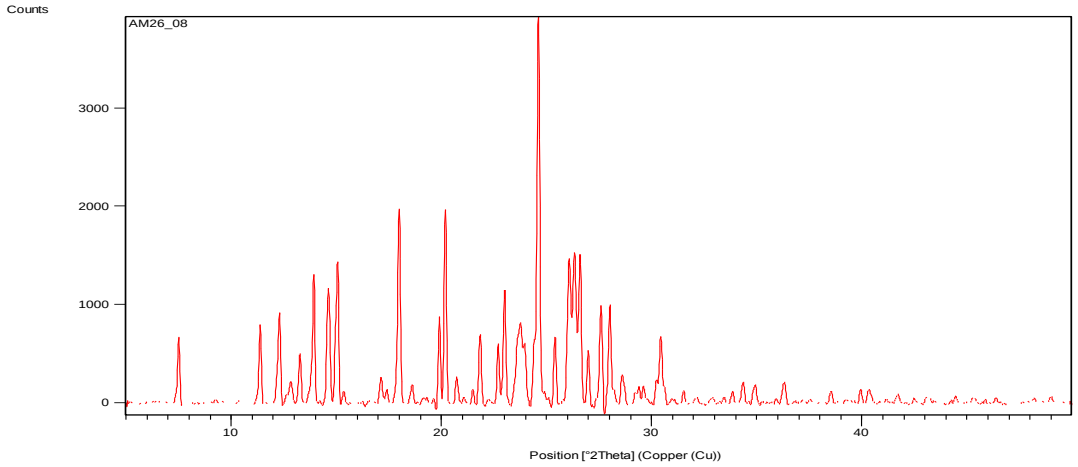

AM26_09 – PAP + 2-chlorobenzoic acid crystallised in acetone at 30°C

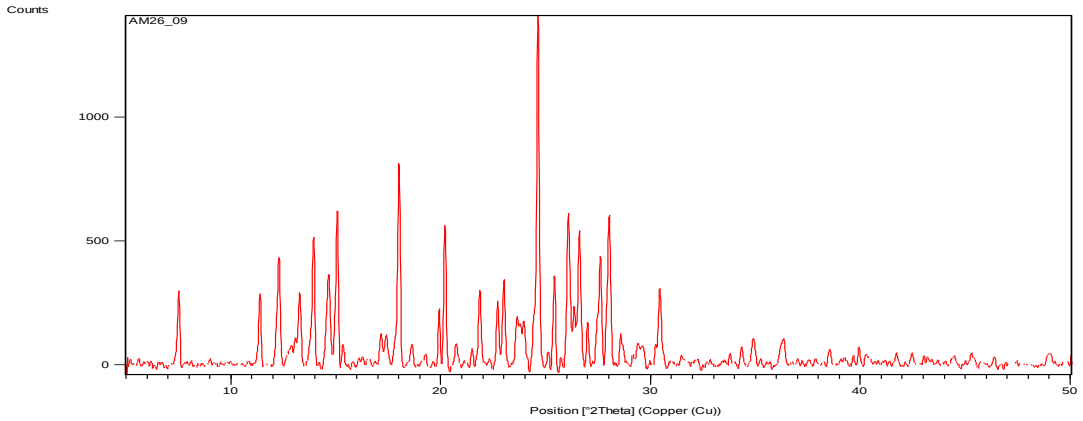

AM26_11 – PAP + 2-chlorobenzoic acid crystallised in ethyl acetate at room temperature

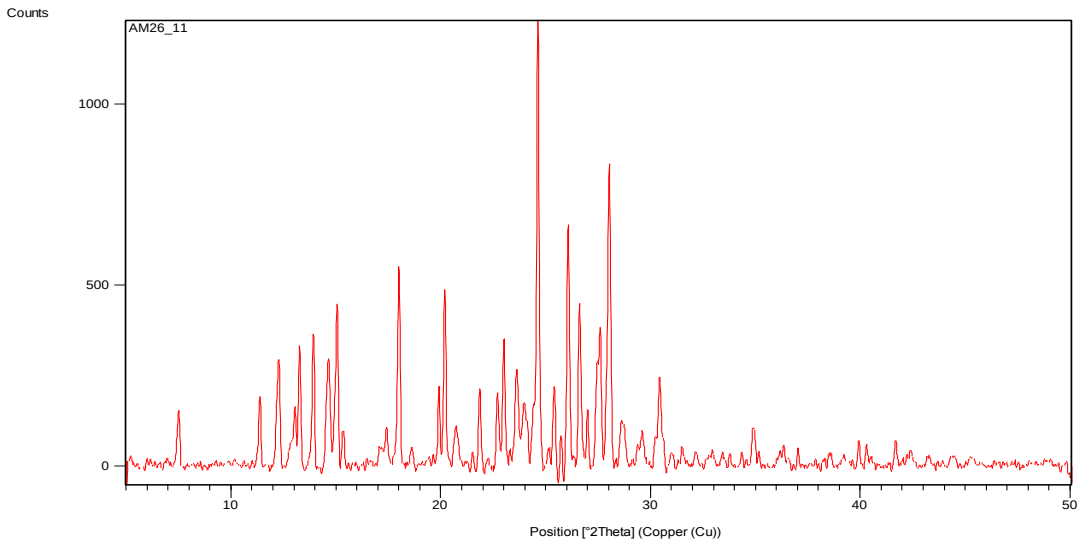

AM26_12 – PAP + 2-chlorobenzoic acid crystallised in ethyl acetate at 30°C

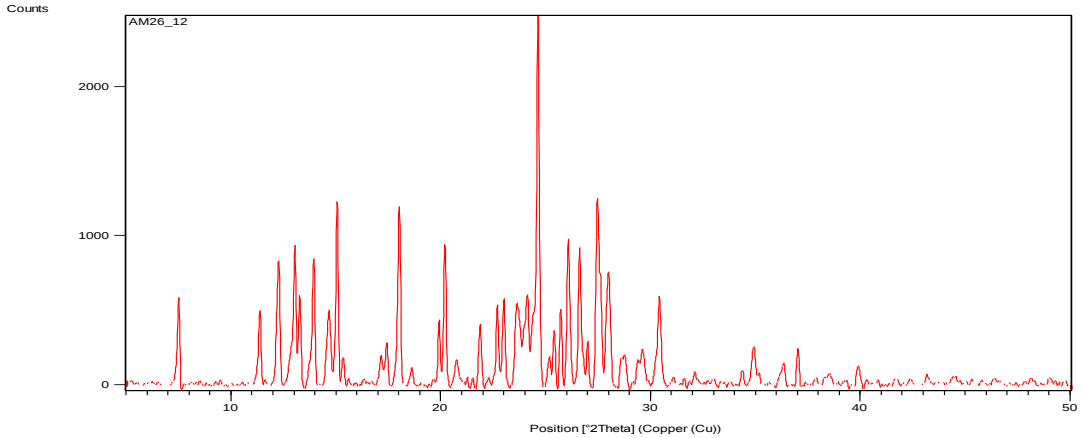

PAP and 3-chlorobenzoic acid

AM25_01 – PAP + 3-chlorobenzoic acid crystallised in methanol at 4°C

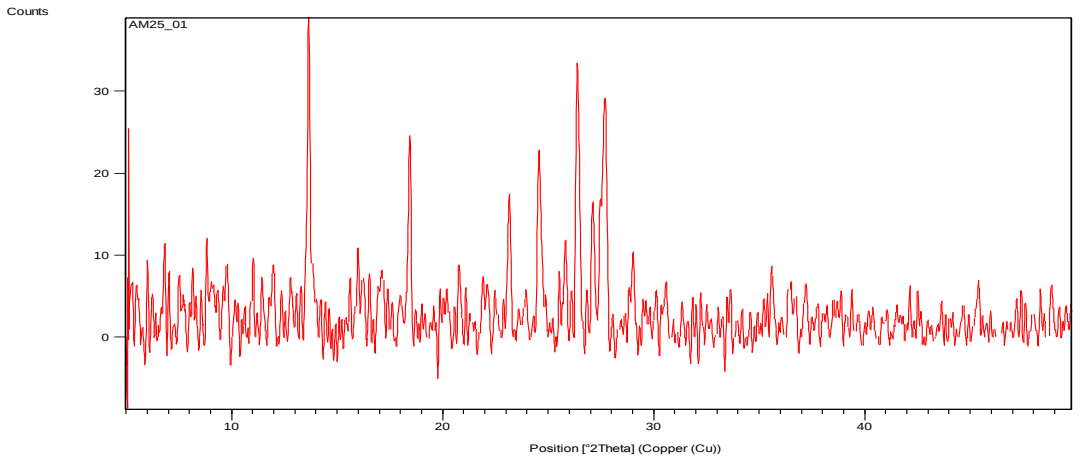

AM25_02 – PAP + 3-chlorobenzoic acid crystallised in methanol at room temperature

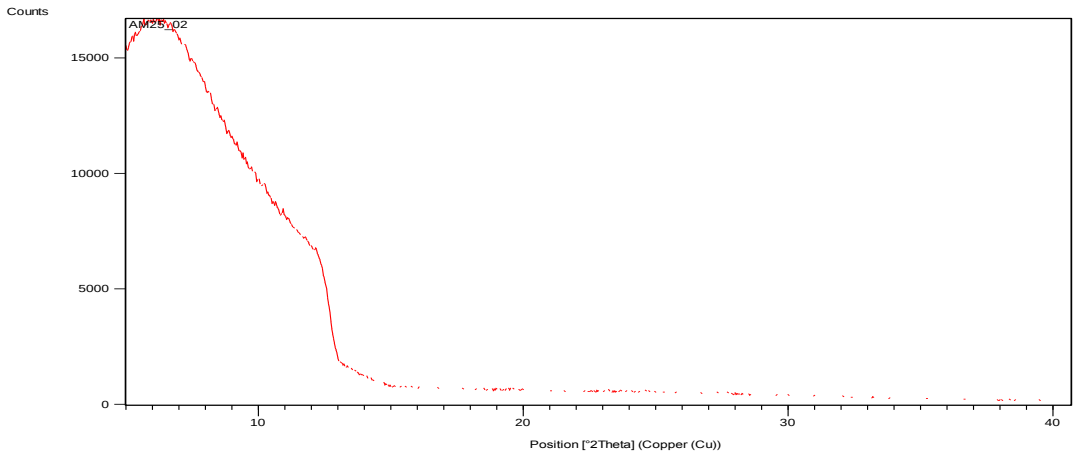

AM25_03 – PAP + 3-chlorobenzoic acid crystallised in methanol at 30°C

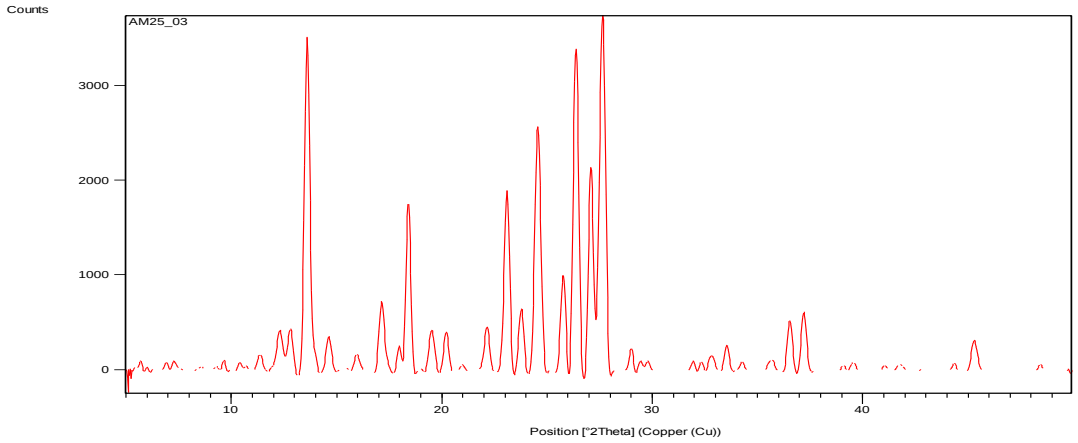

AM25_05 – PAP + 3-chlorobenzoic acid crystallised in ethanol at room temperature

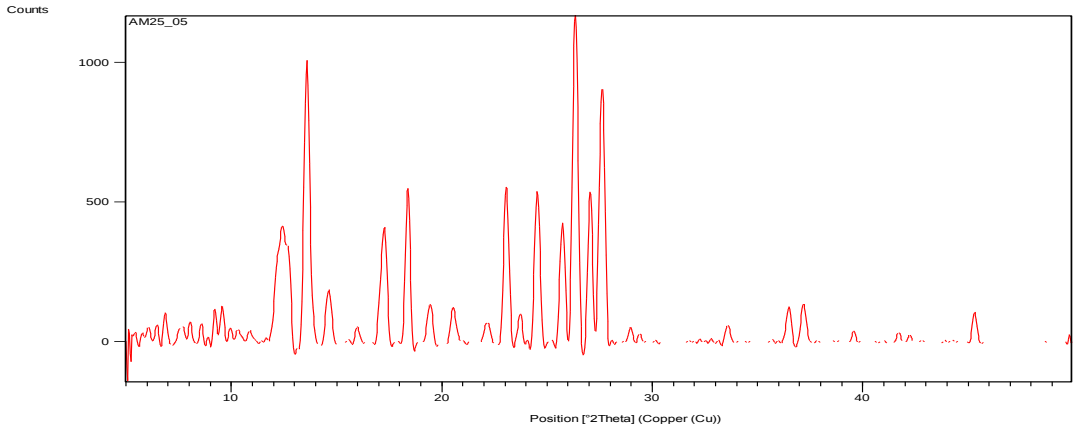

AM25_06 – PAP + 3-chlorobenzoic acid crystallised in ethanol at 30°C

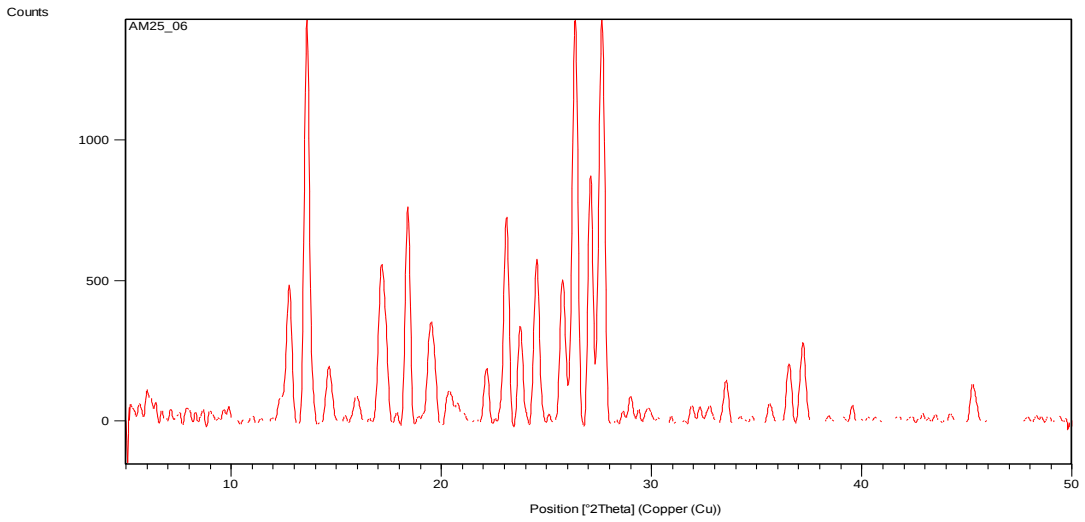

AM25_07 – PAP + 3-chlorobenzoic acid crystallised in acetone at 4°C

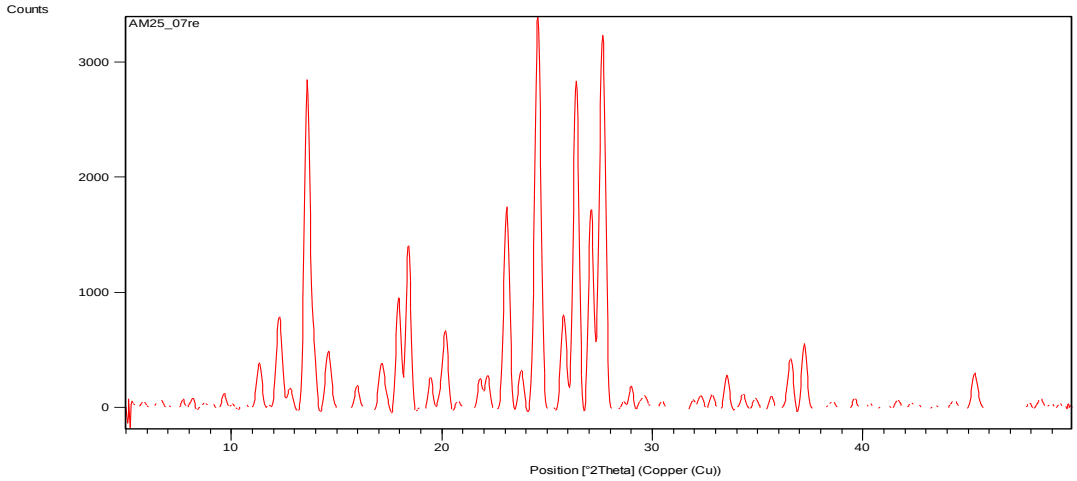

AM25_08 – PAP + 3-chlorobenzoic acid crystallised in acetone at room temperature

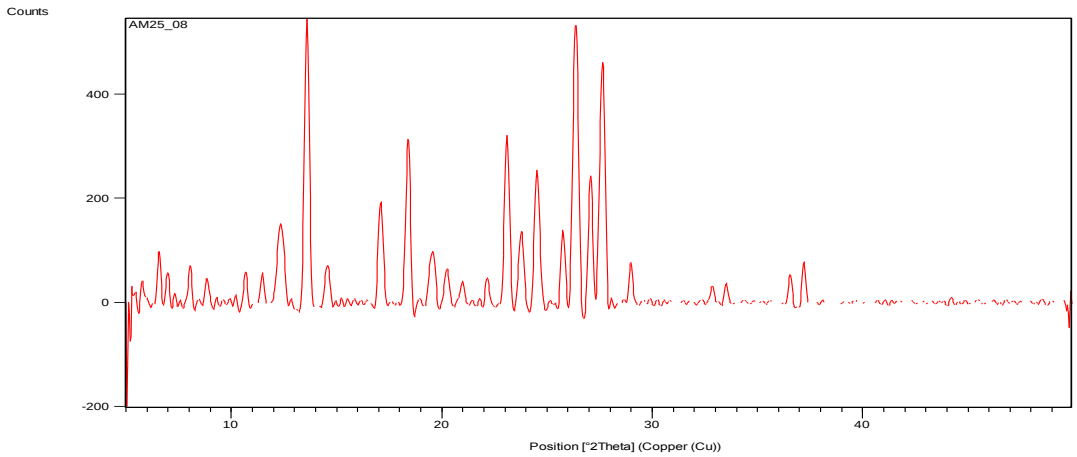

AM25_09 – PAP + 3-chlorobenzoic acid crystallised in acetone at 30°C

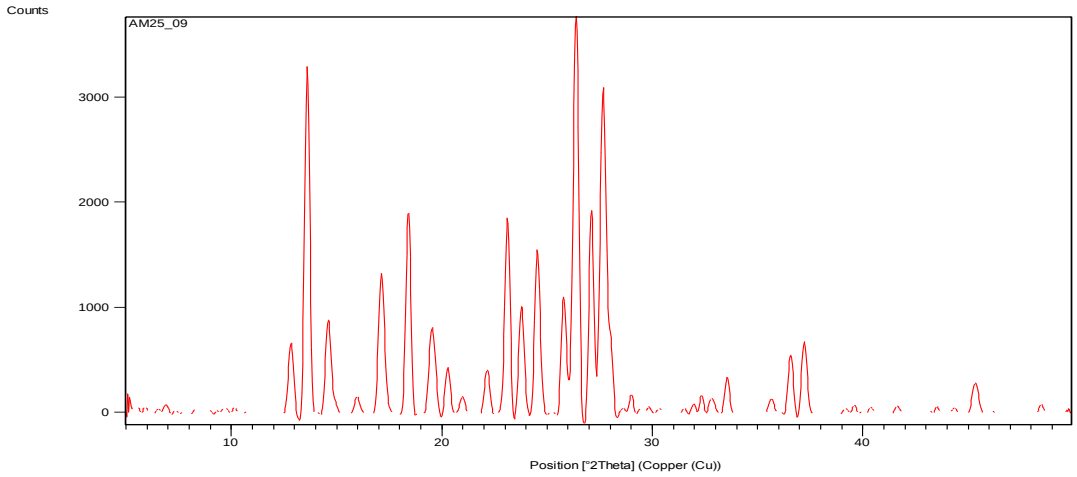

AM25_10 – PAP + 3-chlorobenzoic acid crystallised in ethyl acetate at 4°C

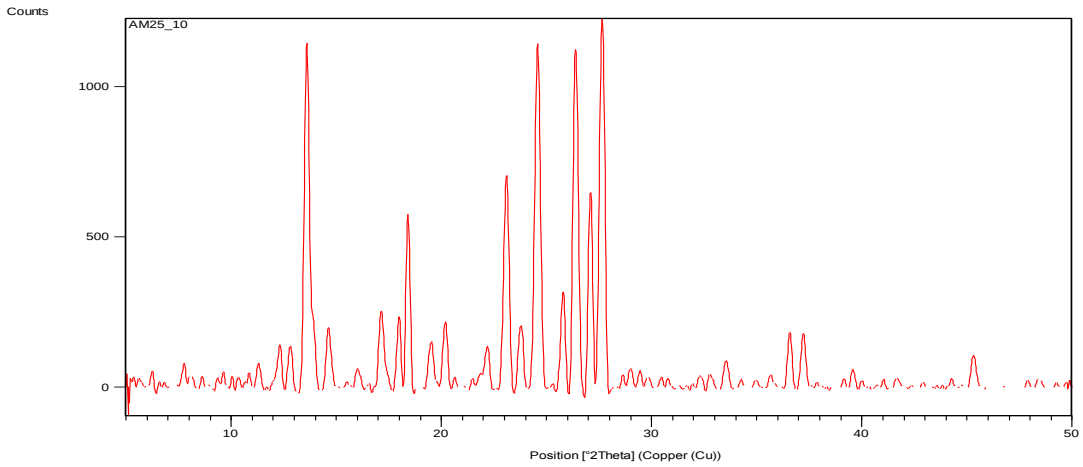

AM25_11 – PAP + 3-chlorobenzoic acid crystallised in ethyl acetate at room temperature

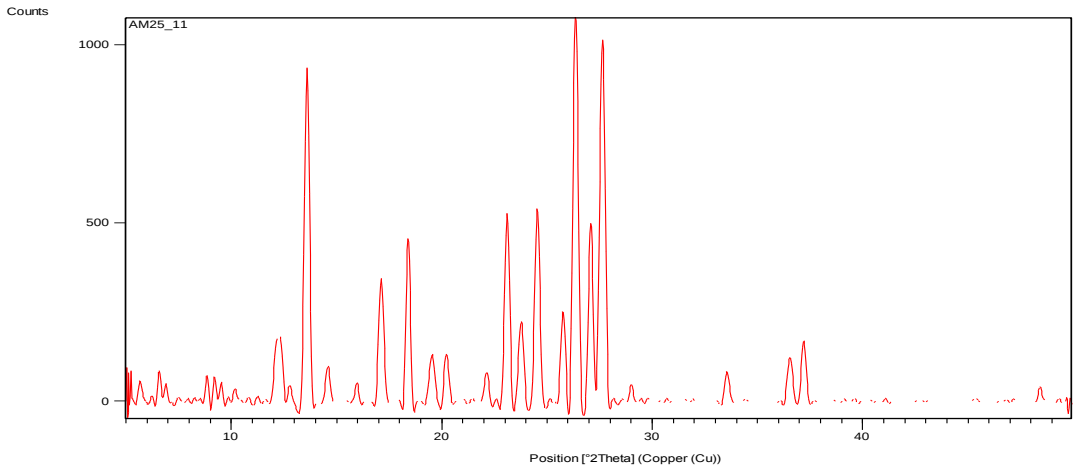

AM25_12 – PAP + 3-chlorobenzoic acid crystallised in ethyl acetate at 30°C

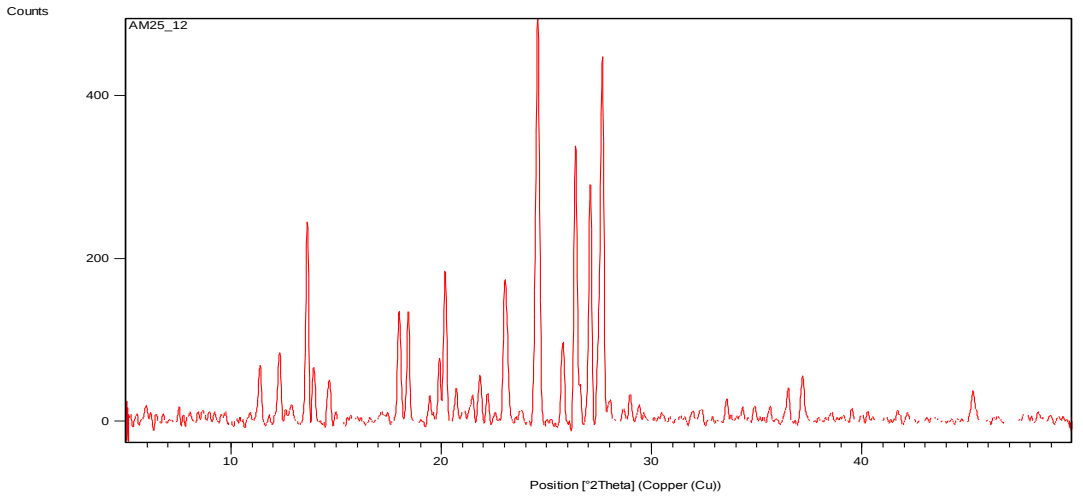

PAP and 4-chlorobenzoic acid

AM27_01 – PAP + 4-chlorobenzoic acid crystallised in methanol at 4°C

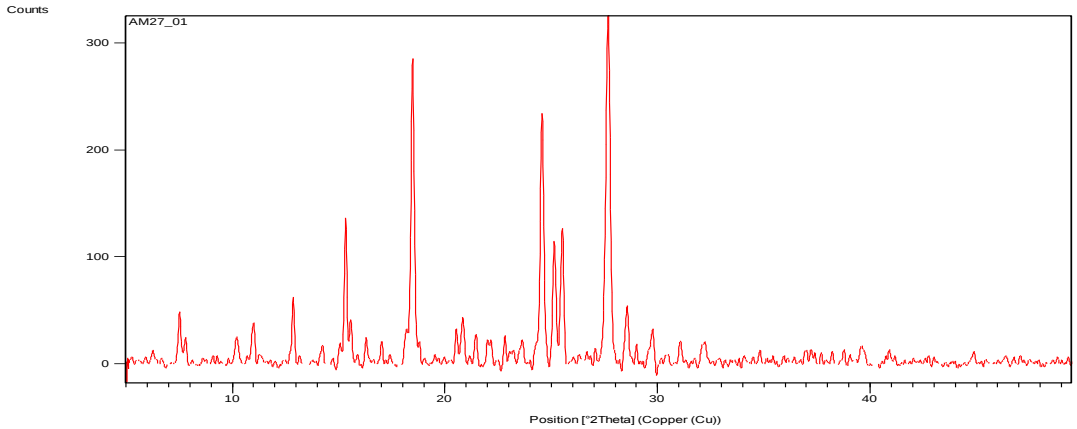

AM27_02 – PAP + 4-chlorobenzoic acid crystallised in methanol at room temperature

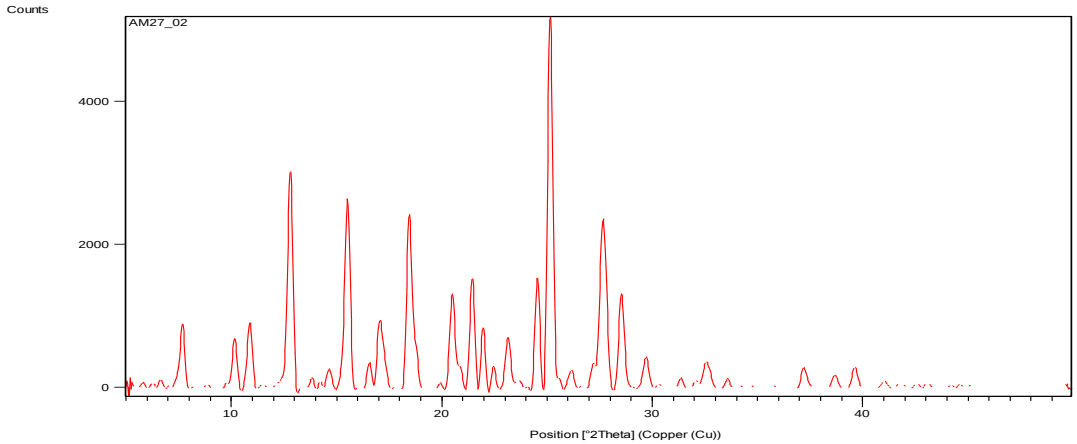

AM27_03 – PAP + 4-chlorobenzoic acid crystallised in methanol at 30°C

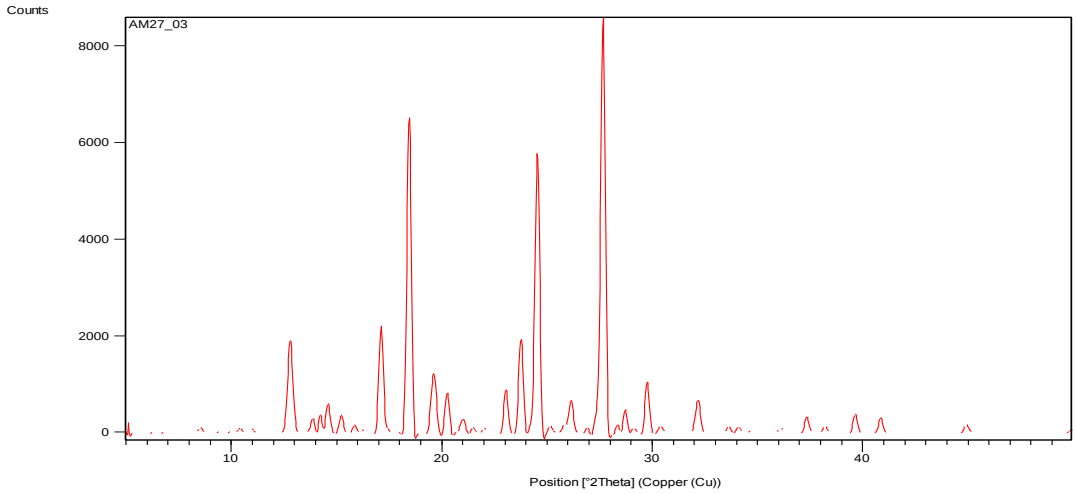

AM27_04 – PAP + 4-chlorobenzoic acid crystallised in ethanol at 4°C

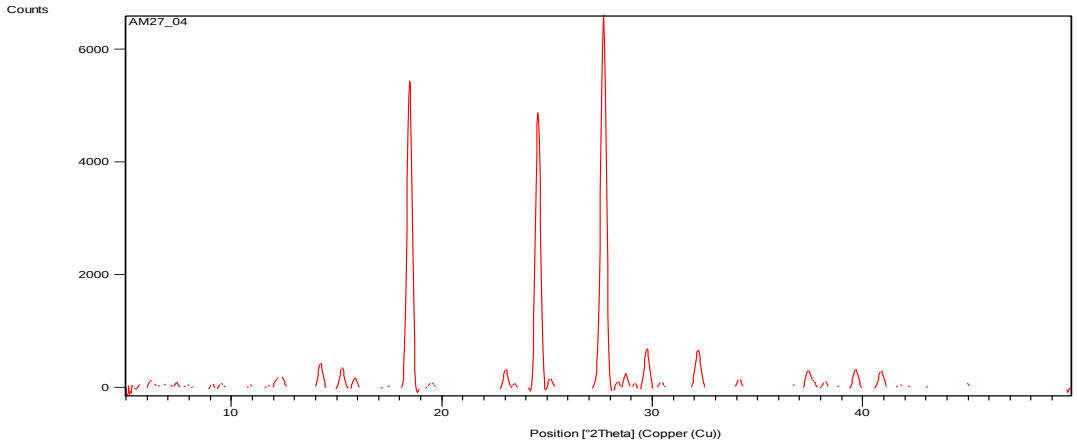

AM27_05 – PAP + 4-chlorobenzoic acid crystallised in ethanol at room temperature

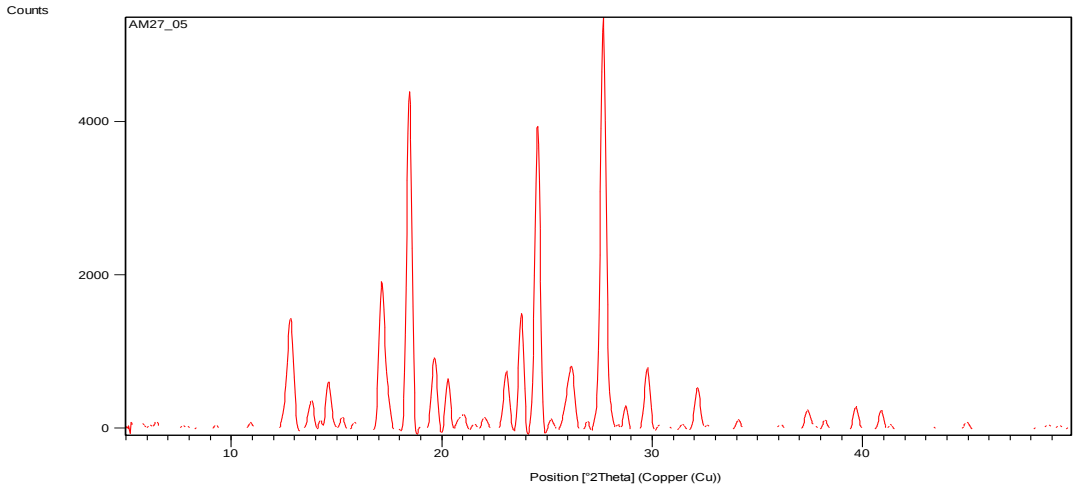

AM27_06 – PAP + 4-chlorobenzoic acid crystallised in ethanol at 30°C

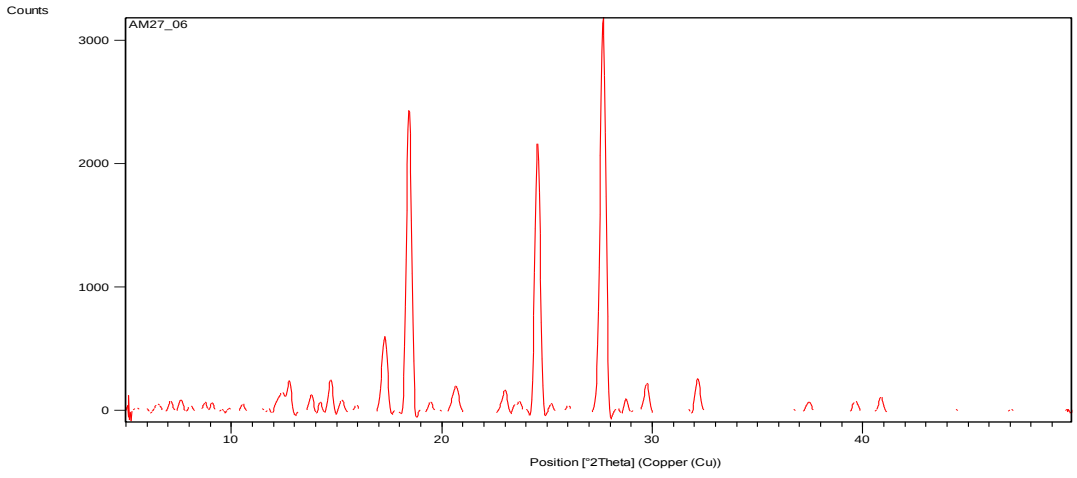

AM27_07 – PAP + 4-chlorobenzoic acid crystallised in acetone at 4°C

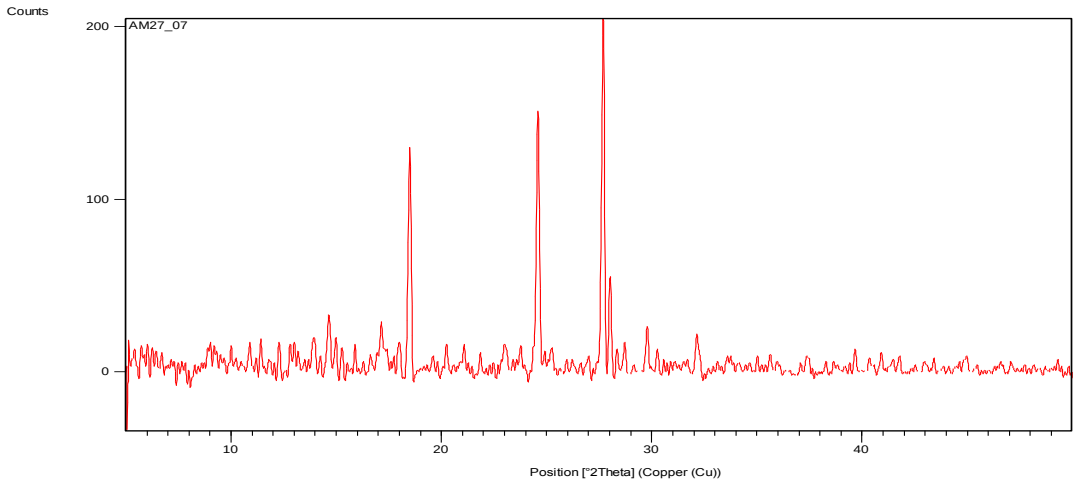

AM27_08 – PAP + 4-chlorobenzoic acid crystallised in acetone at room temperature

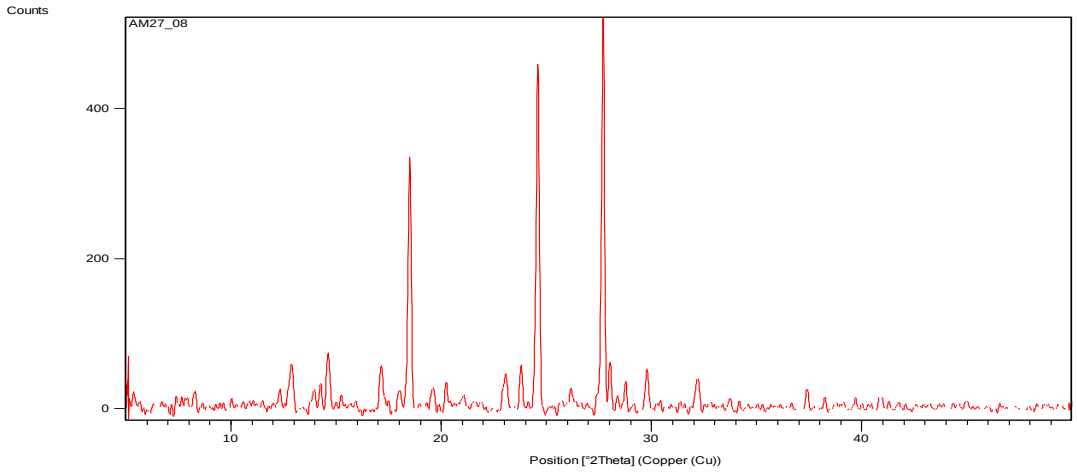

AM27_10 – PAP + 4-chlorobenzoic acid crystallised in ethyl acetate at 4°C

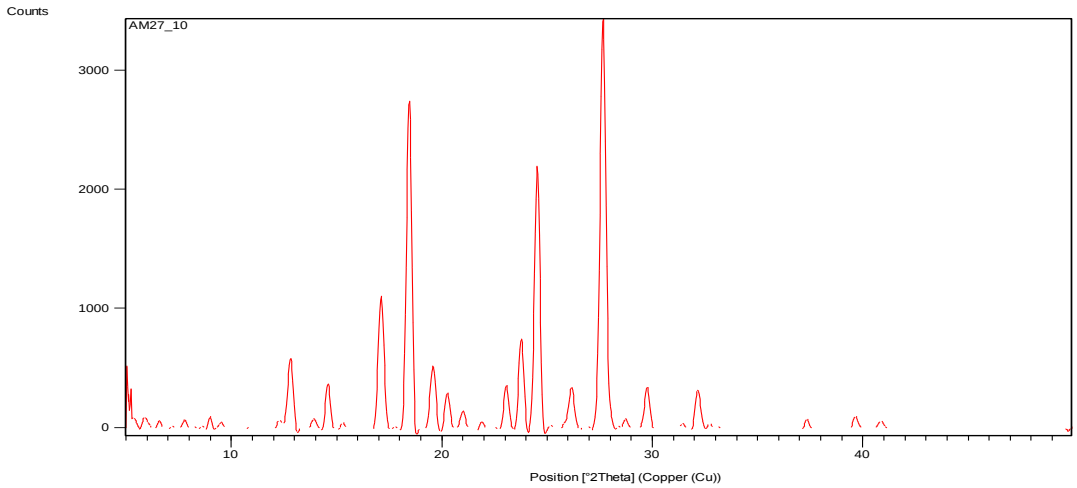

AM27_11 – PAP + 4-chlorobenzoic acid crystallised in ethyl acetate at room temperature

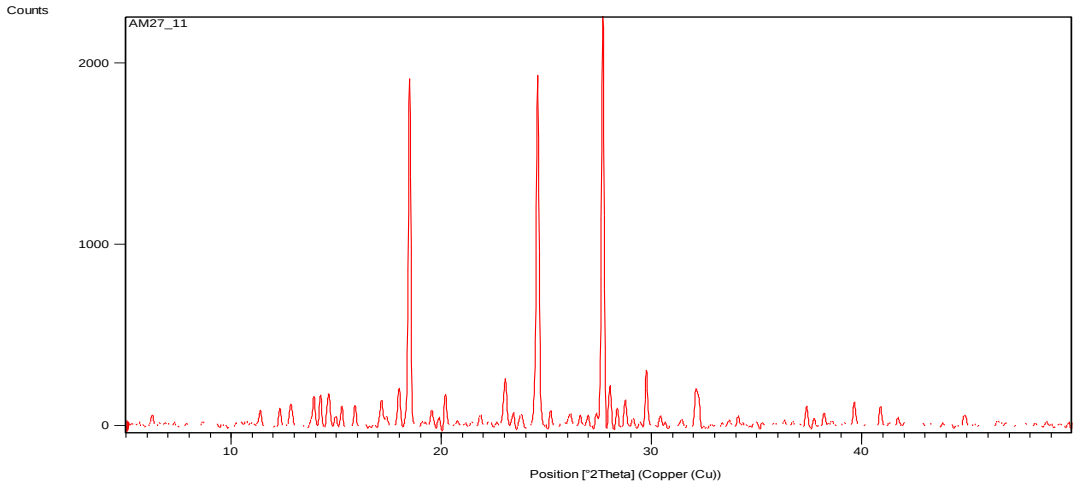

AM27_12 – PAP + 4-chlorobenzoic acid crystallised in ethyl acetate at 30°C

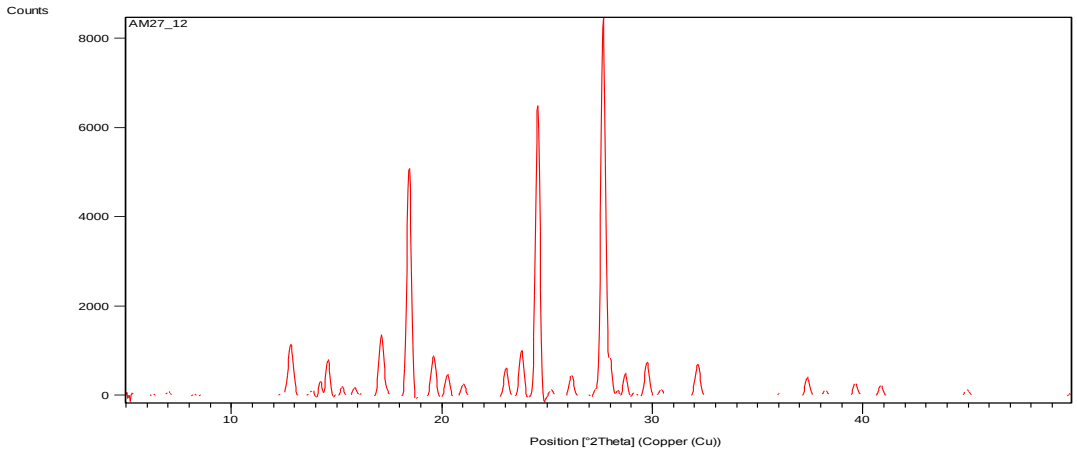

PAP and 1-naphthaleneacetic acid

AM28_01 – PAP + 1-naphthaleneacetic acid crystallised in methanol at 4°C

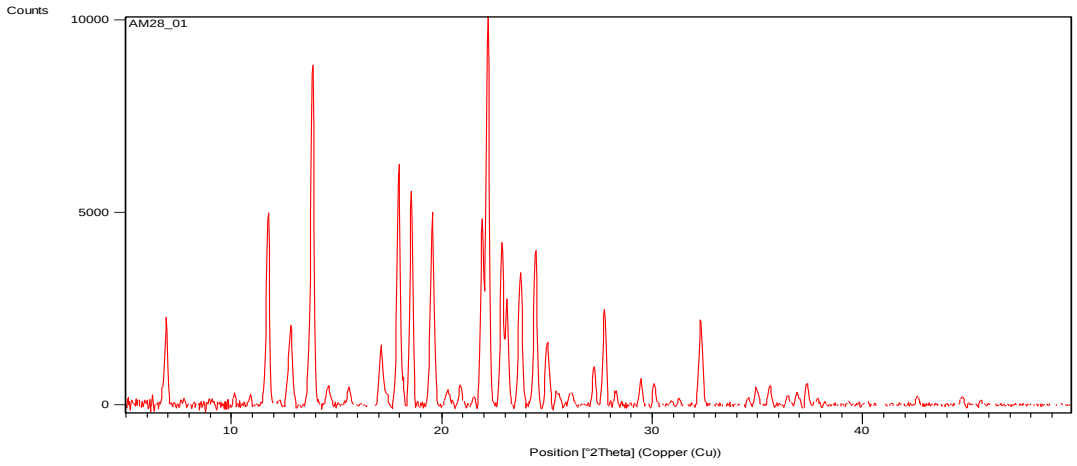

AM28_03 – PAP + 1-naphthaleneacetic acid crystallised in methanol at 30°C

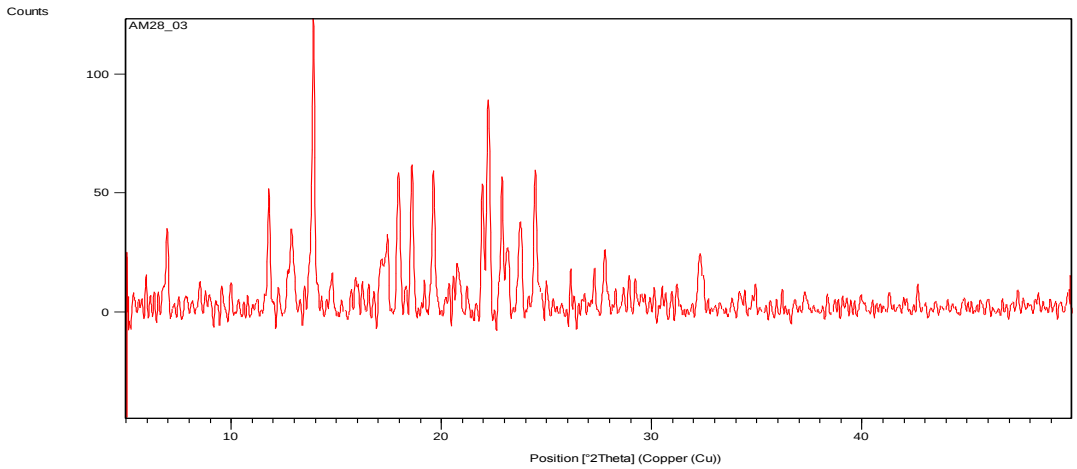

AM28_04 – PAP + 1-naphthaleneacetic acid crystallised in ethanol at 4°C

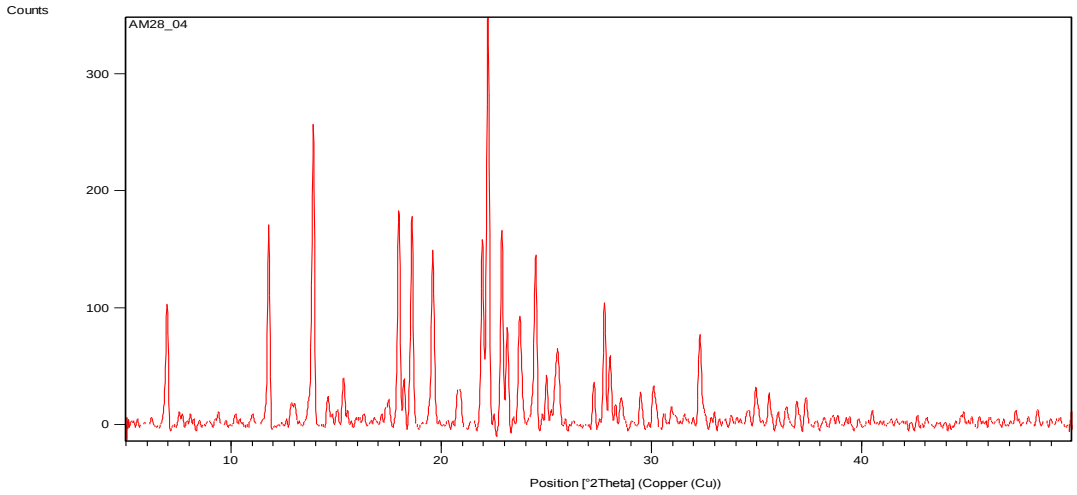

AM28_05 – PAP + 1-naphthaleneacetic acid crystallised in ethanol at room temperature

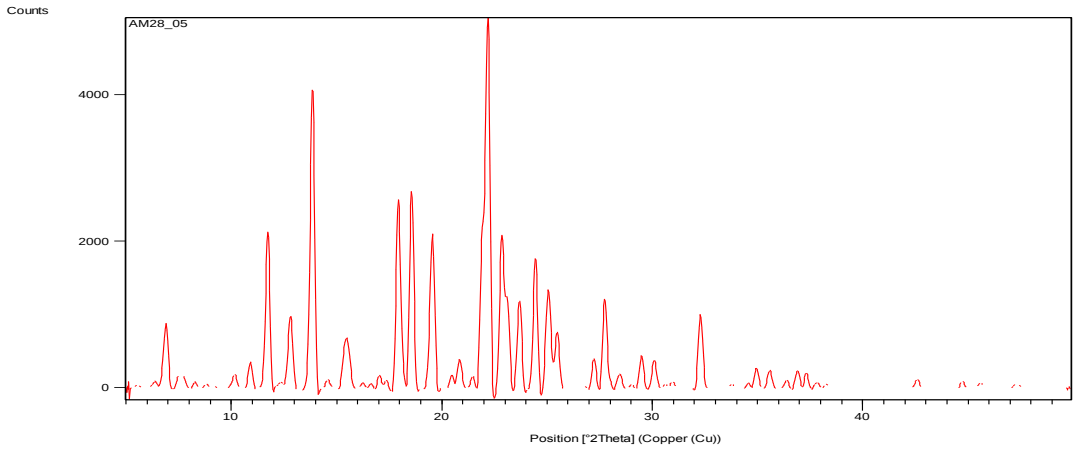

AM28_06 – PAP + 1-naphthaleneacetic acid crystallised in ethanol at 30°C

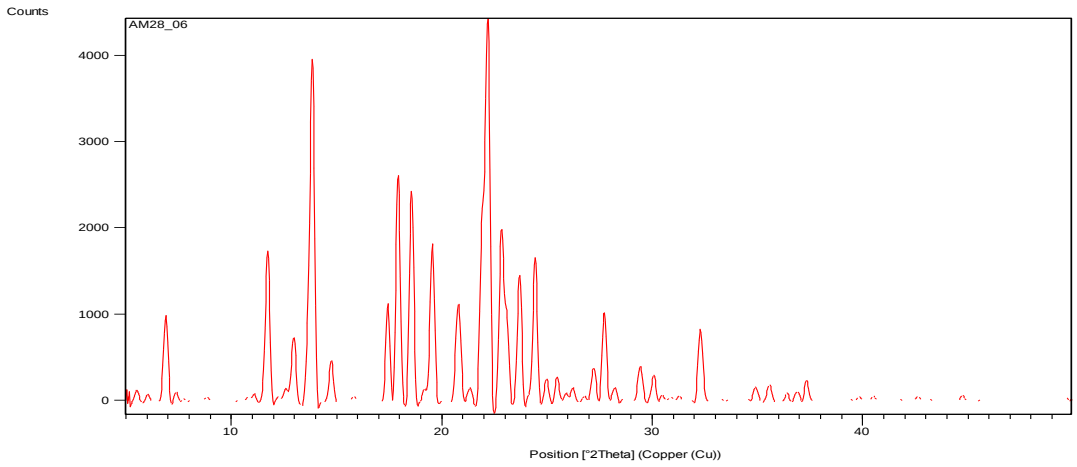

AM28_07 – PAP + 1-naphthaleneacetic acid crystallised in acetone at 4°C

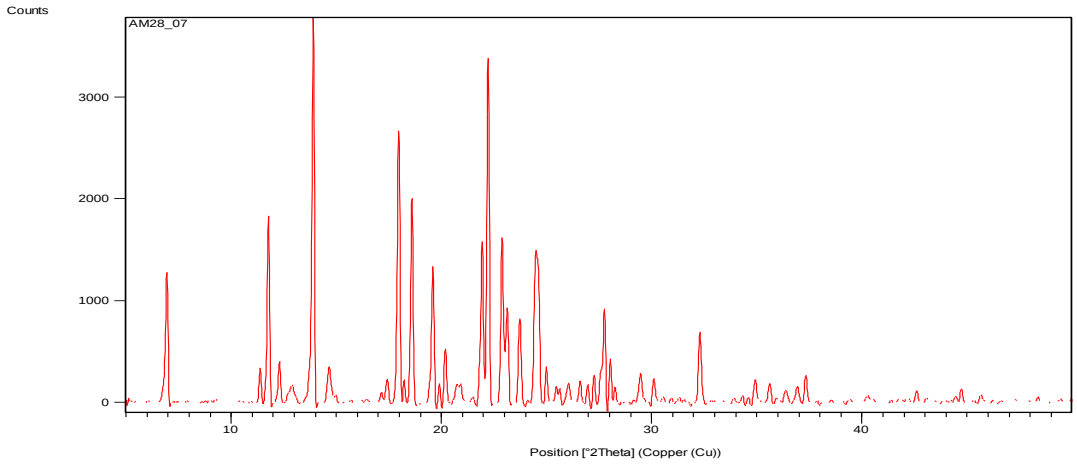

AM28_08 – PAP + 1-naphthaleneacetic acid crystallised in acetone at room temperature

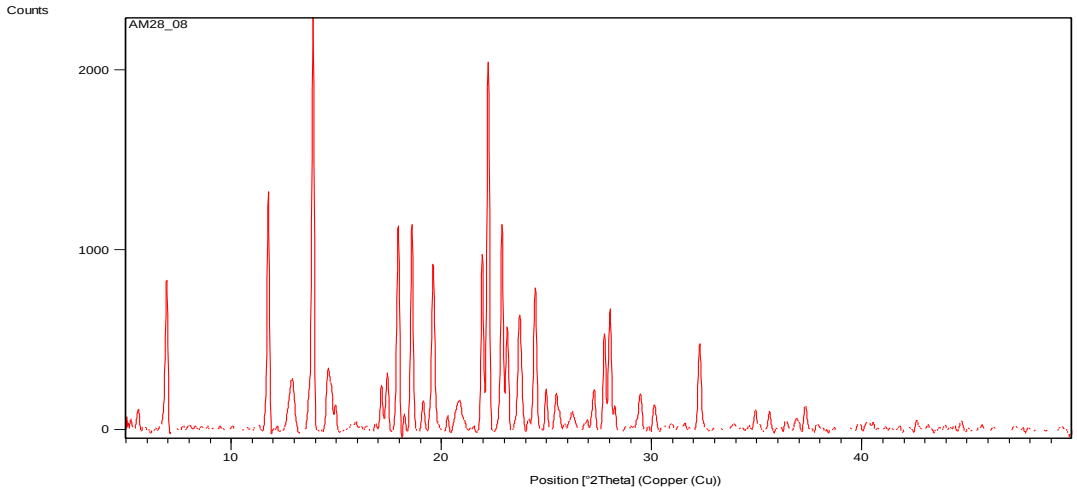

AM28_09 – PAP + 1-naphthaleneacetic acid crystallised in acetone at 30°C

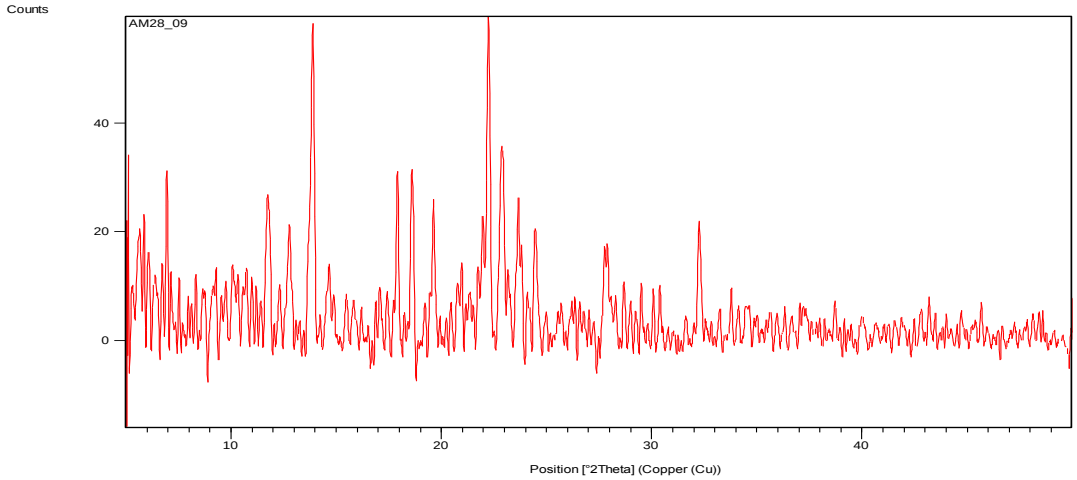

AM28_10 – PAP + 1-naphthaleneacetic acid crystallised in ethyl acetate at 4°C

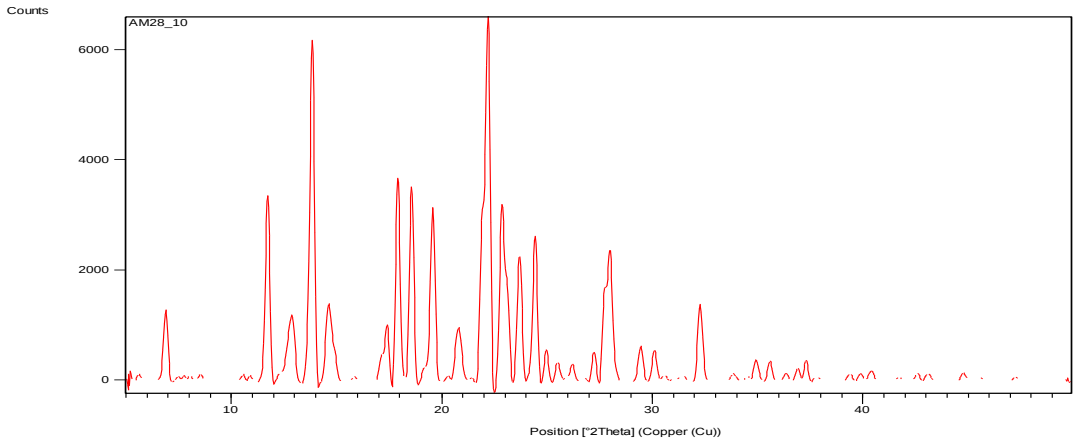

AM28_11 – PAP + 1-naphthaleneacetic acid crystallised in ethyl acetate at room temperature

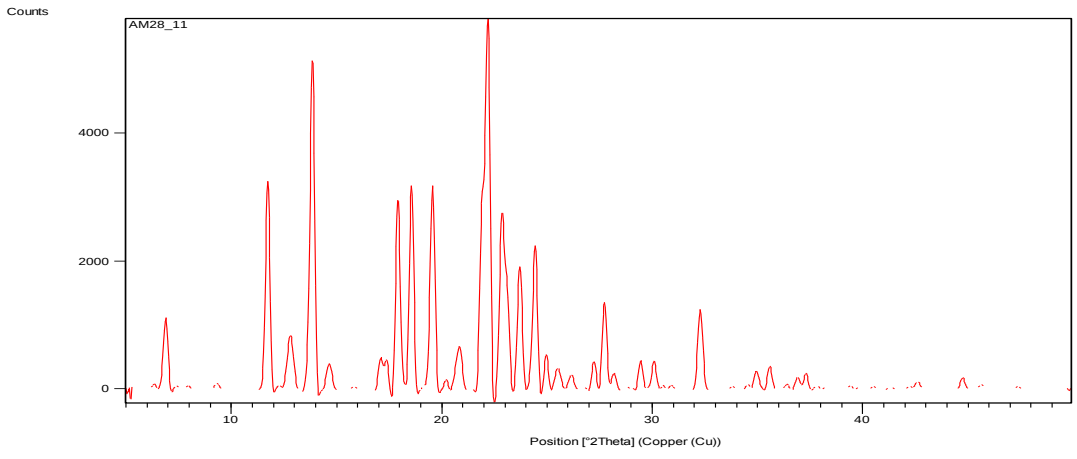

AM28_12 – PAP + 1-naphthaleneacetic acid crystallised in ethyl acetate at 30°C

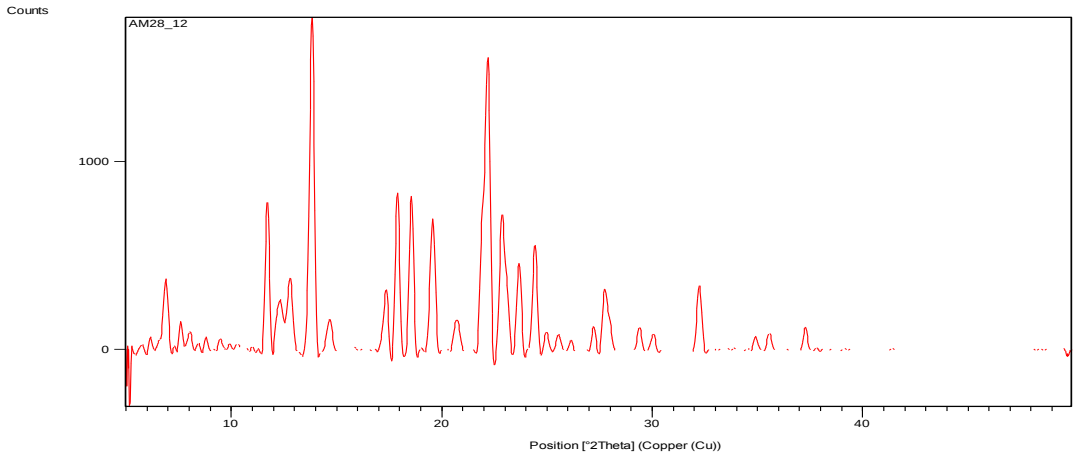

AM28_13 – PAP + 1-naphthaleneacetic acid crystallised in diethyl ether at 4°C

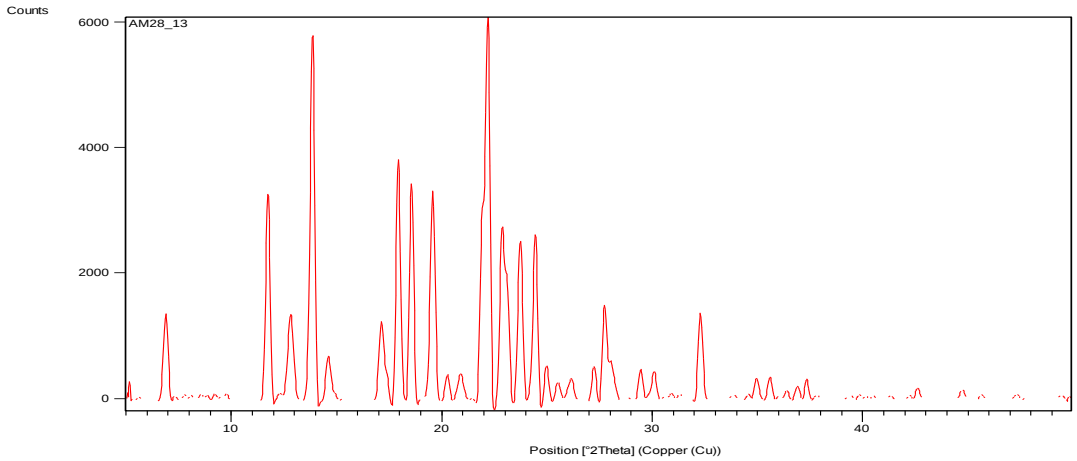

AM28_14 – PAP + 1-naphthaleneacetic acid crystallised in diethyl ether at room temperature

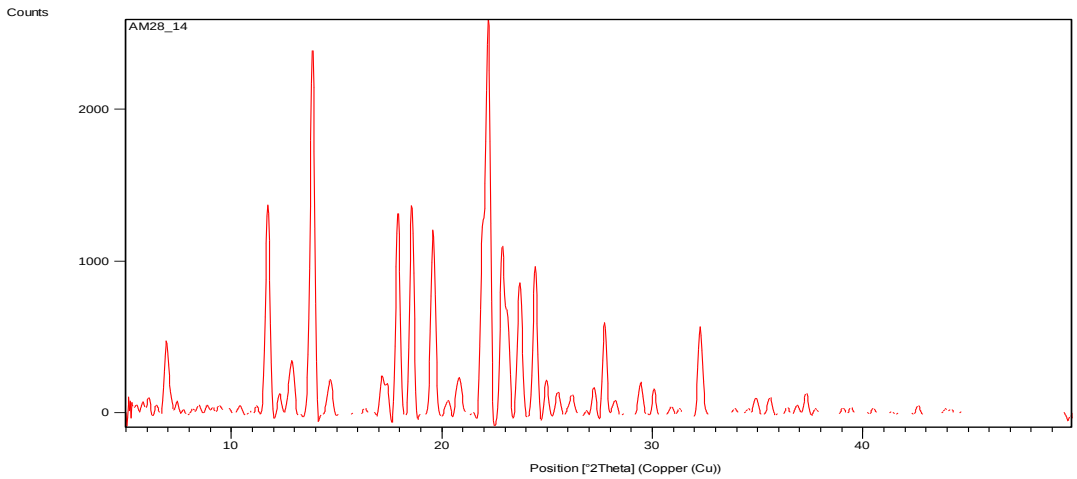

AM28_15 – PAP + 1-naphthaleneacetic acid crystallised in diethyl ether at 30°C

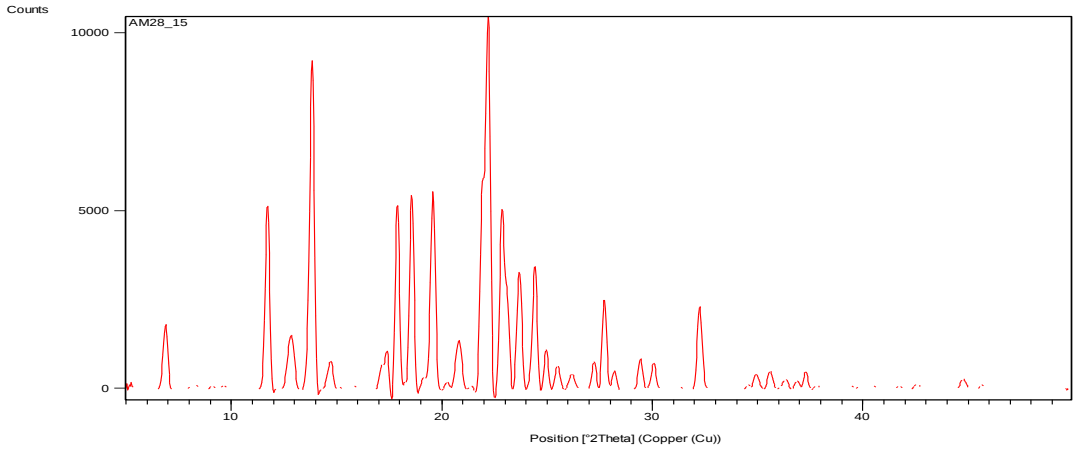

PAP and Salicylic acid

AM29_01 – PAP + salicylic acid crystallised in methanol at 4°C

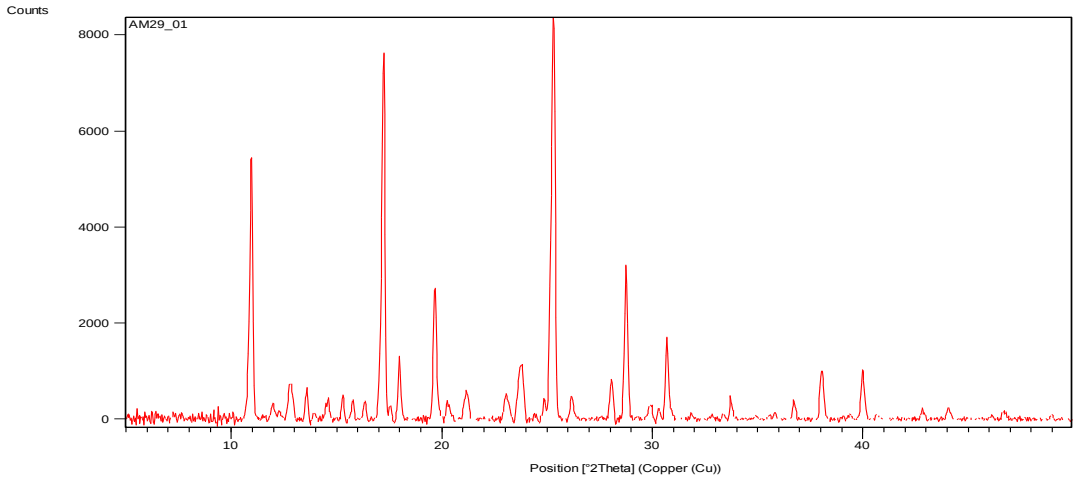

AM29_02 – PAP + salicylic acid crystallised in methanol at room temperature

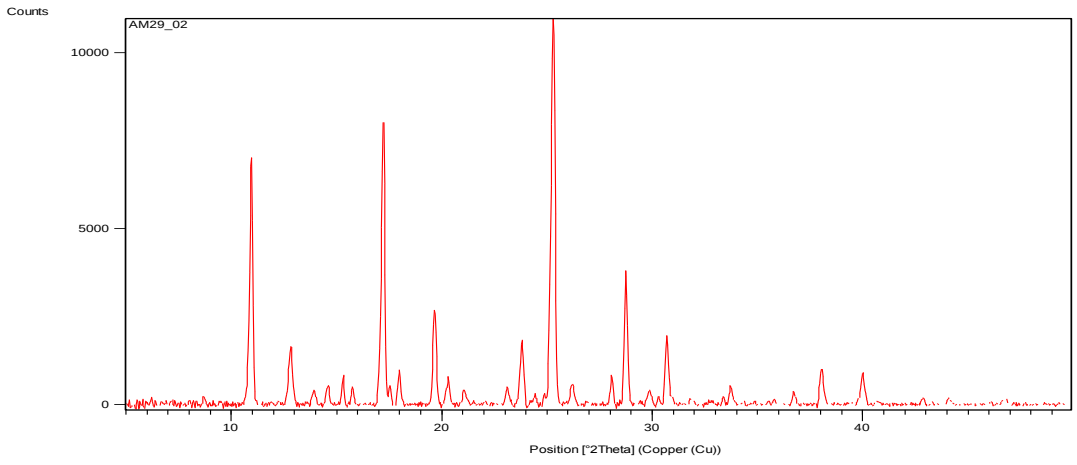

AM29_03 – PAP + salicylic acid crystallised in methanol at 30°C

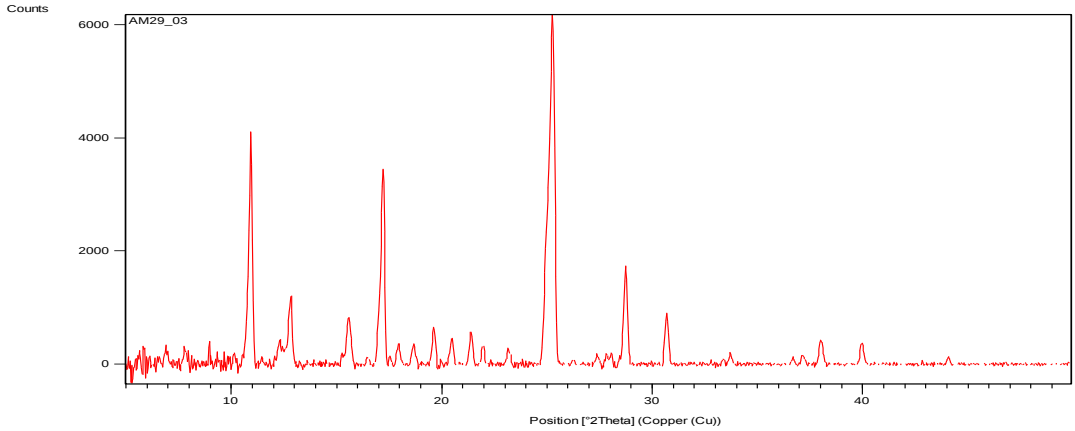

AM29_04 – PAP + salicylic acid crystallised in ethanol at 4°C

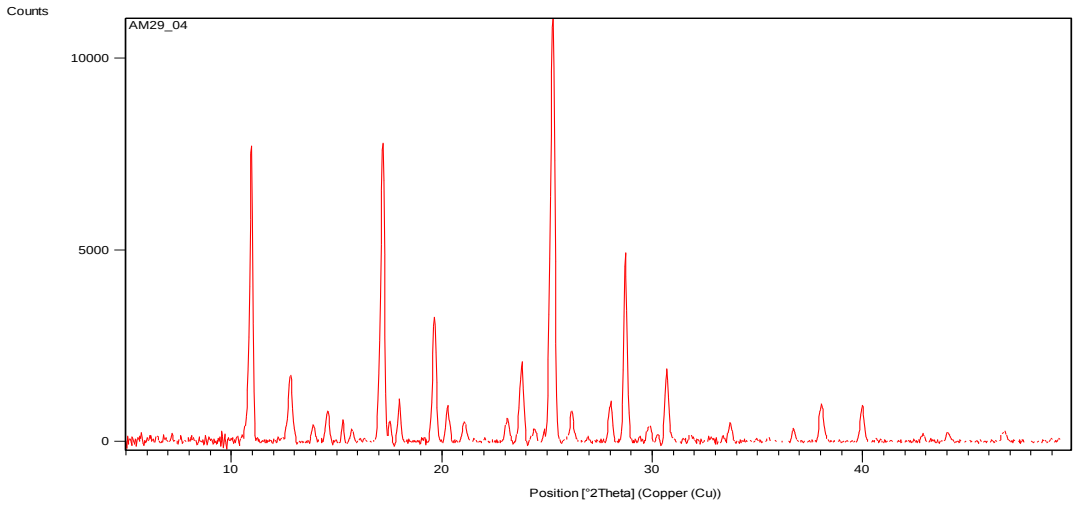

AM29_05 – PAP + salicylic acid crystallised in ethanol at room temperature

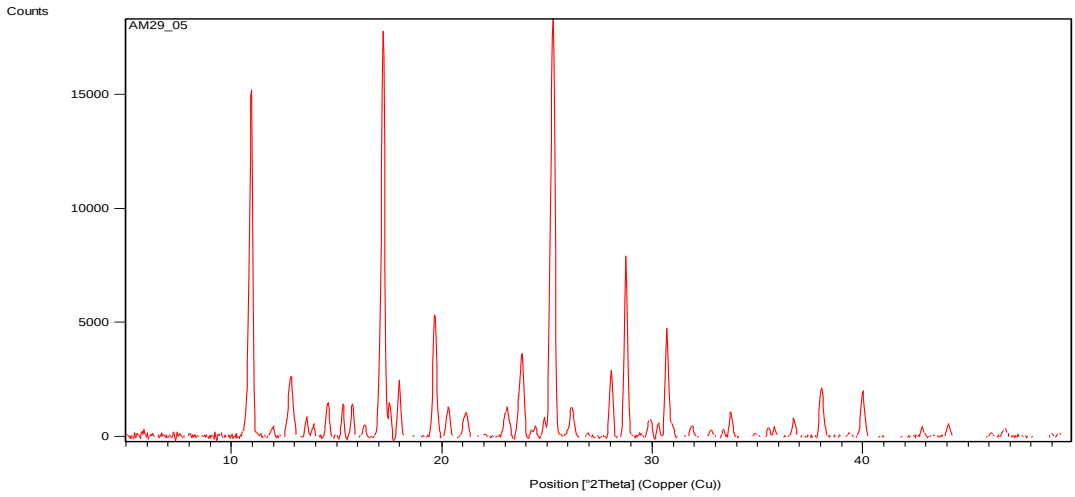

AM29_06 – PAP + salicylic acid crystallised in ethanol at 30°C

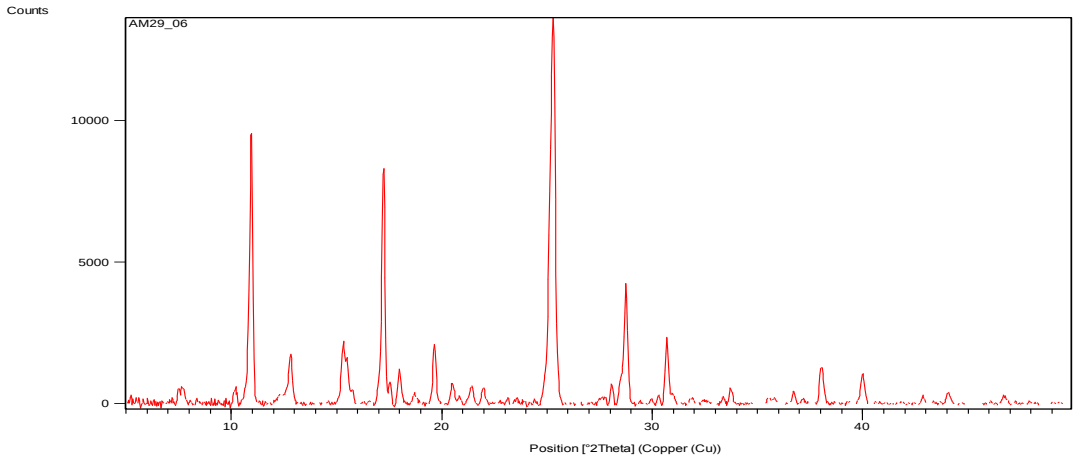

AM29_07 – PAP + salicylic acid crystallised in acetone at 4°C

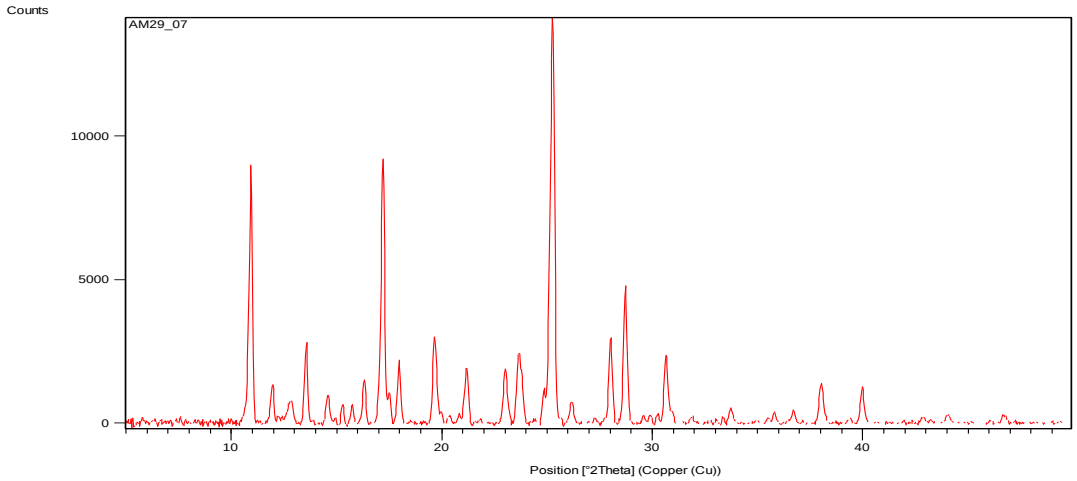

AM29_08 – PAP + salicylic acid crystallised in acetone at room temperature

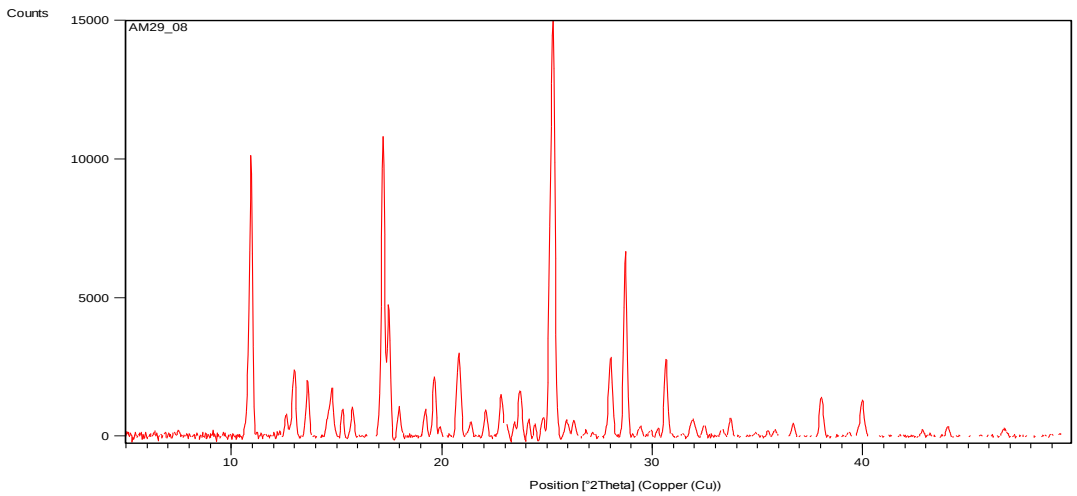

AM29_09 – PAP + salicylic acid crystallised in acetone at 30°C

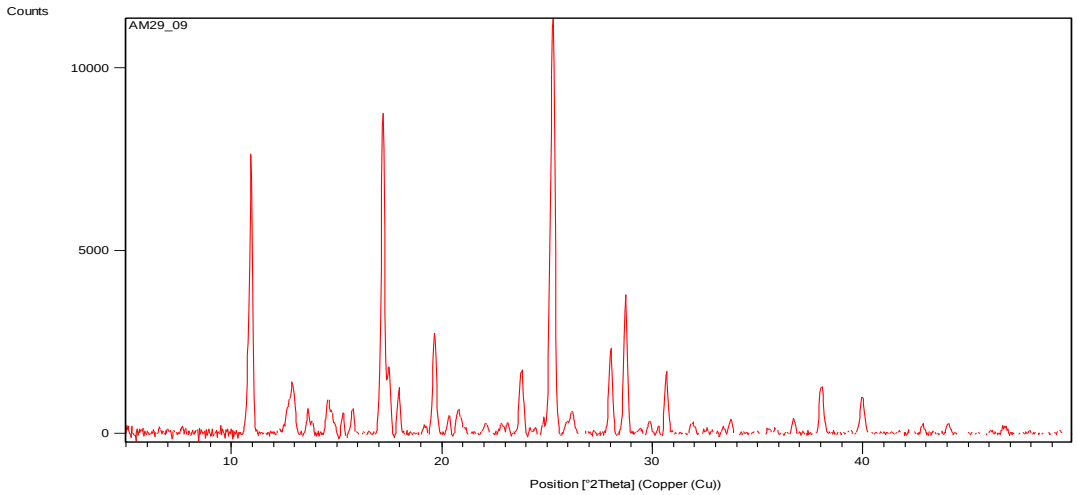

AM29_10 – PAP + salicylic acid crystallised in ethyl acetate at 4°C

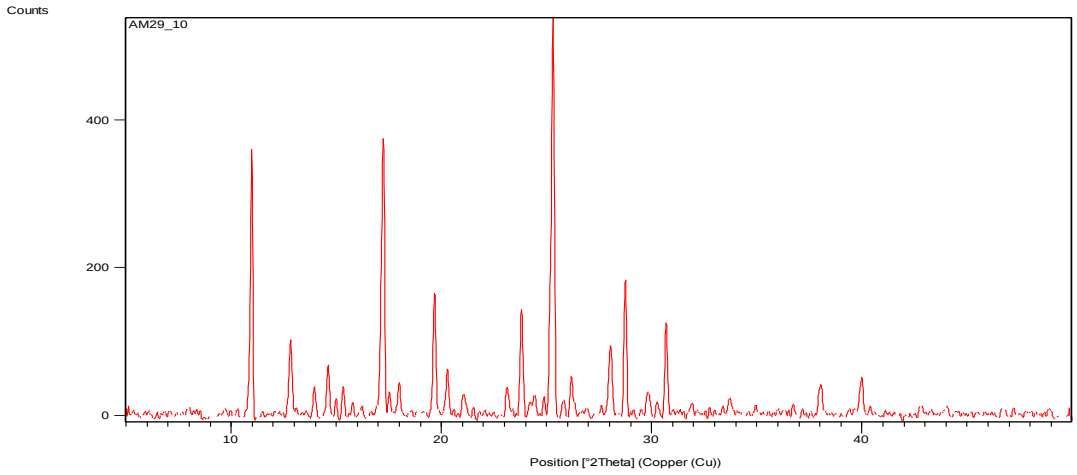

AM29_11 – PAP + salicylic acid crystallised in ethyl acetate at room temperature

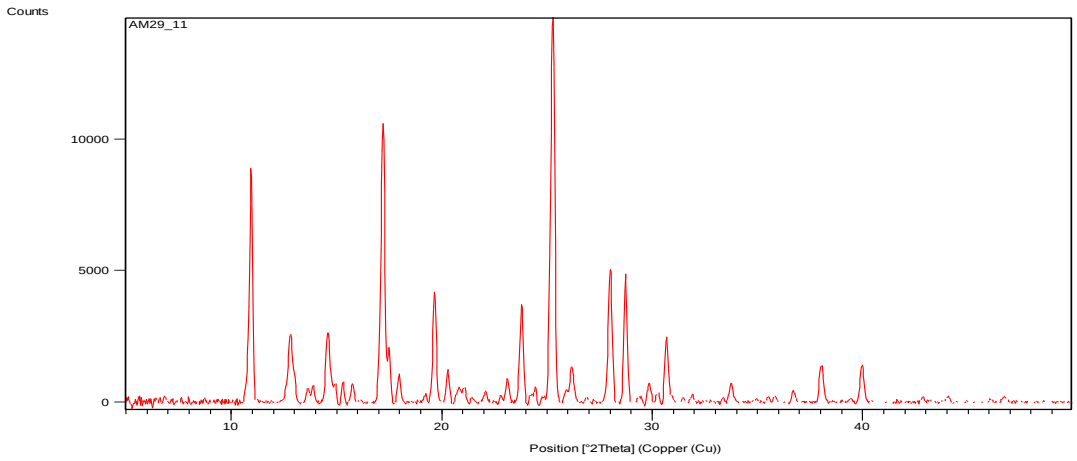

AM29_12 – PAP + salicylic acid crystallised in ethyl acetate at 30°C

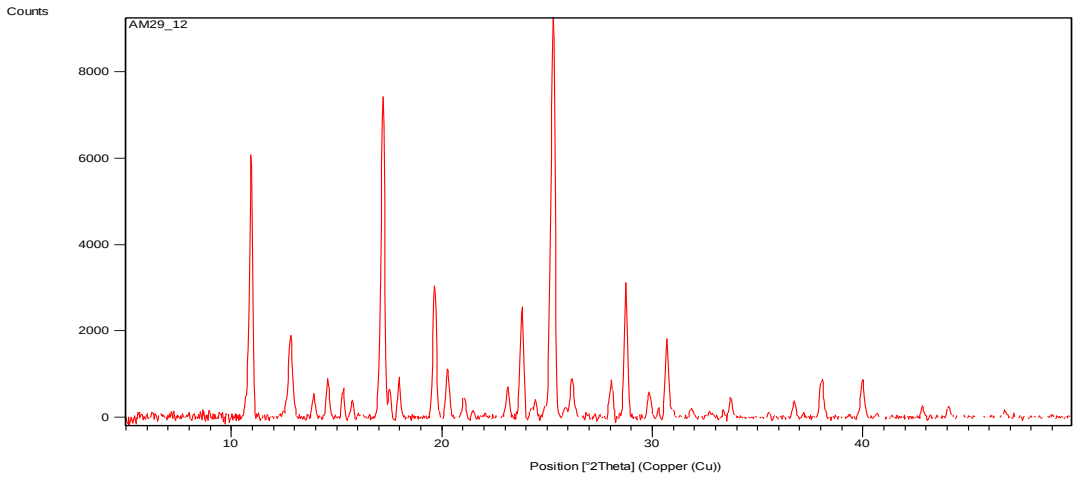

AM29_13 – PAP + salicylic acid crystallised in ethyl acetate at 4°C

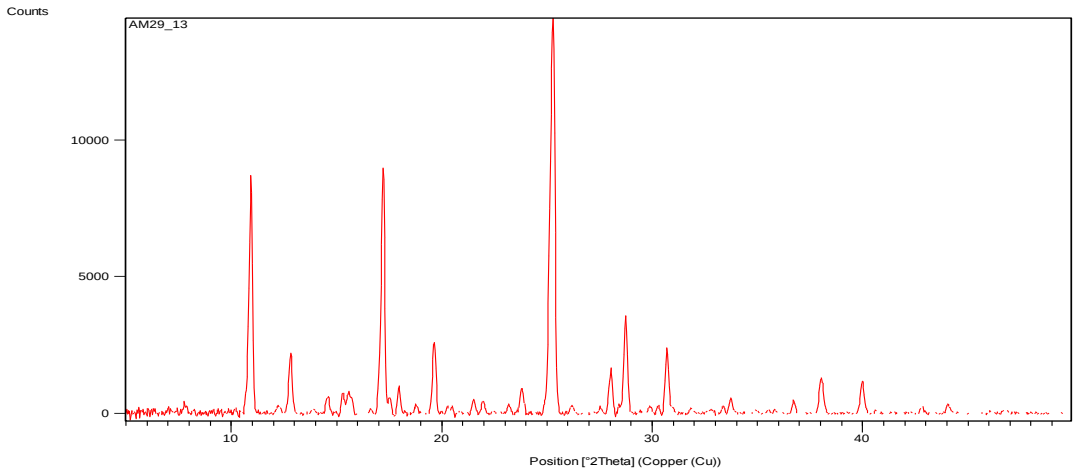

AM29_14 – PAP + salicylic acid crystallised in ethyl acetate at room temperature

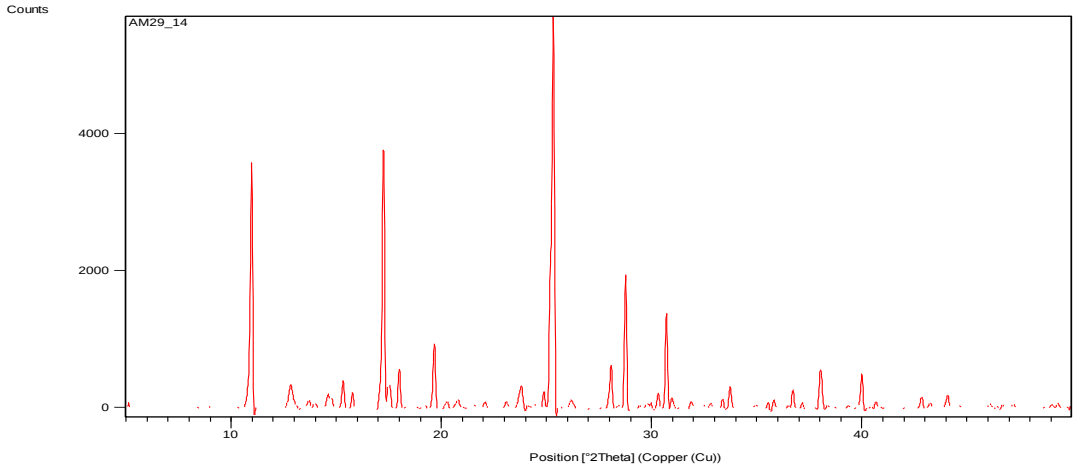

AM29_15 – PAP + salicylic acid crystallised in ethyl acetate at 30°C

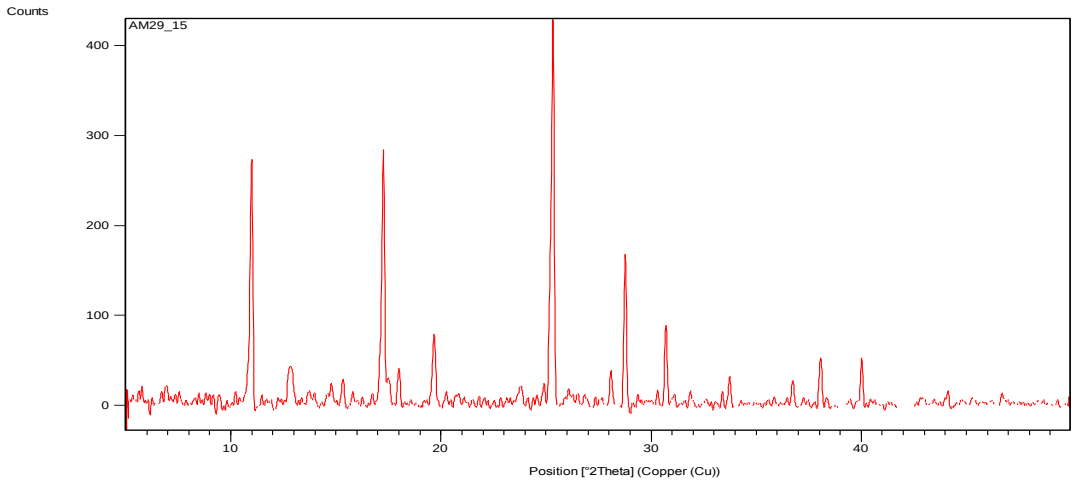

PAP and 3-hydroxybenzoic acid

AM30_01 – PAP + 3-hydroxybenzoic acid crystallised in methanol at 4°C

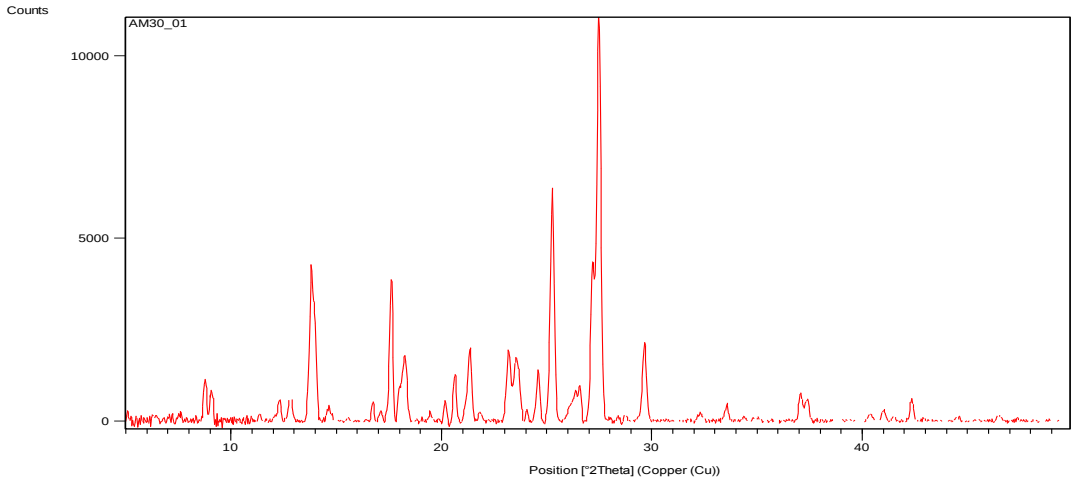

AM30_02 – PAP + 3-hydroxybenzoic acid crystallised in methanol at room temperature

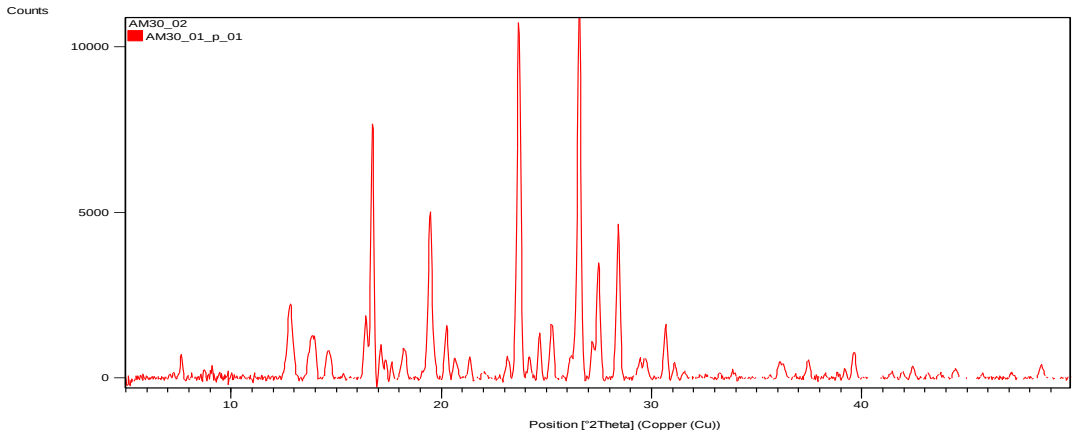

AM30_03 – PAP + 3-hydroxybenzoic acid crystallised in methanol at 30°C

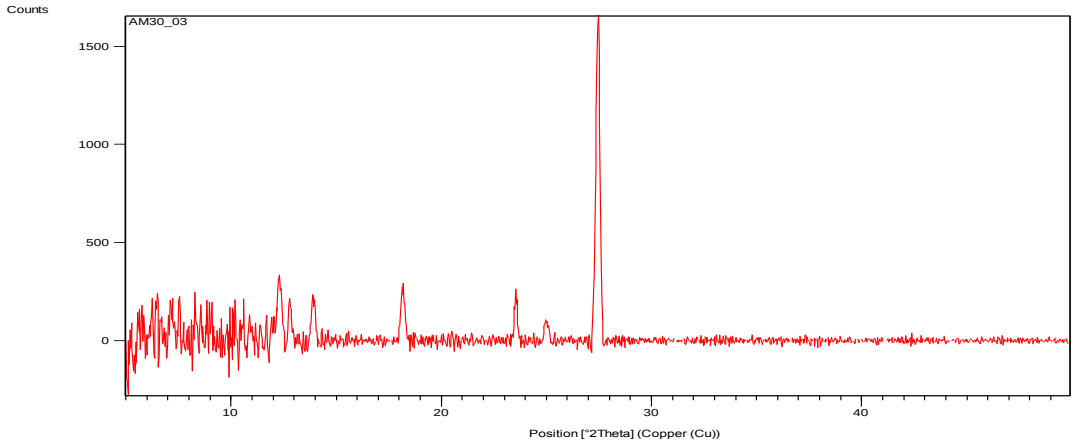

AM30_04 – PAP + 3-hydroxybenzoic acid crystallised in ethanol at 4°C

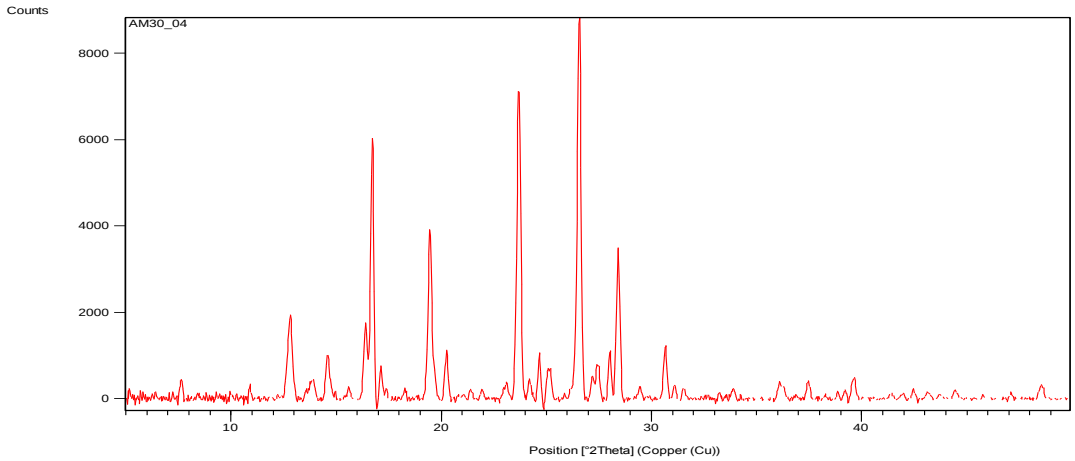

AM30_05 – PAP + 3-hydroxybenzoic acid crystallised in ethanol at room temperature

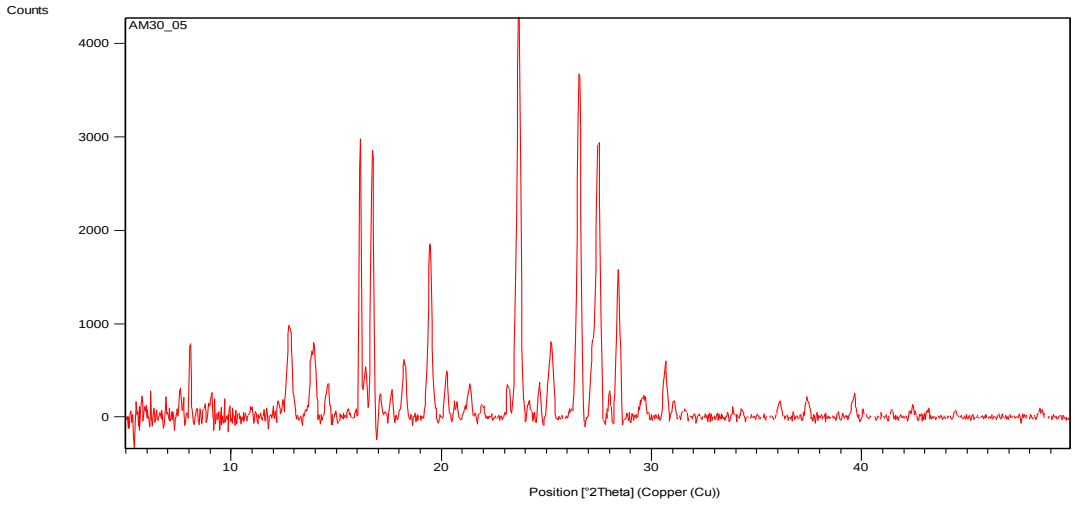

AM30_06 – PAP + 3-hydroxybenzoic acid crystallised in ethanol at 30°C

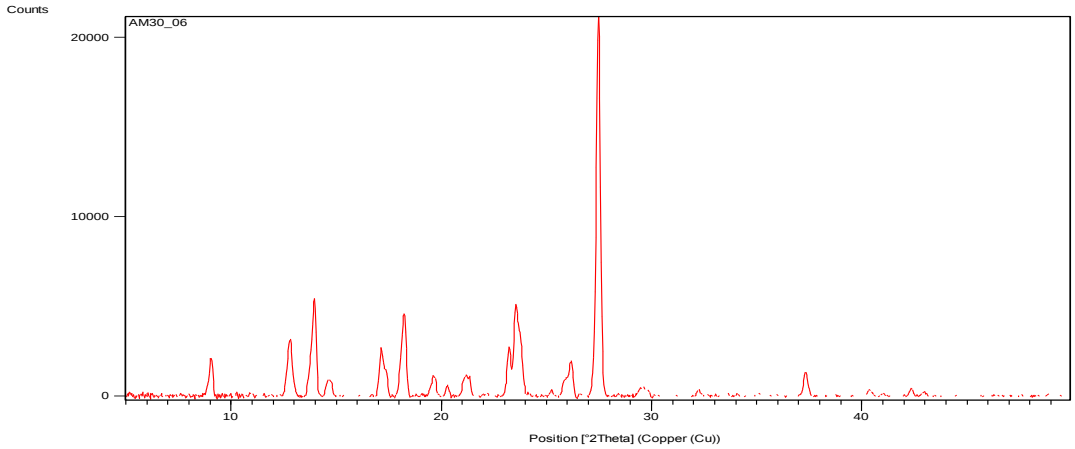

AM30_07 – PAP + 3-hydroxybenzoic acid crystallised in acetone at 4°C

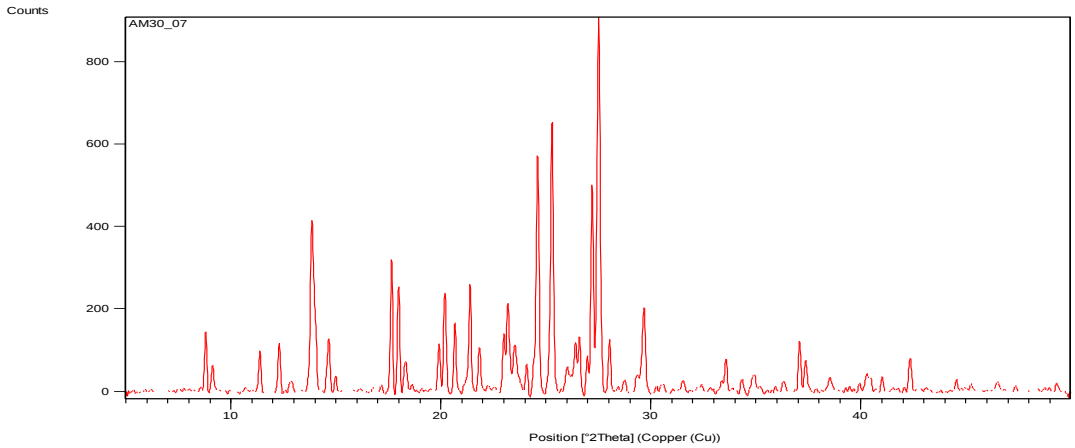

AM30_08 – PAP + 3-hydroxybenzoic acid crystallised in acetone at room temperature

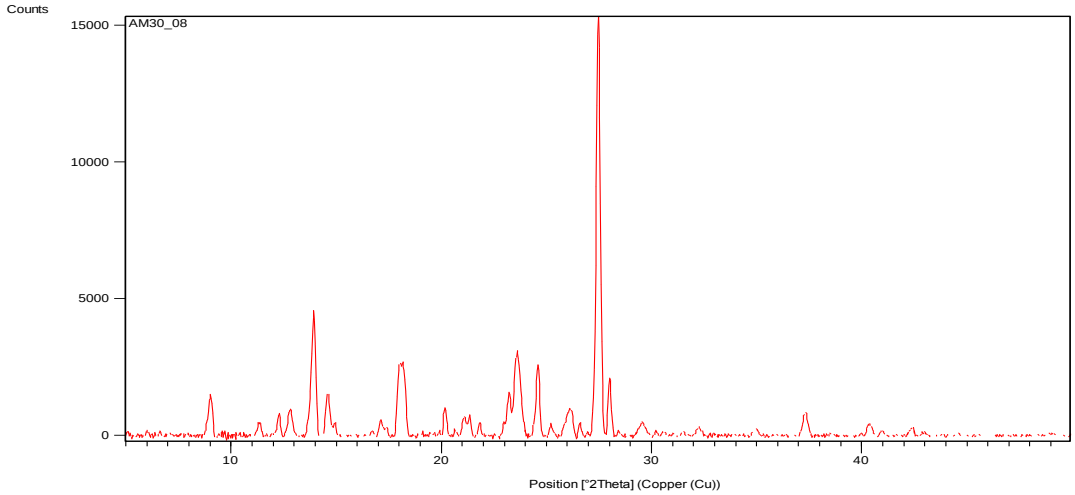

AM30_09 – PAP + 3-hydroxybenzoic acid crystallised in acetone at 30°C

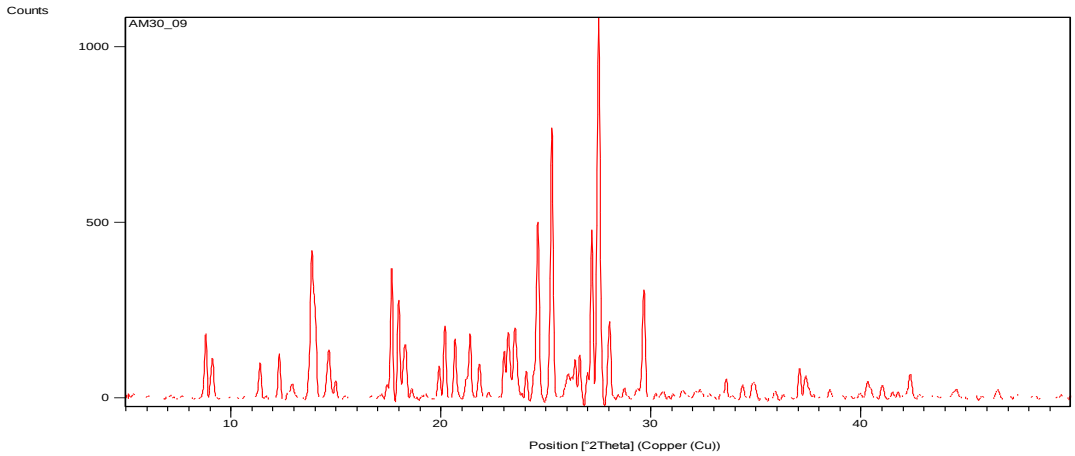

AM30_10 – PAP + 3-hydroxybenzoic acid crystallised in ethyl acetate at 4°C

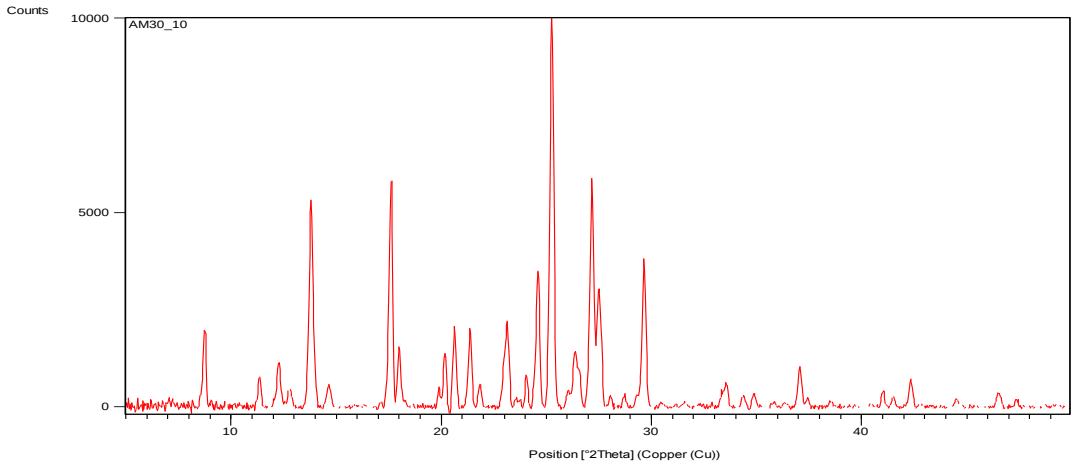

AM30_11 – PAP + 3-hydroxybenzoic acid crystallised in ethyl acetate at room temperature

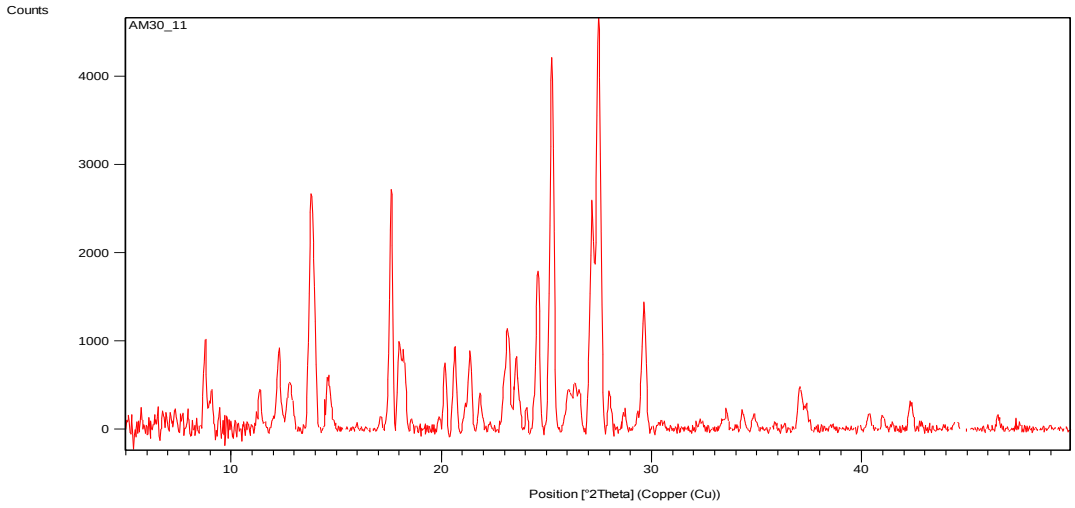

AM30_12 – PAP + 3-hydroxybenzoic acid crystallised in ethyl acetate at 30°C

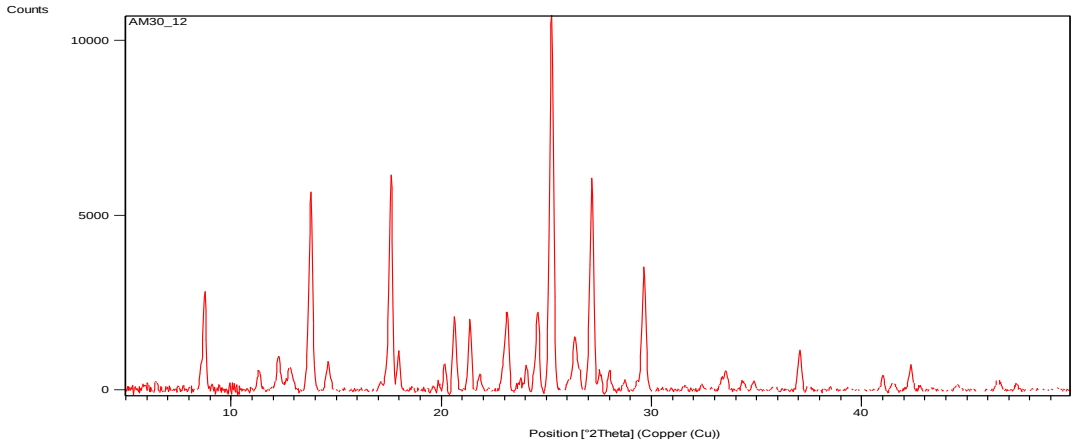

AM30_13 – PAP + 3-hydroxybenzoic acid crystallised in ethyl acetate at 4°C

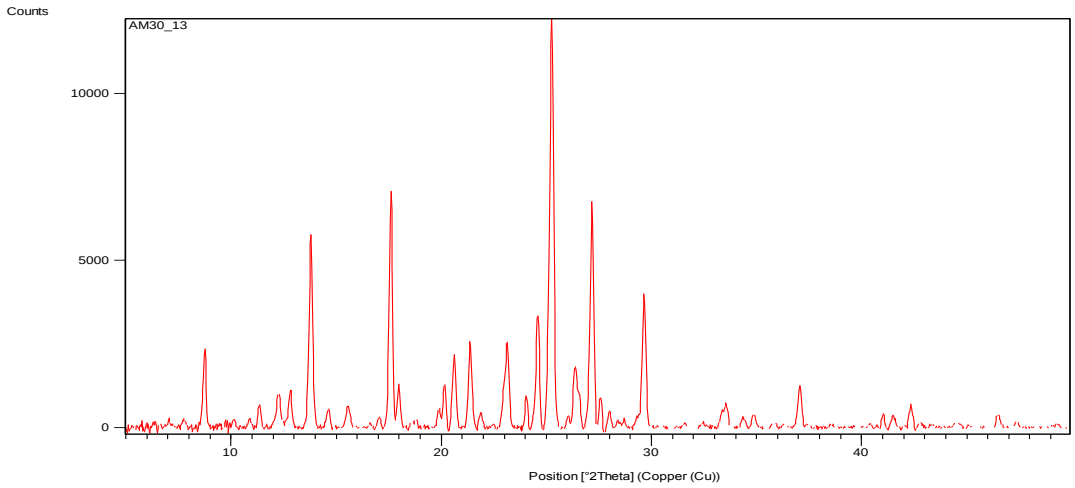

AM30_14 – PAP + 3-hydroxybenzoic acid crystallised in ethyl acetate at room temperature

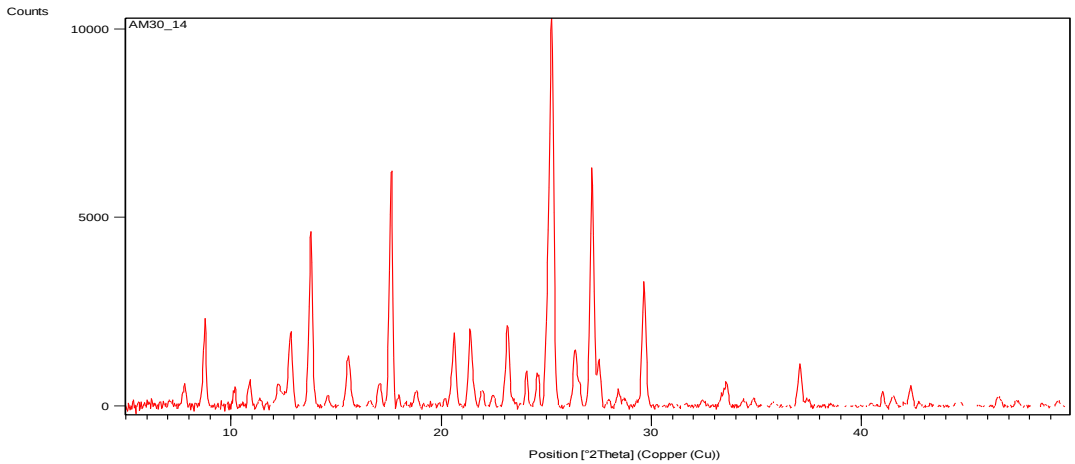

AM30_15 – PAP + 3-hydroxybenzoic acid crystallised in ethyl acetate at 30°C

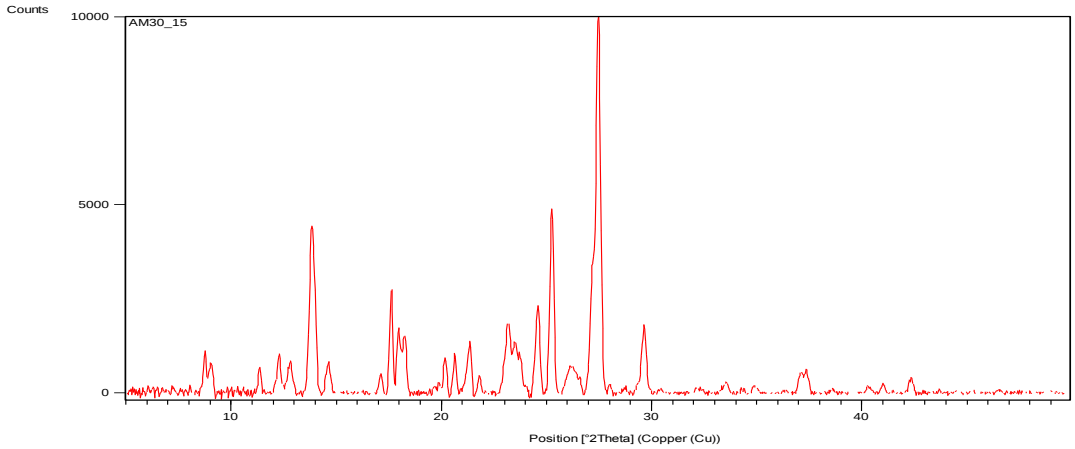

PAP and malonic acid

AM38_14 – PAP + Malonic acid with hydrogen peroxide crystallised in acetone at 4°C

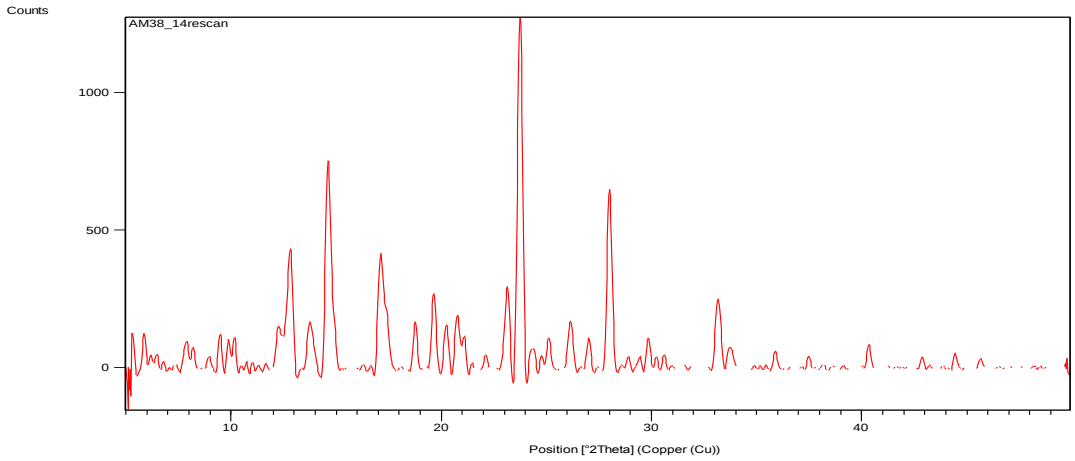

AM38_15 – PAP + Malonic acid with hydrogen peroxide crystallised in acetone at room temperature

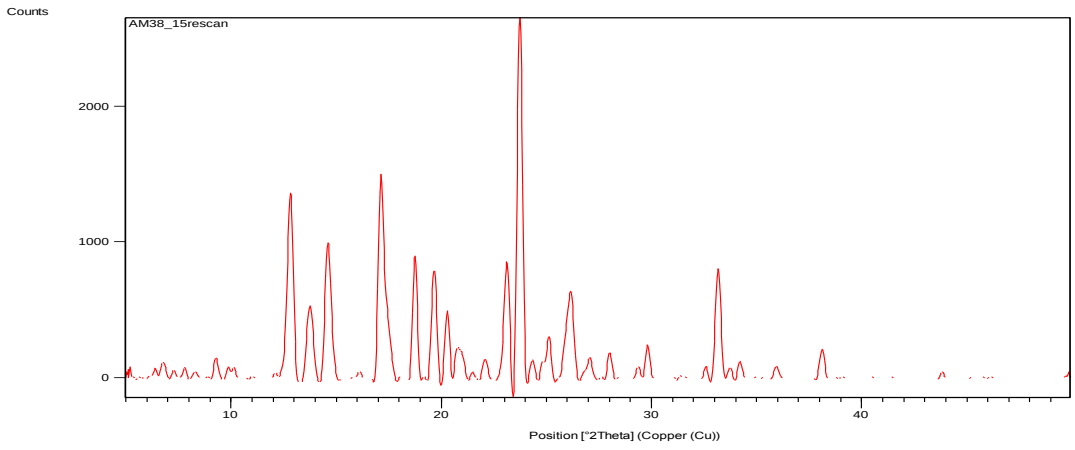

PAP and oxalic acid

AM38_17 – PAP + Malonic acid with hydrogen peroxide crystallised in acetone at 4°C

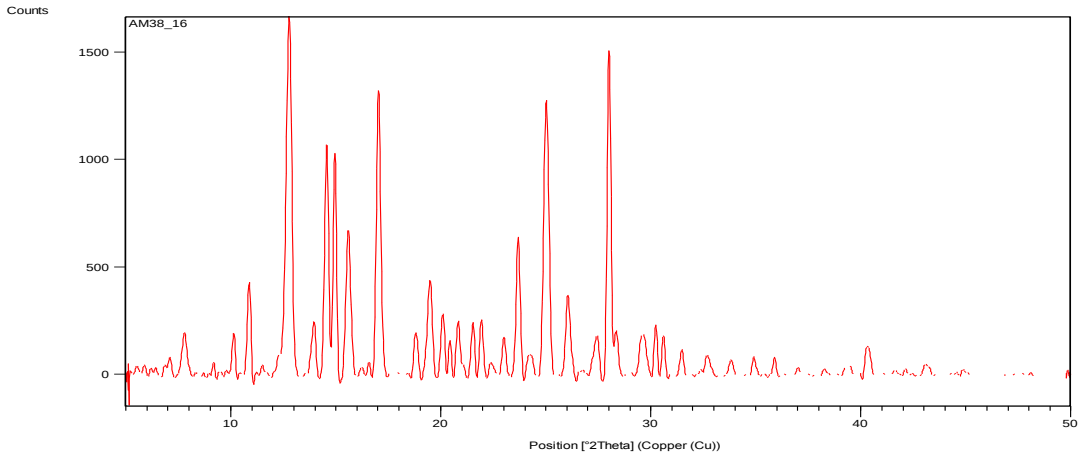

AM38_18 – PAP + Malonic acid with hydrogen peroxide crystallised in acetone at room temperature

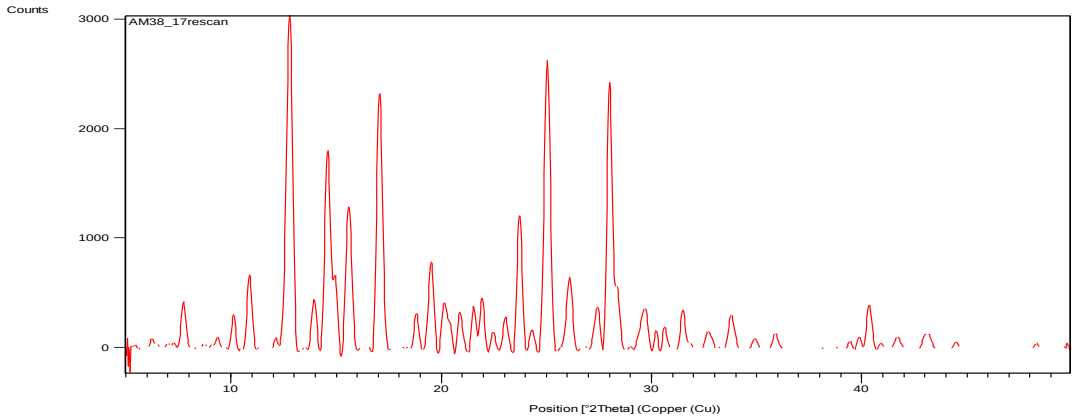

PAP and chloranilic acid

AM66_02 – PAP + chloranilic acid with hydrogen peroxide crystallised in acetone at room temperature

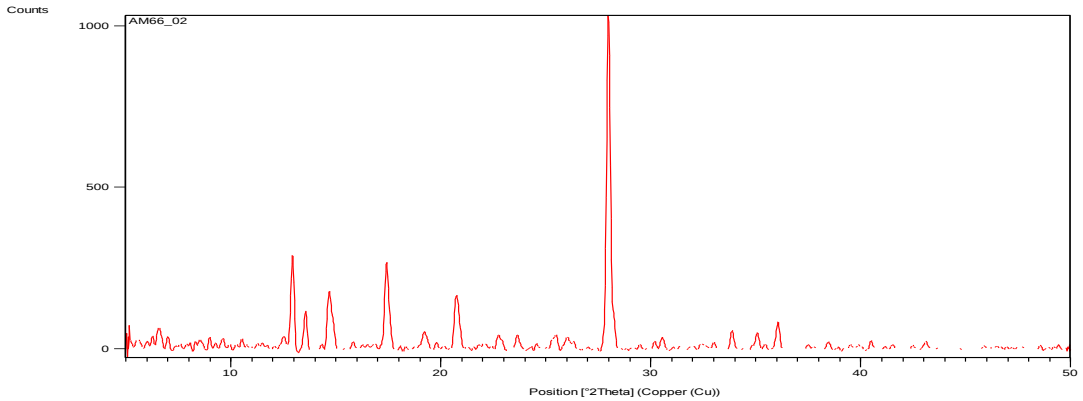

AM66_03 – PAP + chloranilic acid with hydrogen peroxide crystallised in methyl acetate at 4°C

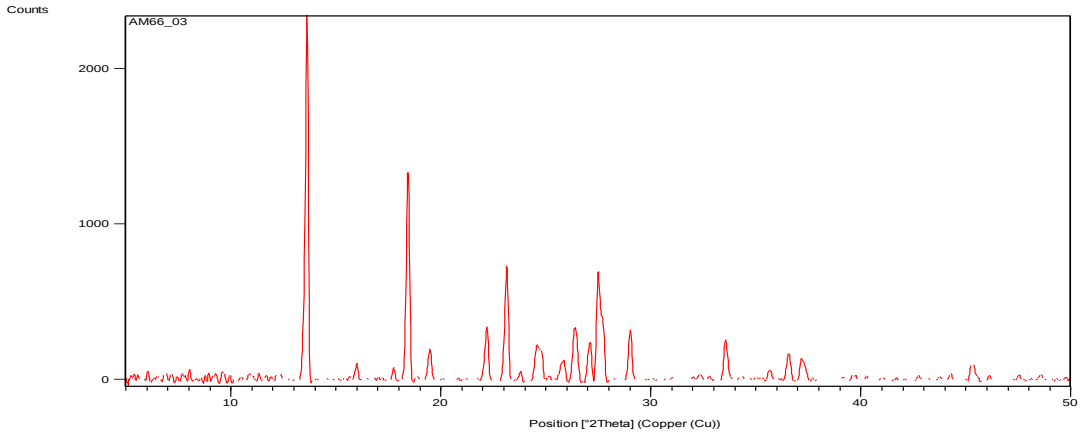

AM66_05– PAP + chloranilic acid with hydrogen peroxide crystallised in ethyl acetate at 4°C

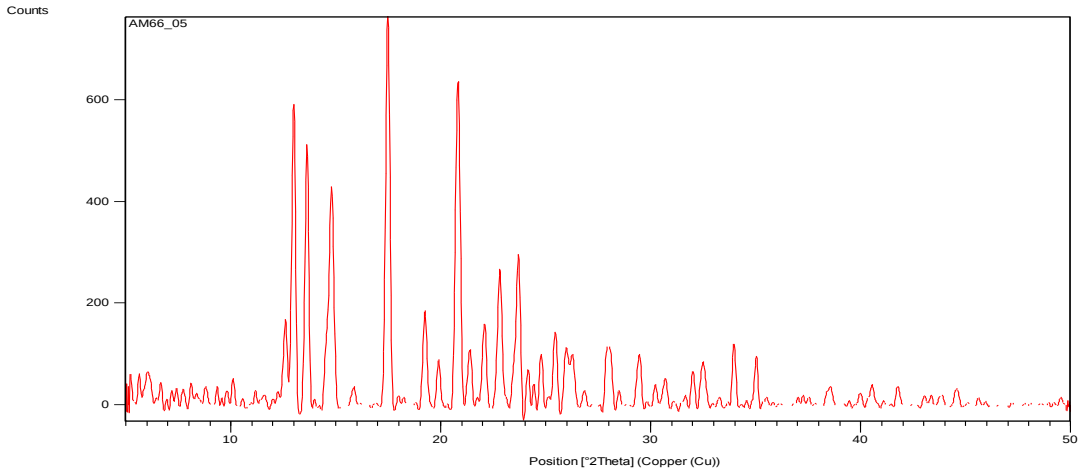

AM66_06 – PAP + chloranilic acid with hydrogen peroxide crystallised in ethyl acetate at room temperature

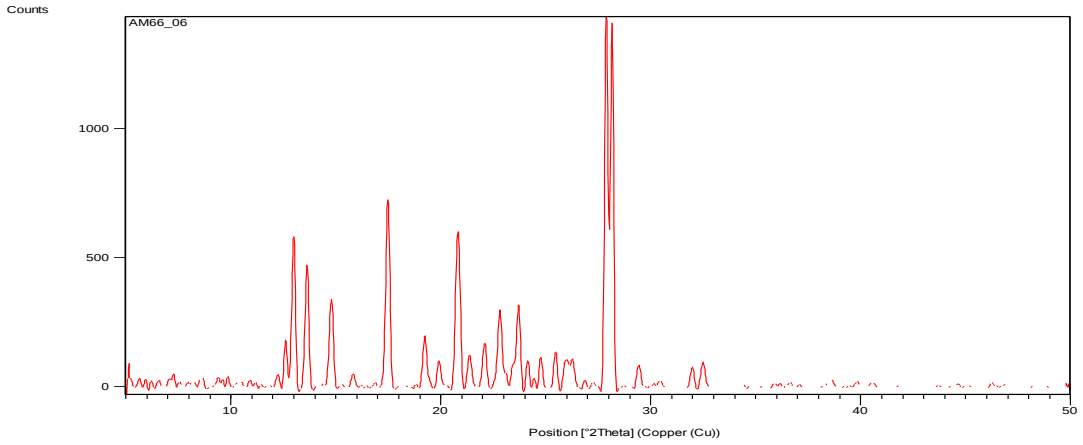

PAP and bromanilic acid

AM67_01 – PAP + bromanilic acid with hydrogen peroxide crystallised in acetone at 4°C

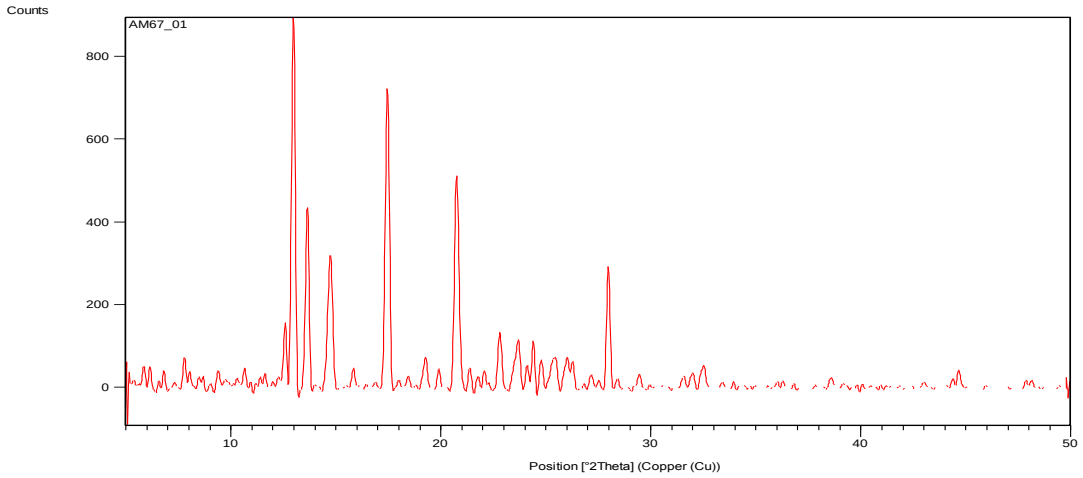

AM67_02 – PAP + bromanilic acid with hydrogen peroxide crystallised in acetone at room temperature

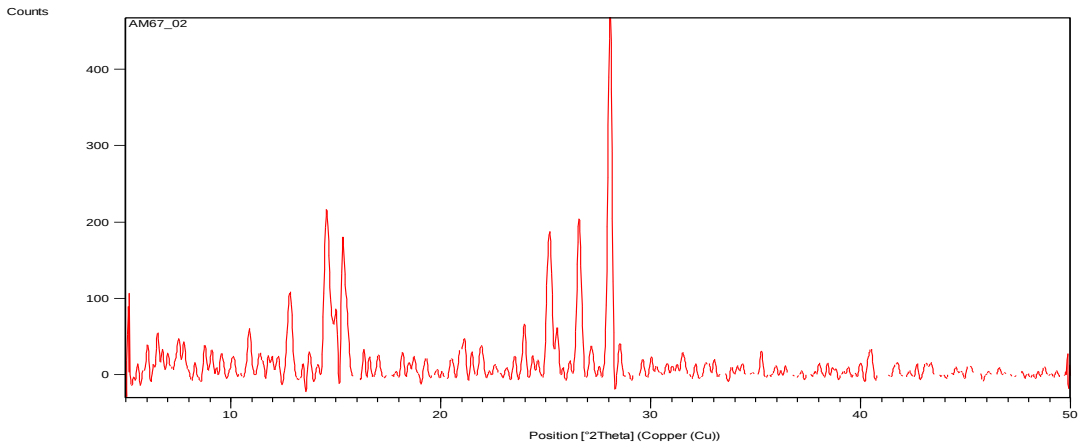

Cocrystallisations with π-π interacting materials

MCPBA and 1,4-Dihydroxybenzene

AM68_02 – MCPBA + 1,4-dihydroxybenzene with hydrogen peroxide crystallised in acetone at room temperature

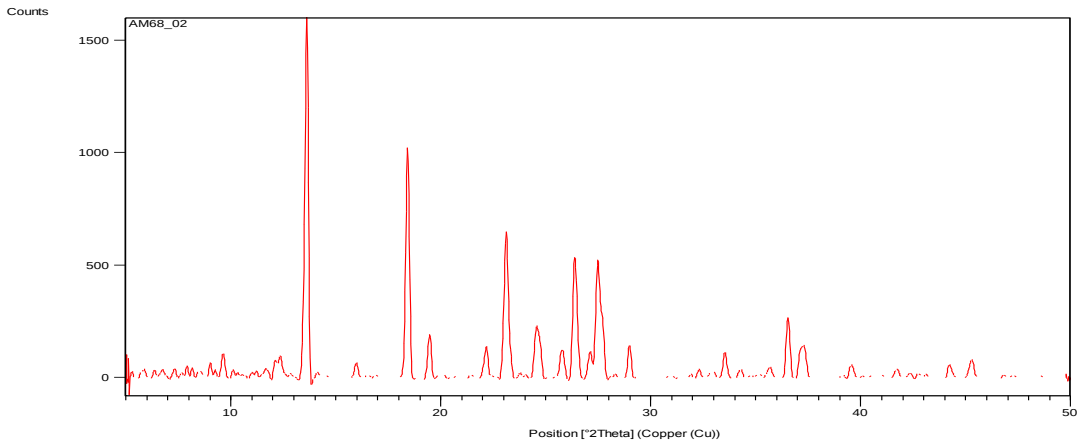

MCPBA and 2-hydroxybenzophenone

AM80_01 – MCPBA + 2-hydroxybenzophenone with hydrogen peroxide crystallised in acetone at 4°C

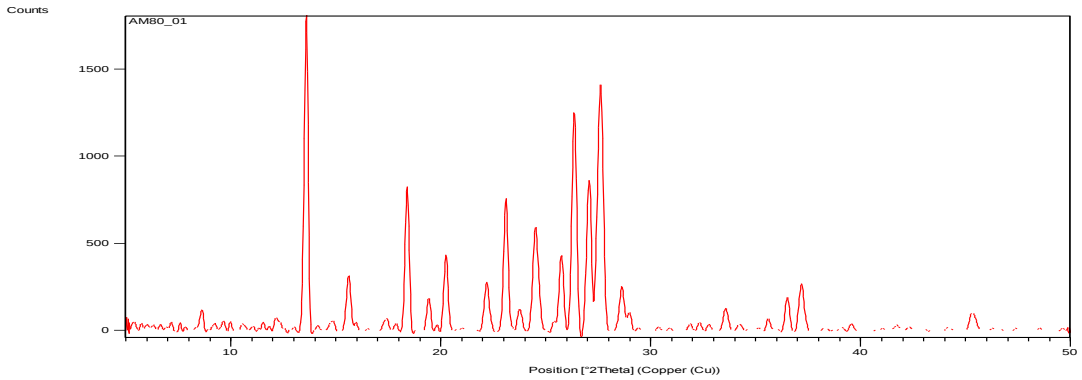

AM80_03 – MCPBA + 2-hydroxybenzophenone with hydrogen peroxide crystallised in methyl acetate at 4°C

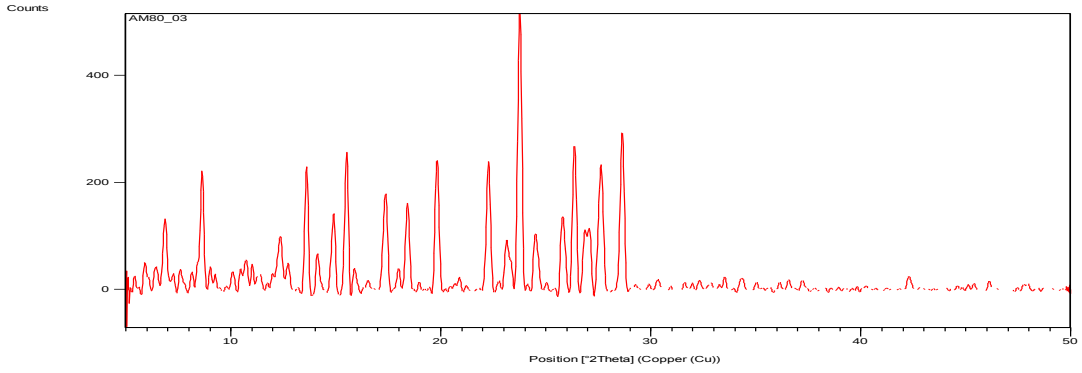

AM80_07 – MCPBA + 2-hydroxybenzophenone with hydrogen peroxide crystallised in diethyl ether at 4°C

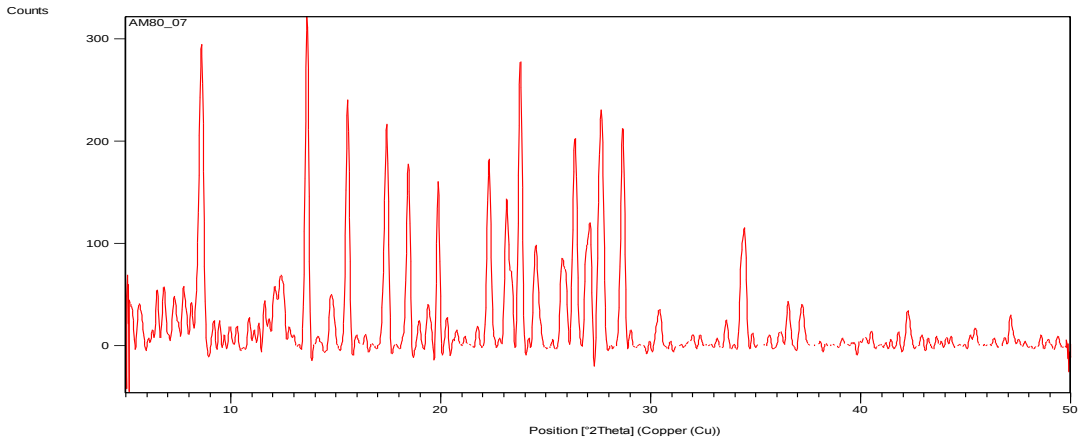

MCPBA and 3-hydroxybenzophenone

AM82_01 – MCPBA + 3-hydroxybenzophenone with hydrogen peroxide crystallised in acetone at 4°C

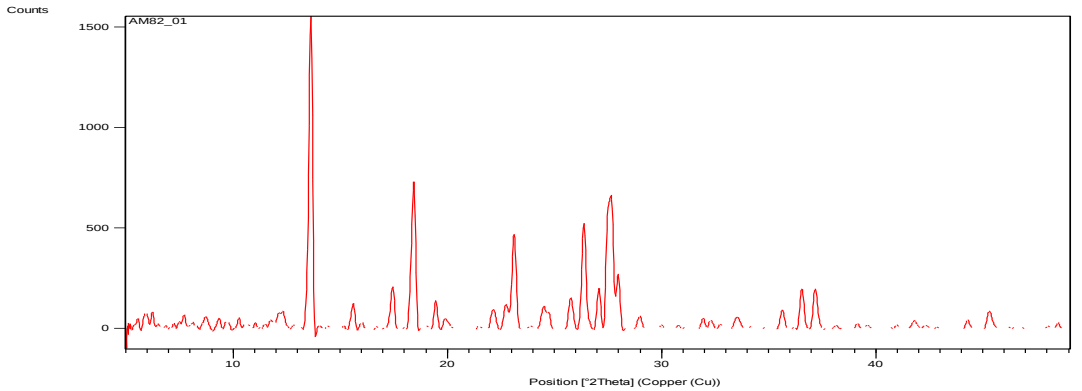

AM82_03 – MCPBA + 3-hydroxybenzophenone with hydrogen peroxide crystallised in methyl acetate at 4°C

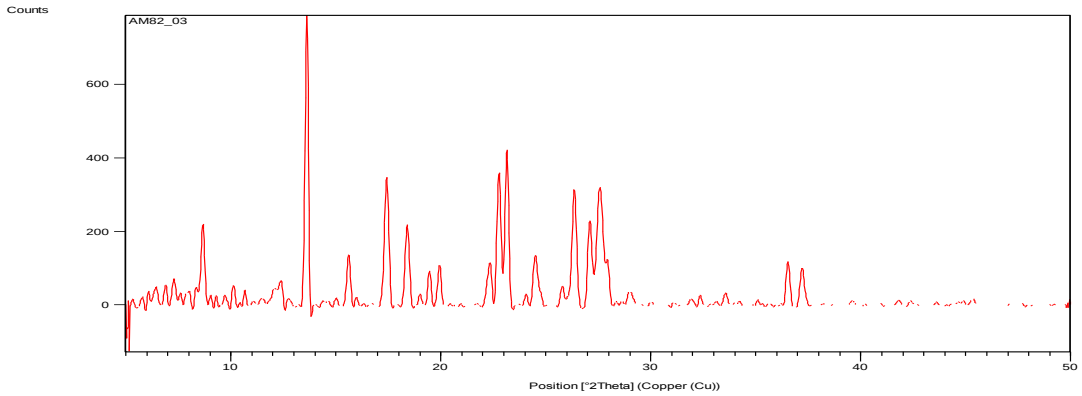

AM82_05 – MCPBA + 3-hydroxybenzophenone with hydrogen peroxide crystallised in ethyl acetate at 4°C

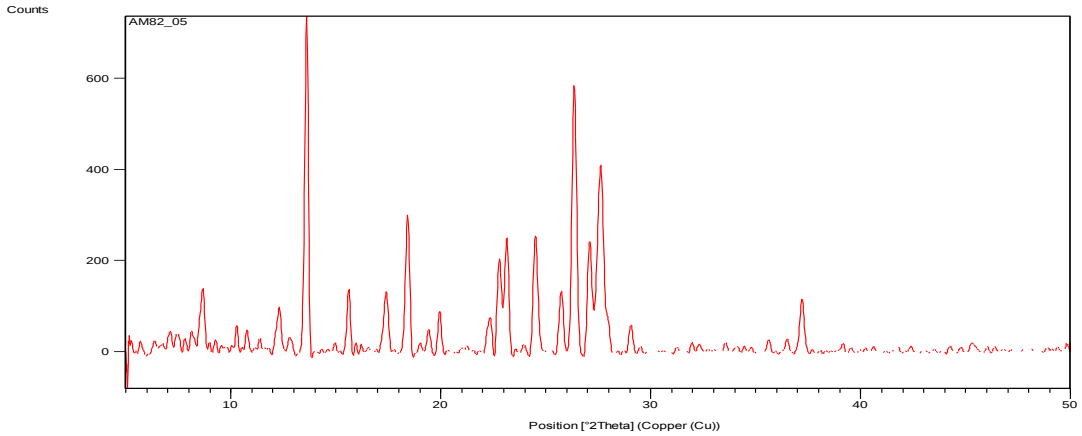

AM82_07 – MCPBA + 3-hydroxybenzophenone with hydrogen peroxide crystallised in diethyl ether at 4°C

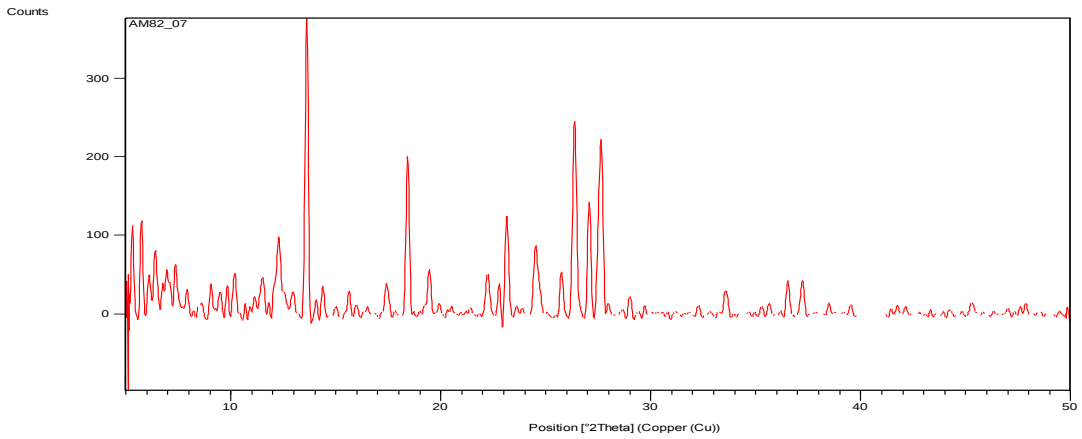

MCPBA and 2-chlorobenzophenone

AM104_05 – MCPBA + 2-chlorobenzophenone with hydrogen peroxide crystallised in methyl acetate at room temperature

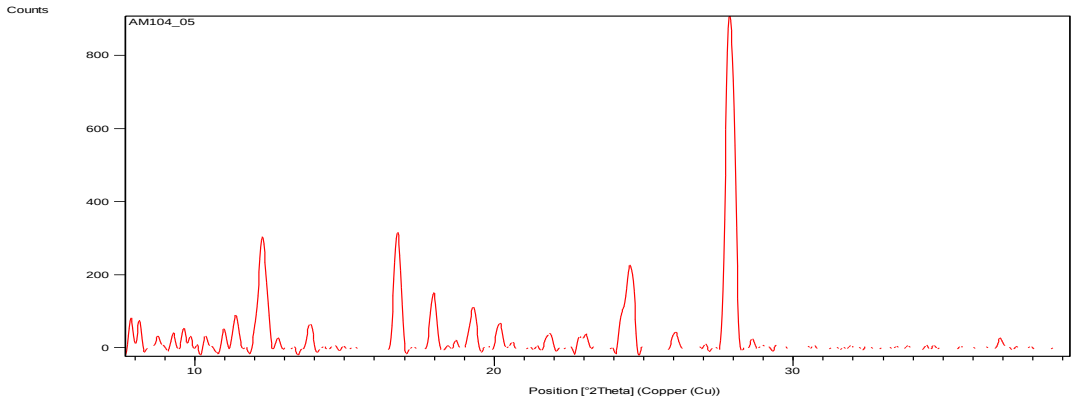

PAP and 2-hydroxybenzophenone

AM81_01 – PAP + 2-hydroxybenzophenone with hydrogen peroxide crystallised in acetone at 4°C

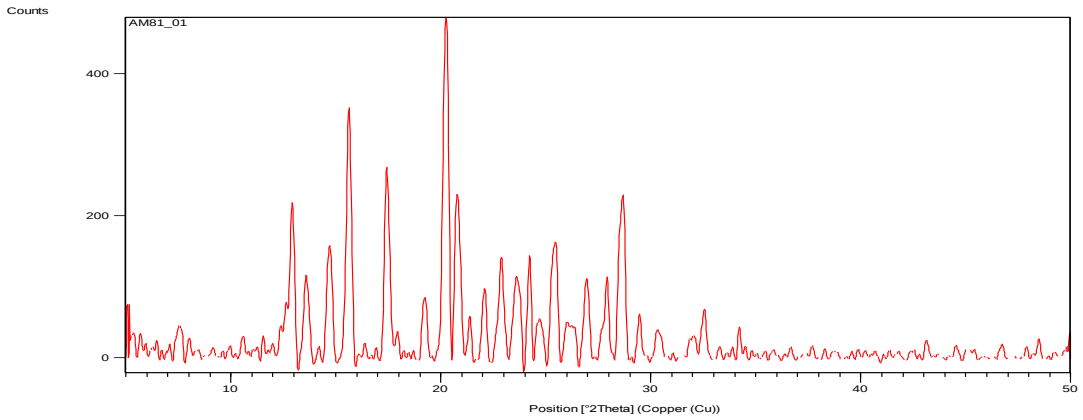

AM81_03 - PAP + 2-hydroxybenzophenone with hydrogen peroxide crystallised in methyl acetate at 4°C

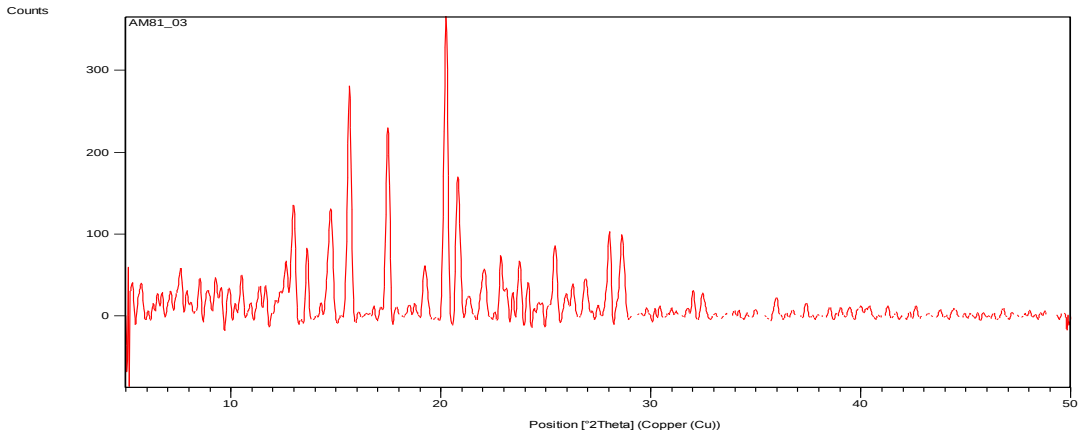

PAP and 3-hydroxybenzophenone

AM83_01 – PAP + 3-hydroxybenzophenone with hydrogen peroxide crystallised in acetone at 4°C

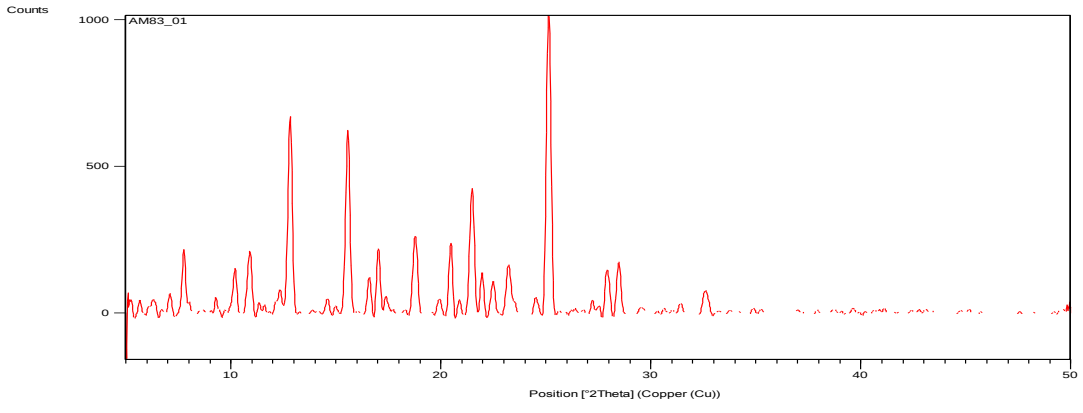

AM83_02 - PAP + 3-hydroxybenzophenone with hydrogen peroxide crystallised in acetone at room temperature

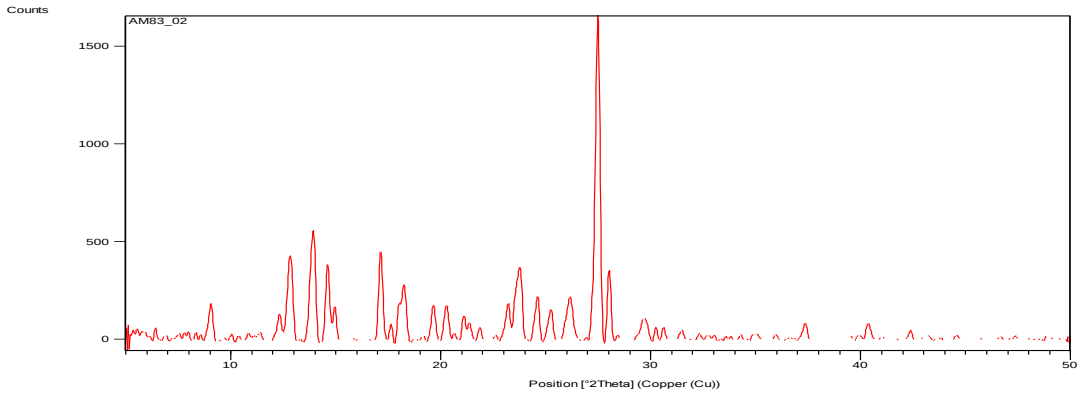

AM83_03 - PAP + 3-hydroxybenzophenone with hydrogen peroxide crystallised in methyl acetate at 4°C

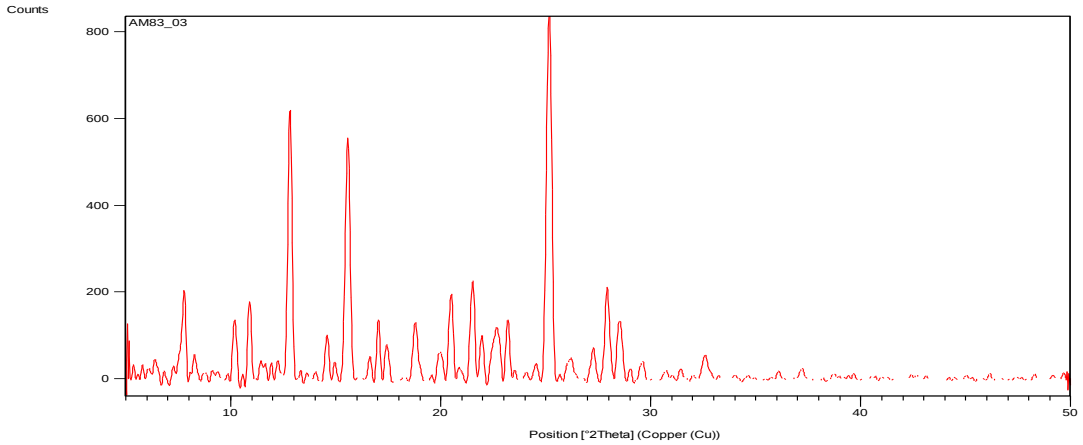

AM83_05 - PAP + 3-hydroxybenzophenone with hydrogen peroxide crystallised in ethyl acetate at 4°C

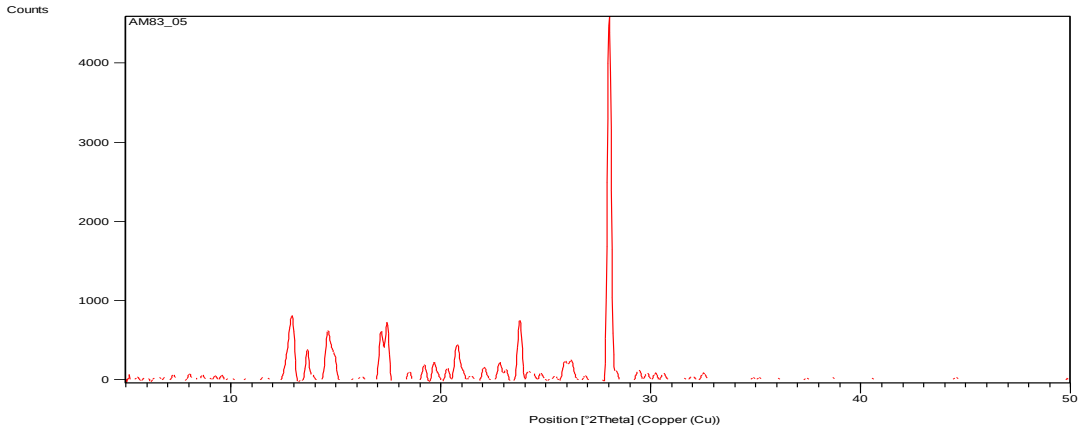

AM83_07 - PAP + 3-hydroxybenzophenone with hydrogen peroxide crystallised in diethyl ether at 4°

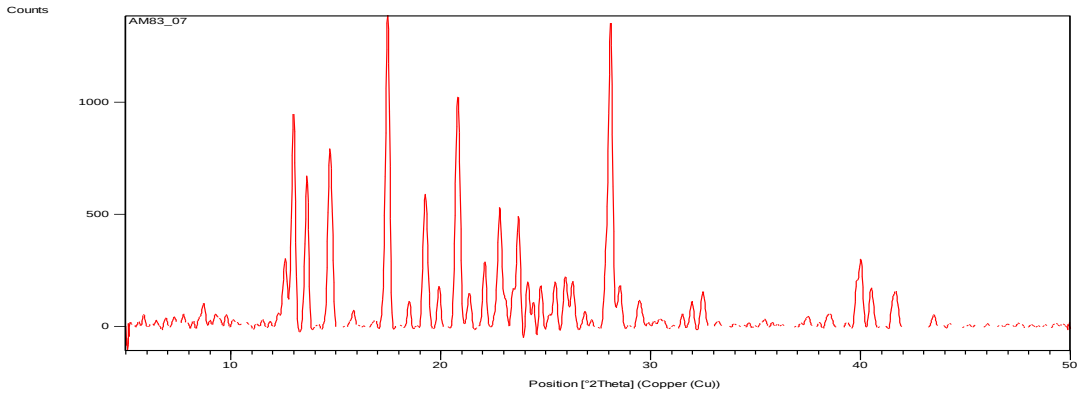

PAP and Benzimidazole

AM31_02 – PAP + Benzimidazole crystallised in methanol at room temperature

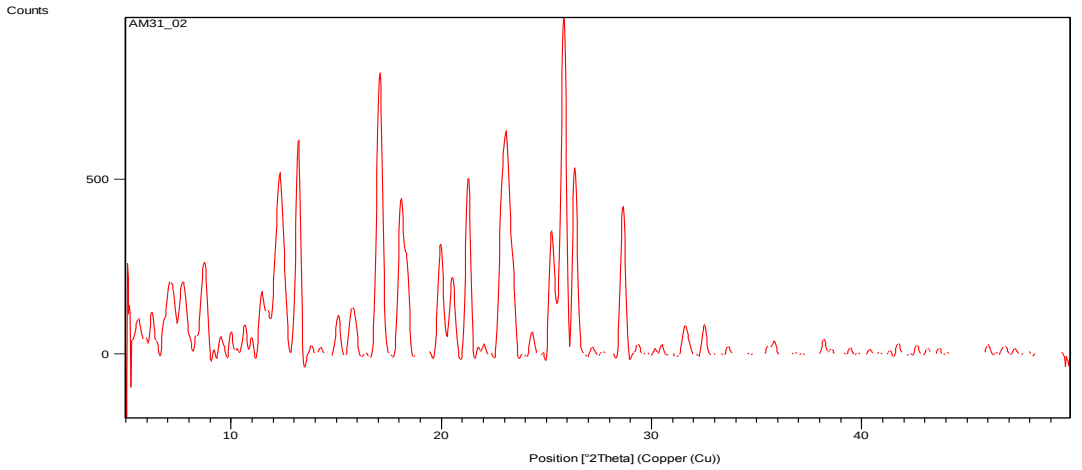

AM31_05 – PAP + Benzimidazole crystallised in ethanol at room temperature

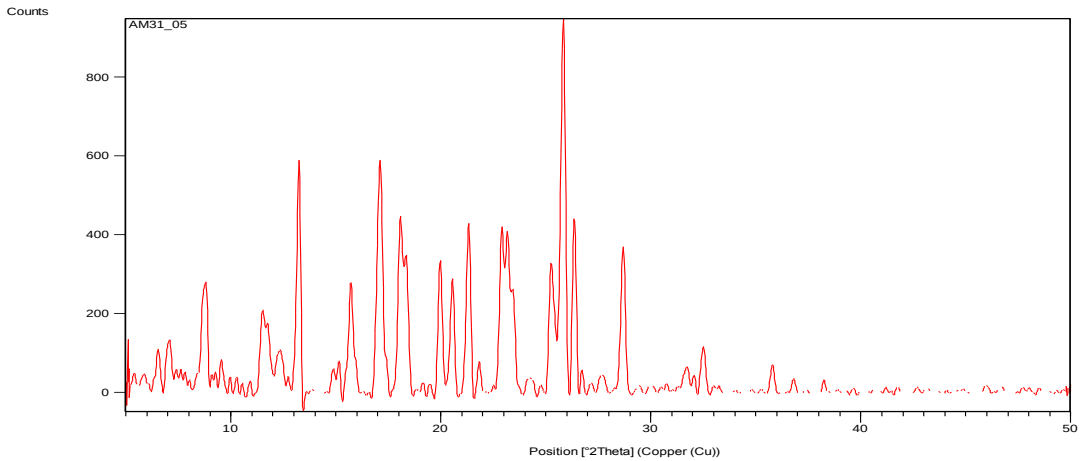

AM31_06 – PAP + Benzimidazole crystallised in ethanol at 30°C

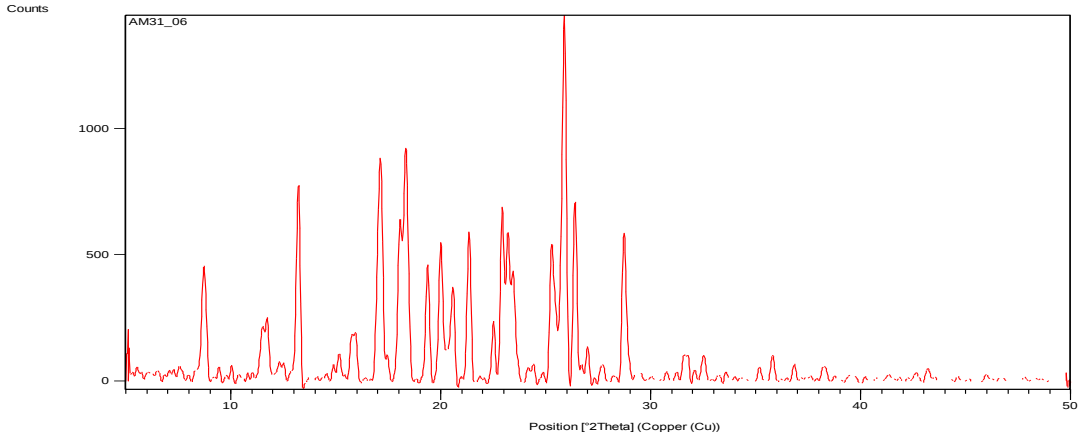

AM31_07 – PAP + Benzimidazole crystallised in acetone at 4°C

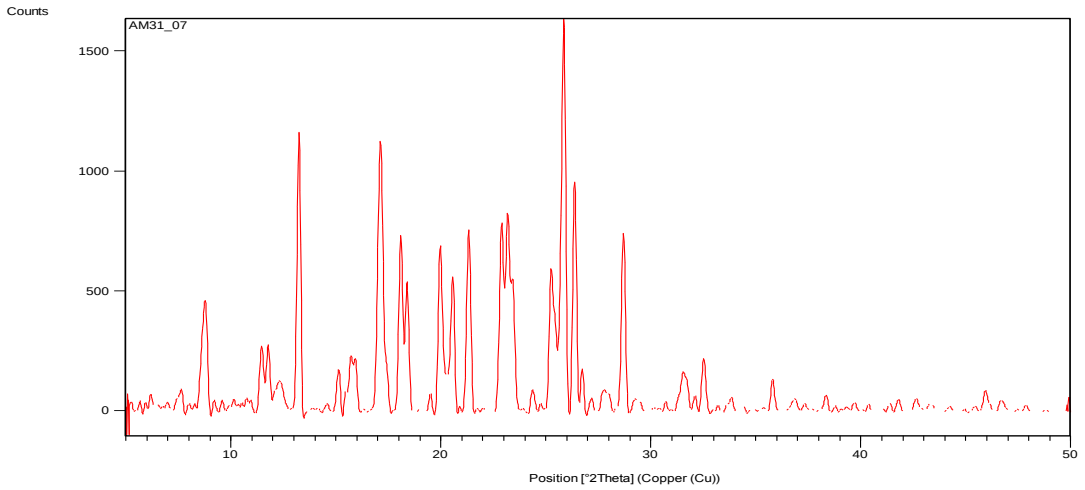

AM31_08 – PAP + Benzimidazole crystallised in acetone at room temperature

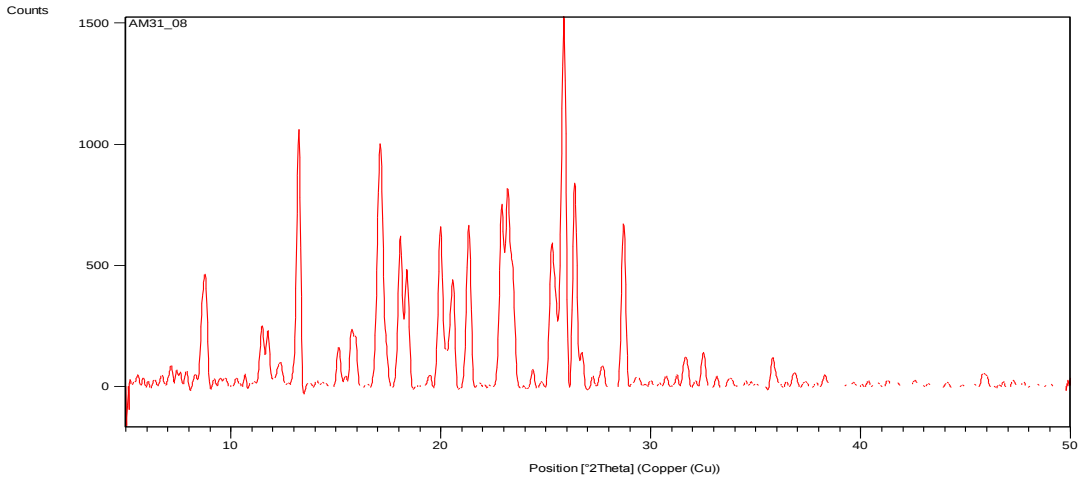

AM31_09 – PAP + Benzimidazole crystallised in acetone at 30°C

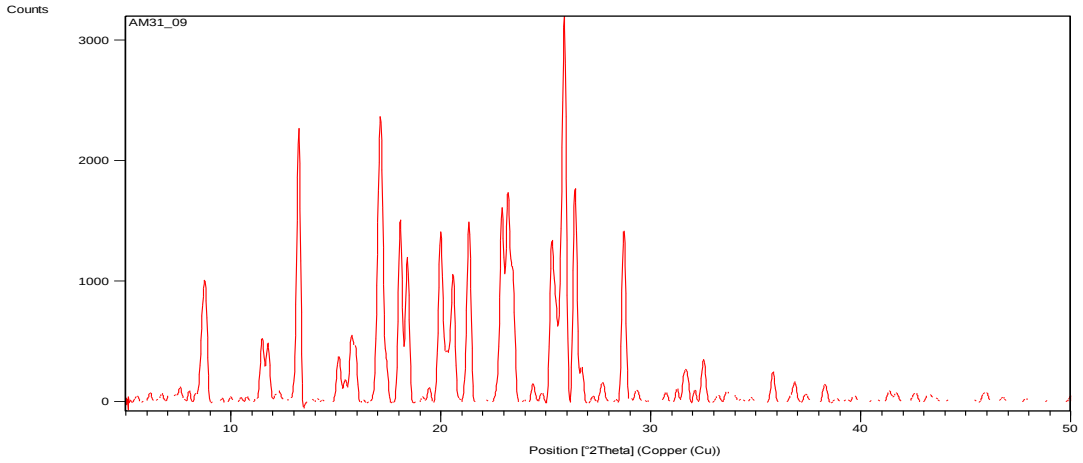

AM31_10 – PAP + Benzimidazole crystallised in ethyl acetate at 4°C

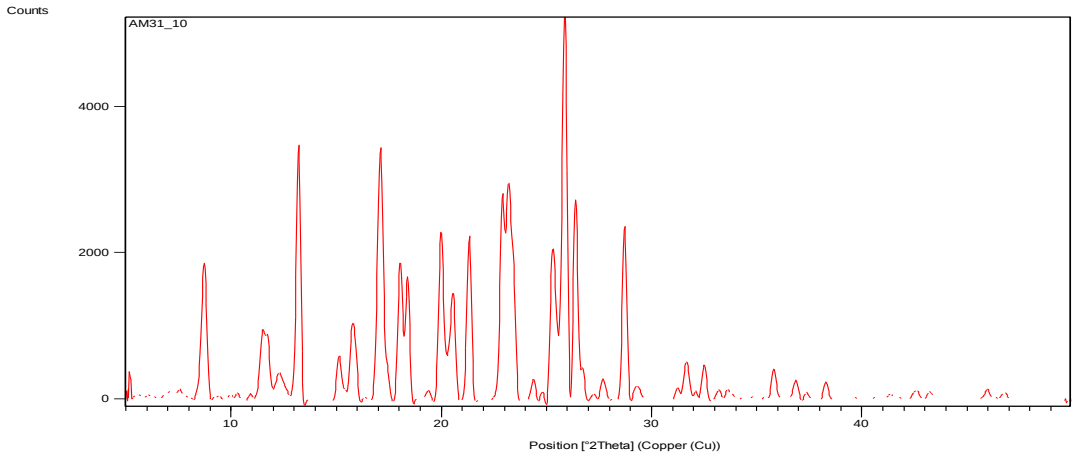

AM31_11 – PAP + Benzimidazole crystallised in ethyl acetate at room temperature

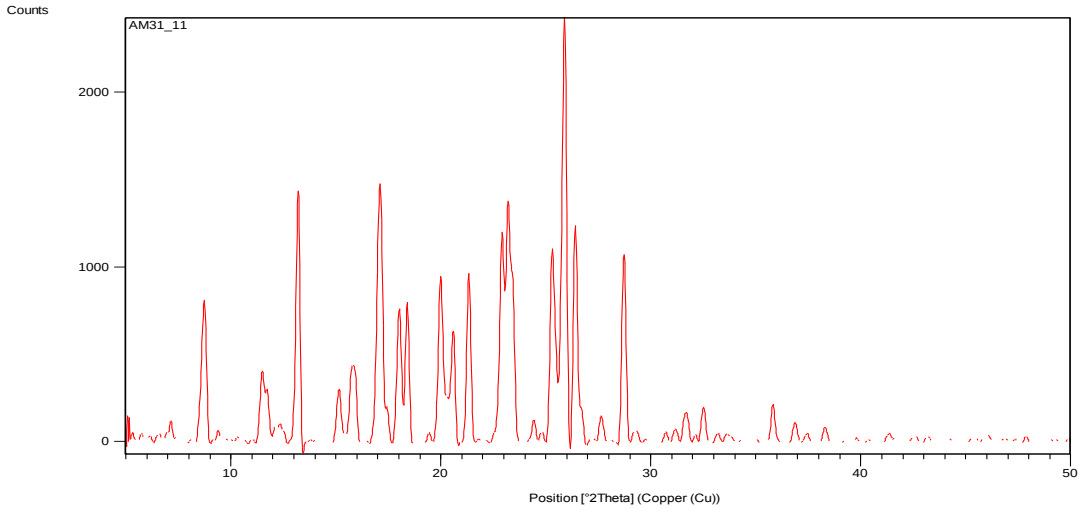

AM31_12 – PAP + Benzimidazole crystallised in ethyl acetate at 30°C

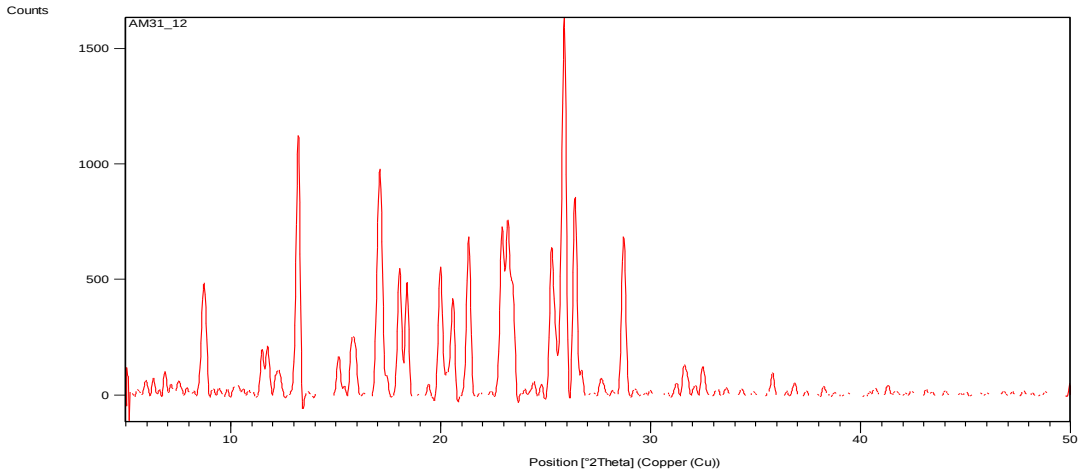

AM31_13 – PAP + Benzimidazole crystallised in diethyl ether at 4°C

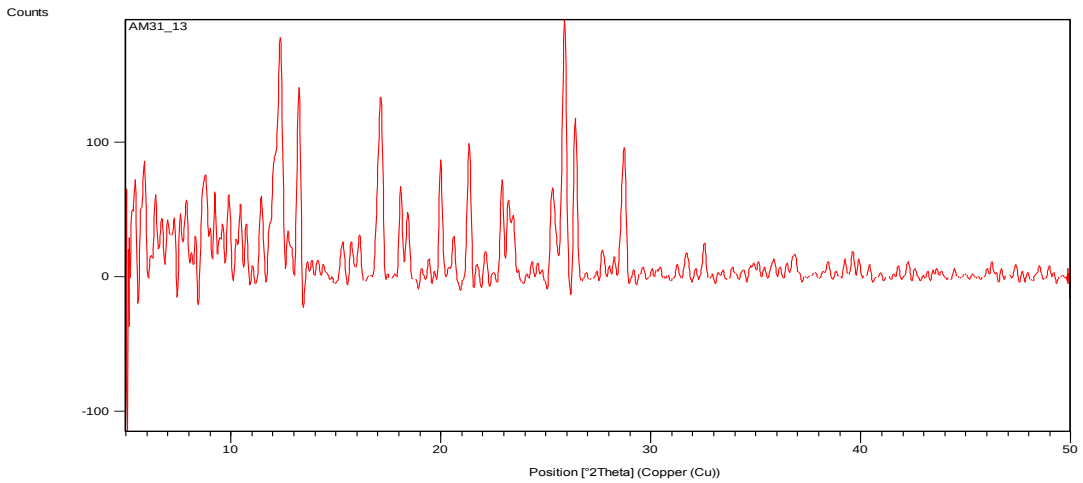

AM31_14 – PAP + Benzimidazole crystallised in diethyl ether at room temperature

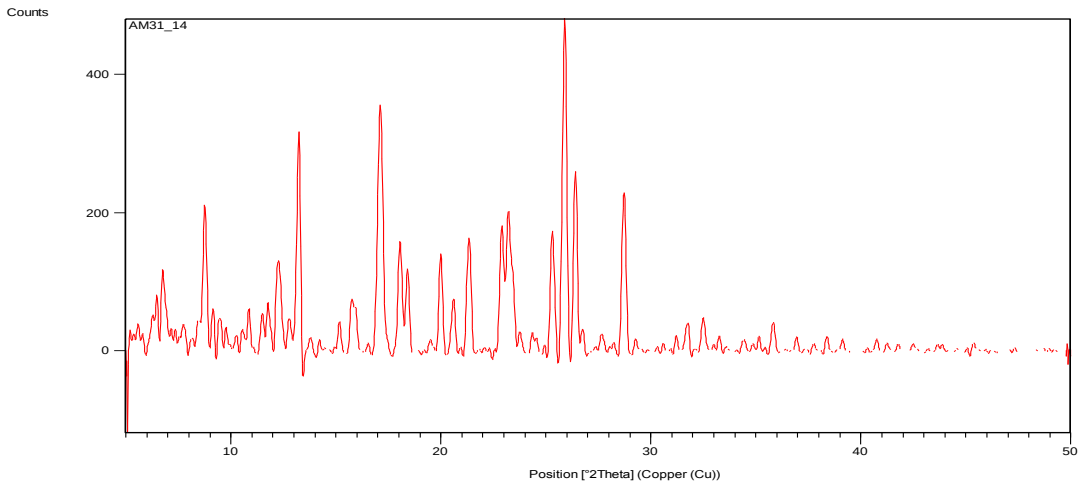

AM31_15 – PAP + Benzimidazole crystallised in diethyl ether at 30°C

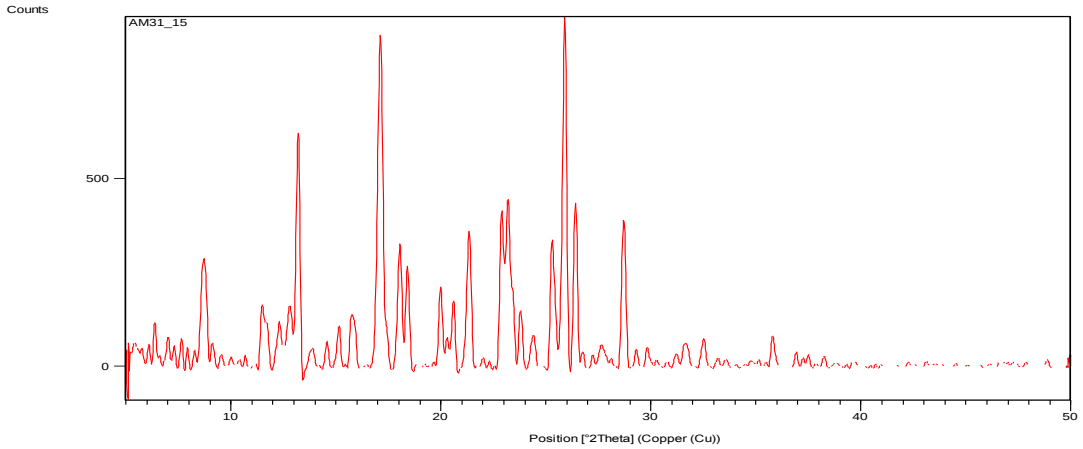

Crystallisations with metals

MCPBA and magnesium chloride

AM50_01 – MCPBA + magnesium chloride with hydrogen peroxide in ethyl acetate at 4°C

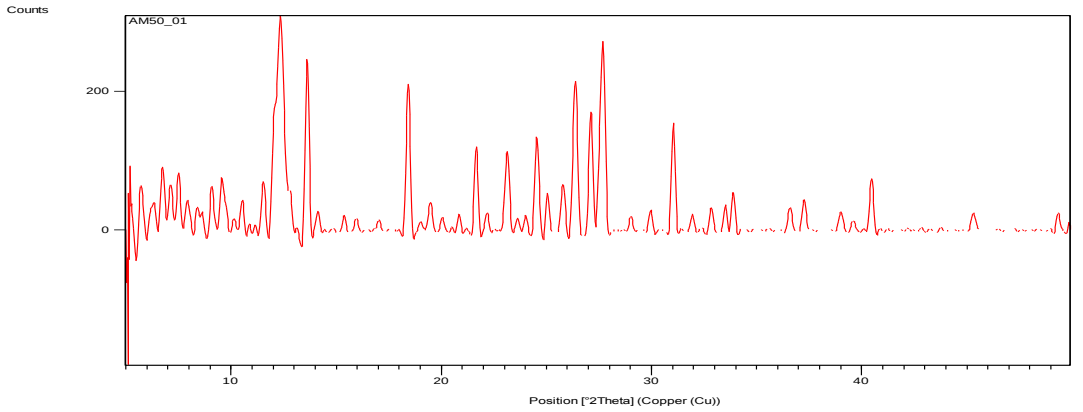

AM50_04 – MCPBA + magnesium chloride with hydrogen peroxide in chloroform at 4°C

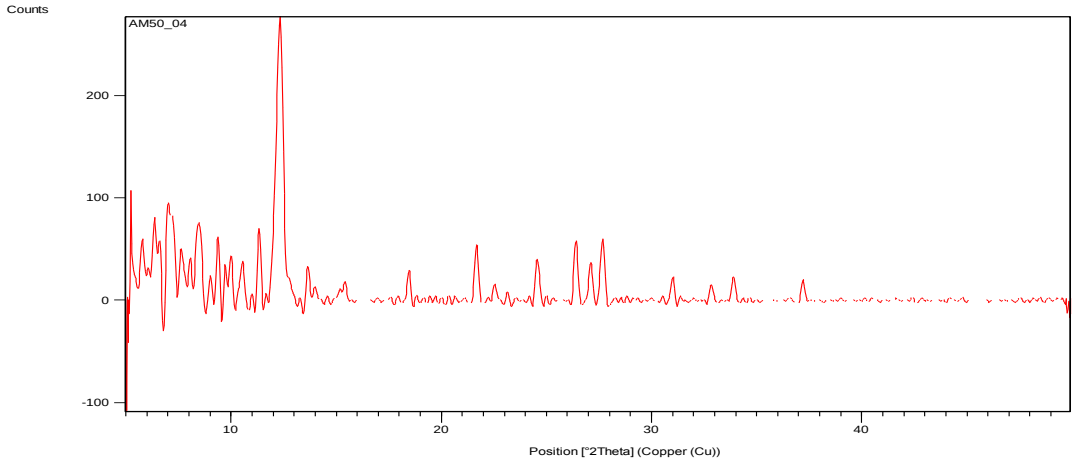

AM50_08 – MCPBA + magnesium chloride with hydrogen peroxide in acetone at room temperature

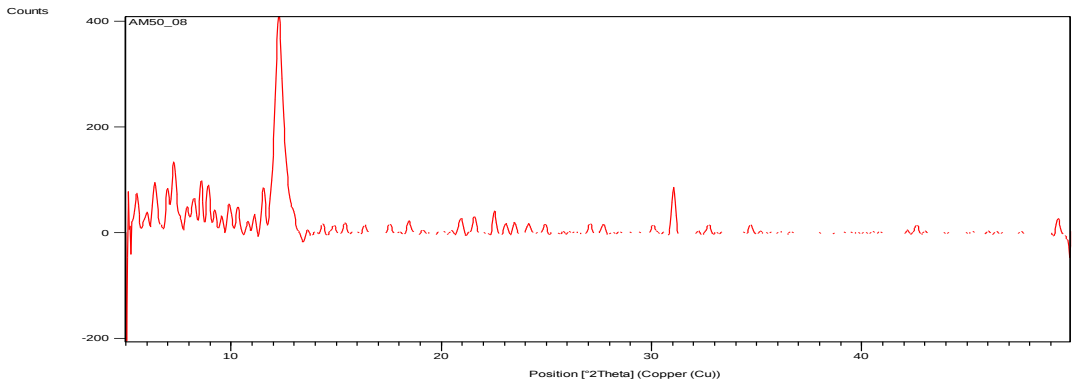

AM50_10 – MCPBA + magnesium chloride with hydrogen peroxide in diethyl ether at 4°C

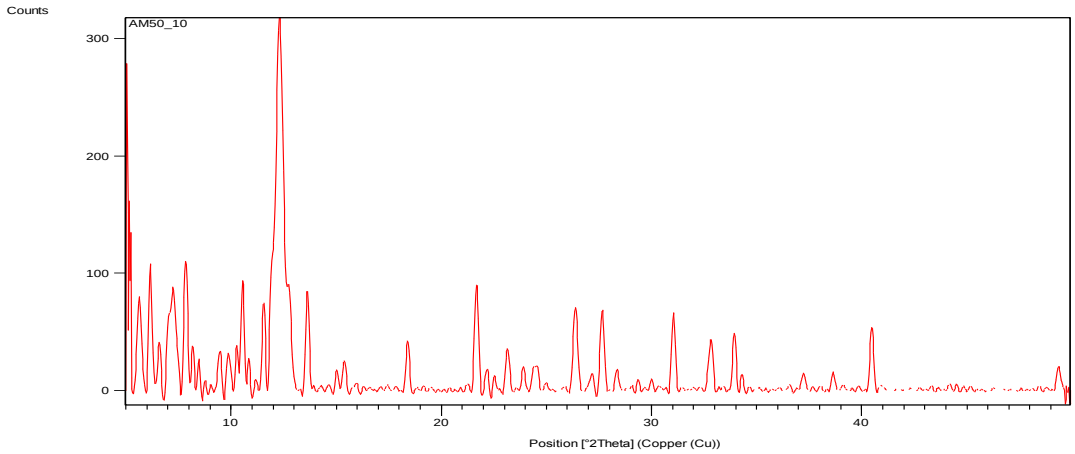

AM50_13 – MCPBA + magnesium chloride with hydrogen peroxide in dichloromethane at 4°C

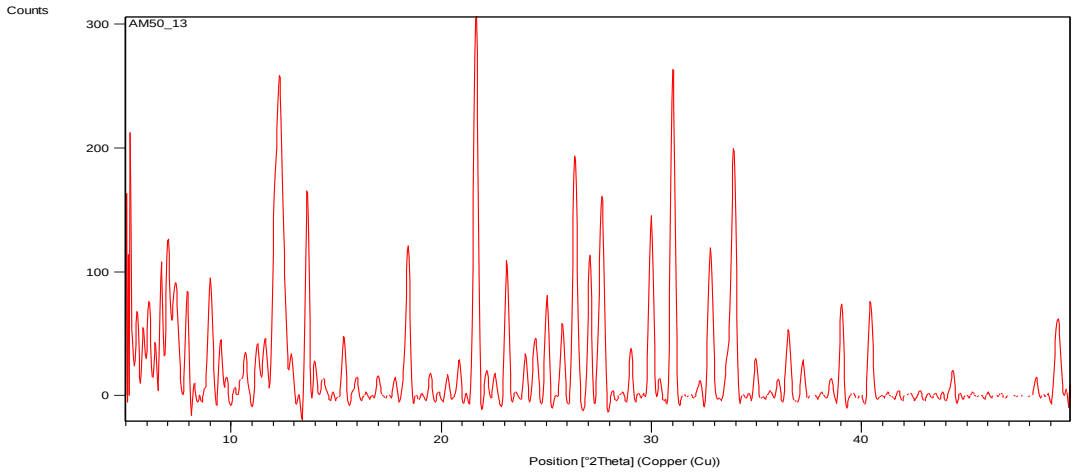

AM50_14 – MCPBA + magnesium chloride with hydrogen peroxide in dichloromethane at room temperature

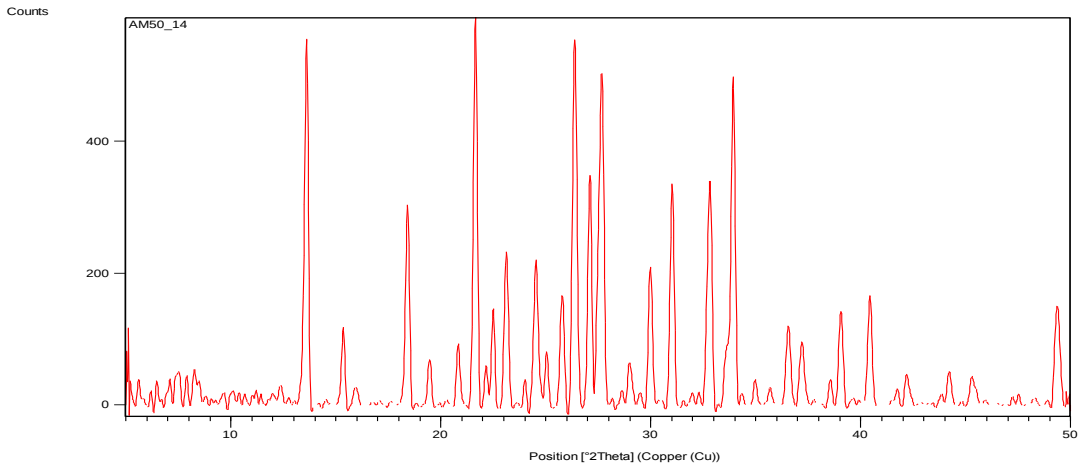

AM50_16 – MCPBA + magnesium chloride with hydrogen peroxide in methanol at 4°C

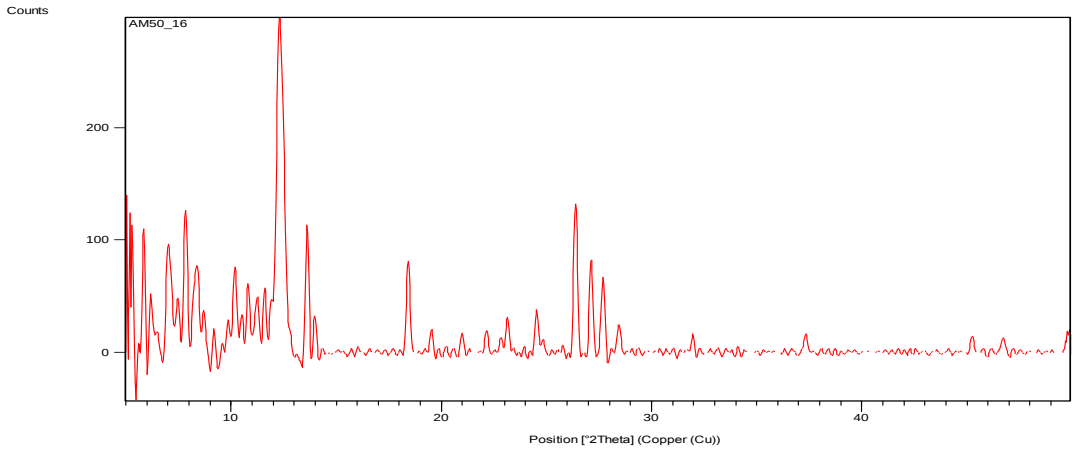

AM50_22 – MCPBA + magnesium chloride with hydrogen peroxide in isopropanol at 4°C

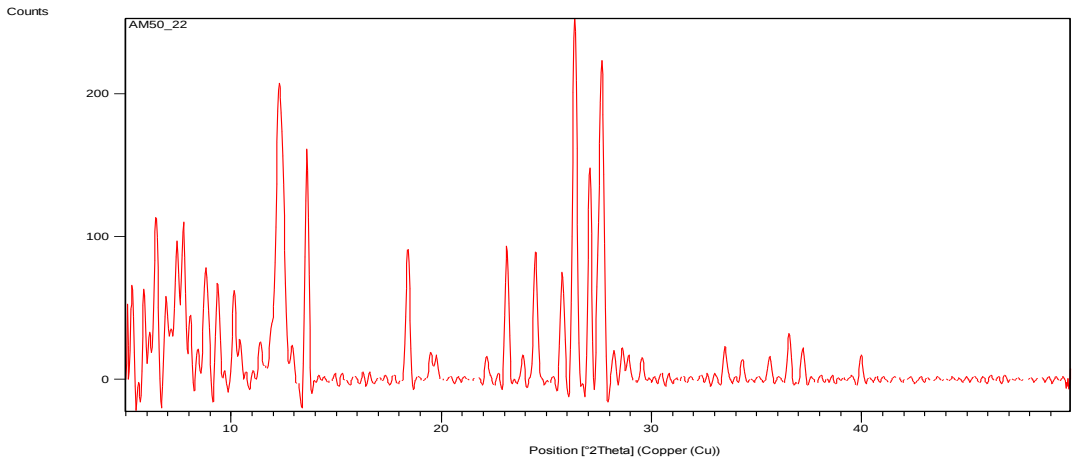

AM50_25 – MCPBA + magnesium chloride with hydrogen peroxide in ethanol at 4°C

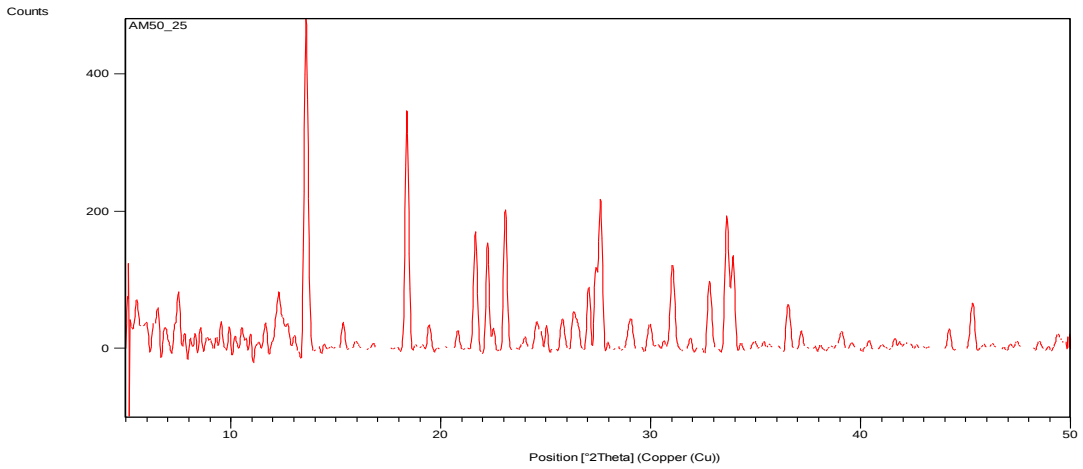

AM50_26 – MCPBA + magnesium chloride with hydrogen peroxide in ethanol at room temperature

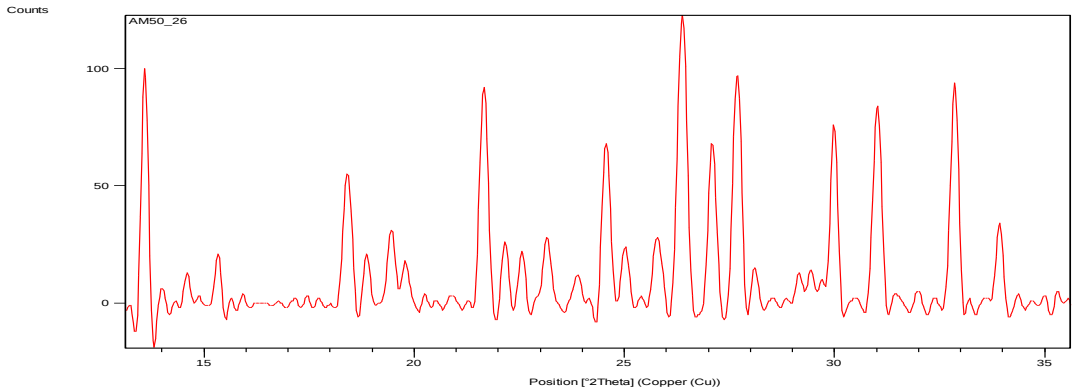

MCPBA and calcium chloride

AM53_01 – MCPBA + calcium chloride with hydrogen peroxide in ethyl acetate at 4°C

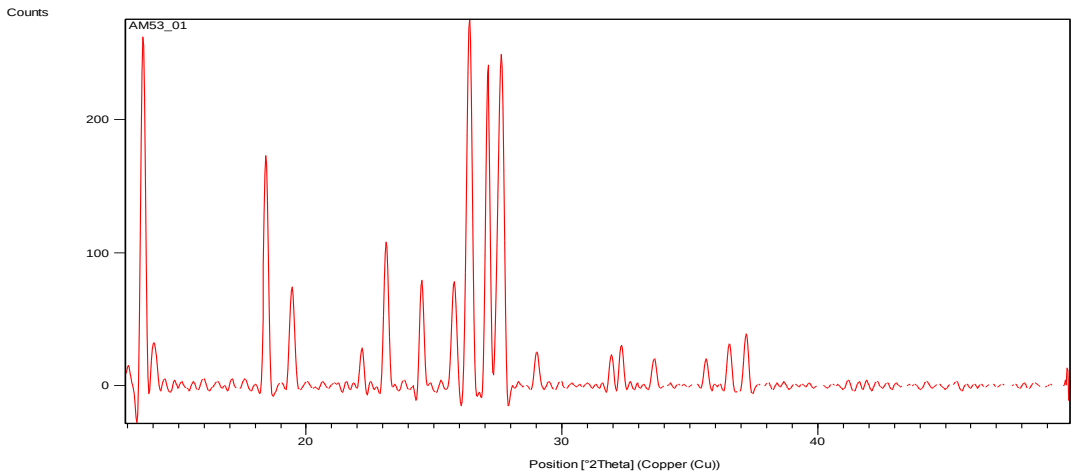

AM53_02 – MCPBA + calcium chloride with hydrogen peroxide in ethyl acetate at 4°C

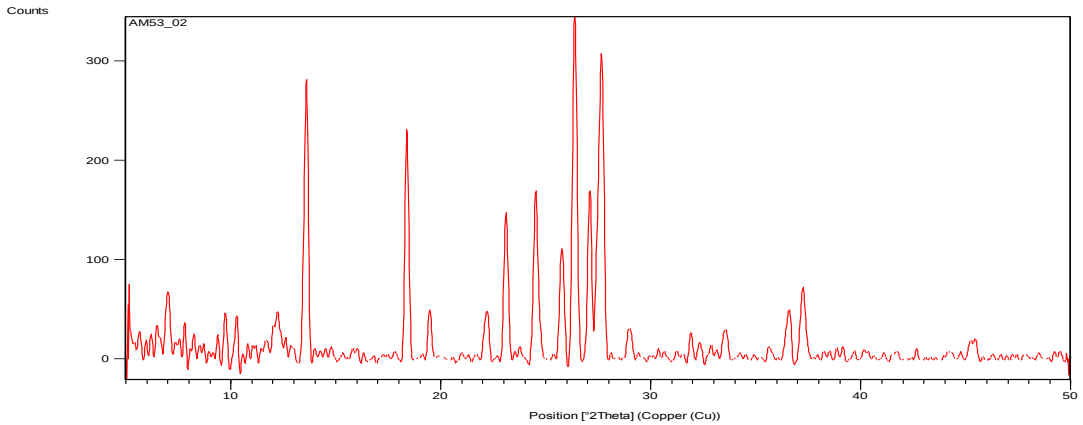

AM53_13 – MCPBA + calcium chloride with hydrogen peroxide in dichloromethane at 4°C

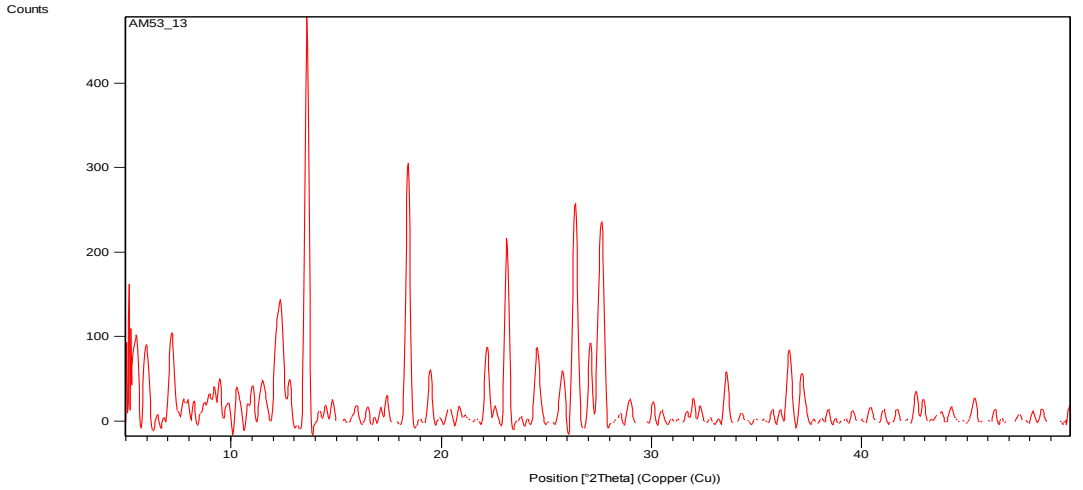

AM53_19 – MCPBA + calcium chloride with hydrogen peroxide in methyl acetate at 4°C

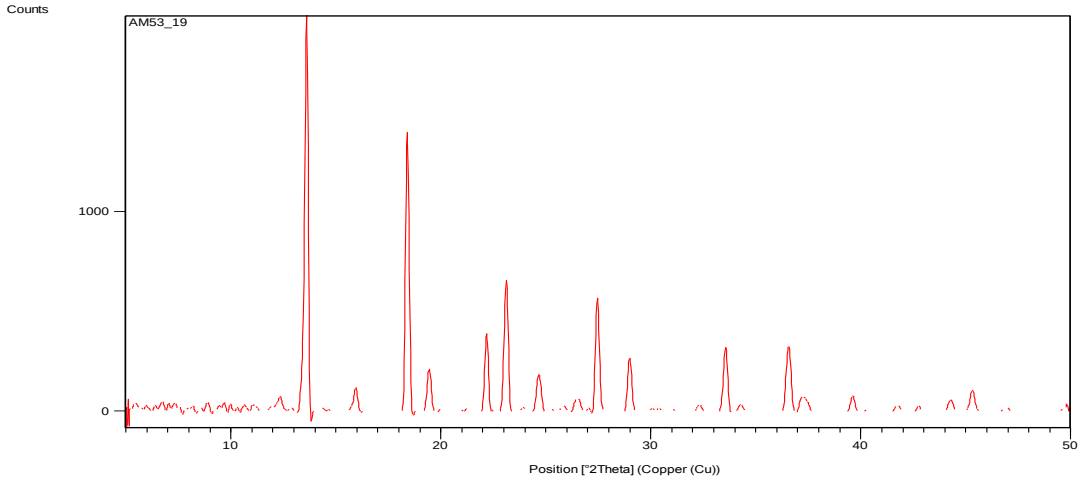

AM53_22 – MCPBA + calcium chloride with hydrogen peroxide in isopropanol at 4°C

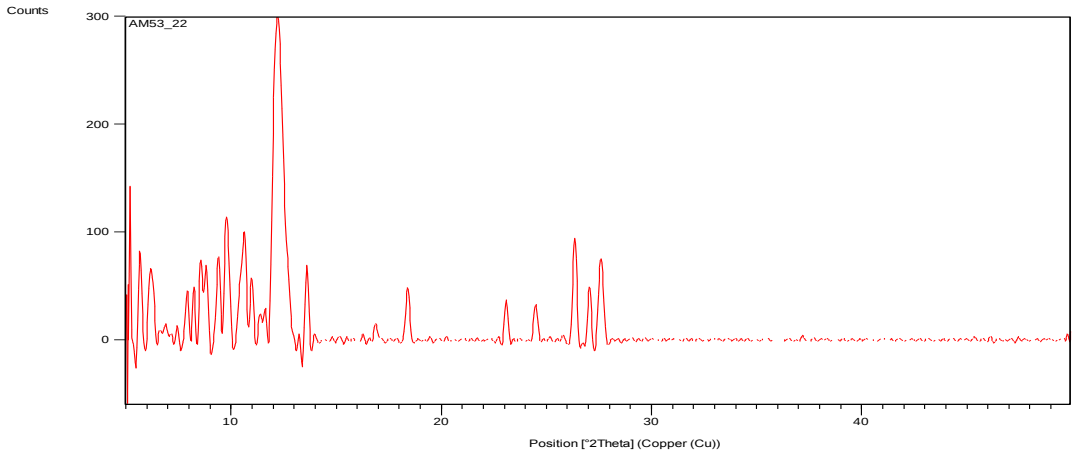

MCPBA and copper chloride

AM86_03 – MCPBA + copper chloride with hydrogen peroxide in methyl acetate at 4°C

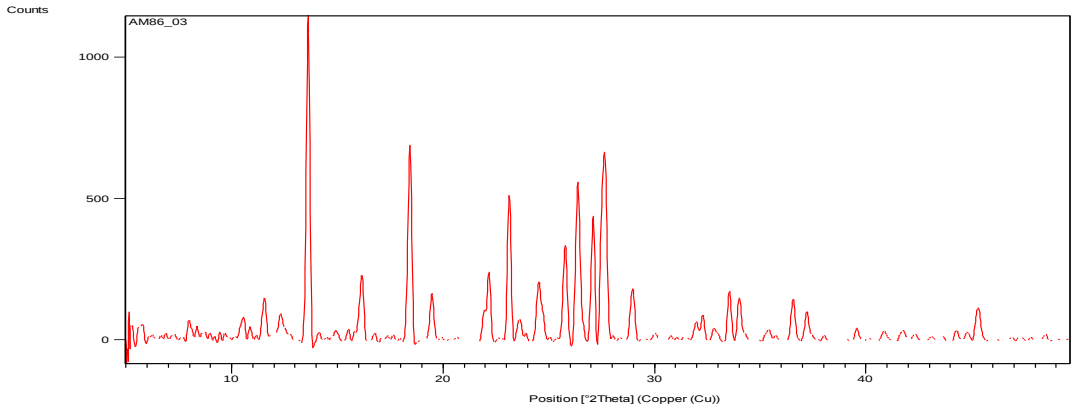

AM86_0 5– MCPBA + copper chloride with hydrogen peroxide in ethyl acetate at 4°C

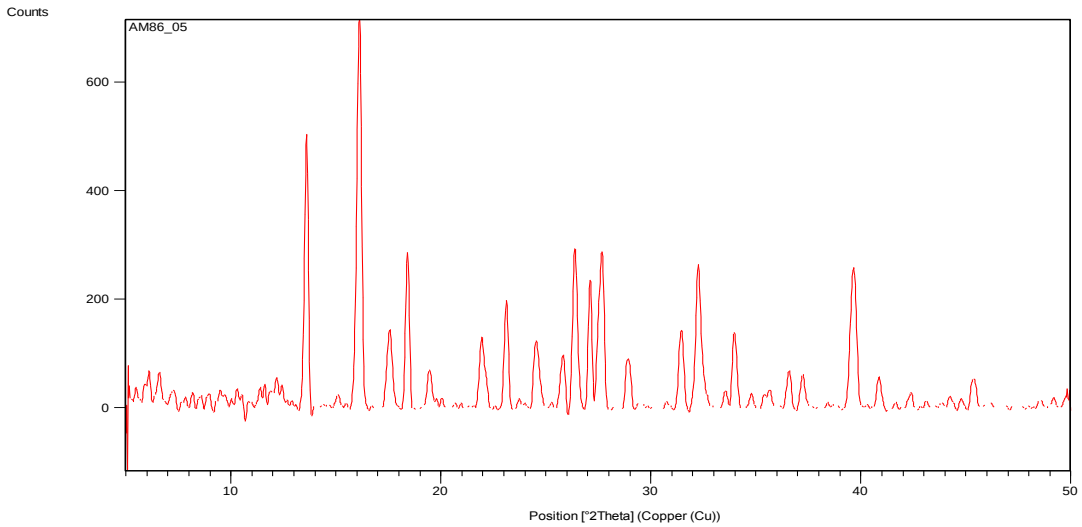

AM86_07 – MCPBA + copper chloride with hydrogen peroxide in diethyl ether at 4°C

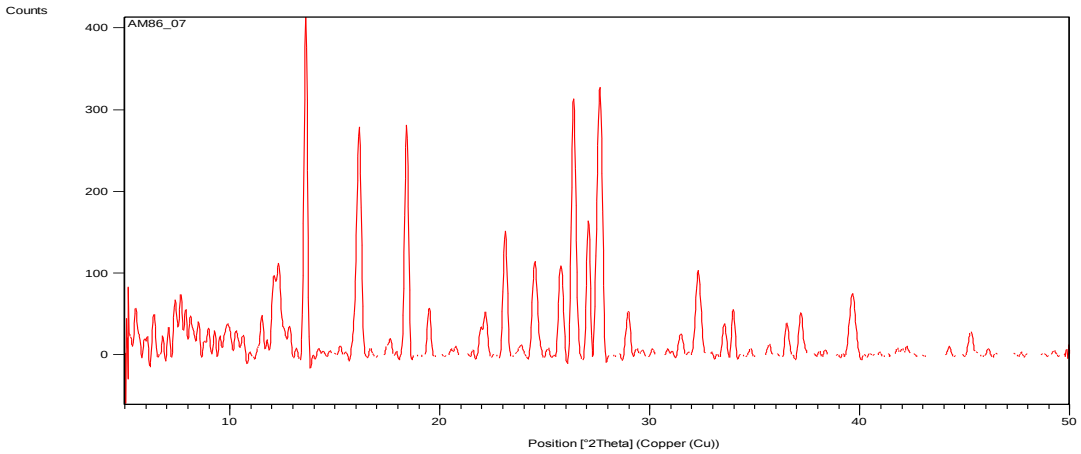

MCPBA and Copper sulfate

AM87_03 – MCPBA + copper sulfate with hydrogen peroxide in methyl acetate at 4°C

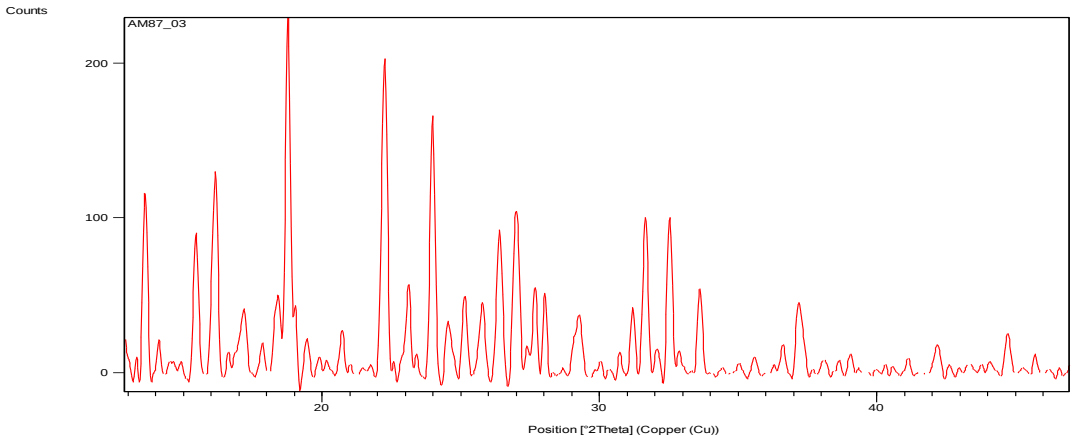

AM87_0 5– MCPBA + copper sulfate with hydrogen peroxide in ethyl acetate at 4°C

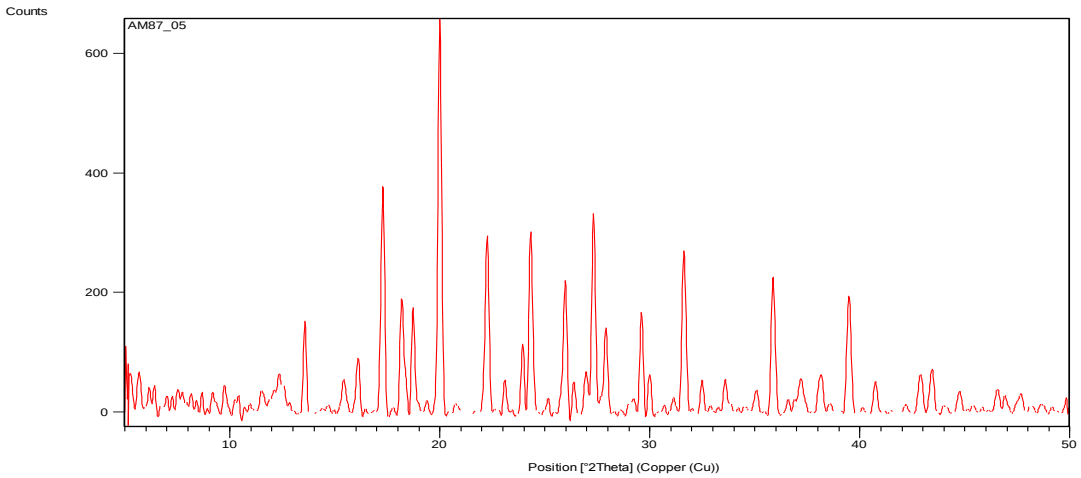

AM87_07 – MCPBA + copper sulfate with hydrogen peroxide in diethyl ether at 4°C

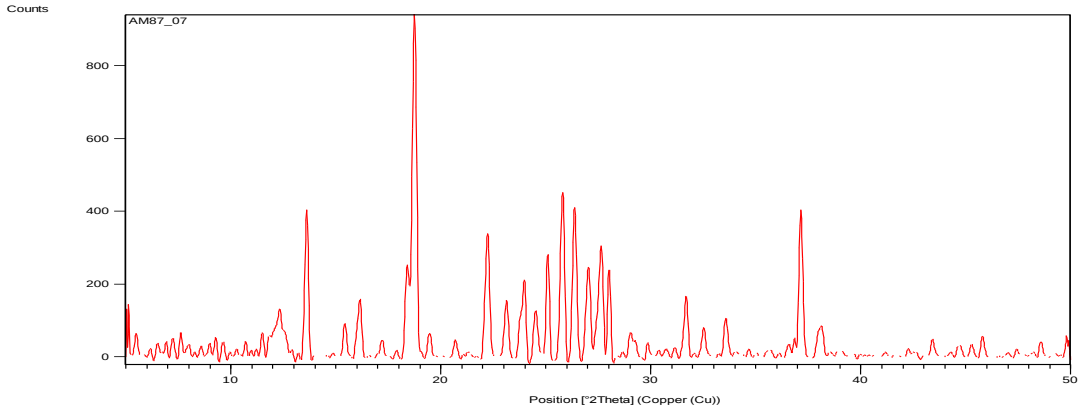

PAP and magnesium chloride

AM51_01 – PAP + magnesium chloride with hydrogen peroxide in ethyl acetate at 4°C

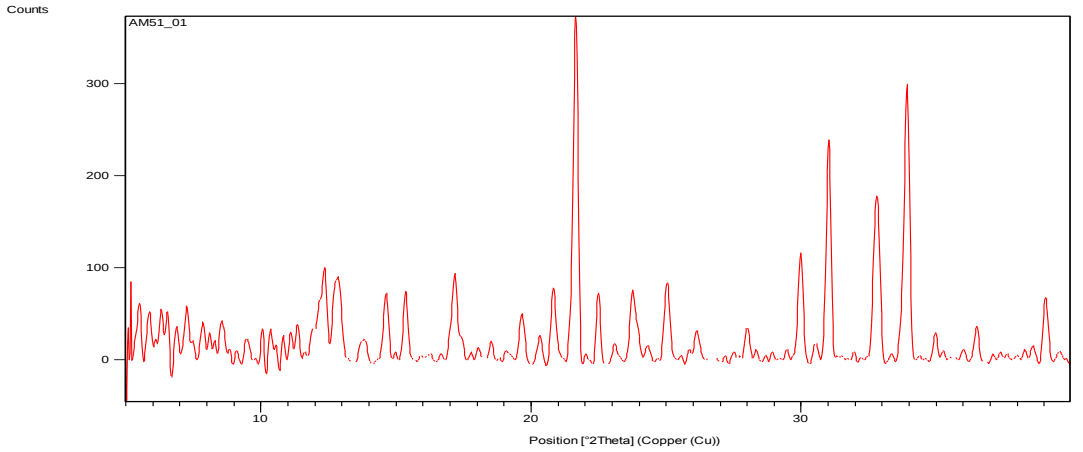

AM51_02 – PAP + magnesium chloride with hydrogen peroxide in ethyl acetate at room temperature

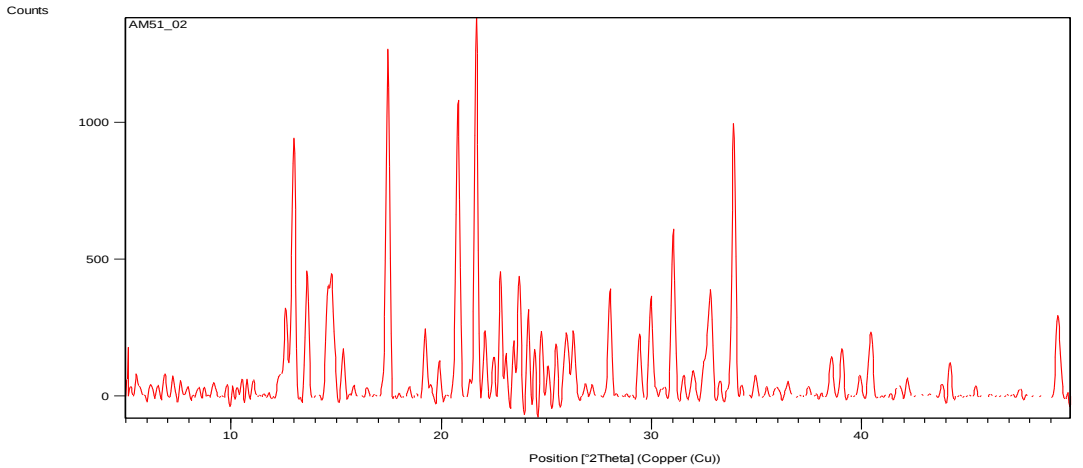

AM51_04 – PAP + magnesium chloride with hydrogen peroxide in chloroform at 4°C

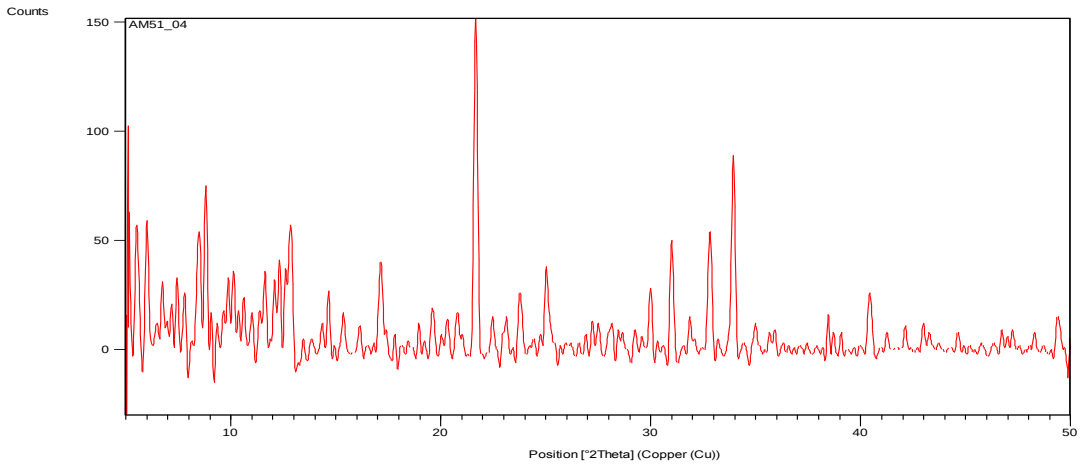

AM51_07 – PAP + magnesium chloride with hydrogen peroxide in acetone at 4°C

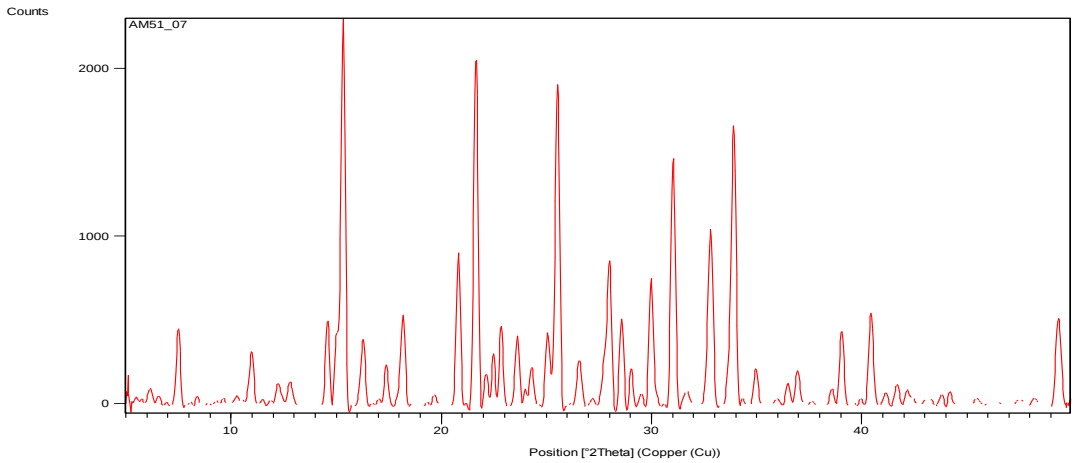

AM51_08 – PAP + magnesium chloride with hydrogen peroxide in acetone at room temperature

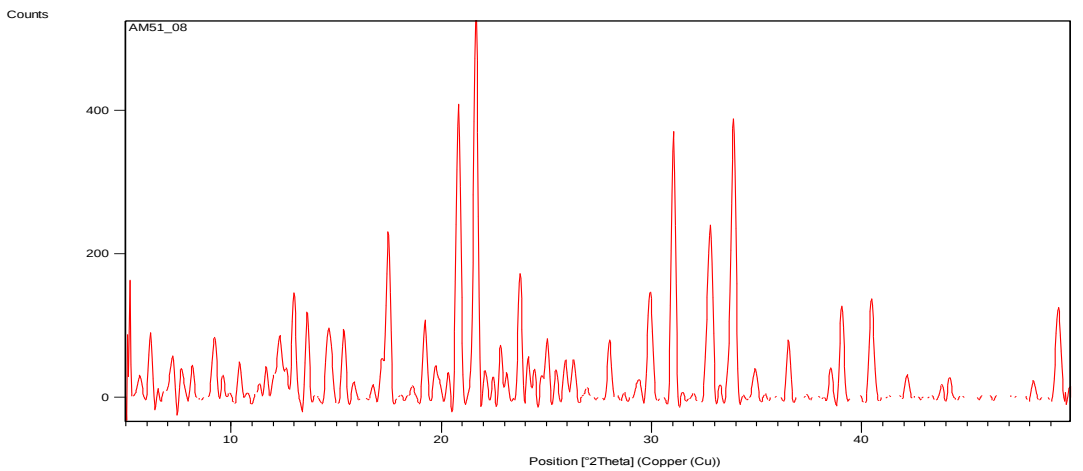

AM51_10 – PAP + magnesium chloride with hydrogen peroxide in diethyl ether at 4°C

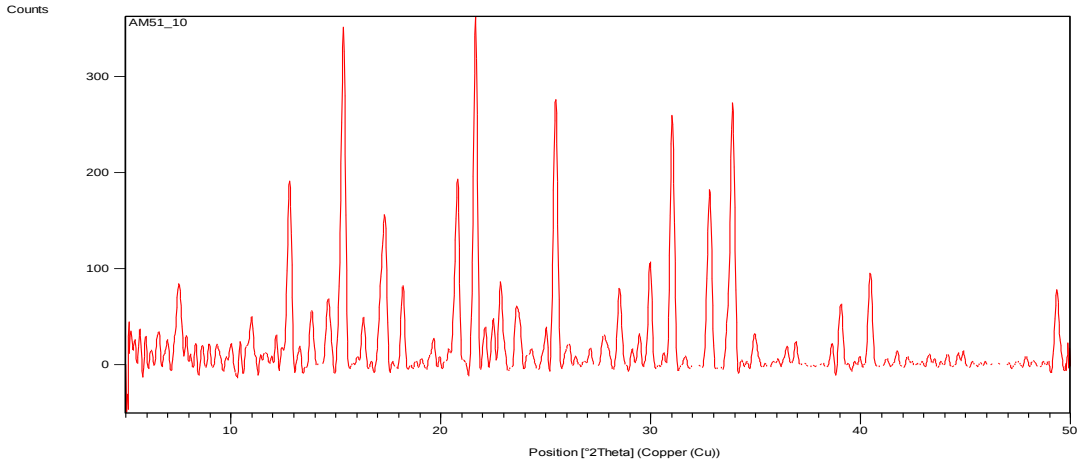

AM51_11 – PAP + magnesium chloride with hydrogen peroxide in diethyl ether at room temperature

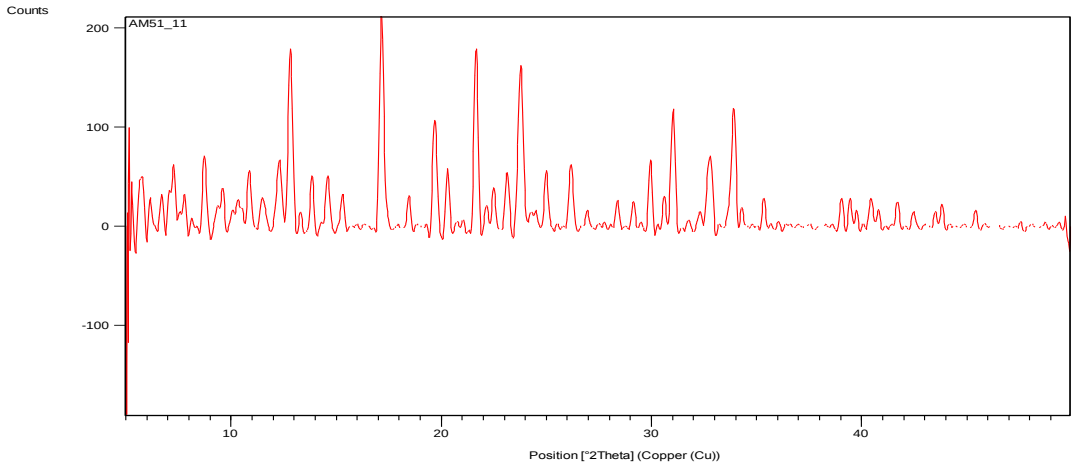

AM51_14 – PAP + magnesium chloride with hydrogen peroxide in dichloromethane at room temperature

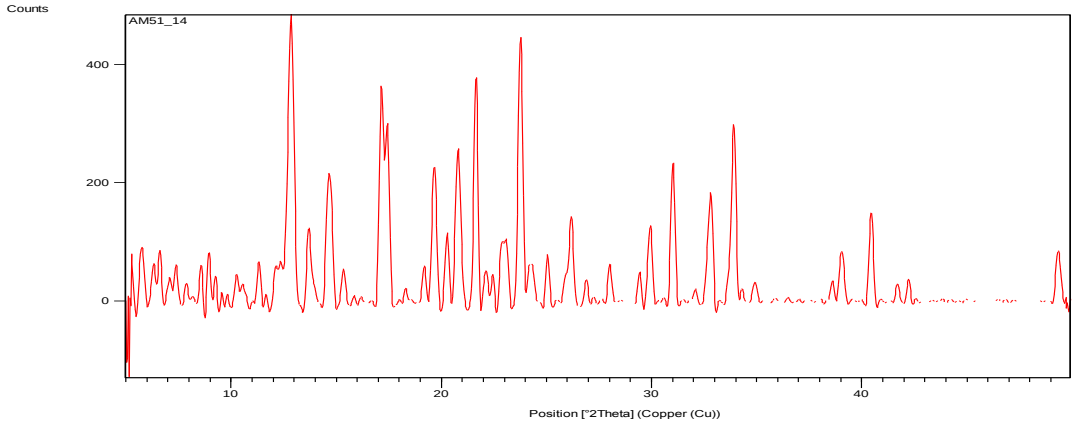

AM51_19 – PAP + magnesium chloride with hydrogen peroxide in methyl acetate at 4°C

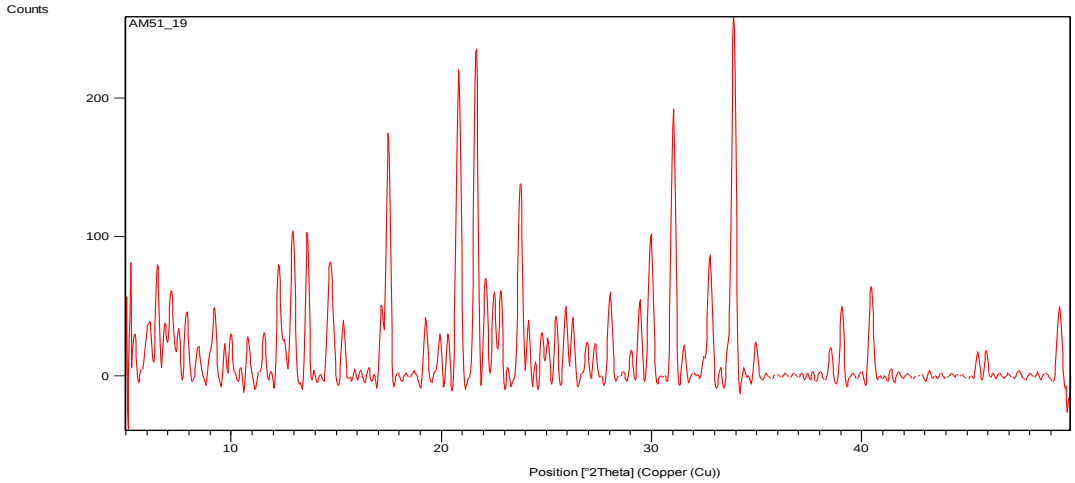

AM51_25 – PAP + magnesium chloride with hydrogen peroxide in ethanol at 4°C

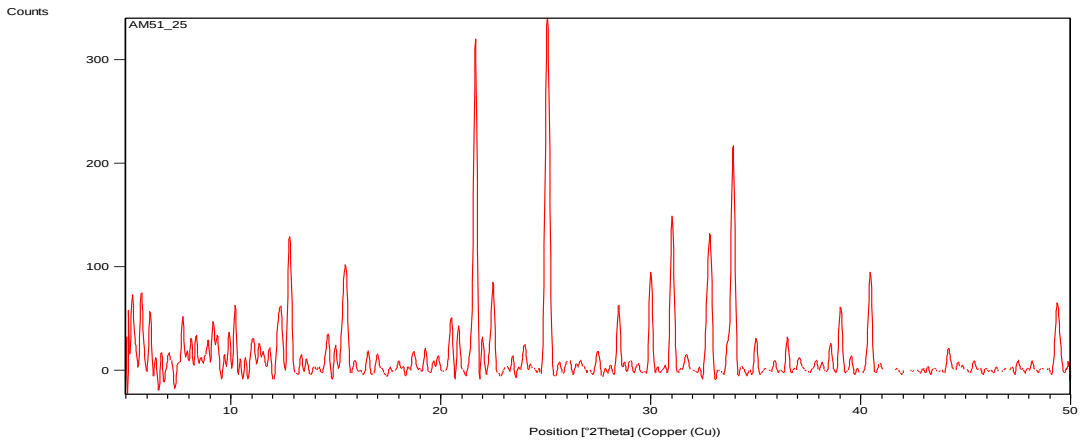

AM51_26 – PAP + magnesium chloride with hydrogen peroxide in ethanol at room temperature

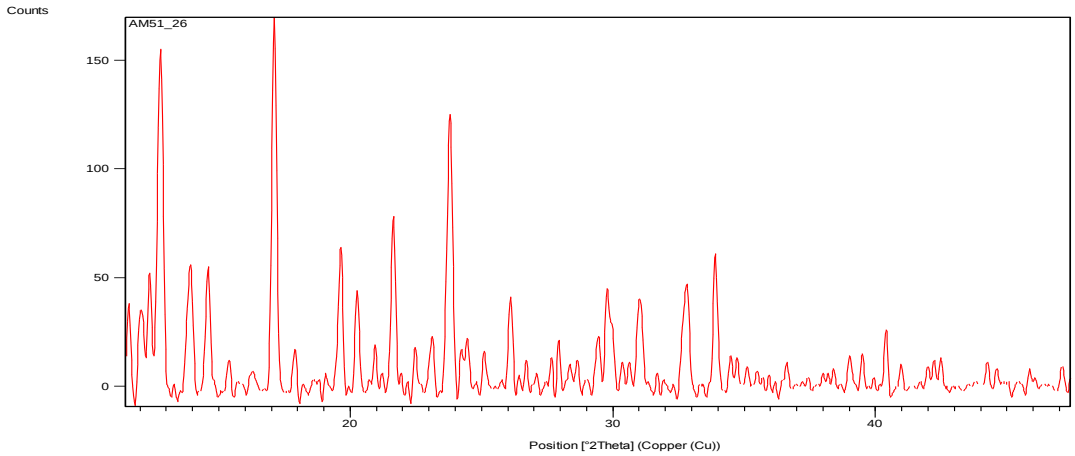

PAP and calcium chloride

AM54_01 – PAP + calcium chloride with hydrogen peroxide in ethyl acetate at 4°C

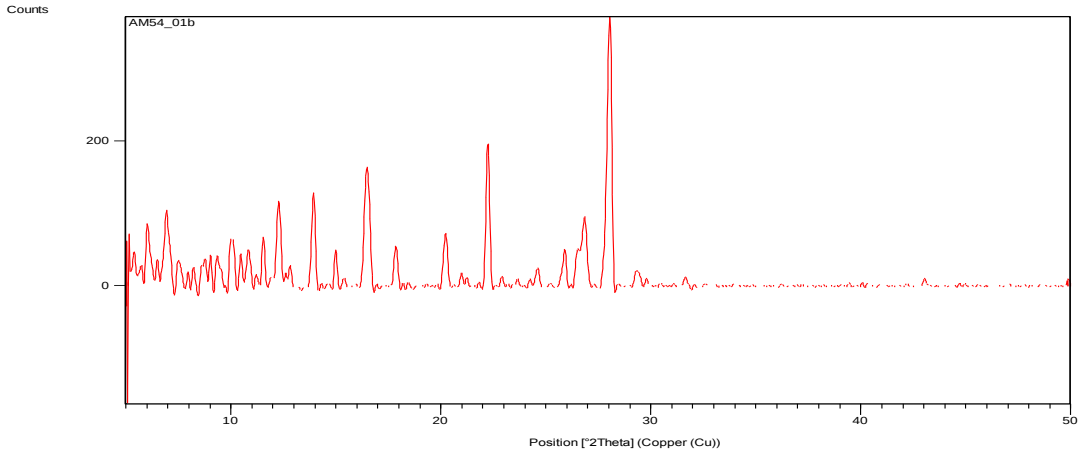

AM54_07 – PAP + calcium chloride with hydrogen peroxide in acetone at 4°C

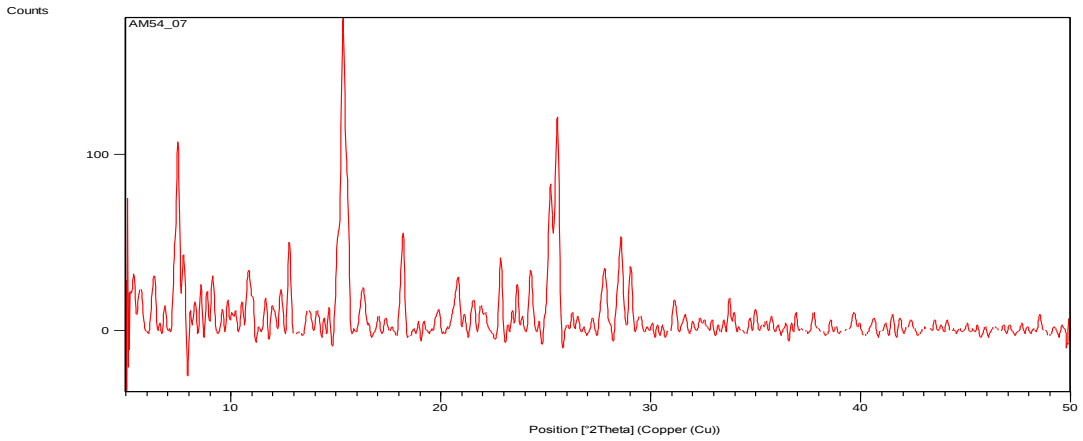

AM54_10 – PAP + calcium chloride with hydrogen peroxide in diethyl ether at 4°C

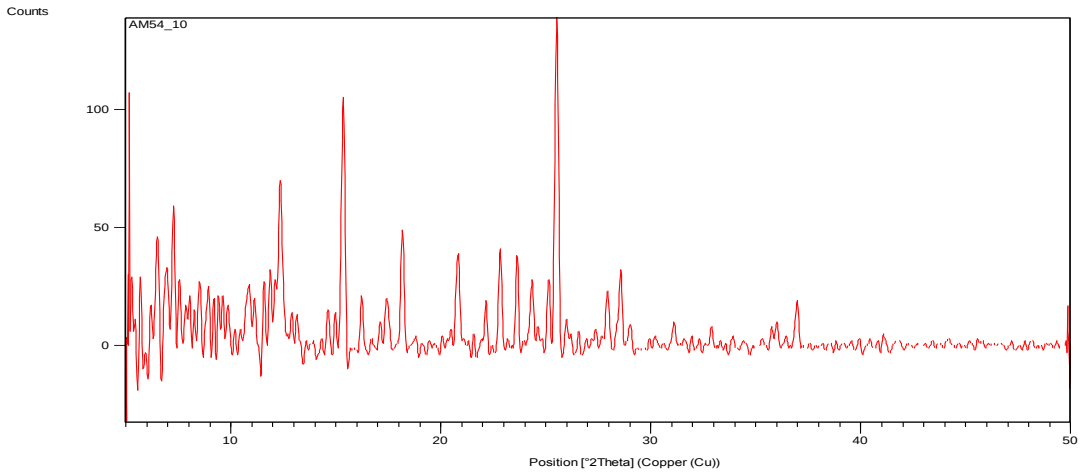

AM54_19 – PAP + calcium chloride with hydrogen peroxide in methyl acetate at 4°C

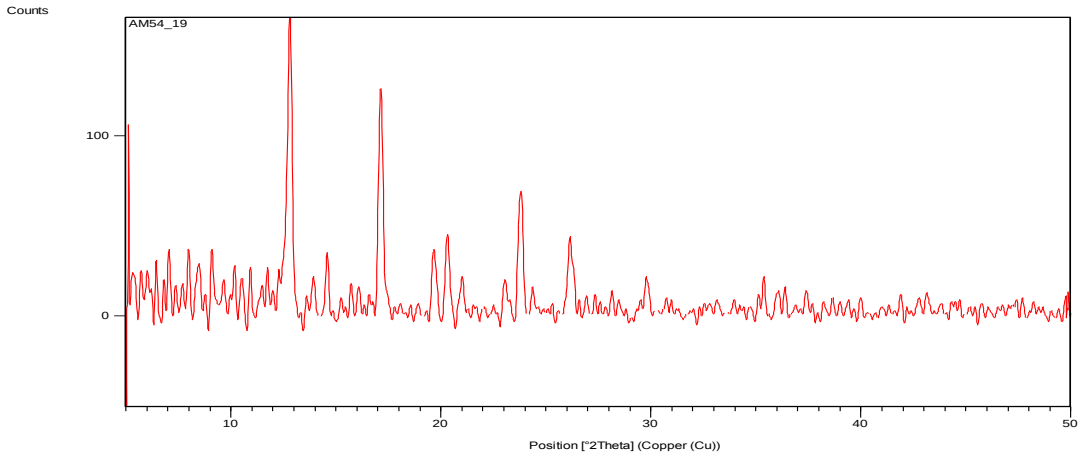

AM54_20 – PAP + calcium chloride with hydrogen peroxide in methyl acetate at room temperature

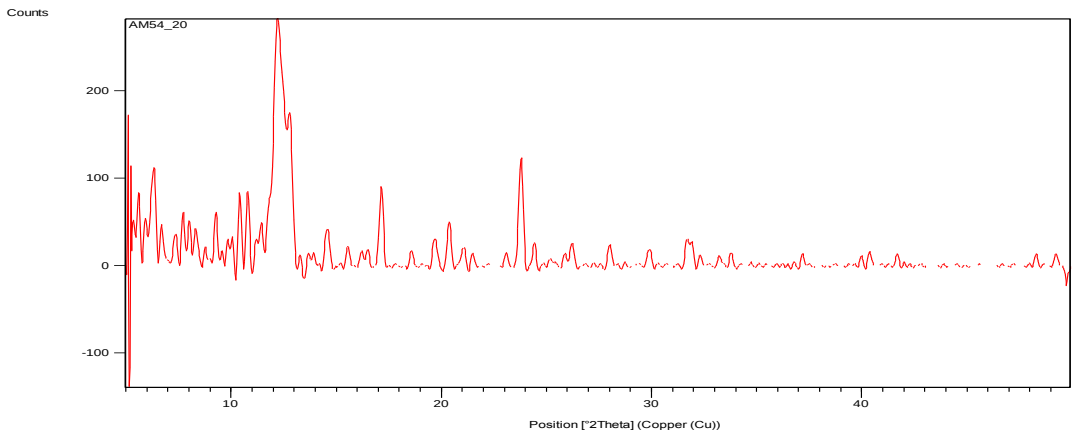

PAP and copper chloride

AM88_01 – PAP + copper chloride with hydrogen peroxide in acetone at 4°C

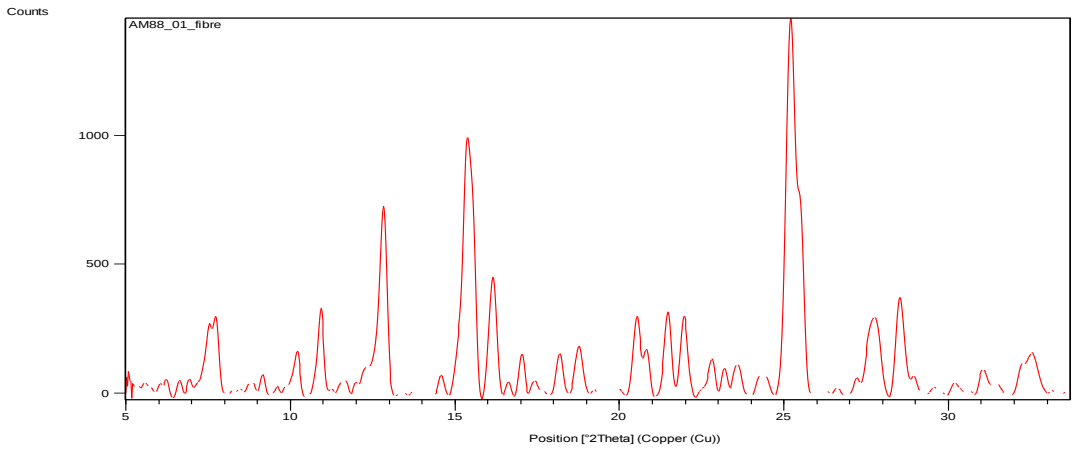

AM88_03 – PAP + copper chloride with hydrogen peroxide in methyl acetate at 4°C

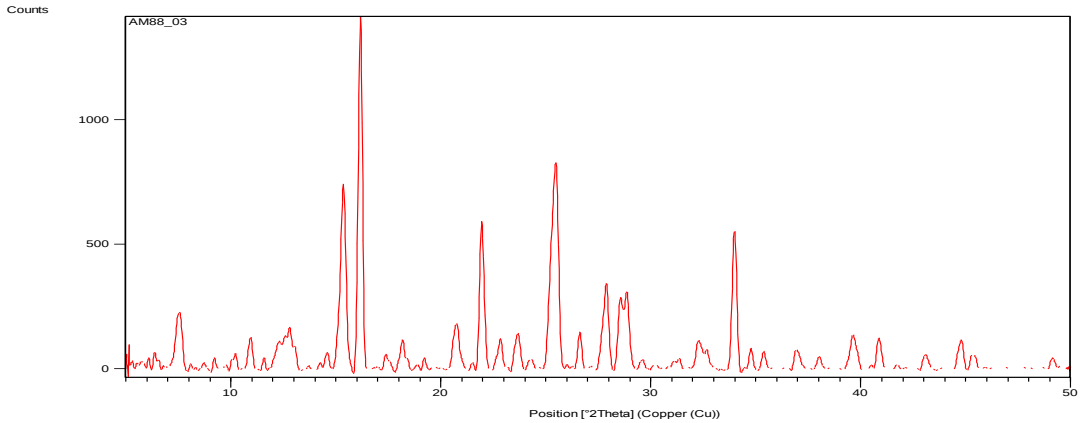

AM88_05 – PAP + copper chloride with hydrogen peroxide in ethyl acetate at 4°C

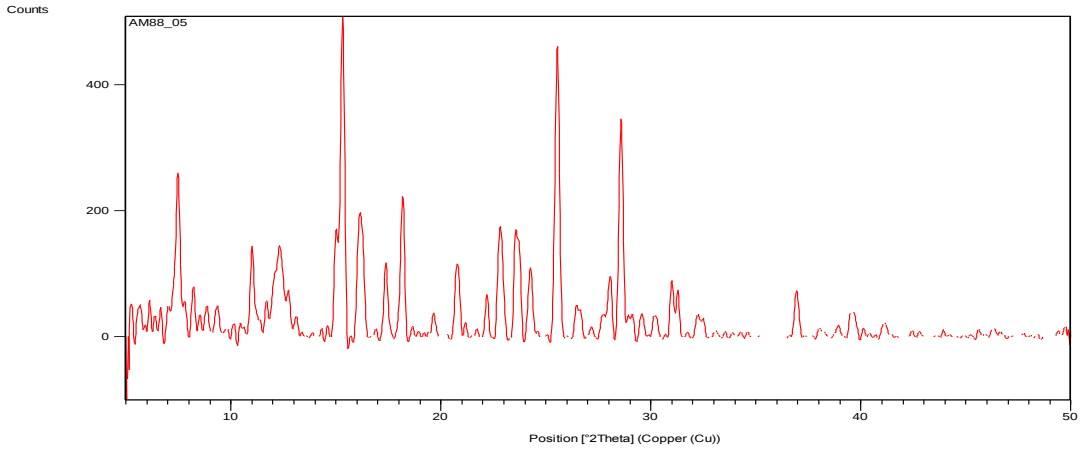

Appendix 3 –Hosting Reactive Peroxides in Layered Materials

XRPD Data

Urea based hosting

Urea and hydrogen peroxide crystallisation

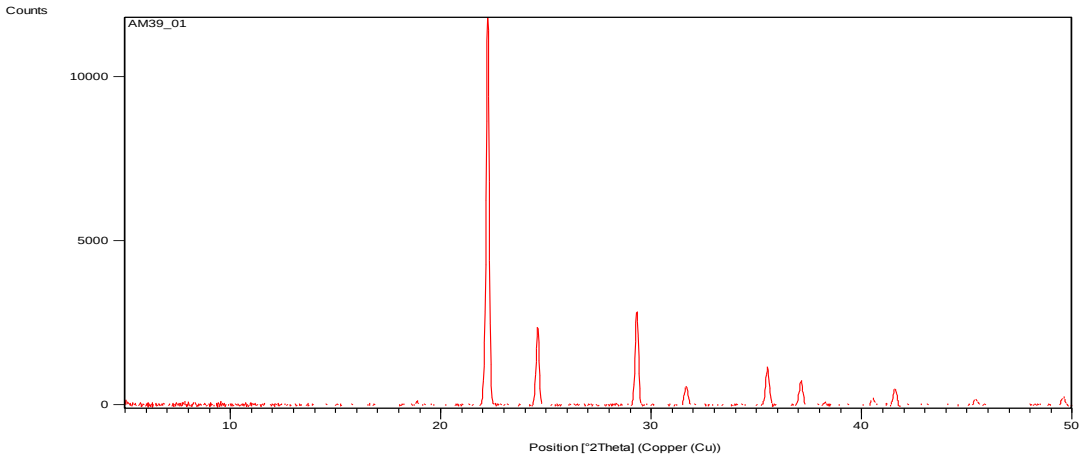

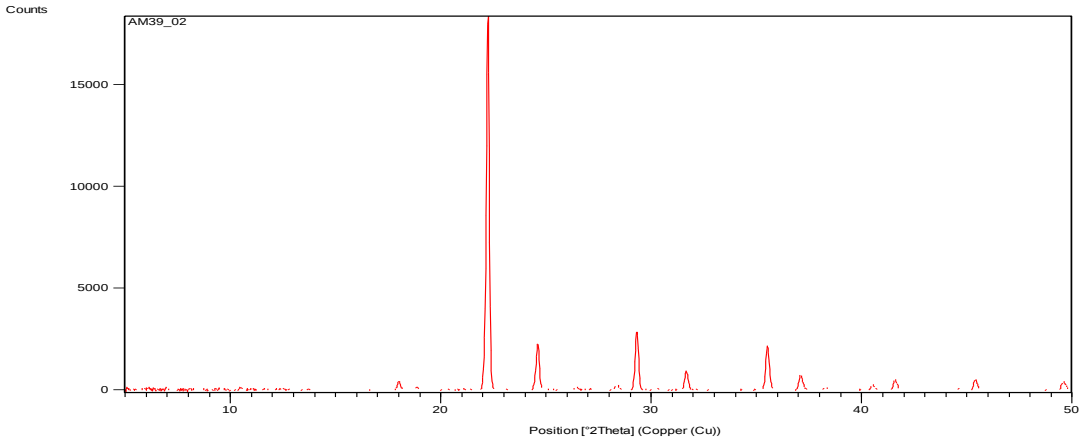

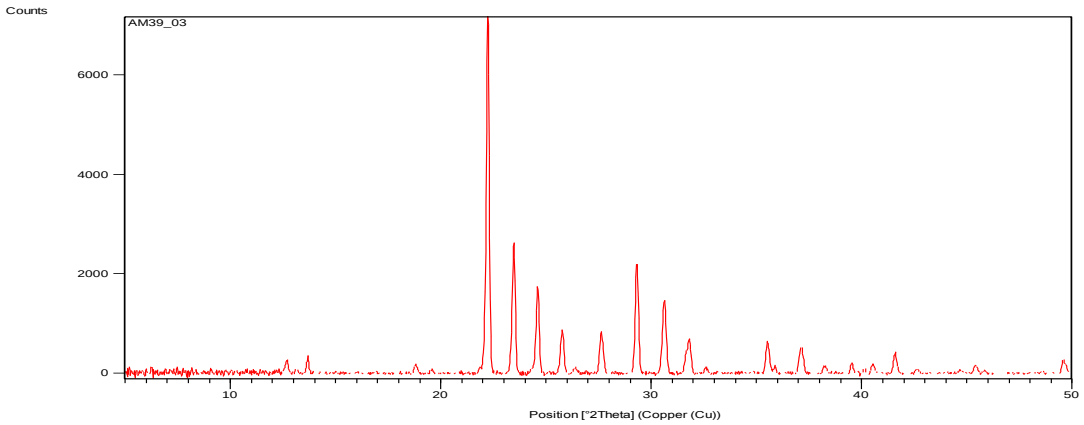
Counts
AM39_03
6000
4000
2000
0
10
20
30
40
50
Position [°2Theta] (Copper (Cu))

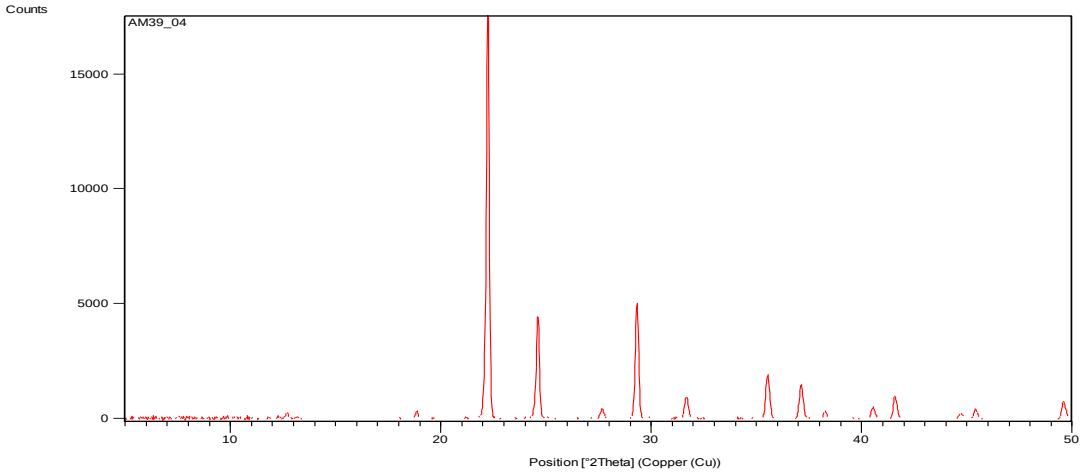
Counts
AM39_04
15000
10000
5000
0
10
20
30
40
50
Position [°2Theta] (Copper (Cu))

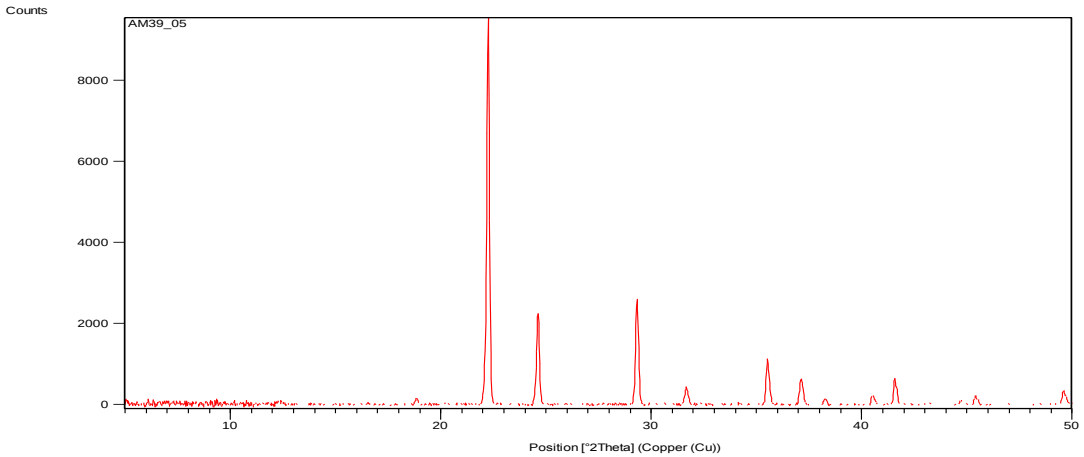
Counts
AM39_05
8000
6000
4000
2000
0
10
20
30
40
50
Position [°2Theta] (Copper (Cu))

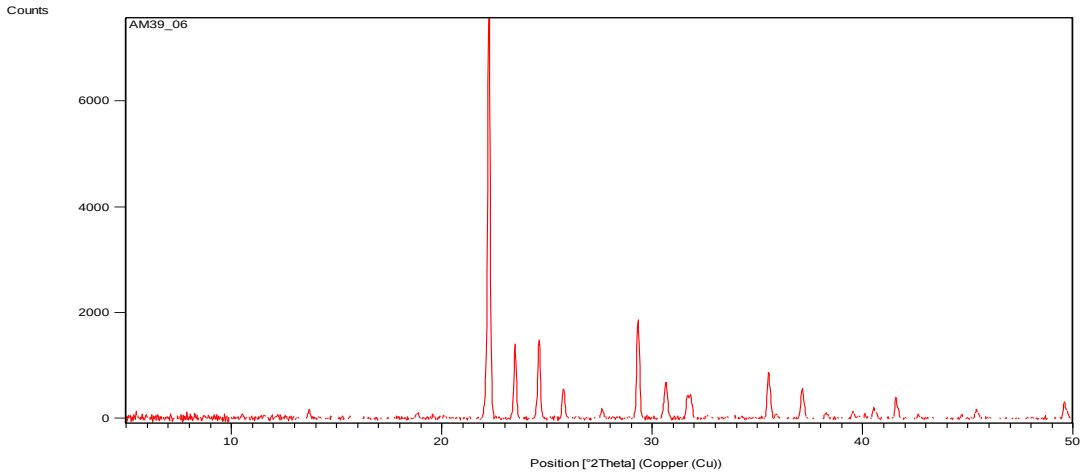
Counts
AM39_06
6000
4000
2000
0
10
20
30
40
50
Position [°2Theta] (Copper (Cu))

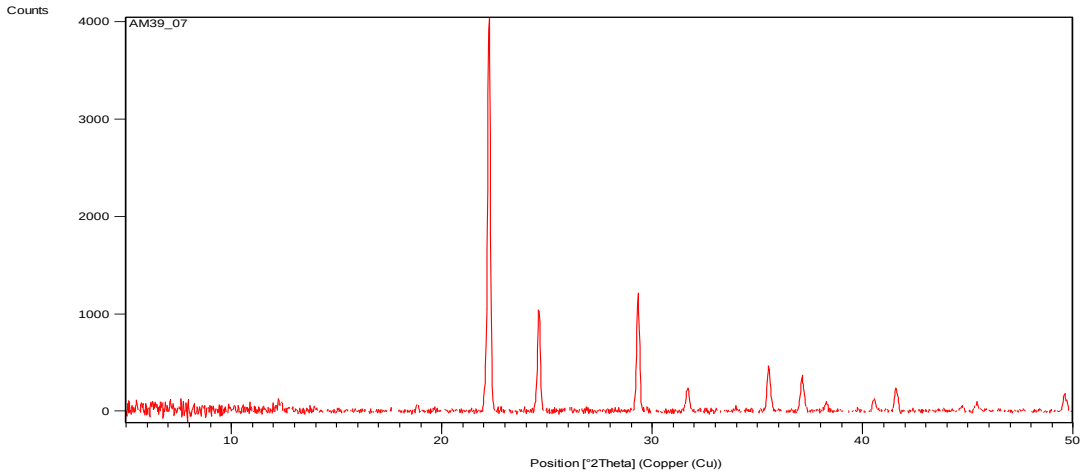
Counts
AM39_07
4000
3000
2000
1000
0
10
20
30
40
50
Position [°2Theta] (Copper (Cu))

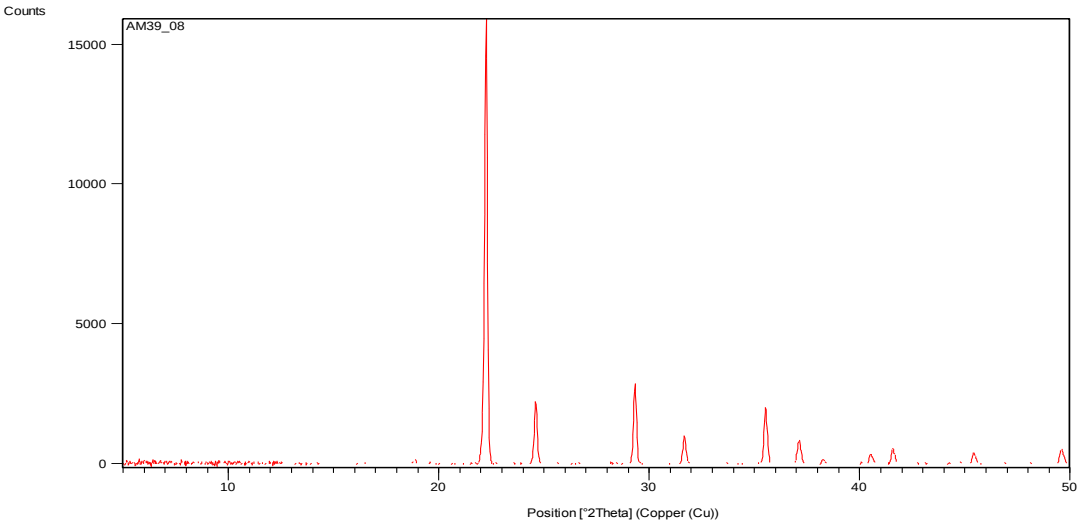
Counts
AM39_08
15000
10000
5000
0
10
20
30
40
50
Position [°2Theta] (Copper (Cu))

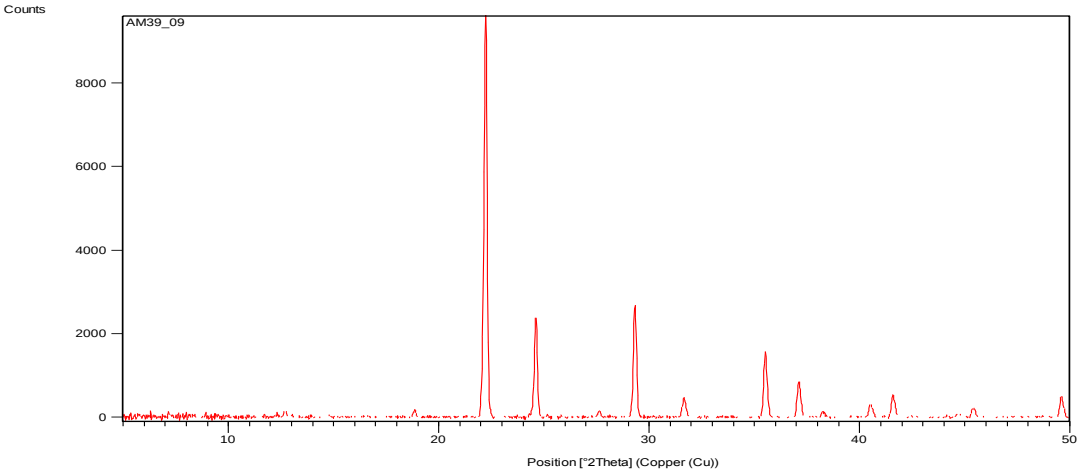
Counts
AM39_09
8000
6000
4000
2000
0
10
20
30
40
50
Position [°2Theta] (Copper (Cu))

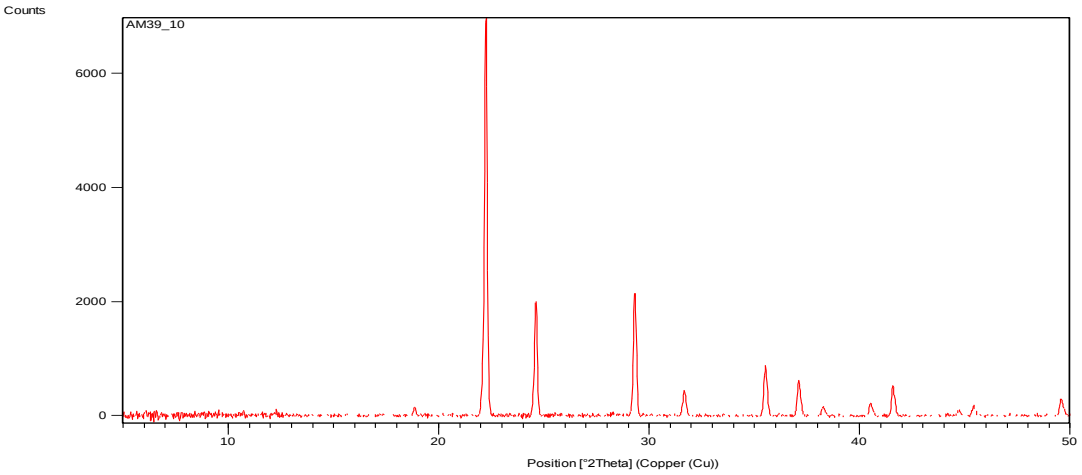
Counts
AM39_10
6000
4000
2000
0
10
20
30
40
50
Position [°2Theta] (Copper (Cu))

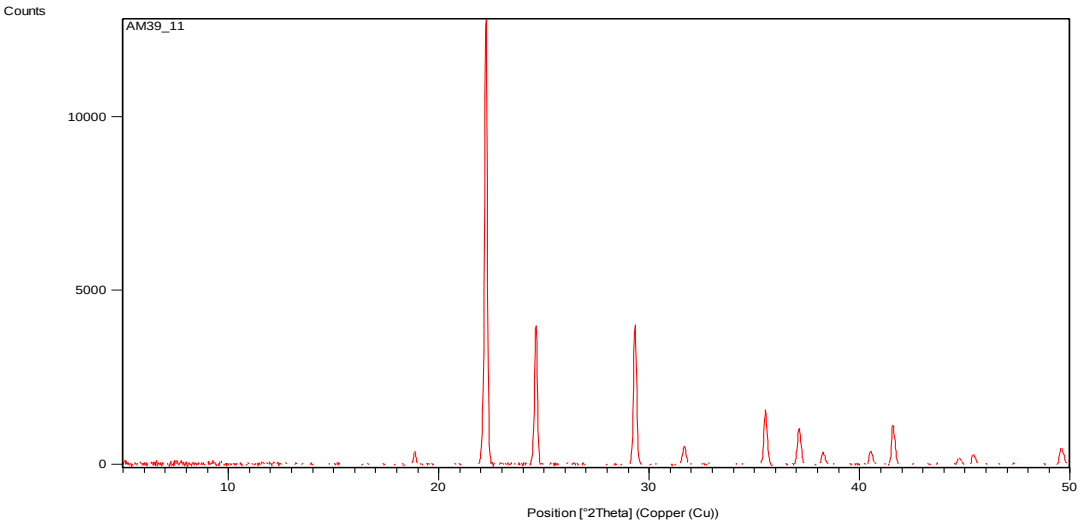
Counts
AM39_11
10000
5000
0
10
20
30
40
50
Position [°2Theta] (Copper (Cu))

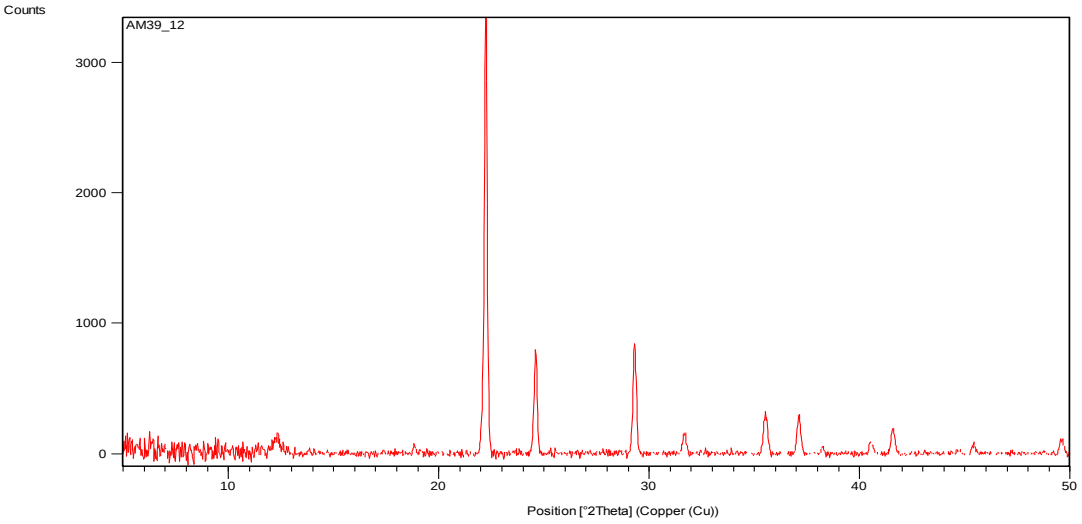
Counts
AM39_12
3000
2000
1000
0
10
20
30
40
50
Position [°2Theta] (Copper (Cu))

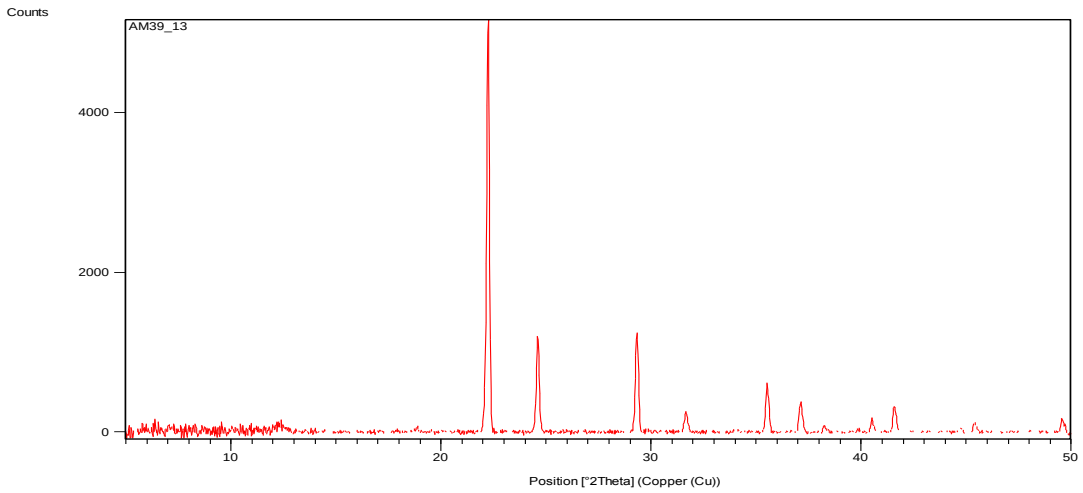

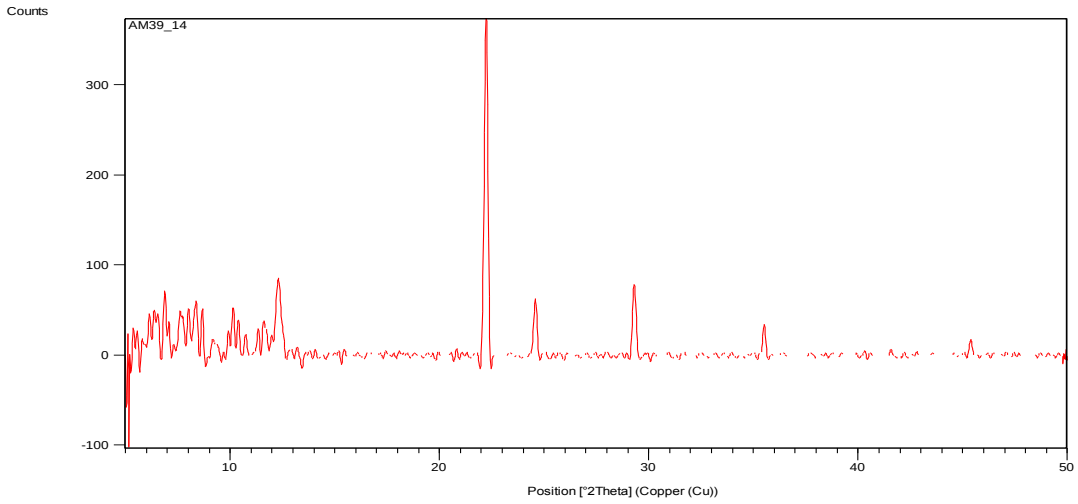

Urea and 6-phthalimidoperoxyhexanoic acid

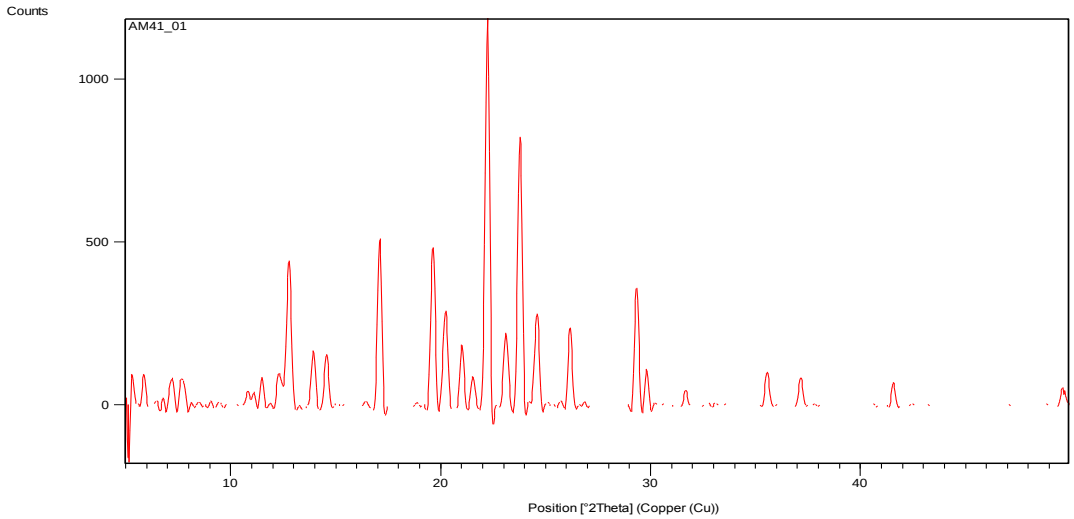

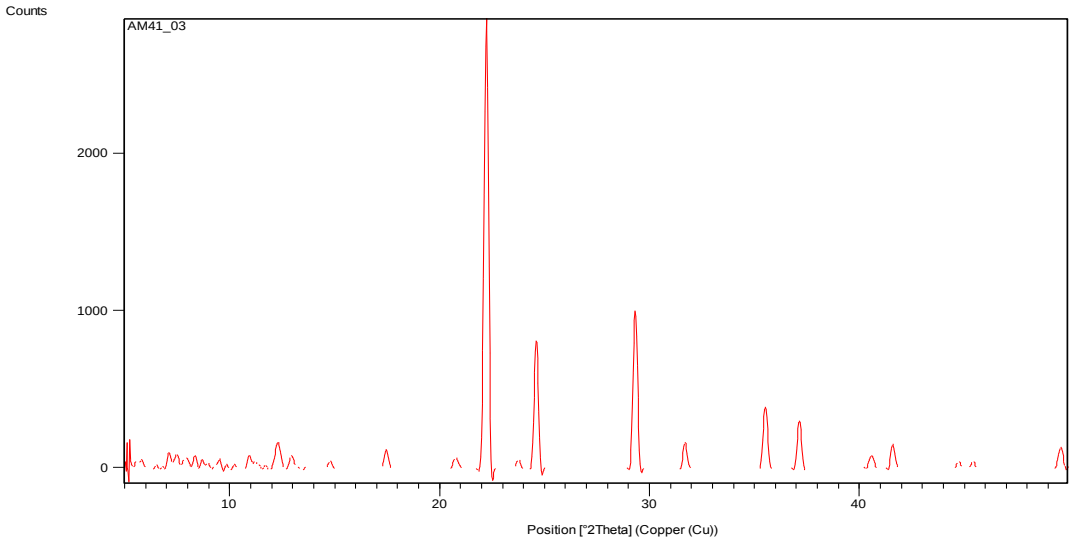
Counts
AM41_03
2000
1000
0
10
20
30
40
Position [°2Theta] (Copper (Cu))

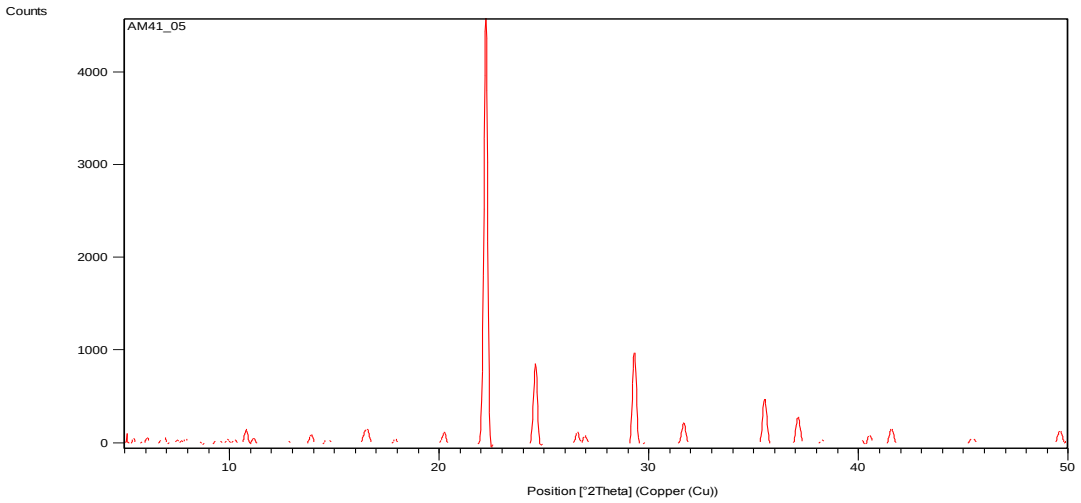
Counts
AM41_05
4000
3000
2000
1000
0
10
20
30
40
50
Position [°2Theta] (Copper (Cu))

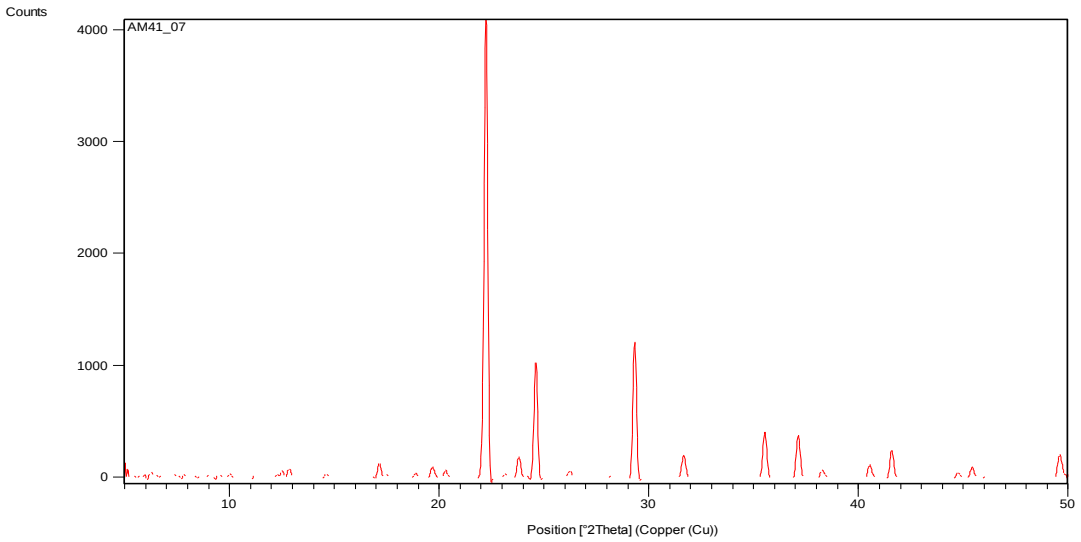
Counts
AM41_07
4000
3000
2000
1000
0
10
20
30
40
50
Position [°2Theta] (Copper (Cu))

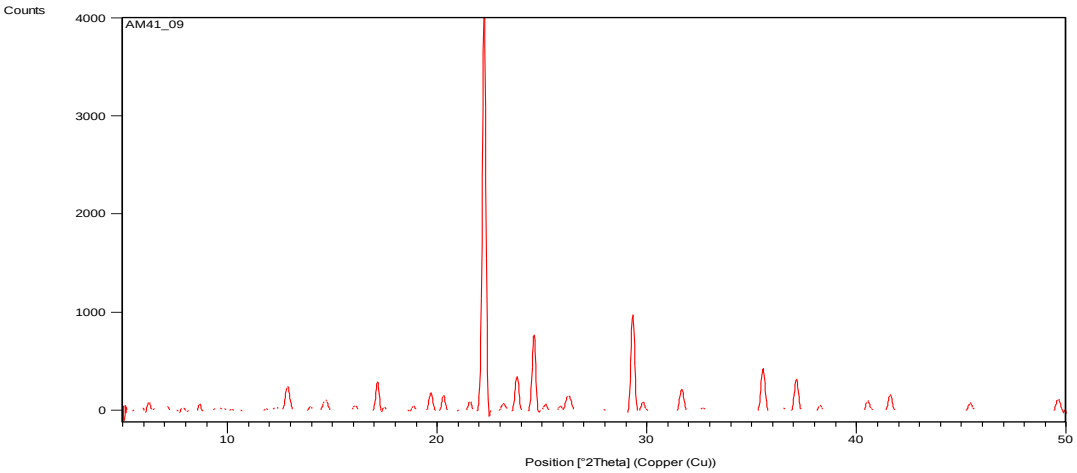

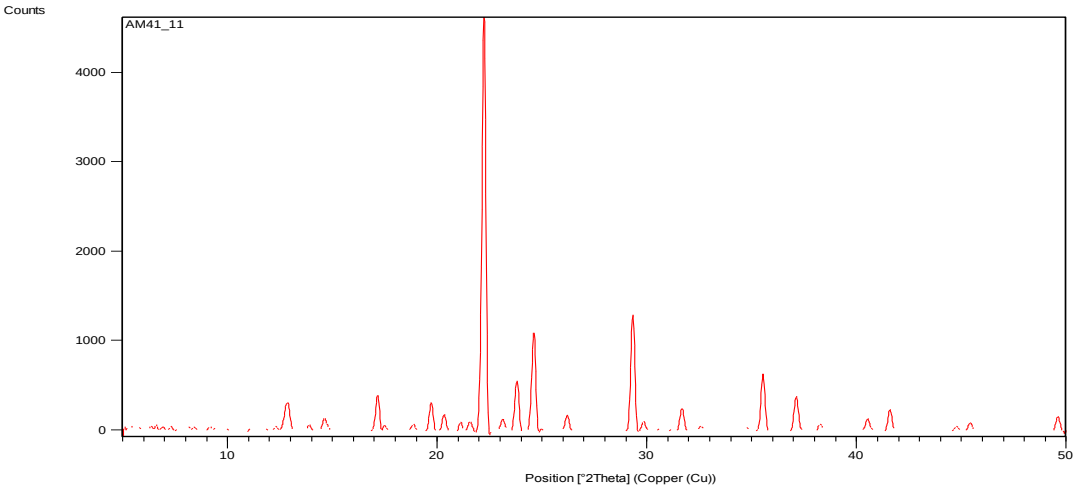

Urea and *meta*-chloroperbenzoic acid

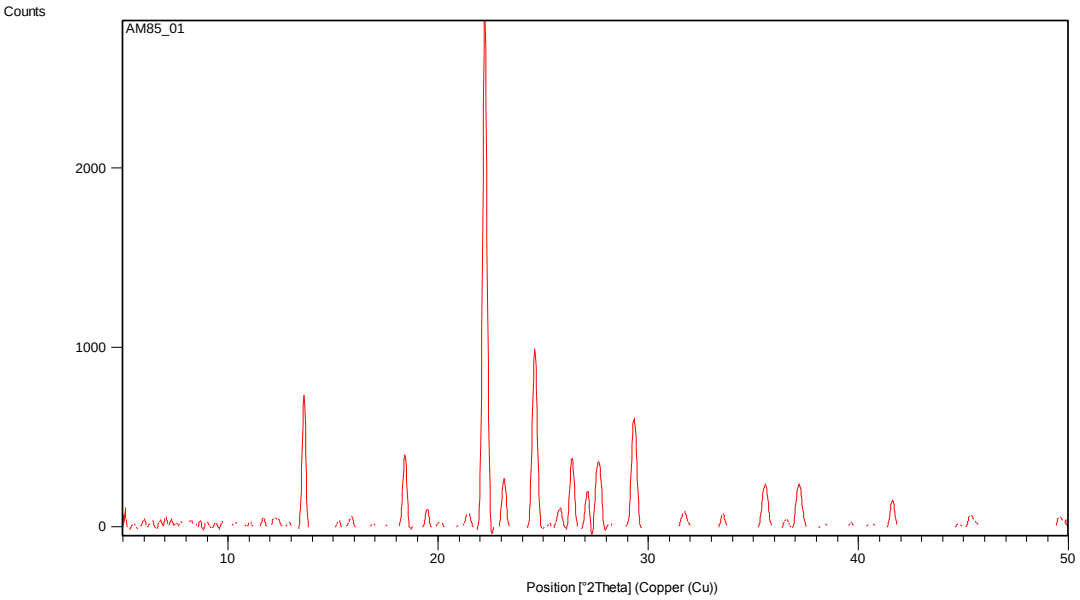

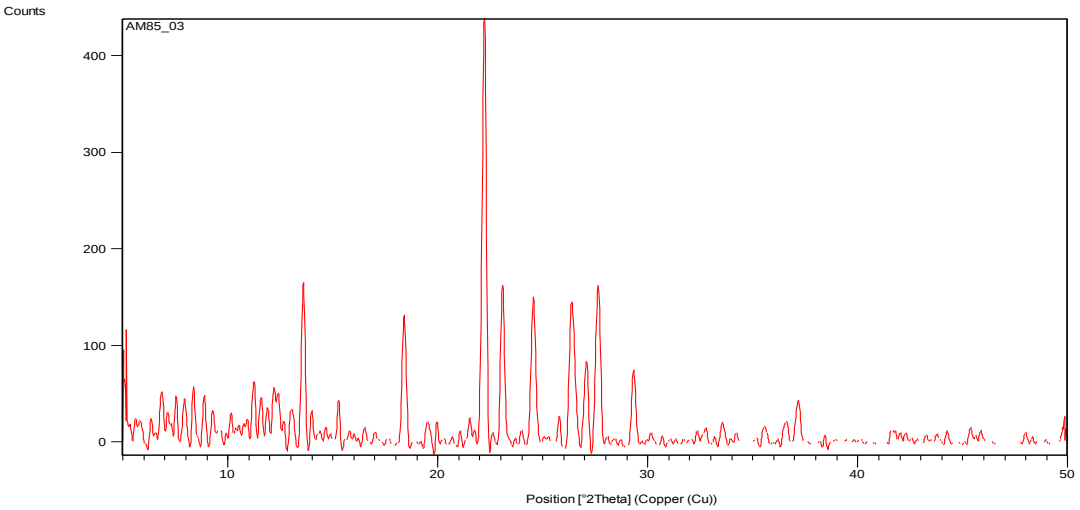
Counts
AM85_03
400
300
200
100
0
10
20
30
40
50
Position [°2Theta] (Copper (Cu))

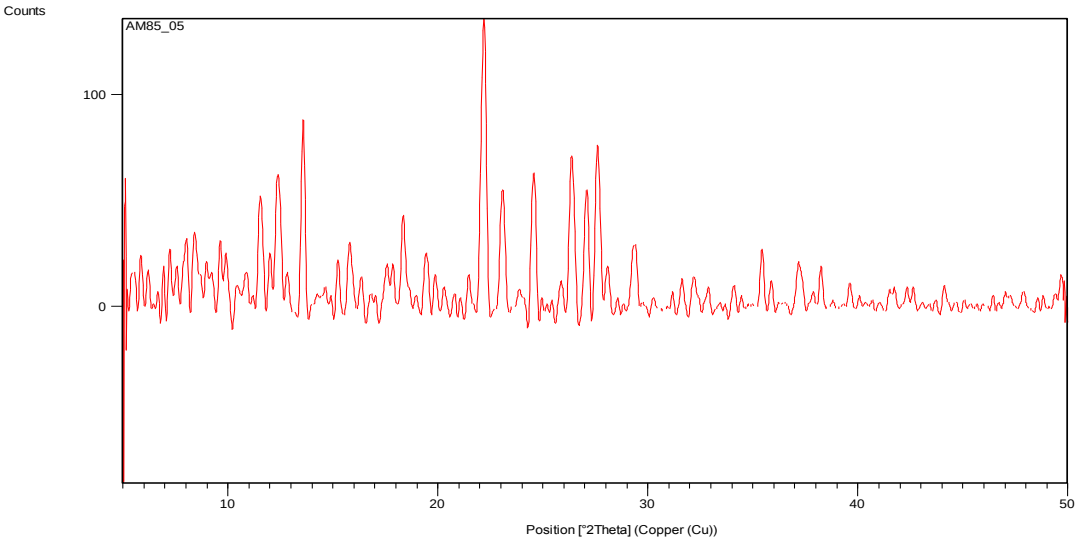
Counts
AM85_05
100
0
10
20
30
40
50
Position [°2Theta] (Copper (Cu))

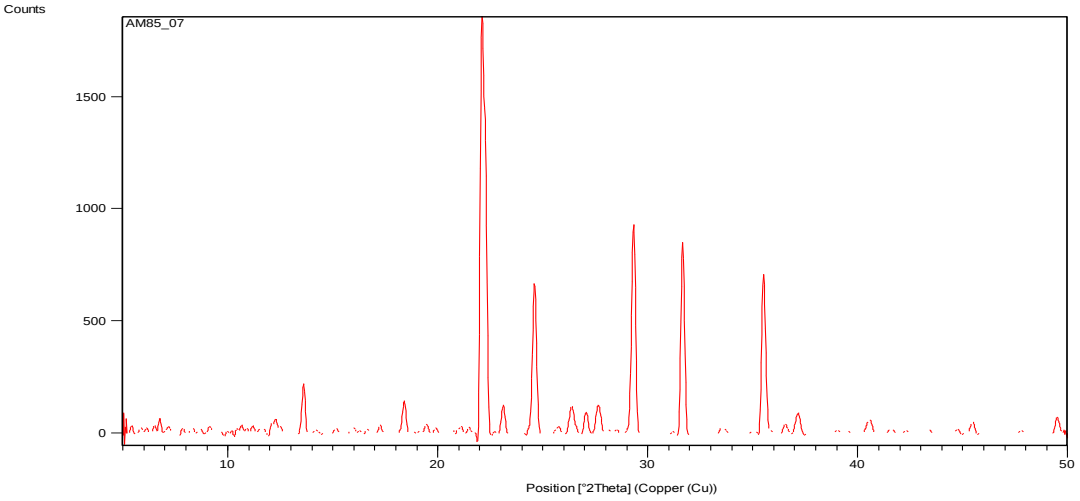
Counts
AM85_07
1500
1000
500
0
10
20
30
40
50
Position [°2Theta] (Copper (Cu))

Clay intercalation

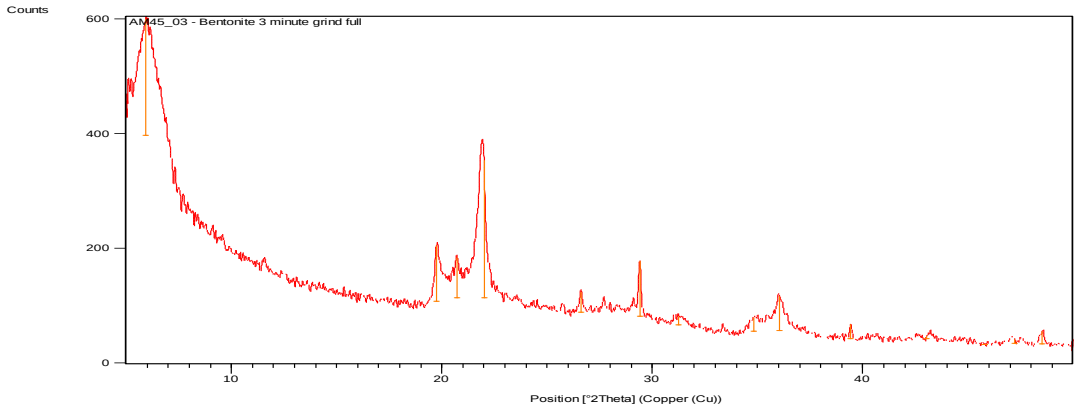

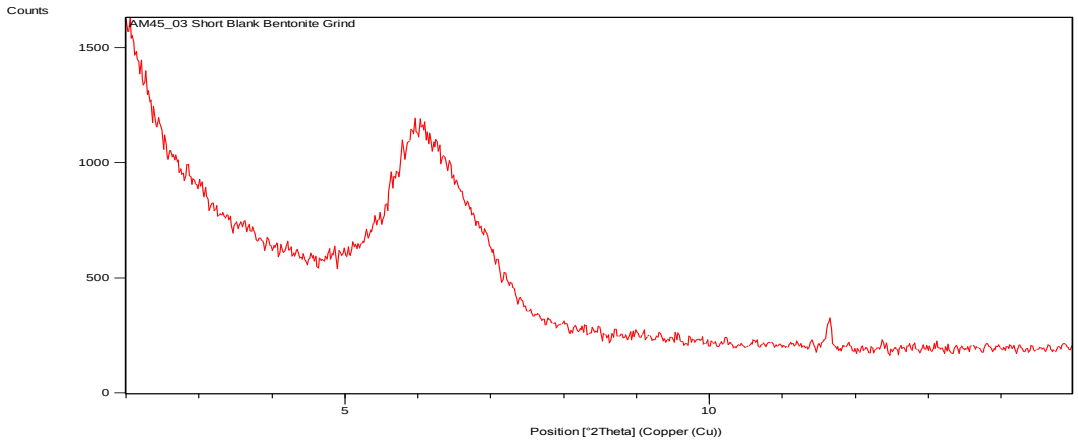

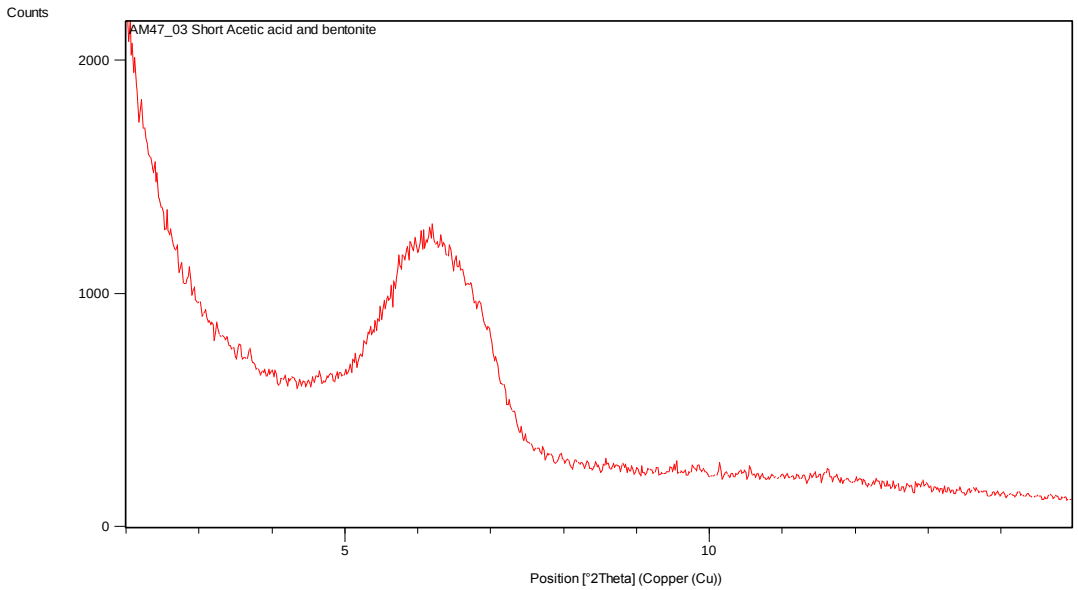

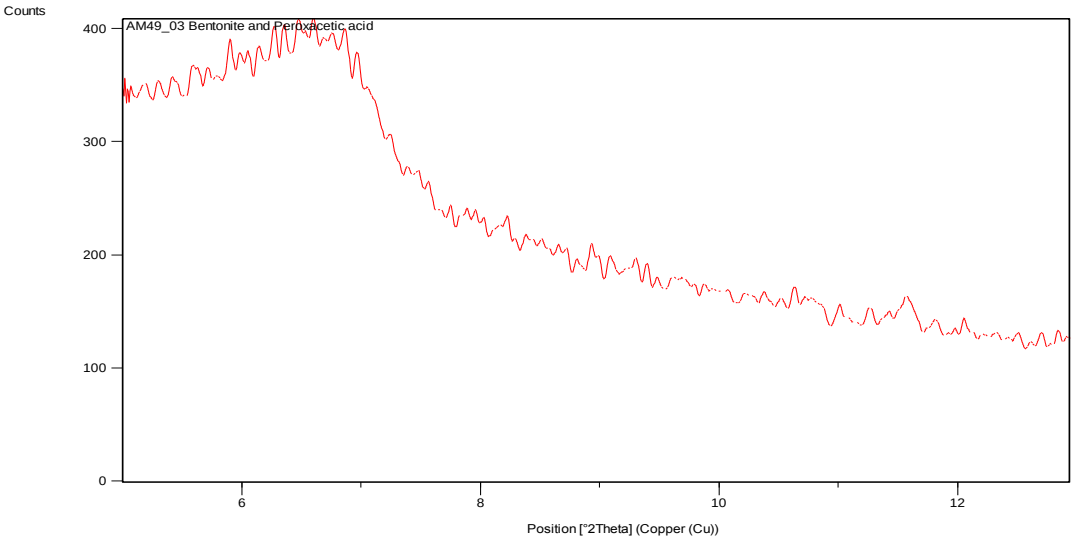
Counts
AM49_03 Bentonite and Peroxyacetic acid
400
300
200
100
0
6
8
10
12
Position [°2Theta] (Copper (Cu))

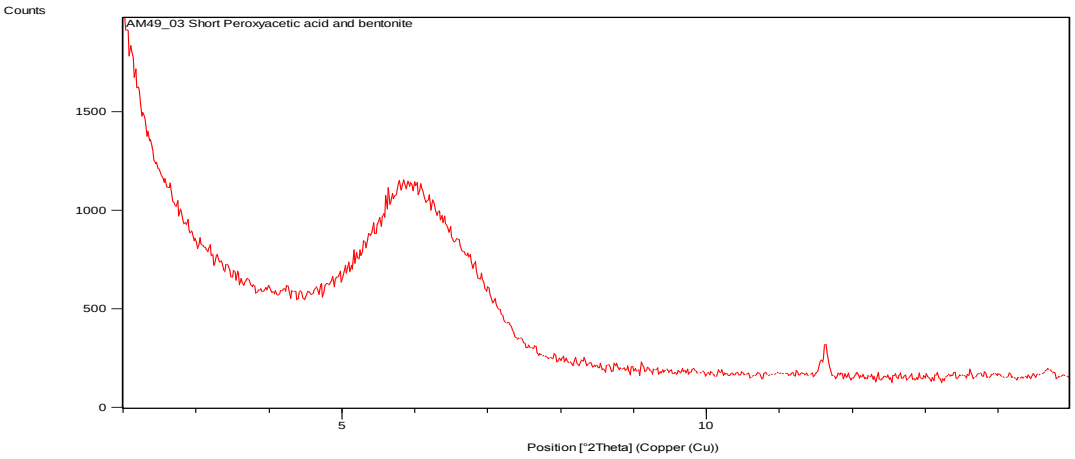
Counts
AM49_03 Short Peroxyacetic acid and bentonite
1500
1000
500
0
5
10
Position [°2Theta] (Copper (Cu))

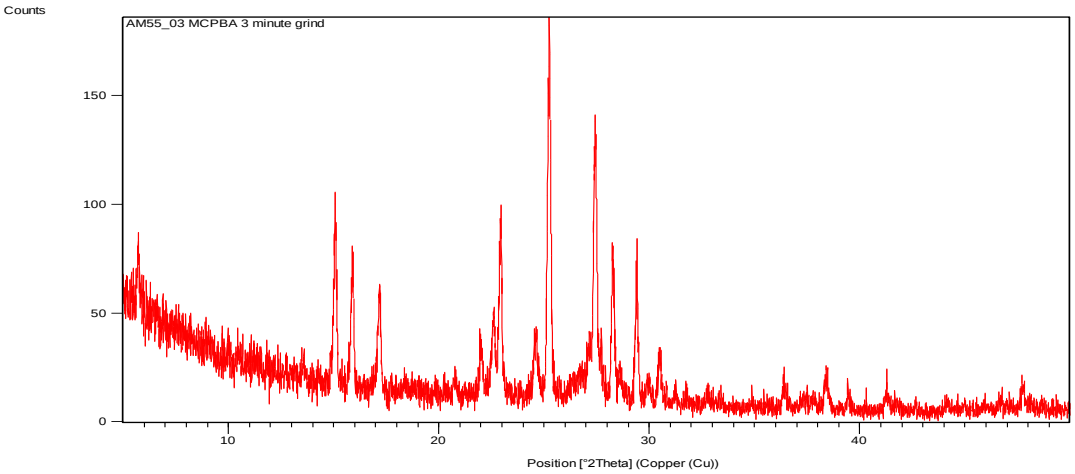
Counts
AM55_03 MCPBA 3 minute grind
150
100
50
0
10
20
30
40
Position [°2Theta] (Copper (Cu))

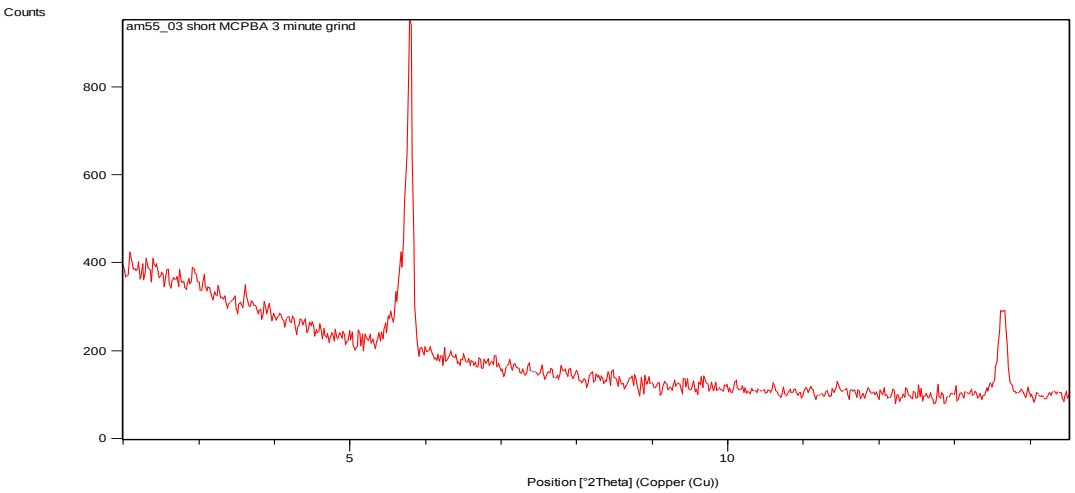
Counts
am55_03 short MCPBA 3 minute grind
800
600
400
200
0
5
10
Position [°2Theta] (Copper (Cu))

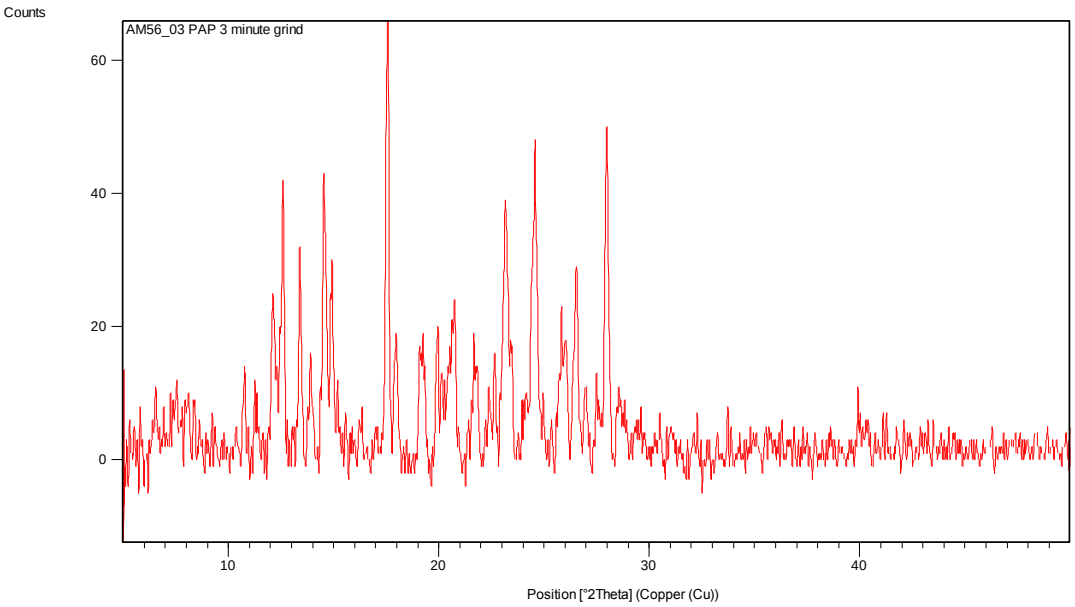
Counts
AM56_03 PAP 3 minute grind
60
40
20
0
10
20
30
40
Position [°2Theta] (Copper (Cu))

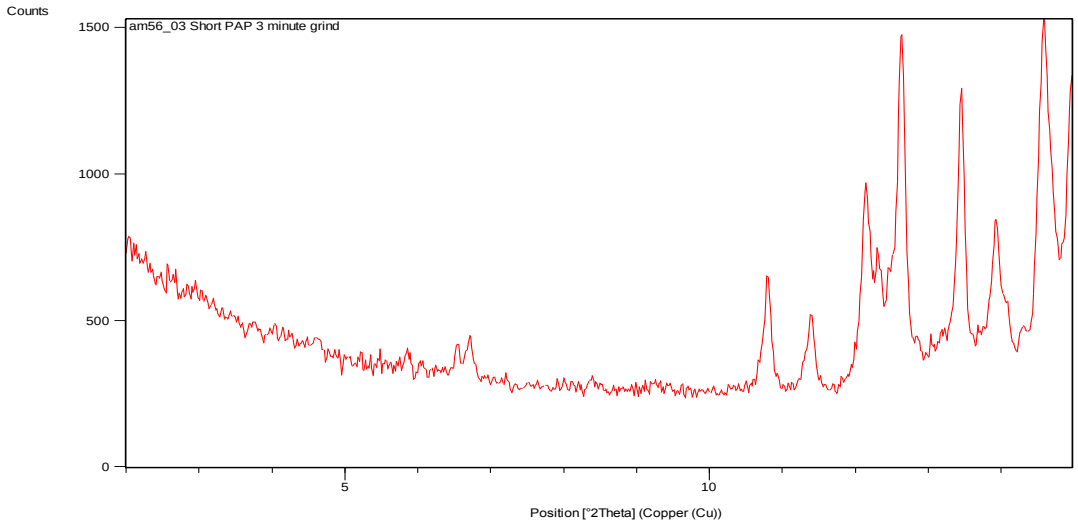
Counts
am56_03 Short PAP 3 minute grind
1500
1000
500
0
5
10
Position [°2Theta] (Copper (Cu))

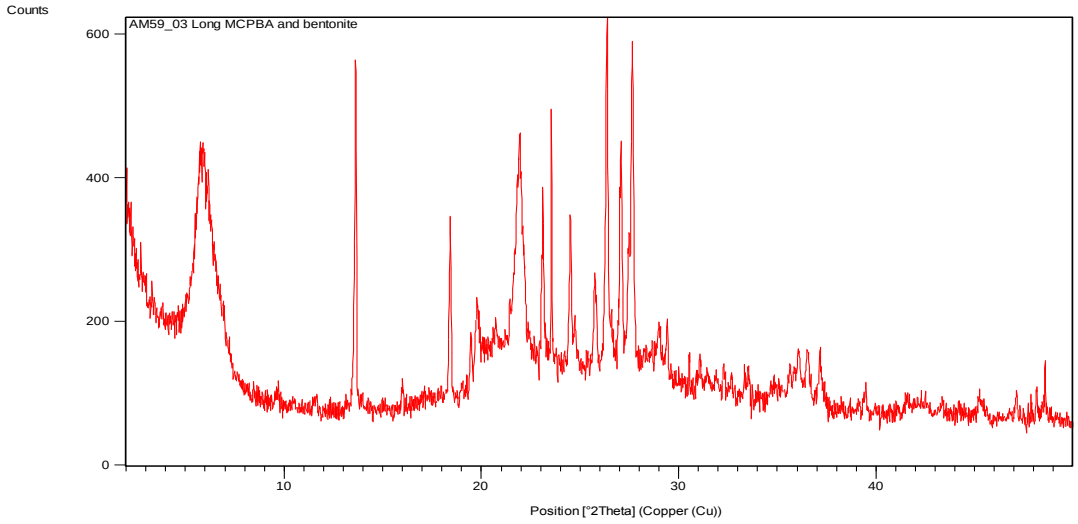
Counts
AM59_03 Long MCPBA and bentonite
600
400
200
0
10
20
30
40
Position [°2Theta] (Copper (Cu))

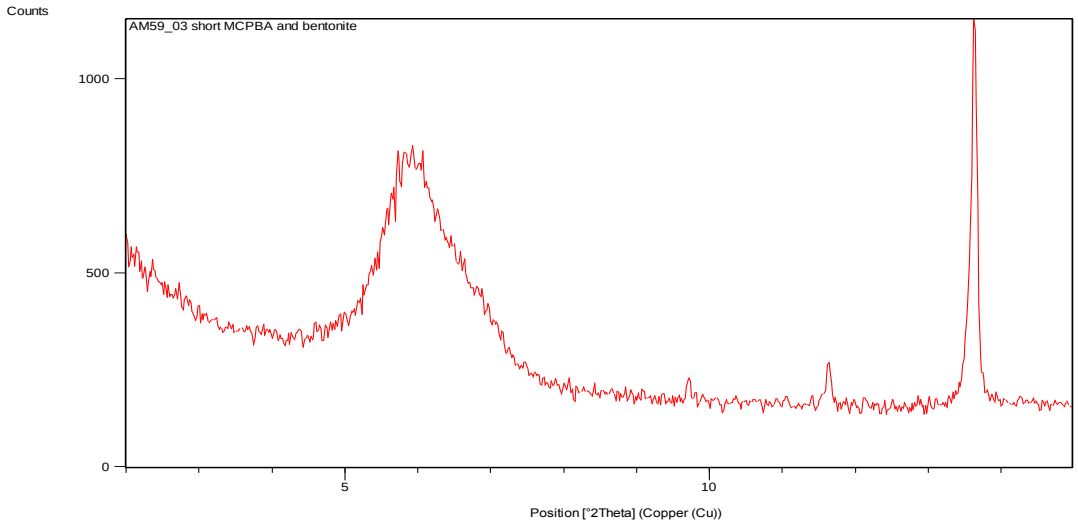
Counts
AM59_03 short MCPBA and bentonite
1000
500
0
5
10
Position [°2Theta] (Copper (Cu))

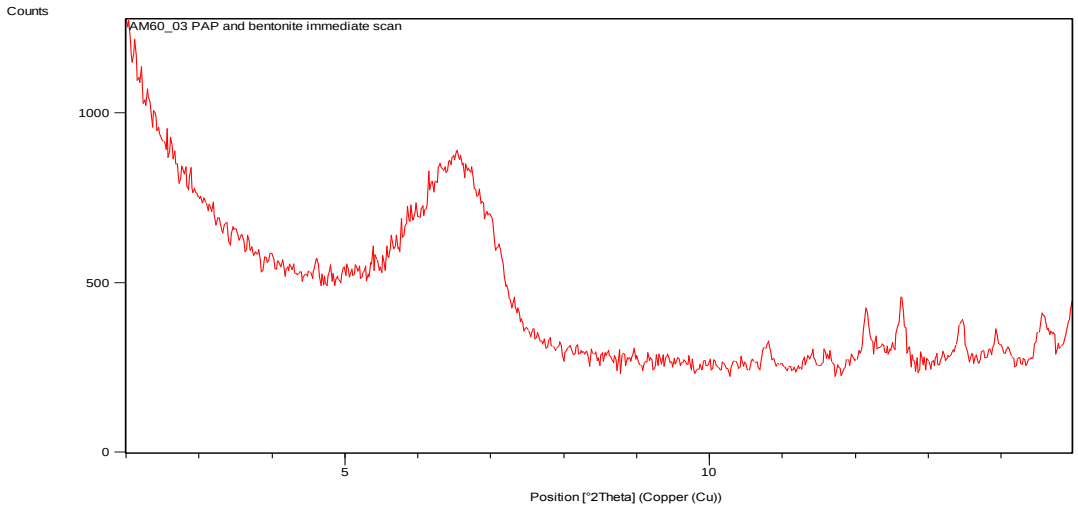
Counts
AM60_03 PAP and bentonite immediate scan
1000
500
0
5
10
Position [°2Theta] (Copper (Cu))

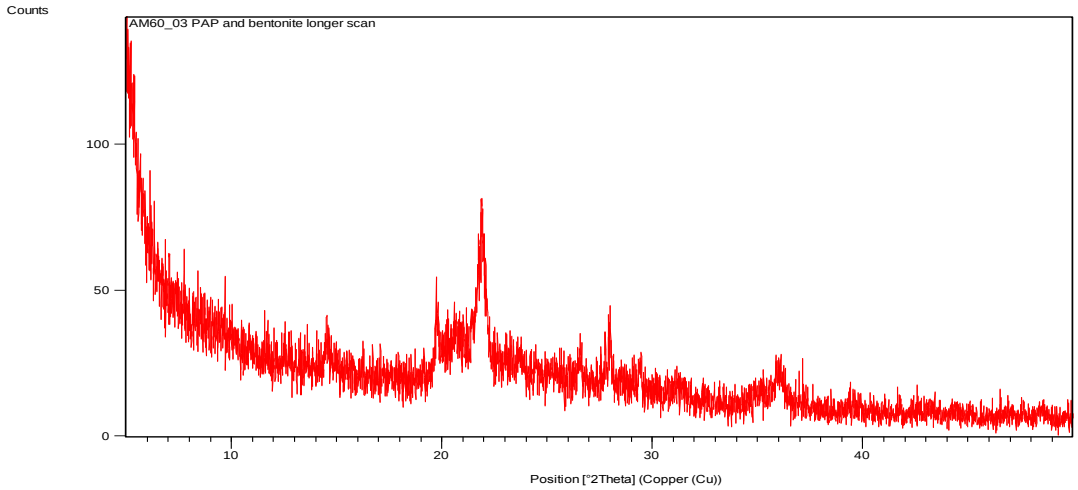
Counts
AM60_03 PAP and bentonite longer scan
100
50
0
10
20
30
40
Position [°2Theta] (Copper (Cu))

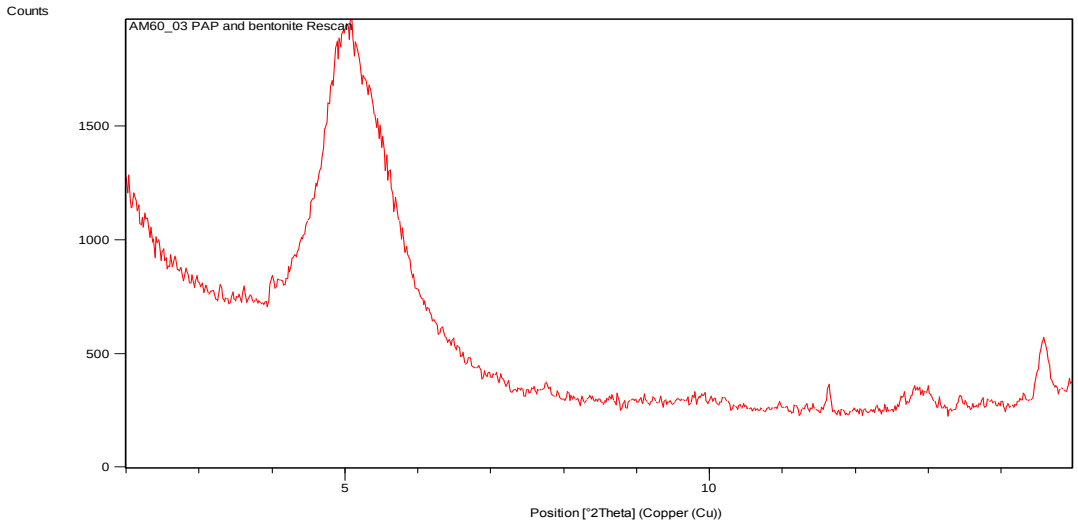
Counts
AM60_03 PAP and bentonite Rescan
1500
1000
500
0
5
10
Position [°2Theta] (Copper (Cu))

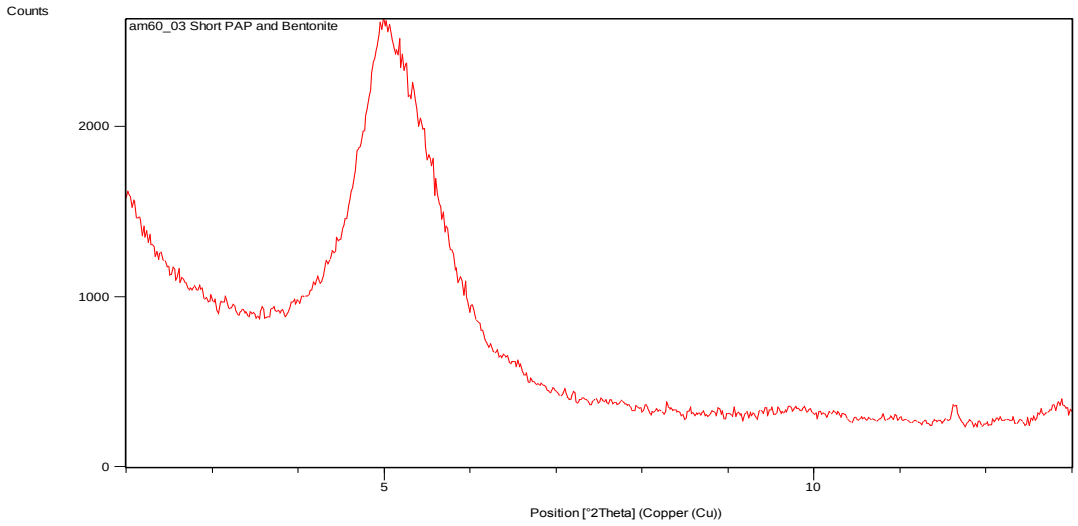
Counts
am60_03 Short PAP and Bentonite
2000
1000
0
5
10
Position [°2Theta] (Copper (Cu))

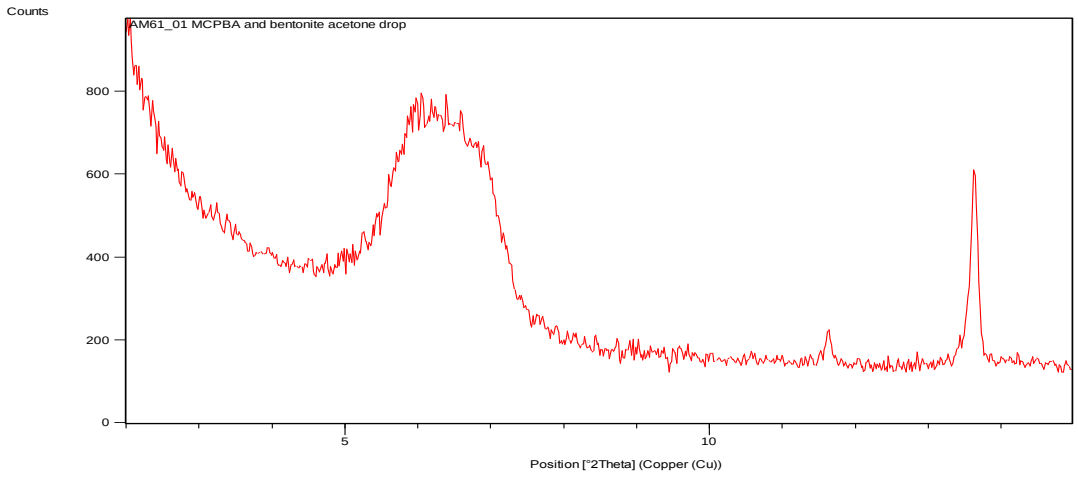
Counts
AM61_01 MCPBA and bentonite acetone drop
800
600
400
200
0
5
10
Position [°2Theta] (Copper (Cu))

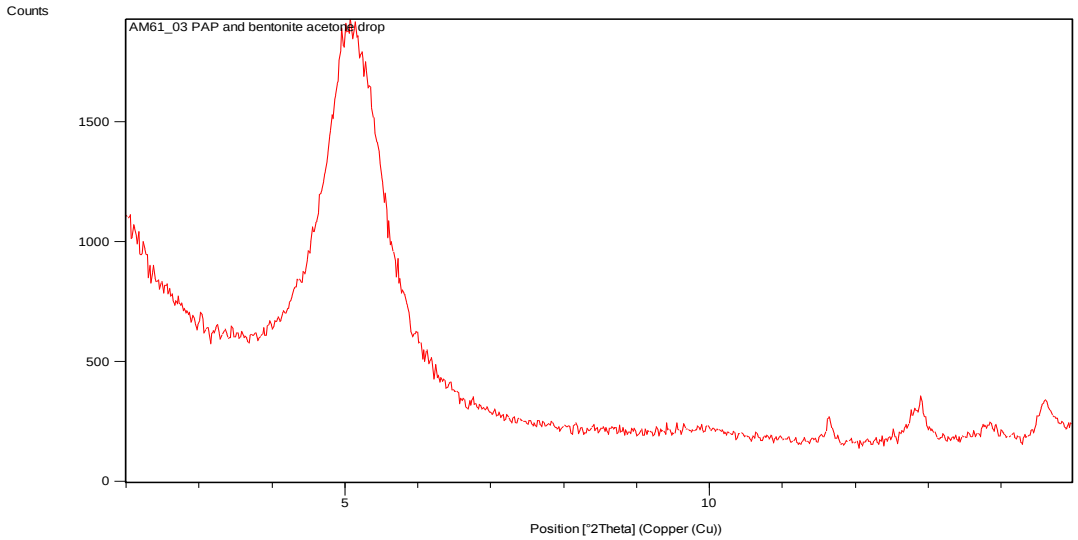
Counts
AM61_03 PAP and bentonite acetone drop
1500
1000
500
0
5
10
Position [°2Theta] (Copper (Cu))

Bentonite and 6-phthalimidoperoxyhexanoic acid incrementing PAP:Bentonite ratio

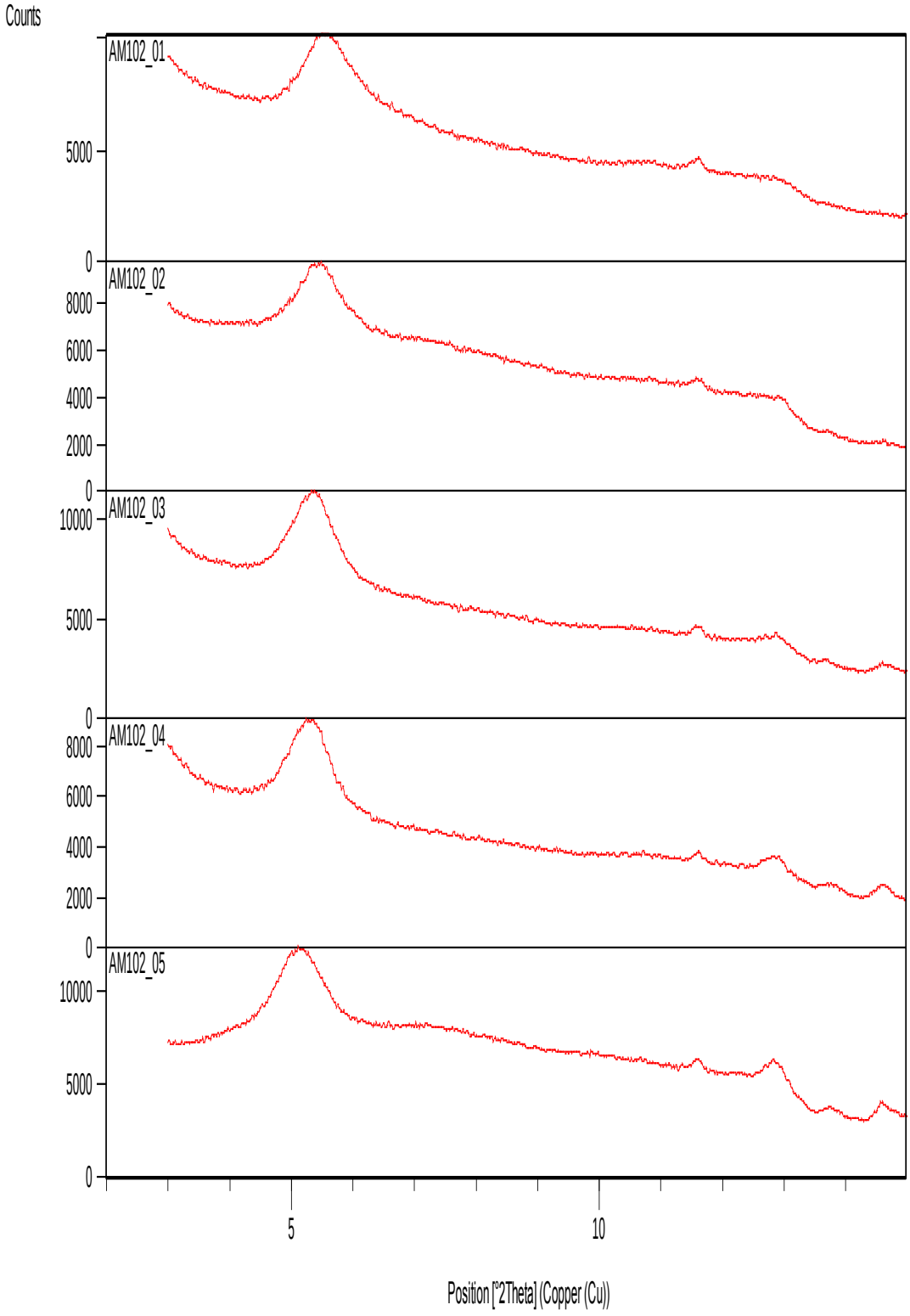

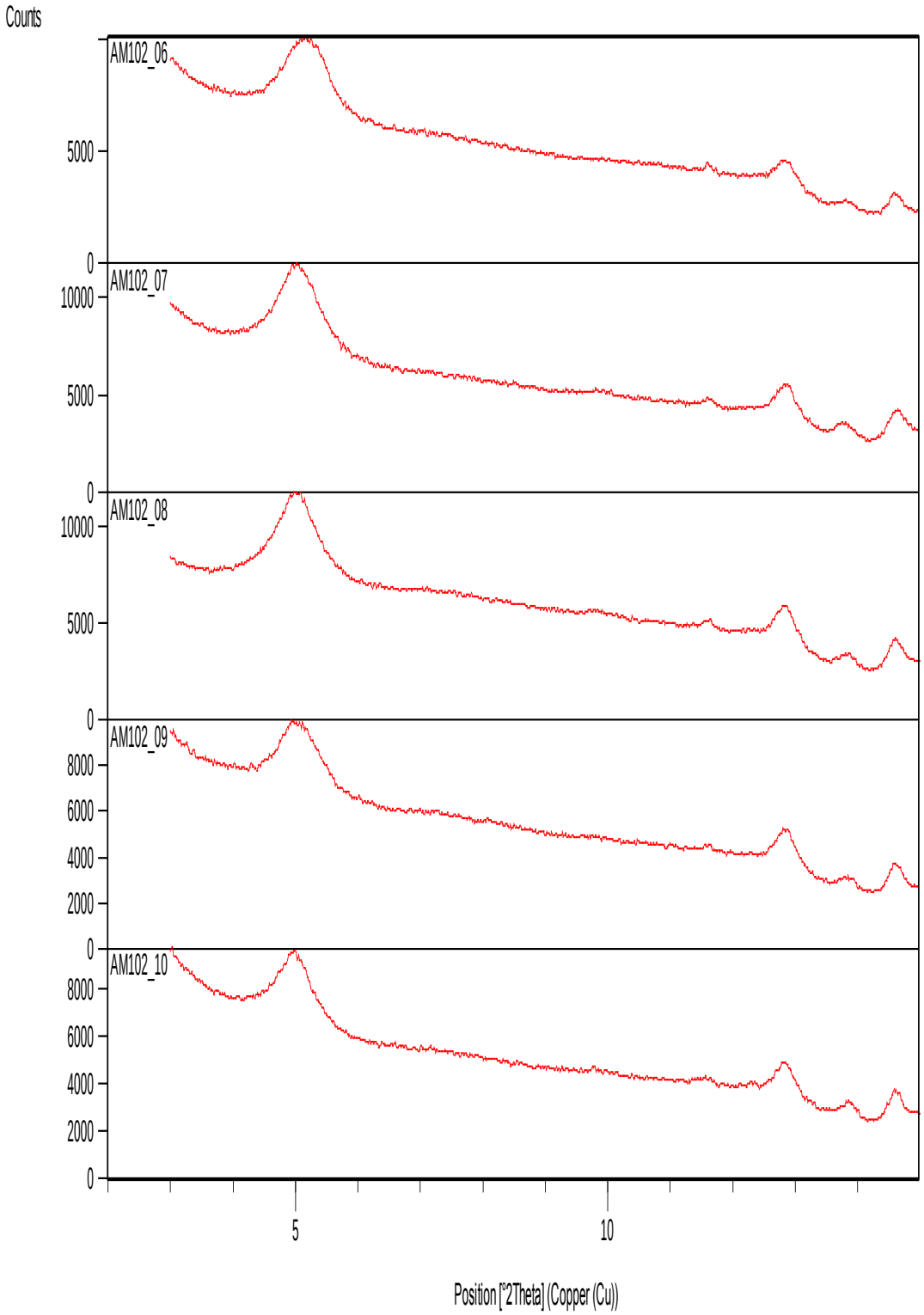
Counts
AM102_06
5000
0
AM102_07
10000
5000
0
AM102_08
10000
5000
0
AM102_09
8000
6000
4000
2000
0
AM102_10
8000
6000
4000
2000
0
5
10
Position [°2Theta] (Copper (Cu))

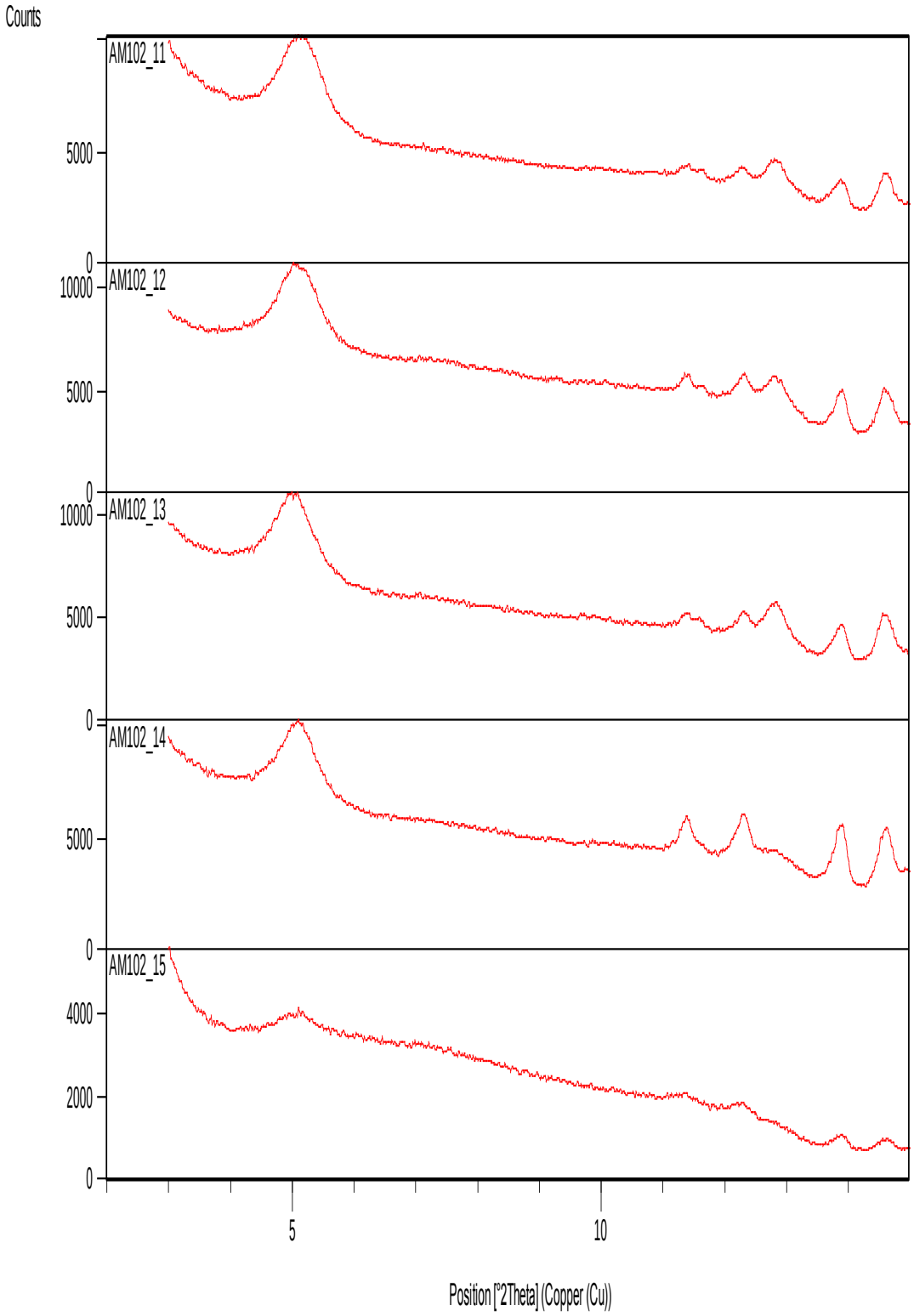
Counts
AM102_11
5000
0
AM102_12
10000
5000
0
AM102_13
10000
5000
0
AM102_14
5000
0
AM102_15
4000
2000
0
5
10
Position [°2Theta] (Copper (Cu))

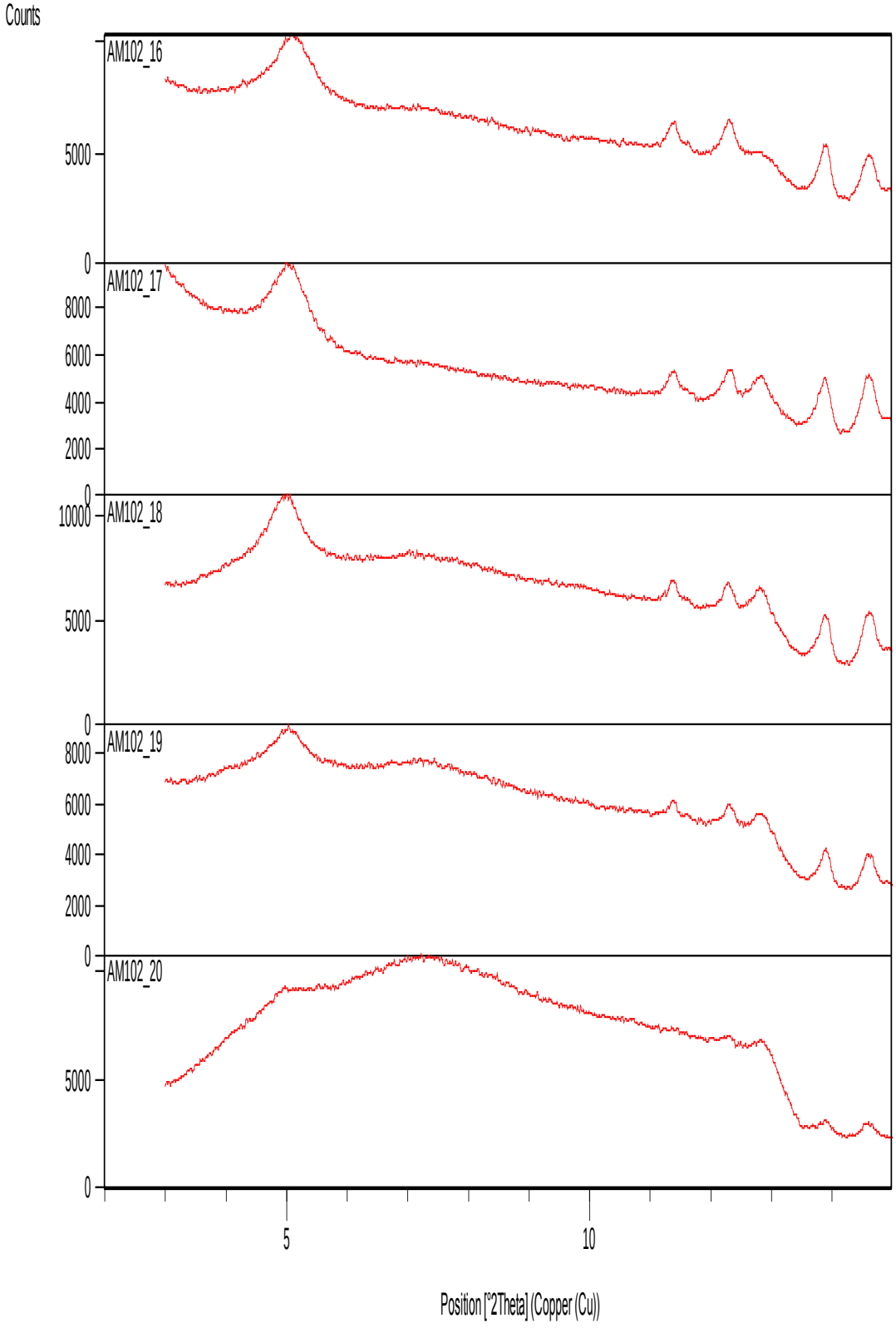
Counts
AM102_16
5000
0
AM102_17
8000
6000
4000
2000
0
AM102_18
10000
5000
0
AM102_19
8000
6000
4000
2000
0
AM102_20
5000
0
5
10
Position [°2Theta] (Copper (Cu))

Bentonite and 6-phthalimidohexanoic acid incrementing Acid:Bentonite ratio

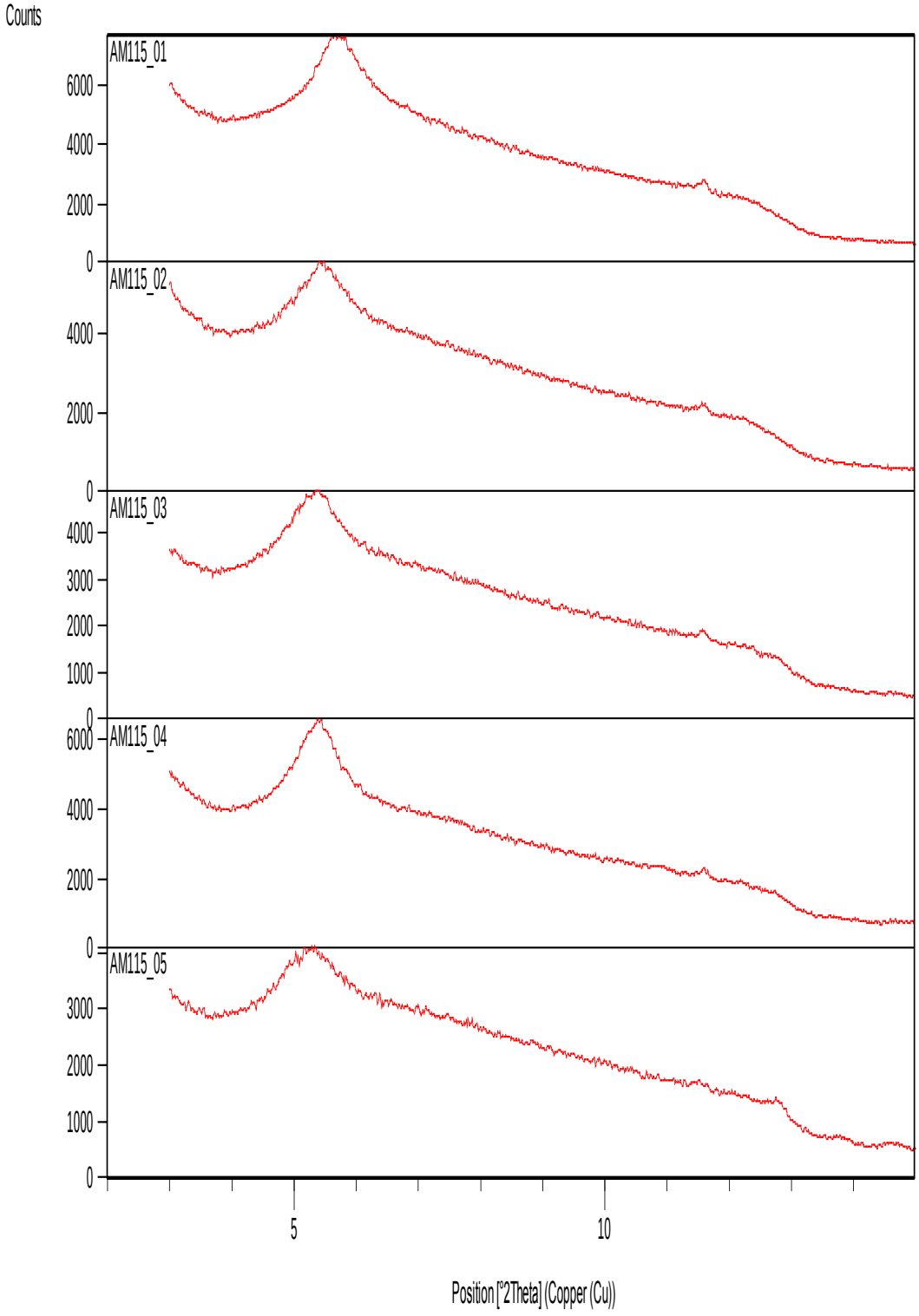

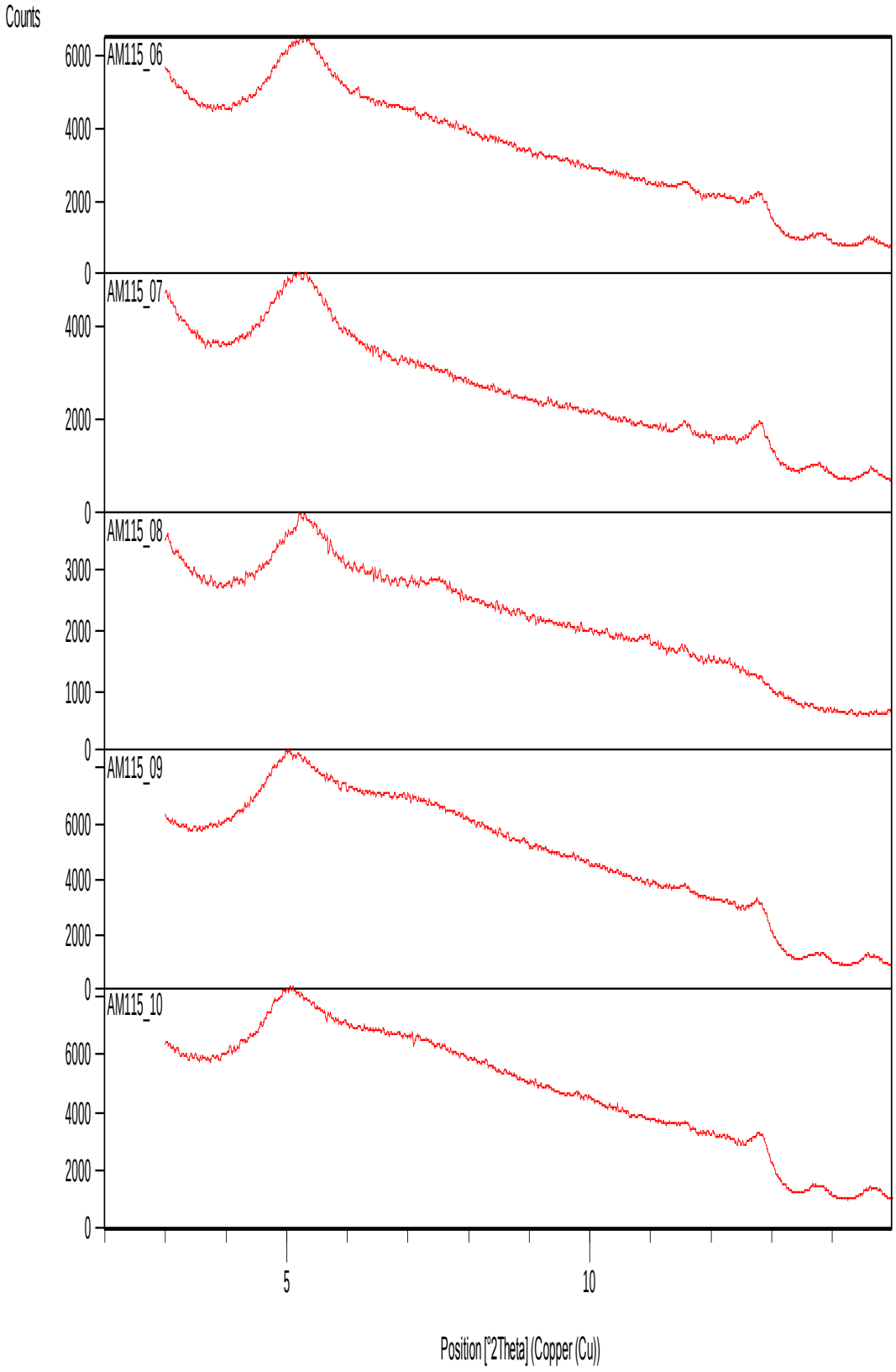
Counts
AM115_06
AM115_07
AM115_08
AM115_09
AM115_10
6000
4000
2000
0
3000
1000
5
10
Position [°2Theta] (Copper (Cu))

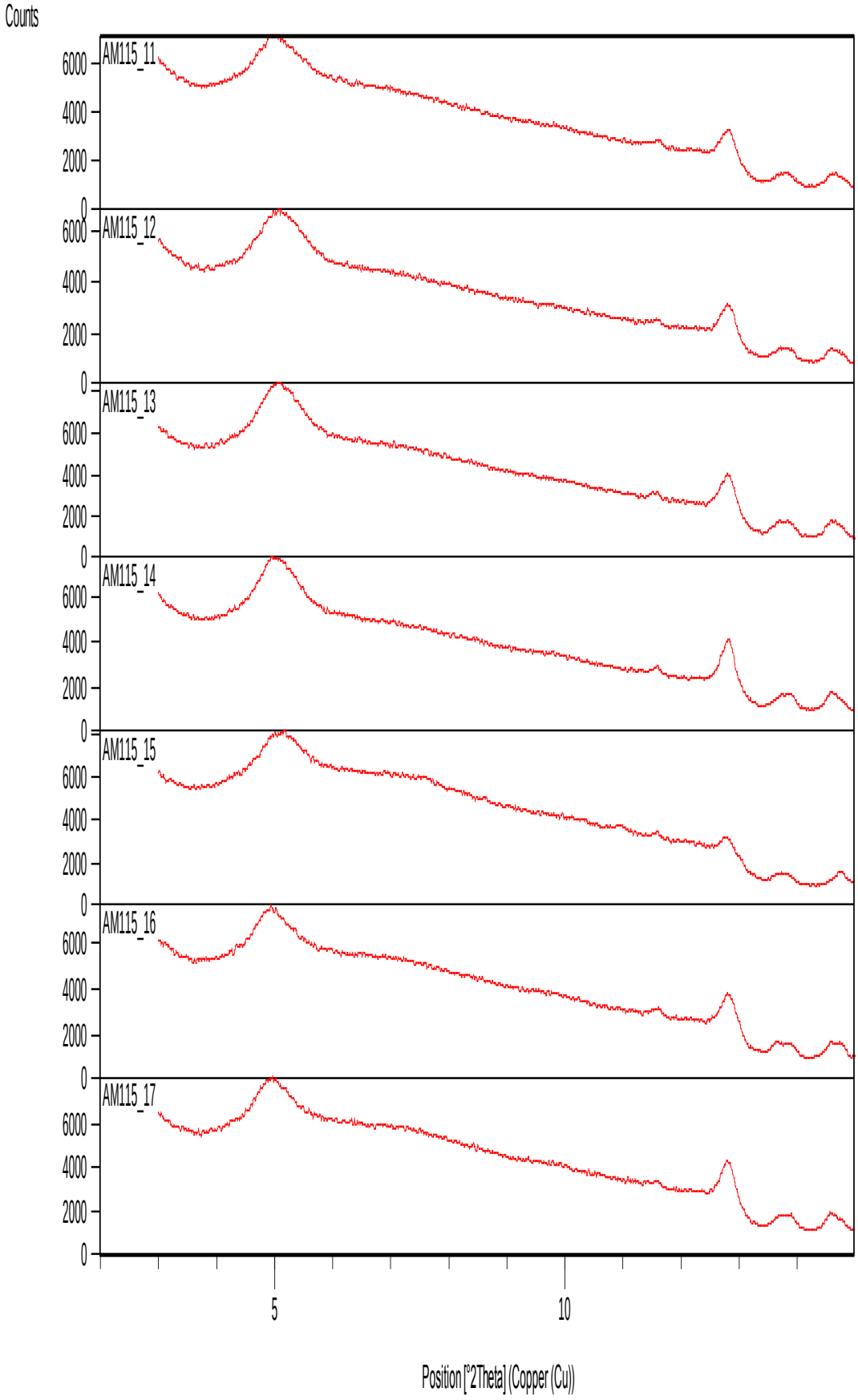
Counts
AM115_11
AM115_12
AM115_13
AM115_14
AM115_15
AM115_16
AM115_17
6000
4000
2000
0
5
10
Position [°2Theta] (Copper (Cu))

Appendix 4 – Cocrystallisation of Agrichemicals

Differential Scanning Calorimetry (DSC) of starting materials

2,4-Dichlorophenoxyacetic acid

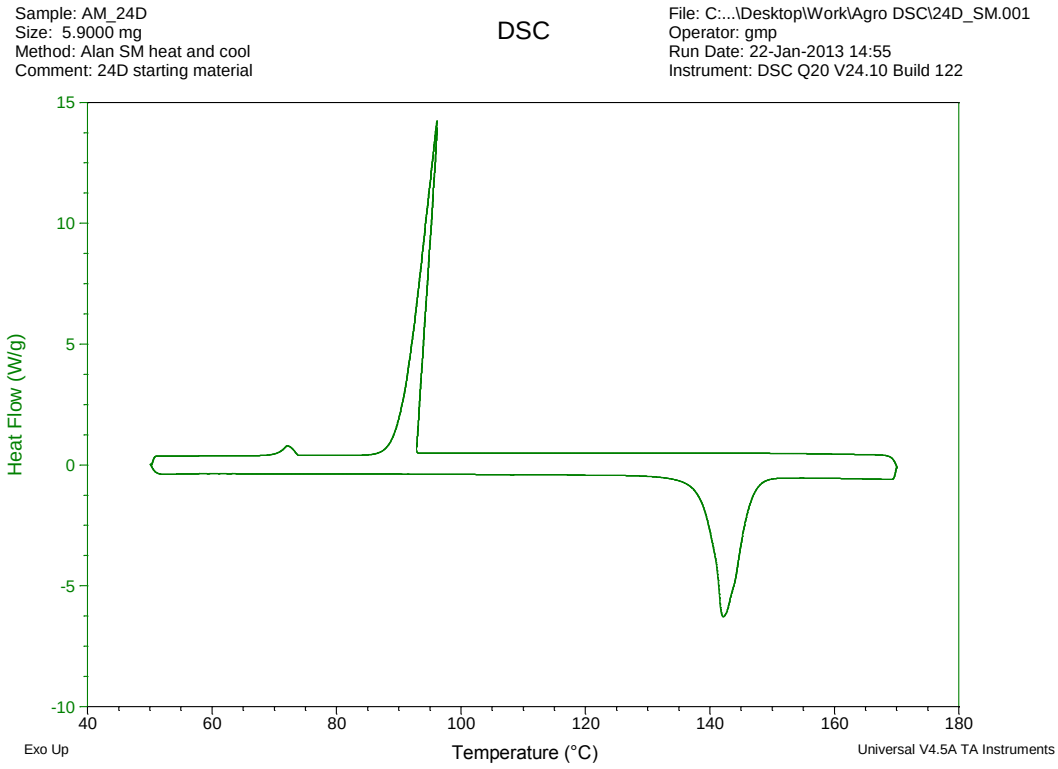

3,4-Dichlorophenoxyacetic acid

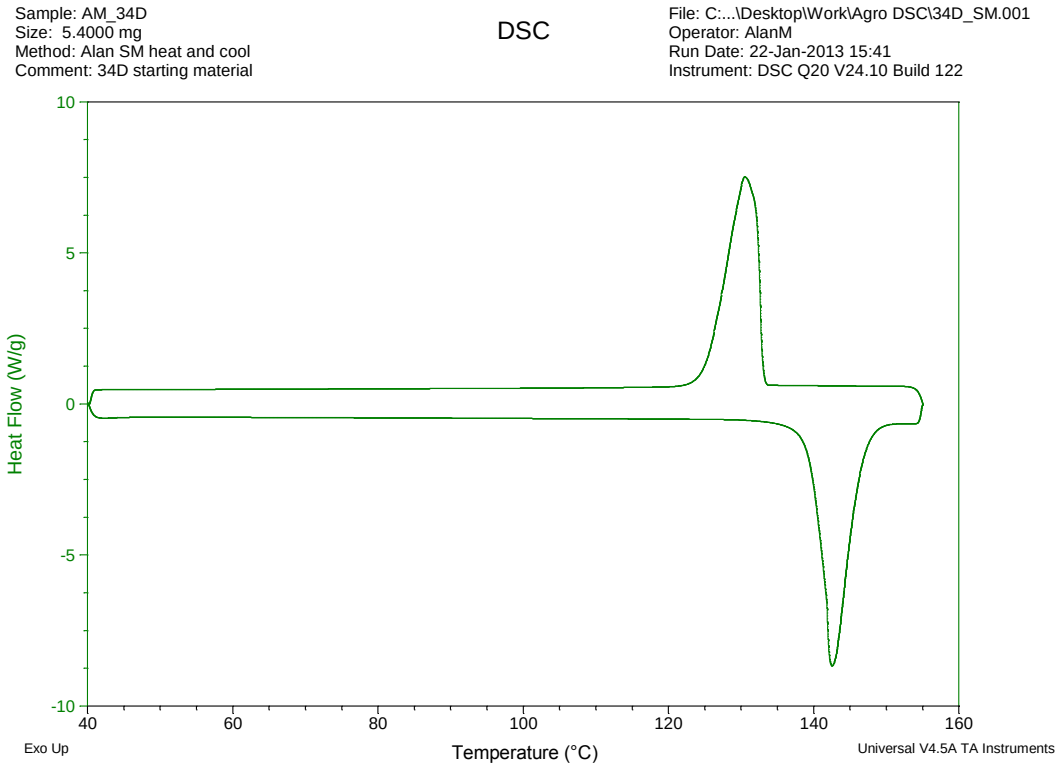

Imidazole

Sample: AM_IMIDAZOLE
Size: 5.4000 mg
Method: Alan SM heat and cool
Comment: IMIDAZOLE starting material

DSC

File: C:...\Work\Agro DSC\IMIDAZOLE_SM.001
Operator: AlanM
Run Date: 22-Jan-2013 16:15
Instrument: DSC Q20 V24.10 Build 122

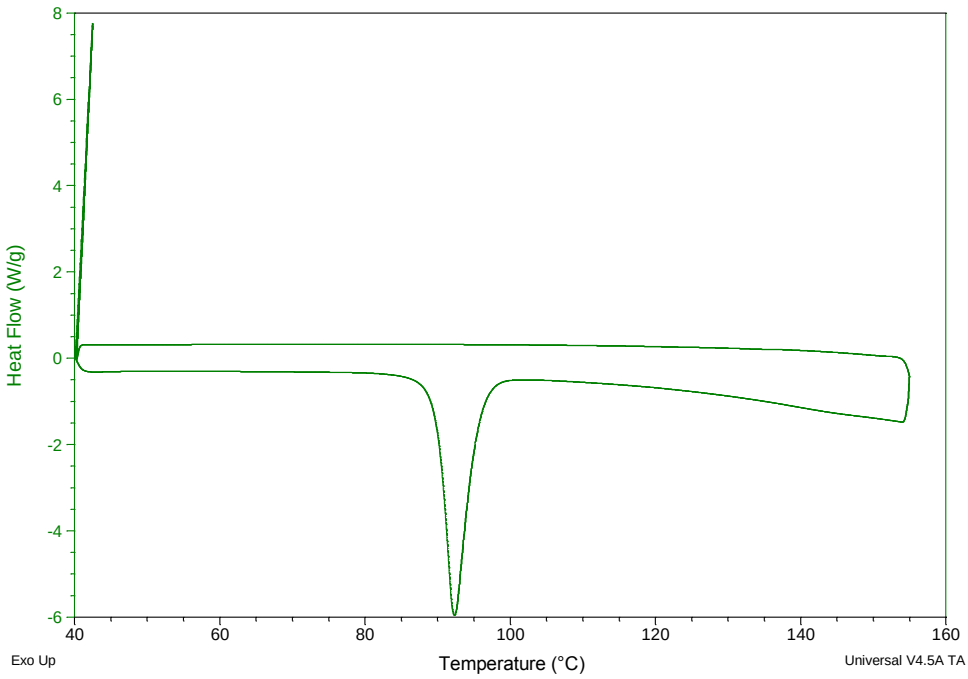

4(5)-Methylimidazole

Sample: AM_METHYLIMIDAZOLE
Size: 6.8000 mg
Method: Alan SM heat and cool
Comment: 4METHYLIMIDAZOLE starting material

DSC

File: C:...\Agro DSC\4METHYLIMIDAZOLE_SM.001
Operator: AlanM
Run Date: 22-Jan-2013 17:45
Instrument: DSC Q20 V24.10 Build 122

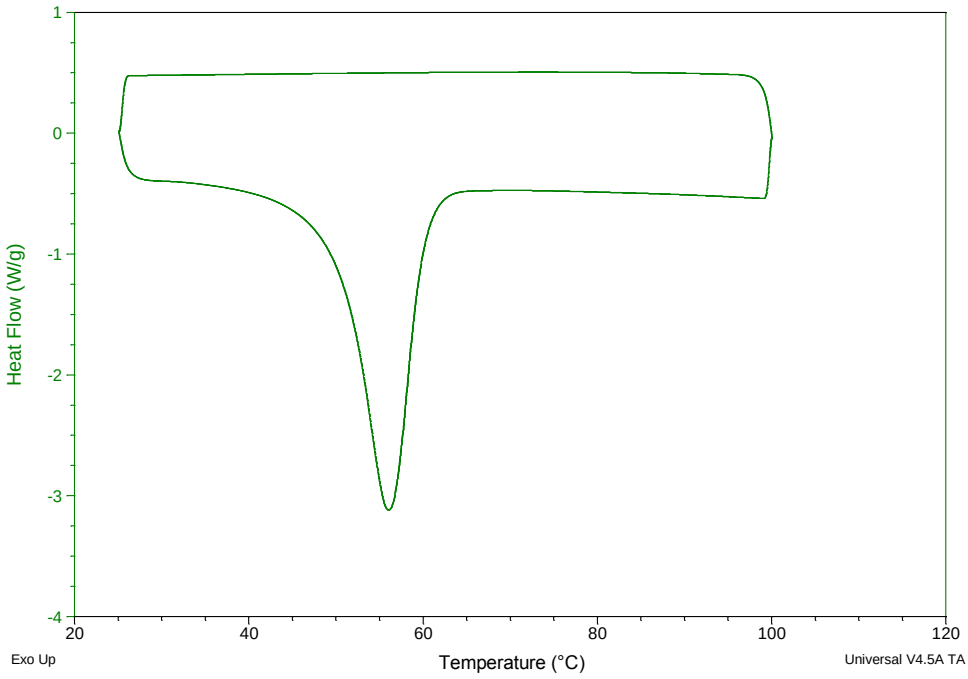

Benzimidazole

Sample: AM_BENZIMIDAZOLE
Size: 3.4000 mg
Method: Alan SM heat and cool
Comment: BENZIMIDAZOLE starting material

DSC

File: C:...\Work\Agro DSC\BENZIMIDAZOLE_SM.00
Operator: AlanM
Run Date: 22-Jan-2013 17:04
Instrument: DSC Q20 V24.10 Build 122

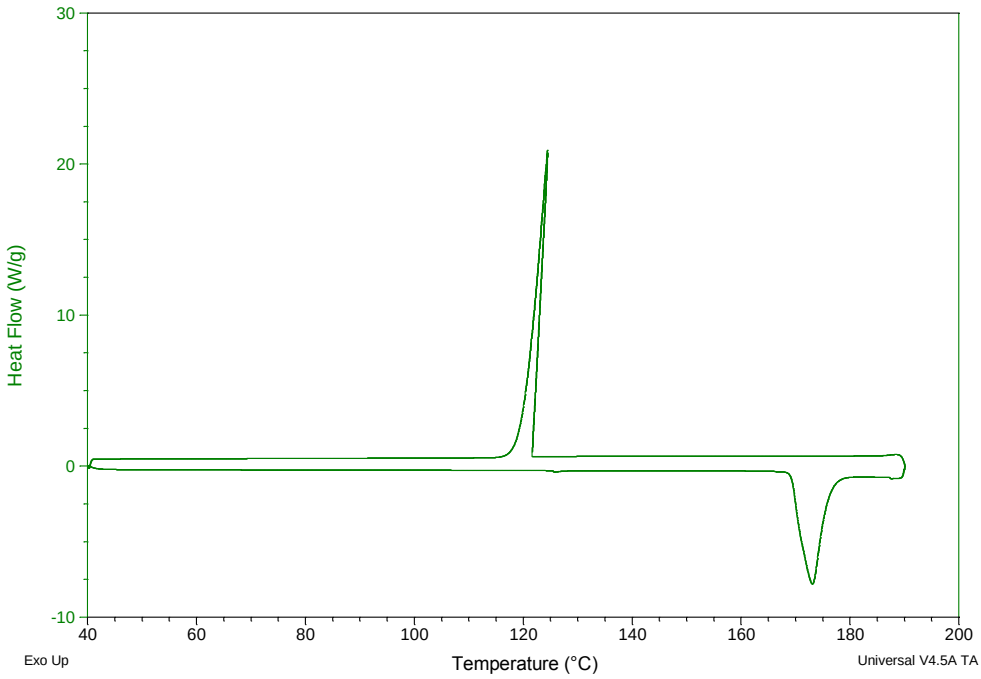

1-Methylbenzimidazole

Sample: AM_1METHYIBENZIMIDAZOLE
Size: 7.6000 mg
Method: Alan SM heat and cool
Comment: 1METHYLBENZIMIDAZOLE starting material

DSC

File: C:...\1-METHYLBENZIMIDAZOLE_SM.001
Operator: AlanM
Run Date: 22-Jan-2013 18:38
Instrument: DSC Q20 V24.10 Build 122

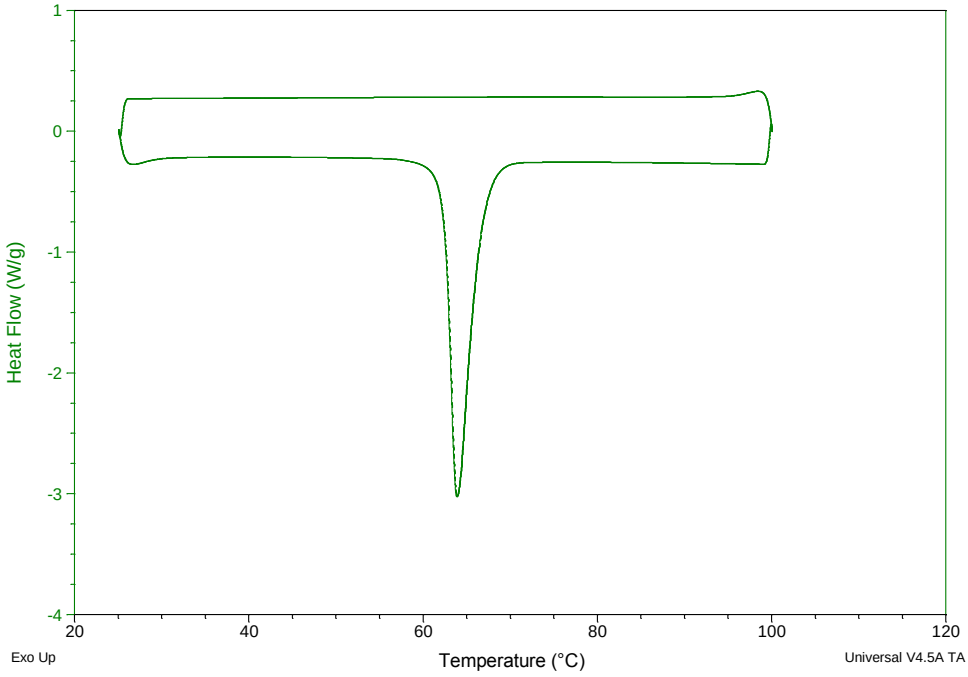

DSC of collected products

2,4-Dichlorophenoxyacetic acid and Imidazole

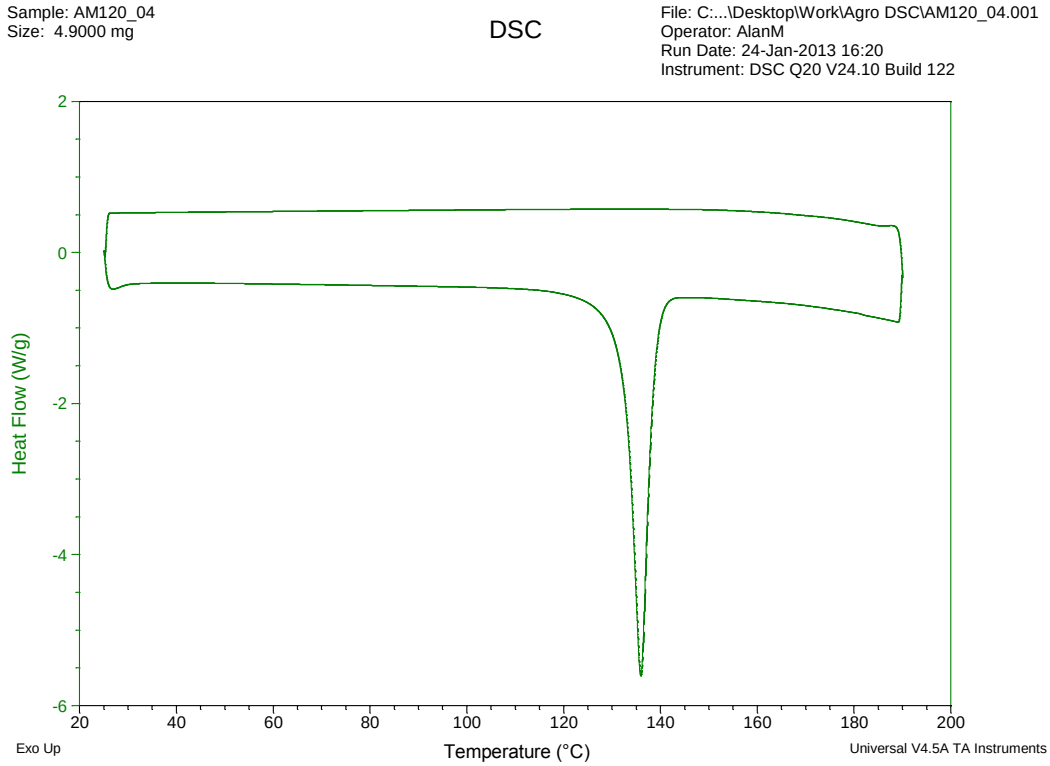

3,4-Dichlorophenoxyacetic acid and Imidazole

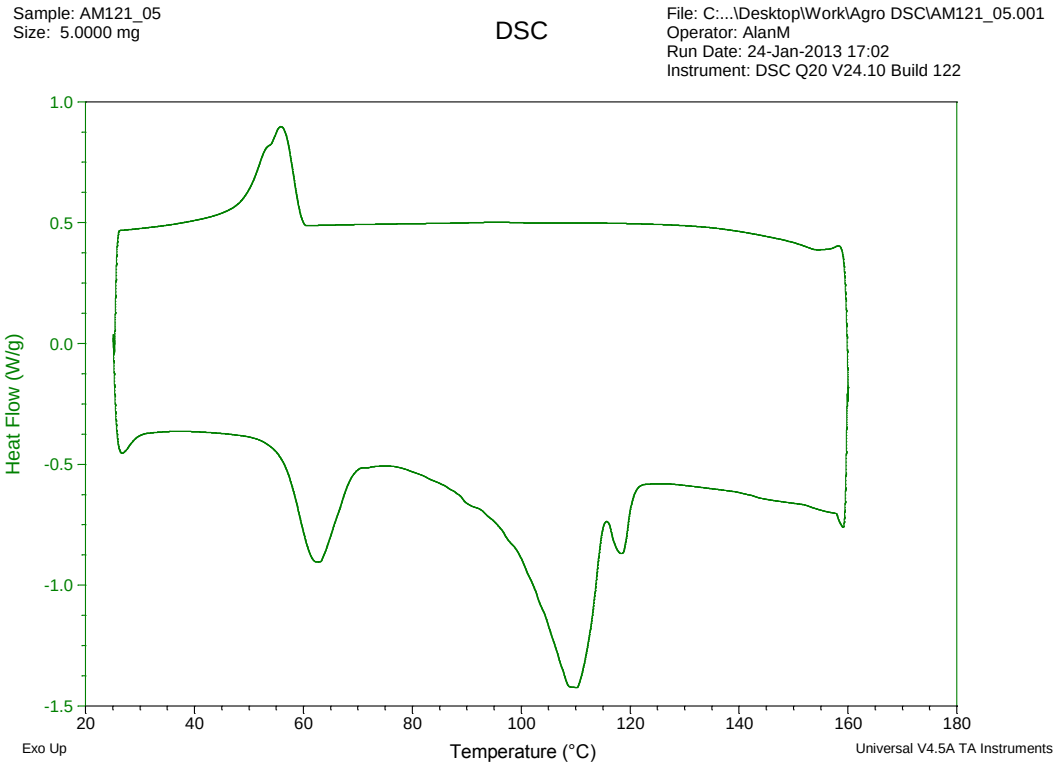

2,4-Dichlorophenoxyacetic acid and 4(5)-methylimidazole

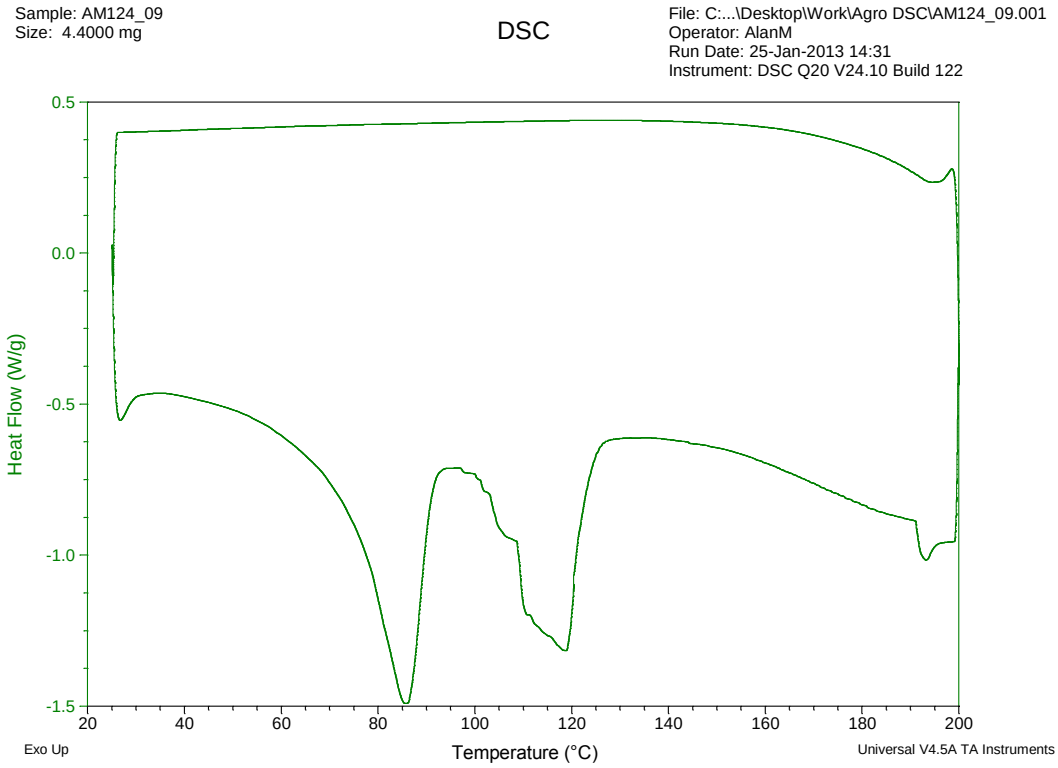

3,4-Dichlorophenoxyacetic acid and 4(5)-methylimidazole

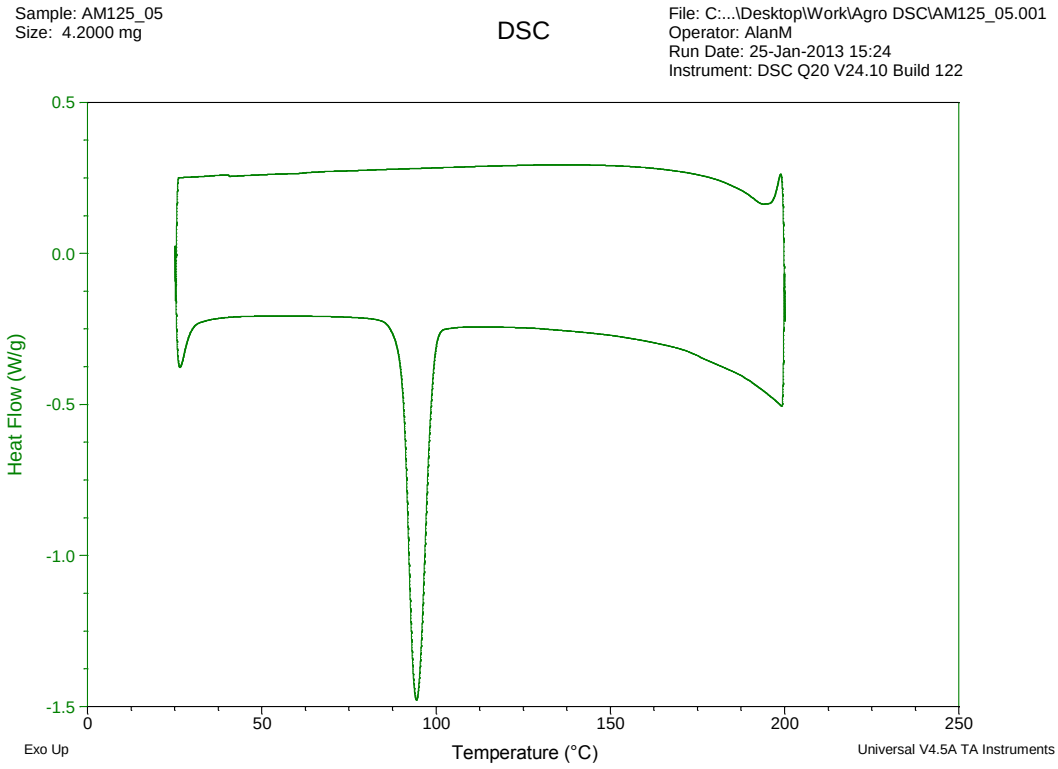

2,4-Dichlorophenoxyacetic acid and benzimidazole

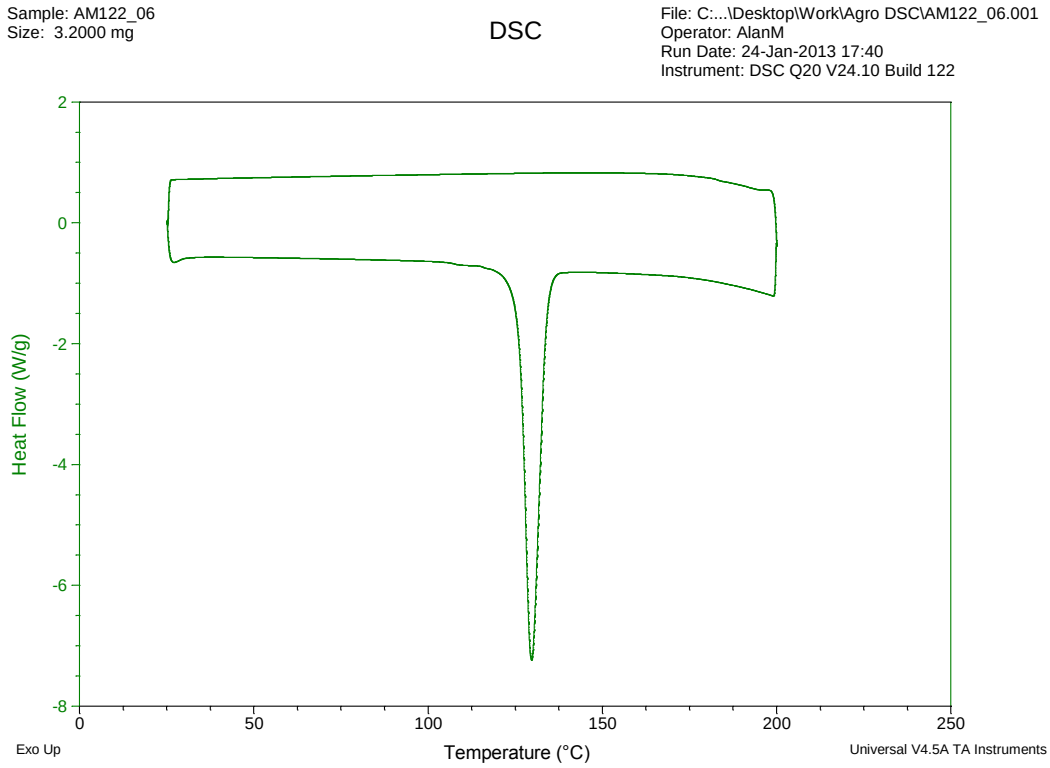

3,4-Dichlorophenoxyacetic acid and benzimidazole

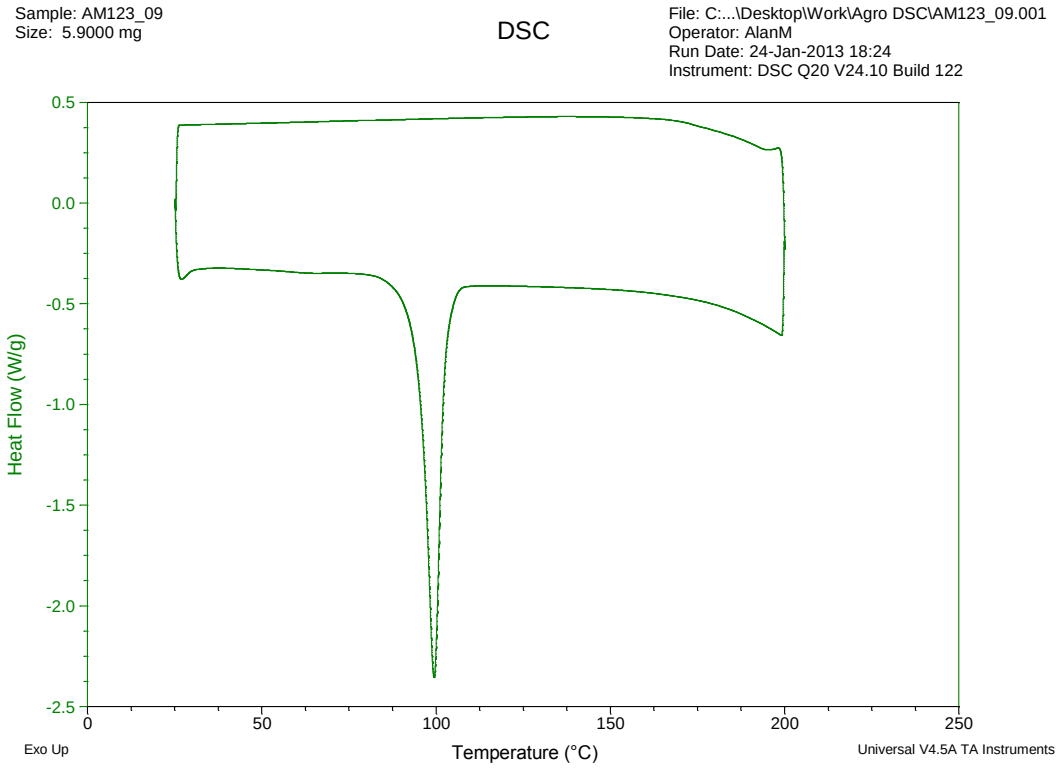

2,4-Dichlorophenoxyacetic acid and1-methylbenzimidazole

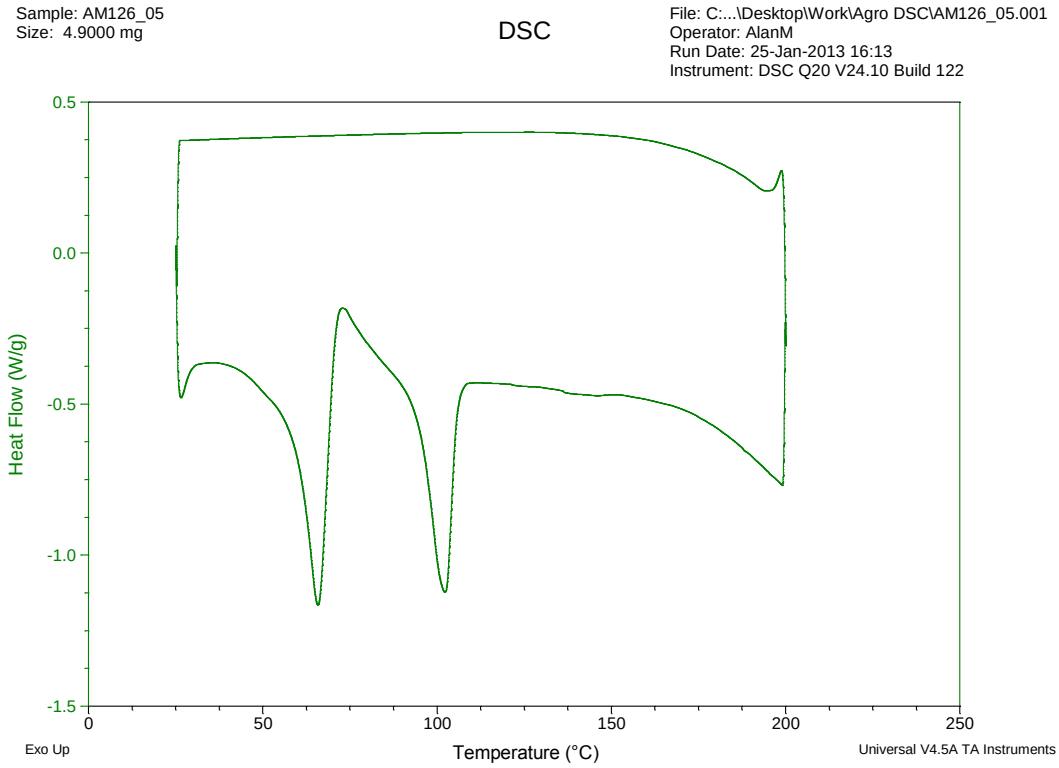

3,4-Dichlorophenoxyacetic acid and 1-methybenzimidazole